

Theoretical Investigation of the Selective Catalytic Reduction of Nitrogen Oxides with Ammonia on Fe/H-ZSM5

Vom Promotionsausschuss der
Technischen Universität Hamburg-Harburg
zur Erlangung des akademischen Grades
Doktor-Ingenieur (Dr.-Ing.)
genehmigte Dissertation

von

Till Brüggemann

aus

Karlsruhe

2012

1. Gutachter: Prof. Dr. Dr. h. c. Frerich J. Keil

2. Gutachter: Prof. Dr. Irina Smirnova

Tag der mündlichen Prüfung: 22.12.2011

Für Katja

Acknowledgements

This work has been accomplished within my time as a PhD student in the Institute of Chemical Reaction Engineering at the Hamburg University of Technology in Germany. Therefore, my special gratitude is dedicated to the head of this institute and my supervisor, Prof. Frerich J. Keil, who gave me the opportunity to work in this field of research, and introduced and taught me the required basics of quantum chemistry and molecular modeling. Furthermore, he supported me in the collaboration with the University of Delaware and always gave me the freedom to set my focus myself while giving advice when needed.

Next, I would like to thank Prof. Dionisios G. Vlachos of the Department of Chemical and Biomolecular Engineering at the University of Delaware for giving me the opportunity to visit his group and for sharing his wisdom in the field of microkinetic modeling. I am very grateful for the fruitful discussions with him and his advice and encouragements related to my work.

Several students have contributed to my work in terms of their Master theses or project works and in this context I would like to thank Marie-Dominique Przybylski, Sayee Prasaad Balaji, Cvetanka Bojkova and Marc-Andreas Christlieb.

The present and former colleagues as well as the permanent staff have always created a pleasant atmosphere in the institute, which brought about a comfortable working environment. I am especially grateful to Niels Hansen, who introduced me to the secrets of Density Functional Theory and always advised me in my work with his fundamental knowledge and experience. Furthermore, I would like to thank my colleagues Sven Jakobtorweihen, Nils Zimmermann, Dennis Chaykin, Aykut Argönül, Diana Tranca and Alexander Rudenko for the nice time, Christina Laarmann and Dr. Achim Bartsch for their support in teaching the practical course, Klaus Mandel for his patient support as a computer administrator and Hermine Oppelaar, the institute's secretary.

Parts of this work are relying on the computing time provided by the "Norddeutscher Verbund für Hoch- und Höchstleistungsrechnen" (HLRN).

Furthermore, I would like to thank my parents and my brother for their steady encouragement and invaluable support during the course of this thesis.

Finally, my entire gratefulness is dedicated to my beloved wife Katja who, besides revising this thesis, always kept the patience to comfort me, to push me, to feed me, to love me and to always say and do the right things even during the most struggling periods of this work.

Contents

I	Basics	1
1	Introduction	3
1.1	Background	3
1.2	Abatement of NO _x	5
1.3	Outline	8
II	Theoretical Background	11
2	Electronic Energy Calculations	13
2.1	Introduction	13
2.2	The Schrödinger Equation	14
2.3	The Born-Oppenheimer Approximation	16
2.4	Electronic Wave Functions	19
2.4.1	The Variational Method	20
2.4.2	Molecular Orbitals	20
2.4.3	Basis Set	22
2.5	The Hartree Fock Method	24
2.6	The Density Functional Theory	28
2.7	Compound Methods	33
3	Reaction Rates and Equilibrium	35
3.1	Potential Energy Surface	35
3.2	Partition Function	39
3.3	Reaction Rates	44
3.4	Application of CHEMKIN	47

III	Selective Catalytic Reduction on Brønsted Acids in H-ZSM5	51
4	Theoretical Investigation of the Selective Catalytic Reduction of Nitrogen Oxides with Ammonia on H-ZSM5	53
4.1	Introduction	54
4.2	Theory	59
4.3	Results and Discussion	62
4.3.1	Formation of NO_2	63
4.3.2	Formation of the Intermediates NH_2NO_x and HNO_y . .	66
4.3.3	Decay of the Intermediates Nitrous and Nitric Acid . .	78
4.3.4	Decomposition of the Intermediates Nitrosamine and Nitramide	92
4.4	Conclusion	97
5	Theoretical Investigation of the Mechanism of the Selective Catalytic Oxidation of Ammonia on H-form Zeolites	99
5.1	Introduction	100
5.2	Theory	103
5.3	Results and Discussion	103
5.3.1	Reaction of NH_3 with O_2	104
5.3.2	Decomposition of HNO	106
5.3.3	Decomposition of NH_2OH	112
5.3.4	Reaction of Nitroxyl with Nitrous and Nitric Acid . . .	117
5.3.5	Pathway for N_2O	120
5.4	Conclusion	122
6	Microkinetic Modeling of the Fast Selective Catalytic Reduction of Nitrogen Oxide with Ammonia on H-ZSM5 Based on First Principles	123
6.1	Introduction	124
6.2	Theory	125
6.3	Results and Discussion	128
6.3.1	Adsorption of Ammonia	129
6.3.2	Modeling of the NO_2 -SCR	132
6.3.3	Modeling of the Fast-SCR	136

6.3.4	Oxidation of Ammonia	141
6.4	Conclusions	143
 IV Selective Catalytic Reduction on Mononuclear Iron Sites in Fe/H-ZSM5		145
7	Theoretical Investigation of the Mechanism of the Oxidation of Nitrogen Oxide on Fe-form Zeolites in the presence of Water	147
7.1	Introduction	148
7.2	Theory	151
7.3	Results and discussion	154
7.3.1	Activity of Iron Exchanged ZSM5 in the Absence of Water	156
7.3.2	Activity of Iron Exchanged ZSM5 in the Presence of Water	169
7.4	Conclusion	182
8	Theoretical Investigation of the Mechanism of the Selective Catalytic Reduction of Nitrogen Oxide with Ammonia on Fe-form Zeolites	185
8.1	Introduction	186
8.2	Theory	189
8.3	Results and discussion	190
8.3.1	Part 1: The Fast SCR	193
8.3.2	Part 2: The NO ₂ SCR	197
8.3.3	Part 3: Impact of Oxygen	203
8.3.4	Part 4: Aspects of SCO and N ₂ O Decomposition	208
8.4	Conclusion	218
9	Microkinetic Modeling of the Selective Catalytic Reduction of Nitrogen Oxide with Ammonia on Fe/H-ZSM5 Based on First Principles	221
9.1	Introduction	222
9.2	Theory	224
9.3	Results and Discussion	226

9.3.1	Modeling of the NO Oxidation	227
9.3.2	Modeling of the NH ₃ Oxidation (SCO)	236
9.3.3	Modeling of the Fast SCR	241
9.3.4	Modeling of the NO ₂ SCR	248
9.3.5	Modeling of the New “Enhanced” SCR	252
9.3.6	Modeling of the Standard SCR	255
9.4	Conclusion	260
V	Backmatter	263
10	Summary	265
A	Supporting Information for Chapter 3	271
B	Supporting Information for Chapter 4	275
B.1	Formation of NO ₂ , NH ₂ NO _x and HNO _y	276
B.2	Decay of HONO and HNO ₃	286
B.3	Decomposition of NH ₂ NO _x	293
C	Supporting Information for Chapter 5	297
C.1	Reaction of NH ₃ with O ₂	298
C.2	Decay of HNO	300
C.3	Decay of NH ₂ OH	304
D	Supporting Information for Chapter 6	309
E	Supporting Information for Chapter 7	335
F	Supporting Information for Chapter 9	337
	Bibliography	361
	Published work	387
	Conferences	389
	Lebenslauf	391

Part I

Basics

1

Introduction

1.1 Background

Catalysis, and by now especially the heterogeneous catalysis, is one of the key technologies of our time^{1,2} and the production of many of the products of our modern world would not be conceivable without it. It was Jöns Jacob Berzelius who, in 1835, was the first to put the basic idea of a catalyst into words, “the body effecting the changes does not take part in the reaction and remains unaltered through the reaction”. He also gave this new concept its name.^{3,4} The history of the industrial application of catalysis dates back to the beginning of the 20th century, when the cooperation of Fritz Haber, Carl Bosch and Alwin Mittasch, which channeled in the famous Haber-Bosch process for the production of ammonia, marked a milestone of the research in this discipline.^{5,6} Back then rather small quantities and only few chemicals were produced by the application of catalysis. Today, however, more than 80 percent^{1,7,8} of all chemical products make use of a catalyst with the highest economical contribution resulting from heterogeneous processes.² Different driving forces and motivations were responsible for the progress in research in this field within the last century. While in the beginning of the 20th century the binding of nitrogen for the use as a fertilizer and the production of explosives from ammonia and nitric acid were the most important application of catalytic processes, the catalytic cracking of petroleum for the production of fuels and polymers dominated the mid-century. By the end of the last century until now the environment has also moved into the center of research interest in heterogeneous catalysis by means of the abatement of

environmental poisons from exhaust gases.³

Recognizing the immense economical potential of catalysis^{2,8} the optimization of existing catalysts as well as the finding of new active materials has become a sector of its own in the chemical industry. However, only by understanding the processes involved in catalysis in detail, a fundamental scientific step can be made in obtaining better catalysts. In the beginning of this field of research most results were obtained by trial and error. The theoretical contributions of Langmuir in 1915^{9,10} with his theories on adsorption and later Hinshelwood in 1927 with the presentation of his kinetic theory,¹¹ however, were responsible for significant improvements because of a better understanding of the functionality of catalysts.³ In addition, when Wheeler¹² in 1951 discovered the impact of diffusion on the activity of catalysts the main influencing factors in heterogeneous catalysis were highlighted, namely mass transport, adsorption and chemical reactions on the catalytic surface. Further significant progress was made with the application of spectroscopic methods¹³ and the analysis of surfaces with scanning tunneling spectroscopy or crystallography.⁸ With the advent of computers and the tremendous development of computational resources the modeling of heterogeneous catalysis has also become feasible and a powerful tool in explaining and predicting several observable phenomena.^{14,15} In fact, today one often refers to three different approaches to understand the governing influences of a catalyst.¹⁶ The first approach is dominated by the analysis of the macroscopic response of a reacting system on pressure, temperature and concentrations. The definition of high throughput experiments (HTE),¹⁷ was a significant development in this field. It allows for the parallelized fast screening of large amounts of potential catalytic active materials as well as the computer guided in depth analysis and characterization of selected catalysts. Alwin Mittasch already used such a kind of screening in order to find an appropriate catalyst for the Haber-Bosch process.¹⁸ The second approach covers the “in situ” application of spectroscopic methods in order to directly visualize intermediates of a reaction. The application of computational based experiments¹⁹ involving quantum chemistry, molecular modeling (Molecular Dynamics or Monte Carlo methods) and microkinetic modeling is referred to as the third way.

Because reactions involve the change of the distribution of electrons in the reacting molecules, the correct description requires an underlying theory that is capable to describe this phenomenon. Such a theory was put down by Erwin Schrödinger in terms of his famous equation in 1926²⁰ which is the backbone of several *ab initio* and semi-empirical models today, capable of describing reactivity. One of the most widely applied methods among them is

the Density Functional Theory (DFT) which has evolved into a working horse in computational chemistry because of its comparatively low computational demand together with reasonable accuracy.^{14,21} More sophisticated and accurate ab initio methods gain importance today but still are restricted to small-scale systems from computational limitations. Climbing on the ladder of time and length scales, in the fields of mass transport in porous structures and adsorption, molecular modeling approaches have been established and contribute to the understanding of these processes.²² The gap between the microscopic evaluation to the macroscopic description of reactor devices is often bridged by the application of microkinetic modeling,²³ which can make use of quantum chemical and molecular modeling results in combination with the application of statistical thermodynamics.

While today the classical and the in situ methods are still dominant, the further development of computational tools and the vast progress in computer power enhances the use of theoretical investigations.²⁴ The ultimate goal would probably be the design from scratch of catalytic devices with all desired properties based on theoretical methods only. However, this would generally require the mapping of the complete energy landscape of a catalyst which is, if ever possible, still decades away.⁸ Nevertheless, the description of reaction pathways in accordance with experiments and the evaluation of reactive patterns for elementary steps on active materials is already possible and significantly increases the understanding of catalytic functionality.²⁵ With that, heterogeneous catalysis will remain a highly integrative science based on the three columns as were outlined, because of its tremendous complexity stretching over several length and time scales. Only a thorough combination of all available resources according to their designated benefits is expected to give the best results in optimizing existing catalysts as well as to facilitate the search for new ones.

1.2 Abatement of NO_x

It has become apparent at the end of the last century that there is a negative impact of exhaust gases of automobiles and industrial production sites on the environment and legislation has been passed to reduce the hazardous and toxicological substances of those gases. With that a new branch of research in heterogeneous catalysis has emerged, dealing with environmental protection.³ One of the important technologies in this field is the abatement of NO_x²⁶ with the prevailing representatives nitrogen oxide and nitrogen dioxide. The main sources of these species are of anthropogenic nature, with the

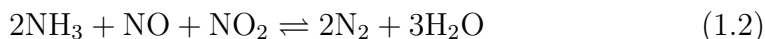
combustion of fossil fuels being the main contributor. This mainly involves the combustion of petroleum in the engines of vehicles as well as the production of electricity in power plants.²⁷ The origin of the nitrogen oxides occurs from the oxidation of molecular nitrogen with oxygen at high temperatures (above 1300K).²⁸ The oxidation of nitrogen bound in the hydrocarbons of the fuel plays only a minor role. Especially in diesel engines the production of nitrogen oxides is significant. Within the industrial sector, a major source of NO_x is the production of nitric acid from the oxidation of ammonia.²⁹

The negative impact of NO_x on the environment can be divided into three main aspects. In the troposphere, they cause the formation of ozone which is responsible for photochemical smog. In the stratosphere, however, they contribute to the depletion of the ozone layer which, here, is in the role of a protecting agent against UV light. Finally, nitrogen oxides are responsible for the formation of acid rain.³⁰ Because of these negative aspects, legislation becomes more and more stringent in most countries to remove nitrogen oxides from exhaust gases.^{27,31} In Europe by now, the so-called EURO V is in effect since 2009 and in the USA the most recent regulations were launched in 2010 which are even more restrictive for heavy duty diesel engines than the European legislation. In fact, the development of tools for the abatement of NO_x already has a long history that started with the three-way catalyst for Otto-engines which is until now probably the best known catalyst worldwide. Because of the stricter legislation the secondary way of reducing emissions of toxic species in exhaust gases remains of high potential for research. With respect to nitrogen oxides the Selective Catalytic Reduction (SCR) has become a key technology besides others.³² Several different catalysts were under investigation in the last two decades as well as different reducing agents.^{28,33} While in the context of diesel engines vanadium-based catalysts have been established, the trend goes more and more to the use of metal-containing zeolites. Here, especially iron or other transition metals, ion-exchanged into the framework of the zeolite, have proven to be of high potential because of their applicability over a wider range of temperatures as well as because of their thermal stability.³⁴ Also, the disposal is less of a problem as compared to the vanadium-based catalysts. Concerning the reducing agent, ammonia has been established from the storage in urea in contrast to hydrocarbons and the reaction follows the following stoichiometry.



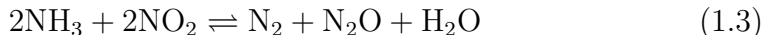
One of the main industrial representatives of this concept is the EnviNO_x[®] process of Uhde, who in cooperation with Süd-chemie, responsible for the iron-containing catalyst EnviCat[®], developed an after-treatment of tail gas from the nitric acid production.

The preparation of these catalysts is, in most cases, based on ion exchange.³⁴ The zeolite, a porous material that is composed of silicon oxide and aluminum oxide tetrahedra,³⁵ contains Brønsted acids to balance the negative charge of the framework aluminum. These can, in general, be exchanged, but during the protocol usually significant amounts of the Brønsted acids either remain or are reformed upon calcination.³⁴ In addition, it is not exactly clear what the exchanged state looks like and what resulting species are responsible for the activity of the catalyst. Several possible structures have been proposed with the mostly accepted assumption of a mixture of mono- and dinuclear species bond to framework aluminum and extra framework iron oxide clusters.³⁶ Because the parent H-form zeolites were also proven to exhibit a significant activity for the SCR, with the ion-exchanged state, a highly complex system is established with at least two different active sites. The complexity as well as the high potential of this reactive system is also reflected in the experimental investigations of the last two decades. Despite ongoing efforts in this field only little is known about the mechanism of the catalyst in terms of a detailed description of the elementary steps and potential intermediates including the contributions of different active sites. However, some interesting features have been discovered, being responsible for subdivisions of the SCR and the related experimental studies. A well-known subsystem is the so-called fast SCR, which received its name from the high activity for the case that equimolar amounts of NO and NO₂ are present in the reactant gas.³⁷ This is true for the vanadium-based catalysts as well as for the H-form and the iron-containing zeolites. The overall reaction stoichiometry is given by:



Because of the significant increase of activity for these reaction conditions over the standard SCR, an effective preoxidation catalyst prior to the fast SCR, which is considered as the essential SCR step, is discussed. However, a further increase of the ratio of NO to NO₂ > 1 even results in a slight decrease of the activity together with the production of unwanted N₂O, proving the active role of NO. For the limiting case of only nitrogen dioxide present in the exhaust gas, large amounts of nitrous oxide were observed.³⁸ For the H-form zeolites even equimolar amounts of nitrogen and nitrous oxide were reported.³⁹ In the case of the iron-containing catalysts such a high ratio is only observed at temperatures between 250° and 300°C and reduces drastically at elevated temperatures.⁴⁰ However, these catalysts, in contrast to the H-form zeolites, are also active for the nitrous oxide decomposition,⁴¹ which could explain these deviating observations. In accordance with the observation of an equimolar production of nitrogen and nitrous oxide from the

principal NO₂-SCR, the following stoichiometric equation can be deduced.



Because of the significantly enhancing contribution of NO₂ in the SCR it was concluded that the oxidation of nitrogen oxide should be the limiting step in the standard SCR mechanism. Finally, also the selective catalytic oxidation of ammonia (SCO)⁴² was found to be catalyzed by iron-containing zeolites and a correlation between the activity for the SCR and the selectivity towards nitrogen in the SCO was observed.⁴³ With that, the selective catalytic reduction of nitrogen oxides with ammonia on iron-exchanged zeolites represents a complex system of ambiguous reactive subsystems that cannot be clarified by experimental methods only. In order to understand the influences of the different active sites in the SCR, it is necessary to understand their activities for all subsystems separately and their capability to produce or remove distinct intermediates. The interest in the clarification of the reaction mechanism results from the impact of this information in order to optimize the catalyst with respect to its preparation or the potential addition of further active sites to increase the velocity of limiting intermediate steps. However, only by evaluating all relevant elementary steps, responsible for the macroscopic behavior of the catalyst, the reaction mechanism of the SCR can be elucidated. The aim of this work is to apply theoretical methods to clarify the governing reaction pathways within the Fe/H-ZSM5 catalyst, taking into account mononuclear iron species and Brønsted acids as active sites for the technically relevant reactive systems. This is supposed to significantly enhance the understanding of the SCR of nitrogen oxides beyond the capabilities of pure experiments.

1.3 Outline

The thesis is subdivided into five parts. In the first part (chapter 1) the background of this work is outlined, covering the general importance of catalysis and the different approaches to understand their functionality as well as a short introduction to the significance of the investigated selective catalytic reduction of nitric oxide. The second part describes the theoretical methods used to analyze the governing chemistry of the SCR on the Fe/H-ZSM5 catalyst. This contains the description of the general idea of quantum chemical methods like DFT, starting with the Schrödinger equation. Furthermore, the background of the relevant statistical thermodynamics and transition state theory is described.

The Fe/H-ZSM5 represents a complex system of at least two different active sites, namely iron and Brønsted acids. The analysis of the mechanism of the SCR on this catalyst was, thus, executed separately for the acid sites and iron in terms of mononuclear iron species. The third part contains the investigations of the mechanism on the H-form zeolite with respect to the Brønsted acids as active sites. The DFT results for the SCR with a focus on the industrially relevant contribution to fast and NO₂ SCR are discussed in chapter 4 and the oxidation of ammonia (SCO) in chapter 5. The quantitative comparison against experimental data and final elucidation of the relevant reactions on the Brønsted acids is then accomplished in terms of microkinetic modeling of the system (chapter 6)

The fourth part is concerned with the role of the mononuclear iron sites in the SCR. Particular emphasis is put on the oxidation of NO to NO₂ in chapter 7 which is believed to be rate-limiting in the SCR and the influence of water is analyzed by using DFT. Furthermore, the mechanisms of the fast and the NO₂ SCR as well as of the ammonia oxidation are thoroughly discussed in chapter 8. Finally, the microkinetic model, containing all calculated reaction steps on the mononuclear iron sites together with the relevant reactions on the Brønsted acids, is applied to compare the simulations against experimental conversion data and to elucidate the relevant reaction mechanisms on the combined catalyst. The influence of the different active sites is discussed (chapter 9).

The fifth part contains the summary of the essential results of this thesis (chapter 10) and additional information is provided in the appendix. All the individual parts are self-contained and include relevant simulation details.

Part II

Theoretical Background

2

Electronic Energy Calculations

In this chapter a short introduction to quantum chemistry and its application in computational approaches with a wide spread in use is provided. Based on the Schrödinger equation, this includes the Hartree Fock method and the Density Functional Theory.

2.1 Introduction

A prerequisite of the description of chemical reactions is the explicit consideration of electrons because they are necessary to describe the fundamentals of reactivity: the breaking and forming of bonds. In contrast to the modeling of macroscopic phenomena, which usually relies on a classical description of the motion of atoms and molecules (e.g. Newton's laws), chemical bonds need a description on the basis of quantum mechanics. While in the beginning of the last century the application of this theory, and especially the Schrödinger equation, was mainly restricted to the most simple systems, today molecular systems of practical use can be studied. This can be attributed to the rapid increase in computational resources but also to the development of additional

techniques which basically imply certain simplifications and approximations regarding the governing quantum chemical equations. In this context, two main branches have been developed: the Hartree Fock method (HF) and the Density Functional Theory (DFT). The HF method allowed for several further improvements leading to very accurate and sophisticated methods. Because this branch generally does not require any additional information but molecular coordinates, the corresponding methods are referred to as *ab initio*. DFT, in contrast, lacks a comparable systematic improvability towards higher accuracy. In addition, within the required functionals, in some cases a fit to experimental or higher level HF data is incorporated and DFT is therefore sometimes argued to not be a true *ab initio* approach. Nevertheless, in most cases DFT exhibits a reasonable accuracy which, in combination with its high efficiency, made it very popular to molecular descriptions in the last two decades. By now there are several excellent textbooks available that cover the scope from basic quantum mechanics to the description of HF and post-HF methods as well as DFT. Those are for example the works of Cramer,¹⁹ Leach⁴⁴ and Jensen.⁴⁵ General introductions to quantum chemistry can be found in the books of Dahl²⁰ and Levine.⁴⁶ More advanced descriptions are outlined in the work of Szabo and Ostlund,⁴⁷ and of Helgaker, Jørgensen and Olsen.⁴⁸

2.2 The Schrödinger Equation

Quantum mechanics allows for the proper description of the behavior of microscopic particles, and applied to chemistry is referred to as *quantum chemistry*.⁴⁶ The general starting point is the governing equation of this concept: the Schrödinger equation in its full time-dependent form.

$$\left\{ -\frac{\hbar^2}{2m} \left(\frac{\partial^2}{\partial x^2} + \frac{\partial^2}{\partial y^2} + \frac{\partial^2}{\partial z^2} \right) + \mathcal{V} \right\} \Psi(\mathbf{r}, t) = i\hbar \frac{\partial \Psi(\mathbf{r}, t)}{\partial t} \quad (2.1)$$

The central part of this partial differential equation (2.1) is the wave function Ψ which contains all possible information of the considered system as well as its evolution in time. Here, the equation is written for a single particle (e.g. an electron) of mass m , defined by the spatial coordinates $\mathbf{r} = x, y, z$ and time t . \mathcal{V} denotes an external field which acts on the system, and \hbar is the Planck's constant divided by 2π . The meaning of the wave function cannot be related to the state of a system as described by classical mechanics which would specify the position of the considered particle and with that violate the Heisenberg's uncertainty relation. In contrast, in 1927, Max

Born⁴⁹ was able to relate the wave function to the *probability* of observing the considered particle around a definite position in space. In most cases of quantum chemistry, the dependency on time can be neglected and the consideration of *stationary-state wave functions* is sufficient. By assuming that the external field is not dependent on time, one easily obtains the time-independent Schrödinger equation which corresponds to the version in which Erwin Schrödinger published it first in 1926.⁵⁰

$$\left\{ -\frac{\hbar^2}{2m} \nabla^2 + \mathcal{V} \right\} \Psi(\mathbf{r}) = E \Psi(\mathbf{r}) \quad (2.2)$$

Here, E is the system energy corresponding to the stationary state wave function Ψ . By denoting the term in brackets on the left-hand side as the Hamiltonian operator \mathcal{H} , the Schrödinger equation reduces to a more simplistic representation.

$$\mathcal{H} \Psi = E \Psi \quad (2.3)$$

With that Ψ is an eigenfunction of the Hamiltonian operator \mathcal{H} with the eigenvalue E . Thus, the main task is to find proper wave functions that solve the equation (2.3) within deterministic boundary conditions. Switching from the special case of one particle to the more general case of quantum chemistry, a molecule with N electrons and K nuclei, the form of equation (2.3) remains unaltered and the Hamiltonian operator can be subdivided into five separate contributions accounting for the kinetic energy of the electrons and the nuclei as well as for the attraction and repulsion of electrons and nuclei with each other. Additional terms could be included to account for contributions from an external electric or magnetic field or relativistic effects which are, however, not relevant in the context of this work.

$$\mathcal{H} = \mathcal{T}_{el} + \mathcal{T}_{nuc} + \mathcal{V}_{el-el} + \mathcal{V}_{nuc-nuc} + \mathcal{V}_{el-nuc} \quad (2.4)$$

The operators for the kinetic energies can be expressed as

$$\mathcal{T}_{el} = - \sum_i^N \frac{\hbar^2}{2m_e} \nabla_i^2 \equiv - \sum_i^N \frac{1}{2} \nabla_i^2 \quad (2.5)$$

and

$$\mathcal{T}_{nuc} = - \sum_k^K \frac{\hbar^2}{2m_k} \nabla_k^2 \equiv - \sum_k^K \frac{1}{2M_k} \nabla_k^2 \quad (2.6)$$

with m_e being the mass of an electron, m_k the mass of the nucleus k and ∇^2 the Laplace operator acting on the i^{th} electron with coordinates \mathbf{r} or on the k^{th} nucleus with coordinates \mathbf{R} . M_k is the ratio of m_k and m_e . The repulsion

of the electrons and of the nuclei among each other is expressed as Coulomb interactions

$$\mathcal{V}_{el-el} = \frac{1}{2} \sum_i^N \sum_j^N \frac{e^2}{4\pi\epsilon_0 r_{ij}} \equiv \frac{1}{2} \sum_i^N \sum_j^N \frac{1}{r_{ij}} \quad (2.7)$$

and

$$\mathcal{V}_{nuc-nuc} = \frac{1}{2} \sum_k^K \sum_l^K \frac{e^2 Z_k Z_l}{4\pi\epsilon_0 r_{kl}} \equiv \frac{1}{2} \sum_k^K \sum_l^K \frac{Z_k Z_l}{r_{kl}} \quad (2.8)$$

Here, e is the charge of an electron, Z is the atomic number, ϵ_0 is the permittivity of vacuum and r are the interelectronic and internucleus pairwise distances. Finally, the pairwise attractive potential between electrons and nuclei is described by

$$\mathcal{V}_{el-nuc} = - \sum_i^N \sum_k^K \frac{e^2 Z_k}{4\pi\epsilon_0 r_{ik}} \equiv - \sum_i^N \sum_k^K \frac{Z_k}{r_{ik}} \quad (2.9)$$

The term on the right hand side of the equations refers to the common notation in atomic units. It should be noted that, because in this general case N electrons and K nuclei are considered, the wave functions become a function of both, the coordinates \mathbf{r} of the electrons and \mathbf{R} of the nuclei: $\Psi(\mathbf{r}, \mathbf{R})$. However, an exact solution of the Schrödinger equation can only be obtained for a few problems, including the “particle in a box”, the harmonic oscillator, the rigid rotator and the hydrogen atom. Therefore, it is necessary to apply certain approximations and techniques to generate solutions to more complex problems like molecules.

2.3 The Born-Oppenheimer Approximation

An exact solution can only be obtained for up to two interacting particles, excluding already the Helium atom. To overcome this limitation, one of the most often applied approximations in quantum chemistry is the *Born-Oppenheimer approximation* (BO) which was proposed by Max Born and Robert Oppenheimer⁵¹ in 1927. The general idea is to decouple the motion of the electrons and the nuclei because of their substantially different mass (the mass of a proton is about 1800 times larger than that of an electron) and the related difference in velocity. It is assumed that, in comparison to the nuclei, electrons move so fast that they instantaneously adjust to any change of the coordinates of the nuclei and with that the electrons move in the field of the fixed protons.⁴⁷ In consequence, the electronic energy can be

calculated for a fixed position of the nuclei. Furthermore, the kinetic energy of the nuclei is considered to be independent of the electrons, the correlation of the motion of electrons and protons is eliminated from the attractive electron-proton potential energy term and the internuclear repulsion term of the potential energy becomes a constant. Mathematically, this idea is represented with a separation of the wave function into an electronic and a nuclear wave function.

$$\Psi(\mathbf{r}, \mathbf{R}) = \Psi_{elec}(\mathbf{r}; \mathbf{R})\Psi_{nuc}(\mathbf{R}) \quad (2.10)$$

The semicolon in the electronic wave function emphasizes that it is not a direct function of the coordinates of the nuclei but depends parametrically on their position. The separate consideration of electrons and nuclei also results in the splitting of the Hamiltonian operator. For the electronic part, the kinetic energy of the nuclei and the internuclear repulsion is neglected. The neglect of the internuclear repulsion is valid because it is deduced to be a constant. An operator acting on a constant solely returns that constant and, thus, its addition just adds to the eigenvalue. The resulting electronic Hamiltonian reads

$$\mathcal{H} = -\sum_i^N \frac{1}{2} \nabla_i^2 + \frac{1}{2} \sum_i^N \sum_j^N \frac{1}{r_{ij}} - \sum_i^N \sum_k^K \frac{Z_k}{r_{ik}} \quad (2.11)$$

with the corresponding electronic Schrödinger equation

$$\mathcal{H}_{elec} \Psi_{elec} = E_{elec} \Psi_{elec} \quad (2.12)$$

The electronic energy is, as a consequence, also parametrically a function of the coordinates of the nuclei as is the electronic wave function. The total energy for the case of the fixed nuclei is then the sum of the electronic contribution and the potential energy of the internuclear repulsion.⁴⁷

$$E_{tot} = E_{elec} + \frac{1}{2} \sum_k^K \sum_l^K \frac{Z_k Z_l}{r_{kl}} \quad (2.13)$$

For the motion of the nuclei, the application of the Born-Oppenheimer approximation leads to the separate Schrödinger equation

$$\mathcal{H}_{nuc} \Psi_{nuc} = E \Psi_{nuc} \quad (2.14)$$

with

$$\mathcal{H}_{nuc} = -\sum_k^K \frac{1}{2m_k} \nabla_k^2 + E_{tot} \quad (2.15)$$

The energy E in the nuclear Schrödinger equation (2.14) corresponds to the molecular energy which would be obtained as the eigenvalue of the unseparated complete Hamiltonian \mathcal{H} . The potential in the nuclear Hamiltonian (2.15) is equivalent to the total energy E_{tot} (2.13).⁴⁷ In fact, this is a very central result far beyond the idea of solely having a simplification for the solution of the Schrödinger equation at hand, because the total energy represents a potential energy surface (PES) for the motion of the molecule including translation, rotation and vibration. These characteristics can be obtained from the solution of the nuclear Schrödinger equation. However, the translation and rotation do not change the internuclear distances and with that the electronic wave function and the internuclear repulsion are independent of the location and orientation of the molecule in space. In addition, concepts like the equilibrium and transition state geometries, which are extensively used in this work, are anchored to the Born-Oppenheimer approximation because they correspond to stationary points on the potential energy surface. Because the BO approximation is often referred to as the adiabatic approximation, it should be noted that in fact it is only a special case. If as the starting point the wave function is expanded as a summation of n products of an electronic and a nuclear wave function (compare eq. (2.10))

$$\Psi(\mathbf{r}, \mathbf{R}) = \sum_n \Psi_{elec,n}(\mathbf{r}; \mathbf{R}) \Psi_{nuc,n}(\mathbf{R}) \quad (2.16)$$

then a set of coupled differential equations is obtained that has to be solved in order to determine the nuclear wave functions.²⁰ The coupling can be expressed in terms of a coupling matrix. In the case that only the diagonal coupling coefficients are considered, one obtains the adiabatic approximation in which the electrons adiabatically follow the motion of the nuclei but not instantaneously as is assumed in the BO approximation. This results in an additional correction term to the BO potential. In the Born-Oppenheimer approximation, as a special case of the adiabatic approximation, the coupling coefficients are neglected completely.⁵²

For most molecules the Born-Oppenheimer approximation is appropriate if the states investigated refer to the lower potential energy surfaces²⁰ (the electronic Schrödinger equation has multiple solutions for each nuclear geometry) and for most cases studied in this work it can be assumed to be valid. However, it breaks down in the cases in which the coupling coefficients of different electronic wave functions cannot be neglected. This is typically the case when different potential energy surfaces come close together at a certain nuclear geometry. This poses a significant problem to model systems that contain reactants and products which, with respect to their spin multiplicity,

are represented by different potential energy surfaces because a surface-to-surface crossing within the BO approximation is permitted. In fact, a model capable to describe such a problem would be required to employ equation (2.16) as the starting point, but finding solutions to general non-adiabatic problems remains restricted to simple systems only.¹⁹ Thus, usually an alternative approach is applied to the problem of “spin-forbidden” chemical reactions by calculating hopping probabilities from one spin surface to another. A typical model for such a probability is the Landau-Zener equation which among others is described in detail by Nakamura⁵³ and Nikitin.⁵⁴ The hopping is thought to take place at a minimum energy crossing point (MECP) which is, in the region of the avoided crossing of two adiabatic potential energy surfaces, described by the crossing of two diabatic surfaces. At the MECP the diabatic representation overcomes the limitation of the Born-Oppenheimer approximation of the resulting wave function to be restricted to only one electronic state. Naturally one would assume that a very flexible high level electronic structure method is needed to obtain MECPs. However, according to Harvey,⁵⁵ in many cases also single-reference methods like DFT are capable to yield reasonable results in this context. Thus, it is assumed that the Born-Oppenheimer approximation is valid throughout all calculations executed in this work with the handling of “spin-forbidden” reactions by using DFT for the finding of approximate MECPs together with surface-hopping probabilities based on the Landau-Zener model. Further detailed descriptions to non-adiabatic phenomena can be obtained from Koseki⁵⁶, Drukker⁵⁷ and Cederbaum et al.⁵⁸

2.4 Electronic Wave Functions

Despite the considerable simplification constituted by the Born-Oppenheimer approximation, the main task of finding electronic wave functions to solve the corresponding Hamiltonian still remains challenging. Because no exact solutions can be obtained for more complex quantum chemical problems, additional approximate methods have to be applied. Besides perturbation theory the variational principle is one of the most widely applied fundamental methods in quantum chemistry to create approximate wave functions. Furthermore, the linear combination of atomic orbitals (LCAO) together with the Slater or Gaussian type orbitals to describe molecular orbitals are crucial developments to obtain approximate solutions to the electronic Schrödinger equation. Finally, the application of Slater determinants ensures the anti-symmetry of the approximate wave functions in poly-electron systems.

2.4.1 The Variational Method

The Rayleigh-Ritz variational method is the basis of many approximate ground state calculations²⁰ and makes use of the variational theorem. By multiplying the Schrödinger equation (2.3) from the left side with the complex conjugate of the wave function Ψ^* and integrating over all space, one obtains the expectation value of the Hamiltonian, the energy E . If the wave function considered corresponds to the ground state of the system (e.g. Ψ_0), then the resulting expectation value is the ground state energy E_0 . The variational method states that the expectation value of any square integrable *trial function* Φ which is a function of the appropriate electronic and nuclear coordinates¹⁹ will be greater than the true ground state energy.

$$E = \frac{\int \Phi^* H \Phi d\mathbf{r}}{\int \Phi^* \Phi d\mathbf{r}} \geq E_0 \quad (2.17)$$

Though this is true in general for the full Schrödinger equation, the further discussion will be confined to the electronic problem as is indicated with the limitation of the integral over only the coordinates of the electrons. The equality of the equation (2.17) only holds for the special case that the trial function is equal to a multiple of the true ground state function $\Phi = c\Psi_0$ with c being an arbitrary complex constant. Thus, the variational principle implies a lower bound of the energy of the ground state that can be obtained with an arbitrary function. The quality of an approximate wave function can be evaluated with respect to its associated energy and the requirement to be as low as possible, which is equivalent to being as close as possible to the true ground state energy. Furthermore, this method allows for the introduction of *variational parameters* in terms of introducing a dependency of the wave function from parameters $\Phi(\alpha, \beta, \gamma, \dots)$. Because this leads to a dependency of the resulting energy on these parameters as well, the application of standard mathematical tools for minimization of the energy leads to a set of variational parameters which correspond to the best representation of the wave function that can be obtained from its underlying form.

2.4.2 Molecular Orbitals

With the variational theorem a method is at hand that allows for the judging and optimizing of the approximate wave functions. This postpones the problem of finding a proper wave function to the task of finding a trial function with an appropriate flexibility from variational parameters and mathematical form. Based on the association of single electrons occupying distinct orbitals,

a straight forward concept is to relate the final wave function (trial function) to molecular orbitals (MOs). The term *orbital* hereby denotes a one-electron spatial function.²⁰ Furthermore, the molecular orbitals are usually described by a combination of different atomic orbitals whose functional form is known from the hydrogenic exact solution of the Schrödinger equation. From these results, atomic orbitals (AOs) can be described with two independent terms in spherical coordinates

$$\phi_{n,l,m} = R_{n,l}(r)Y_{l,m}(\theta, \varphi) \quad (2.18)$$

with R being the radial and Y the angular contribution with the latter referred to as *spherical harmonics*.⁴⁴ The subscripts n, l and m are the principal, the azimuthal and the magnetic quantum numbers. For the molecular orbitals ψ_i typically, a linear expansion of atomic orbitals ϕ_k is used.

$$\psi_i = \sum_{k=1}^K c_{k,i} \phi_k \quad (2.19)$$

Here, ψ denotes a molecular spatial orbital and $c_{k,i}$ is the expansion coefficient of the k^{th} atomic orbital ϕ . The coefficients can be used as variational parameters in the variational method and in the case that they are the only parameters one refers to the approach as the linear variational method. The first approach to assemble the single molecular wave functions to the full solution of the electronic Schrödinger equation is based on Hartree by simple multiplication, which is known as the Hartree product.

$$\Psi_{HP} = \psi_1 \psi_2 \dots \psi_N \quad (2.20)$$

However, it turned out that a further concept, the spin, has to be included when dealing with electrons in atoms or molecules. Originally it was introduced by George Uhlenbeck and Samuel Goudsmit⁵⁹ who suggested that an electron behaves like a spinning top with the z components of the angular momentum being $\pm\hbar/2$. This turned out to be in good agreement with later results from, first, Wolfgang Pauli⁶⁰ and, then, Paul Dirac⁶¹ based on the inclusion of relativistic modifications into the Schrödinger equation. With the spin, an additional quantum number m_s was introduced which only can take the values $\pm 1/2$ with respect to atomic units. With this concept it became possible to explain the experimentally observed fact that only two electrons can occupy one atomic orbital which is manifested in the *Aufbau principle* from Niels Bohr.²⁰ A central cognition, discovered by Dirac⁶² and Pauli,⁶⁰ is that electrons are indistinguishable. This implies that the exchange of any pair of electrons does not change the distribution of the electron density. Together with the interpretation of the wave function by Born, which relates the

square of the wave function to the electron density,⁴⁹ the interchange has to result in either the same or the negative counterpart of the wave function. In the case of electrons as members of the group fermions the latter is true and with that the corresponding wave function is called *antisymmetric*. The spin of the electrons is commonly introduced to the solution of the Schrödinger equation by means of *spin orbitals*. This implies the multiplication of a one-electron spatial wave function with a spin function which results in two spin orbitals per spatial orbital.

$$\chi_i(\mathbf{r}, \varsigma) = \psi_i(\mathbf{r}) \begin{cases} \alpha(\varsigma) \\ \beta(\varsigma) \end{cases} \quad (2.21)$$

Here, χ_i denotes the spin orbital, ψ_i the spatial molecular orbital and α and β are the spin functions of the spin quantum number $m_s \equiv \varsigma$. Both spin functions can only have the values 0 or 1 according to $\alpha(+\frac{1}{2}) = 1$, $\alpha(-\frac{1}{2}) = 0$, $\beta(+\frac{1}{2}) = 0$ and $\beta(-\frac{1}{2}) = 1$.⁴⁴ Creating a correct representation of the wave function that accounts for the required antisymmetry upon exchange of pairs of electrons from these one-electron spin orbitals is ensured by a *Slater determinant*, named after John Clarke Slater.²⁰

$$\Psi(x_1, x_2, \dots, x_N) = \frac{1}{\sqrt{N!}} \begin{vmatrix} \chi_1(x_1) & \chi_1(x_2) & \dots & \chi_1(x_N) \\ \chi_2(x_1) & \chi_2(x_2) & \dots & \chi_2(x_N) \\ \vdots & \vdots & \ddots & \vdots \\ \chi_N(x_1) & \chi_N(x_2) & \dots & \chi_N(x_N) \end{vmatrix} \quad (2.22)$$

In this context N refers to the number of electrons and x_i is a variable that contains both, the coordinates in space and the spin. The term $\frac{1}{\sqrt{N!}}$ is a normalization constant. The Slater determinant can be interpreted as a linear combination of quasi Hartree Products. With the unique properties of a determinant, not only the antisymmetry is at hand, but also the fact that every spin-orbital can be accounted for only once. This is equivalent to *Pauli's exclusion principle* which states that “no two electrons can have the same set of quantum numbers.”

2.4.3 Basis Set

An approximate poly-electronic wave function that accounts for the antisymmetry requirement, and with that for the Pauli exclusion principle, can be created by means of a Slater determinant. The one-electronic spatial wave functions in this determinant can each be written as an expansion of a basis set, which usually consists of atomic orbitals. With the application of

the variational principle on the final poly-electronic wave function, optimal orbitals can be created. Thus, the discussion so far leads to the question of the appropriate basis set on which, eventually, the wave function relies. As already pointed out in equation (2.19), atomic orbitals are a common choice. Slater proposed, on the basis of the exact solution of the hydrogenic atom, a functional form which nowadays is referred to as *Slater type orbitals* (STO).⁶³ In the principle form, they still can be represented as a combination of a spherical harmonic and a radial function as shown in equation (2.18). The radial function $R_{n,l}(r)$ was simplified in comparison to the hydrogenic analytical solution and a correction for the screening of the nucleus from inner shell electrons included.⁴⁴ This leads to the representation

$$R_{n,l}(r) = \left\{ \frac{(2\zeta_{n,l})^{(2n+1)}}{(2n)!} \right\}^{1/2} r^{n-1} e^{-\zeta_{n,l} \cdot r} \quad (2.23)$$

with

$$\zeta_{n,l} = \frac{Z - \sigma_{n,l}}{n} \quad (2.24)$$

ζ is the orbital exponent and depends on the nuclear charge Z , the principal quantum number n and the screening constant σ for which Slater has developed rules dependent on the considered electron orbital. While STOs are reasonably applicable to atomic and diatomic problems, they are not suitable in more complex molecular calculations. This is because of the centering of the atomic orbitals to different nuclei within a molecule which leads to significant problems in the solution of integrals that arise within the calculational scheme of practical applications of the Schrödinger equation like the Hartree-Fock-method. Thus, commonly *Gaussian type orbitals* (GTO) are used in ab initio calculations with the functional form of Gaussian functions to mimic the behavior of the atomic orbitals based on the ideas of Samuel Boys.⁶⁴ This basically implies a change of the linear to a squared dependency of the exponential part in the radial function from r . The general form of the GTO can be represented in Cartesian coordinates as

$$\phi(x, y, z; \alpha, i, j, k) = \left(\frac{2\alpha}{\pi} \right)^{3/4} \left[\frac{(8\alpha)^{i+j+k} i! j! k!}{(2i)! (2j)! (2k)!} \right]^{1/2} x^i y^j z^k e^{-\alpha(x^2+y^2+z^2)} \quad (2.25)$$

α controls the spread of the Gaussian function and i, j and k are integers that describe the character of the orbital and, with that, can, in a wider sense, be related to quantum numbers. This approach significantly simplifies solving the arising integrals in HF-like methods. A drawback in comparison to the STOs, however, is a reduced accuracy of a single Gaussian in describing orbitals because of the functional form. To overcome this problem to a

great extent, usually linear combinations of several Gaussian functions are used to describe one atomic orbital. In general, this leads to the additional variational parameters α_i in the Gaussian exponents and the linear expansion coefficients d_i for each atomic orbital in the basis set and such sets are referred to as *uncontracted* Gaussians.⁴⁴ To reduce the calculational costs, usually the expansion and the exponential coefficients are predetermined and held fixed during a calculation. Such a basis set is then referred to consist of *contracted* Gaussians. One of the early basis sets relied on fitting contracted Gaussians to STOs, which resulted in the labeling “STO-MG” with M being the number of *primitive* Gaussians used.⁶⁵ In fact, for the case of $M = 3$ an optimum balance between accuracy and computational costs was achieved and the corresponding STO-3G basis functions have been assigned for most elements.¹⁹ However, in these basis sets only one *contraction* (series of M Gaussian functions) is used for each occupied spatial orbital and, thus, they are referred to as minimal basis sets. In order to obtain more flexible and accurate basis sets a common approach is to assign more than one function per orbital. In case of two functions, one refers to a *double zeta*, for three functions to a *triple zeta* basis set and so on. This allows for a significant increase in flexibility for calculational schemes like the Hartree Fock method or the Density Functional Theory with the linear expansion coefficients for the combination of multiple functions per orbital being automatically obtained from the applied self consistent field (SCF) calculation. Because the impact of core orbitals on chemical properties is rather small, a further approach is to only apply multiple functions for valence orbitals while describing the inner shell with one function only. In this case, one refers to *split valence* basis sets. Further improvements are possible with *polarization functions* which are based on a higher angular quantum number than the valence orbitals of the considered molecule to account for distortion of the orbitals (e.g. hybrid orbitals). To account for lone pairs in molecules or anionic species, the assignment of additional sets of diffuse functions can be used. In this work we applied the TZVP basis set of Ahlrichs et al.,⁶⁶ which is a triple- ζ split valence basis set with polarization functions. It approximately is equivalent to the 6-311G** basis set in the established writing of Pople et al.⁶⁷

2.5 The Hartree Fock Method

The application of a Hartree product (equation (2.20)) to describe a poly-electronic wave function was the starting point of this method by Hartree. By neglecting the electron-electron repulsion in the Hamiltonian, such a wave function yields the sum of the energies of the individual one-electronic solu-

tions as eigenvalue because of the separability of the Hamiltonian.

$$\mathcal{H} = \sum_{i=1}^N h_i \quad (2.26)$$

$$h_i = -\frac{1}{2}\nabla_i^2 - \sum_{k=1}^K \frac{Z_k}{r_{ik}} \quad (2.27)$$

By including the interelectronic repulsion, the application of the variational principle with a Hartree product as test function still allows for the separation of the Hamiltonian into a set of one-electronic Hamiltonians together with an orbital as eigenfunction.¹⁹ However, the Hamiltonian then includes an additional potential energy term that accounts for the interelectronic repulsion in an averaged way. Because the additional potential energy term in each one-electronic Hamiltonian depends on the charge density of all the other electrons in the system, the set of single equations is not linear anymore and needs to be solved iteratively. Hartree solved this problem with a 'self consistent field' (SCF) approach.⁶⁸ Though this approach allowed to include interelectronic repulsion by still keeping the convenient picture of the final wave function being related to one-electron orbitals, the antisymmetry principle was not fulfilled. Thus, it was straight forward to combine this SCF concept of Hartree with the Slater determinant ensuring the required antisymmetry of the spin orbitals. This was done by Slater⁶⁹ and Vladimir Fock⁷⁰ in 1930, who laid the foundation of the Hartree-Fock (HF) method. The derivation of the Hartree-Fock equations is based on the application of the variational principle on a wave function from a Slater determinant. The minimization of the energy is then executed with the constraint of the orbitals to be orthonormal, which can be done in terms of a Lagrange multiplier. This means that the *overlap integrals* become zero for two different orbitals.⁴⁴

$$S_{ij} = \int \chi_i \chi_j dx = \delta_{ij} \quad (2.28)$$

Within several mathematical manipulations, as are described in detail in several textbooks (e.g. Szabo and Ostlund⁴⁷), a standard eigenvalue form for single orbitals can be obtained.

$$f_i \chi_i = \epsilon_i \chi_i \quad (2.29)$$

The Fock operator f_i is an effective one-electron Hamiltonian for the electron in a poly-electronic system. As in the results obtained by Hartree, the i^{th} fock operator depends on all other electrons $j \neq i$ in terms of an average

potential V_i^{HF} that is experienced by the i^{th} electron because of the presence of the other electrons.

$$f_i = -\frac{1}{2}\nabla_i^2 - \sum_{k=1}^K \frac{Z_k}{r_{ik}} + V_i^{HF} \quad (2.30)$$

The average potential energy can be expressed in terms of the coulomb operator J_j and the exchange operator K_j , which are defined to compute their corresponding integrals.

$$V_i^{HF} = \sum_{j=1}^N \{J_j - K_j\} \quad (2.31)$$

The coulomb operator is defined as

$$J_j(x_1)\chi_i(x_1) = \left[\int dx_2 \chi_j^*(x_2) \frac{1}{r_{12}} \chi_j(x_2) \right] \chi_i(x_1) \quad (2.32)$$

and represents the local potential from an electron in χ_j acting on the electron in χ_i at the position x_1 . The exchange operator is defined as

$$K_j(x_1)\chi_i(x_1) = \left[\int dx_2 \chi_j^*(x_2) \frac{1}{r_{12}} \chi_i(x_2) \right] \chi_j(x_1) \quad (2.33)$$

While the coulomb term already arises in the solution based on a Hartree product as wave function, the exchange term is the result of the antisymmetry of the Slater determinant. It is only defined by its effect when operating on the spin orbital $\chi_i(x_1)$ and involves the effect of an “exchange” of electron 1 and electron 2.⁴⁷ The corresponding exchange integral, which is an energy contribution, reflects the reduced probability of finding pairs of electrons with the same spin close to one another. In fact, there is a finite probability of finding two electrons of opposite spin at the same point in space, but for the same spin this limiting case causes a probability of zero, reflecting the Pauli exclusion principle. Because of the dependency of the single Fock operators on all electrons, again only an iterative solution of this nonlinear problem according to the SCF concept of Hartree is possible. This includes an initial guess of the orbitals from which the average field V^{HF} is calculated. The solution of the eigenvalue problems (2.30) yields then a new set of orbitals. This is continued until self-consistency is reached. A Slater determinant of the N occupied spin orbitals corresponding to the lowest energies, the HF ground state wave function, is the best variational approximation of the ground state of the system that can be obtained from the underlying basis

set and one single determinant.⁴⁷

A significant improvement from a computational point of view was introduced independently by Roothan⁷¹ and Hall⁷² who rewrote the Hartree-Fock equations in terms of matrix algebra. This was done for closed shell systems (all occupied spatial orbitals contain two electrons) by using LCAOs (2.19) for the molecular orbitals. The result can be written in a compact single matrix equation, the Roothan-Hall-equation.

$$\mathbf{FC} = \mathbf{SCE} \quad (2.34)$$

Here, \mathbf{F} is the fock matrix and is related to the one-electron fock operators (2.30). \mathbf{S} contains the overlap integrals with respect to the basis set (2.28). \mathbf{C} represents the expansion coefficients $c_{k,i}$ in the linear expansion of basis functions to molecular orbitals (2.19). Finally, \mathbf{E} is a diagonal matrix that contains the individual orbital energies. The solution is then obtained by a self-consistent-field method because the Fock matrix elements depend on the molecular orbital expansion coefficients. More detailed descriptions of the derivation of the matrix representation of the Hartree-Fock method and its solution can be obtained from Leach⁴⁴ and Szabo and Ostlund⁴⁷.

For the case of an unrestricted open shell system (e.g. radicals), Pople and Nesbet⁷³ have derived the Pople-Nesbet equations based on the idea of applying separate sets of spatial orbitals for electrons with α and β spin.

$$\mathbf{F}^\alpha \mathbf{C}^\alpha = \mathbf{S} \mathbf{C}^\alpha \mathbf{E}^\alpha \quad (2.35)$$

$$\mathbf{F}^\beta \mathbf{C}^\beta = \mathbf{S} \mathbf{C}^\beta \mathbf{E}^\beta \quad (2.36)$$

These two matrix equations are the unrestricted generalization of the Roothan-Hall equation with the single matrices being defined in analogy to equation (2.34), but with the difference to be related to either the spatial orbitals for the α spin ψ_i^α or to the β spin ψ_i^β . Because the two Fock matrices each depend on the expansion coefficients of both spins, the two equations have to be solved simultaneously.

From the variational principle it is known that any trial function will always result in an energy as eigenvalue of the Hamiltonian which is greater than the true energy but the lowest that can be obtained from the applied function. By increasing the flexibility of the trial function, which in the case of a single Slater determinant can be achieved by increasing the size of the basis set, lower and lower Hartree-Fock ground state energies can be obtained until a certain level is reached which is known as the *Hartree-Fock-limit*. This limiting energy, corresponding to an infinite basis set, still will be higher in energy than the true eigenvalue of the Hamiltonian because of the simplifications introduced by the Hartree-Fock method. The major drawback of

this method is the neglect of electron correlation other than the exchange because of the one-electron description. Thus, the great benefit of the HF approximation is not only seen for its own sake, but also as a starting point for more advanced methods that account for the electron correlation. Those non considered correlations arise for example from the correlated motion of each electron with each other, which are 'dynamical correlations'. Furthermore, the restriction in the HF method to a single determinant causes the neglect of 'non-dynamical correlations' in the final wave function. One idea to overcome the limitations of the HF method from a single Slater determinant is, for example, the expansion of the wave function as a linear combination of multiple determinants. Brief descriptions of several post HF methods including the Møller Plesset perturbation theory, Configurational Interaction and the Coupled Cluster Theory can be found in reference [19].

2.6 The Density Functional Theory

The Hartree Fock method, together with the expression of the wave function as a single Slater determinant based on one-electron orbitals, has the great benefit of a resemblance to the intuitive image of independent electrons. However, besides the anchored neglect of correlation contributions to the energy, the Hartree-Fock theory also calculates the full multi-electron wave function which is a rather abstract formalism. In order to overcome both of these limitations, an alternative approach to quantum chemistry has been developed from the attempt to avoid the calculation of the wave function in favor of a more intuitive and observable quantity. Such an observable quantity was manifested in the electron density. The central idea of the resulting Density Functional Theory, in contrast to the HF method, is the attempt to calculate the electronic energy of the system based on the overall electron density distribution. While this concept already dates back to the 1920s and the work of Thomas⁷⁴ and Fermi⁷⁵, the great breakthrough came with the proof of two central theorems by Hohenberg and Kohn in 1964.⁷⁶ The first one is the *Existence Theorem* that states that the ground state density determines the external potential (e.g. the attraction to the nuclei in molecules). Thus, the electron density also determines the Hamiltonian, and the wave function and the energy can thus be computed.¹⁹ It can be said that the electronic energy, E , of the molecule is a unique functional of the density $\rho(\mathbf{r})$. The second theorem states that the density obeys a variational principle and, thus, the essential quantity can be optimized. The energy is

accordingly written as

$$E[\rho(\mathbf{r})] = \int V_{ext}(\mathbf{r})\rho(\mathbf{r})d\mathbf{r} + F[\rho(\mathbf{r})] \quad (2.37)$$

with the first term describing the interaction of the electrons with the nuclei and the second term summarizing the kinetic energy of the electrons and their interaction. The exact ground state density can generally be obtained now from the application of the variational principle on the energy. However, this requires the additional constraint that the integral of the density over all space is equal to the number of electrons, which is a fixed quantity.⁴⁴

$$N = \int \rho(\mathbf{r})d\mathbf{r} \quad (2.38)$$

The striking problem in this approach remained the unknown functional $F[\rho(\mathbf{r})]$ in equation (2.37). In 1965, Kohn and Sham⁷⁷ developed a methodology to overcome this drawback and made the DFT applicable in quantum chemistry. They started with the assumption of a system of non-interacting electrons that have the same overall ground state density as the real system of interest. This allows for the separation of the Hamiltonian into one-electron operators. Thus, as in the HF method, the overall eigenfunction is a Slater determinant of the one-electronic eigenfunctions and the energy is the sum of the one-electronic eigenvalues. The functional $F[\rho(\mathbf{r})]$ is then written as a sum of three terms.⁴⁴

$$F[\rho(\mathbf{r})] = E_{KE}[\rho(\mathbf{r})] + E_H[\rho(\mathbf{r})] + E_{XC}[\rho(\mathbf{r})] \quad (2.39)$$

The first term $E_{KE}[\rho(\mathbf{r})]$ describes the kinetic energy of the non-interacting N electrons with corresponding orbitals ψ_i .

$$E_{KE}[\rho(\mathbf{r})] = \sum_{i=1}^N \int \psi_i(\mathbf{r}) \left(-\frac{\nabla^2}{2} \right) \psi_i(\mathbf{r})d\mathbf{r} \quad (2.40)$$

The second term $E_H[\rho(\mathbf{r})]$ denotes the classical electron-electron repulsion, which is also known as the Hartree electrostatic energy because it already arises in the self-consistent approach of Hartree from the application of a Hartree product (2.20) as wave function. The labels '1' and '2' refer to dummy integration variables over all space to emphasize pairwise interactions summed over all possible electron pairs.

$$E_H[\rho(\mathbf{r})] = \frac{1}{2} \iint \frac{\rho(\mathbf{r}_1)\rho(\mathbf{r}_2)}{|\mathbf{r}_1 - \mathbf{r}_2|} d\mathbf{r}_1 d\mathbf{r}_2 \quad (2.41)$$

The third term, $E_{XC}[\rho(\mathbf{r})]$ is the exchange-correlation energy functional. This term accounts for the contributions of the correlation and the exchange, which are so far neglected in the framework of non-interacting electrons. Furthermore, it also contains the difference between the true kinetic energy and E_{KE} . Finding an appropriate approximation for this term can be seen as the bottleneck of DFT. Because the overall energy of the system in general is *exact*, the combination of equation (2.37) and (2.39) can be interpreted as to define the functional $E_{XC}[\rho(\mathbf{r})]$.⁴⁴

$$E[\rho(\mathbf{r})] = \sum_{i=1}^N \int \psi_i(\mathbf{r}) \left(-\frac{\nabla^2}{2} \right) \psi_i(\mathbf{r}) d\mathbf{r} + \frac{1}{2} \iint \frac{\rho(\mathbf{r}_1)\rho(\mathbf{r}_2)}{|\mathbf{r}_1 - \mathbf{r}_2|} d\mathbf{r}_1 d\mathbf{r}_2 - \sum_{k=1}^K \int \frac{Z_k}{|\mathbf{r} - \mathbf{R}_k|} \rho(\mathbf{r}) d\mathbf{r} + E_{XC}[\rho(\mathbf{r})] \quad (2.42)$$

In equation (2.42) the external potential is written in the appropriate form to represent the interaction of the electrons with the K nuclei. And the electron density $\rho(\mathbf{r})$ of the system is calculated, according to Kohn and Sham, as the sum of the square moduli of the one-electron orbitals.

$$\rho(\mathbf{r}) = \sum_{i=1}^N |\psi_i(\mathbf{r})|^2 \quad (2.43)$$

In analogy with the HF method, introducing the expression of the electron density into equation (2.42) and applying the variational principle results in a set of pseudo-eigenvalue equations which are referred to as the Kohn-Sham equations:

$$h_i^{KS} \psi_i = \epsilon_i \psi_i \quad (2.44)$$

with ϵ_i being the orbital energies and the one-electron Kohn-Sham Hamiltonians being defined as

$$h_i^{KS} = -\frac{1}{2} \nabla_i^2 - \sum_{k=1}^K \frac{Z_k}{|\mathbf{r}_i - \mathbf{R}_k|} + \int \frac{\rho(\mathbf{r}_2)}{|\mathbf{r}_i - \mathbf{r}_2|} d\mathbf{r}_2 + V_{XC} \quad (2.45)$$

V_{XC} represents the functional derivative of the exchange-correlation energy E_{XC}

$$V_{XC}[\mathbf{r}] = \frac{\delta E_{XC}[\rho(\mathbf{r})]}{\delta \rho(\mathbf{r})} \quad (2.46)$$

Because the density is part of the one-electronic Hamiltonian but determined by using the orbitals, which derive from the solutions of the one-electronic

eigenvalue equations, again a self-consistent iteration has to be carried out. In further analogy to the HF method, in the case that the one-electronic orbitals are again expressed as linear expansions of a basis set (e.g. atomic orbitals, compare (2.19)), then the Kohn-Sham equations can be expressed in matrix form similar to the Roothaan-Hall equations.⁴⁴

$$\mathbf{HC} = \mathbf{SCE} \quad (2.47)$$

Apart from the similarities between HF and DFT, they differ with respect to their derivation. DFT is an exact method, but suffers from the problem of containing an unknown operator, the exchange-correlation energy, which has to be approximated. In contrast, HF is an approximate theory which was motivated by the ability to solve the governing equations exactly.¹⁹

The major problem in DFT remains to find an appropriate representation for the exchange-correlation functional. Commonly, this functional is written in terms of an interaction of the electron density and an energy density ϵ_{XC} which is dependent on the electron density.

$$E_{XC}[\rho(\mathbf{r})] = \int \rho(\mathbf{r})\epsilon_{XC}[\rho(\mathbf{r})]d\mathbf{r} \quad (2.48)$$

The most simple approximation is known as the *local density approximation* (LDA) and is based on the model of the uniform electron gas, in which the electron density is constant over all space. It is assumed that the ϵ_{XC} of the inhomogeneous electron distribution at the position \mathbf{r} has the same value as in the homogeneous electron gas, corresponding to an electron density equivalent to ρ at \mathbf{r} . Thus, the real electron density in the vicinity of \mathbf{r} is approximated with a constant electron density with the same value as at \mathbf{r} . The energy density of the uniform electron gas is known accurately from different approaches like quantum Monte Carlo methods⁷⁸ at relevant densities. In most cases, however, the contributions of exchange and correlation are expressed as separate functions. For example, an early attempt by Slater⁷⁹ lead to an exchange energy density

$$\epsilon_X[\rho(\mathbf{r})] = -\frac{9\alpha}{8} \left(\frac{3}{\pi}\right)^{1/3} \rho^{1/3}(\mathbf{r}) \quad (2.49)$$

with α taking a value of 1. The exact solution for the uniform gas results in a value for α of $\frac{2}{3}$.¹⁹ For the correlation energy density, a simple exact solution is not possible but can be obtained from the above stated quantum Monte Carlo-based results by subtracting the exact known exchange term. Functional fits to these values were designed for example by Vosko et al.⁸⁰

The potential V_{XC} in equation (2.45) corresponding to the exchange-correlation energy E_{XC} is obtained from the appropriate first derivative

$$V_{XC}[\mathbf{r}] = \rho(\mathbf{r}) \frac{d\epsilon_{XC}[\rho(\mathbf{r})]}{d\rho(\mathbf{r})} + \epsilon_{XC}[\rho(\mathbf{r})] \quad (2.50)$$

In order to obtain even better approximations to the exchange-correlation energy a common extension to the LDA is to make it not only dependent on the local value of the density but also on its gradient. Such a ‘gradient corrected’ functional is then referred to as *generalized gradient approximation* (GGA). In most cases the correction is introduced by adding a term, depending on the density gradient, to the LDA functional. A functional for the exchange energy from Becke^{81,82} is very popular in this context, which adds a correction term to the standard Slater exchange energy (2.49) by fitting a function to the exact exchange HF energies of the noble gasses. Furthermore, for the correlation, a widely used functional is based on Lee, Yang and Parr (LYP)⁸³ and the combination of the two contributions is known as BLYP functional.

The HF method includes an essentially exact treatment of the exchange energy and, thus, the idea is at hand to combine contributions of HF with DFT. Because a simple addition of HF exchange energies derived from the Kohn-Sham orbitals to the correlation energy of DFT failed, Becke introduced a strategy based on a coupling parameter between the two contributions. This resulted in the establishment of the *hybrid functionals*. The most famous upon these functionals is the B3LYP which is a modification of a 3-parameter⁸⁴ dependent functional proposed by Becke,^{85,86}

$$E_{XC}^{B3LYP} = (1 - a)E_X^{LDA} + aE_X^{HF} + b\Delta E_X^B + (1 - c)E_C^{LDA} + cE_C^{LYP} \quad (2.51)$$

with $a = 0.20$, $b = 0.72$ and $c = 0.81$. The contributions to the overall exchange-correlation energy are E_X^{LDA} the exchange energy from the local density approximation, E_X^{HF} the exact HF exchange energy obtained from the Kohn-Sham orbitals, ΔE_X^B the gradient correction to the exchange energy based on Becke, E_C^{LDA} the local density approximation to the correlation energy from Vosko et al. and E_C^{LYP} the gradient corrected correlation energy functional from Lee, Yang and Parr. The three parameters a , b and c were optimized by Becke by least square fitting of them to experimental data for his 3-parameter functional, which used the PW91⁸⁷ functional instead of the LYP. For the B3LYP, however, no new optimization was performed. Although several exchange-correlation functionals have been derived up to date, the B3LYP remains the most widely used one because it is known to

perform quite well in most cases. The transferability of more recent functionals that are known to be superior for some model cases is, however, usually not known and no other functional has proven yet to perform reliably well over a wide range of systems.⁸⁸ Nevertheless, the careful choice of the exchange-correlation functional can significantly improve the quality of the DFT results. However, the rather crude approximation of it, even including fitting to experimental data to a certain extent, is the reason why the DFT is sometimes described as a semi-empirical method.¹⁹

2.7 Compound Methods

In order to overcome the limited accuracy of the Hartree-Fock method and the Density Functional Theory, several methods, which are essentially improvements on the HF approach and, thus, often called *post-HF* methods, have been established. However, with superior accuracy, the computational demand also increases significantly and many methods can be applied only for rather small systems in practice. To overcome this problem to a certain extent, several compound methods have been established which attempt to achieve high accuracy by combining the results of several different calculations to approximate a single high-level calculation.⁸⁹ Besides the *Gaussian-n methods*, the *Complete Basis Set* (CBS) methods have been shown to give very accurate results. The CBS method is based on Peterson and co-workers⁹⁰ who tried to overcome the inaccuracies related to a truncated basis set. This is achieved by extrapolating from calculations with a finite basis set to the complete basis set limit by computing second-order and infinite-order corrections to the energy. The ‘order’ terminus is related to the Møller Plesset expansion of the energy

$$E = \underbrace{E^{(0)} + E^{(1)}}_{E^{HF}} + E^{(2)} + E^{(3)} + \dots + E^{(\infty)} \quad (2.52)$$

with the 0th and 1st order terms being equivalent to the Hartree-Fock SCF energy. In addition, based on the fact that the contributions of the correlation energy decrease with higher orders of perturbation theory, they concluded that progressively smaller basis sets could be employed for the higher level calculations. For the CBS-QB3 method,^{91,92} applied in this work, as is implemented in Gaussian 03,⁹³ the energy calculation involves, as a sequence of steps, first the geometry optimization and zero-point energy calculation with DFT employing the B3LYP functional and a double- ζ basis set followed by a second order Møller Plesset (MP2) energy calculation at the DFT geometry

with a triple- ζ basis set, together with a CBS extrapolation. Furthermore, a MP4 and a QCISD (quadratic configuration interaction including singles and doubles) energy correction with again only double- ζ basis sets are calculated. The CBS correction is only applied to the second-order perturbation term with the second-order correction and to the higher perturbation terms with the infinite-order correction. The energy terms corresponding to the self-consistent field calculations are assumed to be sufficiently accurate based on the application of the rather large basis set and no extrapolation is performed on them.

3

Reaction Rates and Equilibrium

In this chapter it is outlined how reaction rates and thermodynamic properties are calculated based on statistical thermodynamics for quantum chemically optimized geometries. First, the concept of the potential energy surface is described followed by the introduction of the partition function and the derivation of thermodynamic properties. Finally, the transition state theory and its application to microkinetic modeling is explained.

3.1 Potential Energy Surface

Based on the Born-Oppenheimer approximation, the separation of the motion of nuclei and electrons of a molecule results in the nuclear Schrödinger equation (2.14). The potential for the motion of the nuclei as is denoted in the corresponding nuclear Hamiltonian⁴⁶ (2.15) as E_{tot} defines what is referred to as the potential energy surface (PES). Consisting of the internuclear repulsion and the electronic energy, the PES is a function of only the coordinates of the nuclei in space. Because the position of each atom is defined by

three spatial Cartesian coordinates, the energy as a result is a function of $3N$ coordinates with N being the number of atoms in the molecule. To emphasize this multi-dimensionality, one also refers to the PES as a hyperplane. The application of internal coordinates is a more descriptive mapping of the degrees of freedom of the potential energy. This implies a fixed coordinate system which allows for the description of a molecule in $3N - 6$ ($3N - 5$ for linear molecules) coordinates. Of the complete $3N$ degrees of freedom, the position of the molecule in space is defined by three coordinates with respect to its center of mass.¹⁹ The orientation in space with respect to the coordinate system is defined by three further coordinates (two for linear molecules). The remaining degrees of freedom represent now the positions of atoms relative to each other in terms of bond lengths, bending angles and torsional angles within the molecule. The two-dimensional projection of the hyperplane along the reaction coordinates leads to the common energy diagram⁹⁴ in chemistry (compare Figure 3.1) to visualize reactions and the concept of transition state theory (TST). The 'interesting', *stationary points*⁹⁵ on these

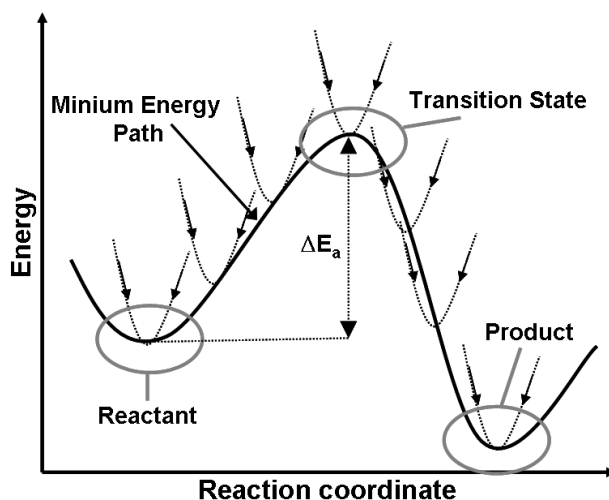


Figure 3.1: Schematic illustration of an energy diagram for a reaction on one PES.

curves are the mathematical extrema in which the gradient of the energy becomes zero. Reactants and products have defined geometries and are related to local minima on the PES in which, besides a zero gradient of the energy, the hessian matrix (second derivatives of the energy) is positive definite. The connecting path between the reactants and products is separated by a saddle point of first order. This corresponds to a maximum in one direction, namely the reaction coordinate, and to a minimum in all remaining

degrees of freedom, describing the lowest barrier which separates the stable reactants and products.¹⁹ Mathematically, this implies an indefinite hessian matrix with one negative (imaginary) eigenvalue and the corresponding eigenvector can be interpreted as the reaction coordinate. The point itself is usually denoted as transition structure. Thus, in general, mapping the complete PES of a set of atoms would represent all possible stable structures in terms of minima as well as the connection and barriers between them defined by saddle points. However, the high dimensionality of the hyperplane⁹⁵ and the anchored computational demand to calculate single point energies referring to one specific geometry do usually proscribe a full mapping of the PES in terms of a reasonable numerical grid.⁴⁴ Thus, one is restricted to the search of local extrema by using numerical algorithms. Because of the vast amount of minima present on a PES, most search algorithms for the minimization of the energy only find the closest local minimum in the vicinity of the starting configuration and chemical intuition for suitable starting geometries is thus required. For the finding of connecting first-order saddle points, global and local algorithms can be distinguished. Global algorithms try to connect the assumed reactant and product states of an elementary reaction step by relaxing a number of aligned configurations to the minimum energy pathway. The nudge-elastic band (NEB)^{96,97} method and the string⁹⁸ and growing string method^{99–102} are typically applied representatives. The crucial benefit of these methods is that as input parameters only minimum energy geometries are required, which results in an approximation for the reaction path and the transition state. The drawback is a rather slow convergence to the minimum energy path and the approximate character of the resulting 'grid' points. Local algorithms like the partitioned rational optimization function (P-RFO)¹⁰³ method, which makes use of the hessian matrix, or the dimer and improved dimer methods,^{104–106} which use minimum mode following, are capable of converging to transition structures. Although, in principle, these local methods can also be started from a minimum geometry resulting in a first-order saddle point, the high dimensionality of the PES makes this rather unreasonable. Not only would one require a significant amount of iterative steps, also it is not predefined to what transition structure the algorithm converges and, thus, to which product state it connects the reactant. Therefore, a combination of both methods is usually applied to obtain transition states that connect predetermined minima. The true reaction pathway can then be determined by a reminimization, starting from a slightly, along the reaction coordinate, perturbed transition structure, applying the steepest descent method.⁴⁴ In the case that reactants and products are located on PESs referring to different spin multiplicities, a description of this spin-forbidden reaction with the above described techniques is not pos-

sible. In fact, the underlying approximation that is required to define the PES, namely the Born-Oppenheimer approximation, breaks down if the two hyperplanes get close to each other. To describe this type of reaction,^{107–110} in analogy to transition state theory on one PES, one can calculate barriers, separating reactants and products on different PESs by finding the minimum energy geometry on the seam of the two related *diabatic* hyperplanes. For simplicity, the diabatic PESs can, in many cases, be approximated by the adiabatic PESs.⁵⁵ Finding this minimum energy crossing point (MECP) requires the minimization of the energy on either of the two PESs with the constraint that the energy is the same on both PESs. Such a constraint is included by the application of a Lagrange multiplier and many algorithms have been suggested in the literature.^{108,111–119}

Minima on the hyperplane can be used to obtain thermodynamic properties of two states relative to each other and the classical motion of the atoms is related to the non-vanishing gradients of the PES for geometries apart from a minimum. Finally, the dynamics of a reaction (kinetics) are related to the transition structure and the height of the energy barrier imposed by the saddle point with respect to the minima it connects.⁹⁵ However, with respect to its origin as the potential of the nuclear Schrödinger equation, it has to be emphasized that the PES is defined at the temperature $T = 0\text{ K}$.⁴⁴ Because the real world relates to finite, non-zero temperatures, it is necessary to impose the impact of temperature on quantum chemical energy calculations to bridge the gap between simulation and macroscopic observables. This can be achieved by the application of statistical thermodynamics on the geometries that represent extrema of the underlying PES. In addition, it has to be noted that the definition of a transition state relates to a first-order saddle point of the Gibbs’ free energy while, in contrast, the transition structure is an extrema on the PES. Despite this discrepancy, the transition structure can be seen as a good approximation to the true transition state but also techniques have been developed like the variational transition state theory^{120–125} that try to account for this deviation.

Following the overall reaction pathway from reactants to products might involve several different routes with different intermediates, but the most probable pathway to be accessed is the lowest in energy. Because an analytical determination of the lowest energy pathway is not possible, the high dimensionality of the PES enforces the manual sampling of pathways.

3.2 Partition Function

Calculating the electronic energy of atoms and molecules is the basis to obtain the potential energy surface within the Born-Oppenheimer approximation that governs the motion of the nuclei. Finding minima and first-order saddle points allows then, in principle, to visualize reactions in terms of relative energies, namely the heat of reaction and the activation energy. However, this discussion still refers to single molecules in contrast to the macroscopic observations of fundamental variables in thermodynamics like enthalpy and entropy or reaction rates. Also the issue of temperature, which relates to $T = 0\text{ K}$ for the QM based PES, has to be solved in order to address measurable quantities. Statistical thermodynamics states the framework that enables to convert single-molecule potentials into ensemble thermodynamic variables and the theory is outlined in diverse textbooks.^{19,61,126–128} The macroscopic state of a system, defined by its boundary conditions, can be interpreted as the time average over the micro state of the system. The micro states are thereby defined by the stationary quantum mechanical eigenstates of the system with energies E_i .¹²⁸ However, the system properties, averaged over time, can also be obtained as the statistical average over all micro states. Thus, the intrinsic energy is the sum over all energies E_i , weighted with the corresponding probability P_i to observe the i^{th} micro state. The list of all micro states is the ensemble.

$$U = \langle E \rangle = \sum_i P_i E_i \quad (3.1)$$

The canonical ensemble is relevant for the calculation of thermodynamic functions corresponding to thermodynamic systems. It is defined by a constant number of molecules N , a constant Volume V and a constant temperature T for all of its single systems. The also as (NVT) ensemble denoted system may exchange energy with the surrounding, but is in thermal equilibrium with it. This leads, in consequence, to a constant, over time averaged, energy $\overline{E}(t)$ which is identical to the internal energy U of the thermodynamic system. However, the system energy fluctuates with time because of random crossings of single systems of different energy E_i . To develop an expression for the statistical distribution of the energy eigenstates of such a single system, Gibbs¹²⁹ considered ensemble micro states of the canonical ensemble to consist of several copies of the single system, each with equivalent number of particles and volume but independent quantized energy eigenstate. The micro states, however, assembled of the single system copies, are restricted to exhibit a constant total energy, differing only in their distribution

of the quantized energy states of the single systems. From relations of the micro-canonical ensemble it is at hand, that each micro state of the canonical ensemble is equally likely to be accessed.¹²⁸ The micro states are then grouped into macro states of the canonical ensemble which are defined by a generalization of the distribution of the energy in the single systems. This implies groups of micro states which contain equivalent amounts of single systems with the quantized energy E_i . The probability to observe a single system in the eigenstate E_i is then equal to the sum over the probabilities to observe a macro state times the probability to observe the state E_i within the macro state.

$$P_i = \sum_j P_j P_i(j) \quad (3.2)$$

P_j is the probability to observe the macro state j and $P_i(j)$ the is the probability to observe the eigenstate E_i in the macro state j . Because the micro states are all equally likely to be accessed, the probability of a macro state is equal to the fraction of micro states that belong to it. For large numbers of micro states of the canonical ensemble, only the macro state with the most probable distribution of micro states needs to be considered in good approximation. Finding the macro state with the maximum number of micro states with the constraint of the boundary conditions of a constant total energy and number of particles within the micro states, in terms of Lagrange multipliers, leads to an expression for the probability of a single system to be in the quantized energy state E_i .¹²⁸

$$P_i = \frac{\exp(-\beta E_i)}{\sum_i \exp(-\beta E_i)} \quad (3.3)$$

The Lagrange multiplier β can be related to the Boltzmann constant and temperature

$$\beta = \frac{1}{k_B T} \quad (3.4)$$

This is a very central result of statistical thermodynamics, stating an exponential dependency of the occupancy of state i to its corresponding energy E_i and temperature. This result is also known as the Boltzmann distribution. The sum in the denominator of equation (3.3) is known as the partition function and can be seen as the fundamental function of statistical thermodynamics comparable to the wave function in quantum mechanics.¹⁹ Thermodynamic functions can, thus, be expressed in terms of averages of single energy states over their distribution (3.3) and eventually be related to solely the partition function Q . The sum in the partition function ranges over all

possible energy levels i .

$$Q = \sum_i \exp\left(-\frac{E_i}{k_B T}\right) \quad (3.5)$$

This implies for the internal energy U , the enthalpy H , the entropy S and the Gibbs' free energy G

$$U = k_B T^2 \left(\frac{\partial \ln Q}{\partial T} \right)_{N,V} \quad (3.6)$$

$$H = U + PV \quad (3.7)$$

$$S = k_B \ln Q + k_B T \left(\frac{\partial \ln Q}{\partial T} \right)_{N,V} \quad (3.8)$$

$$G = H - TS \quad (3.9)$$

However, this still requires to know the quantized energies of the single systems. A common significant approximation is to assume that the single systems consist of non-interacting particles which allows to express the energy E_i as the sum of the energies $\varepsilon(j)$ of the single particles.

$$E_i = \left[\sum_j^N \varepsilon(j) \right]_i \quad (3.10)$$

With that, the thermodynamic functions of an ideal gas can be derived from its atomistic properties. Considering that results in quantum chemistry usually refer to single molecules, the above assumption is crucial to bridge the gap between microscopic and macroscopic properties. With equation (3.10), the partition function of N non-interacting molecules can be expressed as the multiplication of the partition functions corresponding to N single systems that contain only one molecule. In addition, the indistinguishability of the molecules has to be accounted for, and for the case of a much larger number of available quantum states than considered particles the partition function can be approximated as

$$Q(N) = \frac{1}{N!} q^N = \frac{1}{N!} \left[\sum_i \exp\left(-\frac{\varepsilon_i}{k_B T}\right) \right]^N \quad (3.11)$$

The partition function in this form is known as the Maxwell-Boltzmann statistics for ideal gases.¹²⁸ With that, only the quantized energies of the single molecules have to be expressed to obtain the system partition function from

the molecular partition function. In a next step, the molecular energy is assumed to be separable into contributions from translation, rotation, vibration, electronic energy and others. This also affects the molecular partition function to be separable into the corresponding single contributions.

$$\varepsilon = \varepsilon_{\text{trans}} + \varepsilon_{\text{rot}} + \varepsilon_{\text{vib}} + \varepsilon_{\text{elec}} + \dots \quad (3.12)$$

$$q(V, T) = q_{\text{trans}}(V, T) q_{\text{rot}}(T) q_{\text{vib}}(T) q_{\text{elec}}(T) \dots \quad (3.13)$$

The translational partition function can be derived from the quantized energy of translation of the molecule in space, based on the solution of the Schrödinger equation to the problem of a particle in a box.⁶¹

$$q_{\text{trans}}(V, T) = \left(\frac{2\pi M k_B T}{h^2} \right)^{3/2} V \quad (3.14)$$

M is the molecular mass and the volume V can be expressed as RT/P for an ideal gas with pressure P and the ideal gas constant R . The representation of the rotational partition function is commonly derived from the quantum mechanical solution to the rigid rotator. In a good approximation, the partition function of a linear molecule can be written as

$$q_{\text{rot}}(T) = \frac{8\pi^2 I k_B T}{\sigma h^2} = \frac{T}{\sigma \Theta_{\text{rot}}} \quad (3.15)$$

$$\Theta_{\text{rot}} = \frac{h^2}{8\pi^2 I k_B}$$

with I the moment of inertia, Θ_{rot} the rotational temperature and σ the symmetry number of the molecule. The symmetry number represents the number of indistinguishable orientations of the molecule in space.^{130,131} For a non-linear polyatomic molecule, the principle moments of inertia have to be taken into account and the resulting expression for the partition function reads

$$q_{\text{rot}}(T) = \frac{\pi^{1/2}}{\sigma} \left(\frac{T^3}{\Theta_{\text{rot,A}} \Theta_{\text{rot,B}} \Theta_{\text{rot,C}}} \right)^{1/2} \quad (3.16)$$

$$\Theta_{\text{rot,j}} = \frac{h^2}{8\pi^2 I_j k_B}$$

The expressions for the rotational contribution are referred to as the high temperature approximation because they are valid only for the case that $\Theta_{\text{rot}} \ll T$, which is however true for most molecules already at room temperature. The vibrational contribution to the partition function is commonly

derived from the quantum mechanical solution to the harmonic oscillator. By expressing the vibrational motion of the molecule in terms of normal coordinates, a set of independent harmonic oscillators is created. Thus, the vibrational energy can be written as the sum over the contributions of the independent oscillators. The partition function is then written as

$$q_{\text{vib}}(T) = \prod_j^{\alpha} \frac{\exp(-\Theta_{\text{vib},j}/2T)}{1 - \exp(-\Theta_{\text{vib},j}/T)} \quad (3.17)$$

$$\Theta_{\text{vib},j} = \frac{h\nu_j}{k_B}$$

Similar to the rotation, Θ_{vib} defines the vibrational temperature which includes the vibrational frequencies ν_j . The multiplication for N atoms includes $\alpha = N - 5$ vibrational degrees of freedom for linear molecules and $\alpha = N - 6$ for non-linear molecules. Finally, the electronic contribution to the partition function accounts for the contribution of the electrons in the molecule. The energy of the ground state is usually referenced to the ground state of the separated atoms and the depth of the electronic state potential is denoted as D_e . In most cases, the energy difference between the ground state and the first excited state is much larger than $k_B T$ and, thus, the contributions of the excited states can be neglected. However, for few molecules (e.g. NO) the first excited state has to be considered.¹²⁸ The resulting electronic partition function then reads

$$q_{\text{elec}}(T) = g_1 \exp\left(\frac{D_e}{k_B T}\right) + g_2 \exp\left(\frac{-\varepsilon_2}{k_B T}\right) + \dots \quad (3.18)$$

with the degeneracy g_j of the j^{th} electronic state. As the zero of the electronic energy is taken to be the separated atoms in their ground states, also the zero energy of the rotation and vibration has to be fixed. For the rotation this is naturally the ground state of the rigid rotator in which the rotational energy is zero. For the vibration, the zero is taken to be the bottom of the internuclear potential well, and thus the ground state energy of vibration is not zero but $\varepsilon_{\text{vib},j} = h\nu_j/2$ for each independent harmonic oscillator.⁶¹ In consequence, even at $T = 0\text{ K}$, there is a vibrational contribution to the internal energy of a molecule which is

$$U_0 = E_{\text{elec}} + \sum_i^{\text{modes}} \frac{1}{2} h\nu_i \quad (3.19)$$

with E_{elec} being the energy of the stationary point on the PES and the sum over all vibrational modes referred to as the zero-point energy (ZPE).¹⁹

3.3 Reaction Rates

In order to relate the quantum chemical results that define a reaction path on the PES to experiments (e.g. conversion of reactants over temperature), it is necessary to evaluate reaction rates based on them. For the case of an elementary reaction step on one PES with a first-order saddle point separating the two minima, which represent the reactant and the product state, the *transition state theory* (TST) is most widely used to obtain estimates for the rate constants.⁶¹ The theory dates back to the work of Eyring¹³² and Evans and Polanyi¹³³ in 1935. Further developments were reviewed by several authors^{120,134–136} and it is part of most textbooks, related to chemical kinetics.^{8,19,25,61,95,126,128,137} A two-step mechanism is assumed in which, first, the reactants are in equilibrium with the *activated complex* and, subsequently, an irreversible reaction leads to the product state. Thus, the rate of reaction of



can be written in terms of the equilibrium constant between the reactants and the activated complex multiplied with the reaction rate constant of the irreversible step to the product.

$$\frac{dc_P}{dt} = k_2 K_c^\ddagger c_A c_B \quad (3.21)$$

The equilibrium constant is expressed in terms of the partition functions of the reactants and the activated complex. For the latter, in good approximation, the properties of a first-order saddle point of the underlying PES can be used.

$$K_c^\ddagger = \frac{(q^\ddagger/V)c^\circ}{(q_A/V)(q_B/V)} \quad (3.22)$$

c° is the standard state concentration. Because the expressions of the partition functions divided by volume each have the units of molecules per cubic meter, the reference state also has this unit $c^\circ = 1 \text{ molecule/m}^3$. The rate k_2 can be interpreted as the frequency with which the activated complex crosses the top of the barrier and can, thus, be expressed as a one-dimensional translational motion. This leads to the final expression of the rate constant for a generalized stoichiometry

$$k = \frac{k_B T}{h} \frac{(q_{\text{int}}^\ddagger/V)}{\prod_i (q_i/V)} \left(\frac{1}{N_A} \right)^{\Delta_r \nu} \quad (3.23)$$

with q_{int}^\ddagger representing the partition function of the activated complex, but excluding the translational motion over the top of the barrier. This then results in $\alpha - 1$ degrees of vibrational freedom and implies a neglect of the imaginary frequency allocated to the first-order saddle point. The last term in the equation (3.23) includes the Avogadro's number N_A , which, together with the consideration of the stoichiometry in the exponent, accounts for the correct conversion of the units into *moles*. Alternatively, the rate constant can be written in terms of the Gibbs' free energy difference between the reactant state and the activated complex.

$$k = \kappa \frac{k_B T}{h} (c^\circ)^{\Delta r^\nu} \exp\left(-\frac{\Delta G^\ddagger}{RT}\right) \quad (3.24)$$

The term $(c^\circ)^{\Delta r^\nu}$ accounts for the correct units related to the stoichiometry of the reaction. In this context, the standard state concentration is in the units $[mole/m^3]$. In addition, the transmission coefficient κ has been added, which accounts for additional effects like quantum mechanical tunneling.¹²⁸ Furthermore, it allows to account for the possibility that not all activated complexes lead to products, since some may be reflected back to the reactant state. The expressions (3.23) and (3.24) are referred to as the canonical TST which defines the Gibbs' free energy of the activated complex at the first-order saddle point on the PES (the transition structure). The variational transition state theory in contrast moves the reference position along the minimum energy path (MEP) until the rate constant is minimized, which accounts for the difference of the transition structure and the true transition state (the maximum of the Gibbs' free energy along the MEP⁹⁵). A detailed description of the application of this enhancement, for example, is given by Truhlar et al.^{120–124} In this work, only the conventional TST was applied to estimate reaction rates of elementary steps and the transmission coefficient κ was set to one in all cases. In heterogeneous catalysis, besides the ordinary reaction steps on one PES, also the dynamics of adsorption and desorption as well as the crossing of potential energy surfaces of different spin multiplicity have to be accounted for. In general, the desorption can be described in analogy to the conventional TST and pre-exponential factors and activation energies are obtainable from temperature programmed desorption (TPD) experiments.⁸ From computational chemistry the most simple approach is to assume the adsorption to be barrier-less, which results in an activation energy of desorption which is equivalent to the heat of adsorption.¹³⁷

$$k_{\text{des}} = \frac{k_B T}{h} \exp\left(-\frac{\Delta E}{RT}\right) \quad (3.25)$$

The activation energy ΔE represents the zero-point corrected electronic energy. The rate of adsorption is then obtained from the equilibrium constant and the rate constant of desorption according to

$$k_{\text{ads}} = k_{\text{des}} K_{\text{eq}} \quad (3.26)$$

However, this approach assumes the ‘quasi’ transition state to exhibit the same partition function as the adsorbed reactant and, thus, to be of a rather immobile nature. This does not need to be true and the pre-exponential factor might be significantly larger than the standard value $k_B T/h$,⁸ making the equation (3.25) a conservative lower bound estimate of the rate of desorption. An upper bound can be estimated by assuming that the partition function of the ‘quasi’ TST is equivalent to the partition function of the desorbed state. This can be expressed in terms of the Gibbs’ free energy difference between the adsorbed and the desorbed state ΔG in accordance with equation (3.24).

$$k_{\text{des}} = \frac{k_B T}{h} \exp\left(-\frac{\Delta G}{RT}\right) \quad (3.27)$$

Finally, also for the crossing of potential energy surfaces, the formalism of TST can be applied to estimate rate constants for spin-forbidden reactions⁵⁵ and the resulting equation is equivalent to (3.23), using the minimum energy crossing point (MECP) of the two PESs as a reasonable approximation to a transition structure. However, the MECP is only a stationary point on the subspace of the seam of the two PESs, but not on either of them. While calculating translational and rotational contributions to the partition function from the structure of the MECP is straight forward and analogous to a conventional TST, the vibrational contribution requires the calculation of the second derivative of the energy (Hessian). To account for the difference of the partition function between MECP and reactant state, Harvey and Aschi^{108,111} have proposed the calculation of an effective Hessian.

$$\mathbf{H}_{\text{eff}} = \pm \frac{|\mathbf{g}_1|}{|\mathbf{g}_1 - \mathbf{g}_2|} \mathbf{H}_2 \pm \frac{|\mathbf{g}_2|}{|\mathbf{g}_1 - \mathbf{g}_2|} \mathbf{H}_1 \quad (3.28)$$

\mathbf{H}_1 and \mathbf{H}_2 represent the Hessian matrices and \mathbf{g}_1 and \mathbf{g}_2 the gradients of the energy at the MECP on the PESs with spin state ‘1’ and ‘2’. It is derived from the Taylor expansion of a Lagrangian at the MECP as outlined by Koga and Morokuma¹¹² and the signs of the two fractions are dependent on the sign of the Lagrange multiplier. The derivation is shown in Appendix A. Finally, the translational and rotational degrees of freedom as well as the gradient difference $(\mathbf{g}_1 - \mathbf{g}_2)$ have to be projected out of the effective Hessian (see

Page and McIver¹³⁸ for details). The surface thermally averaged hopping probability can be calculated from the Landau-Zener theory according to Eyring and Stearn.¹³⁹

$$\bar{P}_{12} = \int_0^\infty \left(1 - \exp \left\{ \frac{4 \pi^2 H_{12}^2}{h v |\text{grad}(E_1) - \text{grad}(E_2)|} \right\} \right) \frac{\exp(-v^2/2k_B T)}{\int_0^\infty \exp(-v^2/2k_B T) dv} dv \quad (3.29)$$

H_{12} is the spin-orbit coupling energy, v is the mass-weighted velocity of the system at the MECP and $|\text{grad}(E_1) - \text{grad}(E_2)|$ is the absolute value of the difference of the slopes on the PESs ‘1’ and ‘2’ at the MECP, in mass weighted coordinates. The transmission coefficient for the spin inversion is then obtained as

$$\kappa = 2\bar{P}_{12} - \bar{P}_{12}^2 \quad (3.30)$$

Although by now more accurate formulas for the transmission probability of the spin inversion are available (e.g. see Nakamura⁵³), within the accuracy of DFT to calculate relative energies the equation (3.29) is expected to be sufficient for a first estimation of this influence.

3.4 Application of CHEMKIN

In the theoretical investigation of heterogeneous catalytic reactions, quantum chemistry provides the framework to probe the governing potential energy surfaces of the system of interest. Potential reactants, intermediates and products are represented by minima on a PES and the transition states, which connect them, are first-order saddle points. Statistical thermodynamics allows for the derivation of thermodynamic properties of the gas and surface species elucidated from quantum chemistry. Finally, the transition state theory enables to calculate reaction rates for the surface reactions based on the obtained transition structures. For the comparison with experimental data, however, the application of these data sets in a reactor simulation, that allows for a microkinetic description of the surface chemistry, is required. The Fortran package CHEMKIN, which was originally developed by Sandia National Laboratories and is, by now, a commercial software distributed by Reaction Design, provides such a framework. In this work we use the packages CHEMKIN-II¹⁴⁰ for the thermochemistry of the gas phase and SURFACE CHEMKIN¹⁴¹ for the thermochemistry of the surface and the corresponding chemical kinetics. The purpose of these packages is the incorporation of complex chemical kinetics into simulations of reacting flow, although CHEMKIN in its original version is not intended to solve specific

problems but only to provide efficient tools for kinetic modeling. The packages consist of a preprocessor, called interpreter, which reads the provided elementary reaction mechanism and the thermodynamic data of the involved species and stores the information in a linking file. The latter provides all relevant data to a subroutine library that is capable of returning information on elements, species, reactions, thermodynamic properties, and chemical production rates.¹⁴¹ The subroutines may be called by the user's application code.

The relevant information that need to be provided to CHEMKIN is a thermodynamic database that includes all gas phase and surface species, the reaction rates of all elementary steps that represent the reaction mechanism, and the density of active sites. In general, the thermodynamic data base consists of seven parameters for each species, which result from a simultaneous fit of the heat capacity, the heat of formation and the entropy of formation to a polynomial of seven coefficients. This implies for the heat capacity of the k^{th} species at constant pressure

$$\frac{C_{p_k}^0}{R} = a_{1k} + a_{2k}T + a_{3k}T^2 + a_{4k}T^3 + a_{5k}T^4 \quad (3.31)$$

The standard state heat of formation is then given by

$$H_k^0 = \int_0^T C_{p_k}^0 dT \quad (3.32)$$

$$\frac{H_k^0}{RT} = a_{1k} + \frac{a_{2k}}{2}T + \frac{a_{3k}}{3}T^2 + \frac{a_{4k}}{4}T^3 + \frac{a_{5k}}{5}T^4 + \frac{a_{6k}}{T} \quad (3.33)$$

It should be noted that the parameter a_{6k} corresponds to the integration constant and relates to the standard heat of formation at $T = 0K$. In analogy, the standard state entropy is expressed as

$$S_k^0 = \int_0^T \frac{C_{p_k}^0}{T} dT \quad (3.34)$$

$$\frac{S_k^0}{R} = a_{1k} \ln T + a_{2k}T + \frac{a_{3k}}{2}T^2 + \frac{a_{4k}}{3}T^3 + \frac{a_{5k}}{4}T^4 + a_{7k} \quad (3.35)$$

With that, the coefficient a_{7k} is directly anchored to the standard state entropy, only. The thermodynamic database in CHEMKIN allows for the specification of two sets of the seven parameters to account for different temperature regimes. In this work, we have calculated the heat capacities, the standard state enthalpy and the standard state entropy for various temperatures between 50K and 900K and fitted the values simultaneously to the

seven parameters with the algorithm by Spitzer et al.¹⁴². The standard state enthalpy of the surface species has been anchored to the thermochemistry of the gas phase.

The forward reaction rates of all elementary steps have to be provided to CHEMKIN in the format

$$k_{f_i} = A_i T^{\beta_i} \exp\left(\frac{-E_i}{RT}\right) \quad (3.36)$$

A temperature exponent β equal to one yields the Eyring equation and with β equal to zero, the standard Arrhenius equation is obtained. The reverse reaction rate constants are internally calculated by CHEMKIN with respect to the equilibrium constant K_{c_i} for the i^{th} elementary step with

$$k_{r_i} = \frac{k_{f_i}}{K_{c_i}} \quad (3.37)$$

The equilibrium constant is determined from the Gibbs' free enthalpy of the involved species. For all elementary steps we have calculated the rate constants at various temperatures between 250K and 800K and fitted them to either the Arrhenius or the Eyring equation, dependent on the better representation in terms of least squares.

In the reactor simulations, an additional analysis of the reaction mechanisms was conducted in terms of a sensitivity analysis of the pre-exponential factors of all elementary steps. The log-normalized sensitivity coefficient S_{ij} is a measure of the impact of a change in the pre-exponential factor A_j of the j^{th} reaction on the production rate r_i of the i^{th} component (e.g. N_2 in the SCR).¹⁴³

$$S_{ij} = \frac{\partial \ln r_i}{\partial \ln A_j} \quad (3.38)$$

In analogy, the impact of a change of the heat of formation on the production rate of a distinct component can be evaluated for each species in the mechanism. Furthermore, elementary reactions steps that are in partial equilibrium can be determined with the partial equilibrium ratio (PER).¹⁴³

$$\text{PER} = \frac{r_f}{r_f + r_r} \quad (3.39)$$

The PER is defined by the ratio of the forward reaction rate (r_f) of an elementary step, divided by the sum of the forward and the backward (r_b) reaction rate. A value of PER=0.5 implies a partial equilibrium while a value of one or zero implies an irreversible step in either the defined forward or backward direction, respectively.

Part III

Selective Catalytic Reduction on Brønsted Acids in H-ZSM5

4

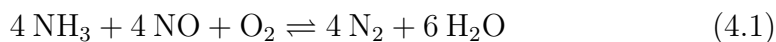
Theoretical Investigation of the Selective Catalytic Reduction of Nitrogen Oxides with Ammonia on H-ZSM5

The selective catalytic reduction (SCR) of NO_x with ammonia in the presence of oxygen has been investigated on a 5 T-atoms containing portion of the H-ZSM5 framework, by using the Density Functional Theory, representing H-form zeolites. The analysis of the potential mechanism was subdivided into a sequence of three parts. First, the intermediates nitrosamine or nitramide together with nitrous or nitric acid are formed from a reaction of ammonia with dimerized nitrogen oxides (N_2O_x with $x = 3, 4$). In this context, different configurations of the dimerized nitrogen oxides were considered (asymmetric (as-) or cis-trans (ct-) for N_2O_3 and asymmetric or symmetric (sym-) for N_2O_4). In addition, it was discriminated between a reaction of the dimerized species with adsorbed ammonia and the decomposition of N_2O_x on a void Brønsted acid, forming an NO_y^+ species prior to a reaction with ammonia. In a second part, the decay of the intermediates nitrous and nitric acid was studied in terms of bimolecular reactions of the acids with ammonia or with each other or their decomposition on a void active site to an NO_y^+ species. Finally, the decomposition of nitrosamine and nitramide into water and nitrogen and

nitrous oxide, respectively, was found to proceed in a “push-pull” mechanism on the Brønsted acids of the catalyst. For all parts, the crossing of potential energy surfaces was considered if necessary. The results of the investigated reaction network are in agreement with the experimental literature.

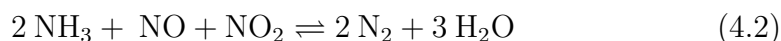
4.1 Introduction

Nitrogen oxides are a major source of air pollution as they cause photochemical smog, acid rain and contribute to the greenhouse effect.¹⁴⁴ They are mainly a product of the combustion of fossil fuels in power plants and automobiles, and emission standards have been legislated to regulate exhaust gases.^{27,28} By now, the most widely applied concept to reduce NO_x (x=1, 2) is the selective catalytic reduction (SCR) with ammonia or hydrocarbons in the presence of oxygen and it has been in the focus of researchers for the last two decades.^{31–33} The generally accepted stoichiometry of the reaction is¹⁴⁵



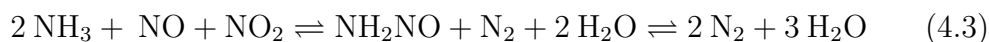
A variety of materials have been reported to exhibit catalytic activity for this reaction and especially vanadium-based^{146,147} catalysts are commercially used in SCR units. Zeolites also show a high activity for the SCR and are particularly promising due to their applicability over a wider range of temperatures. They are more resistant to thermal excursions, and, furthermore, the disposal of used units is less of a problem.¹⁴⁵ Pence and Thomas¹⁴⁸ first reported the catalytic activity of H-mordenite, and subsequently many groups investigated H-form,^{38,39,144,145,148–160} Fe^{161–165}- and Cu¹⁶⁶-exchanged zeolites, among others. Though the Fe-exchanged zeolites show a higher activity than the corresponding H-form in the standard SCR, the latter has not been disregarded by researchers because many experimental results indicate that the main steps of the SCR proceeds on both catalysts with a similar activity. Usually, the Fe-form is prepared by ion exchange, starting with a parent H-form. Since not all Brønsted acid sites are removed, the ion-exchanged catalysts exhibit two different kinds of active sites, iron and

the Brønsted acids.^{161,167} Brandenberger et al.³⁴ even stated an amount of at least 30% of the latter one, no matter what technique was used for the ion-exchange. A crucial finding in the ammonia SCR was the boosting effect of NO₂ upon addition to the reactant gas^{37,38,156,168,169} or via a preoxidation step within the SCR converter, especially at lower temperatures ($\sim 200^\circ\text{C}$). The highest conversion is obtained with a NO₂/NO_x ratio of 50%, which is known by now as the “fast” SCR according to the stoichiometric equation

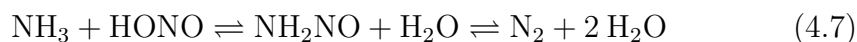


This effect is also valid for vanadium-based catalysts and the H-form zeolites with the difference that the zeolites also show a high activity for an increasing NO₂/NO_x ratio above 50%. However, this leads to a slightly reduced activity and an increased selectivity to unwanted N₂O. The “NO₂-SCR”¹⁷⁰ marks the outer boundary with only NO₂ in the reactant gas. This also leads to the conclusion that NO might be directly involved in the reaction mechanism of the SCR and is not solely a source for NO₂ as an intermediate. While the standard SCR is known to be much slower on the H-form zeolites than on the iron-exchanged catalyst, a significantly high activity was observed for the fast^{37,38,153,157,158,160,161} and the NO₂-SCR.³⁹ This raised the question regarding the influence of the Brønsted acids in iron-exchanged zeolites. Yang and Long¹⁶¹ concluded that the iron in Fe/H-ZSM5 is only responsible for the oxidation of NO to NO₂ while the fast SCR is catalyzed by the Brønsted acids only. Thus, they attributed the difference of the activity for the standard SCR to the NO oxidation which is much faster on the Fe-form than on the H-form.¹⁵⁵ In contrast, Devadas et al.³⁸ and Grünert et al.³⁷ found a higher activity of the iron-containing zeolite for the fast SCR, too. Nevertheless, both groups attributed an at least promoting effect of the Brønsted acid to the activity of the catalyst.^{171,172} Sachtler et al.^{173,174} found that Brønsted acids in BaNa/Y are active for the decomposition of NH₄NO₂ and Grünert et al.³⁷ adapted this as an explanation for the promoting effect in Fe-zeolites. Despite the lower activity as on the iron-form, Halasz et al.¹⁷⁵ showed that the oxidation of NO to NO₂ proceeds much faster on H-ZSM5 than the homogeneous reaction. However, several studies on the H-form suggested, from the observation that NH₃ strongly adsorbs as NH₄⁺ on Brønsted acids, that these sites are blocked for the NO oxidation within the SCR.^{145,150,152} Considering the assumption that also in ion-exchanged zeolites the remaining Brønsted acids have a significant impact on the catalytic performance, the clarification of the mechanism on H-form catalysts should lead to a better understanding of the mechanism of a vast group of commercially interesting products. Though several mechanisms have been proposed to explain the stated phenomena, no clear picture can be drawn yet.

In this chapter, the results of the investigation of the mechanistic details of the SCR of NO with NH₃ on H-ZSM5 are presented based on probing the potential energy surface on a cluster model of this catalyst with the Density Functional Theory. The intention is to clarify the impact of the Brønsted acids in ion-exchanged zeolites. The analysis tries to include most mechanistic suggestions from the experimental literature as well as motivations based on the corresponding gas phase chemistry and related theoretical approaches. Potential reaction pathways are verified from the perspective of lowest energy profiles. An often cited suggestion is based on Eng and Bartholomew¹⁵¹ who proposed that, first a complex is formed by two adsorbed NH₃ molecules on adjacent Brønsted acids together with one NO₂ molecule. Then, an attack by NO should lead to N₂ and H₂O as well as an undissociated complex that remains adsorbed on an acid site. The formation of N₂ and H₂O might be explained by a similar mechanism like the high-temperature gas phase reaction of NO with an amidogen radical (NH₂) via nitrosamine (NH₂NO). A similar explanation was used by Yang and Long.¹⁵⁶ The undissociated complex is assumed to decompose to N₂ and 2 H₂O, whereas the mechanism is unclear. Alternatively, an attack of the complex by NO₂ was stated to form N₂O.

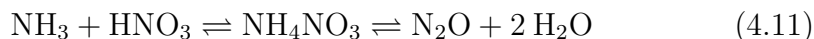
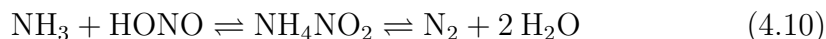


Richter et al.¹⁵² proposed the formation of N₂O₃ for the fast SCR on H-ZSM5 and the subsequent reaction with water to nitrous acid. The latter species is supposed to react with ammonia to water and NH₂NO which further decomposes to nitrogen.



This mechanism is supported by Adelman et al.¹⁷⁶ who reported the formation of N₂O₃ in ZSM5 zeolites after the coadsorption of NO and NO₂. Several authors^{161,170,177} also suggested the formation of ammonium nitrate and nitrite as intermediates. In a series of papers, Tronconi et al. proposed a mechanism for Fe-zeolites^{168–170,178} adapted from Koebel et al.^{146,147} that includes, first, the disproportion of NO₂ in analogy to the mechanism of Richter

et al.¹⁵²

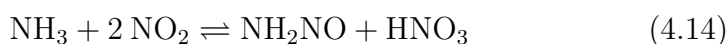


In addition, Tronconi et al. explained the influence of NO as a reducing agent of nitric acid



in the fast SCR and considered this as the rate-determining step of the overall mechanism.

By now, there are also several theoretical studies dealing with reaction mechanisms of the H/N/O system though most apply for the gas phase. However, they can be used as a motivation for the suggestion of analog surface reactions. Anstrom et al.¹⁷⁹ and, later, Soyer et al.¹⁸⁰ investigated the decomposition of NH_2NO to N_2 and H_2O on a V_2O_5 catalyst using DFT calculations and assumed that this reactant should be a key intermediate in the SCR on V_2O_5 . In analogy, Li and Li¹⁸¹ proposed, based on DFT calculations, a mechanism of the decomposition of NH_2NO on the H-ZSM5 by using a very similar push-pull-mechanism like the one used for V_2O_5 . Furthermore, they presented how this intermediate could result from the gas phase reactions



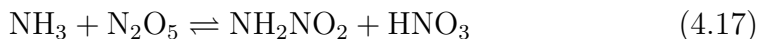
It was assumed for reaction (4.13) that N_2O_3 and for reaction (4.14) N_2O_4 are formed spontaneously from two NO_x molecules. For the case of N_2O_3 , the mechanism was already presented by Hillier et al.¹⁸² and, later, by Morgon et al.¹⁸³. For N_2O_4 an adaptation of this mechanism was used. Furthermore, it was shown for the gas phase that the side product HONO could react to form N_2O_3 and water^{182–185} in accordance with (4.6) or HONO could react with HNO_3 to yield N_2O_4 and water^{181,186} according to (4.9). Besides the hydrolysis of N_2O_4 , Tao and Hanway¹⁸⁷ also studied the hydrolysis of dinitrogen pentoxide leading to two nitric acids, which in terms of the dehydration might be a significant sink of the latter species.



Furthermore, the formation of the potential intermediate species nitramide (NH_2NO_2) was proposed by Musin and Lin¹⁸⁸ from the reaction of ammonia with nitric acid based on DFT calculations. The subsequent decomposition of this species in the gas phase to nitrous oxide and water was investigated by Lin et al.¹⁸⁹



An alternative formation of nitramide was suggested by Frenck and Weisweiler¹⁹⁰ from the reaction of dinitrogen pentoxide with ammonia



Furthermore, Li and Li¹⁸¹ also suggested the formation of NH_2NO_2 from the reaction of symmetric (sym-) N_2O_4 with ammonia in the gas phase

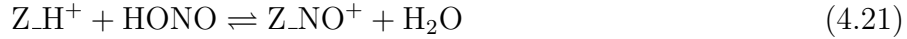
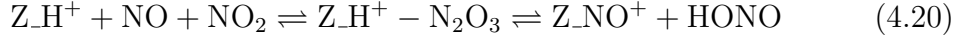


but found this step to be less favorable than the corresponding reaction of asymmetric N_2O_4 to nitric acid and nitrosamine. In addition, Lin et al.^{191,192} theoretically investigated reactions (4.12) and (4.7) and, finally, Li and Li¹⁸¹ proposed the oxidation of NO to NO_2 in the gas phase according to

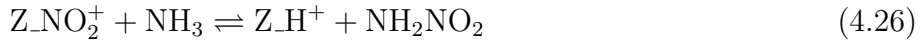
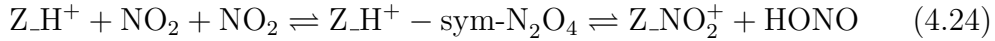
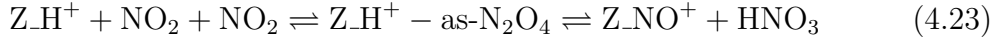


All of the presented mechanisms so far involve as intermediates the formation of a dimerized nitrogen oxide (N_2O_y), nitrous and nitric acid and a species that eventually decomposes to nitrogen or nitrous oxide and water. The latter species are either nitrosamine and nitramide or ammonium nitrate and nitrite. The formation of the acids as key intermediates requires the reaction of the dimerized nitrogen oxides with either adsorbed water or ammonia and subsequently for the decay a reaction of the acids with ammonia or with each other. In contrast to these bimolecular reactions, Richter et al.¹⁵² pointed out that the dehydration of intermediately formed nitrous acid could form the nitrosyl cation NO^+ , which is known from organic chemistry to be capable of attacking amines under the formation of N-nitroso amines. In the simplest case, the reaction of ammonia with NO^+ forms nitrosamine. In fact, the nitrosyl cations in H-form zeolites are well known from several studies on the adsorption of NO_x in these catalysts^{193–196} and correspond to an IR band at 2133cm^{-1} . Lavalley et al.¹⁹³ suggested the formation of NO^+ from the decomposition of N_2O_3 adsorbed on a Brønsted acid by forming nitrous acid. The latter dehydrates then on a second acid site in analogy to

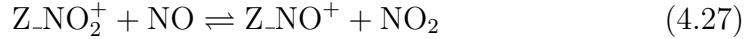
the mechanism proposed by Richter et al.¹⁵². A combination of these suggestions leads to a reasonable reaction pathway for the fast-SCR according to



In analogy, one can suggest the formation of a NO_2^+ species balancing the charge of the zeolite framework as was done by Busca et al.¹⁵⁷. The formation of this species could then either be explained by the decomposition of nitric acid in analogy to reaction (4.21) or by the decomposition of adsorbed N_2O_4 forming nitrous acid in analogy to reaction (4.20).



In analogy to reaction (4.22), the NO_2^+ species can then react with ammonia (4.26) to nitramide (NH_2NO_2) which decomposes to nitrous oxide and water. Finally, an interchange of the two NO_x^+ species according to



is at hand. The significance of the different suggested reaction mechanisms as well as the detailed influence of the catalytic surface is not known. In this chapter, this large network of potential reactions is investigated based on DFT with the aim to find the most probable reaction pathways within the H/N/O system on H-form zeolites that account for the overall mechanism of the SCR in agreement with the experimentally observed phenomena.

4.2 Theory

The ZSM5 (**Z**eolite **S**ocony **M**obil - five) belongs to the group of aluminosilicates which are known as zeolites. They consist of $[\text{SiO}_4]$ and $[\text{AlO}_4]$ tetrahedra, are crystalline and highly porous. The chemical composition of a unit cell of the ZSM5 can, according to Baerlocher et al.,³⁵ be written as $[\text{Al}_n\text{Si}_{96-n}\text{O}_{192}]$ -MFI with $n < 27$ and the pore system can be described as straight pores in one direction with interconnecting zig-zag pores perpendicular to the straight ones (see Figure 4.1). The catalytic active center and

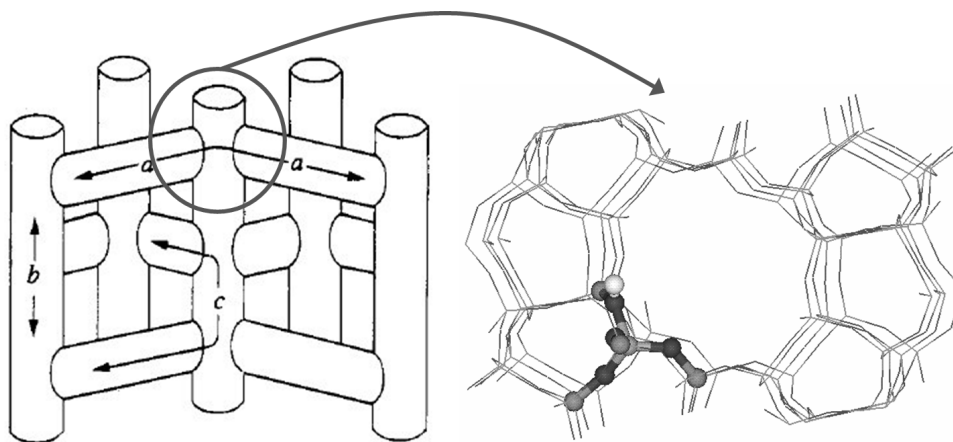


Figure 4.1: Schematic representation of the ZSM5 zeolite, taken from ref. [199], and cluster cut out from the intersection

a part of the zeolite framework was represented by a cluster of 5 T-sites (Figure 4.2, ST A) cut out of the unit cell at an intersection of a straight and a zig-zag pore (Figure 4.1). Therefore, all Si atoms were initially placed at their crystallographic positions, as reported by Olson et al.¹⁹⁷ As there is some evidence that Al is not positioned randomly but prefers the T12 site,¹⁹⁸ we cut our framework cluster from the unit cell, so that it surrounds this site with Al as its center. The terminal Si atoms were saturated with hydrogen, whereas the Si-H bonds are oriented in the direction of the former Si-O bonds. The length of these bonds was set to 1.487 Å, representing the optimal bond length for SiH₄ at the B3LYP/TZVP level of theory. For all calculations on the catalyst, the H-atoms were fixed while other atoms positions were fully relaxed. The Brønsted acid site is the hydrogen bonded to the bridging oxygen atom. All quantum chemical calculations were carried out with the TURBOMOLE suite of programs²⁰⁰ by using gradient-corrected density functional theory (DFT). To represent the effects of exchange and correlation Becke's 3-parameter exchange functional⁸¹ and the correlation functional of Lee, Yang and Parr⁸³ were used (B3LYP). The triple- ζ basis set with polarization functions (TZVP)⁶⁶ was used for all atoms together with a very fine numerical grid size (m5).²⁰¹ Structure optimizations were performed in Cartesian coordinates with an energy convergence criterion of 10^{-7} Ha and the maximum norm of the Cartesian gradient was converged to 10^{-4} Ha/bohr. These specifications were chosen as a reasonable compromise between accuracy and computational expenses. Transition states were localized using a combination of interpolation and local methods. First the grow-

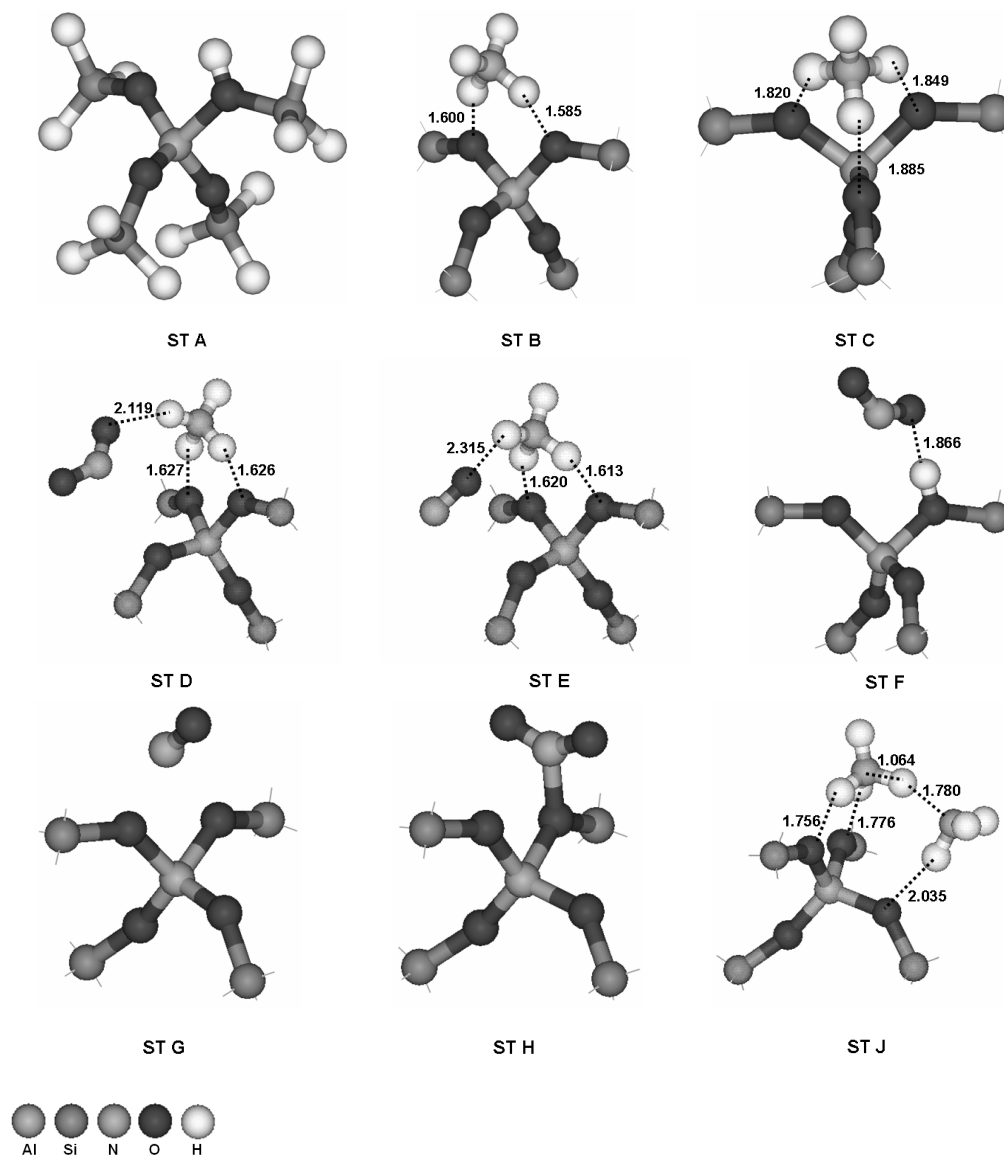


Figure 4.2: T5 cluster model of the acid site in H-ZSM5 (ST A), geometry of the minimum of adsorbed ammonium in the 2H state (ST B) and in the 3H state (ST C), ammonia with coadsorbed NO₂ (ST D) and coadsorbed NO (ST E), adsorbed NO₂ (ST F), NO⁺ (ST G) and NO₂⁺ (ST H), and two NH₃ (ST J). Bond lengths are in Å

ing string-method⁹⁹ was applied in mass-weighted coordinates, leading to an approximate saddle point, once the two ends of the growing string had joined. The refinement of the saddle point was accomplished by the modified dimer method¹⁰⁵ with a gradient-norm convergence criterion of $5 \cdot 10^{-4}$ Ha/bohr. In cases of inaccuracy with this procedure (e.g. more than one imaginary frequency) the PRFO¹⁰³ method was used for further refinement. To confirm that the transition states are connected to the correct energy minima, each transition state was perturbed slightly along the reaction coordinate in the direction of reactant and product. These perturbed geometries were used as starting points for energy minimization which revealed that in all cases the desired energy minimum was found. Because NO and NO₂ are doublets and oxygen is a triplet we considered crossing of seams of PESs in the stepwise adsorption or desorption of these molecules for completion of the mechanisms. Those minimum potential-energy structures on the seam of two PESs were determined with a multiplier penalty function algorithm (see Heyden et al.¹¹⁹ for details). Converged minimum energy crossing point structures had a maximum energy difference on both PESs of less than 10^{-6} Ha. All subsequent structures were then calculated as closed-shell, as the formation of singlet structures revealed lower energies than coadsorbed, but separated, molecules with unpaired electrons.

4.3 Results and Discussion

In the following, the mechanistic details of the reactions (4.5) to (4.27) involving the Brønsted acid of H-ZSM5 as active catalytic site will be presented and discussed, including the crossing of PESs. Besides the oxidation of NO to NO₂ as a precursor, the reactions are distributed into three main groups. In a first part, the formation of the intermediates nitrosamine or nitramide and nitrous or nitric acid via the reaction of dimerized N₂O_y and ammonia is discussed. This includes the reactions of two NO, NO and NO₂ and two NO₂ with adsorbed ammonia as well as an intermediate formation of NO⁺ or NO₂⁺ (Figure 4.2, ST G and ST H) from the decomposition of a dimerized nitrogen oxide on the active site prior to a reaction with ammonia. In a second part, the decay of the intermediates nitrous and nitric acid is discussed. This involves the dehydration reactions of two acids as well as their interaction with adsorbed ammonia. In this context, a discussion on the potential role of ammonium nitrate and nitrite is included. Furthermore, the question of the direction of the interaction of two acids, resulting either in the dehydration or the hydrolysis of the dimerized nitrogen oxides, is addressed. The third part of discussion covers the decomposition of the intermediates nitrosamine

and nitramide. For both, two different pathways are compared. An overview of the investigated reactive network of the H/N/O system is shown in Figure 4.3. All energies stated in this chapter are zero-point energy-corrected (ZPE) electronic energies with respect to single molecules (gas phase) and the empty zeolite framework. For some transition states, only the electronic energy differences to either the reactant or the product were taken into account, because otherwise, with the ZPE-correction, the value was below this state. This effect can occur when rather small electronic energy differences are considered. In these cases, it will be stated as a remark in parentheses including the reference state to which the electronic energy was added.

4.3.1 Formation of NO₂

Tsukahara et al.²⁰² reviewed the chemical kinetics of the gas phase oxidation of nitric oxide and suggested the occurrence of a chain-like transition state (TS) with the sequence O-N-O-O-N-O. Li and Li¹⁸¹ found such a structure from DFT calculations but with a non-planar configuration. In Figure 4.4 the energies of a mechanism for this reaction involving the Brønsted acid as active site as well as of the gas phase mechanism are displayed. The corresponding structures of the catalyzed and the gas phase mechanism, similar to the one proposed by Li and Li, are shown in Figures B.1 and B.10 respectively.

For the catalyzed oxidation of NO we started the mechanism with the adsorption of O₂ on the surface (ST 1). In the next step NO coadsorbs, whereas ST 2 is calculated on the PES with spin multiplicity M_S=4, followed by a crossing of the seam of PESs with M_S=4 and M_S=2. The corresponding structure for this crossing is denoted as SEAM 1 which reveals a shortening of the distance between the N atom of NO and O₂ from 4.8 to 4.0 Å and finally to 2.4 Å for ST 3. This process basically leads to a flip in the spin of the unpaired electron of NO, thus, getting attracted by the oxygen molecule. Then the coadsorption of another NO molecule was considered, leading to M_S=3 as shown in ST 4. Up to that point, the energy profile stays rather constant indicating only a loose binding of the coadsorbed species. The crossing of the SEAM 2 from M_S=3 to M_S=1 leads to a chain-like structure (ST 5) including a drop in energy to -9.8 kcal/mol with respect to the gas phase, indicating a stronger adsorption compared to the single molecules' state. The barrier for this crossing was calculated to be E[‡]=9.8 kcal/mol. In the subsequent transition state (TS 1) the bonds ON-OO shorten whereas the O-O bond in oxygen is prolonged, leading to two NO₂ (ST 6). Here the barrier was E[‡]=5.4 kcal/mol. Finally, SEAM 3 and ST 7 take into account that another crossing of PESs from M_S=1 to M_S=3 is necessary to yield two

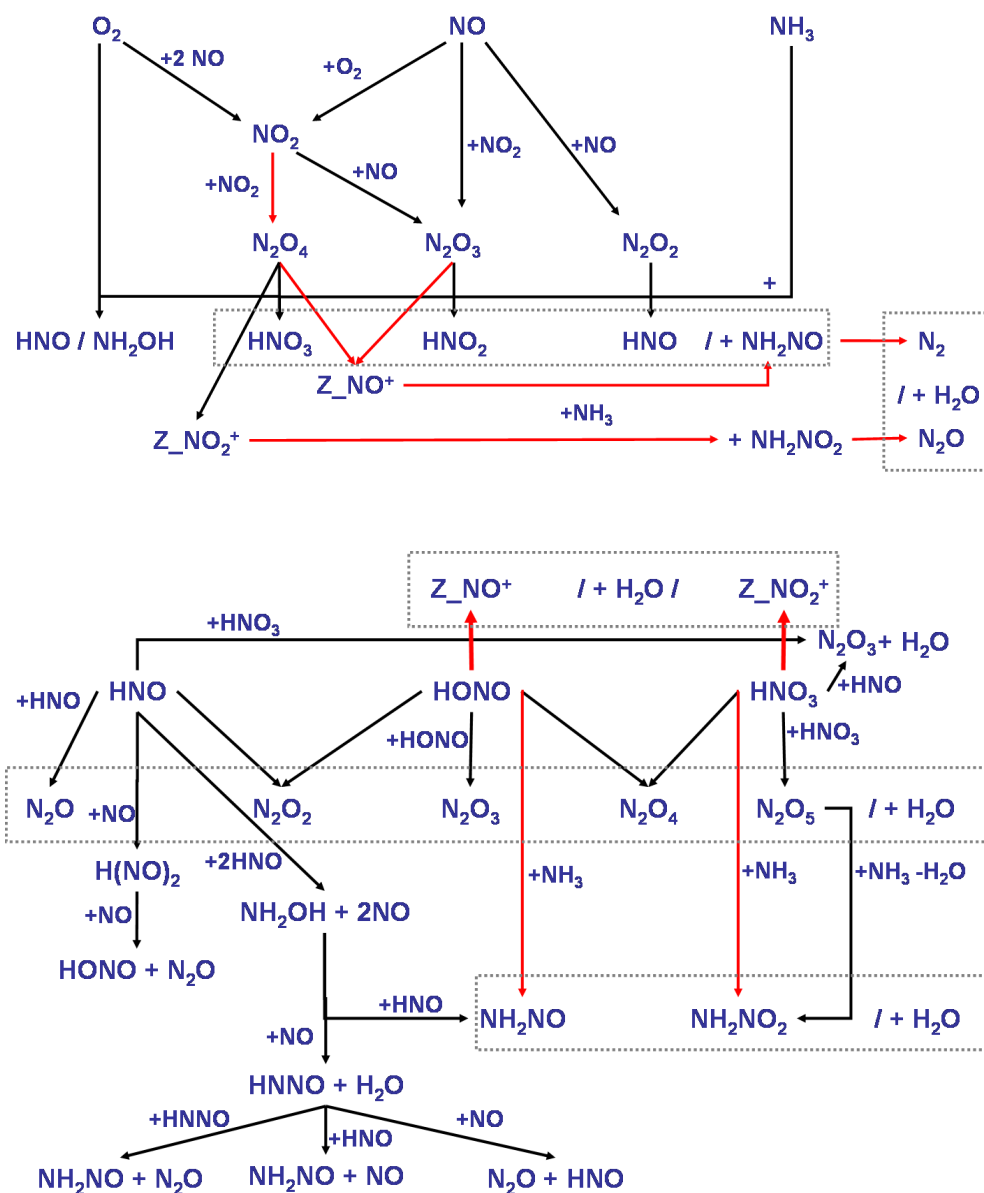


Figure 4.3: Schematic of the combined reaction network of SCO and SCR on H-ZSM5. Fast and NO₂-SCR are accentuated with red arrows. Grey dotted boxes refer to an additional collective product for all encircled reaction steps, which is separated with a slash.

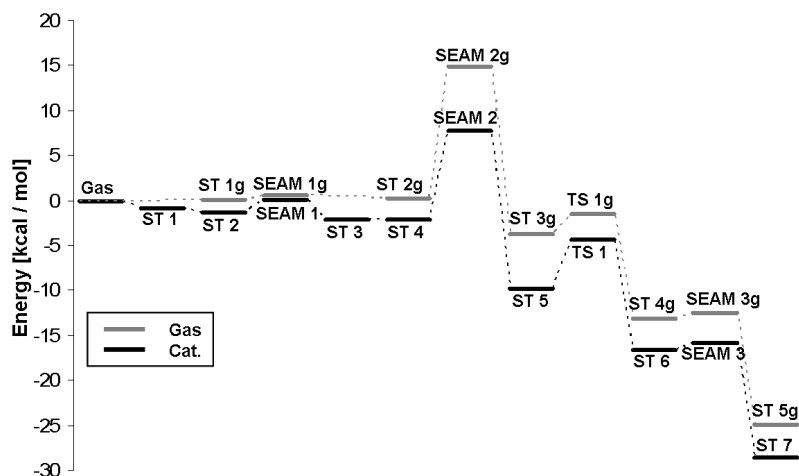


Figure 4.4: Energy profiles for the oxidation of NO with O₂, comparing the catalyzed (Cat.) and the homogeneous (Gas) reaction mechanism. Energies are zero-point corrected.

separate NO₂ molecules. The energy barrier for this process was calculated to be $E^\ddagger=0.7$ kcal/mol, indicating that this last step can be considered as spontaneously running.

For the gas phase reaction (Fig. B.10) ST 1g is on the PES with $M_S=5$, representing three single molecules. We found that a stepwise crossing of the PESs leads to the most favorable energy profile. SEAM 1g is the minimum on the seam of the PESs with $M_S=5$ and $M_S=3$. In the latter state (ST 2g) the distances between the molecules shortened and it should be noted that one NO and the oxygen molecule exhibit similar structures as was observed for the catalyst on the PES with $M_S=2$ (ST 3, Fig. B.1). Again, here the flip of the spin of the unpaired electron of one NO molecule is the effect of the crossing of the seam, whereas the spins of the unpaired electrons in oxygen and the one in the second NO molecule remain in their original configuration. Up to this state, analogically to the catalyzed reaction mechanism, the energy profile (Fig. 4.4) hardly changes, leading to the assumption that the steps prior to ST 2g can be neglected. The crossing of the PESs from $M_S=3$ to $M_S=1$ (SEAM 2g) includes a barrier of $E^\ddagger=14.6$ kcal/mol, being 4.8 kcal/mol higher than the corresponding barrier on the catalyst, and leads to a chain-like structure (ST 3g), comparable to the one on the catalyst. Thus it can be assumed that the benefit of the catalyst here is the facilitation of the formation of the chain-like intermediate structure on the PES with $M_S=1$. Then, via a transition state (TS 1g), exhibiting an energy barrier of $E^\ddagger=2.2$

kcal/mol this step leads to two NO_2 molecules (ST 4g). Finally, again the crossing of PESs with $M_S=1$ to $M_S=3$ was taken into account where an energy barrier of $E^\ddagger=0.65$ kcal/mol needs to be surmounted.

The comparison of the energy profiles of the catalyzed and the homogeneous reaction reveals that the first is favorable due to the overall lower energy. In particular, an enhancement of the formation of the chain like structure has to be taken into account. Although Tsukahara et al.²⁰² stated that from the prior literature it is evident that the homogeneous reaction occurs, our results support the findings of Halasz and Brenner¹⁷⁵ who stated that the oxidation of NO is strongly accelerated by H-ZSM5. Furthermore, their suggestion that the Brønsted acid is the active site for this reaction is in agreement with our findings. The comparison of our gas phase transition state (TS 1g on PES with $M_S=1$) with the one presented by Li and Li¹⁸¹ reveals that from a structural point of view, they agree very well. Considering the energy barriers, Li and Li stated here a value of $G^\ddagger=15.6$ kcal/mol at 373K with respect to the separated reactants (two NO and O_2), whereas our corresponding value is $G^\ddagger=23.7$ kcal/mol. The difference can be explained by the larger basis set used in this work.

4.3.2 Formation of the Intermediates NH_2NO_x and HNO_y

In this part the formation of the potential intermediates nitrosamine and nitramide as well as nitroxyl, nitrous and nitric acid is presented from the reaction of nitrogen oxides with ammonia. This initialization of the main body of the selective catalytic reduction is subdivided into first, the reaction of N_2O_3 with adsorbed ammonia, discriminating between the asymmetric (as-) and the cis-trans (ct-) configuration of the dimerized nitrogen oxide. Secondly, the analogous reaction of N_2O_4 in either the asymmetric or the symmetric (sym-) configuration with adsorbed ammonia is discussed and third, the corresponding reaction of N_2O_2 is considered. Finally, the decomposition of intermediately formed N_2O_x (with $x=3, 4$) on a Brønsted acid, leading to the formation of NO^+ or NO_2^+ prior to a reaction with ammonia or water is analyzed.

Formation of NH_2NO from NO and NO_2 with Adsorbed NH_3

There is agreement in the experimental literature^{151,154,156} that the SCR proceeds fastest for an equimolar NO and NO_2 feed stream. The assumption is self-evident that not only NO_2 plays an important role in the mechanism but also NO. Hillier et al.¹⁸² and Li and Li¹⁸¹ suggested the formation of N_2O_3

as an intermediate in the gas phase, and there is some evidence¹⁷⁶ that this species might occur in zeolites. In the following, we present a mechanism involving this intermediate coadsorbed on the catalyst.

The mechanism starts with the strong adsorption of ammonia as NH_4^+ in the 2H mode²⁰³ ($\Delta E_{\text{ads}} = -18.9$ kcal/mol) and the coadsorption of NO_2 (Figure 4.2, ST B and D). For the coadsorption of NO_2 an adsorption energy of $\Delta E_{\text{ads}} = -2.6$ kcal/mol with respect to adsorbed ammonia was calculated. Figure B.2 illustrates the subsequent species, beginning with the additional coadsorption of NO . In Figure 4.5 the corresponding energies to the structures are shown. ST 1a is calculated on a PES with spin multiplicity of $M_S=3$ and corresponds to a state, where both, NO_2 and NO are considered as separate molecules. The coadsorption of NO hardly affects the structural configurations of the previously coadsorbed NO_2 . Also, the energy profile for ST 1a reveals that NO should be considered a gas phase species. The following minimum on the crossing of the two PESs ($M_S=3$ to $M_S=1$), SEAM 1a, corresponds to the formation of N_2O_3 , with an energy barrier of $E^\ddagger=5.1$ kcal/mol. Within this process, a shortening of the distance between NO_2 and NO takes place, ending at 1.962 Å for ST 2a. This is close to the calculated N-N distance of asymmetric (as-) N_2O_3 (1.864 Å)²⁰⁴, indicating the formation of the latter. In addition, the distance of this molecule to the adsorbed ammonia reduces drastically during the crossing of PESs (O-H from 2.115 over 2.086 to 1.859 Å). Together with a further reduction in energy ($\Delta E_{\text{ads}} = -33.9$ kcal/mol) a stable adsorbed structure can be assumed. In the next step the adsorbed ammonia needs to be activated by reformation of NH_3 via TS 1a. Here, the former NO_2 takes up a proton, briefly forming trans-HONO, whereas the N-N bond in N_2O_3 is enlarged and NH_3 is pushed off the catalyst. Then, the proton is transferred back to the zeolite and the N-N bond length reduces again to nearly the former distance as can be seen in ST 3a. Now, N_2O_3 is adsorbed on the Brønsted acid site but also the short distance between the nitrogen of NH_3 and the one of the former NO molecule (2.333 Å) indicates a rather strong interaction. The activation of NH_3 exhibits the highest barrier in the mechanism with $E^\ddagger=22.5$ kcal/mol. Via TS 2a the bond between NH_3 and NO is formed and a proton transfer from ammonia to the remaining adsorbed NO_2 takes place. This step needs an activation energy of $E^\ddagger=10.7$ kcal/mol followed by a drop in the energy profile down to $\Delta E_{\text{ads}}=-26.9$ kcal/mol for adsorbed NH_2NO and trans-HONO (ST 4a). The next reaction step (TS 3a) is a proton transfer from HONO to NH_2NO which leads to a structure where the latter is adsorbed directly on the Brønsted acid site (ST 5a) and HONO switches to the cis-configuration. Because the configurations 4a and 5a exhibit nearly the same energy, none

of them can be considered superior and, thus, both might occur. The energy barrier for the proton transfer was calculated to be $E^\ddagger=10.8$ kcal/mol.

Furthermore, in Figure B.2 a one step mechanism (b) for the reaction of cis-trans (ct-) N_2O_3 with adsorbed ammonia to yield directly NH_2NO and HONO is illustrated, starting on the PES with $M_S=1$. The NO_2 portion becomes cis-HONO by proton transfer from the ammonia and a bond between the remaining NO and NH_3 forms, including a second proton transfer from NH_3 to the zeolite. It can be seen from the energy profile that the ct- N_2O_3 is less favorable than the as-structure. Furthermore, the activation barrier with $E^\ddagger=26.4$ kcal/mol is 3.9 kcal/mol higher than the highest barrier in the two-step mechanism presented earlier, indicating that the latter is more likely to happen.

For the gas phase reaction, the initial configurations as- N_2O_3 and ct- N_2O_3 were investigated (Figure B.3 a) and b) respectively). The first structure in both cases is calculated on the PES with $M_S=3$ where a slight drop in the energy profile compared to single molecules indicates only a weak intermolecular interaction. In the next step the crossing of the PESs ($M_S=3$ to $M_S=1$) via SEAM 1_{as} for as- N_2O_3 with $E^\ddagger=7.1$ kcal/mol and 1_{ct} for ct- N_2O_3 with $E^\ddagger=7.8$ kcal/mol includes a rotation of the NO_2 molecule, leading to the formation of N_2O_3 . In the case of as- N_2O_3 , the drop in energy corresponding to the formation of the N-N bond exceeds that of ct- N_2O_3 by $\Delta E=6.6$ kcal/mol, indicating that it is the more stable configuration. Next, the formation of an N-N bond between the NO portion of N_2O_3 and NH_3 and a proton transfer from NH_3 to the NO_2 portion via a transition state (TS 1_{as} and TS 1_{ct}) leads to NH_2NO and trans-HONO and cis-HONO respectively. The surmounting of the TS includes an activation energy of $E^\ddagger=15.0$ kcal/mol for as- N_2O_3 and $E^\ddagger=9.4$ kcal/mol for ct- N_2O_3 . For as- N_2O_3 , Hillier et al.¹⁸² reported an activation energy of $G^\ddagger=15.8$ kcal/mol at 298.15 K and Li and Li¹⁸¹ $G^\ddagger=17.8$ kcal/mol at 373 K. The corresponding values of this work at these temperatures are with $G^\ddagger=14.4$ kcal/mol for both temperatures in good accordance. For ct- N_2O_3 Li and Li reported a barrier of $G^\ddagger=14.7$ kcal/mol whereas here, a value of only $G^\ddagger=10.8$ kcal/mol was calculated at 373 K. The difference might be due to the larger basis set used in this work, as the structural properties of the TS compare quite well.

By comparing the energy profiles (Figure 4.5) of the gas phase and the catalyzed reaction, one can see that for the latter the energy always stays below the reference state and also below the energy profile of the gas phase reaction. This is mainly due to the strongly exothermic adsorption of ammonia as ammonium as well as to the exothermic formation of N_2O_3 . Also, the stepwise adsorption of the molecules on the catalyst reveals a high stability

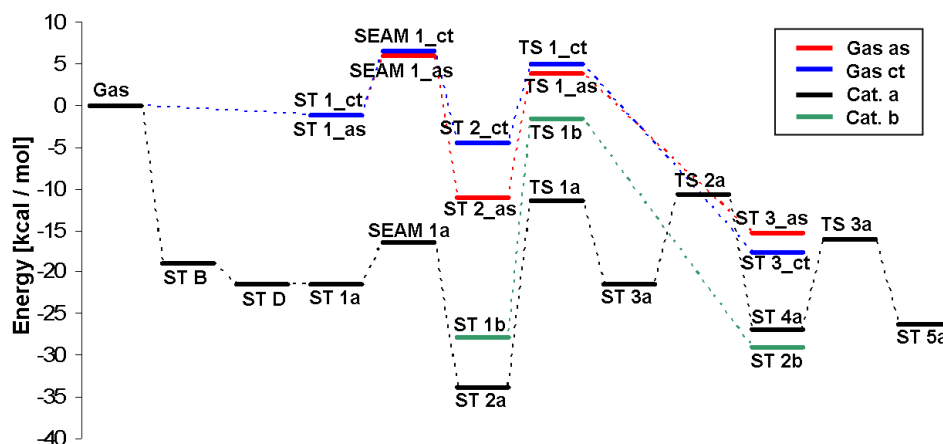


Figure 4.5: Energy profiles for the formation of NH_2NO from NO_2 and NO , comparing the catalyzed two-step mechanism (Cat. a), the catalyzed one-step mechanism (Cat. b), the gas phase mechanism with *as*- N_2O_3 (Gas *as*) and the gas phase mechanism with *cis-trans*- N_2O_3 (Gas *ct*). Energies are zero-point corrected.

of the system whereas in the gas phase the three molecules would need to collide with each other at the same time with the proper orientation for a successful reaction. Though the activation energy in the gas phase for the main reaction is 7.5 kcal/mol for *as*- N_2O_3 and 13.1 kcal/mol for *ct*- N_2O_3 lower than for the catalyzed two-step mechanism the latter is more likely to occur due to the more favorable overall energy profile.

Formation of NH_2NO_x from Two NO_2 with Adsorbed NH_3

Several groups^{38,39,153,158} found that the SCR of NO_2 proceeds on H-form zeolites in the absence of NO and O_2 . Analogous to the proposed mechanism¹⁸² including N_2O_3 as an intermediate Li and Li¹⁸¹ suggested a gas phase reaction pathway by using N_2O_4 as an intermediate structure. Here, a transfer of this basic idea to a catalyzed reaction is presented, comparable to the one for N_2O_3 .

Again the mechanism is started with the adsorption of ammonia as ammonium and the coadsorption of NO_2 (Figure 4.2 ST B and D). The following structures presented refer to Figure B.4 with the corresponding energies of the *as-route* in Figure 4.6. ST 2, calculated on the PES with $M_S=3$ shows the coadsorption of a second NO_2 molecule. From the energy profile it can

be seen that the coadsorption of the two NO_2 molecules is rather weak, compared to the strong adsorption of ammonia. In the next step the crossing of the PESs from $M_S=3$ to $M_S=1$ via SEAM 1 and an energy barrier of $E^\ddagger=19.3$ kcal/mol is considered, which leads to the formation of asymmetric N_2O_4 , coadsorbed on ammonium (ST 3). The drop in energy for this configuration compared to the single NO_2 molecules indicates a more stable state. After the formation of N_2O_4 the activation of NH_4^+ to NH_3 occurs by proton transfer from the ammonium to the NO_3 portion of as- N_2O_4 which then adsorbs as HNO_3 with a hydrogen bridge to the zeolite framework while the NO portion gets closer to the adsorbed ammonia molecule (ST 4a). The transition state (TS 1) that has to be crossed exhibits an energy barrier of $E^\ddagger=19.1$ kcal/mol. Then a slight rearrangement of the adsorbed molecules on the catalyst takes place leading to ST 4b. For this rearrangement, no transition state was found and growing-string-method tests revealed that a barrier between these two states is negligible. In the next step, a bond between adsorbed NH_3 and NO is formed while, simultaneously, a proton transfer from NH_3 to the zeolite takes place (TS 2). This leads to the formation of adsorbed NH_2NO (ST 5). The calculated energy barrier for this process is $E^\ddagger=0.16$ kcal/mol.

For comparison, also the mechanism in the gas phase was investigated, partially following the suggestions of Li and Li.¹⁸¹ The corresponding structures are presented in Figure B.5 a) and the energies in Figure 4.6, denoted with *as*. The mechanism is started with an assembly of the three molecules

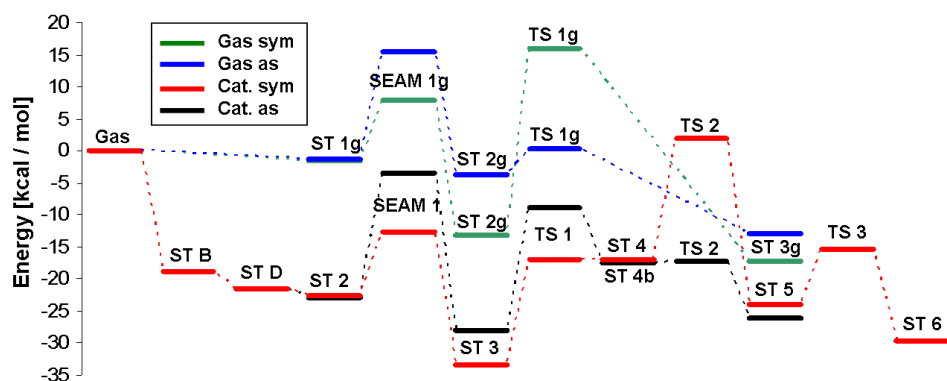


Figure 4.6: Energy profiles for the formation of NH_2NO (as-route) or NH_2NO_2 (sym-route) from two NO_2 , comparing the catalyzed (Cat.) and the homogeneous (Gas) reaction mechanisms. Energies are zero-point corrected.

involved on a PES with $M_S=3$ (ST 1g) leading to a slight drop in energy compared to separated molecules. Then, a crossing of the PESs (SEAM 1g) to $M_S=1$ leads to the formation of as- N_2O_4 (ST 2g), where an energy barrier of $E^\ddagger=20.2$ kcal/mol has to be surmounted. In the next step a bond between NH_3 and the NO portion of N_2O_4 is formed while a proton transfer from NH_3 to the NO_3 portion takes place simultaneously forming HNO_3 and NH_2NO (ST 3g). The energy necessary for this step to proceed was calculated to $E^\ddagger=4.1$ kcal/mol, corresponding to the structure (TS 1g). Li and Li¹⁸¹ only presented a transition state for the formation of the final products starting from N_2O_4 and found an energy barrier of $G^\ddagger=9.5$ kcal/mol at 373K ($G^\ddagger=5.3$ kcal/mol this work at 373K). As the structural properties are in good agreement, the deviation in energy might be due to the larger basis set used in this work. Nevertheless, this barrier is not of such importance since a far higher barrier for the formation of N_2O_4 was observed. Although the reaction pathway for the catalyzed reaction exhibits higher energy barriers than the gas phase reaction its overall energy profile stays below the reference state and the profile of the homogeneous reaction mechanism. This favorable behavior is again due to the strongly exothermic adsorption of ammonia as ammonium ion on the catalyst, releasing enough energy to overcome the subsequent barriers. Also the step by step adsorption of the molecules on the surface has to be seen as beneficial compared to a homogeneous reaction pathway, involving three molecules as initial state.

Besides the reaction via the asymmetric dimerized nitrogen oxide also the mechanism for the symmetric isomer, as was proposed by Li and Li¹⁸¹ for the gas phase, which leads to nitrous acid and nitramide was analyzed. The mechanism on the catalyst is compared to the homogeneous reaction. The structures of the catalyzed reaction are illustrated in Figure B.6 and the energies are shown in Figure 4.6 (sym-route). After the adsorption of ammonia and the coadsorption of NO_2 the coadsorption of a second NO_2 (ST 2) molecule exhibits a low adsorption energy of $\Delta E_{\text{coads}} = -1.0$ kcal/mol which indicates rather a gas phase attack for the subsequent reaction. Because NO_2 is a doublet, the coadsorbed state of structure ST 2 is calculated on the PES with $M_S=3$. Subsequently, the two NO_2 form sym- N_2O_4 (ST 3), coadsorbed on the ammonium ion which includes the crossing of the seam to the PES with $M_S=1$ (SEAM 1). For this process a barrier of $E^\ddagger=9.7$ kcal/mol needs to be overcome and the following drop in energy indicates a more stable structure for the dimerized state than for the single molecules. Then the activation of ammonia takes place as the ammonium ion re-transfers a proton to the catalytic surface to which now sym- N_2O_4 is hydrogen-bonded (ST 4). This step exhibits an energy barrier of $E^\ddagger=16.5$ kcal/mol and leads

to a highly unstable intermediate state as the reverse reaction barrier was calculated to be only $E^\ddagger=0.11$ kcal/mol (electronic energy with respect to ST 4). In the next step via TS 2 and a barrier of $E^\ddagger=18.9$ kcal/mol, nitramide is formed as the one NO_2 forms an N-N bond with the ammonia while the latter releases a proton to the second NO_2 , forming nitrous acid in the cis-configuration (ST 5). Because of the instability of ST 4, enough energy needs to be provided, starting from ST 3, to overcome the internal barrier TS 2 in order to obtain the final products. Thus, lumping these steps together results in an internal energy barrier of $E^\ddagger=35.2$ kcal/mol for the formation of the final products. Finally, also the transfer of the nitrous acid into the more stable trans-configuration was considered by a rotation along the N-O bond (TS 3). This step exhibits a rather low barrier of $E^\ddagger=8.7$ kcal/mol and leads to a slightly more favorable state indicated by a drop in energy of $\Delta E=-5.6$ kcal/mol. Mebel et al.¹⁸⁹ also considered the formation of NH_2ONO as intermediate in their investigation on the reaction of NH_2 with NO_2 in the gas phase. Calculations for the formation of such a structure together with trans-HONO resulted in an activation barrier of $E^\ddagger = 72.7$ kcal/mol making the formation of an N-O bond between the ammonia and NO_2 unlikely (for details see Brüggemann et al.²⁰⁵)

For the corresponding gas phase (Figure B.5 b) the formation of the dimerized structure takes place (SEAM 1g) by crossing the seam from the PES with $M_S=3$ to $M_S=1$ which exhibits an energy barrier of $E^\ddagger=9.4$ kcal/mol. This is similar to the barrier of the catalyzed reaction and it can be concluded from the corresponding structures, that ammonia does not contribute to the formation of sym- N_2O_4 . The subsequent reaction, leading to trans-HONO and nitramide (ST 3g), exhibits an energy barrier of $E^\ddagger=29.2$ kcal/mol which is even less than it was the case for the catalyzed mechanism. Because it is known, that the intermediate N_2O_4 is an unstable structure at elevated temperatures a beneficial contribution of the catalyst can be seen in the step-by-step coadsorption of the single molecules. Nevertheless, a final comparison of the reaction mechanism via sym- N_2O_4 with the proposed reaction via as- N_2O_4 reveals that though the formation of sym- N_2O_4 exhibits a lower energy barrier ($\Delta E=9.6$ kcal/mol) the subsequent reaction with the ammonia needs to overcome a significantly higher barrier ($\Delta E=16.3$ kcal/mol). This indicates, that here the reaction via the asymmetric configuration is more likely to take place, leading to nitrosamine and nitric acid as intermediates.

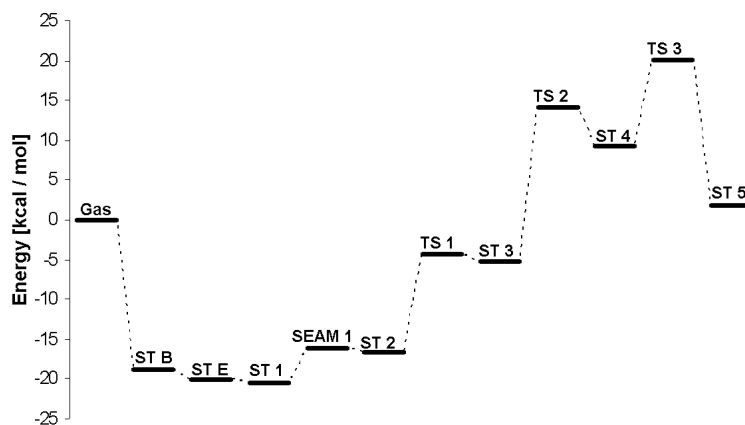


Figure 4.7: Energy profile for the formation of NH_2NO from two NO . Energies are zero-point corrected.

Formation of NH_2NO from Two NO with Adsorbed NH_3

Though there is an agreement in the literature^{38,150,152,157,160} that the SCR of NO hardly proceeds on H-form zeolites in the absence of oxygen, there is no consensus about whether it works at all or not. Figure B.7 illustrates a mechanism dealing with this question. The energies, corresponding to the structures are presented in Figure 4.7. The first energy point corresponds to the adsorbed ammonium and the second to the coadsorbed NO (ST B and E, Figure 4.2). After the rather loose coadsorption of another NO molecule (ST 1) the crossing of PESs from $M_S=3$ to $M_S=1$ (SEAM 1) was considered. This process leads to the formation of N_2O_2 via an energy barrier of $E^\ddagger=4.5$ kcal/mol as can be seen in the reduction of the distance between N-N from the two NO molecules (ST 2). Then, comparable to the cases of N_2O_3 and N_2O_4 , the activation of ammonium to ammonia occurs (TS 1, $E^\ddagger=12.4$ kcal/mol) and N_2O_2 adsorbs on the Brønsted acid site (ST 3). In the next, step a complex forms from NH_3 and N_2O_2 (TS 2) and, simultaneously, a proton transfer from the NH_3 portion to the zeolite as well as from the zeolite to N_2O_2 takes place. This includes the surmounting of an energy barrier of $E^\ddagger=19.4$ kcal/mol. In the last sequence of the mechanism, the N-N bond in the former N_2O_2 of the adsorbed complex (ST 4) is broken (TS 3), leading to the coadsorbed NH_2NO and nitroxyl (HNO) (ST5) by crossing a barrier of $E^\ddagger=10.9$ kcal/mol. Though the single energy barriers are not too high to be unrealistic, the energy profile as a whole (Figure 4.7) reveals that the process is endothermic and exhibits an apparent activation energy of

$E_{\text{app}}^{\ddagger}=20.1$ kcal/mol. This finding still does not cancel out the ability of H-ZSM5 to catalyze this reaction, but in comparison to the energy profiles of the mechanisms of N_2O_3 and N_2O_4 it is less likely to be of relevance.

Fast and NO_2 SCR via NO^+ and NO_2^+

To account for the potential formation of a nitrosyl species on the catalyst as proposed by Richter et al.¹⁵² and Lavalley et al.¹⁹³ the reactions (4.20) to (4.22) are analyzed. The energies are shown in Figure 4.8 and the structures are presented in Figure B.8. The mechanism starts with the weak adsorption of NO_2 on the Brønsted acid (ST1). The subsequent coadsorption of NO reveals only a negligible interaction between the two molecules (ST2). However, only a small barrier of $E^{\ddagger}=1.4$ kcal/mol, associated with the crossing of the seam (S2) from the triplet to the singlet PES, needs to be overcome to form asymmetric N_2O_3 (ST4). Alternatively, the slightly less stable cis-trans N_2O_3 (ST3) is formed by overcoming a barrier of $E^{\ddagger}=4.5$ kcal/mol (S1). Subsequently, the dimerized nitrogen oxide decomposes whereby the NO becomes a nitrosyl ion on the catalytic framework ($\text{Z}^-[\text{NO}]^+$) and the NO_2 takes up the hydrogen from the surface by forming nitrous acid (ST5). In the case of as- N_2O_3 as starting point this process exhibits an activation energy of $E^{\ddagger}=5.3$ kcal/mol (TS1) while a barrier of $E^{\ddagger}=0.1$ kcal/mol (TS2) was calculated for the ct- N_2O_3 . Though the initial formation of the asymmetric dimerized nitrogen oxide is preferred over the cis-trans configuration, the subsequent decomposition of the cis-trans species probably is faster because of the negligible small activation energy. Thus, both pathways can be expected to be accessible. As the next step, the nitrous acid desorbs from the catalyst leaving the $\text{Z}^-[\text{NO}]^+$ (ST6), which involves a heat of desorption of $\Delta E_{\text{des}}=9.7$ kcal/mol. Finally, ammonia adsorbs onto this species (ST8) with a heat of adsorption of $\Delta E_{\text{ads}}=10.8$ kcal/mol prior to the reactive formation of nitrosamine (ST10). The ammonia releases one proton to the catalyst by restoring the Brønsted acid and the remaining amino radical takes up the NO^+ from the surface leading to NH_2NO . The barrier of this step was determined to be $E^{\ddagger}=2.9$ kcal/mol, represented by TS4. Alternatively, water coadsorbs onto the $\text{Z}^-[\text{NO}]^+$ intermediate (ST7) with a heat of adsorption $\Delta E_{\text{ads}}=8.9$ kcal/mol. A subsequent reaction, analogous to the mechanism with ammonia, leads to the formation of nitrous acid (ST9) by overcoming a barrier of $E^{\ddagger}=1.4$ kcal/mol (TS3). Though the latter step is exothermic and only exhibits a rather small barrier, within the framework of the SCR also the reverse reaction could be of significance in terms of a sink for the intermediate produced nitrous acid from the decomposition of N_2O_3 . This is especially of interest because also the reverse barrier is rather low with

$E^\ddagger=5.1$ kcal/mol

In the case of the NO_2 -SCR, the reactions (4.23) to (4.27) are analyzed and the corresponding energy diagram is displayed in Figure 4.9. The structures of all species are shown in Figure B.9. After the coadsorption of two NO_2 (ST1), the formation of a dimerized N_2O_4 takes place by crossing the seam from the triplet to the singlet PES in analogy to the fast SCR. Here, three different structures are possible, a symmetric (sym) (ST3), an asymmetric (as) (ST5) or a cyclic planar (cp) N_2O_4 (ST 2). The lowest barrier was calculated for the first case with a barrier of $E^\ddagger=6.3$ kcal/mol (S3), followed by the cyclic planar isomer with $E^\ddagger=11.6$ kcal/mol (S2) and finally $E^\ddagger=17.7$ kcal/mol (S1) for the asymmetric case. However, the formation of the cyclic planar isomer is less favorable than the asymmetric or symmetric N_2O_4 because of an endothermic reaction in contrast to an exothermic heat of reaction for the latter two cases. The cp- N_2O_4 can be transferred into the asymmetric isomer by overcoming a barrier of $E^\ddagger=8.9$ kcal/mol (TS2), but as can be seen from the energy diagram no benefit can be deduced from this alternative route as compared to the direct formation of the as- N_2O_4 . Also the symmetric isomer can be transformed into the asymmetric one, but because this process exhibits a rather high activation energy of $E^\ddagger=46.1$ kcal/mol (TS1) it can be excluded. Starting from the as- N_2O_4 , the decomposition of the molecule results in the formation of nitric acid and an NO^+ to balance the negative charge of the zeolite framework (ST10). Here the mechanism is in analogy with the $\text{Z}^-[\text{NO}]^+$ formation from the decomposition of N_2O_3 and the barrier, according to the transition state TS4, was calculated to be $E^\ddagger=2.0$ kcal/mol. Finally, the desorption of nitric acid, with a heat of desorption of $\Delta E_{\text{des}}=9.9$ kcal/mol, leaves the nitrosyl ion on the surface for the reaction with ammonia as described above. Similarly, the decomposition of sym- N_2O_4 leads to the formation of nitrous acid together with $\text{Z}^-[\text{NO}_2]^+$. This process exhibits a barrier of $E^\ddagger=24.8$ kcal/mol (TS3) and is endothermic by $\Delta E=18.5$ kcal/mol (ST4). The desorption of the nitrous acid requires then a heat of desorption of $\Delta E_{\text{des}}=7.6$ kcal/mol. In analogy to the reaction with $\text{Z}^-[\text{NO}]^+$, the $\text{Z}^-[\text{NO}_2]^+$ (ST6) can also react with both ammonia and water. In the first case, ammonia only weakly adsorbs with $\Delta E_{\text{ads}}=1.4$ kcal/mol (ST8), but the subsequent reaction exhibits a negligible activation energy of $E^\ddagger=0.6$ kcal/mol (TS7), which leads to the formation of nitramide (ST13). Also in the case of the reaction with water, only a rather small barrier of $E^\ddagger=1.6$ kcal/mol (TS6) was calculated. Similarly to the reaction with ammonia, the heat of adsorption for water is negligible (ST9), but the formation of nitric acid (ST12) is exothermic. Thus, the $\text{Z}^-[\text{NO}_2]^+$ can be seen as a rather short-lived intermediate in the NO_2 -SCR. Finally,

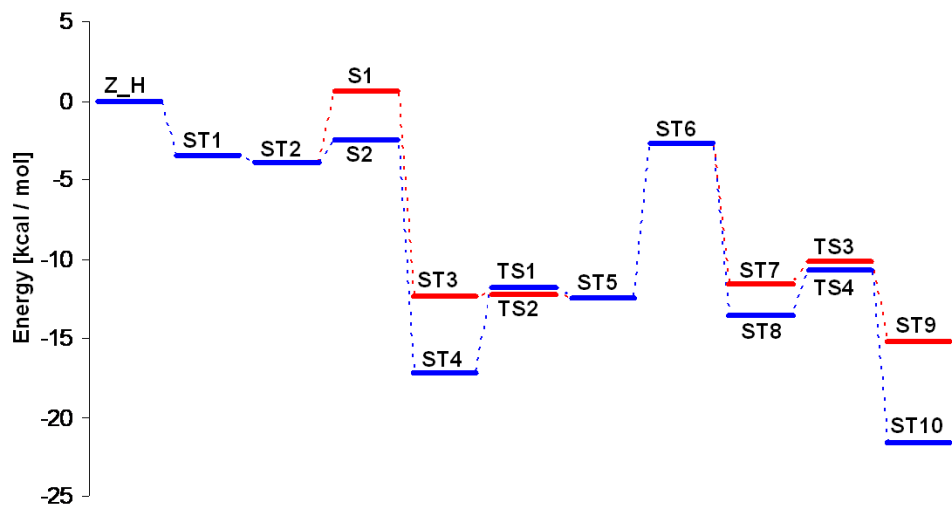


Figure 4.8: Energy profile of the fast SCR mechanism via NO^+ comparing two routes via asymmetric and cis-trans N_2O_3 . Energies are zero-point corrected.

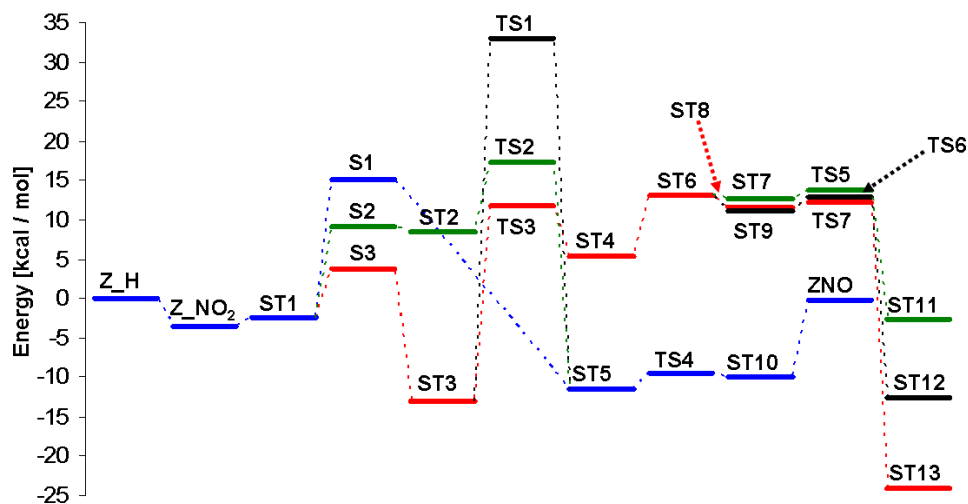


Figure 4.9: Energy profile of the NO_2 -SCR mechanism via NO_2^+ comparing three routes via symmetric, asymmetric and cyclic-planar N_2O_4 . Energies are zero-point corrected.

an interchange between the two NO_x^+ species is also possible. Starting from NO_2^+ , a reaction with NO only exhibits a barrier of $E^\ddagger=1.1$ kcal/mol (TS5) to form NO_2 together with $\text{Z}^-[\text{NO}]^+$ (ST11). Because of the exothermic character of this reaction, this step might only be accessed within the framework of the fast SCR, when both overall reactions, the fast and the NO_2 -SCR, interact with each other. Similar to our discussion on nitrous acid reactions, the nitric acid might decompose into water and NO_2^+ in the reverse direction of the described mechanism involving TS6. This would require to overcome a barrier of $E^\ddagger=25.3$ kcal/mol. Thus, two pathways for the NO_2 -SCR can be deduced from this analysis to be of potential importance, depending on either first the formation of sym- N_2O_4 or as- N_2O_4 . The formation of the symmetric isomer is followed by a rather high barrier for the decomposition into nitrous acid and the NO_2^+ . While nitrous acid decomposes into NO^+ as described in the pathway of the fast SCR, NO_2^+ reacts with ammonia to nitramide. In the case of as- N_2O_4 , the initial barrier for the formation is higher than the corresponding formation of the symmetric isomer, but the subsequent decomposition into NO^+ and nitric acid exhibits only a negligible activation energy. The highest barrier in this process is then the decomposition of the nitric acid with a barrier similar in magnitude to the decomposition of sym- N_2O_4 . In both cases, the stoichiometry leads to the formation of one nitrosamine and one nitramide which results in the equimolar formation of nitrogen and N_2O . This is in good agreement with the experimentally observed values,³⁹ at least at low temperatures. A comparison of the presented pathways for the fast and the NO_2 -SCR in this section reveals, consistent with the experimental literature^{153,156} a higher activity for the fast SCR. Both, the formation of the dimerized nitrogen oxide as well as the decomposition of the resulting acid exhibit a significantly lower barrier for the fast SCR as for the NO_2 -SCR.

In summary, the oxidation of NO was found to be enhanced by the catalyst compared to the gas phase reaction in agreement to the findings of Halasz and Brenner.¹⁷⁵ However, the exothermic character of the adsorption of ammonia is much stronger than the one of oxygen or NO. This leads to the experimentally well-known effect of ammonia blocking the active site for the oxidation of NO and thus the inhibiting influence of NH_3 . For the reaction of NO and NO_2 or two NO_2 with adsorbed ammonia, the main benefits from the catalyst can be seen in the exothermic adsorption of ammonia and in the formation of N_2O_3 or N_2O_4 , lowering the overall energy profiles. Though the formation of symmetric N_2O_4 is favorable over the asymmetric configuration the subsequent reaction to nitramide and nitrous acid exhibits a significantly

higher barrier. Thus, for the NO_2 -SCR it is more likely that as- N_2O_4 reacts with ammonia to nitrosamine and nitric acid. In addition, for both N_2O_y it can be assumed that the successive coadsorption to an ammonium ion and the subsequent reaction to the intermediates should be superior to a homogeneous termolecular reaction. The energy profiles for N_2O_3 and N_2O_4 show that for the coadsorption of the first NO_2 on NH_4^+ there is a sufficiently high drop in energy involved to interpret this configuration as stable. For the following coadsorption of NO or NO_2 , respectively, the additional drop in energy is negligible suggesting that this final step can be considered to be of the Eley-Rideal type, eventually leading to the dimerized structure, coadsorbed on NH_4^+ . A comparison of the above pathways with those via the nitrosyl ion or NO_2^+ reveals that the formation of the dimerized nitrogen oxides is slightly lower in energy in the absence of ammonia. Furthermore, in the presence of ammonia, the first reaction is the activation of the ammonium ion which releases a proton back to the catalytic surface. This step exhibits a rather high intrinsic barrier of ~ 20 kcal/mol. Thus, it can be concluded that the decomposition of the N_2O_y species on the Brønsted acid is favorable with respect to lower activation energies. However, this process requires the presence of a void active site for the adsorption of NO_2 which might exhibit a low probability because of the strong adsorption of ammonia. This leaves an uncertainty whether the initial formation of the intermediates nitrous and nitric acid as well as nitrosamine and nitramide rather takes place from the interaction of nitrogen oxides with adsorbed ammonia or from the prior decomposition on a void active site. Nevertheless, the assumption of Li and Li¹⁸¹ that a main effect of the zeolite is the storage of ammonia and the steady release of it to supply a gas phase reaction is rather unlikely in view of the presented results. For the case of the absence of NO_2 and oxygen in the feed stream, a mechanism for the reduction of NO was shown. The corresponding energy profile is in agreement with the experimental literature that this reaction proceeds rather slowly due to its endothermic character.

4.3.3 Decay of the Intermediates Nitrous and Nitric Acid

In this part the fate of the intermediates nitrous and nitric acid is discussed. The decomposition of the two acids on a Brønsted acid constitutes the first possibility. This is, however, solely the reverse reaction of NO^+ and NO_2^+ with water, as described in section 4.3.2 and, thus, is not discussed again in this context. Furthermore, the potential interaction of the acids with adsorbed ammonia is outlined. Finally, the bimolecular reactions of two nitrous acids,

two nitric acids and of nitrous with nitric acid is analyzed.

Reaction of Ammonia with Nitrous and Nitric Acid

No matter what catalyst is used, the appearance of nitrous and nitric acids as important intermediates and their subsequent reaction with ammonia within the SCR is assumed in several experimental investigations.^{146,152,170} Li and Li¹⁸¹ found a transition state for the catalyzed reaction of NH_3 with HONO on H-ZSM5 but stated at 373 K an energy barrier of $E^\ddagger=46.9$ kcal/mol, which is even higher than the corresponding activation energy found for the gas phase. Lin et al.^{188,191} investigated the reactions for both acids in the gas phase and also considered the two different possible structures of $\text{H}_2\text{N}_2\text{O}_2$ with either an N-N or an N-O bond for nitric acid. Here, a multi-step mechanism for both dehydration reactions as catalyzed by the H-ZSM5 is presented. For the reaction of nitrous acid with ammonia the mechanism starts with the strong adsorption of the latter. All subsequent structures are presented in Figure B.11 with the corresponding energies in Figure 4.10. From the energy profile it is obvious that cis-HONO coadsorbs quite strongly to the ammonium ion ($\Delta E_{\text{coads}}=-13.1$ kcal/mol, ST 1a) indicating a stable state. In the next step via TS 1a the nitrous acid switches its position on the catalyst by enforcing the ammonium ion to release a hydrogen bond with one of the framework oxygen. This step involves a barrier of $E^\ddagger=6.2$ kcal/mol and leads to an eight-member-ring structure (ST 2a), involving the catalytic framework. Within this ring, a proton transfer from the nitrous acid to the catalyst and from the ammonium to the acid takes place next, leading to trans-HONO and NH_3 (ST 3a). This process exhibits an energy barrier of $E^\ddagger=4.0$ kcal/mol (electronic energy only with respect to ST 3a) together with the corresponding transition state structure TS 2a. The subsequent reaction steps are identical with the reaction of hydroxylamine with nitroxyl, which is part of the selective catalytic oxidation (SCO) of ammonia and discussed in detail in the following chapter 5, section 5.3.3. The protonation of the hydroxyl group of the nitrous acid causes the cleavage of its N-O bond (TS 3a) whereas the final splitting into NO and water is accompanied by a rotation of the formed H_2O (TS 4a), representing the highest energetic state in the mechanism. Furthermore, the reformation of a hydrogen bond of ammonia with the catalyst (TS 5a) and, finally, the formation of an N-N bond with the NO, including the regeneration of the Brønsted acid (TS 6a) leads to the products water and NH_2NO . The sequence of elementary reaction steps, starting from the two coadsorbed reactants are all slightly endothermic and have quite low reverse energy barriers up to TS 4a. The two subsequent exothermic steps also exhibit only very low energy barriers. Thus, it can be

concluded from the energy profile that the mechanism of the reaction of ammonia with nitrous acid can be seen as a one step-reaction, starting from ST 1a, via TS 4a to the final products (ST 7a). This lumped process then has to overcome a barrier of $E^\ddagger=26.1$ kcal/mol ($G^\ddagger=24.6$ kcal/mol at 373 K) which is significantly lower than the barrier stated by Li and Li¹⁸¹ for their transition state structure. For the gas phase reaction Lin et al.¹⁹¹ stated for the trans-HONO a value of $E_{\text{app}}^\ddagger=24.6$ kcal/mol and for the cis-form $E_{\text{app}}^\ddagger=26.0$ kcal/mol at the B3LYP/6-311G(d,p) level of theory. These values coincide with results of this work for the gas phase ($E_{\text{app}}^\ddagger=25.8$ kcal/mol, $E_{\text{app}}^\ddagger=26.7$ kcal/mol; for details see Brüggemann et al.²⁰⁵). Nevertheless, in terms of absolute internal values and considering that first ammonium nitrite is formed in the gas phase,¹⁹¹ it becomes obvious that, here, the catalyst enhances the reaction by reducing the intrinsic activation energy by $\Delta E=9.8$ kcal/mol (with respect to cis-HONO) but also because of the strong coadsorption of the two reactants.

For the reaction of ammonia with nitric acid we considered the coadsorption of the latter to the ammonium ion in the 3H state (Figure 4.2, ST C). All structures are shown in Figure B.12 and the energies in Figure 4.10. It can be seen from the energy profile that HNO_3 also coadsorbs quite strongly to the catalyst ($\Delta E_{\text{coads}}=-13.3$ kcal/mol) and we found that this affects the adsorbed state of the ammonium ion, so that the latter releases two hydrogen bonds to the catalytic surface. This effect only occurs if the nitric acid coadsorbs on one of the upper framework oxygen. In the first reactive step (TS 1b) the nitric acid releases a proton to the catalytic surface while the ammonium reorientates to form a hydrogen bond with another framework oxygen as well as with a different oxygen of the remaining NO_3^- . This transition exhibits an energy barrier of $E^\ddagger=2.1$ kcal/mol (electronic energy with respect to ST 2b) and a negligible reverse reaction barrier of $E^\ddagger=0.3$ kcal/mol indicates the instability of the latter structure. The subsequent step returns the ammonium to its original position via TS 2b leading to a product state in which one oxygen atom of the NO_3^- is twice hydrogen-bonded, by the catalyst and by the ammonium (ST 3b). For this process a barrier of $E^\ddagger=4.2$ kcal/mol needs to be overcome leaving a slightly more stable intermediate structure than ST 2b. From the energy profile it can be concluded that the first two steps can be lumped to one step from ST 1b via TS 2b to ST 3b because of the instability of ST 2b. The main step of the mechanism is then finally the cleavage of the internal O-N bond of the NO_3^- as the hydrogen-bonded oxygen gets protonated from the catalyst as well as from the ammonium ion and water is formed (TS 3b). Furthermore, an N-N bond is formed between the released NO_2 and the ammonia, while the latter restores the Brønsted

acid. Here, an internal activation barrier of $E^\ddagger=32.5$ kcal/mol has to be surmounted to receive the final products nitramide and water (ST 4b). The consideration of two further isomers of $\text{H}_2\text{N}_2\text{O}_2$ as proposed by Lin et al.,¹⁸⁸ in terms of the reaction of nitric acid with ammonia as well as a nitro nitrite rearrangement were found to exhibit significantly higher internal energy barriers ($E^\ddagger=88.6$ kcal/mol and $E^\ddagger=81.7$ kcal/mol, respectively). In the case of the gas phase reaction, the barriers for the formation of nitramide and for the formation of the N-O isomer were calculated to be $E^\ddagger=50.9$ kcal/mol and $E^\ddagger=70.8$ kcal/mol respectively, which is in good agreement with values stated by Lin and Musin¹⁸⁸ at the B3LYP/6-311G(d,p) level of theory. Thus, the formation of a NH_2ONO structure in this reaction mechanism can be excluded and for the formation of nitramide the catalyst significantly reduces the energy barrier by $\Delta E=17.5$ kcal/mol.

In the experimental literature^{147,161,169,177} for the reaction of ammonia with nitrous or nitric acid often the intermediate formation of NH_4NO_2 and NH_4NO_3 respectively is proposed. Ammonium nitrite is known to rather easily decompose to nitrogen and water whereas the nitrate is assumed to hinder the DeNO_x catalysis at low temperatures.²⁰⁶ For NH_4NO_2 Morokuma et al.²⁰⁷ have shown from calculations that in the gas phase this species does not exist as ionic geometry and the most stable isomer is the $[\text{NH}_3][\text{trans-HONO}]$. Also for ammonium nitrate no ionic species could be obtained in the gas phase but a molecular complex only (for details see Brüggemann et al.²⁰⁵). Both species form barrier less in the gas phase from ammonia and the corresponding acid. Placing these two structures over the zeolite cluster our calculations revealed that the adsorbed state of NH_4NO_2 corresponds to ST 3a of Figure B.11 and of NH_4NO_3 to ST 3b of Figure B.12 with the energies shown in Figure 4.10. Thus, ammonium nitrite adsorbs with $\Delta E_{\text{ads}}=13.4$ kcal/mol and reacts via TS 4a to nitrosamine and water including a barrier of $E^\ddagger=17.2$ kcal/mol. However, the decomposition into NH_3 and HONO is activated by only $E^\ddagger=1.2$ kcal/mol on the catalyst. In the case of ammonium nitrate the energy of adsorption was calculated to be $\Delta E_{\text{ads}}=-19.2$ kcal/mol and the further reaction to nitramide and water exhibits a barrier of $E^\ddagger=32.5$ kcal/mol (TS 3b). The decomposition to ammonia and nitric acid is activated by $E^\ddagger=5.8$ kcal/mol (TS 2b). These values coincide with the finding that the nitrite species easily decomposes via nitrosamine to nitrogen and water, whereas for the corresponding decomposition of the nitrate via nitramide a significantly higher barrier is observed. Nevertheless, in the scope of the SCR it has to be considered that both, ammonia and the acids adsorb rather strongly to the catalytic surface and thus, the consideration of an alternative route with first the gas phase formation of the nitrite and nitrate prior to

adsorption and decomposition might be misleading. Especially since in both cases the decomposition of the adsorbed complex to ammonia and the acids exhibits only very low barriers.

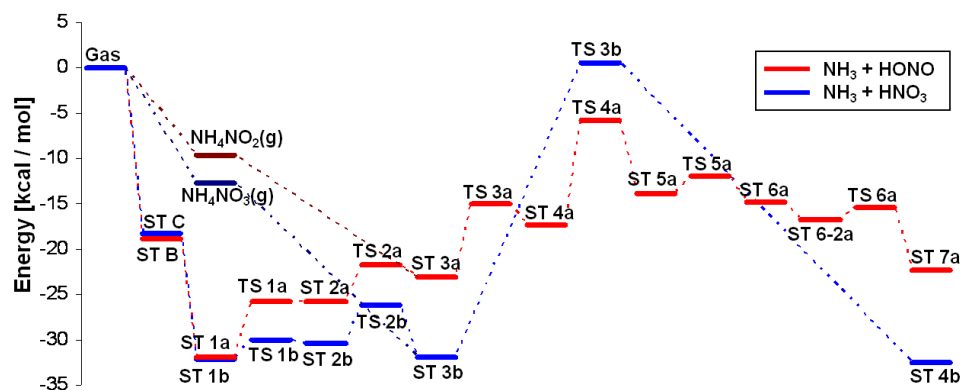


Figure 4.10: Energy profiles for the reactions of cis-HONO and HNO₃ with NH₃. Energies are zero-point corrected.

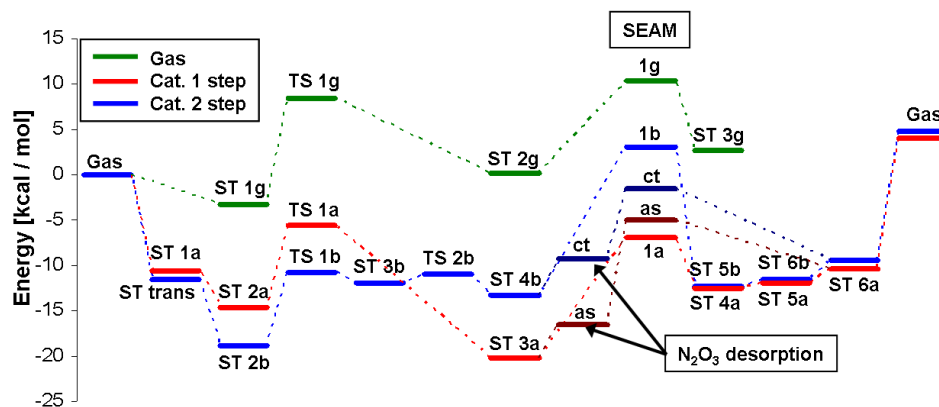


Figure 4.11: Energy profiles for the self-reaction of HONO comparing a one-step, a two-step and the gas phase mechanism. Energies are zero-point corrected.

Dehydration of Nitrous and Nitric Acid

The dehydration reaction of two nitrous acids and of nitrous acid with nitric acid or the corresponding reverse reaction, namely the hydrolysis have been

assumed to be key steps in the SCR by many authors.^{146,152,170,181} But also within the investigations of the atmospheric chemistry these two reactions in terms of the hydrolysis are of high interest because the subsequent photolysis of nitrous acid rapidly leads to the formation of hydroxyl radicals that promote ozone formation.^{208,209} The formation of the two acids is assumed to be heterogeneously catalyzed by urban surfaces or airborne particles.^{210–213} Because of the importance of the two intermediates within different frameworks of the H/N/O system there are also several theoretical studies addressing either the dehydration or the hydrolysis in the gas phase.^{181–186} Nevertheless, the formation or decomposition of the dimerized structures N_2O_3 and N_2O_4 were always considered, if at all, to be barrier less. Furthermore, the hydrolysis of dinitrogen pentoxide was investigated by Tao and Hanaway¹⁸⁷ in the gas phase, because N_2O_5 is known to be a reactive atmospheric constituent that acts as a temporary reservoir for NO_x . Here, the mechanisms of the dehydration of nitrous acid in a self-reaction and with nitric acid as well as the self-reaction of HNO_3 , catalyzed by the Brønsted acid of H-ZSM5 is analyzed and the beneficial influence of the catalyst in comparison to the corresponding gas phase reactions is discussed.

Self-Reaction of Nitrous Acid In the case of the self-reaction of nitrous acid the influence of the configurational state of the reactants, namely the reactions of conformations of cis with cis, trans with trans and cis with trans was analyzed as well as the difference in terms of which isomer adsorbs first (trans or cis). It was observed that the isomeric state of the nitrous acid barely has an impact on the transition barrier; it rather seems to be of importance how the two reactants initially coadsorb on the surface. Furthermore, the zeolite catalyzes the conformational change, whereas the barrier for this process was calculated to $E^\ddagger=4.2$ kcal/mol from trans to cis and $E^\ddagger=2.5$ kcal/mol for the reverse reaction (Figure B.13). This indicates the slightly more stable character of the trans configuration but also that both species are present in the reacting system. Thus here, only the reaction of cis- with trans-HONO, in a one-step mechanism (Figure B.14) and of two trans-HONO in a two-step mechanism (Figure B.15) is presented. The corresponding energies to the structures are shown in Figure 4.11 and the results of the additional investigations on the configurations can be obtained from ref. [205].

For the one-step mechanism the reaction starts with the adsorption of cis-HONO which is exothermic by $\Delta E_{ads}=-10.6$ kcal/mol (ST 1a), and the hydroxyl group of the molecule is twice hydrogen-bonded to the catalyst. The coadsorption of the second nitrous acid in the trans configuration with a

hydrogen bond to the hydroxyl group of the first molecule still accounts for an adsorption energy of $\Delta E_{\text{coads}} = -4.6$ kcal/mol (ST 2a). In the subsequent reaction via TS 1a the hydroxyl group of the cis-HONO is protonated by the second acid and splits off as H_2O while the remaining NO_2 and NO form asymmetric N_2O_3 . With two hydrogen bonds, the water molecule remains quite stable attached to the surface, while the N_2O_3 is only loosely bond to the hydrogen of the water (ST 3a). This elementary step exhibits an energy barrier of $E^\ddagger = 9.1$ kcal/mol and is slightly exothermic by $\Delta E = -5.6$ kcal/mol. As the next step the decomposition of the N_2O_3 species into NO and NO_2 was considered, while still being coadsorbed. This step involves the crossing of the SEAM 1a from the PES with $M_S = 1$ to $M_S = 3$ and an energy barrier of $E^\ddagger = 13.3$ kcal/mol, leaving only the NO_2 hydrogen-bonded to the water (ST 4a). From the energy profile it can be seen for the desorption of NO (ST 5a) that the interaction of the gas phase NO with the coadsorbed NO_2 is negligible ($\Delta E_{\text{des}} = 0.6$ kcal/mol). But also the subsequent desorption of NO_2 only requires a quite low energy of $\Delta E_{\text{des}} = 1.5$ kcal/mol leaving only water on the surface (ST 6a). As an alternative pathway, we also considered the desorption of as- N_2O_3 prior to its decomposition in the gas phase. The release of the N_2O_3 only requires an energy of $\Delta E_{\text{des}} = 3.8$ kcal/mol and the subsequent decomposition (Figure B.17, SEAM as-g) needs to overcome a barrier of $E^\ddagger = 11.6$ kcal/mol which is even slightly less than the corresponding decomposition in the coadsorbed state. Thus, together with the fact that NO_2 only loosely bonds to adsorbed water (ST 5a), it can be concluded that this alternative scenario is more likely to take place. The final desorption of H_2O reveals, that it adsorbs quite strongly on the catalyst with $\Delta E_{\text{des}} = 14.4$ kcal/mol. Overall, the dehydration of cis-HONO with trans-HONO was found to be slightly endothermic by $\Delta E_R = 4.0$ kcal/mol.

The two-step mechanism starts with the adsorption of trans-HONO with an energy of $\Delta E_{\text{ads}} = -11.5$ kcal/mol and also here the Brønsted acid forms a hydrogen bond with the hydroxyl group while the latter bonds with its hydrogen to a neighboring framework oxygen (ST trans, Figure B.13). The coadsorption of a second nitrous acid in the trans configuration with a hydrogen bond to the empty framework oxygen of the T5 Cluster is also quite exothermic with $\Delta E_{\text{coads}} = -7.4$ kcal/mol (ST 2b, Figure B.15). The first elementary reaction step via TS 1b is the protonation of the hydroxyl group of the coadsorbed HONO by the Brønsted acid. This requires the release of the hydrogen bond of the first adsorbed nitrous acid and leads to an enlargement of the N-N bond in the protonated acid from 1.4 Å to 1.9 Å. The latter is now hydrogen-bonded to two framework oxygen (ST 3b). This process is activated by $E^\ddagger = 8.1$ kcal/mol (electronic energy with respect to ST 3b only),

leaving a highly unstable intermediate structure, because the reverse reaction exhibits a barrier of only $E^\ddagger=1.3$ kcal/mol and the subsequent elementary step via TS 2b of only $E^\ddagger=1.1$ kcal/mol (electronic energy with respect to ST 3b only). In this step, the N-N bond in the protonated nitrous acid breaks, while the other HONO restores the Brønsted acid and forms cis-trans- N_2O_3 with the released NO (ST 4b). From the energy profile it can be seen that this product state is less favorable than the corresponding products of the one-step mechanism which mainly results from the higher stability of as- N_2O_3 compared to the cis-trans configuration. Next, the decomposition of N_2O_3 while it still is adsorbed on the Brønsted acid via SEAM 1b was considered. This requires to overcome an energy barrier of $E^\ddagger=16.5$ kcal/mol, leaving nitrogen oxide coadsorbed on the adsorbed water, while the NO_2 can be considered to be released to the gas phase right away (ST5b). The desorption of the NO (ST 6b) only demands an energy of $\Delta E_{\text{des}}=2.1$ kcal/mol. As before in the one-step mechanism, also the desorption of the c-t- N_2O_3 prior to its decomposition in the gas phase was considered. Here, it was also found that this is more likely to happen because of a quite low desorption energy of $\Delta E_{\text{des}}=4.1$ kcal/mol for the dimer. For the decomposition of the ct- N_2O_3 in the gas phase an energy barrier of $E^\ddagger=7.6$ kcal/mol was calculated which is significantly lower than the corresponding one on the catalyst. Furthermore, this barrier is also $\Delta E=4.0$ kcal/mol lower than the barrier for the asymmetric configuration, which supports the fact that the latter species is more stable. Finally, we found here an endothermic reaction energy of $\Delta E_R=4.9$ kcal/mol for the dehydration of two trans-HONO.

A comparison of the energy profiles of the two mechanisms reveals that the two-step mechanism exhibits a slightly lower energy barrier than the one-step mechanism for the dehydration. Nevertheless, for the one-step mechanism this step was found to be exothermic, making the reverse reaction less likely. In fact, here the reverse reaction would require to overcome a barrier being $\Delta E=11.0$ kcal/mol higher than the desorption of as- N_2O_3 . In the case of the two-step mechanism, the desorption even requires slightly more energy than the reverse reaction. Thus, the assumption can be stated, that the two-step mechanism rather describes the hydrolysis while the one-step mechanism favors the dehydration. Nevertheless, from the perspective of the direction of the mechanism it has to be concluded, that none of the NO_x does strongly coadsorb on the water. Thus, it can be assumed that the hydrolysis would in any case require the formation of N_2O_3 in the gas phase prior to coadsorption and reaction with adsorbed water. This dimer structure is quite unstable, whereas the reactants of the dehydration, nitrous acid coadsorb rather strongly to the active site. Thus, in the framework of the SCR, the

dehydration / hydrolysis reaction system can be concluded to serve as a sink for nitrous acid rather than as a source.

For the gas phase, the reaction of a cis- with a trans-isomer of the nitrous acid was analyzed. For the HO-NO bond cleavage in the trans-HONO (TS 1g) a barrier of $E^\ddagger=11.8$ kcal/mol leading to water and ct-N₂O₃ (ST 2g) was calculated which is consistent with the previous works on this gas phase reaction.^{182–184} The decomposition of the N₂O₃ into NO and NO₂ via SEAM 1g ($E^\ddagger=10.2$ kcal/mol) is $\Delta E=2.6$ kcal/mol higher in energy as without the water molecule, resulting from a slight interaction of H₂O with the dimerized structure. It can be concluded, that the catalyst only slightly reduces the activation energy of the dehydration step but not the decomposition of the intermediate N₂O₃. Nevertheless, a beneficial influence of the catalyst for the dehydration has also to be seen in the strong coadsorption of the two nitrous acids prior to reaction.

Reaction of Nitrous with Nitric Acid In the case of the reaction of nitrous with nitric acid the formation of the asymmetric (route “a”, Figure B.19) as well as of the symmetric (route “b”, structures can be obtained from ref. [205]) N₂O₄ as dehydration intermediate was considered, starting in both cases with the more stable trans-configuration for HONO. Furthermore, the results of the catalyzed mechanism are compared to the gas phase reaction with the energies corresponding to the structures presented in Figure 4.12. The mechanism along route “a” is started with the adsorption of trans-HONO where we considered the structure and energy of ST trans of Figure B.13. Then the coadsorption of HNO₃ is slightly exothermic with an energy of $\Delta E_{\text{coads}}=-4.7$ kcal/mol (ST 2a), whereas the nitrous acid is adsorbed to the Brønsted acid and the nitric acid forms a hydrogen bond with its hydroxyl group to another framework oxygen. In the subsequent elementary reaction step, the hydroxyl group of the nitrous acid is protonated by the catalyst while at the same time the nitric acid releases its hydrogen to the catalyst (TS 1a). This process exhibits an energy barrier of $E^\ddagger=5.0$ kcal/mol and leads to a complex structure (ST 3a) that is bond to the catalyst by two hydrogen atoms. Then the protonated hydroxyl group of the complex rotates along the N-O bond of the former nitrous acid (TS 2a) and forms a third hydrogen bond to a further framework oxygen (ST 4a). This rotation only requires to overcome a low energy barrier of $E^\ddagger=0.7$ kcal/mol and the resulting structure can be concluded from the energy profile to be more stable than ST 3a. Finally, the N-O bond of the nitrous acid is cleaved (TS 3a) and as-N₂O₄ is formed together with water. For this, an activation energy of $E^\ddagger=4.2$ kcal/mol was calculated and the N₂O₄ is pushed off the Brønsted

acid, only loosely interacting with the adsorbed water molecule (ST 5a). In order to take into account that N_2O_4 is an unstable species we also analyzed the decomposition of the latter species while still interacting with the catalyst. The crossing of the PES with $M_S=1$ to $M_S=3$ via SEAM 1a exhibits a barrier of $E^\ddagger=20.1$ kcal/mol. In the resulting state the NO_2 molecules can be considered to be in the gas phase, because from the structure ST 6a their distances to the adsorbed water molecule are too large to account for a significant interaction. Furthermore, in the energy profile, we also added the data points of adsorbed water and the bare catalyst to account for the full cycle. This reveals that the overall dehydration process is slightly endothermic by $\Delta E_R=2.3$ kcal/mol. In the same way as the influence of the catalyst on the decomposition of the N_2O_3 species was considered, also here, starting from ST 5a, the desorption of the asymmetric N_2O_4 is taken into account. This only requires an energy of $\Delta E_{\text{des}}=2.1$ kcal/mol indicating the weak interaction with the adsorbed water. The subsequent decomposition into two NO_2 (SEAM 1as, Figure B.18) requires to overcome an energy barrier of $E^\ddagger=19.7$ kcal/mol, which is about the same value that was found for the decomposition in the adsorbed state. This indicates that, in this context the catalyst does not have a beneficial influence and it can be concluded that as- N_2O_4 rather desorbs to the gas phase prior to its decomposition. Thus, for the hydrolysis in turn, the reaction can only take place when as- N_2O_4 forms in the gas phase and reacts with adsorbed water. Though the overall reaction of the dehydration is slightly endothermic and all the barriers of the elementary reactions of the hydrolysis are also low as can be seen from the energy profile, in the framework of the SCR, it seems more likely that the two stable intermediates nitrous and nitric acid dehydrate. This is because they both adsorb rather strongly on the catalyst while N_2O_4 is known to be unstable.

An alternative pathway leading to the formation of sym- N_2O_4 (route “b”) requires the cleavage of the OH group of nitric acid which exhibits a significantly higher barrier than for the corresponding cleavage in nitrous acid. Therefore, this route can be neglected and the mechanistic details are presented elsewhere.²⁰⁵ Though for the reverse direction, the formation of sym- N_2O_4 in the gas phase only exhibits an energy barrier of $E^\ddagger=10.0$ kcal/mol (SEAM 1sym, Figure B.18) while the barrier for as- N_2O_4 is $E^\ddagger=20.4$ kcal/mol (SEAM 1as, Figure B.18), in the subsequent reaction with adsorbed water only the pathway along the asymmetric species is reasonable.

For comparison we also investigated the reaction of HONO with HNO_3 in the gas phase and the energies in Figure 4.12 correspond to the trans-configuration. The cleavage of the N-O bond and the formation of water

(TS 1gt) after the hydroxyl group of HONO is protonated, leading to as-N₂O₄ (ST 2gt) exhibits an energy barrier of $E^\ddagger=8.9$ kcal/mol. For the cis-configuration we calculated a value of $E^\ddagger=9.8$ kcal/mol, leading to the same product state as the trans-pathway. For the decomposition (SEAM 1g) no beneficial influence of the water can be concluded because the calculated barrier of $E^\ddagger=21.1$ kcal/mol is comparable to the value in the absence of water ($E^\ddagger=19.7$ kcal/mol). Thus, also for the hydrolysis in the gas phase, either first the formation of as-N₂O₄ in the gas phase is necessary prior to the reaction with water or a termolecular reaction has to be assumed. Li and Li¹⁸¹ also calculated the dehydration step of nitrous with nitric acid in the gas phase on the B3LYP/6-31G(d,p) level of theory and, with respect to separated reactants, stated activation energies at 373 K of $G^\ddagger=18.8$ kcal/mol and $G^\ddagger=16.6$ kcal/mol for the cis- and trans- configuration respectively. These values are in good agreement with our results ($G^\ddagger=18.3$ kcal/mol and $G^\ddagger=17.4$ kcal/mol). Furthermore, for the reaction of trans-HONO with HNO₃, which leads to sym-N₂O₄ and water, Tao et al.¹⁸⁶ found an energy barrier of $E^\ddagger=28.3$ kcal/mol at the B3LYP/6-311⁺G(2d,p) level of theory. Thus, this reaction is rather unlikely to occur also for the gas phase. A comparison of the results of the catalyst and the gas phase reveals that the catalyst reduces the activation energy but also can be seen as beneficial because of the strong coadsorption of the two reactants prior to the dehydration. Nevertheless, because of the quite low activation energy, it can be assumed that this reaction takes place in the gas phase, too. For the hydrolysis reaction, in both cases the formation of as-N₂O₄ can be considered the bottleneck of the pathway.

Self-Reaction of Nitric Acid For the dehydration of nitric acid, we here include the reaction of N₂O₅ with ammonia as a possible sink for this intermediate for both the catalyst and the gas phase mechanism. On the catalyst the mechanism starts with the exothermic adsorption of one nitric acid and the coadsorption of a second acid. The structures are shown in Figure B.20 with the corresponding energies in Figure 4.13. The coadsorption is nearly as exothermic as the adsorption of the first HNO₃ molecule with $\Delta E_{\text{coads}}=-10.3$ kcal/mol and the two acids form a ten-member ring with the surface with one hydrogen bond between the two reactants and two with the catalyst (ST 1). In the subsequent reaction step the bonding hydrogen between the two reactants is released by the nitric acid that is attached to the Brønsted acid of the surface and protonates the hydroxyl group of the other nitric acid (TS 1). This leads to the cleavage of the HO-NO₂ bond and thus to the formation of coadsorbed water and N₂O₅ (ST 2). The energy barrier for this dehydration

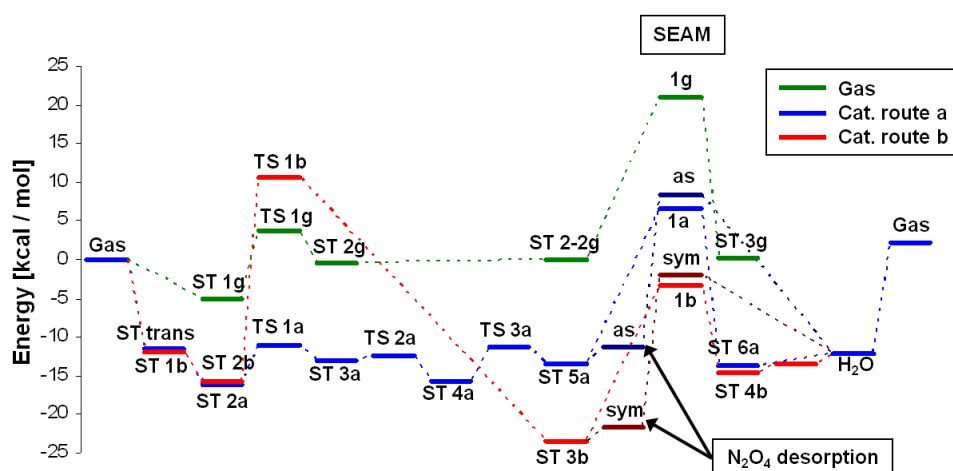


Figure 4.12: Energy profiles for the reaction of trans-HONO with HNO_3 comparing the pathway via as- N_2O_4 and sym- N_2O_4 and with the gas phase mechanism. Energies are zero-point corrected.

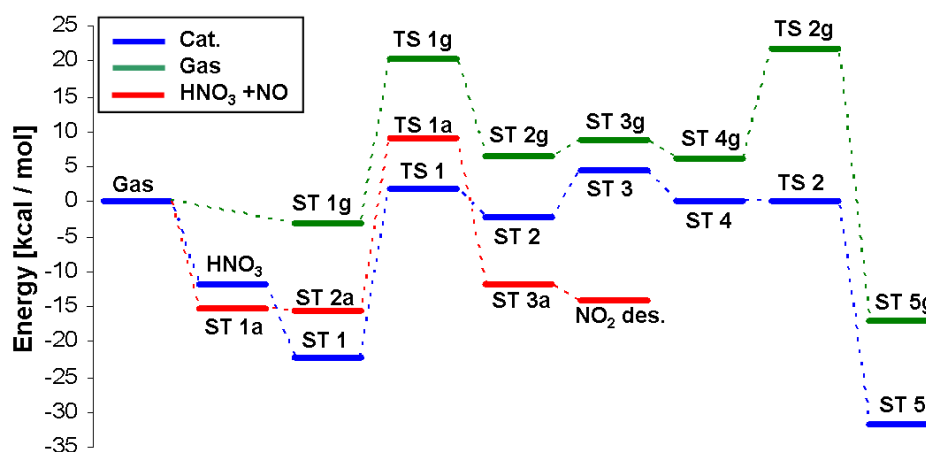


Figure 4.13: Energy profiles for the self-reaction of HNO_3 and the subsequent reaction of N_2O_5 with NH_3 , comparing the catalyzed and the gas phase mechanism. Energies are zero-point corrected.

step was calculated to be $E^\ddagger=24.2$ kcal/mol and the resulting structure has to be considered rather unstable because of a comparably low energy barrier for the reverse reaction with $E^\ddagger=4.1$ kcal/mol. Because N_2O_5 cannot be considered to simply decompose like N_2O_3 or N_2O_4 we here considered first the desorption of water (ST 3) and then the coadsorption of ammonia (ST

4) in order to investigate reaction (4.17) as a potential sink for this dehydration intermediate. The desorption process requires an energy of $\Delta E_{\text{des}}=6.6$ kcal/mol which is only slightly higher than the barrier for the hydrolysis and thus also likely to occur. The coadsorption of ammonia in turn is then slightly exothermic with $\Delta E_{\text{coads}}=4.4$ kcal/mol (ST 4). This was found to be a highly unstable structure as the barrier for the subsequent reaction is negligible with $E^\ddagger=0.006$ kcal/mol. In this reaction step (TS 2), the internal $\text{O}_2\text{N-ONO}_2$ bond is broken again and the ammonia forms with the released NO_2^+ nitramide while at the same time protonates the remaining NO_3^- to recycle one nitric acid. Because this step is quite exothermic with $\Delta E_{\text{R}}=-31.8$ kcal/mol, the reverse reaction can be neglected. Though the dehydration itself as elementary step is endothermic, the subsequent sink of N_2O_5 in the fast reaction with NH_3 makes the overall process very likely to take place. In order to analyze the influence of the catalyst we also investigated the complete pathway in the gas phase. A hydrogen bond between the two reactants (ST 1g, Figure B.21) leads to a slight drop in energy of $\Delta E=-3.1$ kcal/mol as compared to the separated acids. Then, similar to the catalyzed mechanism, the binding hydrogen is transferred from the one hydroxyl group to the one of the other acid inducing the cleavage of the HO-NO_2 bond (TS 1g). This step exhibits an activation energy of $E^\ddagger=23.5$ kcal/mol and leads to dinitrogen pentoxide together with water (ST 2g). A comparison of this barrier with the corresponding one on the surface reveals that the catalyst is not capable to reduce this barrier and a beneficial effect can only be seen in the strong coadsorption of the two reactants prior to the dehydration. For the hydrolysis of N_2O_5 in the gas phase, Hanwa and Tao¹⁸⁷ reported an energy barrier of $E^\ddagger=23.7$ kcal/mol at the B3LYP/6-311⁺⁺G(d,p) level of theory whereas our corresponding barrier is only $E^\ddagger=13.8$ kcal/mol. The difference in energy results here from a different structure found for the transition state. From the corresponding energies to the following exchange of water with ammonia (ST3g and ST4g) it can be concluded that both molecules only slightly interact with N_2O_5 in the gas phase ($\Delta E_{\text{H}_2\text{O}}=-2.3$ kcal/mol, $\Delta E_{\text{NH}_3}=-2.6$ kcal/mol). In the subsequent reaction of N_2O_5 with NH_3 via TS 2g again the internal $\text{O}_2\text{N-ONO}_2$ bond is broken and an N-N bond between the ammonia and the NO_2^+ is formed while at the same time the NO_3^- forms nitric acid (ST 5g). Here, an energy barrier of $E^\ddagger=15.7$ kcal/mol was calculated which is significantly higher than the corresponding one on the catalyst. This reveals that, though the Brønsted acid is not capable to reduce the activation energy for the HO-NO_2 cleavage in the protonated HNO_3 , it considerably enhances the combined pathway of nitric acid dehydration and subsequent reaction with ammonia.

Finally, for the formation of nitrous acid from reaction (4.12) the structures are shown in Figure B.16 and the corresponding energies in Figure 4.13. The mechanism starts with the adsorption of HNO_3 which forms two hydrogen bonds with the surface, one with its hydroxyl group and the other one with the Brønsted acid (ST 1a, $\Delta E_{\text{ads}} = -15.4$ kcal/mol). From the energy profile it can be seen, that an added NO (ST 2a) hardly interacts with the adsorbed HNO_3 and thus the subsequent reaction can be interpreted as one of the Eley-Rideal type. The nitrogen oxide then attacks the hydroxyl group of the nitric acid and the HO- NO_2 bond is broken, while at the same time the NO forms trans-HONO with the released hydroxyl group (TS 1a). This process exhibits an activation energy of $E^\ddagger = 24.6$ kcal/mol and leads to the products nitrous acid and NO_2 . The latter species remains adsorbed on the Brønsted acid (ST 3a). The desorption of NO_2 then leads to a reorientation of the nitrous acid in terms of that its hydroxyl group forms a second hydrogen bond with the Brønsted acid. Because this state is more stable, the desorption of NO_2 appears to be exothermic in the energy profile. Thus, it can be assumed that ST 3a is an unstable state and that NO_2 desorbs to the gas phase right after the reaction. Nevertheless, the reaction barrier in the reverse direction is even slightly lower ($E^\ddagger = 23.0$ kcal/mol) indicating that this reaction is of equal relevance in both directions. An alternative pathway in which NO is oxidized by the non-hydrogen-bonded oxygen of nitric acid turned out to have a significantly higher energy barrier of $E^\ddagger = 38.6$ kcal/mol, making it unlikely to take place. Lin et al.¹⁹² stated an energy barrier of $E^\ddagger = 21.6$ kcal/mol at the B3LYP/6-311++G(d,p) level of theory for the reaction of nitrous acid with NO_2 in the gas phase, which is even slightly lower than our result for the catalyst. This indicates that H-ZSM5 does not positively affect this reaction.

In summary, we investigated the reaction of nitrous and nitric acid with ammonia leading to nitrosamine and nitramide respectively and found a significant reduction of the activation energies compared to the gas phase. Furthermore, the presented mechanisms also cover the decomposition of ammonium nitrite and nitrate. The dehydration of two nitrous acids or of nitrous with nitric acid was shown to exhibit only low energy barriers and a slight enhancement of the catalyst was observed in comparison to the gas phase. In both cases, it was concluded that the intermediately formed dimers N_2O_y desorb to the gas phase prior to their decomposition into NO_2 and NO. Though the dehydration is slightly endothermic, within the SCR it is considered favorable over the reverse reaction because neither NO_2 nor

NO significantly coadsorb to adsorbed water. Thus, the hydrolysis requires the formation of the unstable dimers in the gas phase, whereas in the dehydration both reactants strongly coadsorb to the catalyst. Furthermore, we found that the combination of dehydration of two nitric acids to N_2O_5 and the subsequent reaction with ammonia to HNO_3 and NH_2NO_2 is catalyzed by the H-ZSM5. However, as outlined in section 4.3.2 both, nitrous and nitric acid, can also decompose on the Brønsted acid to NO^+ or NO_2^+ , respectively, and water. In the case of nitrous acid, this decomposition even exhibits a slightly lower energy than the bimolecular self-reaction making the decomposition more favorable. Though the barrier for the decomposition of nitric acid is within the same order of magnitude as the bimolecular reaction of two nitric acids, a severe benefit with respect to entropy can be assumed over the bimolecular reaction which requires the coadsorption of two molecules. Thus, it can be concluded that, in the framework of the SCR, the decay of the intermediate acids most probably is either due to the decomposition on a Brønsted acid or to the reaction with adsorbed ammonia.

4.3.4 Decomposition of the Intermediates Nitrosamine and Nitramide

Besides the intermediates nitrous and nitric acid the pathways outlined in section 4.3.2 also lead to either nitrosamine or nitramide. In this section the influence of the Brønsted acid for the decomposition of these two species into nitrogen or nitrous acid, respectively, together with water is described.

Decomposition of NH_2NO

Several groups^{180,214–216} have investigated the decomposition of NH_2NO in the gas phase on a theoretical basis. These studies all consider a sequence of isomerization steps, leading to nitrogen and water. Anstrom et al.¹⁷⁹ and Soyer¹⁸⁰ examined the influence of hydrogen transfer with a V_2O_5 -based catalyst for this reaction and found a push-pull mechanism, significantly reducing the activation energy barriers compared to the gas phase. Li and Li¹⁸¹ showed that also the H-form catalysts may reduce the activation energies by a similar mechanism. Below, we will compare the two different mechanisms as recalculated in this work on H-ZSM5. Figure B.22 illustrates the resulting structures, whereas in route “a” we followed the approach proposed by Anstrom, in “b” we followed the one from Li, with the corresponding energy profiles in Figure 4.14.

The first structure shows the adsorbed NH_2NO on a free Brønsted acid

site (ST 1) which was the starting point of both prior investigations. A simultaneous proton transfer from the zeolite to the O and from NH_2 to the zeolite with an activation barrier of $E^\ddagger=4.6$ kcal/mol (TS 1, only electronic energy) (Li $G^\ddagger=4.8$ kcal/mol at 373K) leads to trans-HNNOH (ST 2). In the following, a rotation of the molecule in the adsorbed state is necessary in both cases. In route “a” the rotation of trans-HNNOH leads to a structure, where the molecule is bonded to the catalyst via the HN portion and the bridging hydroxyl group of the zeolite to the same N-atom (ST 3a). For this step, an energy barrier of $E^\ddagger=8.3$ kcal/mol corresponding to TS 2a has to be overcome. The following TS 3a is not of relevance for the mechanism because the subsequent reactions should also proceed starting from ST 3a instead of ST 4a, then just involving a different framework oxygen for the following push-pull steps. Thus, this further rotation shown is in purpose of only considering the two initial framework oxygen atoms for this pathway. Soyer et al.¹⁸⁰ neglected this barrier, solely stating the necessity of a desorption-readsorption process. In the next step, a proton transfer from this N-atom to the zeolite and vice versa takes place (TS 4a) with an activation energy of $E^\ddagger=7.1$ kcal/mol. The product (ST 5a) is cis-HNNOH. Subsequently, a rotation along the NO bond in HNNOH via (TS 5a) occurs and the surmounting of $E^\ddagger=5.3$ kcal/mol leads to c-HNNO-t-H (ST 6a). This structure is the same again in both routes.

In route “b” the rotation of trans-HNNOH via TS 2b ($E^\ddagger=10.1$ kcal/mol) leads to a binding of the OH portion to the catalyst framework and the bridging hydroxyl group of the zeolite to the O-atom (ST 3b). Li and Li¹⁸¹ assumed a desorption-readsorption step instead of a rotation and stated an energy barrier of $G^\ddagger=3.4$ kcal/mol for this step. Then, a proton transfer between oxygen and the zeolite (TS 3b) leads to tr-tr-HNNOH (ST 4b) with an energy barrier of $E^\ddagger=2.4$ kcal/mol (Li $G^\ddagger=2.6$ kcal/mol). In the next step, again a rotation of the molecule is considered, yielding tr-tr-HNNOH (ST 5b) bonded to the catalyst with the HN portion. The energy barrier for this process was calculated to $E^\ddagger=5.1$ kcal/mol, corresponding to TS 4b. Li and Li considered this again in terms of a desorption-readsorption process and stated a barrier of $G^\ddagger=2.1$ kcal/mol at 373 K. Another proton transfer (TS 5b) from HN to the zeolite and vice versa with a barrier of $E^\ddagger=6.4$ kcal/mol (Li $G^\ddagger=6.9$ kcal/mol) yields cis-HNNO-t-H (ST 6b). As ST 6a and ST 6b only differ by mirror inversion, the following decomposition was not considered from both starting configurations but only from ST 6a, assuming that this has no influence on the resulting profile. At this point, Anstrom et al.¹⁷⁹ actually considered another desorption-readsorption step leading to a structure with HN being hydrogen-bonded to the zeolite framework and

HO hydrogen-bonded by the bridging hydroxyl group. Li and Li found that such a structure barrier-free decomposes to N_2 and H_2O and could not find a comparable transition state structure. Thus, we considered a reaction step leading directly from adsorbed cis-HNNO-t-H to the decomposed products. TS 6 basically displays another rotation of the molecule on the surface involving an activation energy of $E^\ddagger=9.7$ kcal/mol. The final decomposition step is highly exothermic by $\Delta E=-78$ kcal/mol ending in adsorbed nitrogen and water (ST 7). The comparison of the energy profile (Figure 4.14) of the two mechanisms reveals that route “b” exhibits a slightly more favorable one. It also becomes obvious that the rotation of the molecules on the catalyst cannot be neglected and in route “b” TS 2b and TS 6 even present the highest barriers. Comparable values to those, stated by Li and Li¹⁸¹ by consideration of a desorption-readsorption process instead of a rotation, could not be obtained in our work. Nevertheless, a rotation of an adsorbed molecule seems to be the more realistic viewing of the process rather than a complete removal of the molecule from the catalytic surface, followed by a rotation in the gas phase and a readsorption on the active site. The comparison of the heterogeneous reaction to the corresponding gas phase as reported in the literature^{180,214–216} leads to the finding that both mechanisms exhibit great improvement with respect to activation barriers.

Decomposition of NH_2NO_2

Because of the similarity in structure between nitrosamine and nitramide the assumption is at hand that the catalyst might also enhance the decomposition of NH_2NO_2 with a similar mechanism. Therefore, we probed the PES for NH_2NO_2 according to our previously presented mechanisms on the decomposition of NH_2NO and compare the results with the corresponding gas phase. The latter was also theoretically investigated by Mebel et al.¹⁸⁹ in the context of the combustion of nitramine propellants and the decomposition of ammonium dinitramide (ADN). The structures of the pathway with lower energy is shown in Figure B.23. The corresponding energies of the catalyzed reaction in comparison to the energies of the decomposition of NH_2NO are shown in Figure 4.15.

The mechanism starts with the exothermic adsorption of nitramide ($\Delta E_{\text{ads}}=-15.6$ kcal/mol), which forms two hydrogen bonds with the catalyst, one with the Brønsted acid to an oxygen and one between the amino group of the molecule with a surface oxygen (ST 1, Figure B.23). Then, a proton transfer between the molecule and the catalyst takes place via TS 1 by inverting the origin of the hydrogen for the corresponding bonds (ST 2), which requires an

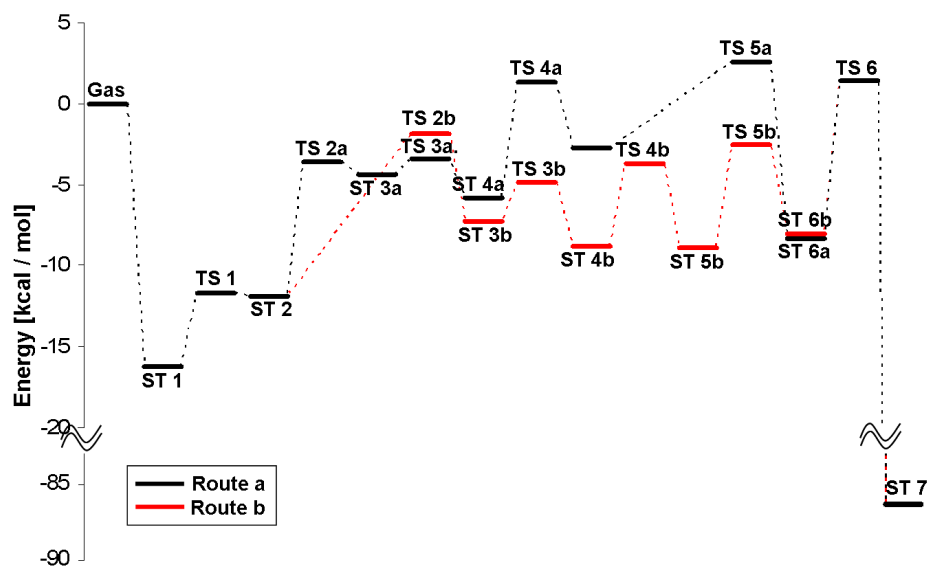


Figure 4.14: Energy profiles for the decomposition of NH_2NO to N_2 and H_2O , comparing two different pathways (route “a” and “b”). Energies are zero-point corrected.

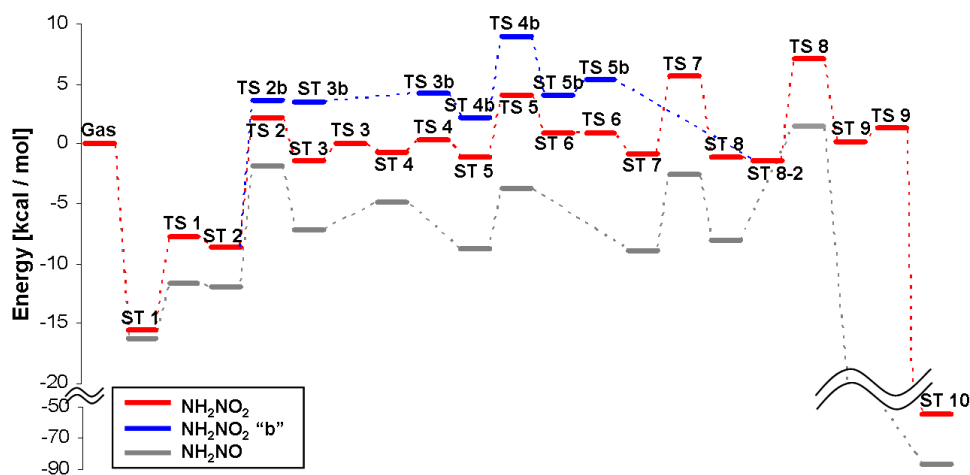


Figure 4.15: Energy profiles for the decomposition of NH_2NO_2 , comparing two different mechanisms with the low energy NH_2NO decomposition. Energies are zero-point corrected.

activation energy of $E^\ddagger=7.8$ kcal/mol (electronic energy with respect to ST 2). In the next step, the molecule rotates in such a way that the hydrogen bond to the former amino group is released (TS 2) and the new hydroxyl group forms a second hydrogen bond with the Brønsted acid (ST 3). This process exhibits an energy barrier of $E^\ddagger=10.7$ kcal/mol. Because the proton transfer via TS 1 only has a rather low reverse reaction barrier, it can be concluded from the energy profile that ST 2 can be neglected and for the step between ST 1 and TS 2 a barrier of $E^\ddagger=17.7$ kcal/mol has to be taken into account. In the next step, the molecule flips via TS 3 from a bend forward into an upright position. This step has to be seen rather from the perspective of completeness than as a mechanistic necessity and the barrier was calculated to be $E^\ddagger=1.5$ kcal/mol. With the subsequent transition state TS 4, a proton transfer between the catalyst and the hydroxyl group takes place which only requires to overcome a barrier of $E^\ddagger=1.0$ kcal/mol. ST 5 is still bond to the surface with two hydrogen atoms. Then, a rotation of the intermediate with respect to the catalyst via TS 5 first leads to the unstable ST 6 where the molecule is loosely bond to the Brønsted acid with its HN portion. A further rotation (TS 6) leads to ST 7, in which the structure is tightly bond to the catalyst by two hydrogen and the hydroxyl group is directed upwards. The first part of the rotation requires a barrier of $E^\ddagger=5.1$ kcal/mol whereas for the second part only a barrier of $E^\ddagger=0.01$ kcal/mol was calculated. This indicates that the rotation can be seen here as one step and ST 6 and TS 6 can be neglected. Subsequently, a proton transfer between the former amino group and the catalyst takes place via TS 7. In the resulting structure ST 8 the hydrogen of the HN portion is directed towards the hydroxyl group of the intermediate. Here, we calculated a barrier of $E^\ddagger=6.5$ kcal/mol for the proton transfer. For the subsequent steps we considered ST 8-2 which is merely the mirror inversion of ST 8. Now, the molecule rotates via TS 8 with respect to the surface, thus, it is bond to the surface twice but with different groups. In ST 9 the HN part forms a hydrogen bond to a free framework oxygen while the hydroxyl group attaches to the Brønsted acid. This rotation is activated by $E^\ddagger=8.4$ kcal/mol and marks the highest point in the energy profile. Then, in a final step, the molecule decomposes into N_2O and water (ST 10) after the protonation of the hydroxyl group by the Brønsted acid. The former amino group restores at the same time the catalytic acid (TS 9). This step requires a barrier of $E^\ddagger=1.2$ kcal/mol (electronic energy with respect to ST 9) and it can be assumed, that after the rotation via TS 8, the intermediate decomposes right away.

Starting from ST 2 for route “b”, two rotations lead to a configuration in which the former amino group is bond to the Brønsted acid. A proton

exchange to this group with the catalyst and an internal rotation of the hydroxyl group then leads to ST 8-2. From the comparison of the energy profiles of the two pathways it can be concluded that, though route “b” is slightly higher in energy, both are accessible because the highest overall barriers with respect to ST 1 (TS 4b and TS 8) deviate only by $\Delta E=1.9$ kcal/mol. Thus, the mechanism is a sequence of rotations of the intermediates with respect to the catalyst and proton exchanges with the catalyst in a push-pull manner, similar to the decomposition of nitrosamine. In fact, the barriers in the energy profile for the decomposition of nitramide and nitrosamine refer to the same structural changes and it can be seen that the pathway for nitramide is only slightly less favorable which is probably because of the more complex structure resulting from the second oxygen.

For the gas phase decomposition first, there is a proton transfer from the amino group to one of the oxygen, forming a hydroxyl group and then a rotation along the N-OH bond takes place. Either a rotation along the N-NH bond or a proton transfer from the hydroxyl group to the second oxygen follows. Both steps lead to an equivalent structure. In the last step, a final proton transfer from the former amino group to the hydroxyl group leads to N_2O and water (Figure B.24). Our results coincide quite well with the structures and energies presented by Mebel et al.¹⁸⁹ at the MP2/6-311G(d,p) level of theory. For the first proton transfer we found the highest intrinsic energy barrier with $E^\ddagger=37.8$ kcal/mol, which is significantly higher than even a lumped barrier on the catalyst from ST 1 to TS 8 ($\Delta E=22.8$ kcal/mol), indicating the high activity of H-ZSM5 for this decomposition. The effect can mainly be seen in the avoidance of bending along the N-N-O or O-N-O angle during the internal proton transfer. For example it can be seen for the first proton transfer from the amino group to the oxygen that in the gas phase this process involves a bending of the corresponding N-N-O angle from $\angle 116.38^\circ$ (ST 1g) to $\angle 102.87^\circ$ (TS 1g) whereas on the catalyst bending is negligible.

4.4 Conclusion

The key steps of the mechanism of the SCR of NO with ammonia in the presence of O_2 on H-form zeolites have been investigated using the Density Functional Theory. Besides the oxidation of NO the reaction scheme can be subdivided into three parts. The first one covers the formation of the principal intermediates nitrous and nitric acid together with nitrosamine and nitramide. The second one deals with the decay of the two acids and the

third one with the decomposition NH_2NO and NH_2NO_2 . For step one, three different pathways were taken into account, starting with two NO_2 molecules, one NO_2 and one NO molecule, and starting with two NO molecules. All mechanisms have been studied on a cluster of 5 T-atoms and the crossing of PESs was considered if necessary. It could be shown that in the absence of oxygen and NO_2 the process barely proceeds, whereas in the other two cases the Brønsted acid site enhances the reaction compared to possible gas phase reactions. However, two potential scenarios have to be discriminated in this context. Either the nitrogen oxides react in dimerized form with adsorbed ammonia or a decomposition of a dimer leads, first, to nitrosyl or NO_2^+ prior to a reaction with ammonia. While the latter scenario exhibits lower intrinsic energy barriers, it might be blocked from the strong adsorbing ammonia as ammonium ion. For the decay of nitrous or nitric acid, three different sinks were discussed, namely the decomposition into nitrosyl and NO_2^+ , respectively, together with water, the bimolecular reaction with adsorbed ammonia or the bimolecular dehydration of two acids. A significant reduction of intrinsic energies was here observed for the reaction of the acids with ammonia, making this pathway favorable at low temperatures, when the active sites are expected to be widely covered with ammonia. The lowest intrinsic barrier for the decay of nitrous acid was however observed for the decomposition into nitrosyl and water on a void Brønsted acid, suggesting this pathway to be most favorable in the presence of free active sites. The analogous decomposition of nitric acid exhibits a significantly higher barrier in the order of magnitude of its dehydration reaction to N_2O_5 . Nevertheless, because the bimolecular reaction does not provide a significant benefit over the decomposition the latter is more probable. Finally, the ability of the catalyst to enhance the decomposition of the intermediates nitrosamine and nitramide into nitrogen and nitrous oxide, respectively, together with water, by several proton transfer steps was illustrated. The main benefit over the gas phase decomposition can be attributed to an avoided internal bending of the molecules due to the proton exchange capability of the catalyst. Thus, we have presented the mechanism of several SCR key steps, accounting for many experimentally observed phenomena and demonstrated the ability of H-form zeolites to enhance these single reactions compared to the gas phase.

5

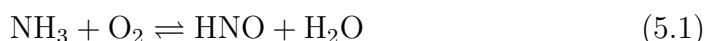
Theoretical Investigation of the Mechanism of the Selective Catalytic Oxidation of Ammonia on H-form Zeolites

The selective catalytic oxidation (SCO) of ammonia has been investigated on a portion of the H-ZSM5 framework which contains 5 T-atoms by using density functional theory, representing H-form zeolites. The mechanism was subdivided into three main blocks: (1) the direct reaction of NH_3 with oxygen, leading either to HNO or to NH_2OH , (2) the decay of nitroxyl (HNO) and (3) the decay of intermediately produced hydroxylamine (NH_2OH). For the decay of HNO and NH_2OH the catalyst is active for reactions with both, NO and HNO, which leads to a reaction network with several energetically similar and accessible pathways. The initial reaction of oxygen with adsorbed ammonia exhibits the highest energy barrier in the mechanism and thus is likely to be the rate limiting step. For all three parts, the crossing of potential energy surfaces was considered if necessary. The investigation of potential reaction pathways of N_2O with NH_3 and NO reveals a low activity of H-ZSM5 for them and thus, they only have a minor relevance within the SCO. The results of the investigated reaction network of the selective catalytic oxidation of ammonia are in agreement with the experimental literature.

5.1 Introduction

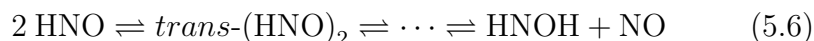
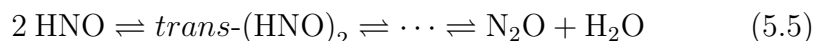
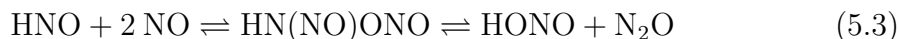
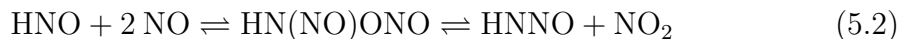
Many chemical processes either use ammonia as a reactant or produce it as a by-product and thus are potential sources of NH_3 slips.^{42,217} As ammonia emissions contribute to the acidification of the environment and its precursors are responsible for the greenhouse effect and city smog, control criteria have become stricter concerning waste stream treatment.²¹⁸ The selective catalytic oxidation (SCO) of ammonia to nitrogen and water is an ideal technology to reduce its concentration in gas waste streams to match legislated emission standards. Ammonia is effectively used in the selective catalytic reduction (SCR) of NO_x ($x=1, 2$).^{43,219–221} In order to prevent ammonia slip, most processes are carried out under non optimal stoichiometric conditions ($\text{NH}_3/\text{NO} < 1$) leading to a loss in NO reduction efficiency. Thus, an SCO step following the SCR of NO would allow for an overall enhanced result. Nevertheless, the SCO of ammonia also has to be considered as a side reaction of the SCR which has to be taken into account when optimizing the performance of waste stream treatment devices.^{145,161,163,178,222} Furthermore, the SCO can be used to remove NH_3 impurities from biomass-derived fuels to prevent the formation of nitrogen oxides during combustion.^{223,224} Many types of materials proved to be active for the SCO of ammonia. Noble metals like Pt, Rh, and Pd exchanged to ZSM5 or supported on Al_2O_3 ,^{225–227} Cu and Fe exchanged to zeolites or supported on Al_2O_3 ^{228–233} as well as Ni,^{234,235} V_2O_5 ²³⁶ based and silver catalysts²³⁷ were investigated. Several catalysts have to face the problem of selectivity because in many cases not only N_2 and H_2O are produced, but also unwanted NO or N_2O . Fe-ZSM5, mainly known as a promising SCR-catalyst also showed high activity for the SCO together with a reasonable selectivity towards N_2 .^{42,43,217,219} In most cases Fe-ZSM5 is produced by ion exchange of the H-form of the zeolite and thus, dependent on the grade of exchange, also leaves Brønsted acids as active centers in the catalyst. Yang and Long²²¹ investigated the SCO of ammonia to N_2 on several different ion exchanged zeolites in comparison to the H-ZSM5. Whereas the H-form produced large quantities of NO, the Fe-ZSM5 showed the highest N_2 yield compared to the other ion exchanged catalysts. Furthermore, they studied the influence of the Si/Al ratio, a parameter that affects the catalyst's surface acidity in different iron containing zeolites.²²⁰ It turned out, that with an increase of this ratio the NH_3 conversion as well as the selectivity to N_2 decreased significantly. Together with the knowledge that a high Brønsted acidity is favorable for ammonia adsorption as NH_4^+ , Yang and Long assumed that this ion plays an important role in the SCO mechanism on Fe/H-ZSM5. They also found a good correlation between the

activity of the investigated Fe-zeolites for the SCR of NO with ammonia and the selectivity of the SCO of NH₃ to N₂. They concluded from this finding that the SCO mainly produces NO and then a reduction to N₂ takes place via the SCR mechanism. Yang and Gongshin^{43,219} verified this coherency between SCR and SCO on the Fe-ZSM5. Furthermore, they concluded the existence of NO and NH₄⁺ ions during the SCO of ammonia and the reaction of the latter with oxygen from FT-IR results. Akah et al.^{42,217} also investigated the SCO on different Fe-zeolites in comparison to the H-ZSM5. Though the H-ZSM5 exhibited a lower activity and selectivity than the iron exchanged catalysts it was also shown that Brønsted acids are needed for a good performance. A synthetically created iron-containing catalyst without any Aluminum in the structure was quite inactive and unselective compared to the Fe/H-ZSM5. Akah et al. assumed that the Brønsted acidity helps in the activation of NH₃ molecules during the SCO. Like Yang and Long²²¹ before, they concluded from their findings that the mechanism of the SCO first leads to NO and the reduction to N₂ is achieved by the mechanism of the SCR. From these results it is obvious that the mechanism of the SCO of ammonia on Fe/H-ZSM5 not only involves the iron but also the Brønsted acids as active sites. Thus, for a complete understanding of this reaction mechanism the influence of both active sites needs to be determined and investigated separately. So far, there are only very few theories available about detailed reaction mechanisms of the SCO in general, including possible intermediate structures. Andrussov²²⁵ stated already in 1926 the assumption that one of the main intermediates of the SCO of NH₃ on Pt is nitroxyl (HNO), which can be illustrated from the stoichiometry of the direct reaction between one NH₃ and one O₂ molecule.



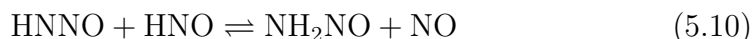
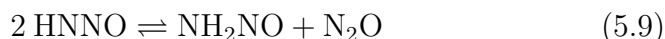
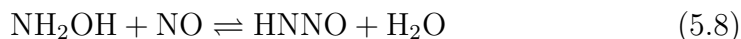
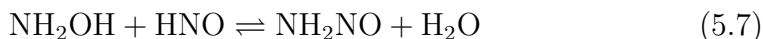
In 1935, Bodenstein^{238,239} extended this mechanism by suggesting the formation of hydroxylamine (NH₂OH). Skreiberg et al.²⁴⁰ who studied the homogeneous oxidation of NH₃ in terms of a kinetic model, also found HNO as one of the most important intermediates. Dixon et al.²⁴¹ stated that, besides HNO and NH₂OH, the isomeric radicals NH₂O and HNOH are also important intermediates in the atmospheric oxidation of ammonia. Cheskis et al.²⁴² experimentally studied the decay rates of HNO at low and high NO pressures in the gas phase. For lean NO conditions they mainly found N₂O as a product and concluded that the reaction of two HNO molecules leads directly to this product by hydrolysis. In the case of NO-rich conditions, a reaction between NO and HNO was assumed and NO₂ was found. Lin et al.^{243–245} theoretically investigated these two cases as well as a reaction of

nitroxyl with NO_2 ²⁴⁶ and stated probable reaction mechanisms.

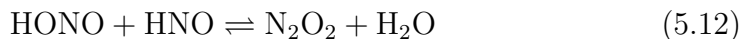


The last two pathways are considered to be competitive and reaction (5.3) is proposed here as a further pathway.

This work focuses on the development of a detailed mechanism for the selective catalytic oxidation of ammonia on H-ZSM5 by probing the potential energy surface on a cluster model of this catalyst on the basis of the density functional theory. Calculations were performed dealing with the proposed reaction to directly oxidize ammonia (5.1) to HNO and water on the Brønsted acid. An additional branch within that reaction also was investigated, leading to NH_2OH due to a further reaction with another ammonia molecule. Furthermore, the system of reactions (5.2) to (5.6) was investigated, including a further step from reaction (5.6) to the potential intermediate hydroxylamine (NH_2OH). In a next step, the decay of NH_2OH is discussed on the basis of reactions (5.7) to (5.11).



The product NH_2NO was shown to decompose to N_2 and H_2O on the H-ZSM5 in the preceding chapter 4. To account for the interaction of intermediates resulting from the SCO and the SCR also the reaction of nitric and nitrous acid with nitroxyl were considered.¹⁹¹



In a final step, we investigated potential pathways for the reduction of N_2O , because this species is experimentally found in traces only. The investigation of the SCO on the H-form zeolite is intended to give insight into the potential role that the Brønsted acid plays in ion-exchanged zeolites like the Fe/H-ZSM5.

5.2 Theory

The applied methodology for the investigation of the SCO mechanism is equivalent to the descriptions in the preceding chapter 4. The catalytic active site and a part of the zeolite framework were represented by a cluster of 5 T-sites (Figure 4.2, ST A) and all Si atoms were initially placed at their crystallographic positions. The terminal Si atoms were saturated with hydrogen, whereas the Si-H bonds are oriented in the direction of the former Si-O bonds and the length of these bonds was set to 1.487 Å. All quantum chemical calculations were carried out with the TURBOMOLE suite of programs²⁰⁰ by using gradient-corrected density functional theory (DFT) with the B3LYP-functional and a triple- ζ basis set with polarization functions (TZVP).⁶⁶ Structure optimizations were performed in Cartesian coordinates with an energy convergence criterion of 10^{-7} Ha and the maximum norm of the Cartesian gradient was converged to 10^{-4} Ha/bohr. Transition states were localized from a combined application of first the growing string-method⁹⁹ and a refinement with either the modified dimer method¹⁰⁵ with a gradient-norm convergence criterion of $5 \cdot 10^{-4}$ Ha/bohr or the PRFO¹⁰³ method. Crossing of seams of PESs in MECPs were determined with a multiplier penalty function algorithm which had a maximum energy difference on both PESs of less than 10^{-6} Ha.

5.3 Results and Discussion

In the following, the mechanistic details of the selective catalytic oxidation of ammonia, involving the Brønsted acid of H-ZSM5 as an active catalytic site, will be presented and discussed in accordance with reactions (5.1) to (5.13), including the crossing of PESs. In order to compare different pathways, dealing with the same reactants, we subdivided the SCO into (I) the formation of HNO, including a branch to NH_2OH , (II) the decomposition of HNO, (III) the decomposition of NH_2OH , (IV) the interaction of nitroxyl with nitrous and nitric acid and finally (V) the potential reaction pathways for N_2O within the system. All energies stated in this work are zero-point energy-corrected electronic energies with respect to single molecules (gas phase) and an empty zeolite framework. For some transition states only the electronic energy differences to either the reactant or the product were taken into account, because otherwise, with the ZPE-correction, the value was below this state. This effect can occur when rather small electronic energy differences are considered. In these cases, it will be stated as a remark in parentheses,

including the reference state to which the electronic energy was added.

5.3.1 Reaction of NH_3 with O_2

Though there is only little known about how the reaction of the SCO proceeds on H-ZSM5 there is an agreement in the literature^{225,238–241} on ammonia oxidation in general that HNO might play an important role as an intermediate. Because this species can be derived directly from a bimolecular reaction between oxygen and ammonia, we investigated the catalyzed reaction (5.1) as a first step (Figure C.1). Furthermore, we investigated the influence of a second ammonia molecule on the reaction (Figure C.2), which resulted, besides an intended change in the energy profile, in an additional reaction branch, directly leading to hydroxylamine. The corresponding energies are displayed in Figure 5.1.

The mechanism starts with the strong adsorption of ammonia as NH_4^+ in the 2H mode ($\Delta E_{\text{ads}} = -18.9$ kcal/mol; Figure 4.2, ST B) and the coadsorption of oxygen (Figure C.1, ST 1a). From the energy profile it can be concluded, that the subsequent interaction between adsorbed ammonia and oxygen can be neglected and thus O_2 rather has to be considered as a gas phase species in this context. Thus, the following direct reaction of gas phase oxygen with adsorbed ammonium can be considered as of the Eley-Rideal type. This first step involves a crossing of the PESs with spin multiplicity of $M_S = 3$ to $M_S = 1$ and ammonium needs to be activated to NH_3 . Subsequently an O-N bond is formed with the oxygen and O_2 takes up the proton from the zeolite surface forming the intermediate species NH_3OOH^+ (ST 2a). For this process, an energy barrier of $E^\ddagger = 40.8$ kcal/mol was calculated and the corresponding structure, the minimum on the seam of the two potential energy surfaces, is denoted with SEAM 1a. ST 2a is $\Delta E = 16.5$ kcal/mol lower in energy than SEAM 1a and thus can be assumed to be a stable intermediate structure that does not instantaneously decompose back to the NH_3 and O_2 . Next, the NH_3 part of the intermediate structure releases one proton to the catalyst and due to a configurational change within the molecule the distance of the OH group of now NH_2OOH to the Brønsted acid of the catalyst is shortened to 2.521 Å (ST 3a). The activation energy to overcome the corresponding TS 1a was calculated to be $E^\ddagger = 7.2$ kcal/mol. In the next step via TS 2a and a barrier of $E^\ddagger = 3.5$ kcal/mol (electronic energy with respect to ST 4a) this distance is even further shortened to 1.734 Å, whereas the intermediate is now not anymore adsorbed to the Brønsted acid with the nitrogen but with the OH group (ST 4a). As a last step, the adsorbed OH group takes up the proton from the zeolite, forming water and the O-O bond is broken. The

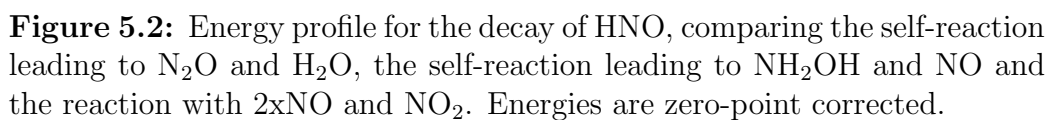
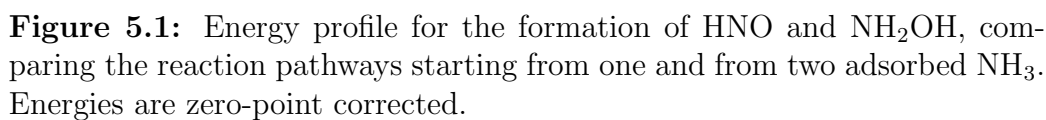
remaining portion of the molecule returns one hydrogen to the catalyst and forms adsorbed nitroxyl (ST 5a). This exothermic step via TS 3a has an activation energy of $E^\ddagger=0.55$ kcal/mol. Basically, as can be seen from Figure 4, TS 2a, ST 4a and TS 3a have very close energies and thus, the step from ST3a to ST5a should rather be considered as one step and the intermediate structure ST4a can be neglected.

An alternative pathway was obtained by starting from two coadsorbed NH_3 molecules (Figure 4.2, ST J). The second ammonia molecule also adsorbs quite strongly as can be concluded from the energy profile ($\Delta E_{\text{ads}}=-13.7$ kcal/mol with respect to ST B) and forms hydrogen bonds with the catalyst and with the prior adsorbed ammonium. TPD experiments^{42,161,217} showed that there are two peaks for ammonia, whereas Long and Yang¹⁶¹ associated the one at higher temperature with NH_4^+ , the other one with coordinated NH_3 . The presented structure ST J might correspond to these findings. The reformation of ammonia from ammonium turned out to be the step with the highest energy barrier not only for route “a” but also for the reactions of NH_3 within the SCR (compare chapter 4). Thus, the motivation for this pathway was the idea to potentially find a reaction mechanism in which this energy barrier is not needed, by starting with a system, where coordinated ammonia already exists in a stable state. Adding oxygen in the next step to the system does not reveal a significant interaction between O_2 and the ammonia complex, with respect to the energy. This indicates, as was the case for route “a” as well, that oxygen can be considered as a gas phase species and the subsequent reaction mechanism is of the Eley-Rideal type. In the next step we considered a crossing of PESs from $M_S=3$ to $M_S=1$ via SEAM 1b, by which the gas phase oxygen enforces the separation of the two ammonia molecules (ST 2b). For this process an energy barrier of $E^\ddagger=36.8$ kcal/mol has to be overcome which is slightly lower than the corresponding barrier for route “a”. In the following step the intermediate structure NH_3OOH^+ (ST 3b) is formed and from the energy profile it is obvious that the energy barrier for this process (TS 1b) can be neglected. Basically, the two processes of crossing the PESs and the formation of bonds between the oxygen with the nitrogen on one side and hydrogen on the other side can be considered as one single step similar to the first step in route “a”. In fact, ST 2b might solely be a product of numerical noise. Now, a proton is retransferred to the zeolite structure (TS 2b), which involves a slight barrier of $E^\ddagger=1.4$ kcal/mol (only electronic energy difference with respect to ST 3b). The desorption of one ammonia molecule ($\Delta E_{\text{des}}=7.4$ kcal/mol) represents the last step, leading from ST 4b to ST 3a (Figure C.1), which further decomposes to HNO and water.

An alternative pathway, starting from ST 4b and leading to two hydroxylamine molecules was investigated and is also accessible from route “a” by considering a coadsorption of ammonia to ST 3a. A slight rotation of the ammonia molecule via TS 3c into an adsorbed state with only one hydrogen-bond to the zeolite (ST 5c) exhibits an activation Energy of $E^\ddagger=0.02$ kcal/mol and thus can be considered barrier less. In the next step the NH_2OOH changes its configuration from trans to cis (ST 6c) and an activation energy of $E^\ddagger=8.9$ kcal/mol (TS 4c) has to be overcome. Then, the OH part from NH_2OOH is released and temporarily forms a hydrogen bond to the catalyst, while the ammonia slightly rotates, being hydrogen-bond to another framework oxygen. Finally, a bond between ammonia and the released OH is formed (TS 5c), accompanied by a proton transfer between the two forming molecules. This implies that the remaining NH_3O part takes up the hydrogen from the former released OH part and releases instead a hydrogen from its nitrogen back to this remaining oxygen atom, which eventually leads to two coadsorbed hydroxylamine molecules. This last step presents for this pathway the highest energy barrier with $E^\ddagger=22.4$ kcal/mol and it can be concluded from the energy profile that the decomposition of the intermediate NH_2OOH into nitroxyl and water is favorable. Nevertheless, the barrier is especially within the context of the formation of the intermediate structure low enough to be overcome and thus the formation of NH_2OH from this pathway is not negligible. A benefit of the second ammonia molecule due to the avoidance of the activation of NH_4^+ to NH_3 was observed within a lower energy barrier. Nevertheless, the decrease in the energy barrier was not as significant as expected because of the necessity to break the formed hydrogen bond within the ammonia complex. Thus, the separation of the formed ammonia complex in addition to the crossing of the PESs and the formation of the intermediate NH_3OOH^+ still exhibits a high energy barrier, close to the corresponding one with only one NH_3 (route “a”). This indicates that the formation of HNO and NH_2OH might be the rate determining step for the SCO of ammonia on H-ZSM5 and the explanation why the catalyst is less active for this reaction than ion exchanged zeolites.

5.3.2 Decomposition of HNO

For the gas phase decay of nitroxyl experimental as well as theoretical studies^{242–245,247} suggested a reaction with either a second HNO molecule or with nitrogen oxide. In the first case, the products N_2O and water were found. Furthermore, Lin et al.²⁴³ proposed the competitive dissociation of the dimer $(\text{HNO})_2$ into the radicals NO and HNOH from theoretical investigation.



For the reaction of nitroxyl with NO Strausz and Gunning^{248,249} and later Holmes and Sundarm^{250,251} suggested the formation of HNO₃ and nitrogen, whereas Lin et al. found this mechanism unfavorable compared to their proposed pathway, leading to HNNO and NO₂. We investigated the decay of HNO on H-ZSM5 by first analyzing the self-reaction of nitroxyl leading to N₂O and water (Figure C.3), as well as a pathway leading to the decomposed products HNOH and NO (Figure C.4). Furthermore, we considered an additional reaction, between HNOH and nitroxyl leading to the more stable hydroxylamine. Because nitrogen oxide is released in the latter reaction, we also investigated the activity of the catalyst for the reaction of HNO with NO and NO₂ (Figure C.5). The corresponding energies to the structures presented in Figures C.3 to C.5 are shown in Figure 5.2.

Self-reaction of HNO, leading to N₂O

The mechanism is started with the adsorption of two nitroxyl molecules on the catalyst. The first one (Figure C.3, ST 0) is fixed by two hydrogen bonds with an adsorption energy of $\Delta E_{\text{ads}} = -9.1$ kcal/mol. The second HNO is only bond by one hydrogen to the unoccupied framework oxygen (ST 1). Its adsorption energy with respect to the first adsorbed molecule is $\Delta E_{\text{coads}} = -4$ kcal/mol and thus it is rather loosely bond. In the next step, the two molecules exothermically dimerize by forming an N-N bond to trans-(HNO)₂ (ST 2). The energy barrier corresponding to that process via TS 1 is negligibly small with $E^\ddagger = 1.0$ kcal/mol and it can be assumed that the dimer forms right away if two nitroxyl molecules are present on the active side of the catalyst. Furthermore, due to the strongly exothermic character of the dimerization by $\Delta E = -30.5$ kcal/mol, a reverse step, leading back to two HNO molecules, is rather unlikely. The following switch in the adsorbed state of the dimer from one framework oxygen to another (TS 2, ST 3) is not relevant for the mechanism but rather presented for the purpose of completion. Nevertheless, as can be seen from the energy profile, such a step only has a low activation barrier ($E^\ddagger = 3.4$ kcal/mol) and thus eventually takes place quite often at reaction temperatures. In the next step, a proton transfer takes place from the catalyst to the oxygen of the dimer and from the nitrogen of the molecule to the zeolite. This proton transfer (TS 3) is activated by only $E^\ddagger = 0.4$ kcal/mol indicating that not the dimer trans-(HNO)₂ but structure ST 4 can be considered as the first rather stable intermediate since the coadsorption of the two nitroxyl molecules. Now, a slight rotation of the molecule on the surface (TS 4a) with an activation barrier of $E^\ddagger = 15.5$ kcal/mol leads to a structure (ST 5a) which enables another hydrogen transfer with the catalyst (TS 5a), involving the two nitrogen atoms. The proton transfer exhibits an

energy barrier of $E^\ddagger=12.1$ kcal/mol and leads to a structure (ST 6a) that is fixed to the catalyst with a hydrogen bond between the reformed N-H part of the molecule and a framework oxygen and a hydrogen bond between the Brønsted acid and the O-H part of the molecule. From this structure another proton exchange with the catalytic surface together with the breaking of the N-O bond via TS 6a and an energy barrier of $E^\ddagger=14.2$ kcal/mol leads to the formation of water and N_2O . This step is exothermically by $\Delta E=-59.6$ kcal/mol and thus can be considered irreversible. With respect to the energy profile, the mechanism can be simplified into the nearly barrierless dimerization of two HNO and a first proton transfer leading to ST 4, then the slight rotation and the subsequent proton transfer leading to ST 6a and finally the decomposition into N_2O and water. The second lumped step then exhibits the highest internal energy barrier which was calculated to be $E_{conc}^\ddagger=22.8$ kcal/mol (ST4 to TS 5a). Furthermore, it becomes obvious from the energy profile that the reaction along this pathway (route “a”) can be considered as to proceed rather fast, because the dimerization already releases enough energy to overcome the subsequent barriers. From theoretical investigations of the corresponding gas phase reaction, Uggerud et al.²⁴⁷ stated an energy barrier of $E^\ddagger=10.5$ kcal/mol for the formation of the dimer indicating, that the catalyst facilitates this formation. Furthermore, the highest internal energy barrier for the most favorable pathway was calculated to be $E^\ddagger=41.3$ kcal/mol, indicating that the catalyst also significantly reduces the energy barriers for proton transfers due to the Brønsted acid. Thus, the presented “push-pull” mechanism of the self-reaction of HNO on H-ZSM5, leading to N_2O and H_2O exhibits great improvement over the corresponding homogeneous reaction with respect to the energy barriers.

Self-reaction of HNO, leading to NH_2OH

Up to structure ST 4 this mechanism is identical to the above presented decomposition to N_2O and H_2O . Then, the molecule changes the state of adsorbance via TS 4b that the hydrogen bond from the Brønsted acid is now not anymore with the molecule’s nitrogen but with the oxygen at the end of the structure (ST 5b). This molecule shift is activated by $E^\ddagger=9.7$ kcal/mol. Because the resulting structure of minimum energy is now only fixed on the catalyst with one hydrogen interaction it can be assumed that it is rather unstable. This is supported by the low energy barrier of $E^\ddagger=0.6$ kcal/mol exhibited by the subsequent rotation of the molecule (TS 5b), leading to a structure, that has two hydrogen bonds between catalyst and molecule (ST 6b). In fact, it can be assumed that the molecule shift directly leads to this structure ST 6b and that the two steps can be considered as one step

because of the negligible second energy barrier. Next, the OH group of the molecule is slightly rotated via TS 6b to structure ST 7b with a barrier of $E^\ddagger=0.1$ kcal/mol and the energy profile indicates that this step can occur in both directions instantaneously. Then, the molecule is rotated along its vertical axis through the displayed transition state (TS 7b), leading to a different adsorbed state of the molecule, where the hydrogenated nitrogen is now twice hydrogen bonded to two framework oxygen atoms (ST 8b). This process exhibits an activation energy of $E^\ddagger=12.9$ kcal/mol and structure ST 8b is only $\Delta E=0.3$ kcal/mol lower in energy than the prior transition state, indicating it to be quite unstable. Then, the molecule takes up the proton from the catalyst and the N-N bond is significantly elongated (TS 8b; N-N=1.73 Å), while the resulting product (ST 9b; N-N=1.83 Å) is bonded to the surface with only one hydrogen. The energy barrier is $E^\ddagger=7.2$ kcal/mol (only electronic energy with respect to ST 9b) and again, the following drop in energy of only $\Delta E=0.2$ kcal/mol on the product side of this step indicates an unstable state for structure ST 9b. Now, the HONH₂ part of the molecule shifts on the catalyst to a new adsorbed state, in which two hydrogen bonds fix it. This results in a rather stable state with respect to the energy profile (ST 10b), whereas the energy barrier for the transition state prior to that structure ($E^\ddagger=1.5$ kcal/mol) is negligible. Thus, the steps from ST 7b to ST 10b have to be lumped into one step in terms of that enough energy must be provided to overcome all intermediate barriers at once, because of the unstable character of ST 8b and ST 9b. This leads to a concerted energy barrier of $E_{\text{conc}}^\ddagger=21.1$ kcal/mol (from ST 7b to TS 9b), presenting the highest internal barrier of the overall process. In fact, the species ST 10b could also be interpreted as hydroxylamine adsorbed on $Z^-[\text{NO}]^+$. Nevertheless, in accordance with reaction (5.4) we further considered the decomposition of the structure into HNOH and NO which includes a switch from the PES with spin multiplicity $M_S=1$ to the one with $M_S=3$. The minimum on the seam of these two surfaces (SEAM 1b) exhibits an energy barrier of $E^\ddagger=9.3$ kcal/mol and the N-N bond is released (ST 11b). As a next step we considered the desorption ($\Delta E_{\text{des}}=6.0$ kcal/mol) of the released NO, while the NH₂O instantaneously forms HNOH by proton transfer with the catalyst (ST 12b). In addition to the fragmentation of the dimer (HNO)₂, corresponding to the gas phase reaction proposed by Lin et al.,²⁴³ we investigated a further reaction step of the remaining HNOH with another nitroxyl molecule leading to the more stable intermediate NH₂OH and NO. Therefore, we considered the coadsorption of HNO as a next step (ST 13b), which exhibits an adsorption energy of $\Delta E_{\text{coads}}=-9.0$ kcal/mol with respect to adsorbed HNOH. In this state, NH₂O reforms from HNOH at present. Then, via TS 10b, HNO releases its proton directly to the nitrogen of the NH₂O, which also takes up the

Brønsted acid from the catalyst to form NH_3OH^+ . This process exhibits an energy barrier of $E^\ddagger=4.4$ kcal/mol and is exothermic by $\Delta E=-29.7$ kcal/mol, indicating that the reverse reaction is unlikely to occur. A comparison of the energy profiles of route “a” and route “b” reveals that these two pathways are competitive and neither one can be concluded to be favorable. In both cases, the initial dimerization releases enough energy to overcome the subsequent barriers and the highest internal barriers are nearly equal, indicating that none of the two processes traps a certain intermediate structure more than the other mechanism does.

Reaction of HNO with NO and NO₂

Cheskis et al.²⁴² found that the decay of HNO in an NO rich environment follows a different mechanism as stated above. Lin et al.²⁴³ proposed the reaction to HNNO and NO₂ whereas Strausz and Gunning²⁴⁸ and Holmes and Sundarm²⁵¹ proposed the production of HNO₃ and N₂. An investigation of these two mechanisms revealed for the first case an internal activation barrier of $E^\ddagger=37.0$ kcal/mol and for the second case a barrier of $E^\ddagger=39.0$ kcal/mol. (For details on the structures see Brüggemann and Keil.²⁵²) In addition an energetically more favorable pathway, leading to N₂O and HONO, was found. Here the mechanism starts with the adsorption of nitroxyl (ST0, Figure C.3) as was the case for the self-reaction of HNO. The addition of an NO molecule then barrierless forms an N-N bond between HNO and NO (ST1c, Figure C.5) which is exothermic by $\Delta E=-13.6$ kcal/mol. Then, another NO is added to the system (ST2c) which, from a configurational point of view, does not interact with the adsorbed intermediate as there is a distance of N-O=3.3 Å. This distance is significantly reduced by considering the crossing of the seam of PESs with $M_S=3$ to $M_S=1$ via SEAM 1c (N-O=2.4 Å) eventually forming a loose bond as can be seen from ST 3c (N-O=1.9 Å). This process needs to be activated with $E^\ddagger=6.8$ kcal/mol and is exothermic by $\Delta E=-11.4$ kcal/mol. Next, we considered a proton transfer of the molecule with the catalyst, leading to a new intermediate isomer with the sequence ONN-OH (ST4c) and the loosely bond NO. The barrier for this proton exchange via TS 1c is $E^\ddagger=1.9$ kcal/mol (only electronic energy with respect to ST3c). In the last step the bond between the OH group and the nitrogen of the intermediate structure is released and forms a bond with the loosely bonded NO (TS 2c). This leads to the final formation of N₂O and trans-HONO (ST 5c) and exhibits an internal energy barrier of $E^\ddagger=8.3$ kcal/mol. Thus, by comparing the energy profiles of the presented pathway with the self-reaction of nitroxyl it can be concluded that the reaction of nitroxyl with NO is slightly more favorable. Especially in the case of an NO-rich environment as is for example

the case in the SCR, it can not be neglected.

For the purpose of completion we also considered the reaction of NO_2 with nitroxyl, which, in the context of the SCO can be considered to be produced from the oxidation of NO. It can be seen from ST 1d (Figure C.5) and the corresponding energy that NO_2 hardly interacts with the adsorbed HNO. In the subsequent reaction step, the proton of the nitroxyl is transferred to the NO_2 , forming cis-HONO (TS 1d) which adsorbs directly to the Brønsted acid, while the released NO desorbs to the gas phase (ST 2d). The barrier that has to be overcome for this process was calculated to be $E^\ddagger=6.2$ kcal/mol and an energy of $\Delta E=-29.1$ kcal/mol is released, making the reverse reaction rather unlikely. For the gas phase reaction of NO_2 with HNO to cis-HONO and NO at the B3LYP/6-311⁺⁺G(d,p) level of theory, Mebel et al.²⁴⁶ only stated an electronic energy difference of $\Delta E=0.4$ kcal/mol between transition state and interacting reactants and found the ZPE-corrected relative energy of it to be $\Delta E=-2.3$ kcal/mol below the reactants. Thus, a distinct conclusion about a beneficial affect of the catalyst from the comparison with these values seems questionable. Nevertheless, even our calculated barrier of $E^\ddagger=6.2$ kcal/mol can be considered small within the H/N/O network and the reaction can be assumed to take place, if the reactants are available.

5.3.3 Decomposition of NH_2OH

Hydroxylamine is known to be a highly reactive compound^{253,254} that can react with other oxides of nitrogen.²⁵⁵ In the following, we present the mechanistic details of the decomposition of this species, catalyzed by the Brønsted acid of the zeolite according to reactions (5.7) to (5.11). For reaction (5.7), two different pathways are presented differing in the adsorbed state of hydroxylamine as either NH_3OH^+ (route “a”, Figure C.6) or NH_2OH (route “b”, Figure C.7) prior to the reaction with nitroxyl. Both states can be considered as existing and the pathway for the interexchange is included in route “b”. Starting from NH_2OH , the reaction with NO according to (5.8) is presented (“c”, Figure C.7) as well as the further branched progress according to reactions (5.9, “d”), (5.10, “e”) and (5.11, “f”). The structures of the latter reactions are presented in Figure C.8 and the corresponding energy profiles of the complete decomposition process are displayed in Figure 5.3.

Reaction of NH_2OH with HNO

The mechanism for route “a” starts with the adsorbed hydroxylamine in the NH_3OH^+ state (ST1, Figure C.7) and the subsequent coadsorption of nitroxyl

(ST2a, Figure C.6). From the energy profile (Figure 5.3) it can be concluded that not only hydroxylamine adsorbs stably on the catalyst ($\Delta E_{\text{ads}} = -20.7$ kcal/mol) but also the coadsorption of HNO ($\Delta E_{\text{coads}} = -7.4$ kcal/mol with respect to the adsorbed NH_2NO) is quite strong. In the next step the nitroxyl releases its proton while the O-N bond within the hydroxylamine breaks (TS 1a). The released OH group takes up the HNO proton and at the same time releases its own proton to the catalyst. Finally, a bond between the adsorbed OH and the NO is formed leading to adsorbed trans-HONO and ammonia (ST 3a). It should be noted that this structure is the same as ST 3a in Figure B.11 for the reaction of ammonia and nitrous acid (compare section 4.3.3) and the subsequent reaction steps are for both systems identical. However, the formation of this structure in this process is the most energy-consuming internal step of route “a”, exhibiting a barrier of $E^\ddagger = 26.6$ kcal/mol, but the energy stays below the reference state of gas molecules and the bare catalyst. Furthermore, this step is exothermic by $\Delta E = -39$ kcal/mol, making the reverse reaction unlikely. Then, the OH group of the nitrous acid again takes up the proton from the catalyst (TS 2a), which leads to the formation of water while the formed O-N bond is broken again (ST 4a). The activation barrier for this process was calculated to be $E^\ddagger = 8.0$ kcal/mol (electronic energy with respect to ST 4a). Next, the water molecule is rotated via TS 3a so that now not the H_2O proton is hydrogen bonded to the ammonia nitrogen but one proton from the NH_3 is interacting with the water oxygen. Furthermore, the NO nitrogen interacts with the ammonia nitrogen as their distance has significantly reduced to 2.2 Å (ST 5a). This change in the arrangement of the system species exhibits an energy barrier of $E^\ddagger = 11.5$ kcal/mol. In the following step, the N-N interaction between NH_3 and NO is further increased as can be concluded from the shortening of the distance to 1.8 Å. Furthermore, a hydrogen bond is formed between the ammonia and the surface by a slight rotation of the latter molecule (ST 6a). The barrier for this step is negligibly small with $E^\ddagger = 1.8$ kcal/mol. ST 6a and ST 7a only slightly differ with respect to the structure and a string calculation between the two structures revealed that the energy barrier is negligible for a potential interchange. Finally, a bond between the NO and the NH_3 is formed and one proton is released to the zeolite surface (TS 5a), leading to NH_2NO and H_2O , adsorbed on the catalyst (ST 8a). The formation of NH_2NO exhibits an activation energy of $E^\ddagger = 1.4$ kcal/mol. Thus, from the energy profile it can be concluded that the reaction proceeds instantaneously starting from TS 3a to ST 8a.

An alternative pathway for this reaction was investigated by first considering a change in the adsorbed state of hydroxylamine. Again, here the

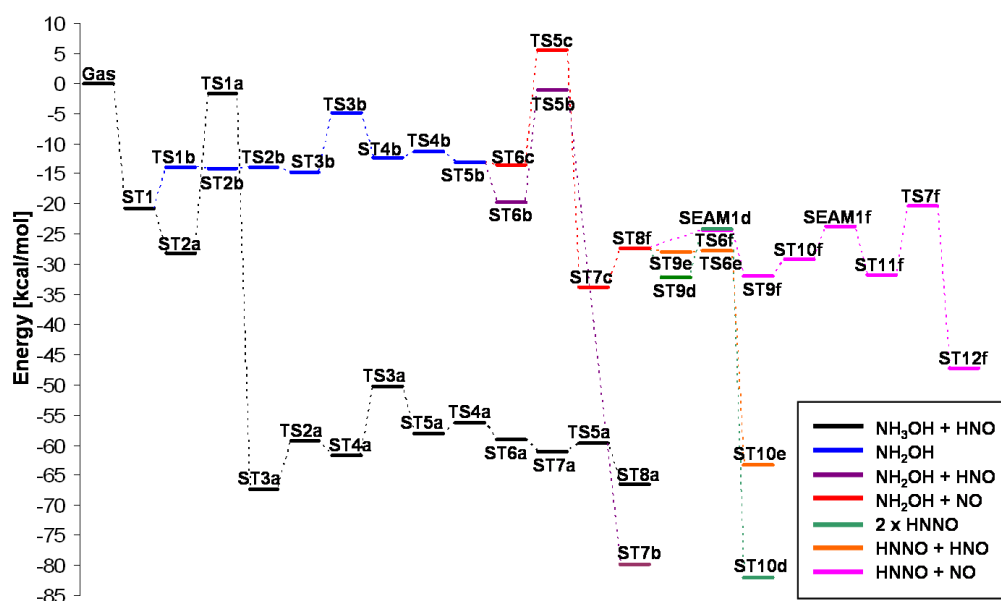


Figure 5.3: Energy profile for the decay of NH_2OH , starting from NH_3OH^+ . Compared are the reactions with HNO , either directly or after prior transformation to NH_2OH and with NO . For the formed HNNO the self-reaction and the reaction with HNO and NO are shown. Energies are zero-point corrected.

starting point is adsorbed NH_2OH in the protonated state (ST 1, Figure C.7), which owes its high stability from two hydrogen bonds of the NH_3 portion of the molecule and one hydrogen bond of the OH part with framework oxygen. A rotation of the molecule (TS 1b), leading to an adsorbed state with only two hydrogen bonds (ST 2b) exhibits an activation energy of $E^\ddagger=6.7$ kcal/mol. A further rotation and a proton transfer of the molecule to the catalyst (TS 2b) is activated by $E^\ddagger=0.2$ kcal/mol (electronic energy with respect to ST 3b) and leads to ST 3b, where only the nitrogen is now hydrogen-bonded to the Brønsted acid. Then, another rotation of hydroxylamine together with a slight shift via TS 3b leads to an adsorbed state where the oxygen of the OH group is hydrogen bond to the Brønsted acid and one proton of the NH_2 portion interacts with one framework oxygen. This process exhibits an activation energy of $E^\ddagger=9.9$ kcal/mol. The following change in the adsorbed state of NH_2OH as presented is only for consistency of the mechanism and the barrier of only $E^\ddagger=0.8$ kcal/mol indicates that this switch proceeds nearly barrierless. Thus, for the change from the NH_3OH^+

state to NH_2OH the process can be merged to one major step, leading from ST 1 over TS 3b to ST 5b. All intermediate reactions can be neglected due to the low energy barriers and from the energy profile it can be concluded that it is not before TS 3b that there is a stable structure that does not directly react back to the NH_3OH^+ state. The activation barrier for this lumped step is $E^\ddagger=15.8$ kcal/mol and endothermic by $\Delta E=7.6$ kcal/mol. This indicates that this interchange has to be considered even at lower temperatures as the internal barrier might already be overcome due to the strong adsorption of the NH_3OH^+ and the reverse barrier of $E_{\text{rev}}^\ddagger=8.2$ kcal/mol is high enough to ensure the short-termed stability of NH_2OH .

Starting from ST 5b we considered the coadsorption of nitroxyl ($\Delta E_{\text{coads}}=-6.7$ kcal/mol with respect to the adsorbed NH_2OH) which forms a hydrogen bond to the framework oxygen but also interacts with the OH part of hydroxylamine (ST 6b). Then, in one step, the O-N bond of NH_2OH breaks, the OH part forms water with the Brønsted acid, the nitroxyl releases its proton to the surface and an N-N bond between NH_2 and NO is formed leading to NH_2NO (ST 7b). This process via TS 5b has to overcome an energy barrier of $E^\ddagger=18.7$ kcal/mol and is exothermic by $\Delta E=-59.9$ kcal/mol. Due to the slightly lower highest internal energy barrier, the second pathway could be considered more favorable although from the higher stability of NH_3OH^+ and the anchored higher availability of this species prior to the reaction with HNO also pathway “a” might be more favorable. Nevertheless, in both cases the energy profiles remain at their highest state below the references state by a comparable value (route “a”: -1.6 kcal/mol, route “b”: -1.1 kcal/mol), indicating that both pathways are accessible.

Reaction of NH_2OH with NO

This reaction pathway is started from adsorbed NH_2OH (ST 5b, Figure C.7), where we considered the addition of an NO molecule to the system (ST 6c). Because there is no interaction between the nitrogen oxide and the adsorbed molecule, as can be seen from the energy profile, the following reaction step can be considered as of the Eley-Rideal type. As with the reaction with nitroxyl, the O-N bond in hydroxylamine breaks and the OH part forms water with the catalyst hydrogen (TS 5c). Furthermore, a bond between the NO and the released NH_2 is formed and finally, the formed species releases one hydrogen to the catalyst, leading to adsorbed water and cis-HNNO (ST 7c). This process exhibits an energy barrier of $E^\ddagger=19.2$ kcal/mol, which is only 0.5 kcal/mol higher as the corresponding barrier for the reaction with HNO indicating the potential importance of this reaction branch especially

under NO-rich conditions.

As a next step, we considered the desorption of water from the catalyst, leaving adsorbed cis-HNNO as the starting point for the three considered branches according to reactions (5.9) to (5.11), which is shown as ST 8f (Figure C.8). The self-reaction of HNNO is presented here representatively as the reaction of one molecule in the cis- and the other one in the trans-configuration. However, similar results are obtained also for other combinations.²⁵² Trans-HNNO coadsorbs to the cis-HNNO ($\Delta E_{\text{ads}} = -4.8$ kcal/mol), by forming a hydrogen bond with one framework oxygen and one with its counterpart (ST 9d). The subsequent reaction step involves the crossing of PESs from $M_S=3$, corresponding to the two radicals HNNO to $M_S=1$, corresponding to NH_2NO and N_2O (ST 10d). The energy barrier, corresponding to the minimum on the seam of the two PESs (SEAM 1d) was calculated to be $E^\ddagger = 8.0$ kcal/mol and the process is exothermic by $\Delta E = -49.9$ kcal/mol, indicating that a reverse step is negligible. In a similar way we investigated the reaction of HNNO with nitroxyl, where again the cis-configuration is considered to be representative for both conformers. Though the addition of the nitroxyl to the system (ST 9e) leads to the formation of hydrogen bonds, a significant drop in energy cannot be obtained from the energy profile. In the following reaction step via TS 6e the HNO releases its hydrogen to the catalytic surface and the HNNO forms NH_2NO by taking up the proton it was adsorbed on (ST 10e). The energy barrier for this step is $E^\ddagger = 0.2$ kcal/mol (electronic energy with respect to ST 9e), indicating that this reaction can be considered to proceed spontaneously as soon as the gas phase nitroxyl hits on adsorbed HNNO. As a last branch we considered the case of an NO-rich environment. For this case, our representative species is in the trans-configuration and thus we also present here the catalyzed change in conformation for the sake of completeness. Starting from the cis-conformation (ST 8f), this change is achieved by proton transfer of the molecule with the catalyst (TS 6f) leading to the trans-HNNO (ST 9f). The activation energy is $E^\ddagger = 2.9$ kcal/mol and the energy profile indicates that the trans-state is slightly favorable. Nevertheless, it can be concluded that both conformers are present in the system not only as products from similar reaction pathways but also due to the presented conformational change. The subsequent investigation of the reaction of trans-HNNO with NO is started from a state where nitrogen oxide is adsorbed on the Brønsted acid and HNNO forms a hydrogen bond with the catalyst (ST 10f). Then, the crossing of the seam of the two PESs with $M_S=3$ to $M_S=1$ takes place via SEAM 1f and the N-N distance of NO to HNNO reduces from 2.870 Å to 1.868 Å (ST 11f). This process is activated by $E^\ddagger = 5.6$ kcal/mol. Finally, a proton transfer between

the molecules and the catalytic surface leads to the formation of nitroxyl and N_2O (ST 12f), by overcoming an energy barrier of $E^\ddagger=11.3$ kcal/mol (TS 7f).

A comparison of the energy profiles of the three branches for the decay of HNNO reveals that the reaction with nitroxyl has to be considered as the most favorable due to its nearly barrierless character, but also the self reaction of HNNO is catalyzed by the H-ZSM5. Although the energy barriers for the reaction with NO are slightly higher, this reaction still has to be taken into account, especially in the view of the motivation for this branch, an NO-rich environment.

5.3.4 Reaction of Nitroxyl with Nitrous and Nitric Acid

In the preceding chapter 4 nitrous and nitric acid have been shown to be key intermediates in the SCR of nitrogen oxides with ammonia on H-ZSM5. Because of the high reactivity of nitroxyl this species might significantly influence the reaction pathways of the fast and the NO_2 -SCR by reacting with its intermediates. Thus, we present here the potential impact of nitroxyl on the two acids with the energies shown in Figure 5.4 and the corresponding structures in Figure C.9 and C.10.

For the case of the reaction of nitrous acid with nitroxyl the mechanism starts with the adsorption of trans-HONO and an energy of adsorption of $\Delta E_{\text{ads}}=-11.5$ kcal/mol. The following coadsorption of HNO (ST 1a, Figure C.9) with $\Delta E_{\text{coads}}=-3.4$ kcal/mol indicates a rather loose state. In the subsequent reaction step, the Brønsted acid protonates the hydroxyl group of the nitrous acid and the HO-NO bond is broken. At the same time, the nitroxyl releases its hydrogen to restore the catalytic surface and forms N_2O_2 together with the released NO^+ . This process via TS 1a exhibits an energy barrier of only $E^\ddagger=1.0$ kcal/mol indicating a fast reaction between the coadsorbed reactants. It is exothermic by $\Delta E=-17.0$ kcal/mol. In the resulting product state, water is bond to two framework oxygen with its hydrogen and the N_2O_2 is hydrogen-bonded to the Brønsted acid and stabilized by the adsorbed water. Furthermore, we considered the decomposition of the N_2O_2 in the coadsorbed state via SEAM 1a including the crossing of PES from $M_S=1$ to $M_S=3$. Here we calculated a barrier of $E^\ddagger=3.0$ kcal/mol that reveals that the dimer is very likely to decompose right away. A minimization on the PES with $M_S=3$, starting from the SEAM 1a, leads to ST 3a in which the two NO still are coadsorbed with the water. Nevertheless, this has to be considered a non-stable state because the desorption of one of the NO directly leads to the reorientation of the water molecule by pushing the remaining NO off the Brønsted acid to which it then bonds (compare ST 6a, Figure

B.14). This adsorption state is significantly more stable for water, thus, the desorption of the two NO appears in the energy profile to be exothermic by $\Delta E_{\text{des}} = -4.3$ kcal/mol. In the case of the corresponding gas phase reaction with nitrous acid in the trans-configuration a hydrogen transfer from the HNO to the hydroxyl group of the nitrous acid (TS 1ag) leads to water and N_2O_2 (ST 2ag). This step exhibits an energy barrier of $E^\ddagger = 17.8$ kcal/mol and it can be concluded that the catalyst tremendously enhances this reaction. The subsequent decomposition of N_2O_2 was then in turn found to be nearly barrier less with $E^\ddagger = 0.07$ kcal/mol via SEAM 1ag leading to two NO and water (ST 3ag). For the dehydration of trans-HONO with HNO, Lin et al.¹⁹¹ found a transition state with an activation energy of only $E^\ddagger = 11.3$ kcal/mol at the B3LYP/6-311⁺⁺G(d,p) level of theory. Nevertheless, this still implies a reduction of the activation energy by one order of magnitude due to the catalyst.

For the reaction of nitroxyl with nitric acid the mechanism starts with the exothermic adsorption of HNO ($\Delta E_{\text{ads}} = -9.1$ kcal/mol; Figure C.3, ST 0) and the coadsorption of HNO_3 with $\Delta E_{\text{coads}} = -7.2$ kcal/mol to the free framework oxygen by forming a hydrogen bond (ST 1b, Figure C.10). Then the hydroxyl group of the nitric acid is protonated by the Brønsted acid, inducing the cleavage of the internal HO- NO_2 bond (TS 1b). This process exhibits an energy barrier of $E^\ddagger = 20.8$ kcal/mol and then leads to the recycling of the Brønsted acid as the nitroxyl releases its proton. Furthermore, the formed water reorientates on the surface by forming a hydrogen bond with the restored Brønsted acid while the released NO_2 and NO combine to ct- N_2O_3 , loosely bond to the adsorbed water (ST 2b). This step is exothermic with $\Delta E = -29.6$ kcal/mol and, thus, the reverse reaction can be neglected. For the subsequent decomposition of the ct- N_2O_3 we found an activation energy of $E^\ddagger = 10.7$ kcal/mol corresponding to the adsorbed state (SEAM 1b). In comparison, the desorption of the ct- N_2O_3 needs an energy of $\Delta E_{\text{des}} = 6.1$ kcal/mol and the gas phase decomposition is activated by $E^\ddagger = 7.6$ kcal/mol. The catalyst does not enhance the decomposition of the dimer structure and it seems more likely, that first the N_2O_3 desorbs to the gas phase prior to its decomposition. The comparison of the two reactions reveals that the nitrous acid is rapidly consumed by nitroxyl, while the nitric acid is considerably more stable. Nevertheless, in the context of nitroxyl being mainly produced within the SCO, which is only of relevance at elevated temperatures, it can be assumed that also the barrier for the reaction of HNO with HNO_3 is easily surmounted.

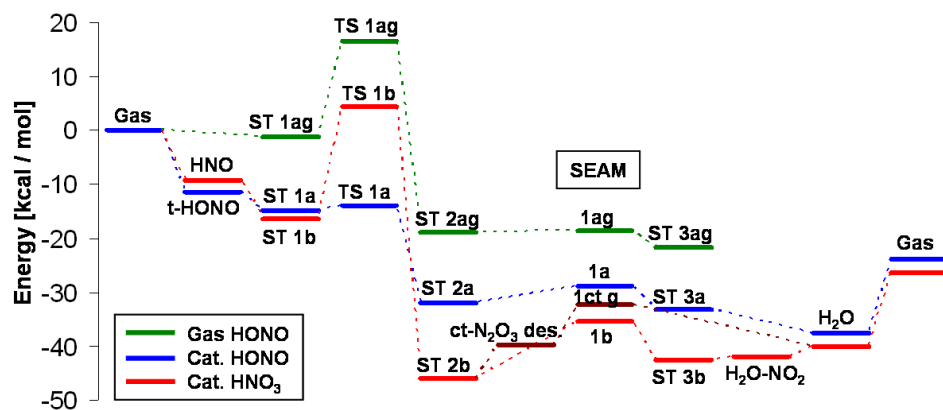


Figure 5.4: Energy profiles for the reaction of HNO with trans-HONO and with HNO_3 , comparing the catalyzed and the gas phase mechanism. Energies are zero-point corrected.

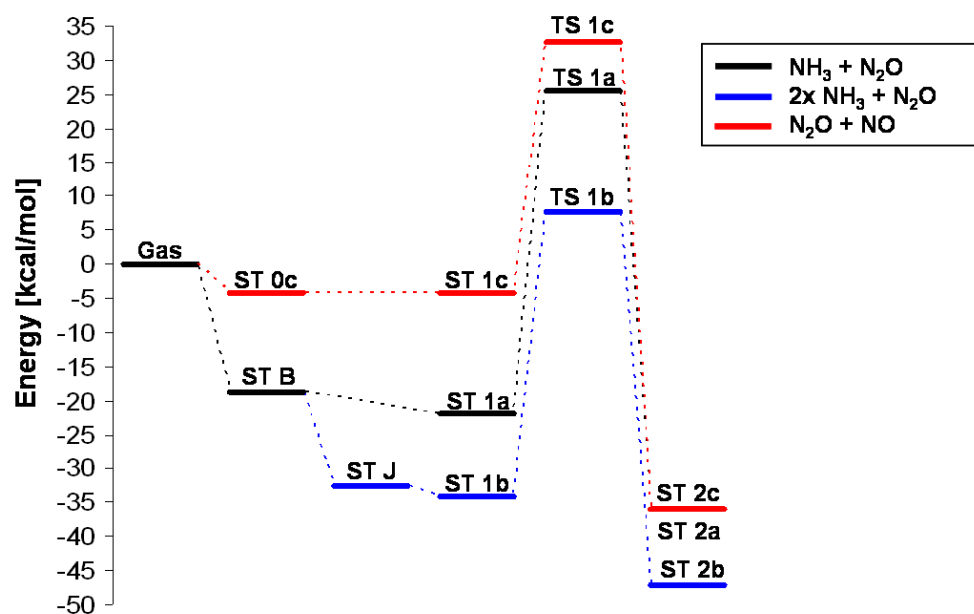


Figure 5.5: Energy profile for the decay of N_2O , comparing the reaction with one and with two adsorbed ammonia molecules and with NO . Energies are zero-point corrected.

5.3.5 Pathway for N₂O

Within the experimental literature N₂O is mentioned to occur in traces only during the SCO of ammonia indicating either that none is produced or that there is a pathway, reducing it to nitrogen. From the so far presented mechanism several reaction branches are potential sources of N₂O and have to be considered to be of relevance. On the other hand, it is known that under certain operation conditions of the SCR significant amounts of N₂O are observed, indicating that the H-ZSM5 is far less active for the SCR of N₂O with ammonia, if at all, than for the SCR of NO. Thus, we investigated the potential reactions of N₂O with ammonia, also considering two adsorbed NH₃ molecules as starting point and the reaction with NO to deal with the question whether there is a potential sink for N₂O in the system. The structures are displayed in Figure C.11 and the corresponding energy profiles are shown in Figure 5.5.

In the first case, we considered the direct reaction of N₂O with adsorbed NH₄⁺ and the starting point is ST B (Figure 4.2). In the subsequent coadsorption of N₂O the oxygen of the latter species slightly interacts with one ammonium hydrogen (ST 1a). Then, the NH₄⁺ is "pushed off" the catalyst into the more active coordinated state, forms a bond with the N₂O oxygen, which is released and takes up the catalyst hydrogen to form NH₃OH⁺ (ST 2a). The molecular nitrogen is directly released to the gas phase. The barrier for this reaction was calculated to be E[‡]=47.5 kcal/mol (TS 1a), indicating that the probability for this reaction to proceed is very low.

As for the reaction of ammonia with oxygen we also examined the potential benefit of two coadsorbed NH₃ (ST J, Figure 4.2) molecules as a starting point for the reaction with N₂O. Again, the oxygen of N₂O slightly interacts with one ammonium hydrogen. Then, the hydrogen bond between the two NH₃ molecules is opened and the coordinated ammonia takes up the oxygen of N₂O, releasing molecular nitrogen to the gas phase. Furthermore, the ammonium releases one hydrogen to the oxygen (TS 1b), leading to NH₃OH⁺ coadsorbed with NH₃ (ST 2b). The barrier in this case is E[‡]=41.8 kcal/mol and thus is slightly lower than for the first case with only one ammonia. A comparison of the energy barriers with those of the reaction of ammonia with oxygen reveals that the reduction of N₂O might play a minor role within the SCO. Compared to the energy barriers within the SCR of NO, on the other hand, these two reactions are negligible.

Finally, we investigated the potential reaction of N₂O with NO, leading to NO₂ and nitrogen. The pathway is started with the adsorption of N₂O ($\Delta E_{\text{ads}}=-4.2$ kcal/mol), where the oxygen of the molecule interacts with the

Brønsted acid (ST 0c). In the next step NO is added to the system, but from the corresponding energy profile it can be concluded that it does not interact with the N_2O and thus can be considered as a gas phase species (ST 1c). Then, NO takes up the oxygen of N_2O which becomes molecular nitrogen that is released to the gas phase and adsorbed NO_2 remains on the surface (ST2c). This process via TS 1c exhibits an activation barrier of $E^\ddagger=36.9$ kcal/mol and is thus the lowest within the investigated pathways for the decay of N_2O . Nonetheless, it has to be taken into account that N_2O adsorbs only weakly on the surface in comparison to ammonia, indicating that this reaction is not necessarily more favorable than the one with ammonia. Furthermore, as is the case for the reaction with NH_3 , this reaction cannot be considered as a significant sink for N_2O in the SCR reaction network.

In summary, from the presented results it can be concluded that the decay of nitroxyl and hydroxylamine are catalyzed by H-ZSM5 leading to different branches that are all accessible, depending on the availability of the reactive gas phase species. For the self-reaction of HNO two energetically similar pathways compete against each other leading either to N_2O or via the radical HNOH to hydroxylamine by releasing two NO. This result is in accordance with the experimental finding that in the SCO of ammonia on H-ZSM5 the main side product is NO. Furthermore, nitroxyl spontaneously forms with NO the intermediate structure $\text{H}(\text{NO})_2$ which reacts with a second NO, leading to the formation of nitrous acid. Thus, produced NO within the SCO can readily be consumed by another pathway but also by the complex reaction network of the SCR. For hydroxylamine, the reaction pathways with nitroxyl or NO are accessible as well, whereas a slight benefit for the first one can be concluded from a lower energy barrier. As the Brønsted acid showed a high activity for the decay of nitroxyl and hydroxylamine, these reaction mechanisms might also play a significant role in the SCO of ammonia in ion-exchanged zeolites like the Fe/H-ZSM5 because of the remaining Brønsted acids in these catalysts. The direct oxidation of adsorbed ammonium can be considered as the rate limiting step in the mechanism. The result is in accordance with the experimental findings that H-ZSM5 is not very active for the SCO and its relevance has to be seen more in the context of the SCR. The consideration of two coadsorbed NH_3 molecules prior to a gas phase attack of oxygen slightly reduced the activation energy. The reaction of N_2O with NH_3 can be concluded to be of no relevance in the view of the SCR of NO due to the high activation energies. Only within the presented reaction scheme for the SCO it might be of at least minor importance as the activation

barriers for the reaction of oxygen with NH_3 reside in the same range. In Figure 4.3 the complex reaction network of the SCO as it was investigated and presented is pictorially summarized together with the mechanism of the SCR.

5.4 Conclusion

The complex network of the selective catalytic oxidation of ammonia on H-form zeolites was investigated using the density functional theory. The reaction mechanism can be subdivided into three parts. The first one is the direct reaction of NH_3 with oxygen, the second is the decay of HNO and the third one is the decay of hydroxylamine (NH_2OH). Within each main part, several branches have been examined as can be obtained from the schematic of the reaction network 4.3. All mechanisms have been studied on a cluster of 5 T-atoms, and the crossing of PESs was considered, if necessary. It was shown that the reaction of ammonia with oxygen either leads to the intermediate nitroxyl or directly to hydroxylamine, whereas both pathways exhibit high energy barriers, indicating that this first part of the mechanism is the rate determining step. For part two, it was demonstrated that the H-form zeolite is highly active for the decay of nitroxyl in either a self-reaction or in the reaction with NO, offering several energetically similar and thus accessible pathways. Also for the decay of hydroxylamine several pathways are accessible for the reaction with either nitroxyl or NO, leading to a highly cross-linked reaction network. Finally, it was shown that H-ZSM5 exhibits only low activity for the reactions of N_2O with NH_3 and NO, indicating their minor relevance within the SCO. Thus, we have presented the complex reaction network of the SCO that accounts for several experimentally observed phenomena.

6

Microkinetic Modeling of the Fast Selective Catalytic Reduction of Nitrogen Oxide with Ammonia on H-ZSM5 Based on First Principles

The reaction mechanism of the fast selective catalytic reduction (SCR) of NO_x on H-ZSM5 has been investigated by means of a microkinetic model based on the DFT calculations presented in chapters 4 and 5. The conversion of NO_x as calculated with our model is in good agreement with experimental data over a wide range of temperature. Reaction path analysis reveals that the activity of the H-ZSM5 for the fast SCR is based on the reaction sequence via $\text{Z}^- [\text{NO}_x]^+$, from the decomposition of N_2O_y and the additional subsequent decomposition of nitrous and nitric acid on void Brønsted acids. The NO_x^+ species then react with ammonia to nitrosamine or nitramide which further decompose to water and nitrogen and nitrous oxide, respectively. At low temperatures also the reaction of nitrous and nitric acid with adsorbed ammonia takes place. Ammonia is concluded to block the active sites at low temperatures while thermodynamic limitations of the equilibrium of the surface species N_2O_y are responsible for the decrease in the conversion of the fast and the NO_2 SCR at high temperatures. Finally, the oxidation of ammonia was found to exhibit only a minor impact on the fast SCR at the applied reaction conditions.

6.1 Introduction

Nitrogen oxides (NO , NO_2), which are mainly produced in the combustion of fossil fuels, are significant air pollutants and stringent emission standards have been legislated to regulate exhaust gases.^{27,28} The selective catalytic reduction (SCR) with ammonia or hydrocarbons has proven to be an effective technology for the abatement of NO_x and has been in the focus of researchers for the last two decades.^{31–33} In particular metal-exchanged zeolites like the Fe/H-ZSM5 were found to exhibit a high activity for this reaction.³⁴ The boosting effect of NO_2 upon addition to the reactant gas^{38,168,169} or via a preoxidation step within the SCR converter was a crucial finding in the ammonia SCR. The highest conversion is obtained with a NO_2/NO_x ratio of 50% which is known by now as the “fast”-SCR. Dosing a ratio above the 50% results in a slightly reduced activity and an increased selectivity to unwanted N_2O . The “ NO_2 -SCR”¹⁷⁰ marks the outer boundary with only NO_2 in the reactant gas. Furthermore, metal-exchanged zeolites were also found to exhibit a significant activity for the selective oxidation of ammonia (SCO),^{42,43,217,218,231} which has to be considered a side reaction of the SCR. However, based on the usual preparation from ion exchange to a parent H-form zeolite, the final catalyst usually exhibits two different active sites, the exchanged metal and the Brønsted acid. Brandenberger et al.³⁴ even stated an amount of at least 30% of the latter one. While the standard SCR is known to be much slower on the H-form zeolites than on the iron-exchanged catalyst, a significantly high activity was observed for the fast^{37,38,153,156,157} and the NO_2 -SCR.¹⁴⁵ Also for the SCO a significant activity was observed on the Brønsted acid sites.^{217,221} Thus, the question regarding the influence of the Brønsted acids in iron-exchanged zeolites has kept high attention amongst researchers. Yang and Long¹⁵⁶ attributed the main SCR reaction to the Brønsted acids only. Though in disagreement with this conclusion, Brandenberger et al.¹⁷² and Grünert et al.¹⁷¹ attributed an at least promoting effect of the Brønsted acid to the activity of the catalyst. This is, according to Akah et al.,⁴² also true for the SCO. Thus, in order to understand the mechanisms of the reactive H/N/O system in iron-exchanged zeolites, analysis of important elementary steps on both active sites, the iron and the Brønsted acid, is crucial. For the H-form zeolite we have presented in chapters 4 and 5 a reaction network for the SCR using density functional theory (DFT) that qualitatively accounts for most experimentally observed phenomena (see Figure 4.3) for both the SCR and the SCO. Nevertheless, only a direct comparison of the theoretically derived mechanisms with experiments allows for a final conclusion of the relevant pathways. Microkinetic

modeling has been applied extensively with success in order to provide insight into the mechanisms of several heterogeneous catalyzed reactions.^{23,143,256–259} Results from first principles methods like DFT can be used to provide the required parameters for a kinetic model which then closes the gap between microscopic and macroscopic quantities. The goal of this work is to establish a microkinetic model based on the results of the chapters 4 and 5 and to probe all elementary steps of the system in a reactor simulation. In comparison with experimental data, this analysis is supposed to provide significant insight into the governing elementary steps of the combined SCR and SCO system on H-ZSM5 and with that to allow for suggestions on interactions of intermediates in the ion-exchanged zeolites in further studies.

6.2 Theory

As the representation of the active site a cluster of 5 T-atoms was used for the screening of the reactive H/N/O system. In order to include, at least to a certain extent, the influence of the pore structure on the reactants and products, energy minimizations were executed for selected species of the complete reactive system on a 23 T-sites containing portion of the catalyst (Figure 6.1) at the B3LYP/TZVP level of theory. From Table D.2 it can be obtained that the impact of the larger cluster on the electronic energy as compared to the 5 T-atoms containing cluster is only relevant if ammonia, water or hydroxylamine is present. The CBS-QB3 level of theory was applied with Gaussian 03⁹³ in order to obtain sufficiently accurate heats of formation for those gas phase intermediates for which no reliable experimental data were available. For the microkinetic modeling, CHEMKIN^{140,141} was employed. The required thermodynamic parameters of the species and the kinetic parameters for the reactions were derived according to standard statistical thermodynamics^{19,61} and transition state theory¹³⁷ on the basis of the DFT results, as outlined in chapter 3. For the ad/desorption processes the theory of absolute rate¹³⁷ was applied for the desorption, assuming the barrier to be equal to the zero-point energy (ZPE) corrected energy difference between the adsorbed and the desorbed state. This implies a barrierless adsorption for which the rate is obtained from the equilibrium constant and the rate of desorption. Such an approach, which relies on the idea of transition state theory, neglects any difference in entropy of the adsorbed state and an assumed transition state of desorption. This, however, can result in a significant underestimation by several orders of magnitude in the pre-exponential factor for loose transition states as outlined by Chorkendorff and Niemantsverdriet.⁸ Assuming that transition states of desorption are rather loose in the case of physisorption,

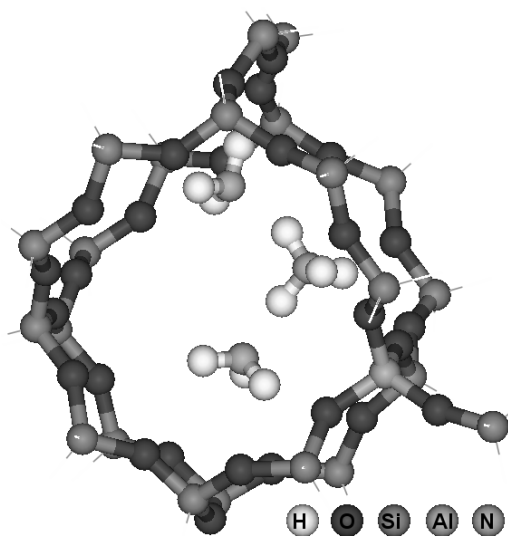


Figure 6.1: T23 cluster model of the acid site in the intersection of a straight and a zig-zag pore of H-ZSM5 with three coadsorbed ammonia molecules. Dangling bonds are not shown.

the corresponding rates of mechanistic relevant steps can be expected to require significant fine tuning. Nevertheless, this approach is expected to yield reasonable first estimates for the model.

The harmonic approximation was applied and contributions for the translational, rotational, vibrational and electronic partition function were considered for all gas phase species while for the zeolite cluster only the vibrational and electronic contributions were included. Enthalpy, entropy and the heat capacity were simultaneously fitted to the in CHEMKIN required seven-parameter polynomial (compare section 3.4) for all species using the algorithm of Spitzer et al.¹⁴² In order to calculate rates for the crossing of PESs, adaptations to adiabatic TST can be used.^{55,109} According to Harvey,⁵⁵ the calculation of the thermal rate constant can be calculated, in good approximation, as the product of a mean probability of surface hopping and a hypothetical adiabatic rate constant resulting from a transition state with the same relative energy and properties of the MECP. While translational and rotational contributions are directly related to the structure of the MECP, the evaluation of the vibrational contribution to the partition function requires the calculation of an effective Hessian as described in section 3.3, equation (3.28). The surface thermally averaged hopping probability can be calculated from the Landau-Zener theory.¹³⁹ However, because the direct comparison

of calculated and experimentally measured reaction rate constants for the decomposition of N_2O_3 and N_2O_4 in the gas phase revealed that the theoretically derived pre-exponential factors of the Arrhenius equation are rather too low, even without the hopping probability, we set the latter in all cases equal to 1. Furthermore, it is known that the accuracy of DFT in the calculation of relative energies as well as for reaction barriers is limited,⁸⁸ usually allowing only for a qualitative analysis of reaction pathways. According to Gokhale et al.,²⁵⁹ DFT can capture the essential aspects of the surface chemistry but fine-tuning usually needs to be done to obtain a reliable microkinetic model. Even though there are quantum chemistry techniques that can provide nearly quantitative results for intrinsic reaction steps, as recently shown by Hansen et al.²⁶⁰ their application to reactive systems with a large number of elementary steps is not feasible because of the high computational costs. To obtain reliable heats of formation of the surface species, the values were anchored to the gas phase species thermochemistry. This was done by relating the heat of formation of the surface species to the corresponding heat of adsorption of a gas phase species on the empty active site. For the latter, the heat of formation was set to $H_f=0$ (denoted as HZSM5 in the thermodynamic database D.4). Because the heat of formation of the gas phase species is, in the best case, experimentally measured or at least calculated with high level methods, inaccuracies in the surface reaction enthalpies, which are computed with the lower DFT level, can be corrected to a certain extent. Furthermore, it is known that the generalized gradient approximation (GGA) functionals in DFT do not include the long-range electron correlations responsible for van der Waals forces. Grimme²⁶¹ has calculated parameterizations for a DFT-D approach to include damped atom pair-wise dispersion corrections of the form C_6R^{-6} for several functionals. To correct the heats of adsorption, we have applied this scheme to all surface species using the results from the 23 T-site containing cluster as far as available and approximated values for the remaining species based on the comparison of the T5 vdW contributions. This was done by either assigning the same vdW values for similar structures, by adding a T23-T5 vdW difference or by adding a T5 contribution to a reference state for which a T23 contribution is available. The applied method is documented for all species in Table D.1. This is a compromise between accuracy and computational costs for the calculations on the larger cluster. Finally, a common assumption for the adsorption is the complete loss of the rotational and translational degrees of freedom of the adsorbate being transferred into vibrational degrees. While this is reasonable for small molecules in chemisorption in the case of physisorption it might lead to a significant underestimation of the entropy of adsorption. A potential technique to overcome this problem is the reassignment of restricted translational and

rotational degrees of freedom in exchange of the corresponding vibrations. Dumesic et al.²⁵⁹ proposed a restricted translation in terms of surface diffusion. Reyniers et al.²⁶² reassigned contributions of the rotation in a zeolite by including the principle moments of inertia representing the as free considered motion of the corresponding gas phase species. For translation, a movement within a plane perpendicular to the active site was considered. The size of this plane was related to a certain extent to the pore diameter and to the size of the zeolite cages. We used the methodology of Reyniers et al.²⁶² to obtain an order of magnitude estimate for entropy corrections for species which are rather loosely adsorbed or coadsorbed. This affects mainly N_xO_y species as well as HNO_z coadsorbed to NO_x^+ (see Table D.1). The applied values are based on calculations for physisorbed NO_2 and asymmetric N_2O_4 for which we obtained entropy corrections $\Delta S_{trans}=3.8$ cal/mol/K and $\Delta S_{trans}=6.6$ cal/mol/K for the 2D translation on a surface of $A^0/N_A=700\text{pm} \times 700\text{pm}$ and $\Delta S_{rot}=3.1$ cal/mol/K and $\Delta S_{rot}=5.6$ cal/mol/K for a 1D rotation at 600K. It should be noted that according to Cramer¹⁹ the exchange of vibrational frequencies by restricted translations or rotations should also affect the contribution to the enthalpy. A low frequency which represents the harmonic oscillator approximation of a frustrated translation or rotation results into a contribution of RT , but the contribution of a free translation or rotation contributes only $0.5RT$ per degree of freedom. Thus, at a temperature of 600K, the exchange of four degrees of freedom leads to an underestimation of the heat of adsorption of $\Delta E=2.4$ kcal/mol. With that, also the assigned heat of formation of the corresponding surface species is affected. Though this value is not significant at first glance it might have a great impact in the case that the overall reaction exhibits a high sensitivity on such an intermediate. Thus, this energy contribution can also be taken into account in the fine tuning of a microkinetic model. Despite the discussed potential corrections that can be applied to improve the model, the uncertainties of the electronic energy as calculated from DFT still remain and with that the rather qualitative nature of the values. Nevertheless, significant insight into the mechanisms of the reactive H/N/O system can be obtained from such an approach.

6.3 Results and Discussion

In this section we compare the results obtained from the microkinetic model with the experimental literature. Reactor simulations were performed in an ideal plug flow reactor with the catalyst being evenly distributed. The number of active sites was calculated based on the mass of the catalyst and its

Si/Al ratio, assuming that the number of aluminum atoms is equal to the number of active sites. The thermodynamic database of the gas phase species in CHEMKIN was obtained either from the database of the Gas Research Institute²⁶³ or created from experimental heats of formations from the literature^{264,265} in combination with calculated contributions from translation, rotation and vibration for the temperature effect. For other gas phase species, for which no experimental values were available, the heats of formation were calculated from related heats of reaction obtained with the CBS-QB3 method. The values of all gas phase species are listed in Table 6.1. For the surface species the heat of formation can be obtained from the thermodynamic data (Table D.4). The reference states for the definition of the heat of formation of the surface species and the calculated corrections are listed in Table D.1. In the column denoted with “extra” the adjustments of the heat of formations within the accuracy of the DFT are stated. The reaction rates of all reversible elementary steps are listed in Table D.3 for the applied direction. All adjustments on the activation energies and pre-exponential factors are stated as “Adjust”.

The subsequent discussion is subdivided into the adsorption of ammonia, the NO₂-SCR, the fast SCR and the oxidation of ammonia.

6.3.1 Adsorption of Ammonia

It is well known that ammonia strongly adsorbs on Brønsted acids by forming ammonium ions.²⁰³ While this is assumed to block the oxidation of NO to NO₂ in the standard SCR,¹⁷⁵ it similarly might also inhibit the fast and NO₂-SCR, depending on the accessed pathways. Therefore, it is expected that the adsorption of ammonia has a significant impact on the reactivity of the SCR. We considered the adsorption of ammonia in three layers in terms of, first, the formation of the ammonium ion NH₄⁺ with a Brønsted acid and, then, the coadsorption of two further ammonia molecules. Based on the implementation of the kinetics of elementary steps in CHEMKIN, the ammonia adsorption is described as a Langmuir type isotherm.

$$a_{NH_3} \left[\frac{mmol}{g} \right] = \frac{K_1 p_{NH_3} + 2K_1 K_2 p_{NH_3}^2 + 3K_1 K_2 K_3 p_{NH_3}^3}{1 + K_1 p_{NH_3} + K_1 K_2 p_{NH_3}^2 + K_1 K_2 K_3 p_{NH_3}^3} \cdot Sites \left[\frac{mmol}{g} \right] \quad (6.1)$$

The isotherm reflects the steady state behavior of the microkinetic model for the ammonia adsorption in the absence of any reaction. Because of its potentially strong impact on the SCR, we analyze here whether the enforced mathematical description of the adsorption in CHEMKIN is capable to describe ammonia adsorption experiments.

Table 6.1: Heat of formation of gas phase species.

	H_f^0 [kcal/mol]
NH ₃	10.97 ^a
NO	21.56 ^b
NO ₂	7.91 ^c
N ₂ O	19.60 ^b
H ₂ O	-57.80 ^a
HNO	23.80 ^c
t-HONO	-18.34 ^c
HNO ₃	-32.10 ^c
NH ₂ OH	-11.19 ^d
NH ₂ NO	17.79 ^d
NH ₂ NO ₂	0.35 ^d
as-N ₂ O ₃	19.80 ^c
ct-N ₂ O ₃	30.25 ^d
sym-N ₂ O ₄	2.19 ^b
as-N ₂ O ₄	9.13 ^d
c-HNNO	53.66 ^d
NH ₄ NO ₂	-38.29 ^d
NH ₄ NO ₃	-55.36 ^d
H ₂ NO	11.21 ^d

^a Taken from ref. [263]^b Taken from ref. [264]^c Taken from ref. [265]^d Calculated with CBS-QB3

In Figure 6.1 the threefold ammonia coadsorption is shown on an intersection of the straight and the zig zag pore of the zeolite, including a framework aluminum. This is in accordance with the experimental literature in which adsorption sites are correlated to the aluminum content^{266,267} of the zeolite and a layer-by-layer adsorption is suggested^{268–272} as is applied here. The experimental heat of adsorption (144–158 kJ/mol,^{273,274} 150 kJ/mol,^{275,276} 145 kJ/mol,²⁶⁷ 128 kJ/mol²⁷¹) is in reasonable agreement with our calculated value (137 kJ/mol) for the ammonium ion formation. Furthermore, Dumesic et al.²⁷⁵ and Gorte et al.²⁶⁷ both found a sharp drop in the heat of adsorption (to 70 kJ/mol and 85 kJ/mol, respectively) with increasing coverage of ammonia on the surface above a certain limit prior to which the heat

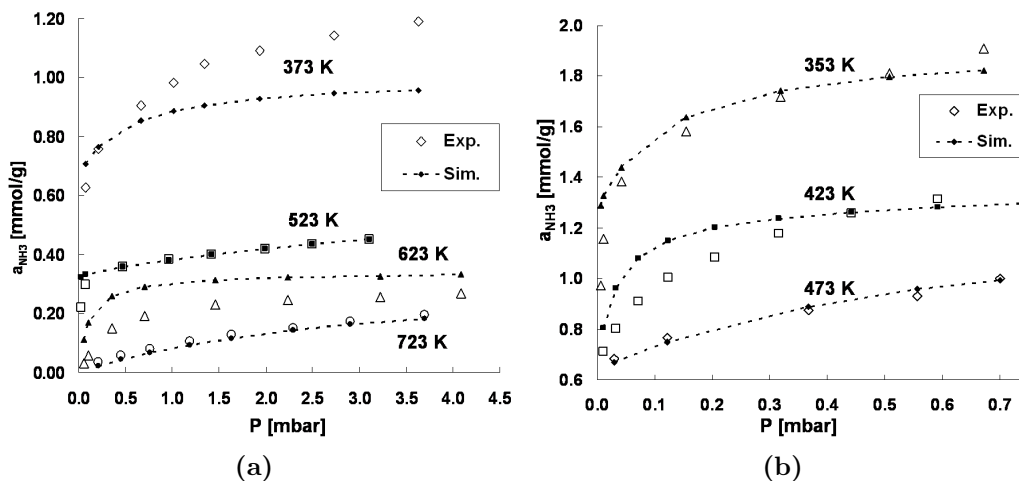


Figure 6.2: Comparison of simulated and experimentally measured adsorption isotherms of ammonia on H-ZSM5. Data in a) corresponds to reference [268] and in b) to reference [276].

remains rather constant. Gorte et al. have correlated this limiting coverage to the number of Brønsted acids available in the catalyst and thus with the formed ammonium ions. For the coadsorption of ammonia to the ammonium ion we calculated a heat of adsorption of $\Delta H_{\text{coads}}=100$ kJ/mol for the first and $\Delta H_{\text{coads}}=68$ kJ/mol for the second molecule. These values are in good agreement with the experimental value, and, thus, can explain the reduced heat of adsorption at higher coverages.

In Figure 6.2 a) and b) the adsorption isotherms from two independent experimental studies^{268,276} are compared to our calculated results of equation (6.1). In both sets, reasonable agreement is obtained with only slight modifications in the thermodynamic data. Specifically, we have used a slightly reduced heat of adsorption for the first ammonia ($\Delta H_{\text{ads}}=127$ kJ/mol), in agreement with the value of Bonelli et al.²⁷¹ For the coadsorption of ammonia, the reduction of heat of formations leads to $\Delta H_{\text{coads}}=95$ kJ/mol for the first and $\Delta H_{\text{coads}}=77$ kJ/mol for the second molecule, in reasonable agreement with the experimental data. However, for both isotherm measurements the Si/Al ratio had to be modified to avoid overestimation of the adsorbed ammonia. For the data of Valyon et al.,²⁶⁸ the ratio was modified from 33.4 to 50 and for Auroux et al.²⁷⁶ from 18 to 26. Therewith, our results suggest that, regardless of the overall aluminum content in the catalyst, a significant fraction either does not contribute to the surface acidity (e.g., extra frame-

work aluminum) or is not accessible by ammonia. This finding is supported by the fact that Auroux et al.²⁷⁶ found an amount of 720 $\mu\text{mol/g}$ of strong acid sites from calorimetric measurements, which correlates well with the modified Si/Al ratio of 26, which corresponds to 640 $\mu\text{mol/g}$. Also Brandenberger et al.¹⁷² observed in the SCR a 21% reduced Brønsted acidity in their H-ZSM5 sample, as was expected from the Si/Al ratio. While heterogeneity of the active sites cannot be excluded, according to Datka and Gil,²⁷⁷ most experimentalists report a rather homogeneous acidity of H-ZSM5.^{267,275,276} At low temperatures ($T=373$ K, Figure 6.2 a) the calculated isotherm suggests the potential coadsorption of even a fourth ammonia molecule. However, the isotherms at 473 and 523 K can also be represented by considering only two layers of ammonia per active site and at 623 and 723 K even the ammonium ions are sufficient. Thus, in the SCR the adsorption in up to two layers is relevant at temperatures above 500 K.

6.3.2 Modeling of the NO_2 -SCR

The kinetic modeling of the NO_2 -SCR is compared to the results of Stevenson and Vartuli³⁹ who used a tubular reactor with an inner diameter of 3.49 mm, a volume of the catalytic bed of 0.41 cm^3 and a length of 4.3 cm. 0.019 g catalyst with a ratio of Si/Al=22 were used at a volumetric flow of 1000 sccm. The composition of the reactant gas was 500 ppm of both, NO_2 and NH_3 , in 1% oxygen and He as balance. Conversions at 300, 350 and 400 °C were reported. Regarding the kinetic parameters of the N_2O_4 formation, comparison of the calculated gas phase decomposition of the symmetric isomer with experimental data²⁷⁸ revealed an overestimation of the activation energy by approximately 5 kcal/mol and a low preexponential factor. Therefore, in all cases, the activation energy of the formation or decomposition of N_2O_4 was reduced correspondingly and the preexponential factor was increased by one order of magnitude for both isomers. Our model was tuned further based on sensitivity analysis of all reactions and the heat of formations of all surface species, as described by Saliccioli et al.¹⁴³ and in section 3.4. The sensitive reaction rates and heat of formations (see Tables D.1 and D.3) were manually adjusted within accuracy to capture approximately the conversion of NO_2 at 350 °C. Figure 6.4 shows the conversion of NO_2 and the fraction of active sites occupied by ammonia and the void sites vs. temperature. Very good agreement between the model and the experimental data is observed. Reaction path analysis reveals that the main path entails adsorption of NO_2 on an empty active site followed by the coadsorption of a second NO_2 and the subsequent formation of as- N_2O_4 . The latter decomposes into $\text{Z}^-[\text{NO}]^+$

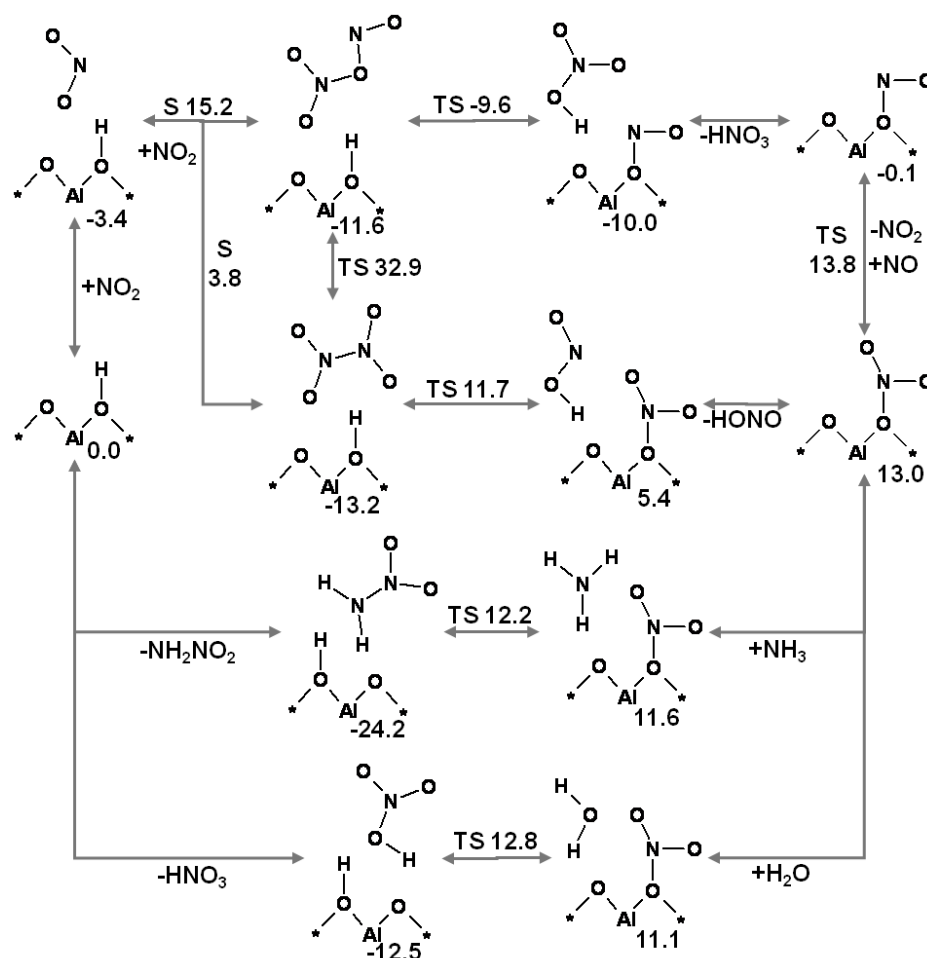


Figure 6.3: Reactive cycle of the NO₂-SCR mechanism including transition states (TS) and minimum energy crossing points (S). Numbers are zero-point-corrected energies relative to the gas phase and the empty catalyst.

and nitric acid, which desorbs to the gas phase. Ammonia then adsorbs to the nitrosyl ion and forms nitrosamine together with the restoration of the Brønsted acid. The nitric acid adsorbs on a free active site and decomposes into $Z^-[\text{NO}_2]^+$ by forming water, which desorbs to the gas phase. In analogy to the nitrosyl ion, ammonia adsorbs on the $Z^-[\text{NO}_2]^+$ and forms nitramide. Nitrosamine and nitramide then decompose into nitrogen and nitrous oxide respectively together with water. The main steps of this mechanism are illustrated in Figure 6.3. A direct reaction of N_2O_4 with the adsorbed ammonium can be neglected over the entire range of temperature. The same

is true for bimolecular reactions of nitric acid. The bimolecular reaction of nitric acid with an ammonium ion, as described in section 4.3.3, only slightly contributes to the decay of the acid at low temperatures. However, a slight reduction of the activation energy of the dehydration step and of the heat of formation of the adsorbed ammonium nitrate leads to a significantly higher contribution of this bimolecular reaction to the reduction of nitric acid up to temperatures of 550 K. Nevertheless, the impact on the overall conversion of NO_2 is negligible. Thus, a significant contribution of this reaction in the NO_2 -SCR mechanism cannot be excluded, but also not proven with our model. Furthermore, under our conditions, the oxidation of ammonia was not found to significantly contribute to the conversion. This somewhat contradicts the observed stoichiometry of Stevenson and Vartuli³⁹ who stated a consumption of about 1.4 mol ammonia per mole NO_2 , which they partially attributed to the SCO. In addition, the lack of the ammonia oxidation in our simulation implies a constant ratio of produced nitrogen to nitrous oxide (equal to one). This is in agreement with the reports of Eng and Bartholomew¹⁵¹ and Busca et al.,¹⁵⁷ but only at 300 °C for the results of Stevenson and Vartuli (they observed a decay of the $\text{N}_2\text{O}/\text{N}_2$ ratio at higher temperatures). This could be due to an additional reaction mechanism relevant in the NO_2 -SCR at elevated temperatures or to the partial decomposition of NO_2 to NO and oxygen, enforced from thermodynamic equilibrium conditions.

From the sensitivity analysis it can be concluded that the rate-limiting step is the desorption of nitric acid from $\text{Z}^-[\text{NO}]^+$ over the entire range of temperature. The dependence of conversion on temperature can be explained based on two main effects. At low temperatures, the reaction is mainly limited by the strong ammonia adsorption, which blocks the active sites. This can be seen in Figure 6.4 where a correlation of the left shoulder of the conversion with the void fraction of active sites is obvious. No other species besides ammonia is present on the surface in significant fraction. The decrease of conversion with elevated temperatures can be traced to the thermodynamic equilibrium of as- N_2O_4 . A partial equilibrium analysis (PE)¹⁴³ over the whole range of temperatures (Figure 6.5) reveals that above 600 K all the steps prior to the rate-limiting nitric acid desorption are in partial equilibrium. The equilibrium surface coverages of the corresponding species vs. temperature show that even though the surface coverage of NO_2 increases up to ~ 750 K, the concentration of the as- N_2O_4 steadily decreases. Accordingly, the concentration of the subsequent intermediate and the reaction rate of the rate-limiting elementary step decrease with increasing temperature.

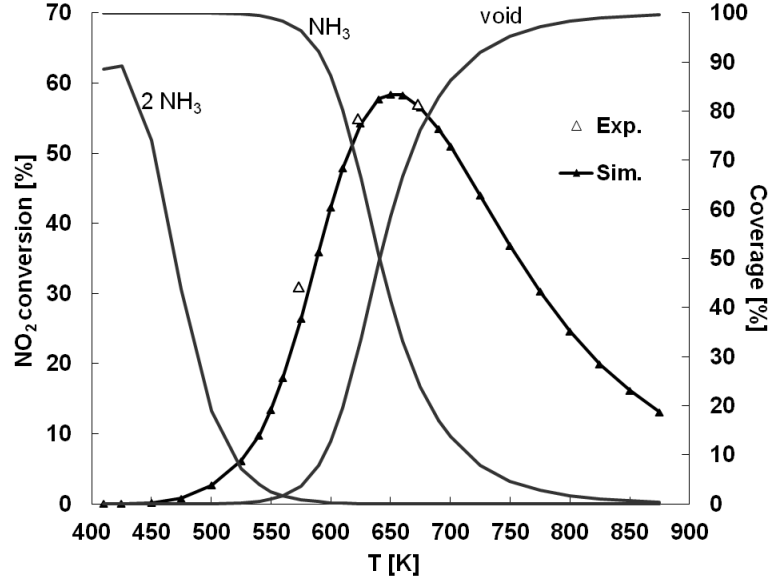


Figure 6.4: Simulated conversion of NO_2 vs. temperature in comparison to data from reference [39]. On the second axis, the coverages of ammonia and the void sites are shown.

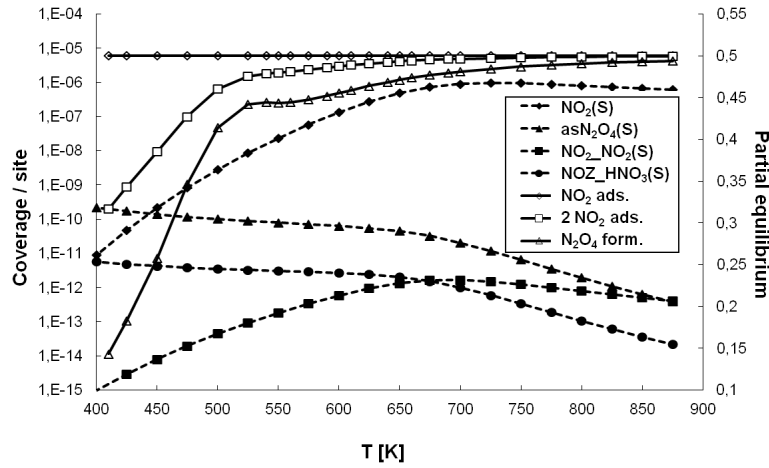


Figure 6.5: Equilibrium fractional coverages per active site of selected surface species in the NO_2 -SCR (dotted lines) at reactor inlet conditions and partial equilibrium conditions for corresponding elementary reaction steps (solid lines).

6.3.3 Modeling of the Fast-SCR

For the fast-SCR we compared our model against the data of Schwidder et al.³⁷ with a tubular reactor of 6 mm inner diameter and an assumed length of 5 cm. The amount of catalyst was 10 mg with a ratio of Si/Al=14 and a flow rate of $Q=183.3$ ml/min. The composition of the reactant gas was 500 ppm NO, 500 ppm NO₂ and 1000 ppm ammonia in 2% oxygen and balance helium. Similarly, as with the NO₂-SCR, comparison of the gas phase decomposition of as-N₂O₃ into NO and NO₂ from experiments²⁷⁸ with our simulations revealed an underestimation of the preexponential factor by an order of magnitude. Thus, we have accordingly adjusted all N₂O₃ decompositions. Further fine-tuning, as described in section 6.3.2, was accomplished without further adjustment of the NO₂-SCR parameters. The resulting model is compared against experimental data in Figure 6.7a). It can be seen that the simulated and the measured conversion curves vs. temperature agree quite well. Yet, our model slightly underestimates at low temperatures whereas above 725 K, the NO₂ conversion significantly deviates. This deviation supports our discussion on an additional reaction step in the NO₂-SCR capable to convert NO₂ without the production of nitrous oxide or the partial decomposition of NO₂ to NO and oxygen. Figure 6.7b) shows the conversion of ammonia in comparison to the combined conversion of NO and NO₂ and the respective experimental data. While in both cases, the fast and the NO₂-SCR require an equimolar conversion of ammonia and NO_x, the combined NO_x conversion curve reflects the ammonia conversion in the absence of its oxidation. Thus, from the deviation of the two curves the influence of the SCO can be seen to be rather small, starting at ~ 600 K. The deviation of the NO_x curve from the experimental data at high temperatures is clearly related to the deviation of the NO₂-SCR described above. It should be noted from Figure 6.7b) that the experimental NO_x conversion is higher than the ammonia conversion over a wide range of temperature. This reflects also the uncertainty in the experimental data set, because even in the absence of the SCO this behavior would require the formation of nitrogen without ammonia which is not plausible at these reaction conditions. To check the influence of a potentially reduced amount of accessible Brønsted acids on the combined NO_x conversion, an additional curve is shown in Figure 6.7b), corresponding to 80% of the amount of active sites derived from the Si/Al ratio. This analysis is done because the ammonia isotherms (section 6.3.1) indicate a reduced amount of Brønsted acids compared to the total aluminum present in the catalyst. The value of 80% is related to the experimentally stated value of Brandenberger et al.¹⁷². It can be seen, that the impact of a reduction of active sites of about 20% on the conversion is small.

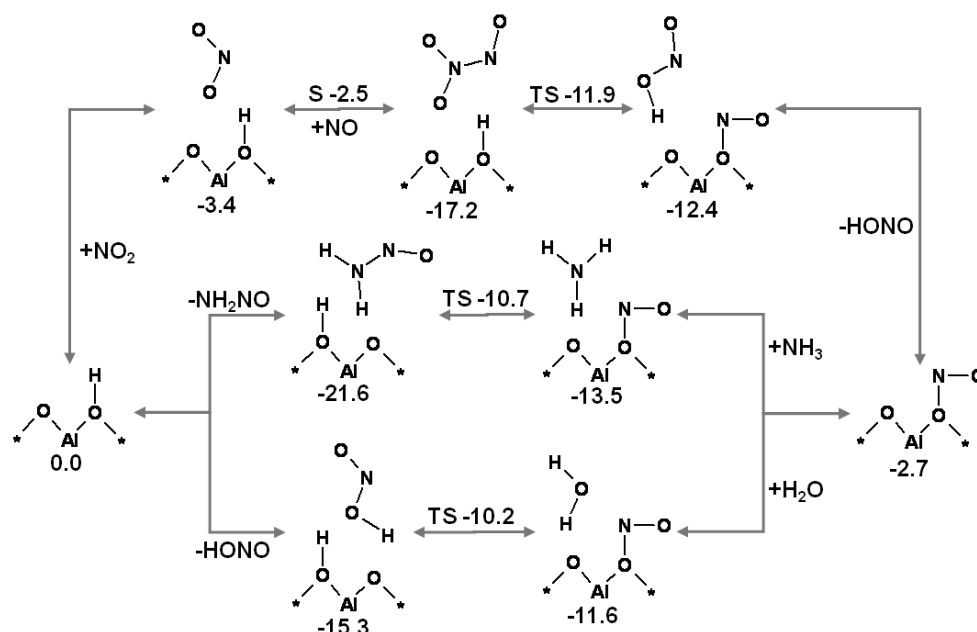


Figure 6.6: Reactive cycle of the fast SCR mechanism including transition states (TS) and a minimum energy crossing point (S). Numbers are zero-point-corrected energies relative to the gas phase and the empty catalyst.

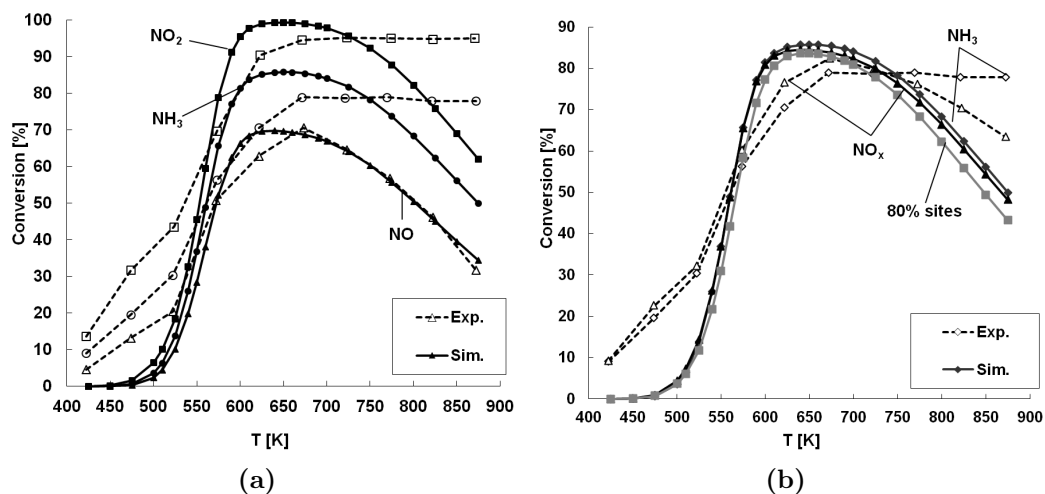


Figure 6.7: a) Simulated conversion of NO, NO₂ and NH₃ vs. temperature in comparison to data from ref. [37]. b) Simulated conversion of combined NO_x and NH₃ vs. temperature in comparison to the data of ref. [37].

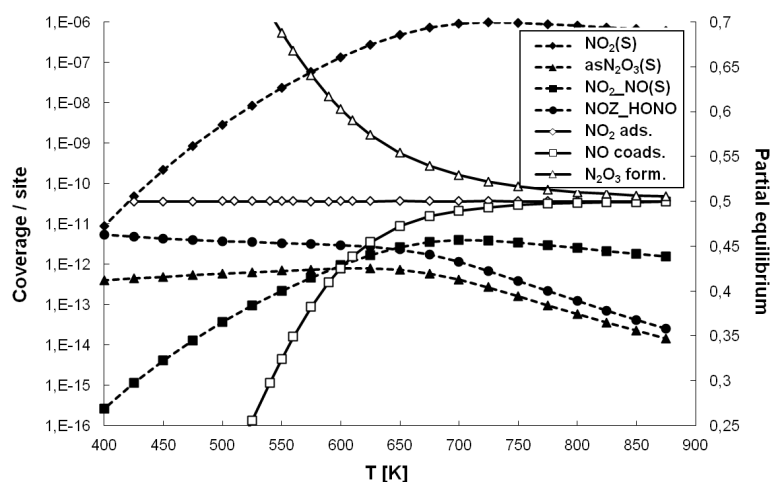


Figure 6.8: Equilibrium fractional coverages per active site of selected surface species in the fast SCR (dotted lines) at reactor inlet conditions and partial equilibrium conditions for corresponding elementary reaction steps (solid lines).

Reaction path analysis indicates that similarly to the NO_2 -SCR pathway, the mechanism proceeds via the adsorption of NO_2 and coadsorption of NO prior to the formation of N_2O_3 . Here, the asymmetric isomer is dominant, though to a certain extent the path via the cis-trans form is accessed, as well. The decomposition of the dimer leads to $\text{Z}^-[\text{NO}]^+$ and nitrous acid, which desorbs. The nitrosyl ion reacts then with ammonia to nitrosamine which decomposes to nitrogen and water. The fate of the nitrous acid is dependent on the temperature. While at elevated temperatures it decomposes on a free active site into the nitrosyl ion and water, at low temperatures, it, at least in part, coadsorbs to an ammonium ion and reacts via ammonium nitrite to nitrosamine and water. The main parts of the mechanism are illustrated in Figure 6.6. In addition, the NO_2 -SCR mechanism, as described in section 6.3.2, also contributes to a certain extent to the conversion of NO_x , but the pathway via N_2O_3 is dominant. The rate-limiting step with respect to the production of nitrogen was found to change with temperature. At low temperatures up to 550 K, the coadsorption of NO to NO_2 prior to the formation of N_2O_3 is limiting. At higher temperatures the desorption of nitrous acid from $\text{Z}^-[\text{NO}]^+$ limits the overall reaction. Furthermore, in the range between 600 and 750 K, the desorption of nitric acid from the nitrosyl ion becomes important, i.e., an increase in the desorption rate causes a reduction of the nitrogen formation. This is obvious in light of this step being rate-limiting for

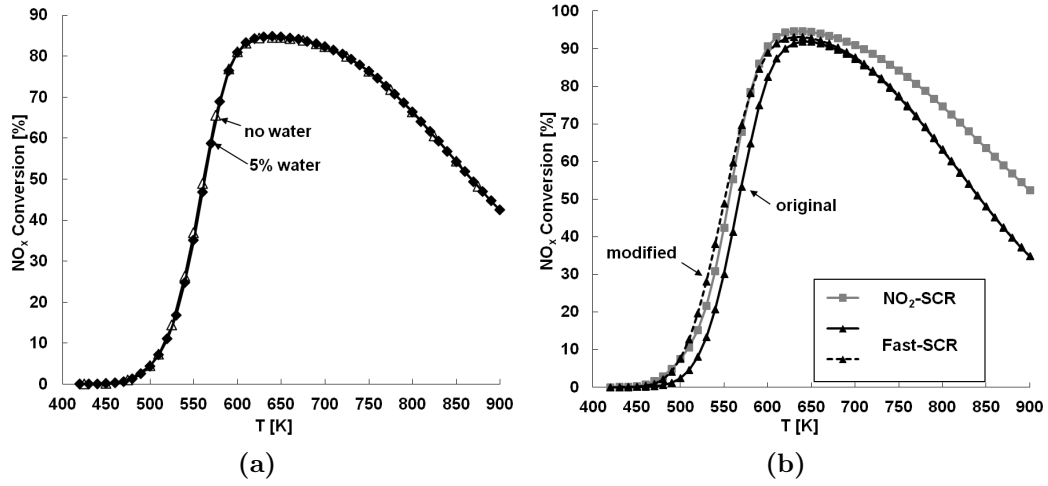


Figure 6.9: a) Influence of 5% water on the conversion of NO_x. b) Comparison of the fast and the NO₂ SCR at equivalent conditions.

the competing NO₂-SCR and given the fact that in this temperature range, NO₂ is nearly completely consumed. Thus, an increase of the NO₂-SCR rate would reduce the fast SCR pathway. The left shoulder of the conversion curve again correlates to the strong adsorption of ammonia, which blocks active sites at low temperatures. At high temperatures, the decreasing conversion is due to the thermodynamic limitation of the N₂O₃ adsorbed on the surface. Similarly to the NO₂-SCR, Figure 6.8 shows that at temperatures above 650 K, adsorption of NO₂, coadsorption of NO and formation of N₂O₃ are in partial equilibrium. The equilibrium concentration of the latter species however, has a maximum between 600 and 625 K after which it decreases and, thus, causes the decrease in overall conversion. Anchored to this observation it appears reasonable to assume that the deviation of the NO₂ conversion is indeed due to the decomposition of NO₂ to NO and oxygen. Because the curvature of the NO conversion is determined from the partial equilibrium it is not expected to change with the NO₂ decomposition. The NO₂ conversion curve in contrast would not be determined by its partial equilibrium condition for the as-N₂O₄ only but also from the rate of decomposition which increases with temperature as the thermodynamic equilibrium shifts towards NO.

In Figure 6.9 a) the influence of 5% water on the conversion of NO_x in the fast SCR is shown and it can be obtained that the impact is negligible. The very slight deviation of the two curves results from an additional blocking of

the active site by water. In Figure 6.9 b) a comparison between the fast and the NO₂ SCR is shown at equivalent conditions (NH₃=NO_x=1000 ppm). For the fast SCR, the elementary steps of the NO₂ SCR have been removed from the model to eliminate their superimposing effect on the conversion and thus to illustrate the activity of the actual fast SCR only. Despite the conclusion drawn from the DFT results and the comparison of the energy diagrams of the two pathways that the fast SCR should be more active than the NO₂ SCR, higher conversions are obtained for the latter. However, by increasing the pre-exponential factor of the rate constant of the coadsorption of NO to adsorbed NO₂ the fast SCR becomes slightly more active than the NO₂ SCR up to the maximum of the conversion curve (dotted line in Figure 6.9 b). It should be noted that within the adjustment of the NO₂ SCR the analog rate of the coadsorption of NO₂ to adsorbed NO₂ was increased as well. Thus, these considerations reflect the qualitative character of our model which only allows for the conclusion that both reactions exhibit a similar activity but not which one is more favorable. For such a conclusion a refinement of the relevant elementary steps with higher order quantum chemical calculations as well as more experimental data for adjustment and validation of the kinetic parameters would be necessary.

In summary of the reaction path analysis for the NO₂ and the fast SCR, it can be concluded that the mechanism, elucidated with our model, combines aspects of several suggestions in the literature for various types of catalysts. The most common sequence of reactions includes the disproportionation of N₂O₄ to nitrite and nitrate and the subsequent reaction of ammonia with these intermediates via ammonium nitrite to nitrogen and via ammonium nitrate to nitrous oxide. The reaction of nitric oxide with a nitrate to nitrite is the key step in the fast SCR. This was suggested by Weitz et al.^{279,280} for Ba-NaY, by Koebel et al.^{146,147} for a vanadium-based catalyst and by Tronconi et al.,^{168,170,281} Kröcher et al.³⁴ and Iwasaki et al.⁴⁰ for Fe-ZSM5. In analogy to these suggestions, we obtained the disproportionation of N₂O₃ and N₂O₄, however, not by forming two acids as would be the case for a reaction with water, but only one acid (nitrous and nitric acid, respectively) together with a nitrosyl ion as balancing charge on the zeolite framework. This is only in agreement with the suggestions of Lavalley et al.¹⁹³. The NO⁺, however, is readily consumed by ammonia to nitrosamine in accord with Richter et al.¹⁵² rather than reacting with water to nitrous acid. The proposed reaction of nitrous or nitric acid with adsorbed ammonia via ammonium nitrite and nitrate was observed to be relevant at low temperatures,

via the additional intermediate formation of nitrosamine for the nitrite, as proposed by Richter et al.,¹⁵² and nitramide for the nitrate. At high temperatures we found the nitrous acid to decompose on a Brønsted acid to nitrosyl, in agreement with Richter et al. and Lavalley et al. and the nitric acid to decompose to NO_2^+ which further reacts with ammonia to nitramide. The suggested reaction of nitric oxide with a nitrate (here nitric acid) was found to not proceed at all. The proposed mechanism by Eng and Bartholomew¹⁵¹ involves the direct attack of nitrogen oxides on adsorbed ammonium ions. This was found not to proceed in our model, although it has to be mentioned that Eng and Bartholomew considered a complex which involves two adjacent occupied active sites. We only considered the reaction on one single Brønsted acid and, thus, the suggestion of Eng and Bartholomew cannot be excluded. Despite the similarities and deviations of our model with the widely suggested mechanism, as stated above, it further has to be noted that these studies mainly refer to ion-exchanged zeolites, or to vanadium-based catalysts. Deriving an analogy or transferring the mechanism to the H-form catalyst is very speculative if one does not want to claim that it mainly proceeds on the same type of site in all catalysts, e.g. the Brønsted acids.

6.3.4 Oxidation of Ammonia

In order to account for the potential influence of the oxidation of ammonia as a side reaction, we have included the SCO reaction mechanism in the discussion on the NO_2 -SCR and the fast SCR. Fine-tuning of this submechanism was carried out by comparing to the data of Akah et al.²¹⁷ The volumetric gas flow was set to $Q=200$ ml/min with a reactant gas composition of 500 ppm ammonia in 2% oxygen and balance helium. Furthermore, 0.1g catalyst with a ratio of $\text{Si}/\text{Al}=15$ was employed, and we assumed a tubular reactor with 6 mm diameter and 5 cm length as in the modeling of the fast-SCR. Figure 6.10 shows the conversion of ammonia vs. temperature. Reasonable agreement between simulation and experiment is found. The mechanism consists of three parts as described in detail in chapter 5. First, oxygen reacts with adsorbed ammonia forming nitroxyl and water. Then, HNO reacts in an intramolecular reaction to NO and adsorbed H_2NO , which after reaction with another nitroxyl molecule leads to hydroxylamine and a second nitrogen oxide. The NH_2OH finally reacts with a third HNO to nitrosamine, which decomposes into nitrogen and water. However, this pathway leads to a deviation in the selectivity of the reaction with respect to nitrogen compared to experiments. While experiments suggest selectivity to nitrogen of about 65%, our model predicts only 50%. Even though we have included poten-

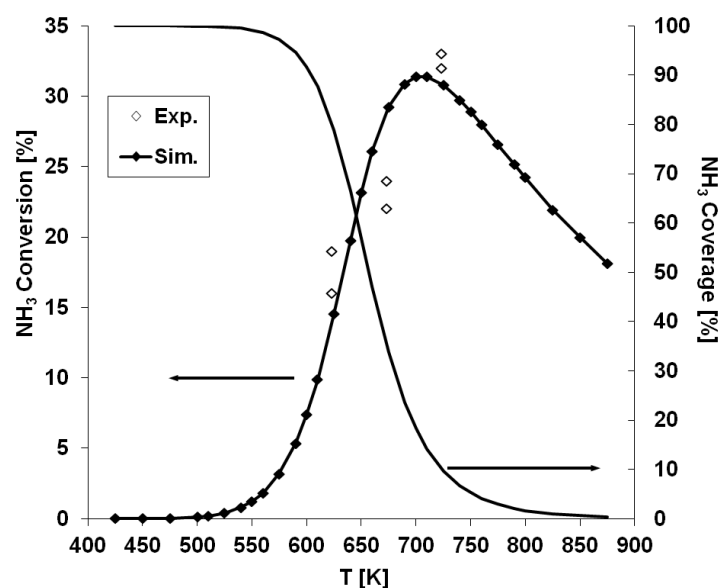


Figure 6.10: Simulated conversion of NH_3 from reaction with oxygen in comparison to data from reference [217].

tial reactions of nitroxyl with NO, none of them was found to be significant at these conditions to account for this deviation. Thus, the most reasonable explanation is oxidation of part of NO to NO_2 followed by the fast-SCR mechanism. Our proposed mechanism for this oxidation as described in section 4.3.1 is however only capable of accounting for the low temperature conversion (compare Halasz et al.¹⁷⁵), but not for the high temperature regime. Nevertheless, the rate-limiting step, the reaction of oxygen with an adsorbed ammonium ion to adsorbed NH_3OOH^+ , was found to be independent of temperature. Thus, the rates of the subsequent steps producing NO and N_2 from the decay of nitroxyl do not significantly influence the overall reaction rate of the SCO and thus, oxidation of a fraction of NO to NO_2 is not expected to significantly change the conversion vs. temperature. Furthermore, in the NO_2 -SCR the oxidation of NO is less relevant because the produced NO directly reacts with NO_2 according to the fast-SCR mechanism. Therefore, it can be concluded that the impact of the ammonia oxidation on the fast and the NO_2 -SCR is only minor and is not expected to account for the observed deviation of the NO_2 -SCR at high temperatures. In contrast to the SCR reactions, the ammonium ion does not block the active sites but actively participates in the reaction. The maximum of the conversion at ~ 700 K is related to the decreasing amount of ammonia adsorbed on the catalyst. The

left shoulder of the curve is related to the rate-limiting initial reaction of oxygen with the adsorbed ammonium ions.

6.4 Conclusions

The mechanisms of the three major sets of the selective catalytic reduction of nitrogen oxides, namely the NO_2 -SCR, the fast SCR and the SCO, were analyzed using microkinetic modeling. The microkinetic model, which includes the DFT-calculated reaction mechanisms of the preceding chapters 4 and 5 showed reasonable agreement with different sets of experimental data. First of all, the crucial adsorption of ammonia on Brønsted acids indicates coadsorption of up to four ammonia molecules on an active site at low temperatures. In addition, our model suggests that only a fraction of the framework aluminum is capable to bind ammonia as ammonium ion. This might be explained by a potential inaccessibility of a certain fraction of Brønsted acids within the microstructure of the zeolite. For the NO_2 -SCR the reaction was found to proceed in the following sequence. First, NO_2 adsorbs and a second NO_2 coadsorbs prior to the formation of $\text{as-N}_2\text{O}_4$ which then decomposes into nitric acid. The latter then desorbs and leaves a nitrosyl ion on the catalyst which subsequently reacts with ammonia to nitrosamine. The nitric acid decomposes on an active site into water and $\text{Z}^-[\text{NO}_2]^+$ which reacts with ammonia to nitramide. Finally, nitramide and nitrosamine decompose into water and nitrous oxide and nitrogen, respectively. Furthermore, at low temperatures, nitric acid potentially reacts directly with an ammonium ion to nitramide and water. The rate-limiting step is the desorption of nitric acid, leaving the nitrosyl ion on the zeolite. The observed maximum in the conversion vs. temperature was related to the blocking of sites by ammonia at low temperatures and to the thermodynamic equilibrium conditions of the intermediate $\text{as-N}_2\text{O}_4$ at elevated temperatures. For the mechanism of the fast SCR, in analogy to the NO_2 -SCR, it was concluded that $\text{as-N}_2\text{O}_3$ is formed as intermediate on the active site, which then decomposes into nitrous acid together with a nitrosyl ion on the zeolite. Here, the decomposition of the acid leads to a second nitrosyl ion or, at low temperatures, the acid directly reacts with an ammonium ion to nitrosamine and water. In addition, the superposition of the NO_2 -SCR causes deviation in NO and NO_2 conversion. At high temperatures, the desorption of nitrous acid from the nitrosyl ion is rate-limiting in analogy to the NO_2 -SCR mechanism while, at low temperatures, the coadsorption of NO to NO_2 prior to the formation of the intermediate $\text{as-N}_2\text{O}_3$ is rate-limiting. The observed maximum can be related to the blocking of the active sites by ammonia at low temperatures and

to the thermodynamic equilibrium of as- N_2O_3 at high temperatures. Finally, the governing pathway of the SCO entails the reaction of oxygen with an ammonium ion to nitroxyl and water and subsequently a self-reaction of HNO , which releases NO to the gas phase and leaves H_2NO on the active site. The latter reacts with another HNO to hydroxylamine followed by the reaction with a third nitroxyl to nitrosamine and water. The limiting factors in this reaction were found to be the initial elementary step between the ammonium ion and oxygen and at high temperatures the thermodynamic limitation of adsorbed ammonia on the active site. The deviation between calculated and experimentally observed selectivity towards nitrogen in the SCO is attributed to oxidation of part of the produced NO to NO_2 followed by the fast SCR mechanism. However, at the present conditions for the SCR, the ammonia oxidation was found to have only a minor impact. Thus, the deviation of the calculated NO_2 -SCR at high temperatures (above 725 K) may be due to an additional reaction mechanism or result from the decomposition of NO_2 to NO and oxygen followed by the accession of the fast-SCR.

In summary, based on first principles' microkinetic modeling, we have elucidated the reaction mechanism of the fast and the NO_2 SCR on H-ZSM5 with Brønsted acids as active sites. The results are to a large extent in agreement with experimental data, and although our model is rather qualitative, several conclusions were drawn beyond experimental findings. Furthermore, high activities of ion-exchanged and H-form zeolites are observed for the fast-SCR at equivalent reaction conditions. Considering the fact that metal-exchanged zeolites usually contain significant amounts of Brønsted acids, superposition of contributions of the two different active sites and coupling in terms of intermediate species or a direct interaction seems reasonable. Assuming a transferability of the H-ZSM5 reaction mechanism to other H-form zeolites, our results might provide new insights and concepts for overall reaction mechanisms of a large group of zeolite-based catalysts.

Part IV

Selective Catalytic Reduction on Mononuclear Iron Sites in Fe/H-ZSM5

7

Theoretical Investigation of the Mechanism of the Oxidation of Nitrogen Oxide on Fe-form Zeolites in the presence of Water

The oxidation of NO to NO₂ by oxygen and the influence of water have been investigated on a portion of the Fe-ZSM5 which contains 5 T-atoms by using the density functional theory. The iron was considered being a mononuclear species. For the main reaction pathway it is most likely that NO initially adsorbs on $Z^{-}[\text{FeO}]^{+}$ forming the nitrite $Z^{-}[\text{FeONO}]^{+}$ which includes a spin change from the septet to the quintet PES. The adsorption of oxygen and the desorption of NO₂ leads to $Z^{-}[\text{FeO}_2]^{+}$ which is attacked by NO from the gas phase. Within another spin change from the septet to the quintet PES, the ligand with the sequence -OONO is formed of which NO₂ desorbs. The latter step is rate-limiting for the overall mechanism. A final spin change restores the initial active site on the sextet PES. At the same time, the nitrite $Z^{-}[\text{FeO}_2\text{N}]^{+}$ and the nitrate $Z^{-}[\text{FeO}_2\text{NO}]^{+}$ are rapidly formed and block the active site. Water leads to the formation of, first, a dihydroxylated iron $Z^{-}[\text{HOFeOH}]^{+}$ and after the reaction with NO or NO₂ to nitrous and nitric acid respectively together with monohydroxylated iron $Z^{-}[\text{FeOH}]^{+}$. The dihydroxylated iron is inactive for the oxidation of NO and the monohydroxylated ex-

hibits a reduced activity as compared to $Z^- [FeO]^+$. The further removal of hydroxyl groups by reaction with NO_x is also accessible, restoring non-hydroxylated iron sites. Furthermore, water also potentially reacts directly with the surface nitrite and nitrate leading to nitrous and nitric acid. This explains the phenomena of a short-term release of significant amounts of NO_2 upon water addition in transient experiments. The results of this work are in agreement with the experimental literature and account for many observed phenomena.

7.1 Introduction

Within the development of technologies to reduce the emissions of pollutants, the abatement of NO_x has become one of the major fields of research.^{27,28} Especially the selective catalytic reduction of NO with hydrocarbons or ammonia has been studied extensively over the last two decades.^{31–33} Besides vanadium-based catalysts, metal-exchanged and, in particular, iron-exchanged ZSM5 have been proven to be very active for this reaction.³⁴ Though the exact mechanism of the SCR is not fully understood, there is an agreement in the experimental literature on the SCR with ammonia that the oxidation of NO to NO_2 is crucial for the SCR and the rate-limiting step of the overall process.^{38,158,222,282,283}



This assumption is mainly supported by the fact that the fast SCR, in which equimolar amounts of NO and NO_2 in the feed stream are reduced by ammonia, is significantly faster than the standard SCR, in which the feed only contains NO and O_2 . Also in case of the SCR with hydrocarbons the oxidation of NO is considered to be of high importance because the hydrocarbons are assumed to react with adsorbed NO_2/NO_3 species,^{284–287} formed in the reaction of NO with oxygen. Because of the obvious importance of this reaction in the SCR systems several researchers also included this topic in their investigations on Fe-ZSM5. Giles et al.²⁸⁸ found in transient experiments

at 350 °C that the catalyst exhibits a high storage capacity for NO₂ and a high activity for the oxidation reaction. Furthermore, they stated an inhibiting influence of water and assumed from transient studies that H₂O replaces adsorbed NO₂ or nitrates. They observed a short-term evolution of both, NO₂ and NO, after adding H₂O to the reactor. Martens et al.^{286,287} fitted several Langmuir-Hinshelwood-Hougen-Watson (LHHW) models to kinetic data and found the best correlation for a type which represents a surface reaction between adsorbed NO and coadsorbed O₂. The fitted adsorption constant for NO₂ was found to be much larger than the corresponding terms for NO and O₂ which leads to the assumption that NO₂ inhibits the reaction due to its strong adsorption. This inhibiting effect was also demonstrated by experiments including NO₂ in the feed, which led to significant lower NO conversion. They also concluded from FTIR and UV-Vis spectra that isolated Fe³⁺ cations and binuclear Fe³⁺ complexes are the active sites for the reaction. Lobree et al.²⁸⁵ concluded from an in situ infrared study that in the SCR with propane NO₂/NO₃ species are the relevant intermediate species and that these are formed from a gas phase reaction of NO with adsorbed oxygen leading either to a nitro or nitrite group adsorbed on FeO or a nitrate group. Delahay et al.²⁸² analyzed several Fe-ZSM5 samples with different iron content and prepared by several methods and found a good correlation between the activity of NO oxidation and NO SCR with ammonia, supporting the assumption of the NO oxidation being the rate limiting step. However, they also found that the activity of the catalysts for the SCR was significantly higher than for the pure NO oxidation, concluding that the NO₂ desorption limits the latter reaction. An NO₂ TPD experiment supported this finding because NO₂ adsorbs strongly on the catalyst, if iron is present, up to a temperature of ~575 K, where the desorption maximum was found. Long and Yang^{155,156} reported the detection of weakly adsorbed NO and more strongly adsorbed NO₂ and nitrate on Fe-ZSM5 in the reacting system of NO with O₂. They also concluded from IR studies that, though the NO₂ formation is much smaller than its consumption by NH₃, the Fe-ZSM5 exhibits a high activity for the NO oxidation. Grünert et al.³⁷ also directly compared the NO oxidation activity with the standard SCR and found, in agreement with Delahay et al.,²⁸² a significant deviation. Kröcher et al.³⁸ studied in pulse experiments the influence of water on the NO oxidation and found an inhibiting effect in agreement with Giles et al.²⁸⁸ Furthermore, they also observed the storage capacity of the catalyst of considerable amounts of NO₂ indicating its strong adsorption. Somewhat contradicting are the results of Olsson et al.²⁸⁹ who measured the NO conversion at increasing temperatures for a kinetic model. They concluded that NO_x is hardly stored on the surface because neither did they observe any time lag between NO_x

inlet and outlet nor any NO_x desorption with increasing temperature.

Another major discussion is related to the structure of the iron, exchanged into the zeolite, and the activity of the different potential species. Most groups support the finding that three major structures have to be considered, namely Fe_xO_y clusters within the pores and bi- or mononuclear iron, directly exchanged to the Brønsted acid of the parent H-form zeolite.^{36,37,290–294} Furthermore, the activity of iron ions chemically anchored to SiO were suggested by Zecchina et al.^{295,296} and recently Rosa et al.²⁹⁷ proposed $[\text{FeO}]^{2+}$, balancing the charge of two framework aluminum atoms, as the active species in analogy to enzymatic systems like P450. However, Lobree et al.²⁹⁸ and Kröcher et al.²⁹⁰ found a 1:1 exchange of Brønsted acids with iron, at least at low iron contents, favoring mono- or binuclear cationic iron species. Nevertheless, there is an ongoing debate about which of the species is responsible for the high activity. Recently, Kröcher et al.³⁶ stated that for the SCR with ammonia mononuclear sites should be considered the most active species at low temperatures up to 300 °C and that binuclear species contribute to the reaction at higher temperatures. In addition, there are several assumptions stated in the literature about stable intermediate structures of the active site, depending on the species considered in the reacting system, e.g. O_2 , NO , NO_2 and H_2O . Thus, Lobree et al.^{285,298} as well as Krishna and Makkee¹⁶⁵ proposed for mononuclear sites $\text{Fe}(\text{OH})_2$ formed from FeO and water, as well as FeO_2 , OFeNO_2 , and the nitrate FeNO_3 . Especially the formation of surface nitrates at low temperatures is proven by many experimental investigations, as stated by Tronconi et al.¹⁶⁹ Based on a theoretical study of NO_2 adsorption on iron exchanged zeolites, Sierraalta et al.²⁹⁹ presented the formation of a nitrite species in which NO_2 is bond to the mononuclear iron ion with both oxygen atoms. Besides this structure, Heyden et al.^{119,300} also found a stable nitrite with only one oxygen bond to the iron as well as the nitrate and dihydroxylated site already mentioned by Lobree et al.^{285,298} Finally, also a single hydroxyl group FeOH was found to be a reasonable representation of the active site.

Because the oxidation of NO is such a crucial step for the SCR of NO with ammonia as well as with hydrocarbons, the aim of this work is to present detailed insight of the reaction mechanism based on density functional theory (DFT). Here we only consider mononuclear active sites, referring to the findings of Kröcher et al.³⁶ that these species are considered most active at low temperatures and thus within the regime where the application of the SCR is wanted. However, a significant contribution of other iron species like the binuclear sites or iron clusters on the oxidation of NO cannot be ruled out. Especially, for the binuclear sites it was shown by Hansen et al.³⁰¹ and

also by Guesmi et al.³⁰² based on DFT calculations that they might have a significant activity for the decomposition of nitrous oxide. However, a micro kinetic modeling study of Hansen et al.²⁵⁸ including both, mononuclear and binuclear, sites suggested the higher activity for the mononuclear sites. This would be in general agreement with the experimental conclusions of Kröcher et al.³⁶ for the SCR. Thus it seems plausible to consider the mononuclear sites as to be most promising also for the NO oxidation.

In accordance with the findings of Heyden et al.³⁰⁰ and the experimentally observed nitrites and nitrates we consider different structures as potential starting points for a catalytic cycle: the structures $Z^-[\text{FeO}]^+$, $Z^-[\text{FeONO}]^+$, $Z^-[\text{FeO}_2\text{N}]^+$, $Z^-[\text{FeO}_2\text{NO}]^+$ and $Z^-[\text{FeOH}]^+$ (Figure 7.1). For reasons of simplicity we will further on denote the structures without the “ $Z^-[\]^+$ ”. We also describe reaction pathways leading to these species. Finally, we analyze the influence of water on the active site and its inhibiting effect as stated by Giles et al.²⁸⁸ and Kröcher et al.³⁸ Addressing the influence of water is especially of importance with respect to the main application of the NO oxidation within the SCR in exhaust gas streams. Not only is water a product of the SCR but it is also usually present in considerable amounts in the exhaust waste gases. Furthermore, because of the pronounced, experimentally observed, deviation in activity between NO oxidation and standard SCR, it is assumed^{37,282} that ammonia rapidly reacts with some intermediates produced in the oxidation cycle. Thus, this study also might provide insight into the most probable state of the active site prior to a reaction with ammonia and with that on the connection between fast and standard SCR. A similar analysis is possible for the SCR with hydrocarbons, considering the experimental finding that the reducing agent reacts with a prior oxidized NO, adsorbed to the active site.

7.2 Theory

The catalytic active center and a part of the zeolite framework were represented by a cluster of 5 T-sites (Figure 7.1, FeO). Therefore, all Si atoms were initially placed at their crystallographic positions, as reported by Olson et al.¹⁹⁷ As there is some evidence that Al is not positioned randomly but prefers the T12¹⁹⁸ site, we cut our framework cluster from the unit cell, so that it surrounded this site with Al as its center. The terminal Si atoms were saturated with hydrogen, whereas the Si-H bonds were oriented in the direction of the former Si-O bonds. The length of these bonds was set to 1.487 Å, representing the optimal bond length for SiH₄ at the B3LYP/TZVP level

of theory. For all calculations on the catalyst, the H-atoms were fixed while other atoms' positions were fully relaxed. The iron was considered as mono-nuclear ions which replace the Brønsted acid site of the parent H-ZSM5. Heyden⁴¹ has shown for two reactions that the change of the electronic reaction energy changes only very little when increasing the cluster size to 17 T-sites at the B3LYP/TZVP level and has concluded that the charge transfer over the zeolite matrix occurs only to a very little extend. In addition we executed a sample calculation for the adsorption of NO on FeO on a 21 T-sites containing cluster that accounts to a certain extent for the pore structure. Also in this case we did not observe a significant influence of the cluster (Figure E.1). Thus, the small T5 cluster is expected to give reliable results of at least qualitative nature. Concerning the chosen T12 site for the aluminum in the ZSM5, there is also no clear evidence about a preferred site. Some early theoretical studies obtain varying results with Fripat et al.^{303,304} and Chakraborty et al.³⁰⁵ suggesting the T12 site, Redondo and Hay³⁰⁶ suggesting the T9 site and Chatterjee and Chandra³⁰⁷ suggesting both, T9 and T12 site to be most favorable. Studies on the influence of the exchanged T-site on properties like the adsorption of probe molecules as done by Zhou et al.³⁰⁸ for MCM-22 show indeed a deviation in adsorption strength on different sites. A related influence on catalyzed reaction barriers on ion exchanged ZSM5 as considered here cannot be excluded. However, we have analyzed the influence of perturbing the O-Al-O angle of the original $Z^{-}[\text{FeO}]^{+}$ cluster, prior to relaxation, and found only a negligible deviation for the heat of adsorption for NO (Table E.1). This suggests qualitatively, that only a minor impact of the chosen T-site on relative energies has to be expected in this study.

All quantum chemical calculations were carried out on potential energy surfaces (PES) with spin multiplicities $M_S=2-8$, by using the gradient-corrected density functional theory (DFT) as implemented in the TURBOMOLE suite of programs.²⁰⁰ Becke's 3-parameter exchange functional⁸¹ and the correlation functional of Lee, Yang and Parr⁸³ were used (B3LYP) to represent the effects of exchange and correlation. The triple- ζ basis set with polarization functions (TZVP) was used for all atoms together with a very fine numerical grid size (m5).²⁰¹ Structure optimizations were performed in Cartesian coordinates with an energy convergence criterion of 10^{-7} Ha and the maximum norm of the Cartesian gradient was converged to 10^{-4} Ha/bohr. Based on studies on density functionals as executed by Truhlar et al.³⁰⁹ or of Ramos et al.⁸⁸ and references therein it is known that the performance of B3LYP has its limitations. However, for a wide range of applications the B3LYP functional was shown to provide reliable results as outlined by Shaik et al.³¹⁰ and references therein for metalloproteins, by Leszczynski et al.³¹¹ for the bond-

ing of atomic oxygen on a ferrous iron center and by Heyden et al.^{119,300,301} for the catalytic decomposition of nitrous oxide on Fe-ZSM5. Thus, the specifications chosen in this work are considered as a reasonable compromise between accuracy and computational expenses.

Transition states were localized using a combination of interpolation and local methods. First, the growing string-method⁹⁹ was applied in mass-weighted coordinates, leading to an approximate saddle point, once the two ends of the growing string had joined. The refinement of the saddle point was accomplished by either the modified dimer method¹⁰⁵ with a gradient-norm convergence criterion of $5 \cdot 10^{-4}$ Ha/bohr or the PRFO method.¹⁰³ To confirm that the transition states are connected to the correct energy minima, each transition state was perturbed slightly along the reaction coordinate in the direction of reactant and product. These perturbed geometries were used as starting points for energy minimization which revealed that, in all cases, the desired energy minimum was found.

Because NO and NO₂ are doublets and O₂ is a triplet, the stoichiometry of reaction (7.1) already dictates the consideration of the crossing of seams of different PESs. Minimization of the surface species on different PESs revealed that the energy differences are usually significant and only the ground state needs to be considered. However, in cases with the two PESs being close to each other, we also considered the crossing of PES in order to obtain the lowest energy pathway for the catalytic cycle overall. For the excited states we considered then only the state of lowest energy which in most cases gives in iron core containing systems with the B3LYP functional relative energies in good agreement to high-level ab initio quantum mechanical calculations.^{311–313} The minimum energy crossing points (MECP) on the seam of two PESs were determined with a multiplier penalty function algorithm (see Heyden et al.¹¹⁹ for details). The converged minimum energy crossing point structures had a maximum energy difference on both PESs of less than 10^{-6} Ha. In order to calculate Gibbs' free energies also for the MECPs we calculated the vibrational frequencies for the partition function based on an effective Hessian as stated by Harvey and Aschi¹⁰⁸ and outlined in section 3.3 equation (3.28).

Energy barriers obtained from transition state search have limited accuracy and are dependent on the applied density functional as outlined by Truhlar et al.³⁰⁹ and Ramos et al.⁸⁸ The same is true for barriers resulting from MECPs but stated by Harvey⁵⁵ to be at least reliable for a qualitative comparison with other reaction pathways. Furthermore, the here described methodology was successfully applied to the investigation of the decomposition of nitrous oxide in Fe-ZSM5 in our institute^{119,300,301} and by Guesmi

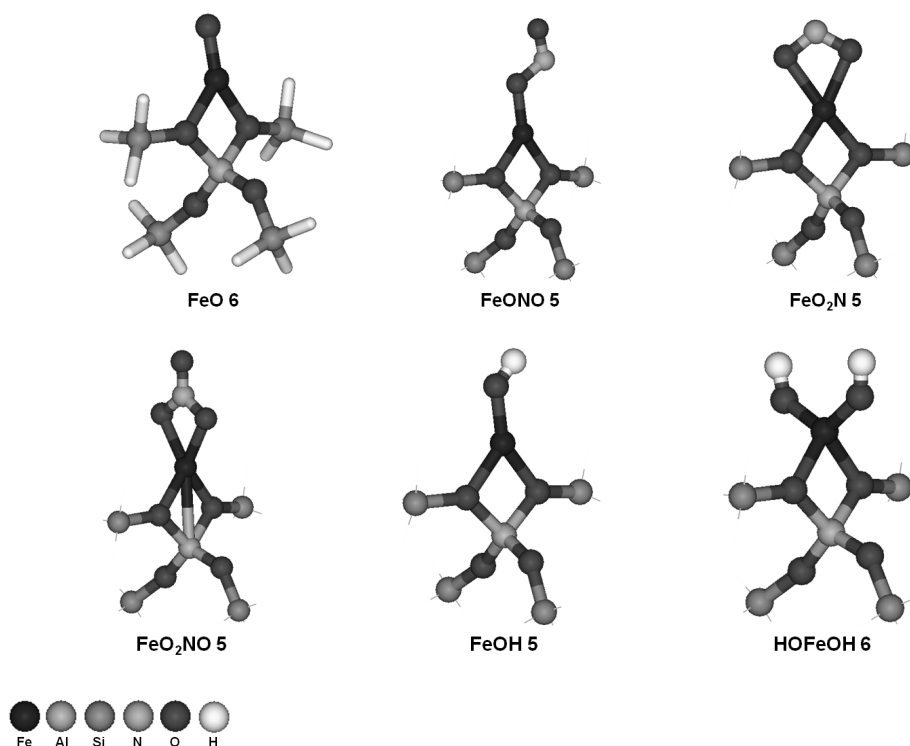


Figure 7.1: T5 cluster model of the different considered active sites of Fe-ZSM5: $Z^-[\text{FeO}]^+$, $Z^-[\text{FeONO}]^+$, $Z^-[\text{FeO}_2\text{N}]^+$, $Z^-[\text{FeO}_2\text{NO}]^+$ and $Z^-[\text{FeOH}]^+$. The numbers correspond to the spin multiplicity of the minimized species. Dangling bonds are not shown.

et al.³⁰² and the results were in both cases to a certain degree even quantitatively in agreement with experiments.^{258,314,315} Thus, it can be assumed that the accuracy of the methodology applied here is sufficient for at least a qualitative analysis of the oxidation of nitrogen oxide on Fe-ZSM5.

7.3 Results and discussion

The mechanism of the oxidation of NO can, in accordance with the stoichiometry of the reaction (equation (7.1)), be interpreted as a sequence of the adsorption of two NO and O₂, the formation of two NO₂ and the subsequent desorption of the formed species. Here, the exact pathway is of interest. Because we only considered mononuclear iron as active sites in this

work, the adsorption of more than two molecules prior to a reaction step leading to NO_2 or an intermediate seemed implausible with respect to space and entropy. Thus, we always started the investigation with either the adsorption of NO and the subsequent coadsorption of O_2 or vice versa, followed by the formation of a first NO_2 and its desorption. Then, the adsorption of a second NO was considered, forming another NO_2 . The desorption of the latter closed the catalytic cycle.

To analyze the appearance of the active site, we first considered the structures FeO , FeONO , FeO_2N and FeO_2NO of Figure 7.1 as the starting points for a catalytic cycle, in accordance with theoretical and experimental findings in the literature. The consideration of a bare iron ion as active site in an oxygen containing atmosphere was concluded to be negligible based on DFT calculations which was also shown by Heyden et al.³⁰⁰ In a second part, we investigated the influence of water on the reaction. This was mainly considered in terms of the formation of hydroxyl groups on the active site and, with that, leading to the monohydroxylated iron (FeOH) as the potential starting point for a catalytic cycle. Furthermore, we included the potential formation of nitrous and nitric acid which provides some insight into the hydrolysis of NO_2 and NO as a side reaction. This is also related to our previous findings on H-form zeolites that these two acids have to be considered as relevant intermediates of the selective catalytic reduction of nitrogen oxides with ammonia (see chapter 4).

As part of the investigations, we also considered the crossing of potential energy surfaces of different spin multiplicities, in order to account for the different spin state of overall reactants and products as well as to find the energetically lowest pathway for the catalytic cycle. Thus, the final results are also supposed to reveal where, within the overall reaction cycle, the crossing of PESs should be considered to be most probable. The labeling of the structures involved naming the ligands to the iron. In the case that three ligands have been considered, one is attached with a minus (“-”). In the case that a molecule is considered as a gas phase species we used an underline character (“_”) to add it to the tag. Here, only the mechanistic overviews and the energy diagrams of the different catalytic cycles are shown. All the energies in the diagrams are zero-point energy-corrected and the values in the overviews are Gibbs’ free enthalpies calculated at 600 K. The black values refer to the structures and the blue values to either transition states or to the barrier for the crossing of a seam between two PESs. The colors of the boxes refer to the spin multiplicity of the PES as follows: white refers to $M_S=3$, green to $M_S=4$, blue to $M_S=5$, yellow to $M_S=6$ and orange to $M_S=7$. In both, energy diagram and overview, the values are given with respect to the stated active

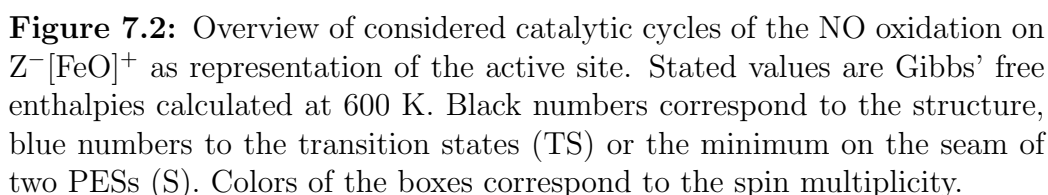
site structure and gas phase molecules as reference. The value of 600K was picked in order to consider the entropic effects of the reaction mechanism at a temperature where also the standard SCR with ammonia shows significant conversions (compare Figure 2, Schwidder et al.³⁷). The structures corresponding to the energy diagrams are illustrated in the supporting information of reference [316]. With respect to the discussion on the accuracy of DFT in general and on the calculation of energy barriers from transition states and minimum energy crossing points as discussed in the section 7.2 it should be emphasized that all the subsequently presented results are of qualitative nature only.

7.3.1 Activity of Iron Exchanged ZSM5 in the Absence of Water

In order to clearly understand the activity of the mononuclear iron centers for the oxidation of NO to NO₂, we first describe in the following sections the potential pathways without the consideration of water. Starting with FeO, we present the formation of the stable nitrite and nitrate structures and discuss their potential activity for the reaction.

Catalytic Cycle on FeO

The energies of this cycle are shown in Figure 7.3. Figure 7.2 provides the overview of the reactive network, including the Gibbs' free enthalpies at 600 K. The ground state of FeO was found to be on the PES with $M_S=6$, which was used as the reference state. The adsorption of oxygen to this structure, leading to OFeO₂ is negligible, as can be inferred from ST 4 in the energy diagram. For the adsorption of NO, leading to FeONO, two different pathways can be considered which include the crossing of two PESs, because the ground state of the product was found to be on the quintet. Either first a spin change of FeO (S 1) to $M_S=4$ (ST 3) takes place, followed by a subsequent adsorption of NO or the crossing of the seam is part of the adsorption itself (S 2). For the first case, a barrier of $E^\ddagger=5.4$ kcal/mol was calculated, while for the second case only $E^\ddagger=0.7$ kcal/mol (electronic energy difference only) was observed. The adsorption process, leading to FeONO (ST 5) is strongly exothermic with a heat of adsorption of $\Delta E_{\text{ads}}=-32.1$ kcal/mol indicating a very stable structure. The desorption of NO₂ from this structure would lead to a bare iron ion but Heyden et al.³⁰⁰ found this to be a very unlikely step because of a very high energy of desorption. For the subsequent adsorption of molecular oxygen a transition state (TS 2) was



found leading to O_2FeONO on the septet PES (ST 7). The calculated barrier with $E^\ddagger = 1.9$ kcal/mol is rather small and also the heat of adsorption with $\Delta E_{\text{ads}} = -4.3$ kcal/mol indicates a rather loose state. As the next step, we considered the desorption of NO_2 for which no transition state was found on the septet PES and the barrier was calculated to be $\Delta E_{\text{des}} = 19.9$ kcal/mol, leading to FeO_2 (ST 12) on the sextet PES. Alternatively, we also investigated the spin change to the quintet PES with a subsequent desorption of NO_2 for this process, followed by another spin change from the quartet structure of FeO_2 to its ground state, because here the energy differences were found to be rather low. The first crossing of the seam (S 3) for O_2FeONO to the potential energy surface with $M_S = 5$ (ST 9) exhibits a barrier of $E^\ddagger = 12.1$

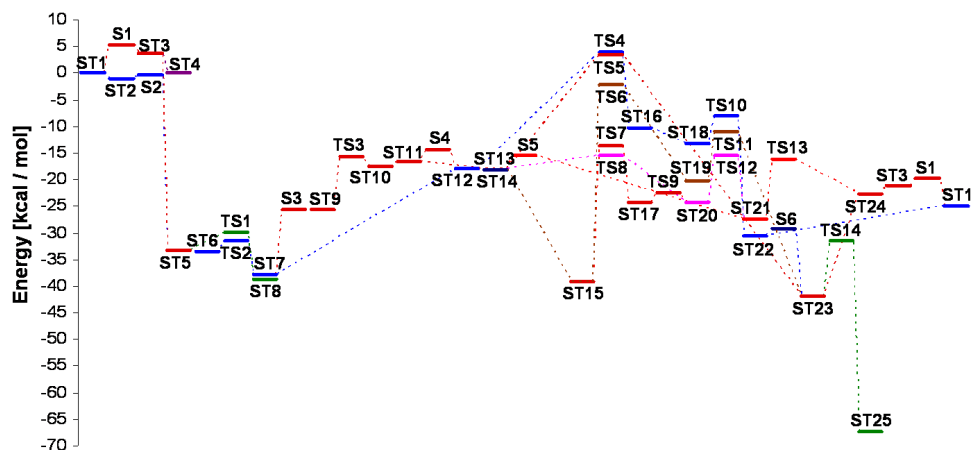


Figure 7.3: Energy profiles for the catalytic cycles of NO oxidation on $Z^-[\text{FeO}]^+$. Energies are zero-point corrected.

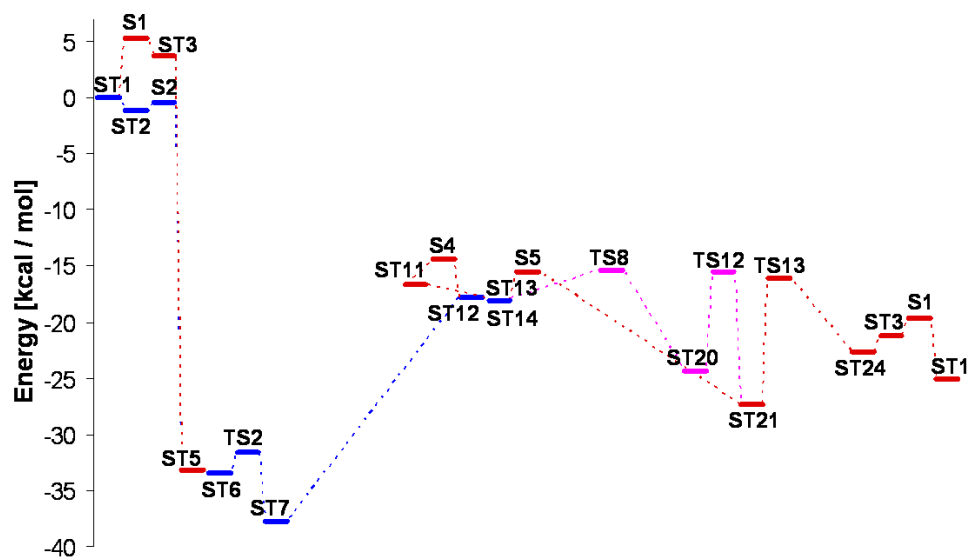


Figure 7.4: Energy profiles of the relevant catalytic cycles of NO oxidation on $Z^-[\text{FeO}]^+$. Energies are zero-point corrected.

kcal/mol, while the reverse barrier is negligible. For the desorption of NO_2 via the transition state TS 3 another barrier of $E^\ddagger=10.0$ kcal/mol needs to be overcome while the desorbed molecule still slightly interacts with the active site, as can be seen from the energy corresponding to ST 10. Finally, the resulting FeO_2 (ST 11) on the quartet PES is only $E=1.2$ kcal/mol higher in energy than the corresponding ground state and a low barrier of $E^\ddagger=2.3$ kcal/mol (S 4) leads to the latter. Thus, the overall energy difference between the two pathways is rather small as can be seen from the energy diagram, and both pathways might be accessible. For the subsequent reaction with NO several different reaction mechanisms were taken into account starting from both spin states of FeO_2 because the quartet and the sextet PES are very close in energy, here. Adding NO to the gas phase leads to nearly the same value for the PES with $M_S=5$ (ST 13) and $M_S=7$ (ST 14), implying a slight interaction between the molecule and the active site on the lower PES, while on the higher one no interaction can be observed. On $M_S=5$ NO adsorbs strongly to the iron forming O_2FeNO (ST 15) with a heat of adsorption of $\Delta E_{\text{ads}}=-21.3$ kcal/mol. Then, in a reaction via TS 7, the NO attaches to the adsorbed oxygen and forms the intermediate FeOONO_ct with the ligand in a cis-trans configuration (ST 17). This process is activated by $E^\ddagger=25.6$ kcal/mol. In a subsequent step with a low energy barrier ($E^\ddagger=1.7$ kcal/mol, TS 9) FeOONO_t (ST 20) is formed with the ligand in the trans-trans configuration and finally a rotation of the NO group with a barrier of $E^\ddagger=8.8$ kcal/mol (TS 12) leads to the trans-cis conformation FeOONO_c (ST 21). In an alternative pathway starting from the quintet O_2FeNO the bond between the two oxygen atoms breaks with a barrier of $E^\ddagger=37.0$ kcal/mol (TS 6), which leads to OFeO-NO (ST 19). Then, subsequently with a barrier of $E^\ddagger=9.2$ kcal/mol (TS 11), the NO releases its bond with the iron and forms adsorbed NO_2 (ST 23). This species in its ground state on the PES with $M_S=5$ has to be considered a rather stable structure because of the low corresponding energy. Furthermore, we also found a reaction of FeO_2 with gas phase nitrogen oxide, leading to the stable structure of OFeONO . This step involves the cleavage of the adsorbed molecular oxygen and the direct formation of adsorbed NO_2 which exhibits an energy barrier of $E^\ddagger=21.4$ kcal/mol (TS 5). Alternatively, the gas phase nitrogen oxide can directly react with the adsorbed molecular oxygen, leading to the -OONO ligand in the trans-trans configuration (ST 20). This step exhibits a low barrier of $E^\ddagger=2.5$ kcal/mol (TS 8). When starting with the sextet PES of FeO_2 (ST 12), the cleavage of the oxygen into OFeO (ST 16) was examined which exhibits a rather high activation energy of $E^\ddagger=21.7$ kcal/mol (TS 4). Nitrogen oxide only loosely interacts here with the iron (ST 18) and thus, the subsequent reaction step via TS 10 ($E^\ddagger=5.0$ kcal/mol), leading to OFeONO (ST 22) on

the septet PES, should rather be seen as a gas phase attack of NO to the active site. The resulting intermediate does not correspond to the ground state but the crossing of the seam from the septet to the quintet PES only exhibits a very low barrier of $E^\ddagger=1.3$ kcal/mol (S 6). Finally, a pathway was found, starting from FeO₂ in its ground state with gas phase NO (ST 14). Here, the spin change (S 5) directly leads to the formation of FeOONO_c (ST 21) on the quintet PES by overcoming a barrier of only $E^\ddagger=2.6$ kcal/mol. In summary it can be stated that, with respect to FeO₂, either the cleavage of the adsorbed molecular oxygen is necessary prior to the reaction with NO leading to OFeONO (ST 23) which involves rather high barriers (TS 4, 5 and 6) or a reaction between gas phase NO and adsorbed molecular O₂ takes place, eventually leading to FeOONO_c with in comparison rather low energy barriers (S 5, TS 8). In the case of coadsorbed oxygen and nitrogen oxide the high barrier of TS 7 can be attributed to the strong prior adsorption of NO.

As last part of the reactive cycle the desorption of the second NO₂ was addressed. Starting from FeOONO_c (ST 21) on the quintet PES, the transition state TS 13 results in the cleavage of the O-O bond of the ligand and NO₂ is formed (ST 24) which only loosely interacts with the remaining FeO. This step exhibits an activation energy of $E^\ddagger=11.2$ kcal/mol. The resulting FeO on the quartet PES easily transforms into its ground state via S 1 as described in the beginning of the catalytic cycle. In the case of OFeONO in its ground state (ST 23) on the quintet PES, either NO₂ desorbs first from the active site, leading to FeO on the quartet PES by overcoming the heat of desorption $\Delta E_{\text{des}}=19.3$ kcal/mol. This requires than the subsequent spin change of FeO into its ground state. Alternatively, the spin change is accounted for via S 6 with a barrier of $E^\ddagger=12.6$ kcal/mol, followed by the desorption of NO₂ on the septet PES with $\Delta E_{\text{des}}=5.6$ kcal/mol. Overall, the latter pathway exhibits a slightly lower barrier.

From the investigation so far, it is most probable that, first, FeONO is formed including the crossing of the seam either prior to the NO adsorption or as the reactive step itself. Then, the adsorption of oxygen is required prior to the desorption of NO₂ on the septet PES, leading to FeO₂. Subsequently, NO reacts from the gas phase with the active site, eventually leading to FeOONO in its cis conformation on the quintet PES. Here again, either first a spin change of FeO₂ is considered prior to a reaction with NO (S 4 and TS 8) or the crossing of the seam already involves the formation of the -OONO ligand via S 5. Finally, the desorption of NO₂ takes place (TS 13) and FeO returns with S 1 to its ground state, closing the catalytic cycle. The energies corresponding to this reduced analysis are presented in Figure 7.4. Furthermore, these

pathways also exhibit the lowest overall Gibbs' free enthalpies at 600 K as shown in Figure 7.2, supporting the concluding remarks, that they present the most probable pathways on FeO as the active site. It is however worth mentioning, that the Gibbs' free enthalpies rather suggest the initial spin change of FeO prior to the first NO adsorption rather than the combined process and for the second NO adsorption favors the combined spin change and -OONO formation over the step by step process.

From the presented results it is obvious, that FeONO has to be considered a rather stable intermediate, which itself might serve as the starting point of a catalytic cycle, at least at low temperatures. A rather low energy barrier of $E^\ddagger=3.3$ kcal/mol (TS1) separates this species from the nitrite FeO_2N on the quintet PES and the transformation is slightly exothermic by $\Delta E=-5.5$ kcal/mol. Furthermore, the nitrate structure FeO_2NO is formed exothermically from OFeONO ($\Delta E=-25.4$ kcal/mol) on the PES with $M_S=5$ after overcoming a barrier of $E^\ddagger=10.5$ kcal/mol (TS 14). Thus, the catalytic cycles on all the three structures have to be further investigated to reveal their influence on the NO oxidation.

Catalytic cycle on FeONO

An overview of the studied mechanism for the catalytic cycle on FeONO in its ground state on the quintet PES is shown in Figure 7.5 which also includes the Gibbs' free enthalpies of the intermediates and the transitions. The energies of the reaction network are presented in Figure 7.6 with the second axis using FeO as the reference state. The cycle on FeONO can be started again either by the adsorption of NO or of O_2 . In the latter case, the transition state TS 1 leads to O_2FeONO (ST 4) on the septet PES and for a following coadsorption of NO a spin change is necessary via S 2 to the quintet PES (ST 9). Up to this point the pathway is identical to the corresponding description in FeO. The coadsorption of NO was found here to be preferred on the molecular oxygen (ST 13) rather than on the iron itself. This results in a heat of adsorption of $\Delta E_{\text{ads}}=-6.9$ kcal/mol with respect to the O_2FeONO ground state. A subsequent reaction via TS 6 with an energy barrier of $E^\ddagger=8.6$ kcal/mol leads to the formation of a -OONO ligand in the trans configuration on the iron (ST 15). Alternatively, first the NO adsorption can be considered on FeONO (ST 3). However, a subsequent crossing of the seam from the sextet to the quartet PES is required for ONFeONO (ST 5) to be in its ground state. The barrier for this process was calculated to be $E^\ddagger=3.1$ kcal/mol (S 1) and the adsorption was found to be significantly stronger than the O_2 adsorption with $\Delta E_{\text{ads}}=-19.0$ kcal/mol. Then, the coadsorption of

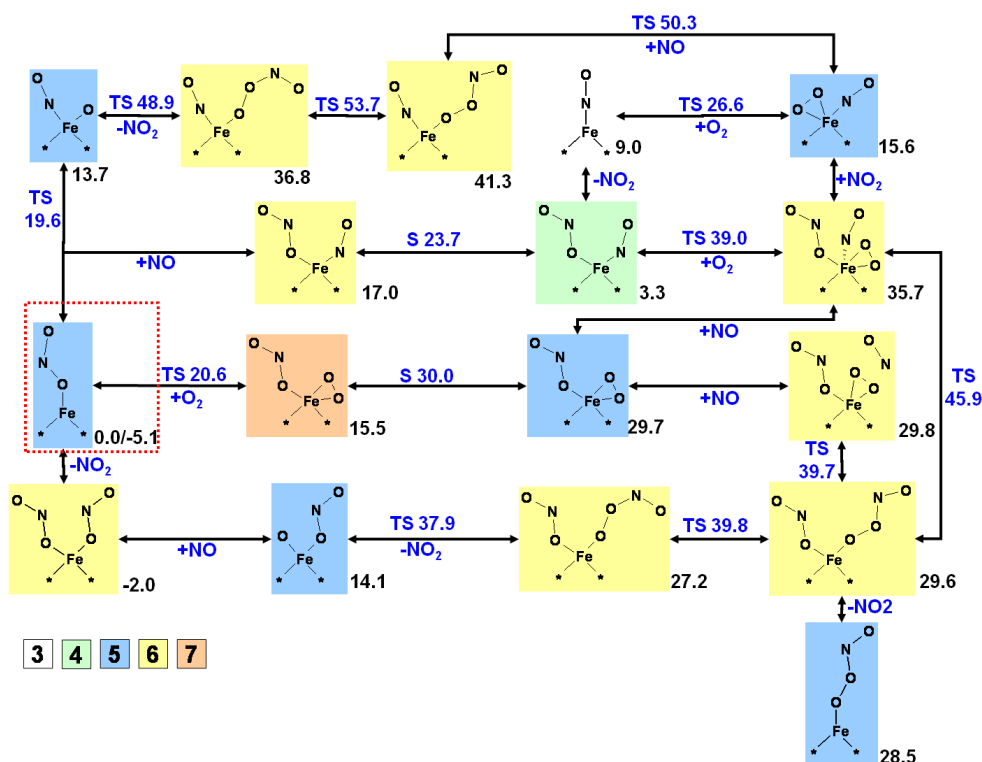


Figure 7.5: Overview of considered catalytic cycles of the NO oxidation on $Z^{-}[\text{FeONO}]^{+}$ as representation of the active site. Stated values are Gibbs’ free enthalpies calculated at 600 K. Black numbers correspond to the structure, blue numbers to the transition states (TS) or the minimum on the seam of two PESs (S). Colors of the boxes correspond to the spin multiplicity.

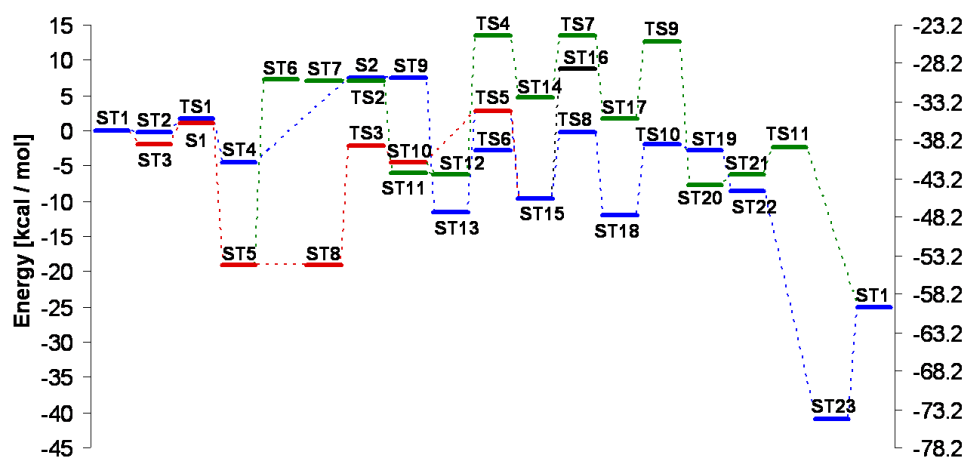


Figure 7.6: Energy profiles for the catalytic cycles of NO oxidation on $Z^-[\text{FeONO}]^+$. Second axis corresponds to $Z^-[\text{FeO}]^+$ as reference state. Energies are zero-point corrected.

oxygen was considered on the sextet potential energy surface which exhibits a barrier of $E^\ddagger=16.9$ kcal/mol (TS 3). Prior to this adsorption oxygen does not interact with the active site at all (ST 8). Interestingly, the adsorption leads to an energetically less favorable state (ST 10) which can be attributed to a loosening of the adsorbed NO. In fact, the energy of O_2FeONO in its ground state (ST 4) is at the same level as ST 10, which indicates that coming from the reversed adsorption sequence, NO coadsorbed on the iron does not exhibit any heat of adsorption. With that, the coadsorption of O_2 has to be rather seen as pushing the NO off the iron only hindered by the barrier of the spin change to the ground state. Nevertheless, a subsequent reaction (TS 5) with an activation energy of $E^\ddagger=7.2$ kcal/mol also leads to the ONFeOONO.t (ST 15). Similar to the results on FeO, a rotation of the -NO of the -OONO ligand results in the cis conformation (ST 18). For this process a barrier of $E^\ddagger=9.5$ kcal/mol (TS 8) needs to be overcome which, in magnitude, is very similar to the corresponding one found for FeO. The release of NO_2 to the gas phase occurs by the cleavage of the O-O bond in the ligand and is activated by $E^\ddagger=10.1$ kcal/mol (TS 10). Structure ST 19 can then be seen as an unstable intermediate, because the removal of NO_2 from ONFeONO (ST 22) is exothermic. In the next step, a second NO adsorbs to the free atomic oxygen on the iron and adsorbed NO_2 is formed (ONFeONO , ST 23) on the sextet PES. This step is highly exothermic with a heat of adsorption of $\Delta E_{\text{ads}} = -32.3$ kcal/mol, indicating a favorable intermediate. Finally, NO_2 desorbs from this structure and closes the catalytic cycle by restoring the active site. Here, the desorption was calculated to require $\Delta E_{\text{des}}=16.0$ kcal/mol.

In addition, the desorption of NO_2 from ONFeOONO.t , leaving the -OONO ligand (ST 16), requires a heat of desorption of $\Delta E_{\text{des}}=18.5$ kcal/mol. This is less favorable than the conversion of the -OONO ligand to the cis conformer and the subsequent release of NO_2 via TS 8 and TS 10 because of a higher barrier. Furthermore, we considered the desorption of NO_2 from the ground state of the intermediate ONFeONO leading to FeNO on the triplet PES (ST 6). Here, the calculated energy difference is $\Delta E_{\text{des}} = 26.3$ kcal/mol. Though this value is rather high, compared to the alternative endothermic coadsorption of O_2 via TS 3, this step might, at least at elevated temperatures, play an important role when the influence of entropy has an increased impact on the Gibbs' free enthalpy. Then, oxygen exothermically coadsorbs to FeNO (ST 11) via the transition state TS 2 and a negligible barrier of $E^\ddagger=0.03$ kcal/mol which presents a cross-over to the FeO cycle. An additional NO does not interact with this species (ST 12) and thus the subsequent formation of the -OONO ligand on FeNO (ST 14) can be seen as of the Eley-

Rideal type. The activation energy for this process is $E^\ddagger=19.8$ kcal/mol (TS 4) and with that considerably higher than the barriers for the formation of this ligand next to the nitrite. Similar as before, a conformational change of the ligand leads to its cis form (ST 17), of which NO_2 desorbs (ST 20). For these steps we found the barriers $E^\ddagger=8.8$ kcal/mol (TS 7) and $E^\ddagger=11.0$ kcal/mol (TS 9), respectively. Finally, the remaining ONFeO (ST 21) on the quintet PES reforms the active site via TS 11 by overcoming a barrier of $E^\ddagger=3.9$ kcal/mol.

An analysis of the Gibbs' free energies in Figure 7.5 supports the finding that the coadsorption of oxygen to ONFeONO is rather unlikely but the desorption of NO_2 to FeNO might be of importance in terms of a crossing to the FeO cycle. However, the subsequent cycle on FeNO itself exhibits rather high Gibbs' free enthalpies making its relevance unlikely. Furthermore, the adsorption of NO to OFeONO, leading to the formation of the dinitrite-iron, is a favorable process also at elevated temperatures. However, the formation of OFeONO via the intermediate formation of the -OONO ligand again leads to rather high values of the Gibbs' enthalpy compared to the cycle on FeO so that these structures have to be considered less likely to occur.

Catalytic cycle on FeO_2N and on FeO_2NO

Because of the similarities of not only the structure itself with a twofold oxygen bond to the iron, but also of the reaction mechanism, we combined the discussion of these two species as potential active sites into one subchapter. In fact, the described mechanisms here are overall nearly identical with the pathway on FeONO, mainly differing by the ligand, which defines the active site. For FeO_2N the overview is shown in Figure 7.7 and the energies are stated in Figure 7.8. The two corresponding Diagrams for FeO_2NO are presented in Figure 7.9 and 7.10. In order to avoid confusion in the following description of the mechanism, we have added the corresponding energies and labels of the structures for FeO_2NO in brackets.

For both active sites, the start configuration has its ground state on the quintet PES. As described before on FeONO, also here the significant intermediate product, resulting from a reaction between one oxygen and one nitrogen oxide, is constituted by an -OONO ligand in the trans configuration. In the case that O_2 adsorbs first, an energy of $E^\ddagger=2.7$ kcal/mol (TS 1) [$E^\ddagger=2.4$ kcal/mol, TS 2] needs to be surmounted. In the resulting adsorbed state however, the oxygen is only very loosely bond to the actives site with a heat of adsorption of $\Delta E_{\text{ads}} = -1.1$ kcal/mol (ST 4) [$\Delta E_{\text{ads}} = -1.8$ kcal/mol, ST 4]. For a subsequent reaction with NO a spin change from the septet to

the quintet PES is required which exhibits a barrier of $E^\ddagger=10.7$ kcal/mol (S 2) [$E^\ddagger=10.7$ kcal/mol, S 2] and results in the excited structure ST 6 [ST7]. The addition of nitrogen oxide results in a significant reduction of energy by $\Delta E_{\text{ads}} = -11.9$ (ST 8) [$\Delta E_{\text{ads}} = -5.8$ kcal/mol, ST 8], due to an interaction of the NO with the adsorbed oxygen. A subsequent reaction with a negligible barrier of $E^\ddagger=0.1$ kcal/mol (TS 4) [$E^\ddagger=0.5$ kcal/mol, TS 4] eventually leads to the -OONO ligand in the trans configuration (ST 10) [ST 10]. In the case that the catalytic cycle is started with the adsorption of NO, a spin change is required from the sextet to the quartet potential energy surface, to obtain the ground state (ST 5) [ST 6]. The corresponding energy barrier for this process is rather small with $E^\ddagger=1.1$ kcal/mol (S 1) [$E^\ddagger=2.0$ kcal/mol, S 1] and the adsorbed state can be considered stable because of the significant heat of adsorption of $\Delta E_{\text{ads}}=-18.7$ kcal/mol on both active sites. In contrast to the mechanism on FeONO, the subsequent formation of the -OONO ligand in this pathway does not require the adsorption of oxygen, but results from a gas phase attack of molecular oxygen. This involves the highest barrier in the catalytic cycle with $E^\ddagger=23.9$ kcal/mol, corresponding to the transition state TS 3 [$E^\ddagger=23.7$ kcal/mol, TS 3]. Though this reaction was concluded in contrast to the FeONO cycle to be of the Eley-Rideal type, it has to be mentioned that, from a structural point of view, this transition state is equivalent to the TS 5 (Figure 7.6). The difference of the reactant state results from the even lower stability of NO and O₂ being coadsorbed on FeO₂N and FeO₂NO as the active sites. Next, the -OONO ligand transforms from the trans into the cis conformation (ST 12) [ST 11], which requires to surmount a barrier of $E^\ddagger=8.7$ kcal/mol (TS 6) [$E^\ddagger=8.9$ kcal/mol, TS 5]. Then, NO₂ is released via the transition state TS 7 with an activation energy of $E^\ddagger=9.9$ kcal/mol [$E^\ddagger=9.7$ kcal/mol, TS 6]. This results in an unstable intermediate (ST 14 and ST 12 respectively), because the subsequent release of NO₂ in the gas phase is exothermic. For FeO₂N, the -OONO ligand might also form a ring structure with the free oxygen binding to the iron. This step exhibits a negligible barrier of $E^\ddagger=1.7$ kcal/mol (TS 8) and the ring structure being slightly lower in energy compared to the loose ligand (ST 13). Also from the ring structure NO₂ can desorb via TS 9 by overcoming a barrier of $E^\ddagger=13.1$ kcal/mol. The NO₂ desorption eventually leads to OFeO₂N (ST 16) [OFeO₂NO, ST 13] on the quintet PES. Then, another NO adsorbs by forming adsorbed NO₂ with the remaining atomic oxygen bonded to the iron which is strongly exothermic by $\Delta E_{\text{ads}}=-34.1$ kcal/mol (ST 17) [$\Delta E_{\text{ads}}=-38.0$ kcal/mol, ST 14]. Finally, the second NO₂ desorbs from the iron by overcoming the heat of desorption $\Delta E_{\text{des}}=14.6$ kcal/mol [$\Delta E_{\text{des}}=14.9$ kcal/mol].

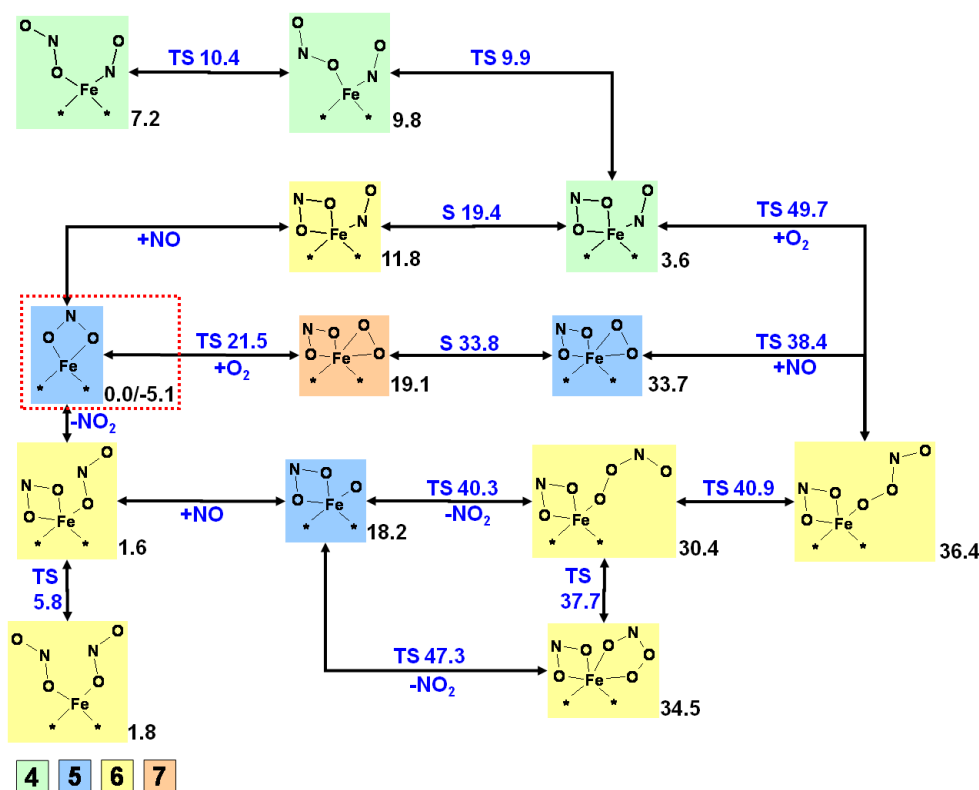


Figure 7.7: Overview of considered catalytic cycles of the NO oxidation on $Z^-[\text{FeO}_2\text{N}]^+$ as representation of the active site. Stated values are Gibbs' free enthalpies calculated at 600 K. Black numbers correspond to the structure, blue numbers to the transition states (TS) or to the minimum on the seam of two PESs (S). Colors of the boxes correspond to the spin multiplicity.

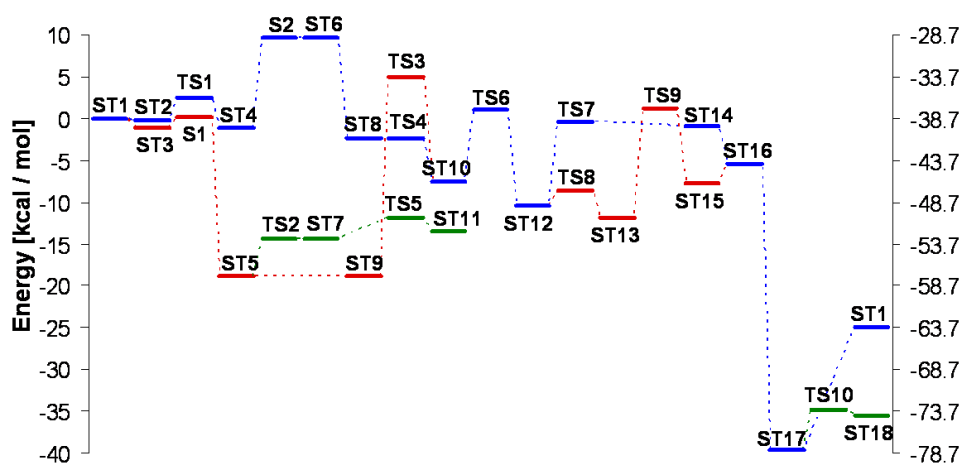


Figure 7.8: Energy profiles for the catalytic cycles of NO oxidation on $Z^-[\text{FeO}_2\text{N}]^+$. Second axis corresponds to $Z^-[\text{FeO}]^+$ as reference state. Energies are zero-point corrected.

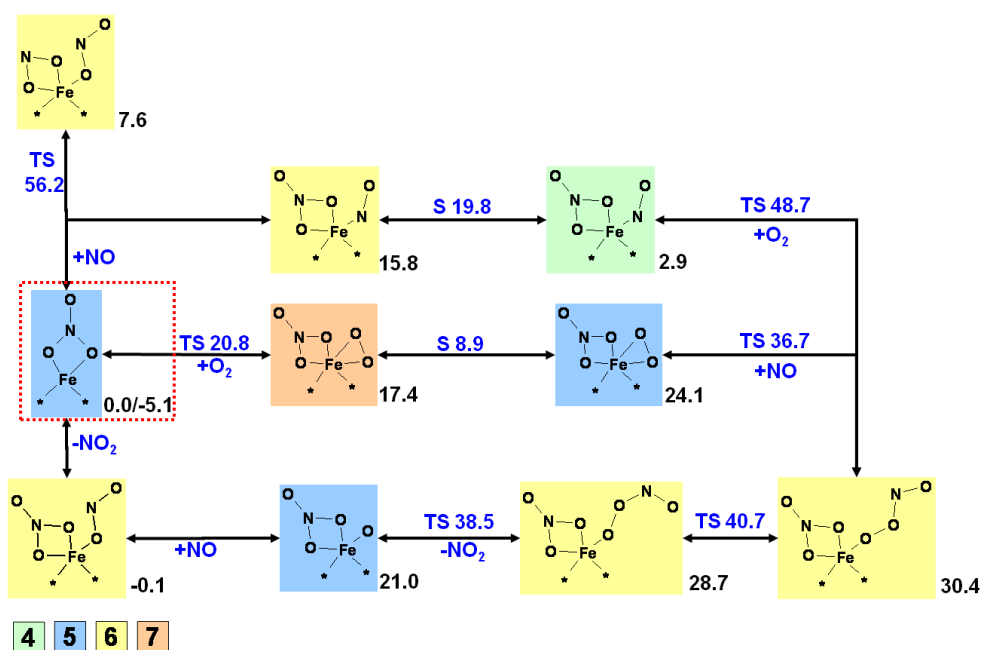


Figure 7.9: Overview of considered catalytic cycles of the NO oxidation on $Z^-[\text{FeO}_2\text{NO}]^+$ as representation of the active site. Stated values are Gibbs' free enthalpies calculated at 600 K. Black numbers correspond to the structure, blue numbers to the transition states (TS) or the minimum on the seam of two PESs (S). Colors of the boxes correspond to the spin multiplicity.

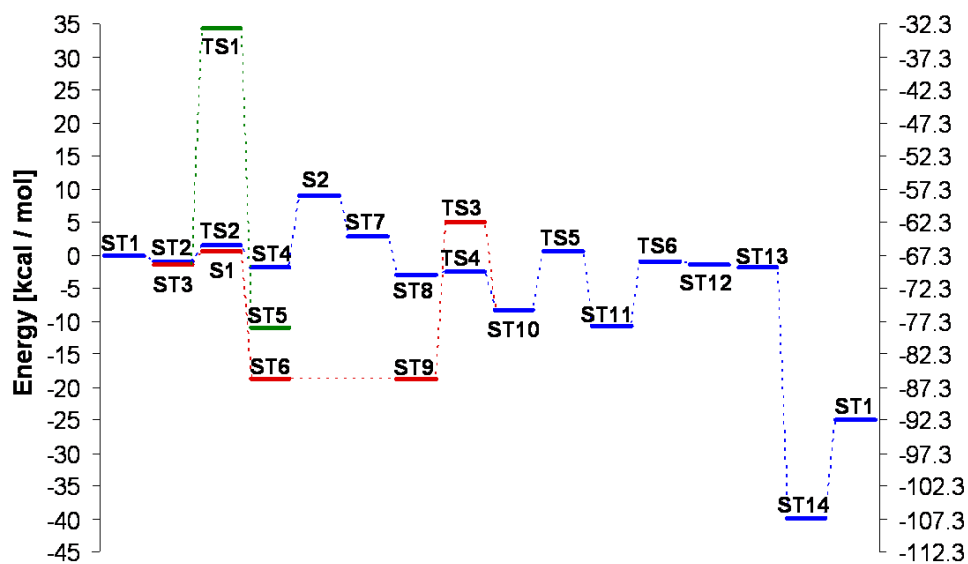


Figure 7.10: Energy profiles for the catalytic cycles of NO oxidation on $Z^-[\text{FeO}_2\text{NO}]^+$. Second axis corresponds to $Z^-[\text{FeO}]^+$ as reference state.

In addition to the catalytic cycle on the two active sites we also found a cross-over for FeO_2N to the corresponding cycle on FeONO . For the transformation of the stable structure ONFeO_2N on the quartet PES into the ONFeONO first the bond between one oxygen atom and the iron is cleaved, leading to a cis conformation of the nitrite ligand (ST 7) by overcoming a barrier of $E^\ddagger=4.4$ kcal/mol (TS 2). Then, a rotation of the nitrite leads to the energetically equivalent trans conformation (ST 11). This process exhibits a barrier of $E^\ddagger=2.6$ kcal/mol (TS 5). Furthermore, NO_2FeONO is transformed into ONOFONO (ST 18) via TS 10 and a barrier of $E^\ddagger=4.9$ kcal/mol. Because a similar transition for the active sites themselves was also found with a rather low barrier (TS 1, Figure 7.3), it can be assumed that both nitrite pathways might interchange within all intermediate structures and the low barriers suggest equilibrium between them. Furthermore, we also found a reaction of gas phase NO with FeO_2NO , leading to adsorbed NO_2 on FeO_2N (ST 5, Figure 7.10) on the sextet PES. This step however exhibits a very high activation energy of $E^\ddagger=35.7$ kcal/mol (TS 1), indicating the high stability of the nitrate. Furthermore, this barrier is within the same magnitude of the barrier for the splitting of the nitrate into OFeONO (35.9 kcal/mol). Thus, this high barrier contradicts somewhat the by Tronconi et al.¹⁶⁹ stated relevance of this reaction for the fast SCR with ammonia because they assumed this step to be fast also at low temperatures (below 140 °C) but blocked by ammonia.

A comparison of the reaction pathways on the two potential active sites with each other but also with the already discussed cycle on FeONO reveals that they all resemble each other not only from the structural perspective but also with respect to their energy profiles. In all cases, the highest internal energy barrier is the reaction of oxygen with ONFeX ($\text{X} = \text{ONO}, \text{O}_2\text{N}$ and O_2NO) with ~ 20 kcal/mol (In the case of ONO the difference between ST 8 and TS 5). Also the subsequent cis-trans change and the NO_2 desorption of the -OONO ligand exhibit similar barriers with ~ 10 kcal/mol. Solely in the case of the initial adsorption of oxygen, the heat of adsorption on FeONO was found to be slightly higher with $\Delta E_{\text{ads}}=-4.5$ kcal/mol compared to -1.0 kcal/mol and -1.7 kcal/mol on FeO_2N and FeO_2NO respectively.

An analysis of the Gibbs' free energies as shown in Figures 7.7 and 7.9 for FeO_2N and FeO_2NO respectively reveals that only the adsorption of NO to the active site is of relevance and oxygen adsorption can be neglected. However, the subsequent reaction with oxygen from the gas phase exhibits significantly high enthalpies for the transition states (49.7 kcal/mol and 48.7 kcal/mol) making such a step rather unfavorable. Also the formation of the ring structure from the cis -OONO ligand can be considered unlikely, because

the slight gain in stability with respect to enthalpy is by far consumed by the corresponding loss in entropy.

It can be concluded from the so far investigated catalytic cycles that starting from FeO as the principal structure the stable structures FeONO, FeO₂N and FeO₂NO can be formed easily also at elevated temperatures. The two nitrite structures are similar in energy and are both present on the surface because they are separated by rather low energy barriers (5-8 kcal/mol). Furthermore, FeONO is a direct intermediate participating in the catalytic cycle on FeO. The nitrate structure, however, is significantly lower in energy compared to the other intermediates and with that has to be considered as very stable. Thus, once formed, elevated temperatures are needed to reduce the nitrate back into a nitrite. The adsorption of oxygen to either the nitrite in the closed form or to the nitrate was found to be very unlikely because of a very low heat of adsorption. The highest barriers on the nitrite and the nitrate structures were found to be the reaction of adsorbed NO with oxygen, leading to the -OONO intermediate which is also shown from the Gibbs' free enthalpies to be the main bottleneck of the catalytic cycles on these structures. On FeO the most probable pathway was concluded to involve the desorption of NO₂ from the O₂FeONO structure and a subsequent reactive adsorption of NO forming the -OONO ligand. It is obvious that the latter ligand is a key species in all the discussed potential active sites so far and it should be pointed out that also Heyden et al.³⁰⁰ considered its cis-configuration in the context of the NO assisted decomposition of N₂O for the same active sites as well as for the hydroxylated iron. The results for the desorption of NO₂ from this species are in close agreement with ours. Overall, it has to be concluded that, especially at high temperatures, the catalytic cycles on both nitrite and the nitrate structures do not contribute significantly to the oxidation of NO. However, at least at low temperatures, the formation of the nitrate is expected to block the active site.

7.3.2 Activity of Iron Exchanged ZSM5 in the Presence of Water

Kröcher et al.³⁸ and Giles et al.²⁸⁸ found water to significantly inhibit the oxidation of nitrogen oxide. Furthermore, there is agreement in the literature,^{38,156,158,282,283} that the NO oxidation is the rate limiting step of the SCR, which itself produces water. With that, a highly connected system is established with the main reaction, the SCR, slowing its rate limiting step down, the oxidation of NO. Thus, the following analysis of the influence of water on the above described reactions also aims to provide an insight into poten-

tial further intermediates and stable structures which might be important adsorption sites for ammonia within the SCR.

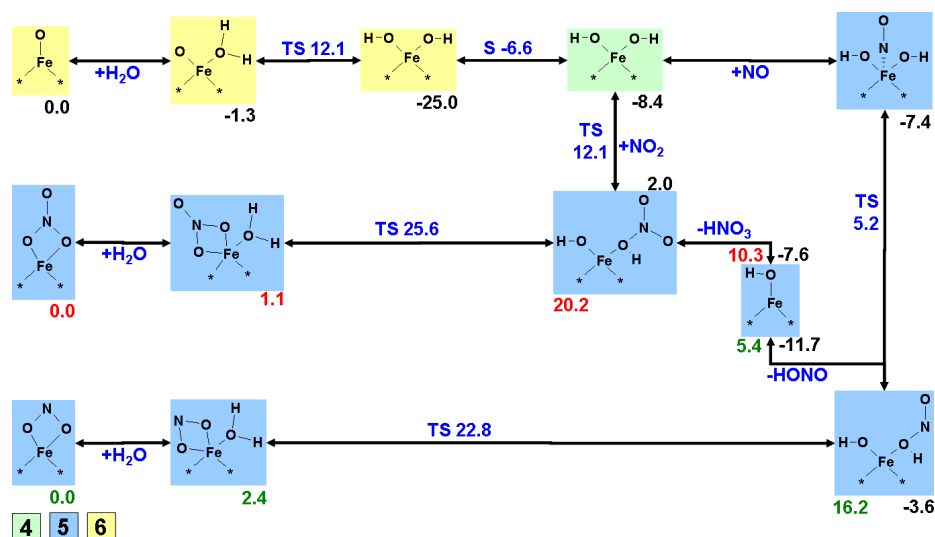


Figure 7.11: Overview of the interaction of water with $Z^-[\text{FeO}]^+$, $Z^-[\text{FeO}_2\text{N}]^+$ and $Z^-[\text{FeO}_2\text{NO}]^+$. Stated values are Gibbs' free enthalpies calculated at 600 K. Black numbers correspond to FeO as reference, green to FeO_2N and red to FeO_2NO . The blue numbers correspond to the transition states (TS) or the minimum on the seam of two PESs (S). Colors of the boxes correspond to the spin multiplicity.

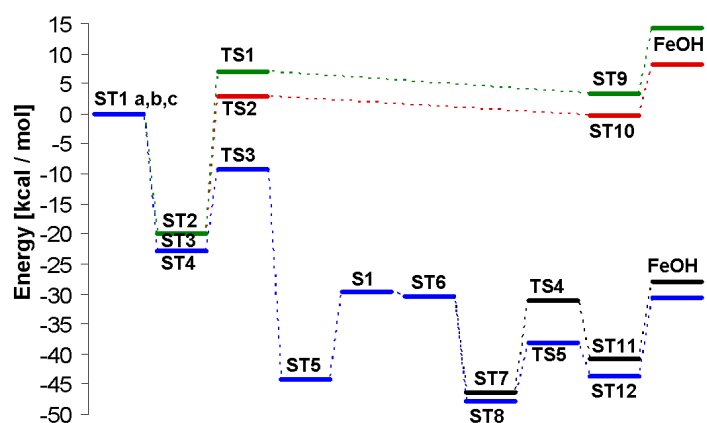


Figure 7.12: Energy profiles for the interaction of water with $Z^-[\text{FeO}]^+$, $Z^-[\text{FeO}_2\text{N}]^+$ and $Z^-[\text{FeO}_2\text{NO}]^+$. Energies are zero-point corrected.

Heyden et al.¹¹⁹ already showed in their theoretical analysis of the influence of water on the activity of mononuclear iron sites for the N_2O decomposition that, in a reaction of FeO with adsorbed water, dihydroxylated sites are created which are rather inactive. Furthermore, they presented a potential reaction of these sites with NO, leading to nitrous acid and monohydroxylated iron which is active for the N_2O decomposition. We also found that the stable structure HOFeOH (Figure 7.1) with the ground state on the PES with $M_S=6$ is easily formed. However, no adsorption of oxygen on this site was observed and the NO adsorption was rather weak. Thus, no catalytic cycle for the oxidation of NO on this site was concluded to be reasonable. However, besides the formation of HOFeOH from water and FeO and the subsequent formation of nitrous acid and FeOH in accordance with Heyden et al.,¹¹⁹ we also provide the reaction of NO_2 with the dihydroxylated iron, leading to nitric acid in Figure 7.11. Finally, we also considered the reaction of water with the stable nitrite FeO_2N and nitrate FeO_2NO , which also leads to FeOH and nitrous and nitric acid, respectively. In the corresponding energy diagram (Figure 7.12) we have set each of the different reference states to zero, allowing for a direct comparison of the single adsorption and reaction steps. In Figure 7.11, we attributed the different reference states by different colors of the stated values of the structures, with black representing FeO, green for FeO_2N and red for FeO_2NO .

The pathways are started with the adsorption of water to the ground state of the considered active site. The highest heat of adsorption of water is obtained for FeO (ST 1a) on the PES with $M_S=6$ with $\Delta E_{\text{ads}}=-22.9$ kcal/mol. In the case of FeO_2N (ST 1b) and FeO_2NO (ST 1c) with $M_S=5$ the heat of adsorption was found to be slightly less but very close to each other with $\Delta E_{\text{ads}}=-19.8$ kcal/mol and $\Delta E_{\text{ads}}=-19.9$ kcal/mol. Then, a hydrogen transfer takes place from the water to an oxygen atom of the respective active site structure. Thus, via TS1 the nitrate (ST 3) is transformed into nitric acid, adsorbed on FeOH (ST 9) by overcoming a barrier of $E^\ddagger=26.9$ kcal/mol. The transition state TS 2 describes the corresponding hydrogen transfer from the water on the nitrite structure (ST 2) to the formation of nitrous acid (ST 10) with a barrier of $E^\ddagger=22.6$ kcal/mol. The higher energy barrier for the hydrogen transfer on the nitrate structure compared to the nitrite indicates that though the process itself is very similar for both, the nitrate is more stable. The lowest barrier for this reaction step is obtained for the FeO as initial site with $E^\ddagger=13.7$ kcal/mol (TS 3) leading to the twofold hydroxylated iron (ST 5) on the PES with $M_S=6$. Furthermore, this step was found here to be strongly exothermic by $\Delta E=-21.3$ kcal/mol while being endothermic for the nitrite and nitrate structures with $\Delta E=19.5$ kcal/mol and $\Delta E=23.3$

kcal/mol, respectively. However, for a further reaction of the dihydroxylated iron with NO or NO₂ a spin change is necessary because the final product, nitrous or nitric acid on FeOH has its ground state on the PES with $M_S=5$ while the reactant state is on the PES with $M_S=7$. This spin change of HOFeOH to the PES with $M_S=4$ via the crossing of the seam S 1 exhibits an energy barrier of $E^\ddagger=14.5$ kcal/mol with the resulting product (ST 6) being $\Delta E=13.9$ kcal/mol higher in energy than the corresponding ground state. Here, NO directly adsorbs to the iron (ST 8) while NO₂ only forms a hydrogen bond with one hydroxyl group (ST 7). The corresponding heats of adsorption with respect to the excited state are $\Delta E_{\text{ads}}=-17.5$ kcal/mol for NO and $\Delta E_{\text{ads}}=-16.0$ kcal/mol for NO₂. Subsequently, the adsorbed species reacts with one of the hydroxyl groups, forming nitrous (ST 12) or nitric acid (ST 11). In the case of NO this involves a barrier of $E^\ddagger=9.5$ kcal/mol (TS 5) and for NO₂ $E^\ddagger=15.1$ kcal/mol (TS 4).

In summary, it is obvious that water easily reacts with FeO, forming the dihydroxylated iron. In the presence of NO or NO₂ this site will be reduced to FeOH by forming nitrous or nitric acid respectively, which, overall, is an exothermic process. On the other hand, the reaction of adsorbed water on the nitrite or nitrate iron, which forms the two acids is endothermic and thus less favorable. This finding is also supported by the Gibbs' free Energies at 600 K as shown in Figure 7.11. Even at this temperature the reaction pathway on FeO via HOFeOH to FeOH is strongly favorable including rather low internal energy barriers while the reactions of the nitrite and nitrate with water have their equilibrium on the side of the reactants. This leads to the conclusion that the inhibiting influence of water mainly can be attributed to the formation of the inactive dihydroxylated iron which eventually transforms into FeOH. The activity of the latter species will be addressed in the following section. Nevertheless, because the nitrite and nitrate were concluded to be very stable surface species, even unfavorable equilibrium conditions might allow for the acid formation considering that the reactants water and surface nitrite and nitrate are present in large amounts. The barrier for the reduction of the surface nitrate with $E^\ddagger=26.9$ kcal/mol is significantly lower (by $\Delta E=8.8$ kcal/mol) than the barrier found for the reaction with NO. Thus, water might indeed have the potential to reduce the surface nitrate. The acids, however, then also might form the inactive surface nitrite and nitrate in the reverse reaction, depending on the amount of FeOH present.

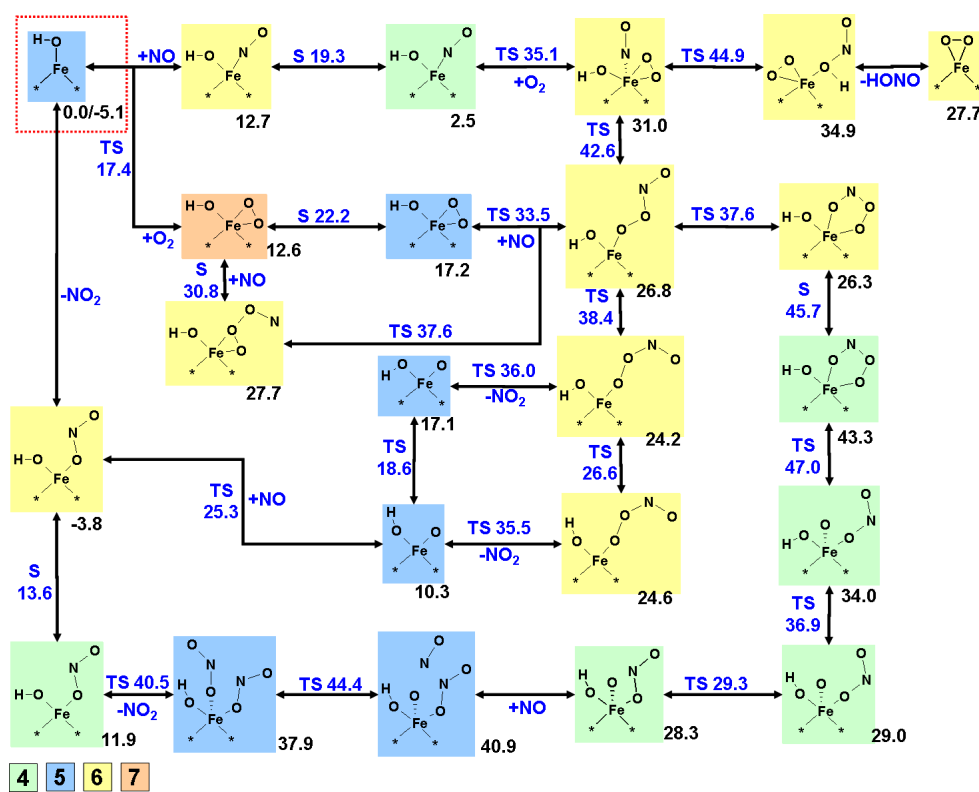


Figure 7.13: Overview of considered reactions in the main catalytic cycles of the NO oxidation on $Z^-[\text{FeOH}]^+$ as representation of the active site. Stated values are Gibbs' free enthalpies calculated at 600 K. Black numbers correspond to the structure, blue numbers to the transition states (TS) or to the minimum on the seam of two PESs (S). Colors of the boxes correspond to the spin multiplicity.

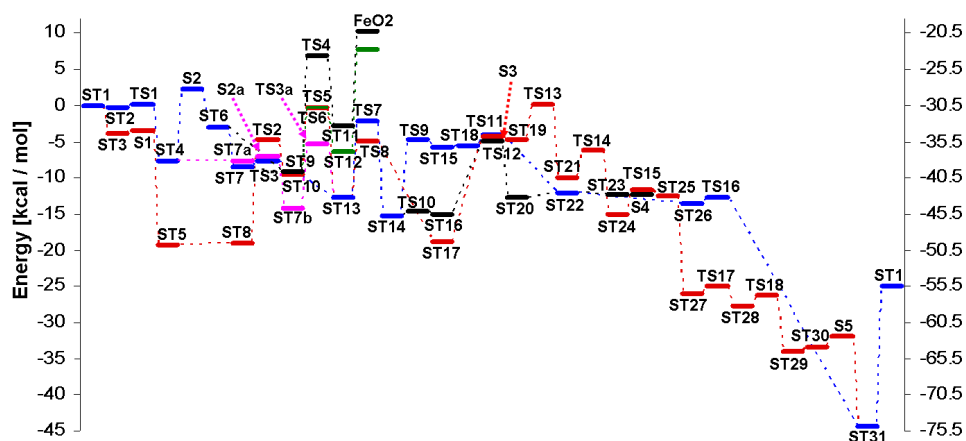


Figure 7.14: Energy profiles for the catalytic cycles of NO oxidation on $Z^-[\text{FeOH}]^+$. Second axis corresponds to $Z^-[\text{FeO}]^+$ as reference state. Energies are zero-point corrected.

Catalytic cycle on FeOH

Because it can be expected from the former discussion that water will lead to the formation of FeOH it is of interest whether this species itself exhibits a high activity for the NO oxidation or rather blocks the active site. Within this study, we also found the potential formation of a nitrate species besides the hydroxyl group. Furthermore, we also included crossings to the non-hydroxylated structures by considering the formation of nitrous and nitric acids, similar to their above discussed formation on the dihydroxylated iron. First, we will discuss the main catalytic cycle which is shown in an overview in Figure 7.13. The corresponding energies are shown in Figure 7.14. The second part discusses the potential nitrate structures and the acid formation.

Main Cycle In a similar way as for the cycle on FeONO, we started the reaction with the adsorption of oxygen onto the ground state of FeOH on the quintet PES. This step here is also an activated process, exhibits a barrier of $E^\ddagger=0.6$ kcal/mol (TS 1) and is exothermic by $\Delta E_{\text{ads}}=-7.3$ kcal/mol (ST 4). Then, prior to a reaction with NO, the crossing of the seam between the septet and the quintet (ST 6) PES is necessary, which includes a barrier of $E^\ddagger=9.9$ kcal/mol (S 2). NO coadsorbs to this excited structure (ST 7) and a reaction with an activation energy of only $E^\ddagger=0.8$ kcal/mol (TS 3) leads to the -OONO ligand in the trans configuration (ST 13). Alternatively, the crossing of the seam can also incorporate the adsorption of the NO, by overcoming a barrier of $E^\ddagger=0.8$ kcal/mol (S 2a). In the adsorbed state NO is here bond to the adsorbed oxygen (ST 7b) on the sextet PES, while on the PES with $M_S=8$ (ST 7a) no interaction between NO and the active site can be observed. Then, the -OONO ligand forms via TS 3a which exhibits a barrier of $E^\ddagger=8.9$ kcal/mol. With that, both pathways for the crossing of the seam, the NO adsorption and the subsequent formation of ST 13 are very similar with respect to their energy barriers and have to be considered as being equally accessible. Again, the -OONO ligand might also be obtained starting first with the adsorption of NO onto FeOH (ST 3). The crossing of the seam from the PES with $M_S=6$ to $M_S=4$ results in the ground state (ST 5), is activated by $E^\ddagger=0.5$ kcal/mol (S 1) and strongly exothermic by $\Delta E=-15.0$ kcal/mol. The subsequent adsorption of oxygen is an activated process including a barrier of $E^\ddagger=14.4$ kcal/mol (TS 2) and is endothermic by $\Delta E=9.5$ kcal/mol (ST 10), which makes this alternative pathway less favorable. Nevertheless, via the transition state TS 5 and a barrier of $E^\ddagger=9.4$ kcal/mol also the -OONO ligand is formed in the trans configuration. The desorption of a first NO₂ was found to occur from the corresponding cis configuration (ST14) and, thus, we have considered the conformational change.

This step requires to overcome a barrier of $E^\ddagger=10.6$ kcal/mol (TS 7). So far, the hydrogen of the hydroxyl group was pointing downwards. For the product of the subsequent desorption of NO_2 however, we found the structure OFeOH on the quintet PES to be more favorable with the hydrogen pointing upwards (ST 22) by $\Delta E=6.6$ kcal/mol. Thus, we considered first the rotation of the hydroxyl group on the $-\text{OONO}$ ligand structure, including a barrier of $E^\ddagger=0.7$ kcal/mol (TS 10). Here, no difference in energy is observed for the upwards pointing hydrogen (ST 16). For the NO_2 desorption via TS 12 a barrier of $E^\ddagger=10.1$ kcal/mol was calculated and from the energy diagram it can be concluded that NO_2 hardly interacts with the remaining OFeOH (ST 20 vs. ST 22). Alternatively, we also considered first the desorption of NO_2 from the downwards pointing hydroxyl group and a subsequent rotation of the latter. Here, the desorption exhibits an activation energy of $E^\ddagger=10.4$ kcal/mol (TS 9) and the rotation of the hydroxyl group $E^\ddagger=1.5$ kcal/mol (TS 11). Thus, from an energetic point of view both pathways are equally accessible. Next, the adsorption of a second NO forms NO_2 adsorbed on the FeOH (ST 31) on the sextet PES. This process is activated by $E^\ddagger=0.9$ kcal/mol (TS 16) and strongly exothermic by $\Delta E_{\text{ads}}=-30.8$ kcal/mol. The final desorption from this structure then restores the initial active site FeOH with a desorption energy of $\Delta E_{\text{des}}=19.4$ kcal/mol.

Besides this very similar pathway as compared to the one on FeONO , we found an additional reactive branch starting from the $-\text{OONO}$ ligand in the trans configuration (ST 13). The formation of a ring structure, being bond with two oxygen to the iron was found via TS 8 by overcoming a barrier of $E^\ddagger=8.0$ kcal/mol which is about $\Delta E=2.5$ kcal/mol lower than the one for the formation of the cis configuration. Also, the resulting structure itself (ST 17) is $\Delta E=3.6$ kcal/mol lower in energy than the cis form. For a following cleavage of the internal O-O bond, leading to NO_2 adsorbed on HOFeO (ST 21), a spin change to the quartet PES is necessary first. The crossing of the seam exhibits a barrier of $E^\ddagger=14.4$ kcal/mol (S 3) and the resulting state with the lower spin multiplicity (ST 19) has to be considered rather unstable because the reverse barrier was calculated to only be $E^\ddagger=0.4$ kcal/mol. The O-O cleavage itself exhibits an activation energy of $E^\ddagger=5.0$ kcal/mol (TS 13) and, thus, the spin change and the cleavage should rather be seen as a combined step with a barrier of $E^\ddagger=19.0$ kcal/mol. In the resulting structure (ST 21) on the quartet PES the adsorbed NO_2 is bond to the iron with one oxygen and in a cis configuration while the hydrogen of the hydroxyl group points downwards. The rotation of the latter group via TS 14 and a barrier of $E^\ddagger=3.9$ kcal/mol leads to the corresponding counterpart which is $\Delta E=5.1$ kcal/mol lower in energy (ST 24). The rotation of the

nitrite group into a trans configuration (ST 25) is slightly endothermic and exhibits a barrier of $E^\ddagger=3.4$ kcal/mol (TS 15). Here, two branches are further possible. A spin change from the quartet to the sextet PES leads to a state in which NO_2 hardly interacts with the remaining HOFeO (ST 23) and, thus, can be considered as in the gas phase. The barrier for this spin change is negligibly small with $E^\ddagger=0.2$ kcal/mol (S 4) and both PESs have nearly the same energy. Thus, this crossover to the previously described pathway (to ST 22) is very likely. However, the adsorption of NO to ST 25 is quite exothermic with $\Delta E_{\text{ads}}=-13.6$ kcal/mol and intermediately forms N_2O_3 with the nitrite (ST 27). Then, two low barrier reactions first lead to the formation of two nitrite ligands (ST 28) and then to the desorption of NO_2 (ST 29). The NO_2 formation exhibits on the quintet PES a barrier of $E^\ddagger=1.0$ kcal/mol (TS 17) and the desorption $E^\ddagger=1.4$ kcal/mol (TS 18). The remaining HOFeONO (ST 30) on the quartet PES was only found with the hydroxyl group pointing upwards. Another spin change to the PES with $M_S=6$ via the seam S 5 and by overcoming a barrier of $E^\ddagger=1.3$ kcal/mol leads to the ground state (ST 31) from which finally the second NO_2 desorbs as described before. Finally, we included in this first part the potential formation of nitrous or nitric acid on FeO_2 , starting from the structure O_2FeOH on the quintet PES (ST 6). For nitrous acid, the reaction is initiated by the adsorption of NO (ST 10) and has to overcome a barrier of $E^\ddagger=9.4$ kcal/mol (TS 5) leading to the adsorbed acid on FeO_2 (ST 12). The desorption requires then an energy of $\Delta E_{\text{des}}=14.1$ kcal/mol. In the case of nitric acid, an adsorption of NO_2 , hydrogen bond to the hydroxyl group, is the initial structure (ST 9). The formation of the acid (ST 11) requires to overcome a barrier of $E^\ddagger=16.1$ kcal/mol (TS 4) and the final desorption step $\Delta E_{\text{des}}=13.1$ kcal/mol. Because in both cases the activation energy as well as the subsequent desorption barrier are within the order of magnitude of the previously discussed reaction pathways, these crossings to FeO_2 in its ground state on the sextet PES have to be considered accessible.

In summary, all the described pathways are quite similar with respect to their energy profiles and none can be excluded. However, the most probable formation of the intermediate -OONO ligand results from first the adsorption of oxygen prior to a reaction with NO because the alternative pathway involves a higher internal barrier. For the desorption of the NO_2 from this ligand, the pathway via the cis configuration exhibits lower barriers than the alternative pathway via the ring configuration and is, thus, considered more favorable. This conclusion is also in agreement with the Gibbs' free energies at 600 K stated in Figure 7.13 with the overall lowest values represented by this pathway. In contrast, the pathway via the ring structure can be con-

sidered to be rather unlikely based on the Gibbs' free energies. With that, we have found a reactive cycle on FeOH for the NO oxidation. However, a comparison of this reactive pathway with the one on FeO as the starting configuration reveals that the Gibbs' free energies are significantly lower for the latter one suggesting its higher activity. In fact, the energies corresponding to the cycle on FeOH resemble strongly those of FeONO as the active site for which the conclusion was already drawn that it is less active than FeO. This finding is in agreement with the experimental results of Giles et al.²⁸⁸ and Kröcher et al.³⁸ who stated an inhibiting influence of water on the NO oxidation.

Surface Nitrate and nitric and nitrous acid formation In the second part of the investigation on monohydroxylated iron we discuss the formation and stability of a nitrate species as well as the further formation of nitrous and nitric acid from the dehydroxylation of the iron. The schematic overview is shown in Figure 7.15 with the energies in Figure 7.16. Here, we started the discussion with the adsorption of NO₂ on HOFeO (ST 1) with hydrogen in the upwards position on the sextet PES (ST 2) and the crossing of the seam (S 1) to the quartet PES (ST 3). These structures are identical with ST 22, ST 23, S4 and ST 25 of the main cycle representing the pathway to the initial structure for the nitrate formation. The latter is then formed in a reaction, starting from HOFeO-ONO on the PES with M_S=4 (ST 4) by overcoming a barrier of $E^\ddagger=4.8$ kcal/mol (TS 1). This step is strongly exothermic by $\Delta E=-28.3$ kcal/mol. The subsequent crossing of the seam from the quartet to the sextet PES only exhibits a barrier of $E^\ddagger=0.1$ kcal/mol (S 2) and leads to the ground state of HOFeO₂NO (ST 5) which lies $\Delta E=17.0$ kcal/mol below the corresponding structure on the PES with the lower spin multiplicity. NO hardly interacts with this structure as can be seen from the negligible adsorption energy corresponding to ST 6. Thus, the subsequent reaction, leading to a nitrite species (ST 16) and NO₂, has to be considered to be of the Eley-Rideal type. The energy barrier calculated for this step is $E^\ddagger=38.0$ kcal/mol (TS 6) and indicates the high stability of the nitrate. The obtained nitrite with two oxygen-iron bonds can then be transferred into the nitrite with only one bond (ST 18) by overcoming a barrier of $E^\ddagger=4.9$ kcal/mol (TS 8). For the nitrate structure we found that the state of the hydroxyl group does not influence the energy and the reaction with NO was considered with respect to a downwards pointing hydrogen. Because we referred to the upwards pointing hydrogen within the main cycle for HOFeONO on the sextet PES, we also calculated the rotation of the hydroxyl group on this structure. The obtained barrier, however, is negligible with $E^\ddagger=0.8$ kcal/mol (TS 9) and

both configurations have nearly identical energies (ST 18 vs. ST19). Finally, the desorption of NO_2 leads to the reformation of the initial FeOH on the quintet PES with a desorption energy of $\Delta E_{\text{des}}=19.4$ kcal/mol. An alternative consumption of the formed nitrate structures starts with the adsorption of NO , bond with the nitrogen to the iron of the quartet HOFeO_2NO . This process involves a heat of adsorption of $\Delta E_{\text{ads}}=-18.5$ kcal/mol (ST 8). From this structure, in a first step, the NO forms nitrous acid, adsorbed on the nitrate (ST 12) by overcoming a barrier of $E^\ddagger=4.6$ kcal/mol (TS 5). In a second step, the NO forms NO_2 with one of the nitrate oxygen, bond to the iron (ST 13), which is readily released to the gas phase, leaving HOFeONO on the quartet PES (ST 15). The activation energy for this process was calculated to be $E^\ddagger=35.2$ kcal/mol (TS 7), being only slightly lower than the corresponding barrier on the sextet PES. Finally, the crossing of the seam to the sextet PES involves a barrier of $E^\ddagger=1.3$ kcal/mol (S 3), which leads to the ground state of HOFeONO (ST 19). With that, we have shown two pathways for the consumption of formed nitrate on the hydroxylated iron. However, both pathways exhibit a rather high internal barrier as a limiting factor which might only be overcome at elevated temperatures. In fact, the obtained internal barriers are very similar in magnitude to the barrier for the consumption of non-hydroxylated iron nitrate, indicating that the hydroxyl group does not contribute to this step.

Besides the reduction of the nitrate species, we also included in our investigation here the potential interaction of NO and NO_2 with the hydroxyl group, forming nitrous and nitric acid, respectively. The reaction pathways are equivalent to the acid formation on HOFeO_2 , which was already described within the main cycle. For HOFeO_2NO we already covered the formation of adsorbed nitrous acid as an intermediate of the nitrate reduction on the quintet PES. The desorption of the acid from this structure (ST 12), leaving FeO_2NO in its ground state, requires a heat of desorption of $\Delta E_{\text{des}}=15.3$ kcal/mol. Similar, the formation of adsorbed nitric acid on the quintet PES (ST 11), starting from adsorbed NO_2 (ST 7), involves a barrier of $E^\ddagger=11.7$ kcal/mol (TS 4) and a heat of desorption of $\Delta E_{\text{des}}=13.8$ kcal/mol. In the case of HOFeO_2N , the formation of the acids required, first, the crossing of the seam from the sextet (ST 16) to the quartet PES (ST 17) prior to the adsorption of NO or NO_2 . This step exhibits an activation energy of $E^\ddagger=15.5$ kcal/mol (S 4), leaving a very unstable state, because the reverse barrier is only $E^\ddagger=0.1$ kcal/mol. It is worth mentioning here that the formation of the acids always takes place on the PES which corresponds to the ground state of the remaining structure after the acid desorption. This is, however, in all cases not the ground state of the structure prior to the adsorption of NO or

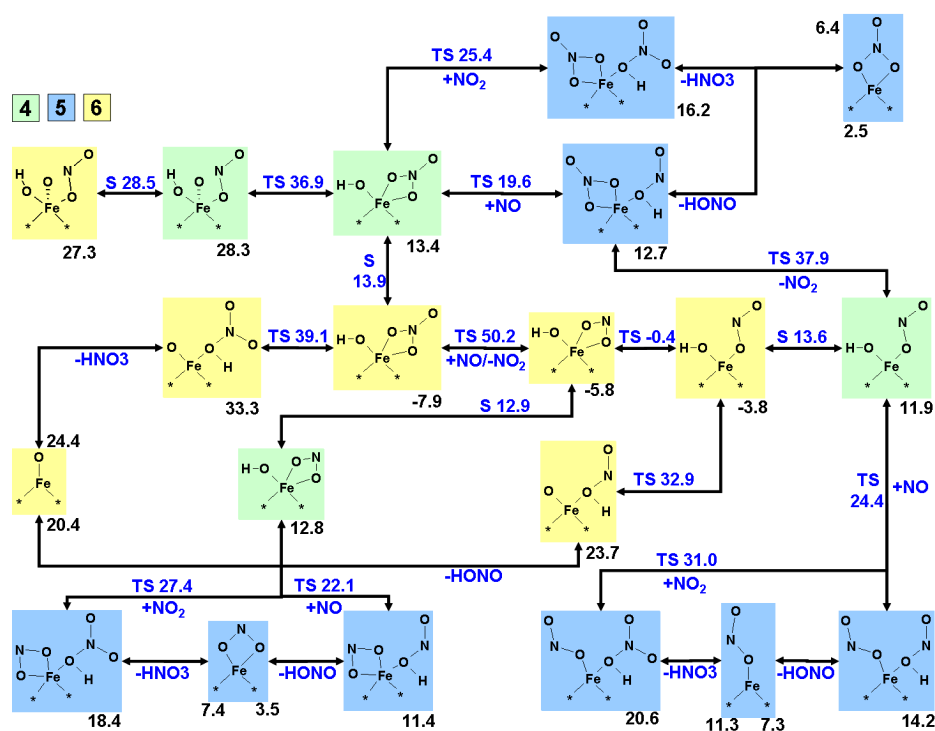


Figure 7.15: Overview of considered reactions including surface nitrate and nitrous and nitric acid formation on $Z^-[\text{FeOH}]^+$ as representation of the active site. Stated values are Gibbs' free enthalpies calculated at 600 K. Black numbers correspond to the structure, blue numbers to the transition states (TS) or to the minimum on the seam of two PESs (S). Colors of the boxes correspond to the spin multiplicity.

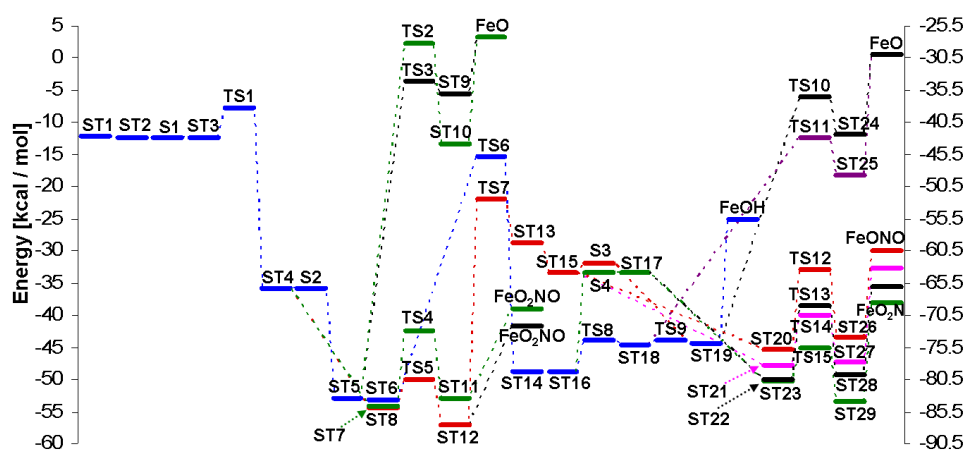


Figure 7.16: Energy profiles for the reactions including nitrate species and nitrous and nitric acid formation on $Z^-[\text{FeOH}]^+$. Second axis corresponds to $Z^-[\text{FeO}]^+$ as reference state. Energies are zero-point corrected.

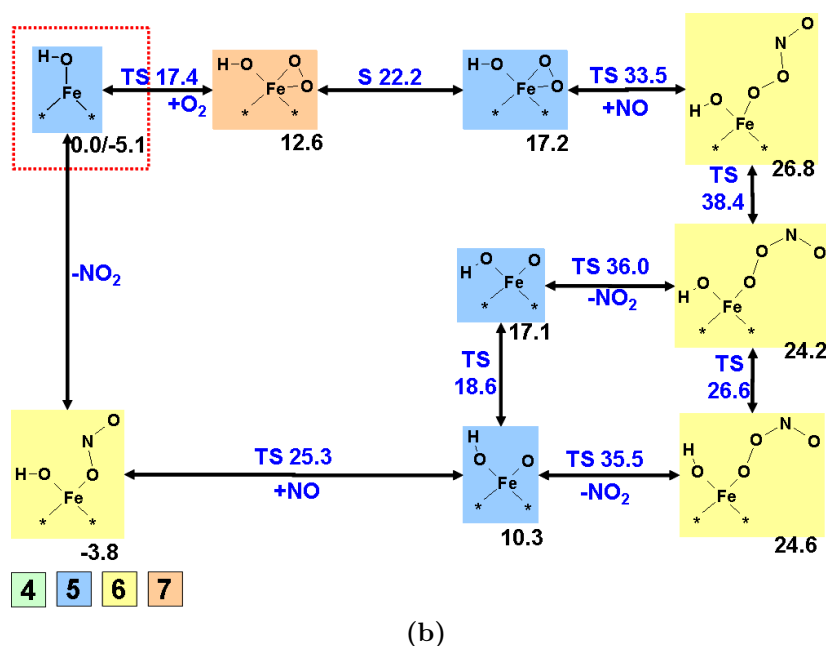
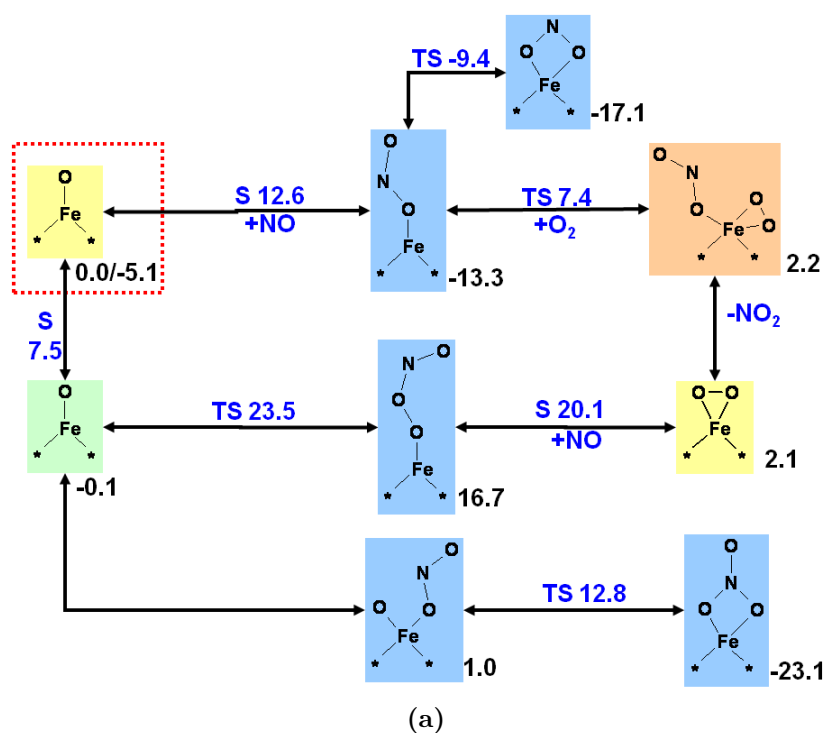


Figure 7.17: Summary of the most probable reaction pathway for the NO oxidation in the a) absence (active site $Z^-[\text{FeO}]^+$) and in the b) presence (active site $Z^-[\text{FeOH}]^+$) of water. Stated values are Gibbs' free enthalpies calculated at 600 K. Black numbers correspond to the structure, blue numbers to the transition states (TS) or to the minimum on the seam of two PESs (S). Colors of the boxes correspond to the spin multiplicity.

NO_2 . After the adsorption of NO to the HOFeO_2N (ST 23) the formation of HONO (ST 29) is activated by $E^\ddagger=5.3\text{ kcal/mol}$ (TS 15) and the desorption requires $\Delta E_{\text{des}}=15.3\text{ kcal/mol}$. In case of NO_2 , the adsorbed state (ST 22) is transferred into the corresponding acid (ST 28) via TS 13 and a barrier of $E^\ddagger=11.4\text{ kcal/mol}$. The desorption requires then $\Delta E_{\text{des}}=14.4\text{ kcal/mol}$. Finally, for HOFeONO on the quartet PES nitrous acid (ST 27) is formed with an activation energy of $E^\ddagger=7.7\text{ kcal/mol}$ (TS 14) starting from adsorbed NO (ST 21) and the desorption of the acid requires $\Delta E_{\text{des}}=14.8\text{ kcal/mol}$. With NO_2 being adsorbed (ST 20), the reaction is activated by $E^\ddagger=12.5\text{ kcal/mol}$ (TS 12) and nitric acid desorbs (ST 26) with a heat of desorption of $\Delta E_{\text{des}}=13.4\text{ kcal/mol}$. In fact, the desorption of the acids are nearly independent of the remaining structures with respect to the heat of desorption. For HONO the value was found to be between 14 and 15 kcal/mol and for HNO_3 between 13 and 14 kcal/mol. But also the activation energies were found to be quite similar and, thus, rather independent of the structure. For nitrous acid the energies are between 4.6 and 9.4 kcal/mol and for nitric acid between 11.4 and 16.1 kcal/mol.

At last, we also analyzed the formation of nitrous or nitric acid without the additional adsorption of NO or NO_2 , starting from HOFeONO and HOFeO_2NO on the sextet PES. Two reaction mechanisms were considered, either the transfer of the hydrogen of the hydroxyl group to the nitrite or nitrate or the transfer of NO or NO_2 from the nitrite and nitrate respectively to the hydroxyl group. The hydrogen transfer exhibits for nitrous acid a barrier of $E^\ddagger=38.5\text{ kcal/mol}$ (TS 10) and for the NO transfer $E^\ddagger=32.0\text{ kcal/mol}$ (TS 11). For nitric acid the barrier for the hydrogen transfer was calculated to be $E^\ddagger=49.3\text{ kcal/mol}$ (TS 3) and for the NO_2 transfer $E^\ddagger=55.3\text{ kcal/mol}$ (TS 2). Thus, for both acids and both cases it has to be concluded that the direct formation of nitrous or nitric acid from the corresponding hydroxylated surface nitrite or nitrate can be excluded because of the rather high energy barriers. However, in the reverse direction, intermediately produced acids easily decompose on FeO, forming the hydroxylated nitrite and nitrate respectively. Also in case of the previously discussed reaction of NO and NO_2 with the hydroxyl groups, the fact that the reaction takes place on the PES of the ground state of the non-hydroxylated surface species suggests that the reverse reaction might be even more important.

Also the calculated Gibbs' free energies in the overview (Figure 7.15) support the results of the discussion so far. It is obvious from the low barriers that the nitrate species will easily form and high temperatures are necessary to shift the equilibrium towards a nitrite form. Also, a reaction with NO involves rather high barriers, making such a step only favorable at high

temperatures. Thus, similar to the case of the non-hydroxylated iron, nitrate species have to be considered to block the active site once they are formed. For the interaction of NO or NO₂ with the hydroxyl group, also at 600 K, the Gibbs' free energies indicate that the equilibrium is on the side of the reactants in their ground state and, thus, does not favor the acid formation.

In conclusion of the results of the influence of water, it is most probable that first inactive dihydroxylated iron is produced which is partially transformed into FeOH by producing nitrous acid. The activity of FeOH itself has to be considered low, compared to FeO as the active site, based on the comparison of the Gibbs' free energies at 600 K. This is in agreement with Giles et al.²⁸⁸ who found at 350 °C a reduction of the steady state conversion from 64% to 29% with respect to NO. Partially, the hydroxyl groups can be removed by the formation of nitrous and nitric acid and with that the further contribution of the FeO as active site cannot be excluded. The removal of formed nitrate species on the other hand is only expected at rather high temperatures, as was also found for the non-hydroxylated iron.

Furthermore, Giles et al.²⁸⁸ have shown in a transient experiment that water, added to the flow of a system in steady state, initially caused a sharp evolution of NO₂ which even exceeded the initial NO concentration. They concluded in accordance with Sachtler et al.²⁸⁴ that water might displace nitrate species on the surface. This is in agreement with our findings that water might react with both structures, FeO₂N and FeO₂NO, forming nitrous and nitric acid and FeOH as shown in Figure 7.11. It can be assumed that in a steady state experiment in the absence of water many active sites will be blocked by either the nitrite or the nitrate species. Thus, by adding water to the system these two reactions exhibit large reactant concentrations. With that, only the question remains about the fate of the nitrous and nitric acid. Either, they reform hydroxylated nitrite and nitrate species, which also includes the release of NO and NO₂, if the acids are adsorbed on FeO₂N, FeONO or FeO₂. Alternatively, they could potentially react with each other in the gas phase or decompose on the Brønsted acids as was shown in chapter 6.

7.4 Conclusion

The reaction mechanism of the oxidation of NO to NO₂ on iron exchanged ZSM5 and the inhibiting influence of water was investigated using the density functional theory. All reaction steps were studied on a cluster of 5 T-atoms, containing a mononuclear iron ion and the crossing of PESs was considered,

if necessary. Starting from $Z^-[\text{FeO}]^+$ we have shown that the stable nitrite structures FeONO and FeO_2N as well as the nitrate FeO_2NO are easily formed, in accordance with the experimental literature.^{155,156,169,285} The conclusion of the most probable reaction pathway is based on a discussion of the activation energies of the single reaction steps and the Gibbs' free energies at 600 K. The reaction involves first the formation of FeONO including a spin change from the septet to the quintet PES. Then, oxygen coadsorbs and NO_2 desorbs, leaving FeO_2 . This species is then attacked by gas phase NO , which again includes a spin change, and a ligand of the sequence $-\text{OONO}$ is formed. From this, finally another NO_2 desorbs and a spin change from the quartet to the sextet PES transfers FeO back into its ground state. In this pathway, the highest barrier is observed for the reactive desorption of the second NO_2 from the $-\text{OONO}$ ligand, thus limiting the overall catalytic cycle. This is in accordance with Delahay et al.²⁸² who stated the assumption that the NO_2 desorption is rate limiting. In contrast, the activity of the nitrite with two oxygen bond to the iron as well as of the nitrate has to be considered negligible. Because of their high stability they block the active site. In the case of the nitrite, the transformation into the active form FeONO only exhibits a low barrier and thus both will exist in equilibrium. The nitrate however, once formed, hardly can be removed, at least at low temperatures. This reduced pathway together with the nitrite and the nitrate formation is shown in Figure 7.17 a).

In the presence of water we found the formation of, first, the dihydroxylated iron and after a reaction with NO or NO_2 the formation of monohydroxylated iron together with nitrous and nitric acid respectively. This is in agreement with the experimental^{285,298} and theoretical^{41,300} findings in the literature. HOFeOH was found to be inactive for the oxidation and FeOH was concluded to exhibit a lower activity for the reaction than FeO . The most probable reaction pathway for the oxidation of NO on FeOH is shown in Figure 7.17 b). The interaction of NO and NO_2 with the hydroxyl group, again producing nitrous or nitric acid, opens a pathway back to the non-hydroxylated iron species. However, a clear conclusion whether the remaining activity of the catalyst in the presence of water is mainly attributed to FeOH as active site or to FeO , including a reduced number of active sites because of blocking effects of the hydroxyl groups, cannot be drawn. Considering the potential surface species for a reaction with ammonia, the stable nitrite and nitrate structures might be the most interesting, which always will be present in an $\text{NO} / \text{NO}_2 / \text{O}_2$ containing system. Also the species observed in the most probable reaction pathway of the NO oxidation are of potential relevance. This includes the active site FeO itself as well as FeO_2 , ONFeO_2 ,

ONFeONO, ONOFeO₂ and finally the species prior to the rate limiting step, FeOONO. Because water is a product of the SCR itself, the formation of the hydroxylated iron species is expected within the framework of the SCR as well. With that, we have presented a theoretical investigation of the NO oxidation on mononuclear iron sites, exchanged into ZSM5, which accounts for many experimentally observed phenomena.

8

Theoretical Investigation of the Mechanism of the Selective Catalytic Reduction of Nitrogen Oxide with Ammonia on Fe-form Zeolites

The selective catalytic reduction of NO with NH₃ has been investigated on a portion of the Fe-ZSM5 which contains 5 T-atoms by using the Density Functional Theory. The iron was represented as a mononuclear species. For the fast SCR and NO₂ SCR it is most likely that ammonia adsorbs on Z⁻[FeO]⁺ and a proton transfer leads to Z⁻[NH₂FeOH]⁺. A subsequent reaction with NO or NO₂ forms nitrosamine or nitramide together with Z⁻[FeOH]⁺, which is probably the most abundant surface species. The reduction of monohydroxylated iron with ammonia leads to Z⁻[FeNH₂]⁺ and water and a final reaction of the amino group with NO₂ to nitrosamine restores the initial site. The intermediates nitrosamine and nitramide can be assumed to decompose on Brønsted acids to nitrogen and nitrous oxide, respectively, together with water. For the increase in selectivity of the NO₂ SCR to nitrogen with temperature, a decomposition of both immediately formed N₂O and NO₂ to NO and oxygen was concluded to be responsible, rather than an additional high temperature pathway. With respect to the decomposition of nitric acid on Z⁻[FeOH]⁺ to dihydroxylated iron and NO₂ followed by the reaction with am-

monia to $Z^-[\text{NH}_2\text{FeOH}]^+$ a mechanistic explanation for the new “enhanced” SCR is also outlined. Finally, the reaction of oxygen with $Z^-[\text{FeNH}_2]^+$, leading first to the radical H_2NO and then via nitroxyl to NO is capable to explain the mechanism of the selective oxidation of ammonia. The results of this work are in agreement with the observed phenomena of the experimental literature.

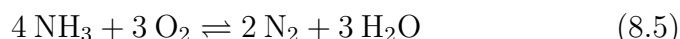
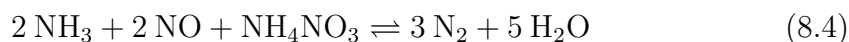
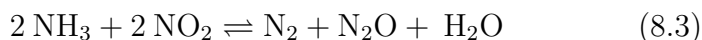
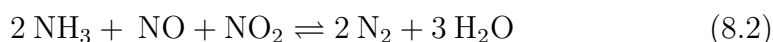
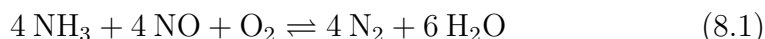
8.1 Introduction

The selective catalytic reduction of nitrogen oxides with ammonia or hydrocarbons has become a key technology in the after-treatment of exhaust gases.^{32,33} Besides the application in the production of nitric acid,²⁹ more stringent legislation for automobiles like the EURO IV and V³¹ have lead to an intensification of research in this field for diesel-engined vehicles. Several materials are known to be active for this reaction, but besides the established V_2O_5 -containing catalysts, by now, metal-containing zeolites appear to be more favorable with respect to durability and activity.³¹⁷ Especially iron-exchanged ZSM5 has been in the focus of research over the last two decades.

Several groups^{34,37,318,319} have examined this catalyst from different perspectives in order to understand its governing parameters, which are responsible for the activity, as well as the mechanisms of its surface chemistry. Several studies concentrate on the impact of different techniques to introduce the metal into the zeolite, covering chemical vapor, liquid and solid ion exchange methods or impregnation.^{293,320–322} The resulting nature of the metal in the final catalyst and the corresponding activity of the exchanged species is also a key aspect of these studies. There is an agreement in the literature that, independent of the applied technique, potentially several different species co-exist, emphasizing mono- and dinuclear iron sites, exchanged to the Brønsted acids of the parent H-form zeolite as well as Fe_xO_y iron clusters.^{323,324} In most studies,^{165,318,325,326} the iron species, resulting from a 1:1 exchange of the Brønsted acids²⁹⁸ are believed to be the active species for the SCR and Kröcher et al.^{36,290} recently stated based on a Poisson distribution analysis that the isolated sites are most relevant at low temperatures, while dinuclear iron sites significantly contribute to the reaction at elevated temperatures. Furthermore, the iron clusters are believed to be especially active for the unwanted oxidation of ammonia.^{164,294} Finally, also the Brønsted acids are

known to be active for the SCR (as discussed in chapters 4 and 6) and their contribution to the reaction remains under debate.^{156,171,172,318,327}

Another key aspect of the investigation on the SCR is the underlying mechanism on the active sites with the intention to better understand the surface chemistry, but also to develop kinetic models to simulate the reaction. This is of certain interest in order to optimize the operating parameters of exhaust gas treatment devices, including heat and mass transfer, but also to develop control devices for optimal ammonia dosage or NO oxidation in diesel oxidation catalysts (DOC).^{328,329} Several macroscopic phenomena are well established by now, including, besides the stoichiometry of the standard SCR (8.1), also the boosting effect of NO₂^{38,40,158} on the reaction, which exhibits a maximum in activity for the ratio of NO₂/NO_x=0.5 and is known as the fast SCR (8.2).



Further increase of this ratio finally leads to the pure NO₂ SCR (8.3), which exhibits a slightly reduced activity as compared to the fast SCR and a significant production of unwanted N₂O is observed. Because the production of nitrous oxide is strongly dependent on temperatures,^{38,40,178} additional different stoichiometric equations are usually attributed with this reaction suggesting different underlying mechanisms.^{170,329} The accepted explanation for the boosting effect of NO₂ on the SCR is the assumption that in the standard SCR the oxidation of NO to NO₂ is required and the rate determining step.^{38,158,282,283,330} With that, the fast SCR can be interpreted to be the true SCR.¹⁶³ However, a discrepancy in this explanation is devoted to the fact that water, which is produced in the SCR, strongly inhibits the NO oxidation^{38,178,288,330} and Fe-ZSM5 was found to be significantly less active for this reaction than for the SCR. Delahay et al.²⁸² suggested that the rate-limiting step of the NO oxidation should be the desorption of NO₂ from the catalyst and that in the SCR this step is circumvented because ammonia directly reacts with the adsorbed species. Similarly, Metkar et al.³³⁰ recently suggested the formation of adsorbed nitrous and nitric acid in the presence of water, which are blocking the NO oxidation. Ammonia is then assumed to react with the acids and, thus, to remove these limiting agents. Nevertheless, the fact that Metkar et al. found similar activities for the SCR and the NO oxidation in the absence of water is in disagreement with Delahay et

al.²⁸² and Schwidder et al.,³⁷ who found significantly lower activities for the oxidation. In the preceding chapter 7, we have outlined that the inhibiting influence of water on the NO oxidation is related to a change of the active site from FeO to FeOH. Furthermore, nitrous and nitric acid were shown to either decompose into an adsorbed hydroxyl group together with NO_x or form a surface nitrite or nitrate, respectively, and are, thus, not expected to remain adsorbed, as stable molecules, on the mononuclear iron sites. With respect to an observed inhibition of the SCR by ammonia,^{169,331} another explanation for the reduced activity of the standard SCR vs. the fast SCR is related to a blocking of the active site for the NO oxidation.^{329,330,332,333} Thus, for the connection between the fast SCR and the standard SCR, a severe interest in the elucidation of the detailed mechanism remains.

Furthermore, Tronconi et al.^{334,335} have established a new reaction system including ammonium nitrate (or nitric acid) as additional reducing agent besides ammonia for the SCR (8.4). They observed a significant enhancement of the SCR, compared to the standard case, but not as pronounced as for the fast SCR. They related the increase in activity to their suggestion that ammonium nitrate is an essential intermediate of the fast SCR. Also, the oxidation of ammonia (SCO) (8.5) was found to be active on Fe/H-ZSM5,^{42,217,221} especially at elevated temperatures and Yang et al.^{43,219,220} observed a correlation between the SCO selectivity towards nitrogen and the SCR activity. Finally, the decomposition of nitrous oxide, as investigated in detail by Heyden et al.,^{119,300,301} and the SCR of nitrous oxide, as studied by Coq et al.^{336–339} and other authors^{340,341} have to be mentioned as part of the complex system of reactions within the SCR as well.

The mechanistic explanation for the standard, fast and NO₂ SCR is dominated by Tronconi et al.^{168,170,281} who proposed a sequence of reactions for iron zeolites in analogy to Koebel et al.^{146,147} for a Vanadium based catalyst. A similar mechanism was stated for a BaNa-Y catalyst by Weitz et al.^{279,280} The key steps which are claimed to be valid also for V₂O₅ and Cu-zeolites involve the disproportionation of two NO₂, leading eventually to ammonium nitrite and nitrate which decompose to nitrogen and nitrous oxide. The rate-determining step in the fast SCR is claimed to be the reaction of NO with a nitrate species to nitrite. The nitrate and nitrite species are also sometimes written in terms of nitric and nitrous acid, involving water in the disproportionation sequence of NO₂.^{34,40} However, the mechanism neglects a discrimination of the coexistence and activity of different active sites and, thus, keeps a rather macroscopic and speculative character despite the formulation of a potential intermediate.

A detailed analysis of the elementary steps within the reactive system of

the SCR on iron as active site that is capable to explain the macroscopically observed phenomena, has so far only been attempted to a small extent by Li and Li.³⁴² Such a study could help to better understand the mechanisms of the single systems and their interaction and serve not at last as a basis for the development of more sophisticated rate expressions for reactor simulations. Nevertheless, tracing surface chemistry to the elementary steps is only possible with theoretical methods like DFT. In chapter 7, we have studied the oxidation of NO on mononuclear iron sites in the absence and presence of water and could explain the difference in activity with respect to a change of the structure of the active site from FeO to FeOH. Also, the key surface species mono- and dihydroxylated iron as well as surface nitrite and nitrate were identified. The choice of the mononuclear species was related to results from Kröcher et al.^{36,290} who suggested these species to be most active in the economically favored low temperature regime and also Grünert et al.^{37,326,343} claimed isolated iron sites to be the active species in the SCR. In continuation of the preceding chapter, the goal of this chapter is to establish a reaction network for mainly the fast and the NO₂ SCR that accounts for the experimentally observed phenomena on mononuclear iron sites. The varying stoichiometry and selectivity of the NO₂ SCR with respect to nitrous oxide is discussed. In addition, the impact of oxygen on ammonia is presented allowing for suggestions on the mechanism of the SCO. Similarly, as the discussion of the H/N/O system on the Brønsted acids as active site (see Part III) the main intermediate gas phase species are assumed to be nitrous and nitric acid as well as nitrosamine and nitramide within the SCR and nitroxyl and hydroxylamine in the SCO. Together with the results of chapter 7 a detailed description of the mechanisms in the SCR based on mononuclear iron sites is outlined.

8.2 Theory

The applied methodology is in close agreement with the one outlined in the preceding chapter 7. The catalytic active center and a part of the zeolite framework were represented by a cluster of 5 T-sites (Figure 8.1, FeO) and all Si atoms were initially placed at their crystallographic positions, as reported by Olson et al.¹⁹⁷ The terminal Si atoms were saturated with hydrogen. The iron was considered as mononuclear ions, which replace the Brønsted acid site of the parent H-ZSM5. All quantum chemical calculations were carried out on potential energy surfaces (PES) with spin multiplicities $M_S=2-8$, by using the gradient-corrected Density Functional Theory (DFT) as implemented in the TURBOMOLE suite of programs²⁰⁰ at the B3LYP/TZVP

level of theory with a very fine numerical grid size (m5).²⁰¹ Structure optimizations were performed in Cartesian coordinates with an energy convergence criterion of 10^{-7} Ha and the maximum norm of the Cartesian gradient was converged to 10^{-4} Ha/bohr. Variations in the choice of the T-site for the aluminum in the zeolite framework as well as in the size of the representation of the catalyst were shown to have little impact on the results, as was outlined in chapter 7. The specifications chosen in this work are considered as a reasonable compromise between accuracy and computational expenses. Transition states were localized from a combined application of, first, the growing string method⁹⁹ and a refinement with either the modified dimer method¹⁰⁵ with a gradient norm convergence criterion of $5 \cdot 10^{-4}$ Ha/bohr or the PRFO¹⁰³ method. Minimizations of the surface species on different PESs revealed that the energy differences between them are usually significant such that only the ground state needs to be considered. However, in cases with two PESs being close to each other, we also considered the crossing of PESs in order to obtain the lowest energy pathway for the overall catalytic cycle. For the excited states we then considered only the state of lowest energy. In iron core containing systems, the B3LYP functional gives results for relative energies between the ground and the lowest excited state which are in most cases in good agreement with high-level ab initio quantum mechanical calculations.^{311–313} Crossing of seams of PESs in MECPs were determined with a multiplier penalty function algorithm which had a maximum energy difference on both PESs of less than 10^{-6} Ha. In order to calculate Gibbs' free energies also for the MECPs, we calculated the vibrational frequencies for the partition function based on an effective Hessian as stated by Harvey and Aschi¹⁰⁸ and outlined in section 3.3 equation (3.28). Energy barriers obtained from transition state search as well as MECPs have limited accuracy and are dependent on the applied density functional.^{55,88,309} However, based on the successful application to the investigation of the decomposition of nitrous oxide in Fe-ZSM5 in our institute^{119,300,301} and by Guesmi et al.,³⁰² which lead in both cases to even quantitative agreement with experiments,^{258,314,315} it can be assumed that the accuracy of the methodology applied here is sufficient for at least a qualitative analysis of the SCR on Fe-ZSM5.

8.3 Results and discussion

The mechanism of the selective catalytic reduction of NO with ammonia can mainly be subdivided into the macroscopic reactions: NO oxidation, the fast SCR, the NO₂ SCR, the ammonia oxidation and the decomposition of

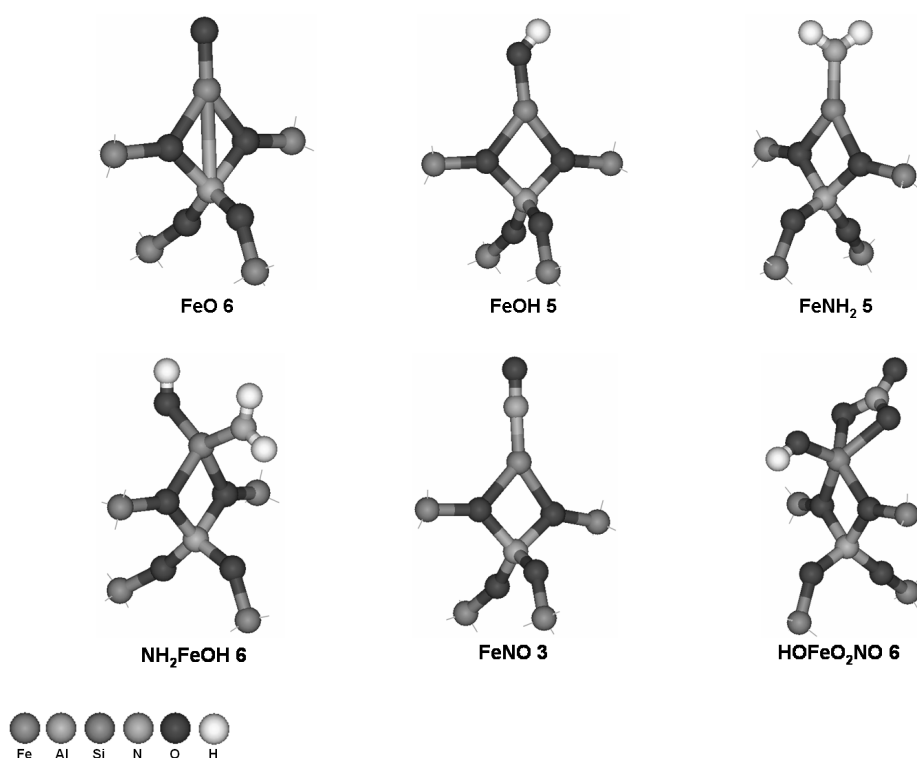


Figure 8.1: T5 cluster model of the significant intermediates of Fe-ZSM5: $Z^-[\text{FeO}]^+$, $Z^-[\text{FeOH}]^+$, $Z^-[\text{FeNH}_2]^+$, $Z^-[\text{NH}_2\text{FeOH}]^+$, $Z^-[\text{FeNO}]^+$ and $Z^-[\text{HOFeO}_2\text{NO}]^+$. The numbers correspond to the spin multiplicity of the minimized species. Dangling bonds are not shown.

nitrous oxide. The NO oxidation was already discussed in chapter 7 and the decomposition of N_2O investigated in detail by Heyden et al.^{41,300,301} In this chapter, the main focus is set on the fast and the NO_2 SCR according to the equations (8.2) and (8.3) with some additional remarks on the ammonia oxidation and the crossover to the nitrous oxide decomposition. With respect to the results of the preceding chapter 7 on the NO oxidation which suggested FeO and FeOH to be the representations of the active sites we neglect other surface species as the starting point of a catalytic cycle. In fact, because hydrogen is introduced into the system by ammonia a clear differentiation between the active site structure, as was done for the NO oxidation, is not possible here. In addition, the interaction of ammonia with the as stable concluded dihydroxylated iron and iron nitrite will be discussed in the context of their appearance in the considered catalytic cycles. In chapter 6, we have

shown that the Brønsted acids are very active for the decomposition of the intermediates nitrosamine and nitramide into nitrogen and nitrous oxide, respectively, together with water. We have assumed that these species are also essential intermediates in the catalytic cycle on the iron as active site and that their decomposition takes place on the acid sites also in the presence of iron. The decomposition on the iron cannot be ruled out, but, within this work, the impact of such an analysis is believed to be negligible. Furthermore, we have shown that nitrous and nitric acids are produced on the Brønsted acids within the fast SCR, but also within the NO oxidation in the presence of water on the iron sites. Thus, we also consider their potential interaction with ammonia on the Fe-ZSM5. Finally, for the oxidation of ammonia on the Brønsted acids, the key intermediates were shown in chapter 5 to be nitroxyl and hydroxylamine and their potential production and consumption on iron sites will be discussed within the framework of the SCR.

The following discussion will be subdivided into four parts. In the first part, we focus on the mechanism of the fast SCR. In the second part, the mechanism of the NO₂ SCR will be covered with respect to the experimental finding of a temperature dependent selectivity of the nitrogen vs. nitrous oxide production. In the third part, we analyze the influence of oxygen on the system other than the NO oxidation. Finally, in the fourth part aspects of the ammonia oxidation as well as the interaction with the N₂O decomposition will be discussed. As part of the investigations, we also considered the crossing of potential energy surfaces of different spin multiplicities, in order to account for the different spin states of overall reactants and products as well as to find the minimum energy pathway (MEP) for the catalytic cycle. The labeling of the structures involved naming the ligands to the iron. In the case that three ligands have been considered, one of them is annotated with a minus ("-"). In the case that a molecule is considered as a gas phase species we used an underline character ("_") to add it to the tag. For all parts, the mechanistic overviews and the energy diagrams of the different catalytic cycles are provided. All the energies in the diagrams are zero-point energy-corrected and the values in the overviews are Gibbs' free enthalpies calculated at 600 K. The black values refer to the structures and the blue values to either transition states or to the barrier for the crossing of a seam between two PESs. The colors of the boxes refer to the spin multiplicity of the PES as follows: purple refers to M_S=2, white to M_S=3, green to M_S=4, blue to M_S=5, yellow to M_S=6 and orange to M_S=7. In both, energy diagram and overview, the values are given with respect to FeO as the active site structure (if not stated differently) and gas phase molecules as reference. The value of 600 K was picked in order to consider the entropic effects of the

reaction mechanism at a temperature at which also the standard SCR with ammonia shows significant conversions.

With respect to the limited accuracy of the DFT in general and on the calculation of energy barriers from transition states and minimum energy crossing points, it should be emphasized that all the subsequently presented results are of qualitative nature only.

8.3.1 Part 1: The Fast SCR

In this part mainly the catalytic cycle of the fast SCR is discussed with FeO (Figure 8.1) in its ground state on the PES with $M_S=6$ as the reference structure. The energies are shown in Figure 8.2 and the schematic overview of the reactions, including the Gibbs' free enthalpies at 600 K, is shown in Figure 8.3. The adsorption of ammonia on this structure was found to exhibit a rather high energy of adsorption of $\Delta E_{\text{ads}}=-26.8$ kcal/mol (ST2) with the ammonia attached to the iron by its nitrogen atom and a hydrogen bond to one of the zeolite framework oxygen. Then, a proton transfer takes place from the adsorbed ammonia to the oxygen leading to an amino group together with a hydroxyl group (ST 4). This step exhibits an energy barrier of $E^\ddagger=23.3$ kcal/mol (TS 1) and is exothermic by $\Delta E=-12.0$ kcal/mol. Thus, two different species (ST2 and ST4) have to be taken into account as the resulting adsorbed state of ammonia on the iron with a heat of adsorption for ST 4 of $\Delta E_{\text{ads}}=-38.7$ kcal/mol. The species so far were calculated on the sextet PES. However, the subsequent reactions with either NO or NO₂ were found to proceed on the quintet PES, which requires, at this stage, a crossing from the ground state sextet to the quartet (ST 5) PES via S2 and a barrier of $E^\ddagger=13.7$ kcal/mol (electronic energy only). The adsorption of NO to this species with the nitrogen bonded to the iron (ST 8) is only weak with respect to the prior ground state. Nevertheless, a subsequent reaction via the TS 5 with a low barrier of $E^\ddagger=3.4$ kcal/mol leads to the formation of nitrosamine, adsorbed on monohydroxylated iron (ST11). Finally, the desorption of NH₂NO with a heat of desorption of $\Delta E_{\text{des}}=8.5$ kcal/mol leads to the ground state FeOH on the quintet PES. Overall, this first formation of nitrosamine was calculated to be exothermic by $\Delta E=-40.3$ kcal/mol. It is at hand that the equilibrium conditions between the ground and the excited state of the intermediate NH₂FeOH dictate only rather small quantities of the quartet species to be available on the catalyst. However, the fact that the ground state is rather stable and the gap between the two states is sufficiently small makes the assumption of the excited state to be present reasonable. Furthermore, the subsequent reaction with NO has to be considered as being fast

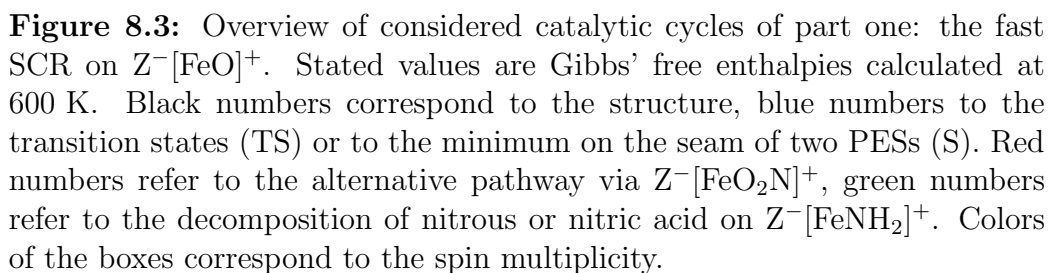
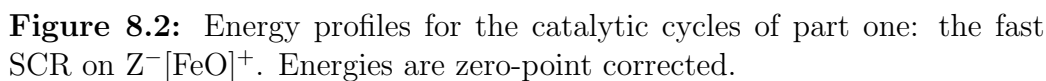
because of the rather low barrier, and, thus, this pathway can be concluded to be accessible. Alternatively, also NO_2 can coadsorb on the excited state of NH_2FeOH , although here the nitrogen dioxide is only hydrogen bonded to the amino group (ST 7). A subsequent reaction in analogy to the formation of nitrosamine results in nitramide adsorbed on the monohydroxylated iron (ST12) by overcoming a barrier of $E^\ddagger=4.6$ kcal/mol (TS 4). The desorption of NH_2NO_2 with $\Delta E_{\text{des}}=11.4$ kcal/mol eventually leads to FeOH . In a next step, ammonia adsorbs on the monohydroxylated iron with, again, the nitrogen bonded to the iron and a hydrogen bond to a framework oxygen with a heat of adsorption of $\Delta E_{\text{ads}}=-20.3$ kcal/mol. Similar as to TS1, another proton transfer from the ammonia to the hydroxyl group takes place forming water coadsorbed to an amino group (ST 14). This step exhibits an activation energy of $E^\ddagger=22.2$ kcal/mol and is in magnitude quite close to the prior proton transfer corresponding to TS1. Then, water desorbs with $\Delta E_{\text{des}}=9.6$ kcal/mol and leaves iron with an amino group on the quintet PES, denoted as FeNH_2 (Figure 8.1). To complete the catalytic cycle of the fast SCR, the adsorption of NO_2 to this species is required, which is strongly bonded to the iron by one oxygen (ST 18, $\Delta E_{\text{ads}}=-24.1$ kcal/mol) on the PES with spin multiplicity $M_S=6$. The subsequent reaction via TS7 leads to the formation of nitrosamine adsorbed on the initial active site FeO (ST19) and exhibits a high barrier of $E^\ddagger=25.8$ kcal/mol. Finally, the desorption of NH_2NO with $\Delta E_{\text{des}}=12.1$ kcal/mol restores the initial active site FeO . Although the second formation of nitrosamine requires to overcome the highest internal barrier of the complete cycle with TS7 and is endothermic by $\Delta E=30.7$ kcal/mol ($\text{FeO} - \text{ST18}$), it has to be pointed out that the species NH_2FeONO has to be considered quite stable while the products nitrosamine and FeO are rapidly consumed. Thus, the equilibrium of this final elementary step will always be dragged to the product site.

Tronconi et al.^{168,170,281} have suggested that the rate-limiting step in the fast SCR should be the reduction of a surface nitrate with nitric oxide to a surface nitrite. We have shown in chapter 7 that such a step exhibits a barrier of $E^\ddagger=35.7$ kcal/mol, which is nearly 10 kcal/mol higher than the highest internal barrier in our pathway. Despite the fact that this result does not allow for a conclusion on the mechanism on iron species of higher nuclearity, for the mononuclear iron sites it clearly indicates that the reaction rather proceeds via the amino groups than the nitrates. From the energy profile (Figure 8.2) it has to be noted that FeOH marks a valley in the catalytic cycle and from this perspective can be assumed to be the dominating surface species. The potential formation of nitramide, from the reaction of NO_2 with NH_2FeOH instead of NO , depicts in the final catalytic cycle the NO_2 SCR

with the stoichiometry of reaction (8.3). Thus, this pathway can be seen as the explanation of the high nitrous oxide production within the NO_2 SCR at low temperatures.

Alternatively, we also considered the adsorption of NO on FeO together with a spin change from the septet to the quintet PES (S 1) leading to an iron nitrite (ST 3) that is bonded with one oxygen to the iron. A low barrier reaction (TS 2) leads then to the more stable nitrite with two oxygen atoms bonded to the iron (ST 6). Up to this point the description of the mechanism is equivalent to the discussion in section 7.3.1 of the preceding chapter 7. Next, ammonia strongly coadsorbs to the nitrite with $\Delta E_{\text{ads}} = -23.6$ kcal/mol (ST 9). A hydrogen transfer from the ammonia to the adsorbed nitrite results in the formation of nitrous acid. The latter remains only hydrogen-bonded to the formed amino group on the iron (ST 10) and finally desorbs with $\Delta E_{\text{des}} = 7.7$ kcal/mol. The formation of the acid, however, requires to overcome a barrier of $E^\ddagger = 33.8$ kcal/mol (TS 3), which is significantly higher than the highest barrier of the formerly discussed pathway. Nevertheless, the exothermicity of the formation of the nitrite and the strong coadsorption of ammonia suggest the formation of ST 9 in reasonable quantities on the catalyst. With that, this pathway cannot be ruled out. However, the analogous reaction of water with the nitrite revealed a barrier of only $E^\ddagger = 22.6$ kcal/mol (see chapter 7) leading to FeOH. Thus, in the presence of sufficient amounts of water, nitrous acid will be produced from the reaction of water with the surface nitrite rather than with ammonia. In transient experiments and in the absence of water, the reaction with ammonia might dominate. An analogous transition state for the reaction of ammonia with FeO_2NO to nitric acid and the FeNH_2 was not found. However, for the reaction of water with the nitrate we found a barrier of $E^\ddagger = 26.9$ kcal/mol which is slightly higher than the corresponding reaction with the nitrite. With respect to the structural similarity of the transition structures for the reaction of the nitrite with either water or ammonia and the reaction of water with the nitrate it can be assumed that a barrier for the reaction of ammonia with the nitrate should also be slightly higher than the corresponding reaction with the nitrite.

In the main pathway FeNH_2 can be interpreted to be a key intermediate and we also considered the interaction of nitrous and nitric acid with this species. Both acids adsorb to it with a bond of the oxygen of the hydroxyl group to the iron and with a hydrogen bond to the zeolite framework (ST 15: nitric acid; ST 16: nitrous acid) with similar heats of adsorption $\Delta E_{\text{ads}} = -12.4$ kcal/mol and $\Delta E_{\text{ads}} = -12.5$ kcal/mol, respectively. Then, via TS 8 and TS 9 the bond between the hydroxyl group of the acid and the corresponding NO_x is broken and NO_2 and NO are released. This step exhibits activation



energies of $E^\ddagger=8.5$ kcal/mol and $E^\ddagger=4.8$ kcal/mol. In the case of the nitric acid, the released NO_2 only remains hydrogen-bonded to the hydroxyl group (ST 21), while for the nitrous acid decomposition the NO forms a bond with the nitrogen to the iron and the species is analogous to ST 8 of the main cycle. From a mechanistic aspect as well as with respect to the energy barriers, the decomposition strongly resembles the decomposition of the acids on monohydroxylated iron, eventually leading to dihydroxylated iron (see section 7.3.2 of chapter 7).

Finally, we also include in this context the interaction of nitroxyl with FeNH_2 which was shown on the H-ZSM5 to be a significant intermediate from the oxidation of ammonia and is expected to be relevant also on iron-containing zeolites. HNO strongly adsorbs with the nitrogen bonding to the iron with $\Delta E_{\text{ads}}=-20.1$ kcal/mol (ST 17). Then, prior to a hydrogen transfer from the nitroxyl to the amino group, a spin change from $M_S=5$ to $M_S=3$ (ST 20) is required, because the final product state (ST 22) has its ground state on the triplet PES and the hydrogen transfer was found to proceed with a slightly lower barrier on this PES. This step exhibits a barrier of $E^\ddagger=8.9$ kcal/mol (S 3, electronic energy only). For the hydrogen transfer, leading to ammonia adsorbed on FeNO (ST 22), a barrier of $E^\ddagger=10.5$ kcal/mol (TS 10) was calculated. Because this step is highly exothermic by $\Delta E=-41.1$ kcal/mol and the two preceding barriers are sufficiently low, it can be assumed that nitroxyl reacts rather fast with the FeNH_2 intermediate, reforming ammonia.

From the Gibbs' free energies in Figure 8.3 it can be seen, in agreement with the above discussion, that the pathway of the fast SCR via first the ammonia adsorption is in favor over the reaction of ammonia with the nitrite because of the lower overall energy barriers. Also the very stable character of the intermediate FeOH can be observed from the low Gibbs' free energy supporting the suggestion of this species to be dominant on the surface. Finally, the importance of the formation of FeNO from the reaction of nitroxyl with the amino group on the iron is supported by the extremely low energy values. Its accessibility is however anchored to the presence of FeNH_2 species in sufficient amounts.

8.3.2 Part 2: The NO_2 SCR

In part one, in the context of the fast SCR, we have outlined a potential mechanism of the NO_2 -SCR leading to equimolar amounts of nitrogen and nitrous oxide. From the experimental literature it is known that the selectivity of this side-reaction towards nitrogen is strongly dependent on temperature^{38,40,170} with a maximum between 250°C and 300°C. Up to the maximum indeed ap-

proximately equimolar amounts of nitrogen and nitrous oxide are observed while at higher temperatures the selectivity drastically shifts towards nitrogen. Tronoconi et al.¹⁷⁰ explained this behavior from first the decomposition of ammonium nitrate to nitrous oxide at low temperatures. Then a reaction of ammonia with surface nitrates as additional NO_2 -SCR mechanism to only nitrogen is suggested to set in at elevated temperatures. Finally, at high temperatures the partial decomposition of NO_2 into NO and oxygen is proposed to make the fast SCR accessible. Also Chatterjee et al.³⁴⁴ and Schuler et al.,³²⁸ assumed different reactions for the NO_2 SCR, within the kinetic modeling of the SCR, to account for the observed change in selectivity. Thus, we probed the PES with respect to an additional pathway only resulting in the production of nitrogen to discuss the potential accessibility to different mechanisms. Furthermore, a strict differentiation between the sub-reactions is not reasonable, because of the crossings of the mechanisms, and thus also the interaction with NO will be discussed in this context. The energies of the reactions are shown in Figure 8.4 and an overview with the Gibbs' free energies at 600 K is shown in Figure 8.5. We start the discussion of the mechanism with the species NH_2FeOH (section 8.3.1, ST 5) on the quartet PES. Besides the interaction with NO_2 leading to nitramide as outlined in the preceding section nitrogen dioxide can also adsorb to this species with an oxygen bonded to the iron (ST 1). However, it has to be pointed out that this adsorbed state is energetically less favorable than the hydrogen bonding to the amino group by $\Delta E=8.3$ kcal/mol. In the subsequent reaction, the N-O bond in the adsorbed NO_2 is broken and nitrosamine forms, adsorbed on OFeOH (ST 2). This step requires to overcome a barrier of $E^\ddagger=12.8$ kcal/mol (TS 1). Although this barrier is sufficiently low to be surpassed in comparison to the highest barrier of the fast SCR, compared to the competing reaction to nitramide ($E^\ddagger=4.6$ kcal/mol) this step is less favorable. Nevertheless, nitrosamine easily desorbs with $\Delta E_{\text{des}}=8.5$ kcal/mol, leaving OFeOH (ST 3) on the quintet PES. Ammonia adsorbs strongly to this species with $\Delta E_{\text{ads}}=-22.7$ kcal/mol (ST 5) with its nitrogen bonded to the iron. For a subsequent transfer of a proton eventually leading to the formation of water, different scenarios were analyzed. For the most straightforward transfer from the ammonia to the hydroxyl group, only on the septet PES a transition state was found. This requires the spin change of the $\text{NH}_3\text{-OFeOH}$ intermediate from its quintet ground state to the excited septet state (ST 6). The barrier for this process was calculated to be $E^\ddagger=16.1$ kcal/mol (S 1, electronic energy only). The proton transfer via TS 3 exhibits a barrier of $E^\ddagger=24.4$ kcal/mol leading to water, adsorbed on NH_2FeO (ST 8) on the septet PES. Because the initial spin change exhibits only a negligible barrier for the reverse reaction to the ground state, the hydrogen transfer should rather

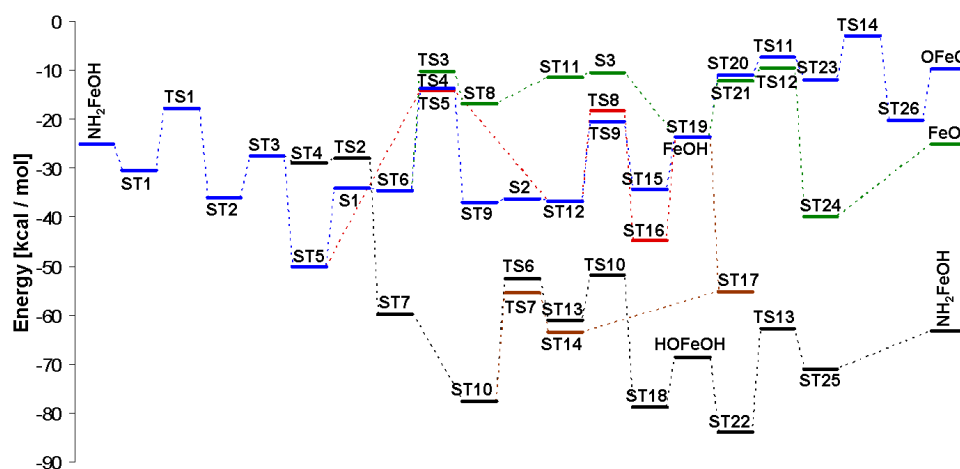


Figure 8.4: Energy profiles for the catalytic cycles of part two: the NO_2 -SCR on $\text{Z}^-[\text{FeO}]^+$. Energies are zero-point corrected.

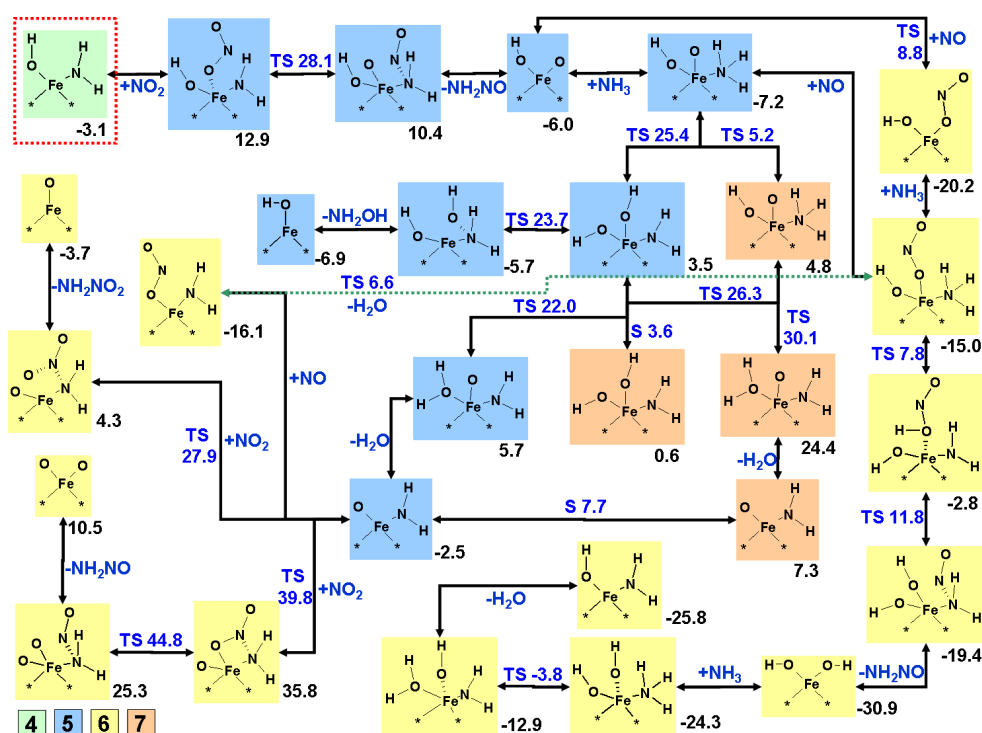


Figure 8.5: Overview of considered catalytic cycles of part two: the NO_2 -SCR on $\text{Z}^-[\text{FeO}]^+$. Stated values are Gibbs' free enthalpies calculated at 600 K. Black numbers correspond to the structure, blue numbers to the transition states (TS) or to the minimum on the seam of two PESs (S). Colors of the boxes correspond to the spin multiplicity.

be seen as a combined step, involving the crossing of the seam S 1 together with the transition state TS 3. This combined step exhibits a barrier of $E^\ddagger=40.0$ kcal/mol and is endothermic by $\Delta E=33.4$ kcal/mol. Therefore, this step is rather unlikely to occur. A subsequent desorption of water (ST 11) and a recrossing to the ground state quintet PES via S 3 to NH_2FeO (ST 19) however only requires to overcome a combined barrier of $E^\ddagger=6.3$ kcal/mol. Alternatively, starting from the excited state ST 6 a slightly lower barrier of $E^\ddagger=20.9$ kcal/mol (with respect to the ground state $E^\ddagger=36.6$ kcal/mol, TS 4) results in a proton transfer to the oxygen, bonded to the iron, forming a second hydroxyl group. Here, the septet PES corresponds to the ground state of this intermediate (ST 9) and though also this elementary step is endothermic, the product state is by $\Delta E=-20.3$ kcal/mol lower in energy than ST 8. Finally, the proton transfer from the ammonia to the free oxygen was also determined on the quintet PES. The barrier for this step was calculated to be $E^\ddagger=36.0$ kcal/mol (TS 5), which is nearly the same value as on the septet PES. The resulting intermediate $\text{NH}_2\text{-HOFeOH}$ on the quintet PES (ST 12) is only by $\Delta E=0.2$ kcal/mol higher in energy as the corresponding ground state (ST 9), and thus, with respect to accuracy of DFT, it cannot be concluded on which PES the true ground state is located. Nevertheless, the barrier from the septet to the quintet PES is negligibly small with $E^\ddagger=0.8$ kcal/mol. Finally, a proton transfer between the hydroxyl groups was considered which, on the quintet PES, requires to overcome a barrier of $E^\ddagger=16.4$ kcal/mol (TS 9) leading, after the desorption of water, to the ground state of NH_2FeO (ST 19). From the energy profile (Figure 8.4) it can be concluded that the formation of water from ammonia and the hydroxyl group of OFeOH is severely more favorable via the intermediate formation of two hydroxyl groups. Although it cannot be excluded that the direct protonation occurs on the quintet PES with a lower barrier, from the prior results it is not expected to be significantly lower than TS 3 to TS 5. Thus, the significance of the interaction of ammonia with the intermediate OFeOH is questionable with respect to the rather high internal barriers.

Besides the final proton transfer between the hydroxyl groups on the quintet PES, the formation of hydroxylamine was considered from the amino group and one of the hydroxyl groups as well. Hydroxylamine was found to be a significant intermediate in the SCO on the Brønsted acids (compare chapter 5) and, thus, this reaction step can be seen as a slight excursion with respect to the ammonia oxidation on iron. NH_2OH is formed on the iron via the transition state TS 8 ($E^\ddagger=18.7$ kcal/mol) and remains strongly adsorbed on the essential monohydroxylated iron (FeOH) with $\Delta E_{\text{ads}}=-21.2$ kcal/mol (ST 16). Thus, the reverse route, starting from FeOH , involving

the decomposition of hydroxylamine via TS 8 to ST 12 and the subsequent formation of water via TS 9 to ST 15 could be of importance in the SCO.

In the energy diagram, ST 17 reflects the species NH_2FeONO on the sextet PES, which forms from the strong adsorption of NO on the oxygen of NH_2FeO (ST19) with $\Delta E_{\text{ads}} = -31.7$ kcal/mol. This species was shown in part one to further react to nitrosamine and FeO. In contrast, the interaction of NO_2 with ST 19, to complete the catalytic cycle of the NO_2 -SCR, was found to be quasi endothermic for two different reactions. It has to be noted in this context that the intermediates ST 20 and ST 21, which both include the interaction with NO_2 , were obtained by descending the minimum energy pathway, starting from the transition states, of the corresponding subsequent reactions. Thus, it can be assumed in both cases that an additional transition to some adsorbed state of NO_2 exists, which is lower in energy than NH_2FeO (ST 19). For the subsequent reactions, however, this is assumed to not be of importance. With ST 20, an adsorbed state of NO_2 is illustrated, which exhibits one bond between its oxygen and the iron on the sextet PES. The subsequent reaction via TS 11 leads to the formation of an additional N-N bond between the adsorbed nitrogen dioxide and the amino group (ST 23). This step exhibits an energy barrier of $E^\ddagger = 3.7$ kcal/mol (TS 11), but, with respect to the prior quasi endothermic adsorption of NO_2 , has to be corrected to $E^\ddagger = 16.1$ kcal/mol. This value can then be interpreted as the barrier of the reaction of NO_2 with NH_2FeO according to an Eley-Rideal type mechanism. The subsequent cleavage of the internal N-O bond of the adsorbed NO_2 results in nitrosamine adsorbed on OFeO (ST 26). The barrier for this step was calculated to be $E^\ddagger = 9.1$ kcal/mol (TS 14). The remaining species OFeO was shown in chapter 7 to easily recombine to FeO_2 and oxygen might desorb after a coadsorption of NO_2 . This corresponds to species ST 3 of part one (Figure 8.2) and the closure of the NO_2 reactive cycle without the production of nitrous oxide is contained in that part. Alternatively, the reaction of NO_2 with NH_2FeO might also lead to adsorbed nitramide on FeO (ST 24) which exhibits even a slightly lower barrier $E^\ddagger = 14.0$ kcal/mol (TS 12) with respect to NH_2FeO . Furthermore, this step is exothermic in contrast to the endothermic pathway to nitrosamine. With that, not only is the initial formation of nitrosamine via TS 1 less likely than the formation of nitramide and the intermediate formation of water via TS 3 to TS 5 questionable with respect to high internal barriers, also the second formation of nitrosamine via TS 11 and TS 14 is less likely than a competing formation of nitramide. From these results, it has to be concluded that the assumption of a pure NO_2 SCR mechanism that avoids the production of nitrous oxide, even at high temperatures, is questionable on mononuclear iron sites. This is also supported

by the corresponding Gibbs' free energies at 600 K as shown in Figure 8.5, which are substantially higher in comparison to the values of part one (Figure 8.3). Thus, it remains indeed most plausible to assume the mechanism of the NO₂ SCR to proceed at low temperatures via the pathway as outlined in part one, including the production of equimolar amounts of nitrogen and nitrous oxide and at elevated temperatures the partial decomposition of NO₂ in accordance with Tronconi et al.¹⁷⁰ and Epling et al.,³²⁹ which enables then the fast SCR mechanism. Furthermore, the decomposition of intermediately produced nitrous oxide could take place at high temperatures and this will be briefly discussed in the fourth part.

Assuming that at high temperatures at least partially the initial step via TS 1 might take place, we also considered the interaction of NO with the resulting intermediate OFeOH (ST 3) on the quintet PES. Already in the preceding chapter 7 this interaction was shown as part of the NO oxidation on monohydroxylated iron, which eventually leads to the formation of a nitrite next to the hydroxyl group (ST 7), is strongly exothermic with $\Delta E = -30.8$ kcal/mol and only exhibits a very small barrier (TS 2, $E^\ddagger = 0.94$ kcal/mol). Thus, this species and the following pathways can also be seen in two further different contexts. First of all, HOFeONO on the sextet PES can be formed from the adsorption of NO₂ on monohydroxylated iron and marks an alternative pathway in the fast SCR as the one outlined in part one. Second, within the standard SCR Delahay et al.²⁸² have stated the assumption that ammonia should react with some intermediate of the NO oxidation. This was intended to explain the observed significant deviations in activity of the catalyst for the NO oxidation and the standard SCR by an avoided desorption of NO₂ in the presence of NH₃. Also at 600 K, the species HOFeONO was shown to exhibit the lowest Gibbs' free energy within the NO oxidation cycle on FeOH (Figure 7.17 b) and could, thus, be the limiting nitrite species assumed by Delahay et al. Ammonia strongly coadsorbs to it (ST 10) with $\Delta E_{\text{ads}} = -17.8$ kcal/mol. Subsequently, two different reactions, involving a hydrogen transfer were considered. The first one involves the transfer from the ammonia to the hydroxyl group, forming water (TS 7) by overcoming a barrier of $E^\ddagger = 22.1$ kcal/mol. The desorption of the produced water leads again to NH₂FeONO (ST 17), which is the precursor of a subsequent formation of nitrosamine. Alternatively, the proton transfer can take place to the adsorbed NO₂ by forming nitrous acid (ST 13). This step exhibits an activation energy of $E^\ddagger = 25.0$ kcal/mol. Either the nitrous acid then desorbs to the gas phase or further reacts from a transfer of its NO group to the amino group, which results in nitrosamine adsorbed on dihydroxylated iron (ST 18). This second step requires to overcome a barrier of $E^\ddagger = 9.1$ kcal/mol.

The desorption of NH_2NO eventually leads to the dihydroxylated iron in its ground state on the sextet PES. In both cases, the proton transfer exhibits a barrier, which is even slightly higher than the hydrogen transfer from ammonia, adsorbed on monohydroxylated iron as described in part one (Figure 8.2, TS 6). Within the fast SCR context, however, this would be the step potentially circumvented by first the adsorption of NO_2 prior to the proton transfer. It has to be concluded that this is from an energetically aspect not beneficial, but it reveals from a mechanistic view that NO_2 also does not block the further reaction. This implies that at lower temperatures the fast SCR indeed might partially proceed via TS7 or TS8. Within the NO oxidation we have already shown that dihydroxylated iron can react with NO_x by forming nitrous or nitric acid. It also might react with ammonia after adsorption of the latter with the nitrogen bonded to the iron (ST 22) and a heat of adsorption of $\Delta E_{\text{ads}} = -15.2$ kcal/mol. A hydrogen transfer from the ammonia to one of the hydroxyl groups results in the formation of water, adsorbed on NH_2FeOH (ST 25) and exhibits a barrier of $E^\ddagger = 21.2$ kcal/mol. This barrier is about 2 kcal/mol lower in energy than the formation of NH_2FeOH from a hydrogen transfer of adsorbed ammonia on FeO, which was the initialization of the fast SCR mechanism of part one. In the preceding chapter 7, we have shown that the formation of dihydroxylated iron from a reaction of FeO with water exhibits in comparison a rather low barrier of $E^\ddagger = 13.7$ kcal/mol and concluded that this species potentially blocks the active site for the NO oxidation in the presence of water. Here, it can be seen that the occurrence of dihydroxylated iron is not expected to inhibit the SCR reaction, because it is removed by ammonia.

8.3.3 Part 3: Impact of Oxygen

Oxygen was shown by Yang et al.¹⁴⁴ to be vital for the standard SCR to proceed on Fe/H-ZSM5 and it is believed that it serves the oxidation of NO to NO_2 as the rate-limiting step^{158,163,282} of the overall reaction prior to accessing the mechanism of the fast SCR. Furthermore, oxygen also causes the oxidation of ammonia as an unwanted side reaction.⁴² This section is intended to discuss on one hand the potential occurrence of a pathway for the standard SCR that is integrated into the described mechanism of the fast SCR rather than assuming a pure combination of the separated sub-reactions, NO oxidation and fast SCR. On the other hand, a potential initialization of the SCO of ammonia is outlined. The energies of all species are illustrated in Figure 8.6 and an overview of the reactions is shown in Figure 8.7. In part one it was shown, that monohydroxylated iron marks, from an energetic point

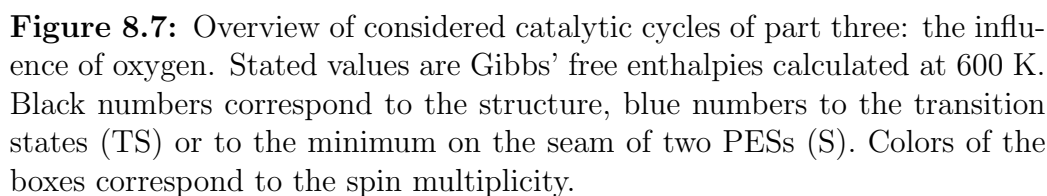
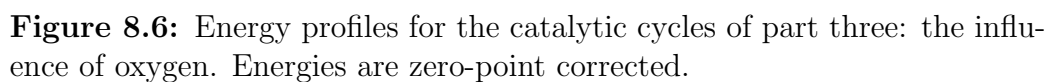
of view, a valley and that the reaction of ammonia with it leads to an amino group (Figure 8.2, FeNH_2) on the quintet PES. Within the presented catalytic cycle of the fast SCR this would be the adsorption site for the NO_2 and thus is the relevant initial species for the consideration of a further pathway of the standard SCR in the absence of nitrogen dioxide. The adsorption of oxygen to this species is activated by a very low barrier of $E^\ddagger=0.4$ kcal/mol (TS 1) and slightly exothermic by $\Delta E=-10.3$ kcal/mol (ST 3). However, in order to further react with a nitrogen oxide, a spin change from the septet ground state to the quintet PES is required. This is in analogy to the mechanism of the NO oxidation on monohydroxylated iron (see section 7.3.2). The crossing of the seam between the two PESs exhibits a barrier of $E^\ddagger=9.2$ kcal/mol (S 2) (electronic energy only) and the excited state (ST 5) is $\Delta E=8.8$ kcal/mol higher in energy than the ground state. The adsorption of NO, bonded with the nitrogen to the iron (ST 10), is rather weak with respect to the ground state precursor. An alternative pathway up to this state was studied based on first the adsorption of NO to the FeNH_2 . The ground state of the species NH_2FeNO was found to be on the quartet PES (ST 4) and, thus, a spin change is required via S 1 and a negligible barrier of $E^\ddagger=0.1$ kcal/mol. The adsorption of NO can be considered to be quite strong with a heat of adsorption to the ground state of $\Delta E_{\text{ads}}=-22.8$ kcal/mol. Oxygen does not interact with this species as can be seen from the energy profile of ST 7 in comparison to ST 4. Thus, the chemisorption of oxygen to the iron is an activated process illustrated with TS 4. This step exhibits an activation energy of $E^\ddagger=15.5$ kcal/mol leading also to ST 10 in which both, oxygen and NO, are coadsorbed on the iron. This alternative pathway to ST 10 appears to be slightly more favorable because of the initial strong adsorption of NO. In a next step, the amino group and the adsorbed NO react by forming an N-N bond, which leads to nitrosamine, adsorbed on FeO_2 (ST14). The barrier for this process is rather low with $E^\ddagger=4.1$ kcal/mol and in analogy to the formation of nitrosamine on FeOH as outlined in part one. The desorption of nitrosamine leads to FeO_2 on the sextet PES.

Alternatively, starting from NH_2FeO_2 on the quintet PES (ST 5), we also considered the interaction of NO in terms of the formation of an -OONO ligand with the adsorbed oxygen in the trans configuration, followed by a conversion to the cis configuration and finally the desorption of NO_2 (not shown). These steps are in complete analogy to the mechanism of the NO oxidation on FeOH and very similar barriers for the three steps on the two different adsorption sites were observed. However, in comparison to the formation of nitrosamine from NO with the amino group no benefit could be deduced.

In the pathway leading eventually to FeO_2 , to this point, the oxygen

only served as an additional adsorbate, not interacting with the formation of nitrosamine. With respect to the strong adsorption of NO on FeNH_2 , it is thus at hand to consider the direct formation of nitrosamine without the coadsorption of the oxygen. The heat of reaction, leading to a bare iron site together with gas phase nitrosamine was calculated to be $\Delta E_{\text{R}}=65.1$ kcal/mol. This value is too high to be reasonable for the reactive system, even at high temperatures and, thus, can be excluded. Alternatively, a second NO could adsorb on NH_2FeNO in its ground state. This, however, was found to require the prior transfer to the doublet PES (ST 6) via the MECP S 3 by overcoming an activation energy of $E^\ddagger=10.4$ kcal/mol (electronic energy only). The subsequent adsorption of NO with the nitrogen bonded to the iron (ST 11) only exhibits a rather small heat of adsorption with respect to the precursor ground state (ST 11 vs. ST 4). Then, nitrosamine forms from the amino group and one of the nitrogen oxides (ST 15) and desorbs, leaving FeNO in its ground state on the triplet PES. The barrier for this process was calculated to be $E^\ddagger=3.8$ (TS 8) kcal/mol, which is again comparable to the formation of nitrosamine on FeOH or on FeO_2 . However, due to the required spin change to the doublet PES prior to the adsorption of NO this pathway is not severely beneficial over the above described pathway. In fact, from the related energies, a higher probability has to be concluded for a re-desorption of the first adsorbed NO over the coadsorption of a second one.

Assuming from the discussion above that FeO_2 on the sextet PES has formed after the reaction of the amino group with coadsorbed NO, the further formation of NO_2 from a reaction with NO was outlined in the context of the NO oxidation on FeO (section 7.3.1). Alternatively, also ammonia can adsorb to this species (ST 16) with $\Delta E_{\text{ads}}=-22.3$ kcal/mol and its nitrogen bonded to the iron. For a subsequent hydrogen transfer, first, the cleavage of the two oxygen atoms in the adsorbed molecule is necessary (ST 17). This requires to overcome a barrier of $E^\ddagger=20.3$ kcal/mol (TS 9), which is only slightly lower than the corresponding cleavage in the absence of ammonia ($\Delta E=1.4$ kcal/mol) and, thus, a beneficial influence of the ammonia cannot be observed. For the proton transfer from the adsorbed ammonia to one of the oxygen atoms (ST 18), we calculated a very high activation energy of $E^\ddagger=45.9$ kcal/mol (TS 10) making this step very unlikely to proceed. Thus, the subsequent formation of hydroxylamine from the remaining amino group and the previously formed hydroxyl group (ST 20) via TS 11 and a barrier of $E^\ddagger=8.6$ kcal/mol might rather be of interest in a different context than from the initial reaction of ammonia with FeO_2 . Alternatively to the proton transfer, NO can coadsorb on one of the oxygen atoms, forming adsorbed NO_2 (ST 19). The ground state of this species is however located on the quintet



PES (ST 22) rather than on the septet and is obtained from a spin change via S 4 ($E^\ddagger=0.6$ kcal/mol, electronic energy only). The adsorption energy to the ground state was calculated to be $\Delta E_{\text{ads}}=-32.0$ kcal/mol. However, the desorption of NO_2 from this species results in an excited state of NH_3FeO on the quartet PES (ST 23) and another crossing of the seam to the sextet PES (ST 26) is required, which exhibits a barrier of $E^\ddagger=6.7$ kcal/mol. Thus overall, the desorption would require to overcome a barrier of $\Delta E_{\text{des}}=30.0$ kcal/mol. NO_2 can however also desorb directly from the excited state of $\text{NH}_3\text{-OFeONO}$ (ST 19), which is an activated process via TS 12 ($E^\ddagger=2.8$ kcal/mol). With respect to the ground state, the NO_2 desorption requires to overcome $\Delta E_{\text{des}}=19.2$ kcal/mol, making the latter pathway more favorable. Finally, we also considered the proton transfer from the ammonia to the oxygen atom on the iron on ST 19 and found the barrier via TS 13 with $E^\ddagger=35.2$ kcal/mol to be substantially less favorable than the desorption of NO_2 . Thus, with respect to the interaction of ammonia with FeO_2 the most favorable pathway resulted eventually solely in the oxidation of NO to NO_2 and it has to be concluded that this rather proceeds in the absence of ammonia directly on FeO_2 via the -OONO ligand as outlined in section 7.3.1.

In summary, the described formation of nitrosamine from adsorbed NO and the initially considered amino group, eventually leading to FeO_2 could be significant in the standard SCR. Integrated into the mechanism of the fast SCR, it allows for the access to the NO oxidation in the absence of water for one further molecule of nitric oxide, which is significantly faster than the NO oxidation on monohydroxylated iron as described in the preceding chapter. This, however, also depends on the fraction of available FeNH_2 on the catalyst, which can only be answered from a microkinetic model, which will be discussed in the next chapter. Furthermore, a major drawback in the considered formation of the intermediate FeO_2 together with nitrosamine remains the necessary initial coadsorption of NO and O_2 on FeNH_2 . With respect to entropy, this is a rather unfavorable process at elevated temperatures, considering that the combined heat of adsorption of the two molecules is rather low (ST10 vs. FeNH_2). In contrast, an interaction of ammonia with FeO_2 can be excluded within the standard SCR. This is also supported by the rather high Gibbs' free energies as shown in Figure 8.7.

While a reaction of the amino group with only NO resulted in a bare iron ion and was energetically excluded, the interaction of the amino group with adsorbed oxygen can potentially be seen as the initialization of the ammonia oxidation. Two different pathways were analyzed in this context. In the first one, the cleavage of the oxygen molecule into two oxygen atoms on the iron (ST 8) was considered, starting from ST5. This process exhibits an activation

energy of $E^\ddagger=34.6$ kcal/mol (TS 2) and is endothermic by $\Delta E=20.1$ kcal/mol. A subsequent formation of a bond between one of the oxygen atoms and the amino group leads to the adsorbed radical H_2NO (ST 13) by overcoming a barrier of $E^\ddagger=8.9$ kcal/mol (TS 5). The rather high desorption energy with $\Delta E_{\text{des}}=28.0$ kcal/mol of the radical, resulting in FeO on the quartet PES indicates the high stability of the adsorbed state. Alternatively, we found a mechanism for the formation of the H_2NO radical from first the formation of a bond between the amino group with the oxygen molecule. Here, the barrier is significantly lower with $E^\ddagger=23.4$ kcal/mol (TS 3) leading to a state, in which an $-\text{OONH}_2$ ligand is twofold bonded to the iron with the nitrogen and one oxygen (ST 19). Breaking the iron-nitrogen bond exhibits a barrier of $E^\ddagger=6.7$ kcal/mol (TS 6) and the final desorption of H_2NO also leads to FeO on the quartet PES. The produced radical was already shown on the H-form catalyst to be a significant intermediate in the NH_3 oxidation (see chapter 5) and its further decomposition will be discussed in the fourth part. It can be concluded that the formation of this radical is significantly more favorable from the reaction via the $-\text{OONH}_2$ in analogy to the mechanism of the NO oxidation shown in chapter 7. Although the energy profiles in Figure 8.6 as well as the Gibbs' free energies at 600 K shown in Figure 8.7 indicate that the formation of H_2NO is not favorable over the pathway to FeO_2 within the SCO these steps might be significant and at temperatures above 600 K also become dominating because of the impact of entropy.

8.3.4 Part 4: Aspects of SCO and N_2O Decomposition

In part three, we have shown with respect to the influence of oxygen that the radical H_2NO can be formed from a reaction of the intermediate FeNH_2 of the fast SCR with O_2 . Because this radical also occurs within the SCO of ammonia on the Brønsted acids (see chapter 5), we assumed its formation on the mononuclear iron site to mark the potential initialization of the SCO on iron. In this part, we focus on the fate of H_2NO and outline potential pathways that account for the SCO of ammonia and involve, in analogy to the results on the Brønsted acids, also the formation of the intermediate nitroxyl. Furthermore, in part one, the formation of nitrous oxide in the NO_2 -SCR from the formation and decomposition of nitramide was discussed. As it is known that N_2O decomposes on Fe-ZSM5,^{119,300–302,315} but is also reduced in a SCR with ammonia,^{336–339} we also outline here some aspects of the fate of nitrous oxide. This should, however, rather be seen in the context of the NO_x -SCR than as standing for itself. An overlap to the SCO is evident in view of the explanations of Coq et al.³³⁶ for the mechanism of the N_2O -SCR,

which involves the oxidation of ammonia from the released oxygen of nitrous oxide.

For the potential decay of the radical H_2NO and the subsequently produced nitroxyl, we considered the interaction with first FeO and then with FeOH. For the interaction with FeO, the energies are shown in Figure 8.8 and the overview in Figure 8.9. The adsorption of H_2NO on FeO ($M_S=6$) in its ground state with the oxygen bonded to the iron exhibits a quite high heat of adsorption of $\Delta E_{\text{ads}}=-23.8$ kcal/mol (ST 1). However, on the septet PES this species OFeONH_2 does not represent the ground state, and the crossing to the quintet PES is required. The barrier for this step was found to be negligible with $E^\ddagger=0.3$ kcal/mol (electronic energy only) and the final ground state on the quintet PES (ST 3) is only $\Delta E=0.7$ kcal/mol lower in energy than on the septet PES. In fact, based on DFT, such a small difference is not sufficient to conclude the true ground state but this is not of significant relevance within the qualitative discussion on the reaction mechanism. Subsequently, a proton transfer from the H_2NO to the oxygen of FeO takes place, which involves an energy barrier of $E^\ddagger=5.6$ kcal/mol (TS 2) and is exothermic by $\Delta E=-18.8$ kcal/mol. This leads, in consequence, to nitroxyl being adsorbed on monohydroxylated iron (ST 5) with its oxygen bonded to the iron. The final desorption of nitroxyl requires to overcome the heat of desorption $\Delta E_{\text{des}}=12.2$ kcal/mol. Besides its interaction with FeNH_2 as shown in part one, the produced nitroxyl can also interact with FeO. However, for the adsorbed nitroxyl as well as for the subsequent reaction, we found the ground state to be on the quartet PES. In the preceding chapter 7 we have shown that FeO on the quartet PES is only slightly higher in energy than the ground state ($\Delta E=3.8$ kcal/mol, ST 2) and the barrier for the crossing is rather low as well ($E^\ddagger=5.4$ kcal/mol, S1). Nitroxyl adsorbs then rather strongly to FeO with $\Delta E_{\text{ads}}=-23.9$ (ST 4) with respect to the ground state of the initial active site. In fact, similar as for H_2NO , it can be assumed that nitroxyl also directly adsorbs to FeO on the sextet PES and that a subsequent MECP can transfer the reactant OFeHNO to the required quartet PES, but this is believed to be of minor significance in this context. Similarly, also H_2NO could have been considered to directly adsorb to the quartet FeO, leading to ST 3. Nevertheless, the hydrogen transfer from the adsorbed nitroxyl in OFeHNO to the free oxygen leads to the ground state of NO, adsorbed on monohydroxylated iron (ST 6). This step is strongly exothermic by $\Delta E=-49.5$ kcal/mol after overcoming a barrier of $E^\ddagger=16.5$ kcal/mol (TS 1). For the desorption of nitric oxide, however, another spin change to the sextet PES is required, because monohydroxylated iron is in its ground state on the quintet PES. This barrier via S 3 was calculated to be $E^\ddagger=15.8$ kcal/mol

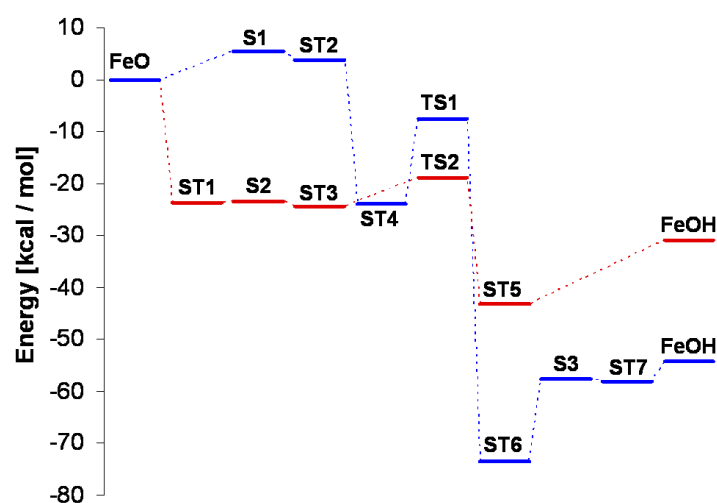


Figure 8.8: Energy profiles for the decay of H_2NO and HNO on $\text{Z}^-[\text{FeO}]^+$. Energies are zero-point corrected.

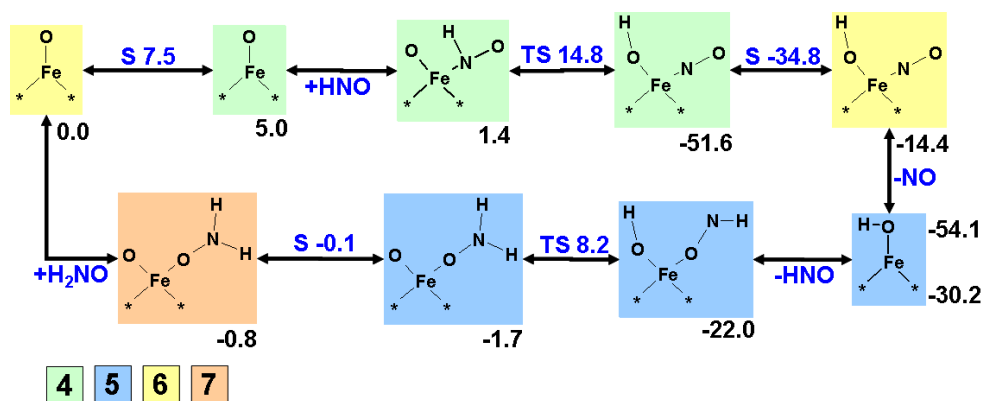


Figure 8.9: Overview of the decay of H_2NO and HNO on $\text{Z}^-[\text{FeO}]^+$. Stated values are Gibbs' free enthalpies calculated at 600 K. Black numbers correspond to the structure, blue numbers to the transition states (TS) or to the minimum on the seam of two PESs (S). Colors of the boxes correspond to the spin multiplicity.

and NO then subsequently desorbs. With that, it was shown that immediately produced H_2NO easily decomposes on FeO to monohydroxylated iron and nitroxyl. The latter potentially reacts with another FeO to nitric oxide and FeOH. Also the Gibbs' free energies, as shown in Figure 8.9, reveal that both pathways exhibit rather low barriers and are strictly exothermic making

them very likely to occur. Produced NO can be consumed further within the mechanism of the standard SCR. The main bottleneck in the context of the SCO, however, has to be seen in the low probability of FeO being present as a free site for the adsorption because the high concentrations of the reactant ammonia make it certainly more likely to be blocked by the latter.

Furthermore, we have analyzed the interaction of the two intermediates H_2NO and HNO with monohydroxylated iron. The corresponding energies are displayed in Figure 8.10 and the schematic overview is shown in Figure 8.11. In contrast to all prior discussed pathways, the energies in both figures are here calculated with respect to FeOH as the active site rather than FeO . The radical H_2NO adsorbs to the FeOH with its oxygen bonded to the iron and a heat of adsorption of $\Delta E_{\text{ads}} = -19.5$ kcal/mol (ST 1) representing the ground state of the adsorbed species on the sextet PES. For a subsequent reaction, it was found necessary to consider a spin change to the quartet PES which is, however, only slightly higher in energy (ST 4). Also the barrier for the crossing was found to be rather low with $E^\ddagger = 1.9$ kcal/mol (S 2). Then, a reaction with nitric oxide forms nitrosamine together with HOFeO . From the energy profile it can be concluded that NO hardly interacts with the surface species (ST 5) and, thus, the reaction can be interpreted to be of the Eley-Rideal type. For the barrier of the cleavage of the O-N bond in the adsorbed radical H_2NO together with the simultaneous formation of a N-N bond with the gas phase nitric oxide a value of $E^\ddagger = 19.3$ kcal/mol (TS 1) was obtained. After the desorption of nitrosamine, the remaining HOFeO could react with another NO to form NO_2 together with monohydroxylated iron. However, the high Gibbs' free energy at 600 K for the transition state suggests that this formation of nitrosamine is rather unlikely. The reason can be seen in the required coadsorption of two molecules prior to the reaction causing a high loss in entropy in the transition state as compared to the reactant state. Alternatively, we considered the decomposition of the adsorbed H_2NO . In a first step, starting from ST 4, the radical forms a second bond to the iron with its nitrogen (ST 6). The barrier for this process is $E^\ddagger = 11.1$ kcal/mol (TS 3) and the product is only slightly higher in energy by $\Delta E = 4.9$ kcal/mol. The cleavage of the internal O-N bond (ST 10) in contrast was found to be highly endothermic by $\Delta E = 33.8$ kcal/mol, dictating in addition a quite high energy barrier for this step with $E^\ddagger = 42.7$ kcal/mol (TS 4). Although a subsequent adsorption of NO on the free atomic oxygen (ST 14) and the subsequent desorption of NO_2 from the remaining NH_2FeOH is strongly exothermic the intermediate formation of the HOFeO-NH_2 (ST 10) is rather unlikely and can be excluded. This is also expressed in the high Gibbs' free energies for this pathway as shown in Figure 8.11. Finally, the proton transfer from

the adsorbed H_2NO to the hydroxyl group on the iron remains, leading to coadsorbed water and nitroxyl. For this process two different pathways were analyzed on the quartet PES. The first one starts from ST 4, in which the radical is only bonded to the iron with its oxygen. The proton transfer exhibits a barrier of $E^\ddagger=20.2$ kcal/mol (TS 6, electronic energy only) and the resulting product has to be considered rather unstable because of a negligible reverse barrier. In fact the desorption of water from this product state (ST 11) was found to be endothermic (ST 11 vs. ST 13), which suggests a further reaction step prior to the water desorption. Alternatively, the proton transfer and the desorption of water to the gas phase can be interpreted as a combined step. The second pathway starts with a proton transfer from the twofold bonded radical (ST 6) which includes a barrier of $E^\ddagger=19.5$ kcal/mol (TS 5). The resulting product state (ST 12) requires a heat of desorption for the water of $\Delta E_{\text{des}}=15.1$ kcal/mol (ST 13). The remaining nitroxyl on the iron can be exchanged with oxygen by coadsorption of the latter (ST 16) and desorption of HNO to FeO_2 which is part of the NO oxidation pathway. Overall, both pathways for the proton transfer are energetically similar and can be accessed. Also with respect to the Gibbs' free energies at 600 K it has to be concluded that the most probable decay of H_2NO on monohydroxylated iron results from the proton transfer to the hydroxyl group eventually forming nitroxyl. In comparison to the analog proton transfer on FeO, however, the barrier is significantly higher and thus the impact of this pathway remains anchored to the surface concentrations of FeO and FeOH.

A slightly different behavior was found for the interaction of nitroxyl with the monohydroxylated iron. It also adsorbs quite strongly to the active site ($\Delta E_{\text{ads}}=-20.3$ kcal/mol, ST 2) with its nitrogen bonded to the iron. Then, a spin change from the quintet to the triplet PES is required prior to the subsequent reaction because the final product has its ground state on the lower PES. The crossing of the seam exhibits a barrier of $E^\ddagger=12.1$ kcal/mol (S 1, electronic energy only) and the excited state (ST 3) is $\Delta E=10.9$ kcal/mol higher in energy than the ground state. In the subsequent reaction, a proton transfer from the nitroxyl to the hydroxyl group takes place, which leads to water adsorbed on FeNO (ST 8) on the triplet PES. For this transfer, a barrier of $E^\ddagger=7.0$ kcal/mol needs to be overcome and a reverse reaction is rather unlikely because of its strong exothermicity ($\Delta E=-31.2$ kcal/mol). Finally, water desorbs, leaving FeNO as the surface species. In fact, this pathway is in close analogy to the reaction of nitroxyl with FeNH_2 , as described in part one, with respect to both, the mechanism and the corresponding barriers. Furthermore, the combined barrier of spin inversion (S 1) and proton transfer is with $E^\ddagger=17.9$ kcal/mol quite similar to the barrier of the proton transfer on

FeO. Thus, for the decay of nitroxyl the impact of available surface concentrations, as was outlined for H_2NO , is less significant. The produced FeNO can be transferred back to FeO within the mechanism of the NO oxidation as outlined in the preceding chapter 7. Alternatively, a reaction with the radical H_2NO can take place after its strong adsorption ($\Delta E_{\text{ads}} = -21.5$ kcal/mol) with the oxygen bonded to the iron (ST 9). The formation of an N-N bond between the amino group of the adsorbed radical and the NO leads to the formation of nitrosamine, which remains bonded with a nitrogen to the iron (ST 15). This step exhibits a barrier of $E^\ddagger = 12.5$ kcal/mol (TS 7) and the final desorption of nitrosamine ($\Delta E_{\text{des}} = 20.9$ kcal/mol) restores FeO in the quartet state. This final process certainly might be of significant impact for both, the further decay of the radical H_2NO and the intermediately produced surface species FeNO, as can be also concluded from the low Gibbs' free energies in Figure 8.11. However, the high oxygen concentrations in the reactant feed gas of the SCO make the consumption of FeNO from O_2 more probable. Nevertheless, starting from the production of the radical H_2NO as described in part three, the consumption of ammonia to first nitroxyl and then to NO can be concluded to be a reasonable explanation of the mechanism of the SCO in accordance to the suggestions of Akah et al.²¹⁷ and Yang et al.²¹⁹ A closure of the reactive cycle is obtained with respect to the production of FeNH_2 , as the precursor to the H_2NO formation, as outlined in part one. Produced NO is consumed in the pathway starting from FeO via FeOH to finally FeNH_2 .

For the decay of nitrous oxide, as is produced in the NO_2 -SCR, the release of its oxygen to the catalytic surface is the most reasonable concept as was shown by Heyden et al.^{119,300} In Figure 8.12, the schematics with the corresponding zero-point corrected energies (red) and the Gibbs' free energies at 600 K are shown for this step on the initial sites FeO, FeOH and FeNH_2 . While the barrier for the oxygen release is severely higher on FeO with $E^\ddagger = 31.1$ kcal/mol they are rather similar for the two other species (FeOH: $E^\ddagger = 21.8$ kcal/mol; FeNH_2 : $E^\ddagger = 19.3$ kcal/mol). Thus, for the latter two species, the barriers are within the order of magnitude of the two highest internal barriers within the presented fast and NO_2 -SCR mechanism in part one and, with that, can be concluded to be accessible. With respect to the fact that in part one, monohydroxylated iron was concluded to probably be the most abundant intermediate, at elevated temperatures, the decay of nitrous oxide on this species to a certain extent is likely. Heyden et al.³⁰⁰ have shown for the NO assisted N_2O decomposition on mononuclear iron sites that a crucial step is the decomposition of NO_2 on HOFeO via an -OONO ligand. The initial surface species was the product of the oxygen release of

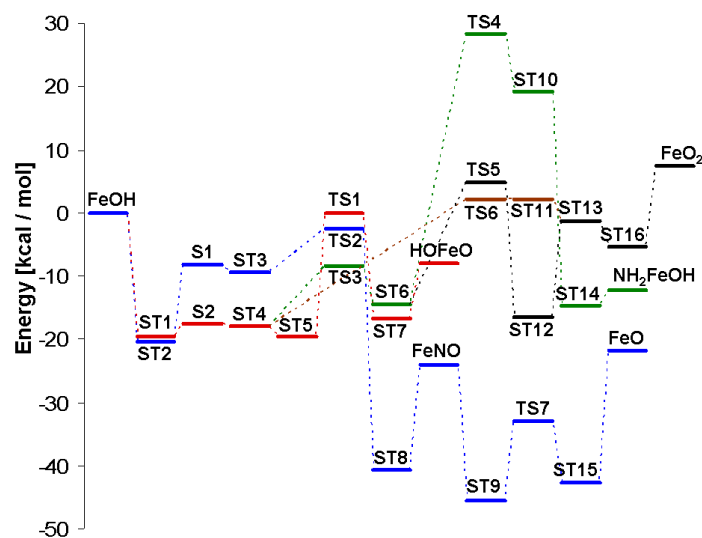


Figure 8.10: Energy profiles for the decay of H_2NO and HNO on $\text{Z}^-[\text{FeOH}]^+$. Energies are zero-point corrected.

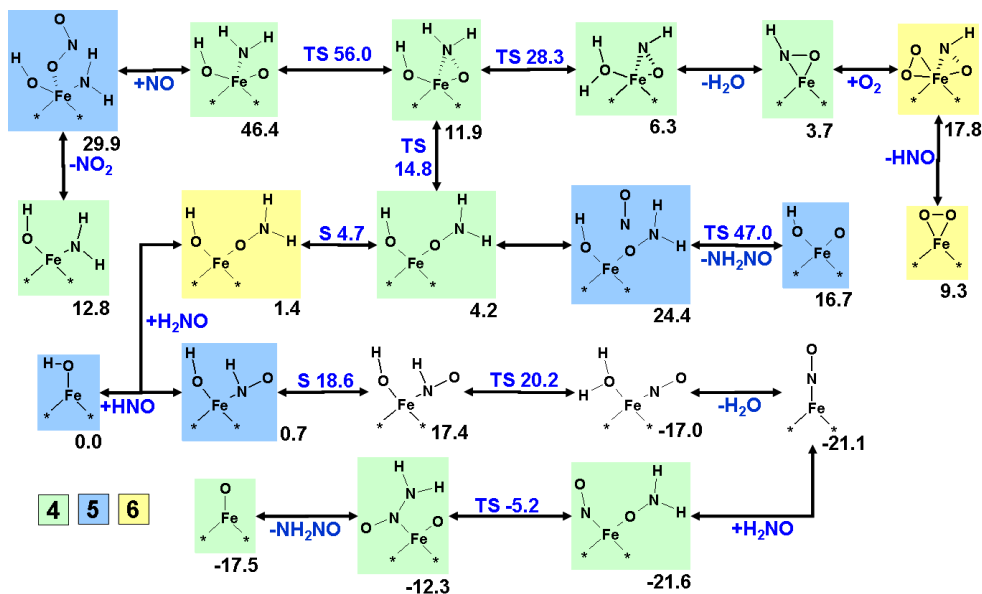


Figure 8.11: Overview of the decay of H_2NO and HNO on $\text{Z}^-[\text{FeOH}]^+$. Stated values are Gibbs' free enthalpies calculated at 600 K. Black numbers correspond to the structure, blue numbers to the transition states (TS) or to the minimum on the seam of two PESs (S). Colors of the boxes correspond to the spin multiplicity.

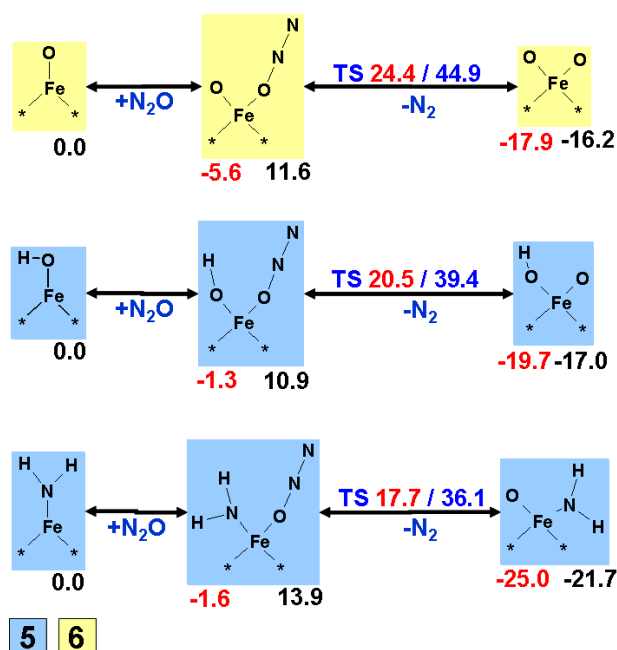


Figure 8.12: Overview of the decay of N_2O on $\text{Z}^-[\text{FeO}]^+$, $\text{Z}^-[\text{FeOH}]^+$ and $\text{Z}^-[\text{FeNH}_2]^+$. Stated values are zero-point corrected energies (red) and Gibbs' free enthalpies calculated at 600 K. Black numbers correspond to the structure, blue numbers to the transition states (TS) or to the minimum on the seam of two PESs (S). Colors of the boxes correspond to the spin multiplicity.

N_2O on FeOH . In fact, this step via the $-\text{OONO}$ ligand also marks a crucial point in the NO oxidation on FeOH as described in chapter 7, although in the reverse direction. However, it can be derived from this analysis, that in the NO_2 SCR the decreasing selectivity to nitrous oxide with increasing temperature can be related to two different reactions. The thermodynamic equilibrium dictates the decomposition of NO_2 to NO and oxygen to a certain extent. On the other hand, formed nitrous oxide might decompose on monohydroxylated iron forming HOFeO together with nitrogen. This latter produced surface species, however, is also the adsorption site for a second NO_2 molecule within the decomposition cycle of nitrogen dioxide on FeOH . With that, a mixture of NO_2 and N_2O decomposition, with the latter making use of the significantly higher activity of the NO assisted pathway, can be deduced to explain the decrease in observed nitrous oxide in the NO_2 SCR with increasing temperature.

In summary, we have studied several pathways on the basis of the DFT within the SCR of NO_x with ammonia on Fe-ZSM5. Iron was represented as mononuclear iron sites and it was assumed that NH_2NO_x are essential intermediates that decompose on the Brønsted acids as shown in chapter 6. In part one, a low energy pathway was presented in accordance with the stoichiometry of the fast SCR. In analogy, a pathway for the NO_2 SCR, leading to equimolar amounts of nitrogen and nitrous oxide, can be concluded to be equivalent to the fast SCR in its main steps, but to differ in the formation of one nitramide from a reaction of a surface amino group with NO_2 rather than the formation of nitrosamine from NO. For the fast SCR, Li and Li³⁴² have proposed a pathway that also leads to the intermediate formation of nitrosamine and involves mononuclear FeO and FeOH. However, as essential steps, they assumed the coadsorption of NO and ammonia on FeO and FeOH prior to a direct formation of nitrosamine. The initial adsorbed state of NO on FeO, as presented in their work, was concluded in chapter 7, section 7.3.1 to be highly unstable, because only a low barrier of $E^\ddagger=3.9$ kcal/mol needs to be overcome to form the significantly more stable nitrite. Thus, the initial state of the mechanism has to be considered rather unlikely to be available for the subsequent coadsorption of ammonia. Furthermore, with respect to the loss of entropy from adsorption, the assumption of the coadsorption of two molecules prior to a reaction, as done by Li and Li, is less likely than the here outlined mechanism which always considers, first, the formation of an amino group on the iron prior to a subsequent interaction with NO_x . For the change of selectivity in the NO_2 SCR towards molecular nitrogen with increasing temperature, it was found in part two that an additional reaction mechanism, leading directly to N_2 , is unlikely to proceed. This behavior can rather be explained by a combined decomposition of intermediately produced N_2O and of the reactant NO_2 into NO and oxygen as outlined in part four. In part three, a potential reaction mechanism for the standard SCR, integrated into the steps of the fast SCR, was addressed. Nitrosamine might be formed after the coadsorption of NO and oxygen on FeNH_2 . This can be interpreted to be in accordance with Schwidder et al.,³⁷ who concluded from the observed strong deviation between NO oxidation and standard SCR activity that the latter might not solely be a combination of NO oxidation followed by the fast SCR. Although our proposed mechanism would circumvent this crude combination of sub-reactions in series, some doubt is left with respect to an unfavorable impact of entropy for the required coadsorption of NO and O_2 . A final conclusion on this question can only be drawn from microkinetic modeling of the system as will be discussed in chapter 9. In addition, we have also shown that from a reaction of oxygen with the FeNH_2 the intermediate radical H_2NO can be formed, which further decom-

poses to nitroxyl and eventually is reduced to NO as outlined in part four. Thus, the formation of the H_2NO can be seen as the potential initialization of the SCO with the intermediately formed NO being consumed within the standard SCR. This is in agreement to the conclusions of Akah et al.^{42,217} and Yang et al.²¹⁹ who proposed, first, the oxidation of ammonia to nitric oxide and its subsequent consumption by ammonia to molecular nitrogen within the standard SCR.

The proposed mechanisms for the SCR schemes in the literature are all quite similar.^{34,40,168,170} It is assumed that ammonium nitrate and nitrite or surface nitrates and nitrites are formed, which are created from the disproportionation of two NO_2 . The reduction of the nitrates by NO is believed to be the rate-determining step in the fast SCR. In reference to the preceding chapter 7, section 7.3.1 we have outlined that such a step exhibits a significantly higher barrier than the highest internal barrier in our proposed mechanism. Thus, it was concluded that the significant role of the nitrate reduction as stressed by Tronconi et al.¹⁶⁸ is rather unlikely. Also, the concept of the disproportionation of two NO_x and the formation and decomposition of ammonium nitrite and nitrate rather fits to our mechanism concluded for the fast and NO_2 SCR on the Brønsted acids as outlined in chapter 6 than to the outlined pathway on the iron sites. However, it has to be emphasized that our presented mechanism only refers to the analysis of mononuclear iron sites, while on dinuclear iron or iron clusters the mechanism could be completely different.

Furthermore, Tronconi et al.^{334,335} have presented a new “enhanced” SCR in which, besides ammonia, also ammonium nitrate is applied as reducing agent and they observed a significantly higher conversion as for the standard SCR. An explanation of this mechanism can also be derived from our mechanism as outlined in part one within the assumption that evaporated ammonium nitrate decomposes into ammonia and nitric acid. Following the sequence of steps in Figure 8.3, it is at hand that from two ammonia molecules and one NO the species FeNH_2 is easily produced together with water and nitrosamine. Then, nitric acid adsorbs to this species and releases NO_2 to the gas phase, which restores the species NH_2FeOH for the reaction with another NO. Eventually, again the species FeNH_2 is produced, which now reacts with the previously released NO_2 . After the desorption of the produced nitrosamine to the gas phase the catalytic cycle is closed. Thus, the schematic directly also explains the new “enhanced” SCR within the observed stoichiometry (equation (8.4)). Alternatively, the nitric acid could also adsorb on monohydroxylated iron forming dihydroxylated iron after the release of NO_2 . In part two, it was shown that ammonia reacts with the dihydroxylated iron by forming water and again the intermediate NH_2FeOH .

8.4 Conclusion

The reaction mechanism of the selective catalytic reduction of nitrogen oxide on iron-exchanged ZSM5 was investigated using the Density Functional Theory. All reaction steps were studied on a cluster of 5 T-atoms, containing a mononuclear iron ion. The crossing of PESs was considered, if necessary. While the NO oxidation, which is considered as the rate-determining step of the standard SCR^{38,158,282,283,330} was already discussed in detail in chapter 7, we have presented here a mechanism for the fast and NO₂ SCR starting from $Z^-[\text{FeO}]^+$ as a representation of the active site on the sextet PES. It was concluded that most probably, first, ammonia adsorbs to the active site and a proton transfer takes place to the oxygen forming an amino group next to a hydroxyl group. Then, either NO or NO₂ react with this intermediate forming nitrosamine or nitramide respectively and monohydroxylated iron remains. The reaction with another ammonia results in the formation of water and an amino group remains on the iron. The latter finally reacts with NO₂ to nitrosamine and the active site is restored. Nitrosamine and nitramide are assumed to decompose on Brønsted acids into nitrogen and nitrous oxide, respectively, together with water. To account for the increasing selectivity of the NO₂-SCR to nitrogen over nitrous oxide with temperature, we concluded that not an additional reaction mechanism, leading directly to only nitrogen, is responsible for this behavior. It is rather the result of an interacting combination of nitrous oxide decomposition and NO₂ decomposition from thermodynamic limitations,^{170,329} on monohydroxylated iron. In this context, the analogy to the NO assisted nitrous oxide decomposition was outlined.³⁰⁰ Furthermore, it could be shown that the additional consideration of the decomposition of nitric acid on either the $Z^-[\text{FeNH}_2]^+$ or on monohydroxylated iron also allows for the explanation of the mechanism of the recently proposed new “enhanced” SCR.³³⁴ For the impact of oxygen, starting from the intermediate surface species $Z^-[\text{FeNH}_2]^+$, the formation of the radical H₂NO was proposed to mark the initialization of the selective catalytic oxidation of ammonia on the catalyst. The radical was shown to further decompose to nitroxyl and eventually lead to NO. Nitric oxide might then further be consumed within the mechanism of the SCR in accordance with the experimental literature.^{217,219} Finally, we have also discussed an alternative pathway for the standard SCR, integrated into the scheme of the fast SCR rather than requiring the NO oxidation separately. Starting from the intermediate $Z^-[\text{FeNH}_2]^+$, after the coadsorption of NO and O₂ the reaction of the amino group with nitric oxide forms nitrosamine. The remaining adsorbed oxygen reacts with NO to NO₂, which is released and restores the

initial active site. Thus, only half of the separate NO oxidation is required, but takes place via the mechanism of the water-free NO oxidation, which is significantly faster than on monohydroxylated iron. The impact of such an additional pathway can however only be revealed from microkinetic modeling. With that, we have presented a theoretical investigation of the SCR of NO with ammonia on mononuclear iron sites, exchanged into ZSM5, which accounts for many experimentally observed phenomena.

9

Microkinetic Modeling of the Selective Catalytic Reduction of Nitrogen Oxide with Ammonia on Fe/H-ZSM5 Based on First Principles

The reaction mechanism of the Selective Catalytic Reduction (SCR) of NO_x on Fe/H-ZSM5 has been investigated by means of a microkinetic model based on the DFT calculations presented in the chapters 7 and 8 together with the model on the Brønsted acids described in chapter 6. The conversion of NO_x ($x=1, 2$) as calculated with our model is in good agreement with experimental data over a wide range of temperature. The NO oxidation proceeds via an -OONO ligand and the negative impact of water relates to the switch of the active site from $\text{Z}^+[\text{FeO}]^+$ to less active $\text{Z}^+[\text{FeOH}]^+$. The fast and the NO_2 SCR proceed via the formation of amino groups on the iron, which subsequently react with NO_x to NH_2NO_x . Nitrosamine and nitramide decompose on the Brønsted acids to nitrogen and nitrous oxide respectively. In both sub-reactions the Brønsted acids exhibit a strong impact on the conversion between 500 K and 700 K. The lower activity of the NO_2 SCR in comparison to the fast SCR is related to the production of nitric acid on the Brønsted acids that cause blocking nitrates on the iron sites. The new “enhanced” SCR appears to bear aspects of both, the fast and the NO_2 SCR. The decompo-

sition of added nitric acid releases NO_2 , which makes the fast SCR accessible, but also causes the consumption of an additional molecule of NO . At low temperatures, the nitric acid forms blocking surface nitrates in analogy to the NO_2 SCR. The fast SCR and the related NO_2 and “enhanced” SCR appear to be catalyzed by mononuclear iron sites only. The simulations of the standard SCR and the ammonia oxidation (SCO), however, were only in agreement with experiments for catalysts with low iron loading, suggesting an important contribution of dinuclear iron sites and iron clusters for these reactions. The SCO proceeds on the mononuclear iron sites via the intermediate H_2NO , which reduces to nitroxyl and eventually to nitric oxide. The latter is consumed within the SCR. At low temperatures, the Brønsted acids exhibit a significant influence owing to the formation of nitroxyl, which then decomposes on the iron sites. The standard SCR was found to be in agreement with the believed combination of NO oxidation and fast SCR in series only at low temperatures. At elevated temperatures, an increase in conversion is anchored to aspects of the SCO.

9.1 Introduction

The abatement of NO_x from exhaust gases has become a major field in environmental research reflecting the more stringent legislation established within the last decade.³⁴⁵ Caused mainly by sources like power plants or automobiles, catalysis is widely applied to reduce polluting compounds.³⁴⁶ While for gasoline engines the three-way catalyst (TWC) is well established, for diesel engines, the SCR with ammonia on zeolite based catalysts has been accepted.³¹ Especially iron exchanged ZSM5 is known for its high activity and durability.³¹⁷ While the SCR on various catalysts is already in the focus of research for more than two decades^{32,33} and correspondingly many phenomena have been elucidated by now, a detailed understanding of the mechanism on iron-exchanged zeolites is still missing. This certainly is attributed to the

significant complexity of the reactive system.

From the preparation of the catalyst by ion exchange to a parent H-form zeolite, at least two different active sites are available, namely the iron and the remaining Brønsted acids. Kröcher et al.³⁴ stated an amount of at least 30% of the latter to remain in the catalyst independent of the applied ion exchange method. In addition, there is an ongoing debate of the active structure of the iron with a certain agreement^{165,318,325,326} by now that mainly mono- and dinuclear iron centers, 1:1 exchanged to the former Brønsted sites, are responsible for the activity of the catalyst for the SCR. Kröcher et al.^{36,290} recently concluded the isolated iron sites to be most active at temperatures up to 300 °C, while the dinuclear sites are claimed to significantly contribute to the activity at higher temperatures. The influence of the Brønsted acids, in contrast, remains under debate,^{171,172,318,327} although the well known fast and NO₂-SCR proceed with significant activity on the iron-free zeolite, too.^{37,39,156}

Besides the complexity of the underlying catalyst itself, the reactive system also includes several macroscopic reactions that are known to co-exist. The fast SCR is the most relevant, which corresponds to a ratio of NO₂/NO_x=0.5 in the reactor inlet and its name reflects the significantly enhanced activity over the standard SCR in the absence of external NO₂.^{37,38,158,319,333} Furthermore, it is believed that the oxidation of NO to NO₂ is the rate-limiting step^{38,158,282,283,330} in the standard SCR with a subsequent access to the fast SCR mechanism. However, a pure feed of NO₂ without NO, which is denoted as NO₂ SCR, exhibits a reduced reactivity as compared to the fast SCR and produces, dependent on the temperature, significant amounts of nitrous oxide.^{38,40,178} Finally, also the selective catalytic oxidation (SCO) of ammonia is known to be of certain relevance on the iron zeolite catalysts as a side reaction.^{42,217,347}

Recently, several experimental studies^{289,328,330,333,344,348,349} included modeling of the SCR system based on fitting of rate expressions for the different observed relevant macroscopic reactions. The rate expressions for the standard SCR usually include, to some extent, the coarse mechanistic suggestions of Tronconi et al.^{168,170,281} or similar ones from Brandenberger et al.³⁴ or Iwasaki et al.⁴⁰ Special attention is also ascribed to the adsorption of ammonia to reflect its strong adsorption on the acid sites and to account for an inhibition effect, observed at low temperatures.^{328,344} While those models are suitable for the application in reactor design, analysis of the contribution of the macroscopic reactions or the parametrization of ammonia supply devices,³²⁸ their transferability to a catalyst other than the investigated one, is very limited because of the neglect of different active sites and their relat-

ive amounts. Although, some more detailed suggestions like the intermediate formation of ammonium nitrite and nitrate³¹⁹ are usually incorporated in the applied rate expressions, it has to be noted that this can also be interpreted to provide an increased mathematical flexibility together with sufficient fit parameters to reproduce the experimental data.

Microkinetic modeling is, in general, capable to elucidate not only the detailed reaction mechanism in agreement with macroscopic observable phenomena, but also allows for the transferability to different catalysts, provided that all necessary elementary steps on all active sites are included. The parametrization of such a microkinetic model can be achieved by the application of quantum chemical tools like the DFT in combination with statistical thermodynamics as was done in several studies so far.^{23,143,256–259} In chapter 7 and 8, we have outlined in detail potential mechanisms that cover the oxidation of NO, the fast and the NO₂ SCR, the new “enhanced” SCR from Tronconi et al.^{334,335} as well as the oxidation of ammonia on mononuclear iron sites based on the DFT. In chapter 6, we have presented the microkinetic modeling of the SCR on the H-form zeolite. The aim of this chapter is to apply the obtained DFT results for the isolated iron sites in a microkinetic model together with the prior results on the Brønsted acids. This leads to a comprehensive consideration of two different active sites in the complete reaction system of the SCR on Fe/H-ZSM5. From this approach it is expected to obtain detailed information about the exact mechanism of all the macroscopic observable sub-reactions, including the impact of the two different active sites, in accordance with the experimentally observed phenomena. Besides a better understanding of the performance of Fe/H-ZSM5, the results of this study are also aimed to allow for the establishment of more profound coarse grained mechanisms for kinetic fitting as well as to serve as the basis for a refinement of the relevant reaction steps from higher level ab initio methods.

9.2 Theory

The applied methodology in this chapter is in close agreement with the descriptions in chapter 6. As a representation of the active site a cluster of 5 T-atoms was used for the screening of the reactive H/N/O system with a mononuclear iron oxide balancing the negative charge of the zeolite framework, caused from an aluminum in the T12 position. For the microkinetic modeling, CHEMKIN^{140,141} was employed. The required thermodynamic parameters of the iron surface species and the kinetic parameters for the

corresponding reactions were derived according to standard statistical thermodynamics^{19,61} and transition state theory¹³⁷ on the basis of the DFT results, as outlined in chapter 3. To account for the influence of the Brønsted acids in the complete catalyst, the relevant reaction mechanisms, as concluded in chapter 6, were applied here, too. The thermodynamic data for the gas phase species are the same as in chapter 6. For the ad- and desorption processes the theory of absolute rate¹³⁷ was applied for the desorption, assuming the barrier to be equal to the zero-point (ZPE) corrected energy difference between the adsorbed and the desorbed state. This implies a barrierless adsorption for which the rate is obtained from the equilibrium constant and the rate of desorption. Because of the neglect of any difference in entropy of the adsorbed state and an assumed transition state of desorption, this approach has to be considered as a conservative approximation, but is expected to yield reasonable first estimates for the model. The harmonic approximation was applied to account for the vibrational contributions for the zeolite cluster, together with its electronic energy. Enthalpy, entropy and the heat capacity were simultaneously fitted to the in CHEMKIN required seven-parameter polynomial for all species using the algorithm of Spitzer et al.¹⁴² (see Table F.2). Approximations for the rates of the crossing of PESs can be calculated as the product of a mean probability of surface hopping and a hypothetical adiabatic rate constant resulting from a transition state with the same relative energy and properties of the minimum energy crossing point (MECP).⁵⁵ For the evaluation of the vibrational contribution to the partition function at the MECP, an effective Hessian as described in section 3.3, equation (3.28) was applied. For the surface thermally averaged hopping probability, the Landau-Zener theory,¹³⁹ in terms of equation (3.29) was used for those elementary steps which were concluded to contribute to the overall reaction from reaction path analysis. The required spin orbit coupling energies were estimated with $H_{12}=825$ J/mol based on the results from Danovich and Shaik³⁵⁰ for the oxidative activation of H_2 by FeO^+ . This approach, though only roughly approximating the hopping probabilities \bar{P}_{12} , was also successfully applied by Heyden et al.^{119,314} in the microkinetic modeling of the related nitrous oxide decomposition on Fe-ZSM5 as well as recently by Bell et al.³⁵¹ The transmission coefficient was then obtained according to¹³⁹

$$\kappa = 2\bar{P}_{12} - \bar{P}_{12}^2 \quad (9.1)$$

However, in the case that the electronic energy differences were low between the excited state and the MECP, similarly as to regular transition states on one PES, the consideration of the zero-point error correction from the effective hessian sometimes resulted in a slightly negative activation energy. In

those cases, usually also the consideration of the hopping probability caused a negative activation energy in the fitting to standard kinetic expressions and, thus, both contributions were neglected. Although the accuracy of DFT in the calculation of relative energies and for reaction barriers⁸⁸ is limited, according to Gokhale et al.,²⁵⁹ it at least captures the essential aspects of the surface chemistry but fine-tuning usually needs to be done to obtain a reliable microkinetic model. Even though there are quantum chemical techniques that can provide nearly quantitative results for intrinsic reaction steps, as recently shown by Hansen et al.,²⁶⁰ their application to reactive systems with a large number of elementary steps is not feasible because of the high computational costs. To obtain reliable heats of formation of the surface species, the values were anchored to the gas phase species thermochemistry. This was done by relating the heat of formation of the surface species to the corresponding heat of adsorption of a gas phase species on the empty active site. For the latter, the heat of formation was set to $H_f=0$. For the iron species, the empty active site corresponds to $Z^-[\text{FeO}]^+$ on the sextet PES (denoted as FeO_6 in the thermodynamic database in Table F.2) and is denoted for the empty Brønsted acid as HZSM5. It should be noted that with respect to the uncertainties of the electronic energy as calculated from DFT and the rather small representation of the active site, the final model keeps a qualitative character to a certain extent and should rather be seen as a detailed screening for relevant elementary steps, which can further be optimized. In addition, the final model only accounts for mononuclear iron sites and Brønsted acids, but the influence of other species, especially dinuclear iron sites, remains speculative. Nevertheless, significant insight into the mechanisms of the reactive H/N/O system can be obtained from such an approach.

9.3 Results and Discussion

The microkinetic model was applied in reactor simulations in an ideal plug flow reactor with the catalyst being evenly distributed. For the comparison to the results of the experimental literature, the number of active sites was anchored to the mass of the catalyst and its Si/Al ratio, assuming that the number of aluminum atoms is equal to the number of Brønsted acids. The active iron sites were assumed to be mononuclear species, ion-exchanged to the Brønsted acids and the amount was related to the stated Fe/Al fraction. The thermodynamic database of the gas phase species and for the surface species on the Brønsted acids is the same as used in chapter 6. For the surface species related to the mononuclear iron sites, the heat of formation

can be obtained from the thermodynamic data (Table F.2). Adjustments on the heat of formations of relevant species are outlined in the text of the corresponding reactions where it was conducted. The reaction rates of all reversible elementary steps on the iron sites are listed in Table F.1 for the applied direction together with any adjustments (column “Adjust”). The following discussion is subdivided into five parts. First, the oxidation of NO to NO₂ and the influence of water on this reaction will be discussed. Second, the oxidation of ammonia as a side reaction is studied. The third part will cover the fast SCR with special emphasis on the influence of the Brønsted acids in the system vs. the iron. In the fourth part, the NO₂ SCR is analyzed with special attention on the temperature dependence of the selectivity towards nitrogen as well as to the observed reduced activity in comparison to the fast SCR. In a fifth part, we comment on the new “enhanced” SCR and, finally, the mechanism of the standard SCR is discussed. The specifications of the simulated experiments are summarized in Table 9.1, assuming a tubular reactor. However, for a quantitative comparison with experimental data, exact information about the applied catalyst is necessary with respect to the Si/Al ratio, the iron content and the absolute mass, as well as of the applied conditions, flow and feed gas composition and parameters of the reactor. Thus, despite the immense amount of experimental literature available on the SCR on Fe-ZSM5, only few papers contain sufficient information to qualify for direct comparison.

9.3.1 Modeling of the NO Oxidation

There is a wide agreement in the literature that the oxidation of NO to NO₂ is the crucial step in the standard SCR and is considered to be rate-limiting for the overall process. However, the activity of the catalyst for the NO oxidation was found to be significantly lower than for the standard SCR,^{37,282} although Metkar et al.³³⁰ recently observed similar activities for both reactions. The fact that water significantly inhibits the NO oxidation is beyond controversy.^{163,288,330} Within the SCR, which mainly produces water and nitrogen, this would imply that the SCR itself slows the rate-limiting step down. Delahay et al.²⁸² suggested that in the NO oxidation, the NO₂ desorption is rate-limiting and that in the standard SCR ammonia directly reacts with the adsorbed nitrogen dioxide. Metkar et al.³³⁰ suggested that, in the presence of water, nitrous and nitric acid block the active site for the limiting NO oxidation and are removed by ammonia in the standard SCR. Finally, Schwidder et al.³⁷ proposed that the SCR might not solely be a combination of NO oxidation and subsequent fast SCR, but exhibits

Table 9.1: Specifications of the simulated experiments assuming a tubular reactor of length l and diameter d .

Rxn	Si/Al [-]	Fe/Al [-]	m_{cat} [mg]	\dot{V} [cm ³ /min]	d [mm]	l [cm]	NH ₃ [ppm]	NO [ppm]	NO ₂ [ppm]	O ₂ [%]	H ₂ O [%]	Ref.
NO ox	11.4	0.75	140	100	6	5 ^a	-	1000	-	5	-	[288]
NO ox	10	0.193	50	500	6 ^a	5 ^a	-	1000	-	2	-	[155]
NO ox	13.5	0.3	901	7810	169	4	-	1000	-	10	-	[172]
NO ox	16.4	0.49	20	138.3	6 ^a	5 ^a	-	2000	-	3	-	[282]
NO ox	13.5 ^a	0.3 ^a	901	7810	169	4	-	1000	-	10	5	[163]
SCO	15	0.08	100	200	6 ^a	5 ^a	500	-	-	2	-	[42]
fast SCR	14	0.18	10	183.3	6	5 ^a	1000	500	500	2	-	[37]
NO ₂ SCR	14	0.18	10	183.3	6	5 ^a	1000	-	1000	2	-	
st. SCR	14	0.18	10	183.3	6	5 ^a	1000	1000	-	2	-	[37]
st. SCR	13.5	0.02	901	7810	169	4	1000	1000	-	10	5	[36]

^a Assumed parameters

a complete different mechanism. This illustrates the demand for a detailed understanding of the mechanism of the NO oxidation in order to understand its influence in the SCR. First we present the kinetic modeling in the absence of water and then discuss the impact of water on the active site and the reaction pathway.

For the case of the water-free NO oxidation, we compared our results to four independent sets of experimental data from the literature.^{155,172,282,288} Our model was slightly adjusted in comparison to the set of data from Delahay et al.,²⁸² based on a sensitivity analysis¹⁴³ of all reactions and the heat of formations of all surface species. This method was also applied in chapter 6 for the reactions on the Brønsted acids. With respect to the surface species, the tuning resulted in an increase of the heat of formation of the surface nitrite $Z^-[\text{FeO}_2\text{N}]^+$ by $\Delta E=2$ kcal/mol. Adjustments on the reaction rates are outlined in Table F.1 in “NO oxidation on FeO”. The comparison between our model and the four sets of data is shown in Figure 9.1 a) to d). In all four cases, a good agreement between simulation and experiments is observable and with that over a wide range of conditions. Only at elevated temperatures, a slight tendency to overestimate the conversion is present. The limitation of the conversion at high temperatures is clearly related to the thermodynamic equilibrium between NO and NO₂ in the gas phase. While the data represented in a), b) and c) correspond to steady state conversions, the data in d) was obtained from temperature programmed surface reaction (TPSR). It can be assumed that in the high temperature regime no equilibrium between the surface and the gas phase is reached, explaining the experimentally observed higher production of NO₂ than thermodynamically allowed.

Reaction path analysis reveals that the mechanism for the conversion is dependent on temperature. At low temperature the dominating pathway starts with the adsorption of NO on the active site FeO by forming the nitrite FeONO, which subsequently transfers to the more stable nitrite with two oxygen bonded to the iron (FeO₂N). Then, another nitric oxide coadsorbs on the nitrite and NO₂ desorbs after first transforming back to the more loose bonded state. Now, oxygen coadsorbs to the remaining FeNO and the nitric oxide is released back to the gas phase from which it directly attacks the oxygen by forming an -OONO ligand in the cis-conformation. The desorption of a second NO₂ from this ligand restores the active site and the catalytic cycle is closed. It should be noted that the somewhat unconventional desorption of NO prior to its attack on the oxygen is probably an artifact of the implementation of the reactions. It should be interpreted as the suggestion that in the reactant state, prior to the -OONO ligand formation, nitric oxide rather interacts with the adsorbed oxygen than with the iron. The direct reaction

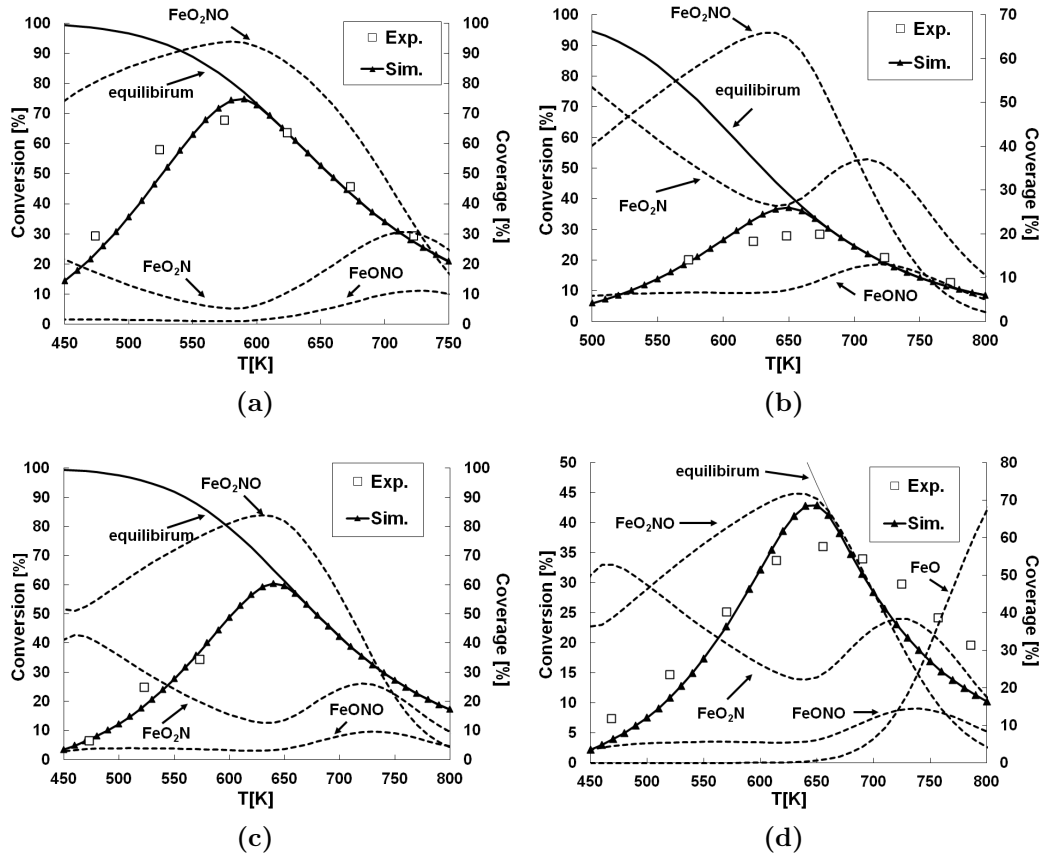


Figure 9.1: Simulated conversion of NO and coverage of the dominant surface species vs. temperature in comparison to data from a) Giles et al.²⁸⁸ b) Long and Yang¹⁵⁵ c) Brandenberger et al.¹⁷² and d) Delahay et al.²⁸²

pathway to the characteristic ligand with NO adsorbed on the iron in the reactant state hardly contributes to the conversion at all. While the initial nitrite formation and the final -OONO formation from FeO_2 with NO prevail over the whole range of temperature, the amount of nitrite that transfers into the more stable configuration becomes less. This is related to the higher degree of mobility which, with respect to entropy, becomes more favorable with increasing temperature. Thus, oxygen coadsorbs more dominantly to the nitrite, which desorbs as NO_2 to the gas phase. The schematic of the described reactions together with the corresponding spin multiplicities are shown in Figure 9.2 a).

A sensitivity analysis revealed that the rate-determining step for the NO

oxidation is the desorption of NO_2 from the $-\text{OONO}$ ligand. This is true over the complete range of temperature and independent of the conditions applied. Furthermore, it is apparent from Figure 9.1 that the dominating species on the surface is the nitrate FeO_2NO . Because it does not contribute to the reaction at all, it blocks the active site, in agreement to the conclusions drawn in chapter 7 based on the DFT results. The rate of reduction of this species by nitric oxide to a nitrite species was found from the reaction path analysis to be up to ten orders smaller in magnitude than the rate-determining step in the catalytic cycle. Thus, even with respect to the rather qualitative character of our model, from the DFT results a significant contribution of such a step as suggested by Tronconi et al.¹⁶⁸ as the rate-limiting step of the fast SCR has to be excluded based on this result. The shape of the surface coverage with the nitrate over temperature is clearly anchored to the production of NO_2 and can be interpreted as an equilibrium concentration with respect to the gas phase. Furthermore, the surface coverages of the two nitrite species FeONO and FeO_2N are shown. The elementary reaction step for the transformation between these two species was found to be in partial equilibrium over the whole range of temperature. From the shape of the concentrations, the temperature dependence of the mechanism can be explained. At low temperatures, the more stable nitrate is dominant and the probability of nitric oxide to coadsorb on it is significantly higher than that oxygen adsorbs on FeONO . With that, the following reaction pathway is also predetermined. At higher temperatures, the equilibrium between the two nitrites shifts in favor of the more loose state anchored to the shift of the attribute “more stable” to “more restricted with respect to entropy” for FeO_2N . This also enables the shift in the dominance of the mechanism responsible for the NO oxidation via the intermediate O_2FeONO . In addition, it can be seen that the surface concentrations of the nitrites are limited by the dominant nitrate species, which also explains their maximum above 700 K when the reduced production of NO_2 , from the thermodynamic limitation, also reduces the nitrate surface coverage. Furthermore in this regime, the initial active site FeO (compare Figure 9.1 d) becomes the dominant surface species when the gain in entropy from the desorption of nitric oxide from the nitrites outbalances the heat of desorption.

For the NO oxidation in the presence of water, no sufficiently defined set of experimental data was available for comparison with our model. However, Kröcher et al.¹⁶³ have shown the influence of water in comparison to the water-free case on an unspecified, commercial catalyst and later¹⁷² measured the conversion in the absence of water for a well-defined catalyst at the same conditions (compare Figure 9.1 c). A comparison between the two experi-

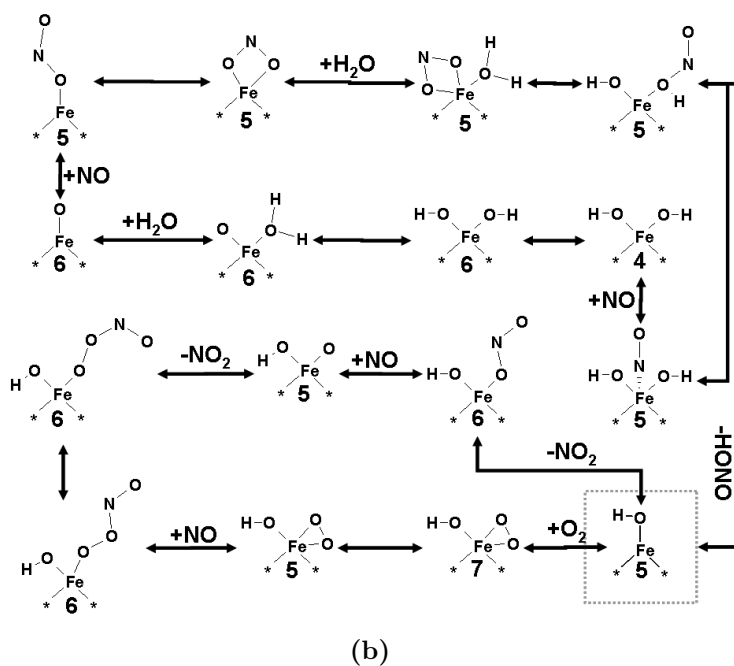
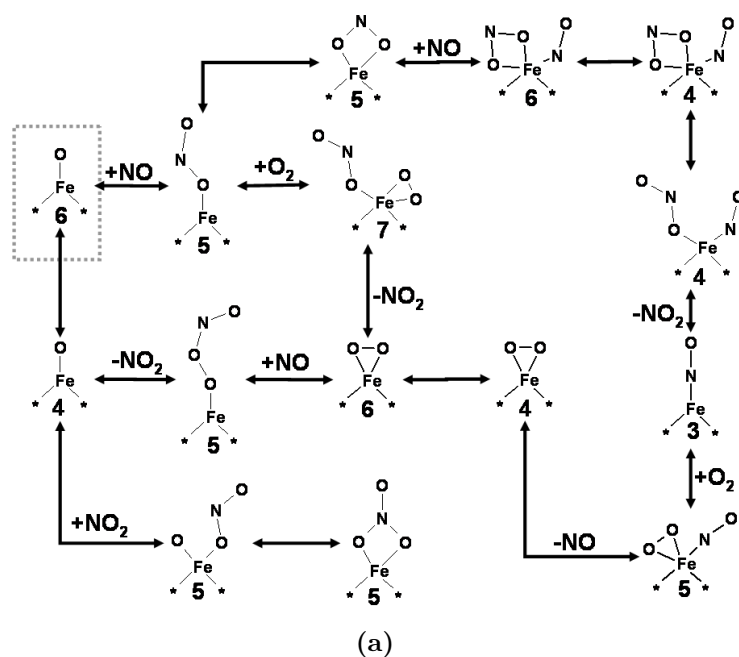


Figure 9.2: Schematic of the relevant reaction pathways in the oxidation of NO to NO₂ in a) the absence and b) the presence of water. Numbers refer to the spin multiplicities of the species.

mental data sets in comparison to our model, parametrized according to the well-defined catalyst shows that, as a rough approximation, the two catalysts can be assumed to be equivalent. Thus, the influence of water on the well-defined catalyst should accordingly be very similar as on the commercial one. In consequence we have adjusted the essential surface species and reactions to obtain the conversion at approximately 750 K measured by Kröcher et al.¹⁶³ Within the fine tuning, the heats of formation of HOFeOH on the sextet and FeOH on the quintet PES were increased by $\Delta E=3$ kcal/mol, of $\text{O}_2\text{FeOH_NO}$ on the sextet PES reduced by $\Delta E=-2$ kcal/mol and of HOFeOONO_t on the sextet reduced by $\Delta E=-1$ kcal/mol. Adjustments on the reaction rates are outlined in Table F.1 in “NO oxidation on FeOH”. In Figure 9.3 a), the comparison between the two data sets, based on the different catalysts and the impact of water, is shown together with the results of our model. Furthermore, the surface coverages of the dihydroxylated and the monohydroxylated iron are shown for the case of the presence of water. In Figure 9.3 b), the conversion in the presence of water is shown comparing the results of the complete catalyst with a virtually only iron containing catalyst.

It can be seen that a very good agreement of the model with the experimental data is obtained. It is true that this comparison is somewhat arbitrary from the perspective that the specifications of the catalyst are not known and are only assumed to be similar to the one used in the model. However, from the comparison of the water-free experiment with our model, it is at hand that the assumption of similar catalysts is reasonable. Furthermore, it should be noted that the fine tuning of our model was executed with respect to only one experimental conversion measurement at 750 K. The subsequent agreement with the data set over the complete temperature range proves the validity of the approach.

From reaction path analysis, it can be obtained that over the complete range of temperature the conversion follows the same mechanism with monohydroxylated iron functioning as the active site. First, oxygen adsorbs on the iron and then reacts with NO by forming the characteristic -OONO ligand in the trans configuration. After a transfer to the cis-isomer, the desorption of NO_2 takes place and another nitric oxide forms with the remaining oxygen atom on the iron a nitrite. The desorption of this second NO_2 closes the catalytic cycle. The pathway is outlined in the schematic of Figure 9.2 b). From Figure 9.3 a), it can be obtained that the dominating surface species are the di- and the monohydroxylated iron. With respect to the fact that the dihydroxylated iron is inactive, for the NO oxidation it becomes obvious that the activity in the presence of water is anchored to the available monohydroxylated surface species and is blocked, especially at low temperat-

ures by HOFeOH . At elevated temperatures, the monohydroxylated species becomes thermodynamically more favorable causing its higher availability as active site. The maximum in the conversion curve results from the required adsorption of oxygen on the monohydroxylated iron. Although the content of FeOH significantly increases with temperature, the concentration of HOFeO_2 decreases again above 800 K, which can be explained by the increasing influence of entropy at higher temperatures, favoring the desorbed state. Finally, also in the presence of water, the thermodynamic limitation of the NO oxidation determines the conversion at even higher temperatures. The rate-limiting step of the reaction was found to be the internal conversion of the $-\text{OONO}$ ligand from the trans- to the cis-configuration.

It should be noted that, in the so far discussed model, we have included the reactions on the Brønsted acid that were found relevant in the fast SCR (compare chapter 6). In addition, the conversion in the absence of the contribution of the Brønsted acids is presented in Figure 9.3 b) (●, “w/o Z-H”) and a significant deviation between the two conversion curves is apparent at low temperatures. The reason for this deviation is the production of nitrous acid on the Brønsted acids from the decomposition of N_2O_3 , which further decomposes on the monohydroxylated iron by forming the dihydroxylated species. This reduces the amount of available active sites significantly for the case of the consideration of the full system in comparison to the only iron-considering catalyst. In Figure 9.3 b), the concentration of HONO in the reactor outlet is shown over temperature for both cases. The deviation in conversion is eliminated, as soon as the production of this species is the same for both catalysts at temperatures above 640 K. While the consideration of the Brønsted acids is obviously required in our model to correctly account for the conversion curve, an uncertainty remains if there really is a negative influence of the Brønsted acids or if this is only an artifact of our model, resulting from an underestimated production of HONO on the iron species.

The discussion so far did not address the nuclearity of the iron species. Good agreement between the model and experimental data was obtained for various iron loadings. However, especially at high iron loadings, also other species than the mononuclear ones are present.²⁹⁰ In Figure 9.4, the impact of the Fe/Al ratio is shown in comparison to the conversion curve in the absence of water for the specifications as in Figure 9.1 d). It can be seen that a further increase in iron does not significantly further enhance the conversion, while a decrease of Fe has a more pronounced impact. It could be suggested from this result that the NO oxidation is dominated by mononuclear iron species and that in the modeling of catalysts of higher iron contents the amount of present active sites is overestimated which, however,

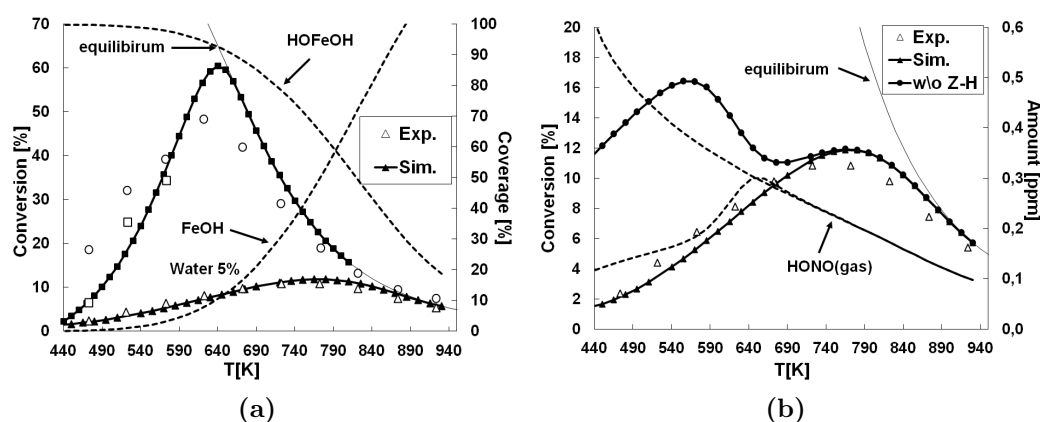


Figure 9.3: a) Simulated conversion of NO in the absence and presence of water in comparison to experimental data of a specified catalyst (\square ref. [172]) and an unspecified catalyst (\circ and Δ ref. [163]) and surface coverages of the dominant surface species vs. temperature. b) Impact of Brønsted acids on the NO oxidation in the presence of water vs. temperature.

then only has a minor impact. Alternatively, it could be suggested that iron species of higher nuclearity exhibit a similar activity for the NO oxidation, which makes the distinction between the sites dispensable.

In summary, the reaction mechanism for the NO oxidation was elucidated for both cases, in the absence and in the presence of water. The strong inhibiting influence of water on the system is related to the formation of dihydroxylated iron species from the reaction of water with FeO, which are inactive for the NO oxidation. The reaction itself proceeds on the monohydroxylated iron species, which exhibits a lower activity for the reaction, as was already concluded from the comparison of the energy profiles of the two mechanisms in chapter 7. To explain the discrepancy of the activity of the Fe-ZSM5 for the NO oxidation and the standard SCR, Delahay et al.²⁸² assumed that the rate-limiting step of the NO oxidation is the desorption from NO_2 and that ammonia reacts with the adsorbed species to eliminate the desorption step in the SCR. Although the rate-limiting step was found in the absence of water to be the desorption of NO_2 from the -OONO ligand the coverage of this species is negligible. In the presence of water, which is a product of the SCR, the surface is dominated by the hydroxylated iron species and, thus, it is more likely that ammonia reacts with these than with a surface nitrite. Furthermore, also no adsorbed nitrous or nitric acid are obtained as relevant surface species in contrast to the suggestions of Metkar

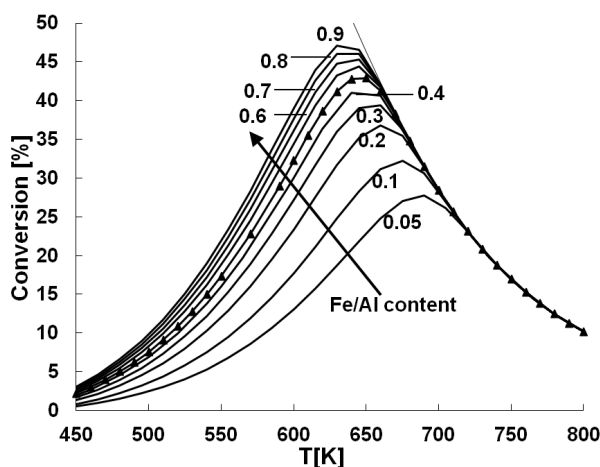


Figure 9.4: Impact of the iron content on the conversion of NO to NO₂ in the absence of water.

et al.³³⁰ It could be argued that the general idea of ammonia retransferring the active site to the more active FeO within the SCR still might be plausible in view of the results of the preceding chapter 8. It was shown, based on the DFT, that the fast SCR mechanism includes both species, FeO and FeOH and that ammonia also reacts with the dihydroxylated iron species. However, the energy profile of the fast SCR suggested that, again, the monohydroxylated iron species will be dominating and the more active FeO is probably not available in sufficient amounts for the NO oxidation. A more detailed discussion on that issue is presented in the subsection on the standard SCR.

9.3.2 Modeling of the NH₃ Oxidation (SCO)

The oxidation of ammonia is known to be an unwanted side reaction of the SCR, which is also fairly well catalyzed by the Fe-ZSM5.²²¹ However, within the after-treatment of applications that use ammonia, the SCO was also found useful to prevent ammonia slip. The benefit of the iron-exchanged zeolite for this reaction is the favorable selectivity towards nitrogen as opposed to noble metal containing catalysts that produce NO and N₂O in significant amounts.⁴² From a mechanistic aspect, this beneficial selectivity is related to the parallel proceeding SCR, which is capable to convert intermediately produced nitric oxide to nitrogen.^{217,219} This is supported by Yang et al.^{43,220} who found a good correlation between SCR activity and

SCO selectivity towards nitrogen. In analogy to the discussion of the relevant active site species for the SCR, also within the SCO it can be assumed that different species are involved with differing activity. Akah et al.²¹⁷ concluded that binuclear iron sites are responsible for the oxidation of ammonia to nitrogen, while Fe_2O_3 clusters predominately cause nitric oxide. This is in agreement with the conclusion of Long and Yang²²⁰ that a low ratio of Si/Al together with a high iron content is favorable for the SCO. Also Brandenberger et al.³⁶ concluded that the ammonia oxidation is primarily catalyzed by lower clustered oligomers and most likely binuclear species, based on the correlation of statistically estimated iron species concentrations with activity. Thus, it is at hand that our model, which only accounts for the mononuclear iron sites, is not the best choice to describe the SCO in general. However, Akah et al.⁴² analyzed a catalyst with a very low iron content ($\text{Fe}/\text{Al}=0.08$, $\text{Si}/\text{Al}=15$) for which, in comparison to a similar catalyst from Brandenberger et al.,³⁶ the conclusion can be drawn that a high fraction of about 80% of the iron is present as monomeric species. Furthermore, Akah et al.²¹⁷ also observed an enhancing influence of the Brønsted acids with respect to activity and selectivity and although the H-ZSM5 was found to be less active and selective for the SCO, (compare chapter 6, section 6.3.4) its interaction with the iron is not known. Here, we compare our model against the data presented from Akah et al.⁴² to analyze the impact of the Brønsted acids and the mononuclear iron sites on the SCO. We have adjusted the heat of formations of essential surface species and relevant reaction rates to obtain approximately the conversion at 725 K measured by Akah et al.⁴². This resulted for the surface species in an increase of the heats of formation of the sextet NH_2FeOH by $\Delta E=2$ kcal/mol and of the HOFeH_2NO by $\Delta E=3$ kcal/mol and in a reduction for the quintet species NH_2FeO_2 and FeOONH_2 by $\Delta E=-3$ kcal/mol. Adjustments on the reaction rates are outlined in Table F.1 in “SCR on Fe-ZSM5; Part 4”. From the comparison in Figure 9.5 a), a reasonable agreement between the model and the experimental data can be observed. However, not a distinct smooth curve of S-shape is obtained but rather a double S-shape. This already indicates the overlapping of two different mechanisms to be responsible for the conversion, dependent on temperature. Whether this effect truly exists, with respect to the potential observability on a catalyst that only exhibits mononuclear iron sites, or rather is an artifact of our model, which does not sufficiently smoothly account for the crossing between mechanisms, cannot be concluded. However, also the data presented by Metkar et al.³³⁰ for the ammonia oxidation can be interpreted in terms of the occurrence of two different regimes with a sharp bend upwards at approximately 400°C.

From reaction path analysis, the main contribution of the ammonia oxidation interestingly starts on the Brønsted acids with the oxidation of ammonia to nitroxyl. In chapter 6, this was concluded to be the rate-limiting step in the SCO on H-ZSM5. However, the subsequent bimolecular reactions of nitroxyl on the acid sites do not proceed at all anymore in the presence of the iron. The nitroxyl mainly adsorbs on the monohydroxylated iron and, by a proton transfer, forms FeNO together with water, which desorbs. To a certain extent, the analogous reaction takes place on FeNH₂ with the reformation of ammonia together with FeNO. To this surface species oxygen coadsorbs and nitric oxide as intermediate is released to the gas phase, leaving FeO₂. Parts of the NO (approximately half of it) is oxidized to NO₂ via the formation of the -OONO ligand from the reaction with FeO₂. The produced NO₂, in turn, decomposes within the reverse mechanism of the NO oxidation on FeO as described in the preceding section 9.3.1. In detail that implies coadsorption of the NO₂ on another FeO₂, desorption of oxygen which leaves the nitrite FeONO and, finally, the desorption of nitric oxide. Thus, the immediately produced NO₂ solely serves to consume the surface species FeO₂. Ammonia coadsorbs to the eventually produced FeO and forms NH₂FeOH, which reacts with nitric oxide to nitrosamine. After the desorption of the latter, monohydroxylated iron is restored. Nitrosamine eventually decomposes on the Brønsted acids to nitrogen and water. At elevated temperatures, the initialization of the SCO on the Brønsted acid is reduced because of the decreasing amount of adsorbed ammonia on these sites. The correlation of this effect can be seen in the change of the conversion curve from convex to concave at the onset of a steep decrease in ammonia coverage on the acid sites (Figure 9.6 a). An additional mechanism sets in on the iron sites to further convert ammonia to nitrogen. Parts of the monohydroxylated iron are transferred in a reaction with ammonia to FeNH₂ by proton transfer to the hydroxyl group and the subsequent desorption of water. To this species oxygen coadsorbs and via a chain-like ligand, similar to the one in the NO oxidation, -OONH₂, the radical H₂NO is released to the gas phase. Next, it adsorbs on a free FeO, but with the oxygen now bonded to the iron, and transfers a proton to the free oxygen leading to nitroxyl adsorbed on FeOH. The remaining consumption of the nitroxyl is analogous to the low temperature behavior. However, related to the increasing formation of water, now also parts of the FeO are not only consumed by ammonia, but also by water, producing dihydroxylated iron, which further leads to the formation of nitrous acid on monohydroxylated iron. Furthermore, parts of the immediately formed nitrite FeONO transform into the more stable nitrite FeO₂N, which reacts with water to FeOH and nitrous acid. The fate of the thus produced HONO is anchored to the increasing number of free Brønsted acids

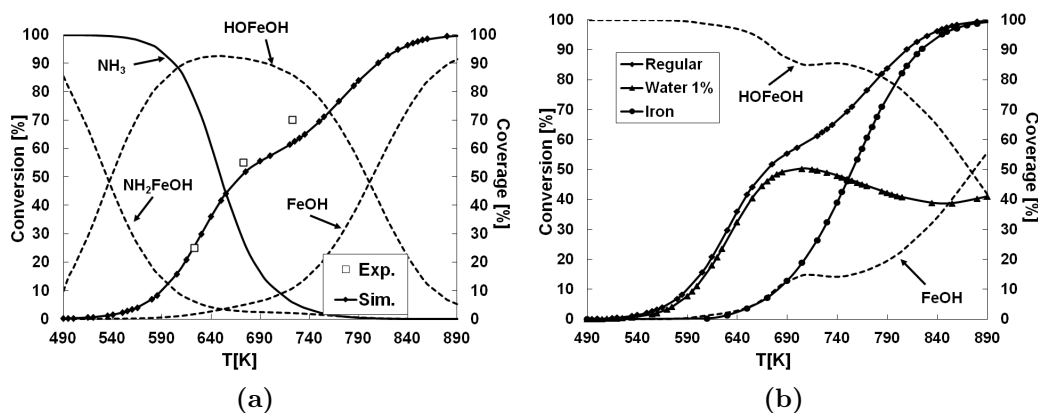


Figure 9.5: a) Simulated conversion of NH_3 and coverage of the dominant surface species vs. temperature in comparison to data from Akah et al.⁴² b) Impact of Brønsted acids and water on SCO. Surface coverage refers to simulated water influence.

from ammonia desorption. It decomposes into water and NO^+ on the zeolite and further reacts with ammonia to nitrosamine. The relevant reactions on the iron are represented in the schematic of Figure 9.6. The pathway from FeNO to finally FeO is outlined in Figure 9.2 a) and the formation of nitrous acid from the interaction of water with FeO_2N and from nitric oxide with dihydroxylated iron is shown in Figure 9.2 b). Nevertheless, the transfer from the low to the high temperature mechanism is a rather smooth function and both pathways coexist over a wide range of temperature. The kink in our conversion curve is thus the representation of a narrow temperature window in which the activity for the low temperature mechanism decreases faster than the activity of the high temperature mechanism increases. The dominating surface species on the iron sites is, over a wide range of temperatures, the dihydroxylated iron. At low temperatures, it is not as dominant because of the lack of water from the ammonia conversion. Thus here, NH_2FeOH is dominant, which can be interpreted as adsorbed ammonia on FeO . At high temperatures, a shift towards the monohydroxylated iron takes place resulting from an increased reactivity of both, ammonia and nitric oxide with the dihydroxylated iron.

In Figure 9.5 b) the conversion of ammonia is shown for only the iron sites in comparison to accounting for both active sites. While above 850 K the iron sites are the only relevant species, the significant impact of the Brønsted acids is apparent below that temperature. Furthermore, it is known^{163,330}

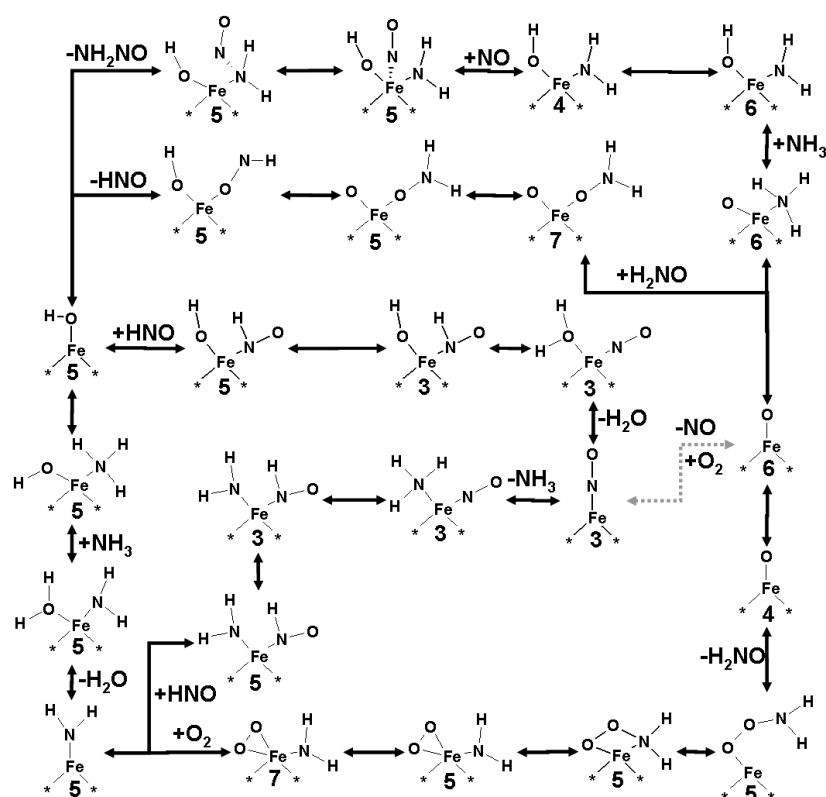


Figure 9.6: Schematic of the relevant reaction pathways in the oxidation of NH_3 . Numbers refer to the spin multiplicities of the species.

that water has an inhibiting influence on the SCO. The impact of 1% water on the ammonia conversion is also shown in Figure 9.5 b). While the influence is rather moderate at low temperatures, at high temperatures, it even causes a decrease in conversion with temperature. This can be explained with the shown coverages of the iron sites. Here, the dominance of the dihydroxylated iron is significantly more pronounced, which suppresses the onset of the iron-catalyzed formation of H_2NO and its subsequent transfer to nitroxyl. At low temperatures, the production of the nitroxyl is governed by the Brønsted acids and the decomposition of this intermediate on the iron is only slightly influenced by water. However, the formation of nitrous acid as outlined for the regular high-temperature mechanism is now significantly present over the whole temperature range with its decomposition on the Brønsted acids. It should be noted that the experiments of Devadas et al.¹⁶³ and Metkar et al.³³⁰ in the presence of water did not result in a decrease of ammonia conversion at elevated temperatures. Furthermore, while a comparison with

the low iron-containing catalyst yielded reasonable agreement to experiments, the performance of a catalyst with significantly higher iron content, as also presented by Akah et al.,⁴² could not be simulated. Both deviations support the analysis of Brandenberger et al.³⁶ that the SCO is mainly catalyzed by iron species other than the mononuclear sites. This, however, does not mean, that there is no contribution from the mononuclear iron sites, but solely that the impact of these sites is less pronounced than the influence of other iron species. With that, the reduction in activity from water could, in fact, still be related to the break down of the contribution of the mononuclear sites, although this conclusion remains rather speculative in the absence of related experimental data.

9.3.3 Modeling of the Fast SCR

It is well established that NO₂ exhibits a boosting effect on the activity for the selective catalytic reduction of nitric oxide with ammonia with a maximum at equimolar amounts of NO and NO₂, known as the fast SCR.^{37,38,319,333} This finding was a main contributor to the suggestion that in the standard SCR the NO oxidation is the rate-limiting step¹⁵⁸ and Kröcher et al.¹⁶³ even concluded the fast SCR to be the true SCR. In diesel engines, this boosting effect is available because of the installation of preoxidation units prior to the addition of ammonia as reducing agent in exhaust gas treatment.^{170,329} In any case, the fast SCR can be interpreted as the central part within the SCR. Schwidder et al.³⁷ concluded that mononuclear iron sites are sufficient for the activity of Fe-ZSM5 for the fast SCR. Furthermore, the fast SCR also proceeds on the Brønsted acids with significant activity,^{37,38,156} but the influence of these sites in the iron exchanged catalyst is not known. Finally for the fast SCR, Iwasaki et al.³³³ observed a change in apparent reaction order of ammonia at low temperatures from positive to negative and Tronconi et al.¹⁶⁹ found a blocking effect of ammonia from transient experiments. In this section, we compare our model against the data from Schwidder et al.³⁷ to elucidate the governing mechanism for the fast SCR. In addition, the impact of the two different active sites is analyzed based on a variation of the iron content as well as from simulating a virtually Brønsted acid-free catalyst. We adjusted our model to approximately obtain the experimentally measured NO conversion at 525 K based on a sensitivity analysis of the heats of formation and the reaction rates. The values for the quintet NH₂FeOH-NO and for the quartet HOFeO-ONO_{tu} have been reduced by $\Delta E = -3$ kcal/mol and for the sextet HOFeO₂NO increased by $\Delta E = 3$ kcal/mol. Adjustments on the reaction rates are outlined in Table F.1 in “SCR on Fe-ZSM5; Part 1”.

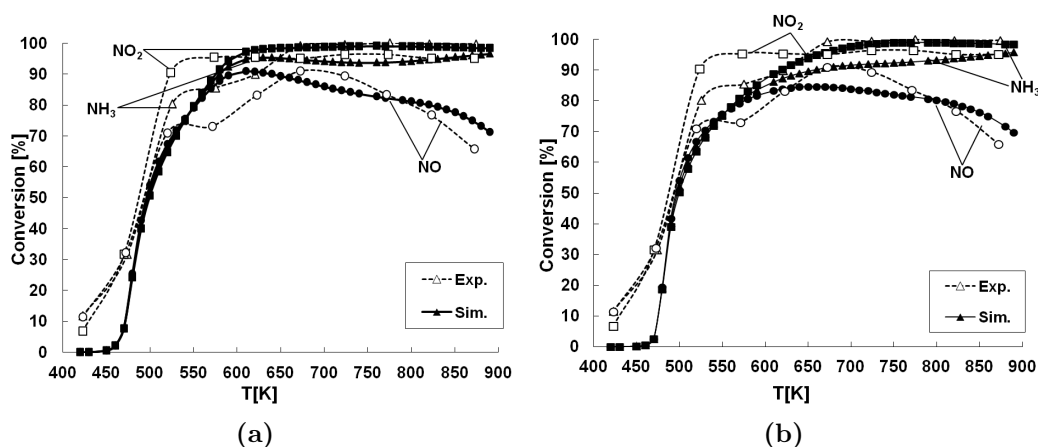


Figure 9.7: Simulated conversion of NH_3 (Δ), NO (\circ) and NO_2 (\square) vs. temperature in comparison to data from Schwidder et al.³⁷ a) Iron and Brønsted acids b) Only Iron.

In Figure 9.7 a) the comparison between the experiment and the microkinetic model is shown. Good agreement between the conversion curves for NO , NO_2 and NH_3 can be observed over the complete range of temperature. Above 650 K, experiments suggest that the conversion of NH_3 should be slightly higher than the NO_2 conversion, which is related to the more dominant oxidation of ammonia. In our model, this is not the case but can be explained by the fact that we only considered the mononuclear sites. It can be assumed that in the true catalyst species of higher nuclearity also exist which cause the oxidation of ammonia, as was discussed in the preceding section 9.3.2. Furthermore, the stoichiometry of the fast SCR suggests a one-to-one consumption of NO and NO_2 . The deviation, as is observed at elevated temperatures in the simulation as well as in the experimental data, can be related to the NO_2 SCR which proceeds in parallel, as will be further discussed in the subsequent section 9.3.4. In Figure 9.7 b) the comparison of only the contribution of the iron sites with the experimental data is shown. While in general also for this case a quite good agreement can be stated, there is a region between 500 K and 700 K in which the Brønsted-free catalyst represents the increase in conversion too shallowly as compared to the curves accounting for both active sites. Thus, our data clearly shows that there is a non-negligible contribution from the Brønsted acids on the fast SCR.

From reaction path analysis, it is obtained that the mechanism on the iron

proceeds mainly via the adsorption of ammonia on FeO, followed by a proton transfer to NH_2FeOH . This species reacts with nitric oxide to nitrosamine adsorbed on monohydroxylated iron. Another ammonia molecule coadsorbs to the latter and a hydrogen transfer leads to the formation of water on FeNH_2 . The amino group is consumed after the coadsorption of NO_2 , followed by the formation of a second nitrosamine. The original active site FeO is restored upon desorption of the NH_2NO . Because of the fact that both species, FeO and FeOH, are accessed within the reactive cycle it is rather arbitrary which species is denoted as the representation of the active site. For the initialization of the formation of NH_2FeOH , which reacts further with nitric oxide, two further pathways via the intermediate formation of dihydroxylated iron are also accessed. Partially, water decomposes directly on FeO to form HOFeOH . Furthermore the surface nitrite FeO_2N is formed from the adsorption of nitric oxide on FeO, prior to a reaction with water, leading to nitrous acid. The latter decomposes again on monohydroxylated iron, resulting in the dihydroxylated iron together with gas phase NO (compare schematic in Figure 9.2 b). The dihydroxylated iron is then consumed by ammonia to the intermediate NH_2FeOH . This shows that, here, the dihydroxylated iron does not block the active site as was the case in the NO oxidation in the presence of water and neither does a nitrite species concentrate on the surface. Furthermore, the barrier for the formation of the intermediate NH_2FeOH from the reaction of ammonia with FeO is even slightly higher than for the hydrogen transfer of ammonia to dihydroxylated iron. The relevant reactions on the iron as active site are shown in the schematic of Figure 9.8.

In the presence of both active sites, it is at hand that also the mechanism of the H-ZSM5 is accessed and parts of the NO_x are converted via the intermediate formation of NO^+ from the decomposition of N_2O_3 and N_2O_4 on the Brønsted acids, because of the large amount of available active sites. While at approximately 500 K this contribution is, to a large extent, blocked by the strong adsorption of ammonia, its impact increases steadily. In fact, at about 600 K nearly 75% of the conversion of the NO_x proceeds on the Brønsted acids. That does not imply that without the acids the conversion would be significantly less, which can be seen in Figure 9.7 b) to not be the case, but solely that in this regime the pathway via the Brønsted acids is more favorable. A further interaction between the two active sites takes place via the intermediately formed nitrous and nitric acid. At low temperatures, acids, formed on the Brønsted centers, partially decompose on FeOH to form the dihydroxylated iron, which reacts further with ammonia to NH_2FeOH . At high temperatures, however, produced nitrous acid from the reaction of water with the nitrite FeO_2N decomposes partially on the Brønsted acids to

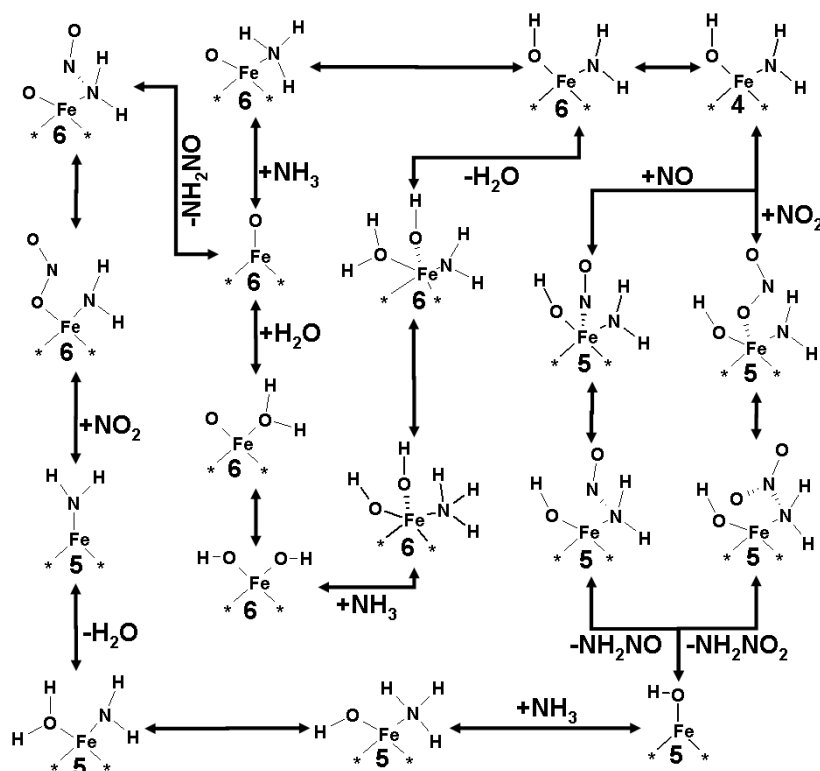


Figure 9.8: Schematic of the relevant reaction pathways in the fast and NO_2 SCR. Numbers refer to the spin multiplicities of the species.

water and NO^+ , which further reacts with ammonia to nitrosamine. Despite the impact of the Brønsted acids, the coadsorption of nitric oxide to the species NH_2FeOH prior to the formation of nitrosamine was found to be the rate-determining step on iron as the active site. This indicates that a significant further increase in nitrogen production is anchored to the iron sites. In Figure 9.9 a), the conversion of NO_x ($\text{NO} + \text{NO}_2$) is shown for the cases of only iron sites, only the H-ZSM5 and the combined catalyst in comparison to the data from Schwidder et al.³⁷ The difference in the conversion curves points out again the impact of the Brønsted acids in contrast to the iron sites within the region between 500 K and 700 K. Below and above this temperature, the conversion curves of the true and the “only iron” catalyst coincide, illustrating the fact that, here, the contribution of the Brønsted acids is negligible. From the comparison with the curve of the H-ZSM5, it is apparent that the positive influence of the Brønsted acids on the Fe/H-ZSM5 coincides with the regime of maximum activity of the H-ZSM5. In Figure 9.9

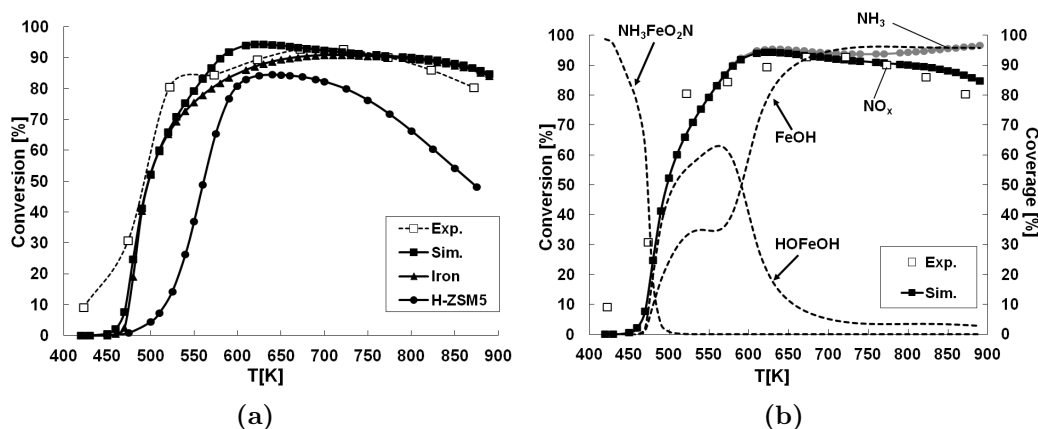


Figure 9.9: a) Simulated conversion of NO_x on the iron sites only, on the Brønsted acids only and on the combined catalyst in comparison with experimental data (ref. [37]) vs. temperature. b) Comparison of simulated NH_3 and NO_x conversion and coverage of the dominant surface species vs. temperature.

b), the dominant surface species on the iron sites are shown together with the NO_x conversion of the regular case. At the very low temperatures, prior to which an observable conversion takes place, the surface is covered with ammonia adsorbed on the nitrite FeO_2N . Here, mainly the nitrite blocks the active site because the reaction with ammonia is not yet active. As soon as the conversion of NO_x is initiated, the surface transfers to mono- and dihydroxylated iron species, with a peak of the latter at approximately 560 K. This is the regime when sufficiently amounts of water are present from the increased conversion of ammonia to form the dihydroxylated species. At higher temperatures the monohydroxylated iron is the only dominant surface species. In addition, the conversion of ammonia is shown in comparison to the NO_x conversion. While in the fast SCR the stoichiometric conversion of ammonia and NO_x equals one, the deviation of the two curves, starting slightly at 600 K and becoming significant above 700 K, marks the onset of ammonia oxidation. From comparison with the experimental data this effect should be more strongly pronounced. This underestimation of the ammonia oxidation illustrates again the limited capability of mononuclear iron sites to catalyze the SCO.

The analysis of the influence of the iron content on the conversion is shown in Figure 9.10 in comparison to the original catalyst ($\text{Fe}/\text{Al}=0.18$). Overall,

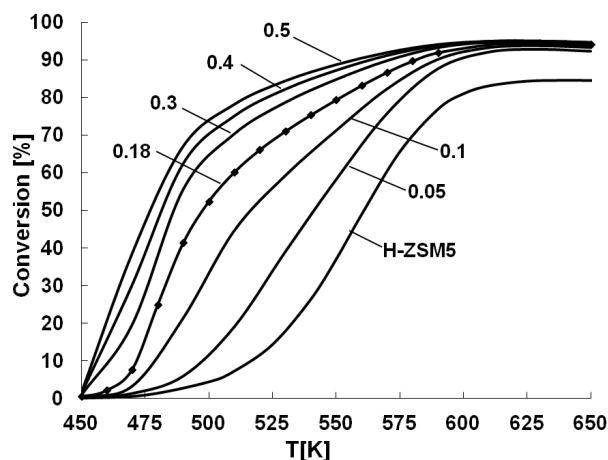


Figure 9.10: Simulated conversion of NO_x with varying iron content. Numbers refer to the Fe/Al ratio.

the influence is rather moderate. However, a reduction of the iron content appears to cause a stronger pronounced decrease in activity than an increase does rise the conversion at lower temperatures. Thus, with a certain amount of mononuclear iron sites present in the catalyst, high conversions can be achieved in the fast SCR and a further increase of the iron content has a rather low impact. This is in agreement with Schwidder et al.³⁷ who, for the fast SCR, found the difference in iron content for three catalysts prepared by liquid ion exchange to be nearly negligible. The fact that our model is in good agreement with the experimental data, even though it only accounts for the mononuclear iron sites, strongly supports the suggestion of Schwidder et al.³⁷ that only mononuclear iron sites are required for the fast SCR. Epling et al.³²⁹ recently found from spatial resolution experiments that while the fast and the NO_2 SCR proceed in parallel, the onset of the standard SCR will be negligible until the reactants for the fast SCR are consumed. Thus, even for zeolites containing a very high amount of iron no significant increase in activity for the fast SCR can be obtained because only the mononuclear sites contribute to the conversion and their sensitivity to the iron content appears to be rather low. The fact that there already is a strong impact of the rather small addition of iron (Fe/Al=0.05) in comparison to the parent H-ZSM5 is, in turn, in agreement to the finding of Schwidder et al.³⁷ and Devadas et al.³⁸ that iron also contributes to the reaction of the fast SCR and does not only serve for the oxidation of NO to NO_2 .

To analyze the reported ammonia inhibition effect at low temperatures,

its concentration was varied at 470 K from 300 to 2000 ppm in analogy to the experiment of Iwasaki et al.³³³ for the above discussed set up. In Figure 9.11 a), the conversion over the ammonia concentration is shown for both cases, the catalyst with both active sites, iron and Brønsted acids and the catalyst with only iron as active site. While the only iron catalyst shows a decrease in NO_x conversion over the complete range, the catalyst with both active sites is in perfect agreement with the behavior reported by Iwasaki et al.³³³ First, an increase of the conversion with ammonia concentration up to a maximum slightly before the correct stoichiometric concentration is obtained, followed by a decrease in conversion. The reason for this behavior can be related to the steady state surface coverages. While the conversion requires the monohydroxylated sites, at low ammonia content, the surface is covered with the nitrate species FeO_2NO and HOFeO_2NO , which block the active site. The interesting fact is that the nitrates result from the decomposition of nitric acid on the iron, which is produced from the decomposition of N_2O_4 on the Brønsted acids. With lower ammonia concentration in the feed, the acid sites are less strongly blocked by adsorbed ammonia at this temperature and, thus, catalyze the decomposition of N_2O_4 . Thus, with increasing ammonia concentration the production of nitric acid on the Brønsted acids is reduced and less surface nitrates are formed on the iron. A further increase of ammonia causes the dominating adsorption of ammonia on the nitrite FeO_2N , which blocks the active site as ammonia is not sufficiently capable to reduce the nitrite at this temperature. This again causes the decrease in conversion. With only the iron sites present as active sites, the formation of nitrates is rather negligible as can be seen in Figure 9.11 b) and, thus, at low ammonia content, the monohydroxylated iron sites dominate with an increased conversion. With higher ammonia concentrations, however, it is this additional production of nitrous and nitric acids on the Brønsted centers which serve as shuttles for hydroxyl groups and cause a higher flexibility in the system, making the combined catalyst superior over the only iron-containing catalyst. Furthermore, the additional conversion on the Brønsted acids also causes a higher concentration of water, which triggers the consumption of the surface nitrite and, with that increases the number of unblocked active sites.

In summary, it was shown that the mechanism on the mononuclear iron sites, starting from FeO , involves the intermediate formation of amino groups from adsorbed ammonia, which further react with NO_x to nitrosamine. Within the mechanism, water is produced directly on the iron from the interaction of ammonia with monohydroxylated iron and dihydroxylated iron sites are easily consumed by ammonia rather than blocking the active site. Furthermore, it was shown that between 500 K and 700 K the reaction on the

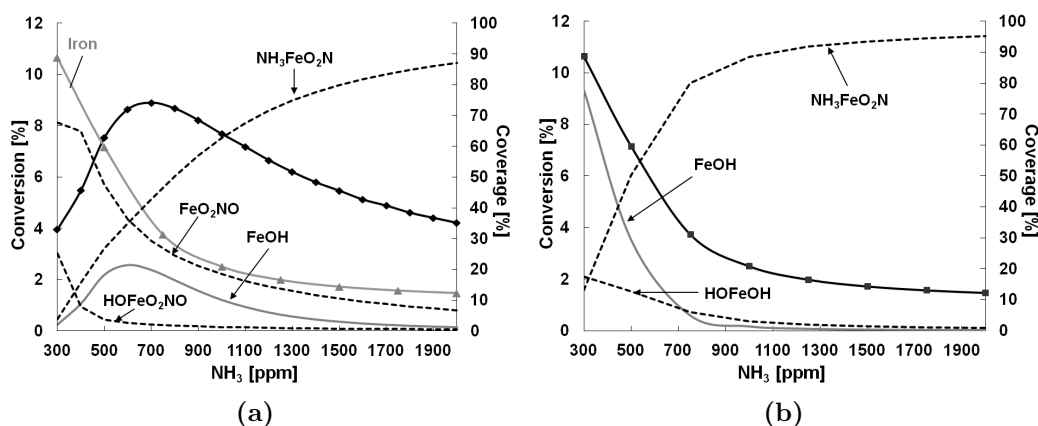


Figure 9.11: Influence of ammonia concentration on the conversion of NO_x at 470 K and on the coverage of the dominant surface species. a) Both active sites b) Only iron.

Brønsted acids significantly contributes to the overall conversion and cannot be neglected. Besides the obvious additional conversion of NO_x, the interaction between the active sites with respect to production or consumption of nitrous and nitric acid was highlighted. In agreement with the data of Schwidder et al.,³⁷ the iron content was shown to only have a moderate impact on the activity and it can be assumed that mainly mononuclear iron sites are responsible for the catalysis of the fast SCR. However, the by Tronconi et al.^{168,170,281} claimed significance of a reaction of nitric oxide with a surface nitrate as rate-limiting step could not be confirmed. Although present to a certain extent at low temperatures, the nitrates were not found to contribute to the reaction path. In fact, their proposed reaction mechanism for the fast SCR via the disproportionation of N₂O₄, the formation of ammonium nitrite and the decomposition of the latter has strong resemblance to the mechanism on the Brønsted acids as described in chapters 4 and 6. On the mononuclear iron sites, however, the reaction appears to require the intermediate formation of amino groups on the surface.

9.3.4 Modeling of the NO₂ SCR

The impact of NO₂ was not only found to be enhancing in the limit from NO₂/NO_x = 0 to 0.5, but to exhibit a maximum in the equimolar ratio of NO and NO₂ denoted as the fast SCR. Further increase of the NO₂ content is known to decrease the activity of the catalyst compared to the fast SCR

and to cause the production of nitrous oxide.^{38,40,178,352} At the boundary of the pure NO₂ SCR, the lowest activity and the highest production in N₂O is observed for the case of NO₂/NO_x ≥ 0.5. However, the production of nitrous oxide was found to exhibit a maximum at medium temperatures with nearly equimolar amounts to nitrogen, followed by a significant decrease at high temperatures. Based on the proposed mechanism from Tronconi et al.¹⁷⁰ the production of nitrous oxide is explained from the decomposition of ammonium nitrate. Furthermore, they speculate about the direct consumption of surface nitrates with ammonia to nitrogen, representing an additional NO₂ SCR mechanism. At high temperatures, the further increase in selectivity to nitrogen is attributed to the decomposition of NO₂ to NO, followed by the access of the fast SCR. Iwasaki et al.⁴⁰ further suggested the increased reduction of produced nitrous oxide from a N₂O SCR. For the H-ZSM5, we have shown in chapter 6 that the production of nitrous oxide is related to the decomposition of nitric acid on Brønsted acids to NO₂⁺ prior to the formation of nitramide from a reaction with ammonia. The latter decomposes to N₂O and water.

To elucidate the mechanism on the iron-containing catalyst, we used the same set up as applied in the fast SCR and discussed the results on a qualitative basis with the experimental literature. In Figure 9.12 a), the conversion of NO₂ is shown in comparison to the fast SCR for the case of only the iron being the active site and for both active sites. In agreement with the experimental literature, the activity is lower as compared to the fast SCR with respect to a higher light-off temperature. Similarly as for the fast SCR, the impact of the Brønsted acids on the conversion of NO₂ is observed at moderate temperatures between 550 K and 700 K. At lower temperatures, the only iron-containing catalyst appears even slightly superior. At high temperatures, from the overlap of the two conversion curves, it can be concluded that only the iron sites are responsible for the conversion. For the mechanism on the iron sites, we found a strong resemblance to the mechanism of the fast SCR from reaction path analysis. From the interaction of ammonia with either FeO or the dihydroxylated iron, the intermediate NH₂FeOH is formed after a proton transfer. NO₂ reacts with this species by forming adsorbed NH₂NO₂ on monohydroxylated iron. The nitramide decomposes on the Brønsted acids to nitrous oxide and water. The remainder of the mechanism is equivalent to the fast SCR. Ammonia reacts with FeOH to FeNH₂ followed by the reaction of another NO₂, which forms nitrosamine and restores the active site. Thus, the striking difference is the formation of one nitramide rather than a nitrosamine. The details are outlined in the schematic of Figure 9.8 together with the mechanism of the fast SCR. This,

however, dictates the equimolar formation of nitrogen and nitrous oxide. The change of this ratio is anchored to the decomposition of NO_2 into NO and O_2 on FeOH in the reverse direction as described for the oxidation of NO in section 9.3.1. To a rather small extent, also produced nitrous oxide decomposes on monohydroxylated iron leading to HOFeO , which is part of the decomposition pathway of NO_2 . Thus, the N_2O decomposition produces the precursor of the subsequent decomposition of a NO_2 molecule. From a mechanistic aspect, this correlates with the decomposition of nitrous oxide in the presence of NO as outlined by Heyden et al.³⁰⁰

In the presence of both active sites, however, the reaction is, at low temperatures, mainly catalyzed by the Brønsted acids via the decomposition of asN_2O_4 to NO^+ and nitric acid. The latter decomposes to a certain extent on the Brønsted acids but also on the iron sites, which mainly causes the formation of surface nitrates. At slightly higher temperatures, the nitric acid behaves similar to the nitrous acid in the fast SCR by forming dihydroxylated iron from the decomposition on FeOH . In this moderate temperature regime, also the nitrates decompose and release NO_2 . This is represented by the surface coverages shown in Figure 9.12 a) as well. At low temperatures, the iron species are nearly completely covered with nitrates (FeO_2NO and HOFeO_2NO), which are further enforced from the production of nitric acid on the Brønsted acids. At medium temperatures, the nitrates decompose or react with water to nitric acid. Furthermore, the decomposition of nitric acid on monohydroxylated iron forms, to a large extent, dihydroxylated iron, making it the dominating species. Also in this regime, the contribution of the Brønsted acids is dominating the reaction. Similarly, as for the fast SCR, this does not imply that the reaction cannot proceed on the iron, but solely that it is more favorable on the Brønsted acids in this temperature range. It is at hand that also the rate-determining step in this regime is anchored to the Brønsted acids with the adsorption of ammonia on NO^+ , while at higher temperatures the adsorption of NO_2 to NH_2FeOH becomes dominant. Finally, at high temperatures, the surface is covered with the monohydroxylated iron sites. The lower activity of the NO_2 SCR, as compared to the fast SCR, can be related to the fact that, at low temperatures, surface nitrates form on the iron and block it as active site. This is further enhanced by the production of nitric acids on the Brønsted acids, which then decompose on the iron sites to nitrates. At moderate temperatures, the two surface nitrates are still formed from a first decomposition of nitric acid on FeOH to FeO_2NO and the decomposition of a second nitric acid on this species by releasing a NO_2 . This causes the second observed nitrate HOFeO_2NO , which further decomposes to NO_2 and HOFeO . Thus, at elevated temperatures, the formed nitrates only

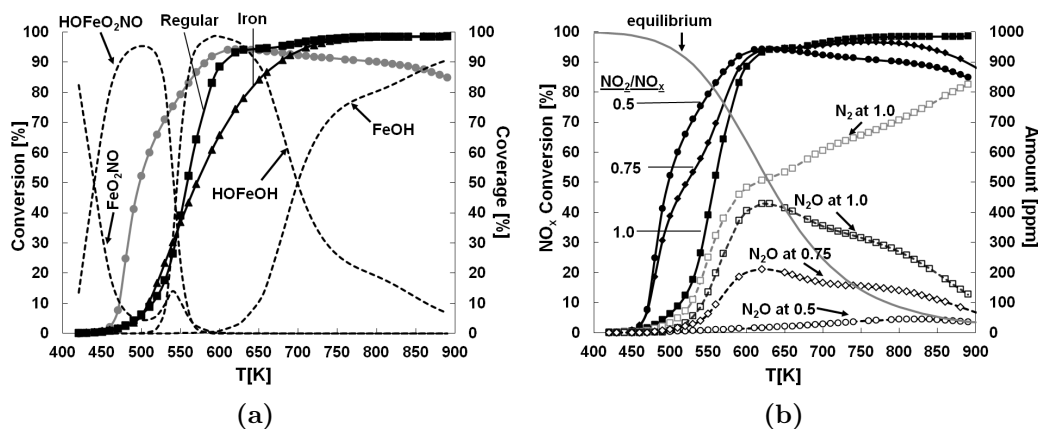


Figure 9.12: a) Simulated conversion of NO₂ on the iron sites only and on the full catalyst in comparison with the simulated NO_x conversion in the fast SCR and coverage of the dominant surface species vs. temperature b) Comparison of simulated NO_x conversion at different NO₂/NO_x ratios and corresponding production of N₂O vs. temperature.

serve in the decomposition of nitric acid back to the reactant NO₂, without directly contributing to the conversion to nitrogen. The schematic of this sequence is illustrated in Figure 9.13.

In Figure 9.12 b), the conversion of the fast SCR, the NO₂ SCR and an intermediate case with a ratio of NO₂/NO_x=0.75 is shown together with the corresponding production of nitrous oxide versus temperature. In agreement with the experimental literature,^{38,40,170,178} the activity decreases with an increase of the NO₂/NO_x ratio together with an increase of the N₂O production. The somewhat twisted shape of the curve of the conversion corresponding to a ratio of 0.75 is clearly related to the difference in activity of the fast and the NO₂ SCR. At low temperatures, the shape is governed by the fast SCR mechanism, because the NO₂ SCR is not yet active. With increasing temperature and activity, the shape more and more adapts to the NO₂ SCR mechanism, because the further increase of NO_x conversion is anchored to it. Also the formation of nitrous oxide in the NO₂ SCR is in general agreement with the experimental data,^{38,40} with the maximum strictly related to the increasing conversion and an absolute value between 40% and 50% of the converted reactants. To further emphasize the difference in nitrogen versus nitrous oxide production, we have included the N₂ production curve in Figure 9.12 b) for the NO₂ SCR together with the equilibrium curve for NO₂ and NO. The deviation of the N₂ and N₂O curve below 530 K results to a

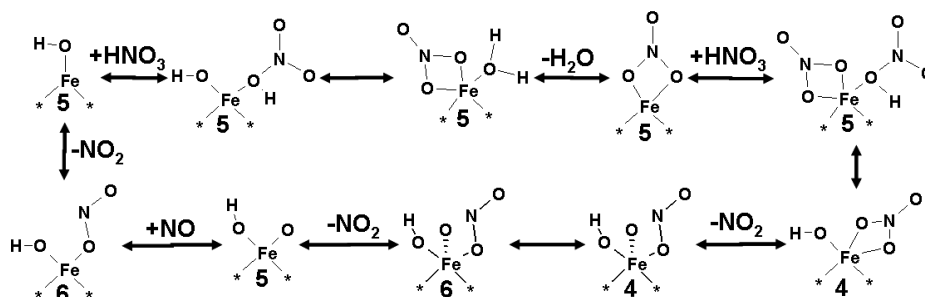


Figure 9.13: Schematic of the formation of nitrates from HNO_3 decomposition. Numbers refer to the spin multiplicities of the species.

certain extent from non-decomposed nitric acid and might be an artifact of our model. However, above this temperature, the deviation is caused by the decomposition of NO_2 to NO and oxygen making the fast SCR mechanism accessible. While at the low temperatures, this effect is still rather low, its impact significantly increases with temperature when the equilibrium further shifts to the favor of nitric oxide. Thus, our model suggests that the true mechanism of the NO_2 SCR should be seen in close analogy to the fast SCR with an equimolar production of nitrogen and nitrous oxide. The macroscopically observed deviation from this ratio mainly results from the decomposition of NO_2 to NO . A further partial decomposition of produced N_2O , as described above, or a further benefit from the N_2O -SCR cannot be excluded, however, an additional mechanism for the direct conversion of NO_2 to only nitrogen with ammonia appears not to be required.

9.3.5 Modeling of the New “Enhanced” SCR

Recently, Tronconi et al.^{334,335} have proposed a new reaction system for the SCR, applying ammonium nitrate as additional reducing agent besides ammonia. They found a significant increase in activity at low temperatures in comparison to the standard SCR, which was even close to the fast SCR. The benefit of such a system is the rather simple supply of the ammonium nitrate in aqueous solution and its availability. It was pointed out that injecting such an additional boosting agent might be superior to an upstream oxidation catalyst that partially transforms the nitric oxide to NO_2 for the fast SCR. In fact, they also found the same result for the injection of nitric acid, which corresponds in its stoichiometry to equation (8.4) by considering the ammonium nitrate to decompose into ammonia and nitric acid. Assuming a

barrierless decomposition in the gas phase for the ammonium nitrate, we simulated the conversion of NO according to the stoichiometry of equation (8.4) and compared the result to the fast and the NO₂ SCR. It should be noted that for the reason of accurate comparison, we also included the ammonium nitrate in the ammonia conversion balance as well as in the NO_x balance. While this is at hand for ammonia with respect to the decomposition of ammonium nitrate, it also has to be considered that nitric oxide accounts for a NO₂ molecule and, thus has to be included into a NO_x balance. In Figure 9.14 a), the comparison between the reactive systems is shown. It can be seen that up to 600 K, a significant conversion is obtained, similar as to the fast SCR in agreement with the observation from Tronconi et al.^{334,335} in a stoichiometric consumption of ammonia and the combined NO_x (Figure 9.14 b). Interestingly, between 510 K and 580 K, the conversion curves of the fast and the enhanced SCR come very close to an overlap. Also, the production of nitrous oxide is rather low up to 600 K in agreement with Tronconi et al.³³⁵ However, above 600 K the NO_x conversion exhibits a maximum and decreases together with a significant increase in the production of nitrous oxide. Already the low amounts of N₂O below 600 K are related to the decomposition of nitric acid on the Brønsted acids according to the NO₂ SCR mechanism on H-ZSM5 as shown in chapter 6 and the subsequent formation and decomposition of nitramide. Above this temperature, the desorption of ammonia unblocks large amounts of Brønsted acids for the decomposition of nitric acid as can be seen in Figure 9.14 b) from the good correlation of the decreasing ammonia coverage and the decreasing NO_x conversion. Whether this is an artifact of our model resulting from an overestimation of nitric acid decomposition on the Brønsted acids cannot be concluded, because only experimental data up to 350 °C is published. However, by taking into account that the low temperature regime is the one of interest for application and the good qualitative agreement with experiments in this regime, it can be concluded that our model appears suitable to explain the mechanism of the new enhanced SCR as well.

From reaction path analysis, it can be obtained that on the iron sites the catalytic cycle involves, first, the adsorption of nitric acid on monohydroxylated iron sites. In parts, it decomposes in terms of the release of NO₂, leaving dihydroxylated iron. The latter reacts with ammonia, as outlined in the fast SCR schematic, to NH₂FeOH and then with nitric oxide to nitrosamine and monohydroxylated iron. Summarizing this short cycle, the nitric acid from the ammonium nitrate has two effects. From its decomposition on FeOH, it causes the formation of the relevant precursor for the reaction with nitric oxide of the fast SCR. In addition, an NO₂ molecule

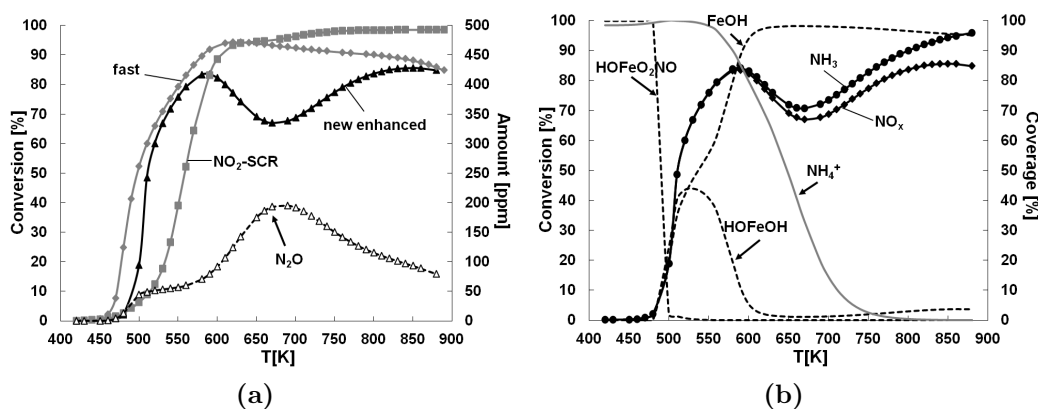


Figure 9.14: Simulated NO_x conversion of the new “enhanced” SCR. a) In comparison with simulated fast and NO₂ SCR together with the N₂O production vs. temperature. b) In comparison to the ammonia conversion and with the coverage of the dominant surface species vs. temperature. NH₄⁺ refers to the Brønsted acids.

is released, which, within the fast SCR stoichiometry, consumes a second nitric oxide in agreement with the overall stoichiometry of the enhanced SCR. In addition, nitric acid also decomposes on FeOH via the surface nitrates FeO₂NO and HOFeO₂NO as outlined in the preceding section 9.3.4 and shown in Figure 9.13. Here internally, mainly NO₂ is produced, with the decomposition of two molecules nitric acid forming three molecules of NO₂. The benefit from this decomposition results from the caused oxidation of one NO to NO₂. Because each of the NO₂ molecules causes in turn the consumption of one nitric oxide in the fast SCR, the balance of the overall stoichiometry is obtained again: two nitric acids consume four nitric oxide molecules. With that, from a mechanistic point of view, the enhanced SCR can be interpreted as a mixture of the fast and the NO₂ SCR by accessing the relevant pathways of both reactions. It is at hand that the interaction with the Brønsted acids also here proceeds in analogy to the mechanisms outlined for the fast and the NO₂ SCR. In 9.14 b), we have included the coverages of the dominant surface species. Clearly related to the nitric acid from the ammonium nitrate, the surface is blocked with surface nitrates at low temperatures. This is in close analogy to the NO₂ SCR and can also be seen as the reason why the enhanced SCR is less active than the fast SCR. At intermediate temperatures, the dihydroxylated iron sites appear and, finally, the mononuclear sites dominate the surface at high temperatures. In

the moderate regime the surface organization strongly resembles the one of the fast SCR, which further supports our interpretation of the enhanced SCR being a mixture of the NO_2 and the fast SCR. With that, our results strongly suggest that also the enhanced SCR mainly proceeds on mononuclear iron sites. The increase in conversion at high temperatures is related to the onset of ammonia oxidation and the standard SCR as well as the partial decomposition of produced nitrous oxide on monohydroxylated iron to HOFeO , which further causes the oxidation of NO to NO_2 (see Figure 9.13). This last part can be interpreted in the view of the N_2O SCR.

9.3.6 Modeling of the Standard SCR

The standard SCR is commonly separated into diverse subsystems with the center piece represented by the fast SCR and the rate-determining step represented by the oxidation of NO .^{38,158,282,283,330} The NO_2 SCR, responsible for the production of unwanted nitrous oxide, and the SCO, responsible for the unwanted additional consumption of ammonia, are rather considered as side reactions that have to be accounted for. Thus, in general, the combination of a correct mechanism for the NO oxidation with the fast SCR should be capable to account for the standard SCR. However, from the observed discrepancy between activity of NO oxidation and standard SCR doubts have been stated towards such a simplistic combination. Delahay et al.²⁸² suggested the reaction of ammonia with adsorbed NO_2 in terms of a nitrite to overcome this discrepancy. Metkar et al.³³⁰ recently claimed that the NO oxidation is only less active than the standard SCR in the presence of water and that ammonia neutralizes the water inhibition by reaction with adsorbed nitrous and nitric acid on the iron sites. Schwidder et al.,³⁷ in contrast, rather assumed a complete different mechanism in the standard SCR as compared to the fast SCR. Furthermore, the nature of the present iron species appears to be of significance. While the fast SCR can be concluded to predominantly proceed on mononuclear iron sites as suggested by Schwidder et al.³⁷ and supported by our model in section 9.3.3, Brandenberger et al.³⁶ concluded that above 300°C the contribution of dinuclear iron sites becomes significant in the standard SCR.

To analyze the impact of the mononuclear iron sites and the Brønsted acids on the standard SCR, we compared our model with the same set-up as for the fast SCR against the corresponding data from Schwidder et al.³⁷ as well as against the conversion for a catalyst of very low iron content of Brandenberger et al.³⁶ The results are shown in Figure 9.15 a) and b). In comparison to the data from Schwidder et al.,³⁷ it becomes apparent that

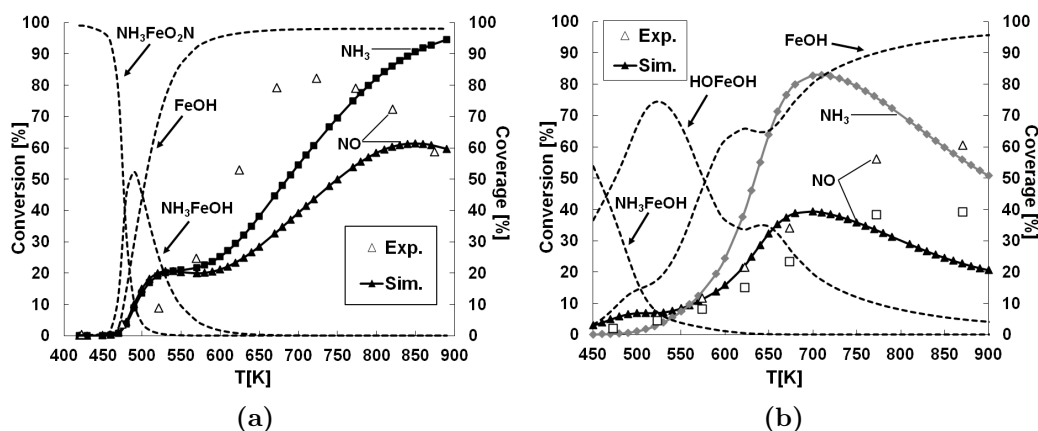


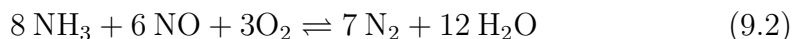
Figure 9.15: Simulated NO and NH₃ conversion in the standard SCR and the dominant surface species vs. temperature. In comparison to a) Schwidder et al.³⁷, b) Brandenberger et al.³⁶

a description with only the mononuclear iron sites is not capable to reproduce the conversion correctly. Only up to a temperature of about 575 K, an agreement is observed while at higher temperatures a significant underestimation of our model is obtained. This is, however, in perfect agreement with the conclusions of Brandenberger et al.³⁶ who related the contribution of the mononuclear iron sites to the conversion in the standard SCR to below 300°C. The real catalyst with an exchange degree of Fe/Al= 0.18 certainly exhibits to a large extent also dinuclear iron sites and probably even clusters of higher nuclearity. Thus, as a first conclusion, in contrast to the fast SCR, the standard SCR certainly also requires iron species other than mononuclear iron sites to exhibit a significant activity. The real catalyst used for the simulation of the conversion shown in Figure 9.15 b), however, exhibits nearly exclusively mononuclear iron sites with an exchange degree of Fe/Al= 0.02 according to Brandenberger et al.³⁶ And in fact, a very good agreement of our model with the experiments is obtained for the NO conversion up to 675 K. Above this temperature, several aspects might be responsible for the increasing deviation. First of all, also the H-ZSM5 becomes active and contributes to the conversion as is shown by Brandenberger et al.³⁶ As a rough approximation, we have subtracted this contribution from the data for the Fe-ZSM5 and added these data points (□) to the graph. Our conversion curve comes quite close to the reduced data-point at 775 K. Because a correct accounting for the standard SCR is not included in our model, the deviation starting above 675 K could partially be attributed to a conversion

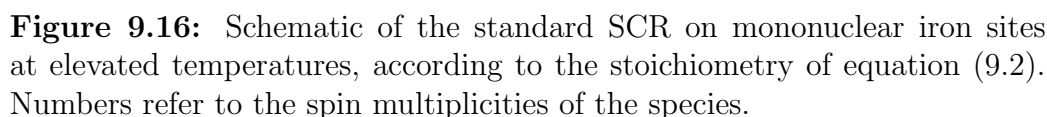
on the Brønsted acids. Furthermore, a decrease in conversion is observed with our model above 700 K. By also taking into account the significantly higher conversion of ammonia at this temperature, it is obvious that here the ammonia oxidation plays a distinct role. The latter, however, was found to exhibit a decreasing behavior at elevated temperatures in the presence of water with our model. Because the modeling here contains 5% water in the feed, the decreasing conversion can be explained from the relation to the ammonia oxidation. It has to be noted that the standard SCR is known to be rather insensitive to water in the feed.^{38,178,330} However, no experimental data is available that also certifies this finding for only mononuclear iron sites and, thus, it remains highly speculative whether this behavior of our model is just an artifact or truly existing, as was already discussed in the context of the SCO. Finally, even in a catalyst of very low iron exchange degree, as compared to here, it cannot be excluded that also higher clustered iron species are present that become sufficiently active at the higher temperatures to account for the deviation between our model and the experiment.

Nevertheless, assuming that our model accounts at least qualitatively correct for the standard SCR on mononuclear iron sites, some interesting aspects can be concluded from the reaction path analysis. In the absence of water, which was modeled in the case of 9.15 a), the mechanism in the low temperature regime (~ 500 K) can indeed be summarized by the oxidation of NO to NO₂ on monohydroxylated iron sites as described in section 9.3.1 and the subsequent fast SCR. Although the oxidation proceeds on the monohydroxylated sites, which corresponds to the lower activity in the presence of water, a severe difference to the simulation of only the NO oxidation is observed in the representation of the active site. While for the NO oxidation the surface was mainly covered with inactive dihydroxylated iron sites, here, with the onset of the conversion, the monohydroxylated sites dominate nearly exclusively. Thus, ammonia also causes a significant increase of available active sites for the NO oxidation from the reaction with HOFeOH to NH₂FeOH. However, an interaction of ammonia directly with adsorbed NO₂, as created in the oxidation cycle, was not observed. At temperatures above 600 K, the NO conversion curve in our model exhibits a bend upwards together with the onset of the deviation to the ammonia conversion curve. The bend in the NH₃ conversion is obviously related to its oxidation, but interestingly, this also causes an increase in the NO conversion. With increasing temperature, the mechanism shifts further away from the assumed combination in series of NO oxidation and fast SCR. The detailed mechanism, responsible at the elevated temperature, mainly includes three cycles, starting on monohydroxylated iron as shown in the schematic in Figure 9.16. First, ammonia

transfers the FeOH to FeNH₂ and water desorbs. Then, oxygen reacts with that species to FeO, releasing the radical H₂NO as was described in the context of the SCO. The transfer of FeO back to monohydroxylated iron follows the partial mechanism of the fast SCR in a reaction with ammonia and NO via NH₂FeOH. In a second cycle, the radical H₂NO adsorbs on FeOH and after a proton transfer water is released, leaving nitroxyl adsorbed on iron (FeHNO). After the coadsorption of oxygen and the desorption of the nitroxyl FeO₂, an intermediate of the NO oxidation cycle in the absence of water, remains. A reaction with NO forms NO₂ and the remaining FeO is again transferred to FeOH. In the third cycle, nitroxyl decomposes on FeOH to water and FeNO. The latter is then, by exchange with oxygen, transferred to FeO₂ and the released NO oxidized to NO₂, which again leaves FeO. Within these three cycles, two molecules NO₂ are produced, which consume two further molecules of NO within the fast SCR. In combination, this leads to the following stoichiometry for this superimposing SCR mechanism,



Because the first and the third cycle were also relevant in the SCO of ammonia as described in the section 9.3.2, this pathway can be interpreted that NO is burned in the fire of the ammonia oxidation. The significant benefit of this pathway is the reformation of surface species that can be directly consumed from nitric oxide, namely FeO and FeO₂ with the first one being relevant in the fast SCR and the second one in the high activity NO oxidation mechanism in the absence of water. This is also the severe benefit over the ammonia oxidation itself, because, here, the NO is externally provided and does not need to be produced as an intermediate as was outlined in section 9.3.1. With that, it is also at hand that the rate-limiting step at ~700 K is with the reaction of oxygen and FeNH₂ to H₂NO related to the SCO mechanism. However, also on the Brønsted acids the oxidation of ammonia takes place leading directly to nitroxyl. Because this species only causes the slight benefit of the third cycle, but not of the first and the second one, this partial oxidation leads to a less beneficial stoichiometry for the SCR. In fact, for the SCO, we found the formation of H₂NO on the iron site to be suppressed in the presence of water. This is also the case in the comparison of our model against the data of Brandenberger et al.³⁶ for the standard SCR at elevated temperatures. Furthermore, this is emphasized by the high amount of dihydroxylated iron sites (Figure 9.15 b). Thus, the further increase in NO conversion is here only related to the oxidation of ammonia on the Brønsted acids and the accession of the third cycle. This also causes the significantly more pronounced deviation in the conversion curves of NO and NH₃ in comparison to the absence of water (Figure 9.15 a).



In summary, it has to be concluded from the analysis of the standard SCR that in contrast to the fast SCR, iron species of higher nuclearity are essential for a high activity. This is in agreement with the observations from Brandenberger et al.³⁶, but also by Long and Yang¹⁵⁵ who found a ratio of Fe/Al=0.193 to be optimal in the SCR performance and with that a catalyst that exhibits diverse iron sites. With respect to the mechanism for mononuclear iron sites, the general agreement of the NO oxidation to be the rate-limiting step, followed by the fast SCR is only true at low temperatures, anchored to low conversions. But also here, the oxidation proceeds on monohydroxylated sites, which were found to be the less active sites for the NO oxidation in the presence of water. In contrast to the assumption of Metkar et al.,³³⁰ ammonia only exhibits the capability to increase the available amount of these sites, but does not cause the NO oxidation to proceed on the representation of the active site in the absence of water (FeO). At elevated temperatures, our simulation strongly suggests the occurrence of a complete different reaction scheme, related to the oxidation of ammonia via the radical H_2NO and in accord to the stoichiometry of equation (9.2). This supports the conclusion of Schwidder et al.,³⁷ who suggested that the standard SCR might indeed follow a complete different pathway than the combined NO oxidation and

fast SCR. Furthermore, it would answer the question on the observed discrepancy of the NO oxidation and standard SCR activities. Nevertheless, it has to be emphasized that the results discussed here only apply to mononuclear iron sites and the mechanism on other iron species might be significantly different. Whether on those sites a pathway is also accessed that is related to the ammonia oxidation remains speculative.

9.4 Conclusion

Based on the DFT calculations as described in chapters 7 and 8, a microkinetic model for the selective catalytic reduction of NO with ammonia on Fe/H-ZSM5 has been established, which, in combination with the results from chapter 6, accounts for the contribution of mononuclear iron sites as well as of the Brønsted acids. For the oxidation of NO to NO₂ in the absence of water, the mechanism proceeds on $Z^-[\text{FeO}]^+$ via the intermediate formation of an -OONO ligand and is inhibited by the formation of surface nitrates (schematic 9.2 a). In the presence of water, the surface coverage changes by forming inactive dihydroxylated iron together with monohydroxylated iron sites, which then function as active sites with a lower activity than $Z^-[\text{FeO}]^+$. The mechanism proceeds in this case in close analogy to the water-free reaction with the difference of the additional hydroxyl group bonded to the iron (schematic 9.2 b). Interestingly in this case, the Brønsted acids were found to exhibit a negative impact on the NO oxidation at low temperatures, resulting from the production of nitrous acid that causes an increase in the blockage of the iron sites by dihydroxylated iron. For the oxidation of ammonia, an agreement with experimental data was only obtained for a catalyst with low iron content correlated to the dominance of mononuclear iron sites. This emphasizes that the ammonia oxidation rather proceeds on higher nuclear iron species. On mononuclear sites, the mechanism proceeds via, first, the formation of the radical H₂NO from the interaction of an amino group $Z^-[\text{FeNH}_2]^+$ with oxygen. This is then further reduced to nitroxyl and, finally, to NO and consumed by ammonia (schematic 9.6). At low to intermediate temperatures, the conversion of ammonia to nitroxyl mainly takes place on the Brønsted acids, which are further consumed on the iron sites. A severe negative impact of water was observed related to the suppression of the formation of H₂NO on the iron sites. For the fast SCR on the iron, we found the mechanism to be initialized on $Z^-[\text{FeO}]^+$ by, first, the formation of an amino group from the interaction with ammonia ($Z^-[\text{NH}_2\text{FeOH}]^+$), followed by a reaction with NO to nitrosamine. The resulting monohydroxylated iron site is transferred with ammonia to the amino group containing iron $Z^-[\text{FeNH}_2]^+$, which reacts with

NO_2 to a second nitrosamine. The NO_2 SCR mechanism is in close analogy with the fast SCR, differing in the formation of nitramide from a reaction of NO_2 with the first amino group rather than nitrosamine (schematic 9.8). Nitrosamine and nitramide both decompose on the Brønsted acids to water and nitrogen and nitrous oxide, respectively. In both cases, the Brønsted acids were found to significantly enhance the conversion in a temperature window between approximately 500 K and 700 K. Furthermore, nitrous and nitric acid interact between the two active sites with respect to their production and consumption. This implies, at low temperatures for the fast SCR, that nitrous acid, produced on Brønsted acids, decomposes on the iron sites to either surface nitrite or to dihydroxylated iron by releasing nitric oxide. In the NO_2 SCR, it is mainly nitric acid, produced on the Brønsted acids, that decomposes to nitrates on the iron sites. This was also concluded to be the reason for the higher activity of the fast SCR over the NO_2 SCR, because at low temperatures the nitrates block the active site stronger than the nitrite. However, a reaction of nitric oxide with a surface nitrate, which was suggested by Tronconi et al.¹⁶⁸ as the rate-determining step in the fast SCR, was found to be of no relevance. The nitrates formed in the NO_2 SCR decompose to gas phase NO_2 and atomic oxygen, bonded to the iron, at elevated temperatures. At intermediate temperatures, the governing surface species are the dihydroxylated iron sites, which, in contrast to the NO oxidation in the presence of water, do not inhibit the reaction but are consumed by ammonia. At high temperatures, the monohydroxylated iron sites are dominant. For the increase in selectivity to nitrogen over nitrous acid in the NO_2 SCR with temperature, the decomposition of NO_2 to NO and oxygen, followed by the access to the fast SCR, was found to be responsible. The results suggest from comparison to experimental data that mononuclear iron sites are most likely to be the active species for the fast and the NO_2 SCR. Also, the simulation of the new “enhanced” SCR was qualitatively in agreement with the experimental literature and the mechanism exhibits aspects of both, the fast and the NO_2 SCR. At low temperatures, the formation of surface nitrates, in analogy to the NO_2 SCR via nitric acid causes a reduced activity. The decomposition of the nitric acid releases, in turn, NO_2 and causes the oxidation of NO to NO_2 , making the fast SCR mechanism accessible. In conclusion, also this enhanced SCR probably proceeds on mononuclear sites only. The standard SCR was, however, found to require the consideration of higher nucleated iron sites as well. Furthermore, a combination of NO oxidation and fast SCR mechanism in series is only relevant at low temperatures for mononuclear iron sites. At elevated temperatures, aspects of the ammonia oxidation cause an increasing conversion via the intermediate formation of H_2NO , which results in a modified stoichiometric equation (9.2).

Our model was shown to be capable of accounting for many experimentally observed phenomena and emphasizes the importance of the consideration of both, the iron and the Brønsted acid as active sites. Especially the deviation in the standard SCR with respect to experimental data also reflects the necessity to differentiate the contributions of different iron sites in the establishment of a quantitative model. However, the additional accounting for iron species of higher nuclearity is at least as demanding as the analysis of relevant reaction pathways on the mononuclear iron sites, as shown here and in chapter 7 and 8, and is with that beyond the scope of this work. Despite a remaining qualitative character of our microkinetic model, the results are believed to contribute significantly to the understanding of the extremely complex chemistry of the SCR.

Part V

Backmatter

10

Summary

In this thesis, the Selective Catalytic Reduction (SCR) of NO_x ($x=1, 2$) with ammonia in the presence of oxygen on Fe/H-ZSM5 has been investigated by means of the Density Functional Theory (DFT) and microkinetic modeling. Two different active sites, namely Brønsted acids and mononuclear iron sites, have been accounted for and their influence has been discussed. The results are of relevance for the better understanding of the performance of one of the most important catalysts in the exhaust gas treatment of nitric acid production plants and diesel-engined vehicles. The methodology of using the DFT in combination with microkinetic modeling belongs to the field of multiscale modeling and, in this work, serves the purpose of a vast screening of potentially significant reactions in order to elucidate the most relevant ones. The complexity of the system requires the subdivision of the reactive H/N/O system into the oxidation of NO to NO_2 , the fast and the NO_2 SCR and the oxidation of ammonia, which mainly gather to the standard SCR.

For the reaction mechanism of the SCR on the Brønsted acids, a key aspect was found to be the formation and consumption of the intermediates nitrous and nitric acid and nitrosamine and nitramide. The formation of the intermediates was probed in two different scenarios. Either the reaction of a dimerized nitrogen oxide species (N_2O_y ; $y=3,4$) with adsorbed ammonia leads directly to nitrous or nitric acid together with nitrosamine, or the decomposition of N_2O_y on a free Brønsted center results in the acid together with nitrosyl on the zeolite framework. The latter is consumed by ammonia to nitrosamine. While the second scenario exhibits slightly lower internal energy barriers, the strong adsorption of ammonia as ammonium ion on the

Brønsted acids was concluded to exhibit the capability of blocking this pathway. For the fate of the acids, bimolecular dehydration reactions between two acids, the reaction with adsorbed ammonia and the decomposition on Brønsted acids to nitrosyl from nitrous acid or to NO_2^+ from nitric acid were considered. While the bimolecular dehydrations appeared not to be beneficial in comparison to the corresponding gas phase reactions, the barriers in the reaction with ammonia were significantly reduced by the catalyst. The lowest barriers, however, were obtained for the decomposition on the Brønsted acids. In analogy to the nitrosyl, a reaction of NO_2^+ with ammonia leads to nitramide. It was concluded that at low temperatures the reaction of the acids with adsorbed ammonia to nitrosamine or nitramide and water are most probable because of the presence of large amounts of ammonium, while at higher temperatures the decomposition of the acids dominates. Finally, the decomposition of the intermediates nitrosamine and nitramide to nitrogen and nitrous oxide, respectively, exhibit significantly lower barriers than in the gas phase because of an avoided internal bending in the proton transfer.

For the SCO, as a side reaction, the studied mechanism can essentially be separated in three sequences. First, nitroxyl is formed from the initial oxidation of adsorbed ammonia, then HNO reacts in a bimolecular reaction via H_2NO to hydroxylamine and, finally, a reaction between the two intermediates leads to nitrosamine. Because nitric oxide is also produced in the pathway for the decay of nitroxyl, the potential energy surface for the interaction between NO and the intermediates was analyzed.

Based on the DFT results, reaction rates were calculated from the transition state theory and the temperature dependency of the enthalpy and entropy of the surface species from statistical thermodynamics. Microkinetic modeling, including all calculated elementary steps, has shown that the fast and the NO_2 SCR proceed via the decomposition of the dimerized nitrogen oxide on a void Brønsted acid and are blocked by adsorbed ammonia at low temperatures. The decay of the nitrous and nitric acid was confirmed to be dependent on temperature, with a consumption from adsorbed ammonia at low temperatures via ammonium nitrite and nitrate and the decomposition to nitrosyl and NO_2^+ at high temperatures. The decomposition of the intermediates nitrosamine and nitramide to nitrogen and nitrous oxide takes place instantaneously at all temperatures. For both cases, the shape of the conversion curve was found to be anchored to the blocking of the active site by ammonia at low temperatures and to the thermodynamic limitation of the formation of the dimerized nitrogen oxide N_2O_y at high temperatures. The onset of the ammonia oxidation was found to be anchored to the initial

formation of the intermediate nitroxyl and at high temperatures limited by the decreasing amount of adsorbed ammonia present on the surface for reaction. Its contribution to the conversion at fast SCR conditions is, however, of minor importance.

Within the SCR on iron exchanged zeolites, the oxidation of NO to NO₂ is believed to be rate-determining. On mononuclear iron sites, we studied the NO oxidation for the two cases of absence and presence of water with DFT. In both cases, a catalytic cycle, involving the intermediate formation of an -OONO ligand and a nitrite was concluded to be the most probable pathway based on the internal energy barriers and the corresponding Gibbs' free energies at 600 K. While the reaction proceeds in the absence of water on Z⁻[FeO]⁺, in the presence of water the active site changes to monohydroxylated iron Z⁻[FeOH]⁺. The internal barriers and Gibbs' free energies were found to be higher on the latter suggesting its lower activity. In addition, the stable but inactive surface nitrates and dihydroxylated iron sites were concluded to exhibit the capability of blocking the active sites. Furthermore, the interaction of water with surface nitrites and nitrates as well as of NO_x with hydroxyl groups was shown to open a vast range of potential reactions involving the essential intermediates of the SCR, nitrous and nitric acid.

For the fast and the NO₂ SCR, a similar reaction pathway on mononuclear iron sites was outlined, which involves both active species of the NO oxidation, Z⁻[FeO]⁺ and Z⁻[FeOH]⁺. The interaction of ammonia with the first one results in the formation of an amino and a hydroxyl group. The reaction of either NO or NO₂ with the amino group leads to nitrosamine or nitramide, respectively. Both intermediates are assumed to decompose on Brønsted acids, also in the presence of iron. The interaction of a second ammonia with the monohydroxylated iron again forms an amino group and releases water. The reaction of NO₂ with the remainder amino group leads to a second nitrosamine and restores the catalytic surface. An additional high-temperature mechanism for the NO₂ SCR to only nitrogen was concluded to be unlikely because of higher internal barriers. Instead, the decomposition of NO₂ and partially of the formed N₂O is responsible for the decreasing amount of produced nitrous oxide with increasing temperature. The mechanism of the more recently introduced new "enhanced" SCR,^{334,335} including ammonium nitrate as additional reducing agent, could also be explained from the proposed mechanism of the fast SCR together with the decomposition of nitric acid on the iron sites. Finally, aspects of the ammonia oxidation on mononuclear iron sites were highlighted in terms of the formation of, first, the radical H₂NO from oxygen and the amino group containing iron Z⁻[FeNH₂]⁺

and its further reduction to nitroxyl and eventually to nitric oxide.

Microkinetic modeling of the NO oxidation on the catalyst, which contains mononuclear iron sites, confirmed, in comparison to experimental data, the mechanism via the -OONO ligand, suggested from DFT. In the absence of water, the dominating surface species is the blocking nitrate and surface nitrites, which however participate in the reaction mechanism. In the presence of water, the dominating surface species is the blocking dihydroxylated iron besides active monohydroxylated iron sites. For the correct description in the presence of water at low temperatures, however, the contribution of the Brønsted acids was found necessary to be accounted for in terms of the additional production of nitrous acid, which causes blockage of the active sites. Also for the fast and the NO₂ SCR, mononuclear iron sites appeared to be reasonable representatives for the active iron species. The reaction proceeds along the pathway as concluded to be relevant from the DFT results. However, the conversion of NO_x on the Brønsted acids was in both cases found to be relevant between 500 K and 700 K. Furthermore, the two active sites communicate via nitrous and nitric acid in terms of the local variation of their formation and decomposition with temperature. Thus, the lower activity of the NO₂ SCR is mainly the result of the formation of surface nitrates on the iron from the decomposition of nitric acid formed on the Brønsted acids. The new “enhanced” SCR from Tronconi et al.^{334,335} could be interpreted as a mixture of fast and NO₂ SCR mechanism. The release of NO₂ from nitric acid decomposition makes the fast SCR accessible, but the formation of surface nitrates in analogy to the NO₂ SCR makes it less active than the fast SCR. In the context of this interpretation, the “enhanced” SCR can be concluded to only require mononuclear iron sites as well. Both, the SCO and the standard SCR, however, were only found in agreement with experiments for comparison with low iron-containing catalysts for which the assumption of a dominance of mononuclear iron sites is reasonable. This supports suggestions from the literature that for these reactions higher nuclear iron species are required. Nevertheless, for the conversion of ammonia on the mononuclear sites a severe interaction with the Brønsted acids was observed. At low temperatures, the intermediate nitroxyl is mainly produced on the acid sites and decomposes on the iron. At elevated temperatures, the nitroxyl is also produced on the iron sites via the radical H₂NO. A remarkable conclusion had to be drawn for the standard SCR on mononuclear sites. The widely accepted suggestion that the NO oxidation to NO₂ is rate-determining and followed by the fast SCR was only found to be true at low temperatures, anchored to low conversions. At elevated temperatures, a new mechanism, related to the ammonia oxidation with the intermediate formation of H₂NO,

becomes relevant.

The results of this work are capable of explaining many experimentally observed phenomena, although not all. The importance of the consideration of more than one representative of the active site was already emphasized in terms of the interaction between Brønsted acids and mononuclear iron sites, but certainly iron species of higher nuclearity have to be considered as well to account for the full catalytic capabilities of the introduced iron. In this context, special emphasis should be laid on the standard SCR and the SCO. The screening and highlighting of relevant elementary reactions and surface species should allow for the derivation of better kinetic expressions for fitting to experimental data. It further presents the starting point for higher level calculations on a reduced set of reactions for a refinement of the model. Finally, established opinions on the mechanism of the SCR should be reconsidered in the light of these results, especially with respect to the in the literature suggested importance of the surface nitrates in the mechanism of the fast SCR and the role of the NO oxidation in the standard SCR.

A

Supporting Information for Chapter 3

In this section the derivation of the effective Hessian (3.28) as outlined in section 3.3 is presented. In addition to the original formula an analogous equation is derived which accounts for the in this work applied method to find the minimum energy crossing point.

Here, we show the derivation of the effective Hessian as was proposed by Harvey et al.^{108,111} based on the work of Koga and Morokuma.¹¹² In addition, we show the corresponding derivation for the algorithm applied in this work for finding minimum energy crossing points. Basis is the Lagrangian equation L for the determination of the MECP

$$L(\mathbf{R}, \lambda) = E_1(\mathbf{R}) - \lambda (E_1(\mathbf{R}) - E_2(\mathbf{R})) \quad (\text{A.1})$$

by minimizing the energy E_1 on one PES with the constrained that the energies are identical on both PESs at the coordinates \mathbf{R}^* of the MECP. The PESs only differ in the assigned spin state. At the MECP the energy E_1 and the Lagrangian L are equal and with that their respective Taylor expansions in the vicinity of this point with a displacement $\Delta\mathbf{S}$ along the hyperline of the crossing of the PESs (seam). The seam can be defined as the $3N - 7$ dimensional subspace of both PESs with the vector

$$\mathbf{x} = \nabla E_1(\mathbf{R}) - \nabla E_2(\mathbf{R}) = \mathbf{g}_1 - \mathbf{g}_2 \quad (\text{A.2})$$

being orthogonal to the seam at the MECP. The derivatives of the Lagrangian with respect to the coordinates \mathbf{R} are

$$\frac{\partial L(\mathbf{R}, \lambda)}{\partial \mathbf{R}} = \nabla_{\mathbf{R}} L(\mathbf{R}, \lambda) = \mathbf{g}_1 - \lambda \cdot (\mathbf{g}_1 - \mathbf{g}_2) = 0|_{\mathbf{R}=\mathbf{R}^*} \quad (\text{A.3})$$

$$\begin{aligned} \frac{\partial^2 L(\mathbf{R}, \lambda)}{\partial \mathbf{R}^2} &= \nabla_{\mathbf{R}}^2 L(\mathbf{R}, \lambda) = \nabla_{\mathbf{R}}^2 E_1 - \lambda \cdot (\nabla_{\mathbf{R}}^2 E_1 - \nabla_{\mathbf{R}}^2 E_2) \\ &= \nabla_{\mathbf{R}}^2 E_1 \cdot (1 - \lambda) + \nabla_{\mathbf{R}}^2 E_2 \cdot \lambda \end{aligned} \quad (\text{A.4})$$

With these expressions the Taylor expansion of the energy E at the MECP can be written as

$$\begin{aligned} E_1(\mathbf{R}^* + \Delta\mathbf{S}) &= L(\mathbf{R}^* + \Delta\mathbf{S}, \lambda^*) \\ &= L(\mathbf{R}^*, \lambda^*) + \Delta\mathbf{S}^T \cdot \nabla_{\mathbf{R}} L(\mathbf{R}^*, \lambda^*) + \frac{1}{2} \cdot \Delta\mathbf{S}^T \cdot \nabla_{\mathbf{R}}^2 L(\mathbf{R}^*, \lambda^*) \cdot \Delta\mathbf{S} \\ &= E_1(\mathbf{R}^*, \lambda^*) + \frac{1}{2} \cdot \Delta\mathbf{S}^T \cdot \nabla_{\mathbf{R}}^2 L(\mathbf{R}^*, \lambda^*) \cdot \Delta\mathbf{S} \end{aligned} \quad (\text{A.5})$$

by noticing that the first derivative of the Lagrangian at the coordinates of the MECP is zero as a requirement of the definition of this point to be a minimum on the hyperline of the crossing PESs. Thus, in the Taylor expansion of the energy E_i on either of the two PESs the second derivative of the energy, and with that the Hessian, can be expressed in terms of the

second derivative of the Lagrangian which combines contributions from both PESs according to (A.4). Finally, only the Lagrange multiplier needs to be determined. It is directly obtained if the corresponding search algorithm (A.1) for finding of the MECP is applied. However, it can also be calculated independently of the algorithm from equation (A.3). λ cannot be obtained directly from this equation, but only its absolute value by making use of the norm of the two gradients.

$$\begin{aligned} \mathbf{g}_1(\mathbf{R}^*) &= \lambda^* \cdot (\mathbf{g}_1(\mathbf{R}^*) - \mathbf{g}_2(\mathbf{R}^*)) \\ |\mathbf{g}_1(\mathbf{R}^*)| &= |\lambda^*| \cdot |\mathbf{g}_1(\mathbf{R}^*) - \mathbf{g}_2(\mathbf{R}^*)| \\ |\lambda^*| &= \frac{|\mathbf{g}_1(\mathbf{R}^*)|}{|\mathbf{g}_1(\mathbf{R}^*) - \mathbf{g}_2(\mathbf{R}^*)|} = \frac{|\mathbf{g}_1|}{|\mathbf{x}|} \end{aligned} \quad (\text{A.6})$$

In analogy, the separation of the two gradients prior to applying the norm yields in combination with (A.6)

$$|1 - \lambda^*| = \frac{|\mathbf{g}_2(\mathbf{R}^*)|}{|\mathbf{g}_1(\mathbf{R}^*) - \mathbf{g}_2(\mathbf{R}^*)|} = \frac{|\mathbf{g}_2|}{|\mathbf{x}|} \quad (\text{A.7})$$

The reintroduction of the Lagrange multiplier in equation (A.3) allows for the determination of its correct sign. Inserting the two expressions (A.6) and (A.7) in (A.4) results in the expression of the effective Hessian (3.28). However, from a practical point of view it is straight forward to only calculate the value of the Lagrange multiplier together with its sign and then directly apply it in (A.4) rather than calculating the absolute value of $(1 - \lambda)$, as well. The latter case would also require the distinction of cases in order to obtain the correct sign for the difference.

In this work we applied an algorithm with the governing equation for the Lagrangian

$$L(\mathbf{R}, \lambda) = E_1(\mathbf{R}) + E_2(\mathbf{R}) - \lambda (E_1(\mathbf{R}) - E_2(\mathbf{R})) \quad (\text{A.8})$$

which minimizes the sum of the energies of the two PESs with the constraint that the energies are equal at the coordinates of the MECP. This results in the corresponding derivatives

$$\frac{\partial L(\mathbf{R}, \lambda)}{\partial \mathbf{R}} = \nabla_{\mathbf{R}} L(\mathbf{R}, \lambda) = \mathbf{g}_1 + \mathbf{g}_2 - \lambda \cdot (\mathbf{g}_1 - \mathbf{g}_2) = 0|_{\mathbf{R}=\mathbf{R}^*} \quad (\text{A.9})$$

$$\begin{aligned} \frac{\partial^2 L(\mathbf{R}, \lambda)}{\partial \mathbf{R}^2} &= \nabla_{\mathbf{R}}^2 L(\mathbf{R}, \lambda) = \nabla_{\mathbf{R}}^2 E_1 + \nabla_{\mathbf{R}}^2 E_2 - \lambda \cdot (\nabla_{\mathbf{R}}^2 E_1 - \nabla_{\mathbf{R}}^2 E_2) \\ &= \nabla_{\mathbf{R}}^2 E_1 \cdot (1 - \lambda) + \nabla_{\mathbf{R}}^2 E_2 \cdot (1 + \lambda) \end{aligned} \quad (\text{A.10})$$

For the Taylor expansion, it has to be kept in mind that the Lagrangian minimizes the sum of the energies of the two PESs.

$$\begin{aligned}
 E(\mathbf{R}^* + \Delta\mathbf{S}) &= \frac{1}{2}L(\mathbf{R}^* + \Delta\mathbf{S}, \lambda^*) \\
 &= \frac{1}{2} \left\{ L(\mathbf{R}^*, \lambda^*) + \Delta\mathbf{S}^T \cdot \nabla_{\mathbf{R}}L(\mathbf{R}^*, \lambda^*) + \frac{1}{2} \cdot \Delta\mathbf{S}^T \cdot \nabla_{\mathbf{R}}^2L(\mathbf{R}^*, \lambda^*) \cdot \Delta\mathbf{S} \right\} \\
 &= E(\mathbf{R}^*, \lambda^*) + \frac{1}{4} \cdot \Delta\mathbf{S}^T \cdot \nabla_{\mathbf{R}}^2L(\mathbf{R}^*, \lambda^*) \cdot \Delta\mathbf{S} \quad (\text{A.11})
 \end{aligned}$$

For the Lagrange multiplier one obtains the absolute value

$$|\lambda^*| = \frac{|\mathbf{g}_1(\mathbf{R}^*) + \mathbf{g}_2(\mathbf{R}^*)|}{|\mathbf{g}_1(\mathbf{R}^*) - \mathbf{g}_2(\mathbf{R}^*)|} \quad (\text{A.12})$$

and with that for the effective Hessian of the MECP

$$\mathbf{H}_{\text{eff}} = \frac{1}{2} \left\{ \left(1 - \left[\pm \frac{|\mathbf{g}_1 + \mathbf{g}_2|}{|\mathbf{g}_1 - \mathbf{g}_2|} \right] \right) \cdot \mathbf{H}_1 + \left(1 + \left[\pm \frac{|\mathbf{g}_1 + \mathbf{g}_2|}{|\mathbf{g}_1 - \mathbf{g}_2|} \right] \right) \cdot \mathbf{H}_2 \right\} \quad (\text{A.13})$$

Both expressions, equation (3.28) and (A.13) yield the same result in the frequency analysis of the MECP. Though the equation of Harvey et al.^{108,111} is simpler at first, depending on the applied algorithm, it might make sense to derive an alternative expression as shown here and to use the optimized Lagrange multiplier from the MECP search algorithm. Furthermore, this approach allows for the validation of the Lagrange multiplier or the application of a corresponding equation like (A.6) or (A.12) to obtain a better start value in the search algorithm. It should be pointed out that the gradients and second derivatives are used in mass weighted coordinates.

B

Supporting Information for Chapter 4

This appendix contains the structures of the minima, transition states and minimum energy crossing points between two potential energy surfaces corresponding to the discussion of the selective catalytic reduction on H-form zeolites in chapter 4

B.1 Formation of NO_2 , NH_2NO_x and HNO_y

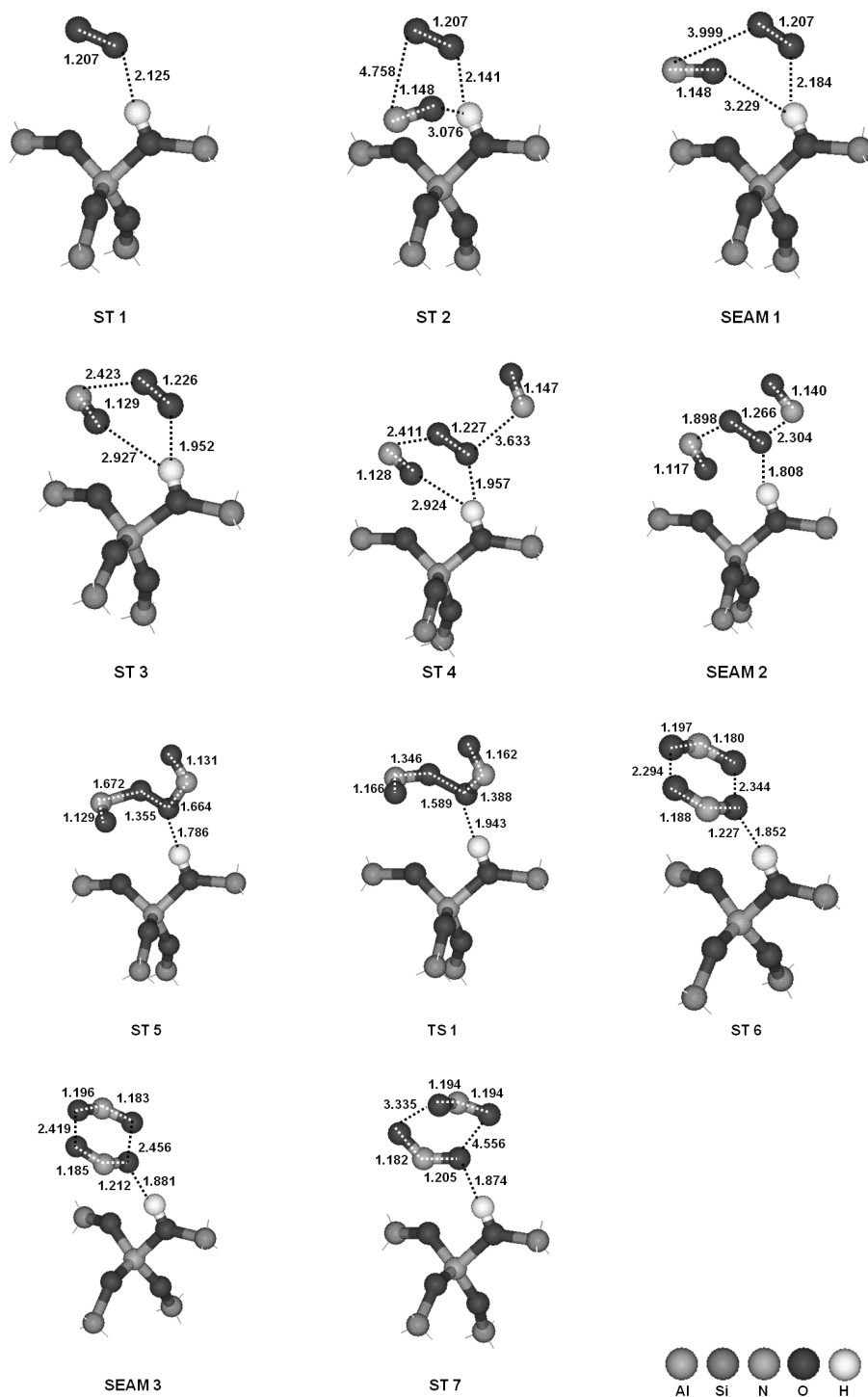


Figure B.1: Geometries of the minima (ST), transition states (TS) and minima on the seam of two PESs (SEAM) in the oxidation of NO with O_2 over the zeolite cluster. Bond lengths are in Å. Dangling bonds are not shown.

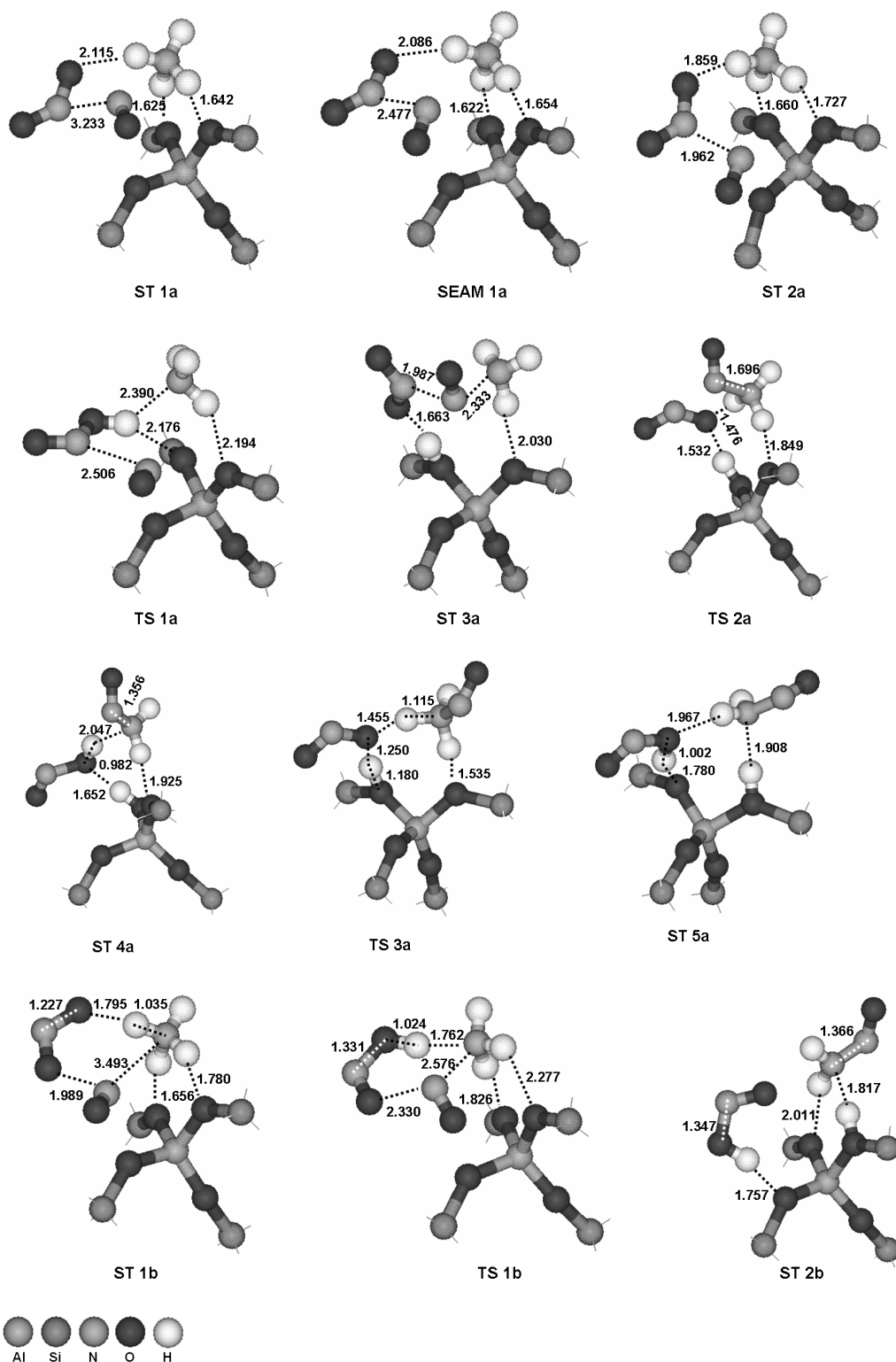


Figure B.2: Geometries of the minima (ST), transition states (TS) and minimum on the seam of two PESs (SEAM) in the formation of NH_2NO from NO_2 and NO in a two-step mechanism over the zeolite cluster. Bond lengths are in Å. Dangling bonds are not shown.

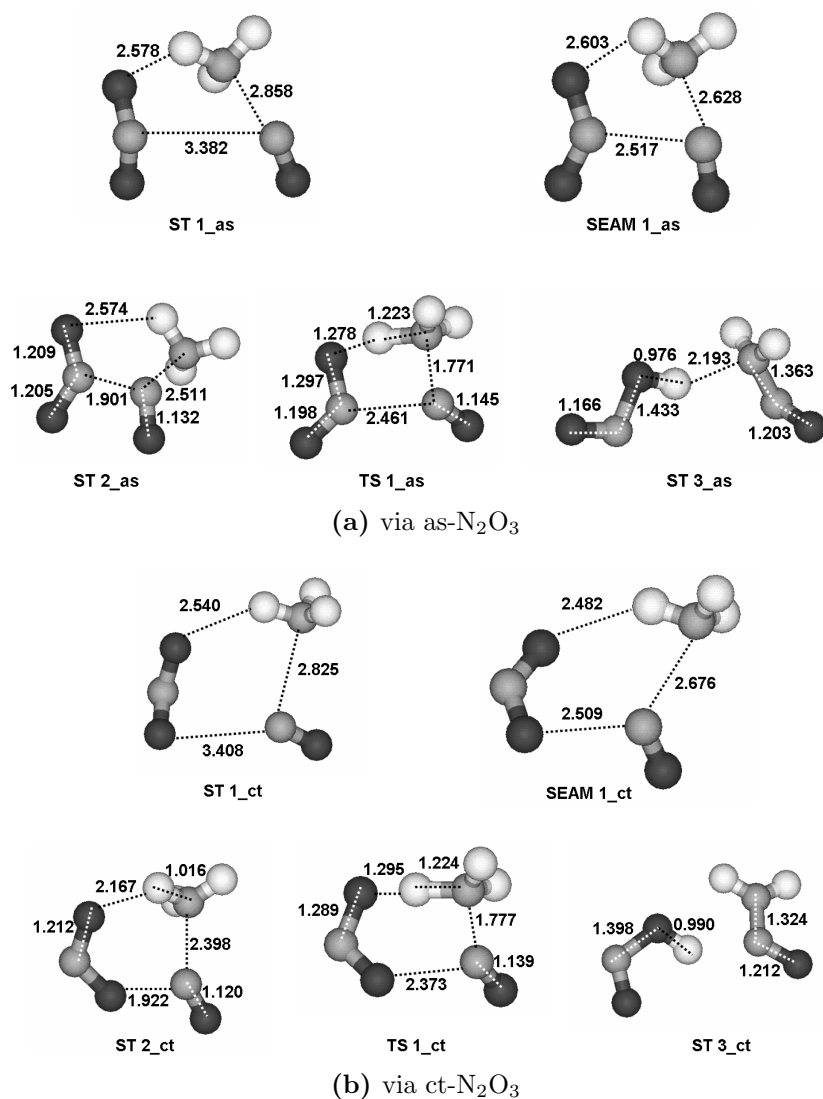


Figure B.3: Geometries of the minima (ST), transition state (TS) and minimum on the seam of two PESs (SEAM) in the homogeneous formation of NH_2NO from NO_2 and NO . Bond lengths are in Å.

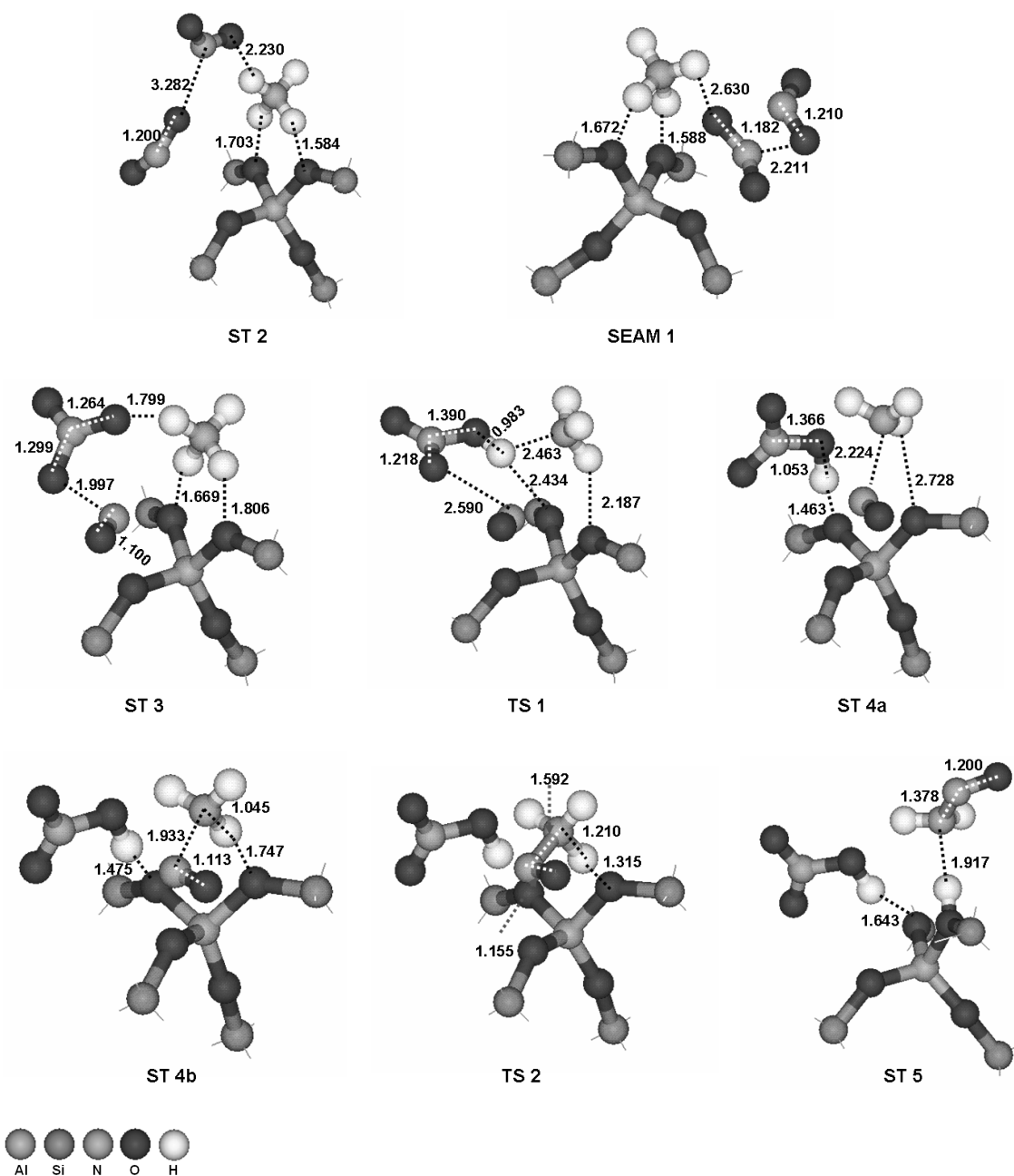


Figure B.4: Geometries of the minima (ST), transition states (TS) and minimum on the seam of two PESs (SEAM) in the formation of NH_2NO from two NO_2 in a two-step mechanism over the zeolite cluster. Bond lengths are in Å. Dangling bonds are not shown.

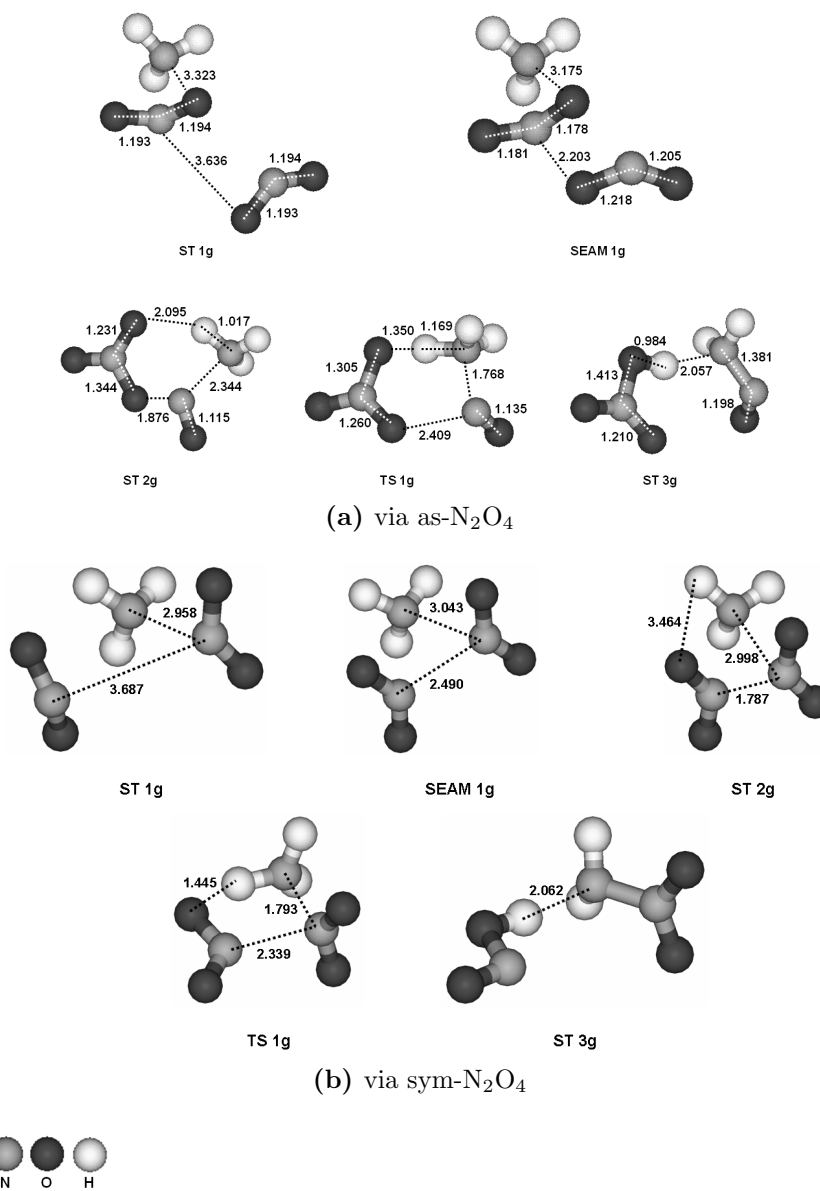


Figure B.5: Geometries of the minima (ST), transition state (TS) and minimum on the seam of two PESs (SEAM) in the homogeneous formation of NH_2NO or NH_2NO_2 from two NO_2 . Bond lengths are in Å.

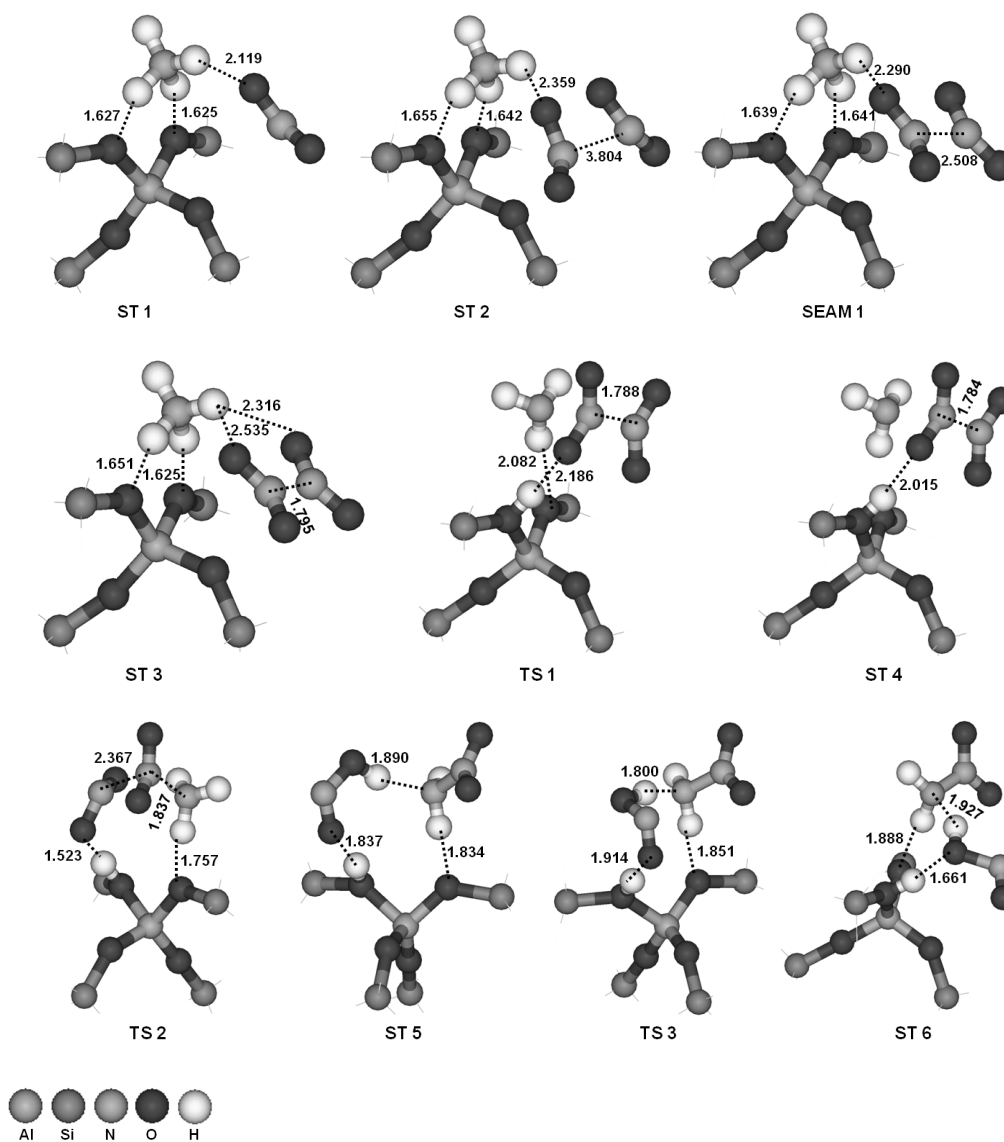


Figure B.6: Geometries of the minima (ST), the transition states (TS) and the minimum on the seam of two PESs (SEAM) in the reaction of sym- N_2O_4 with NH_3 over the zeolite cluster. Bond lengths are in Å. Dangling bonds are not shown.

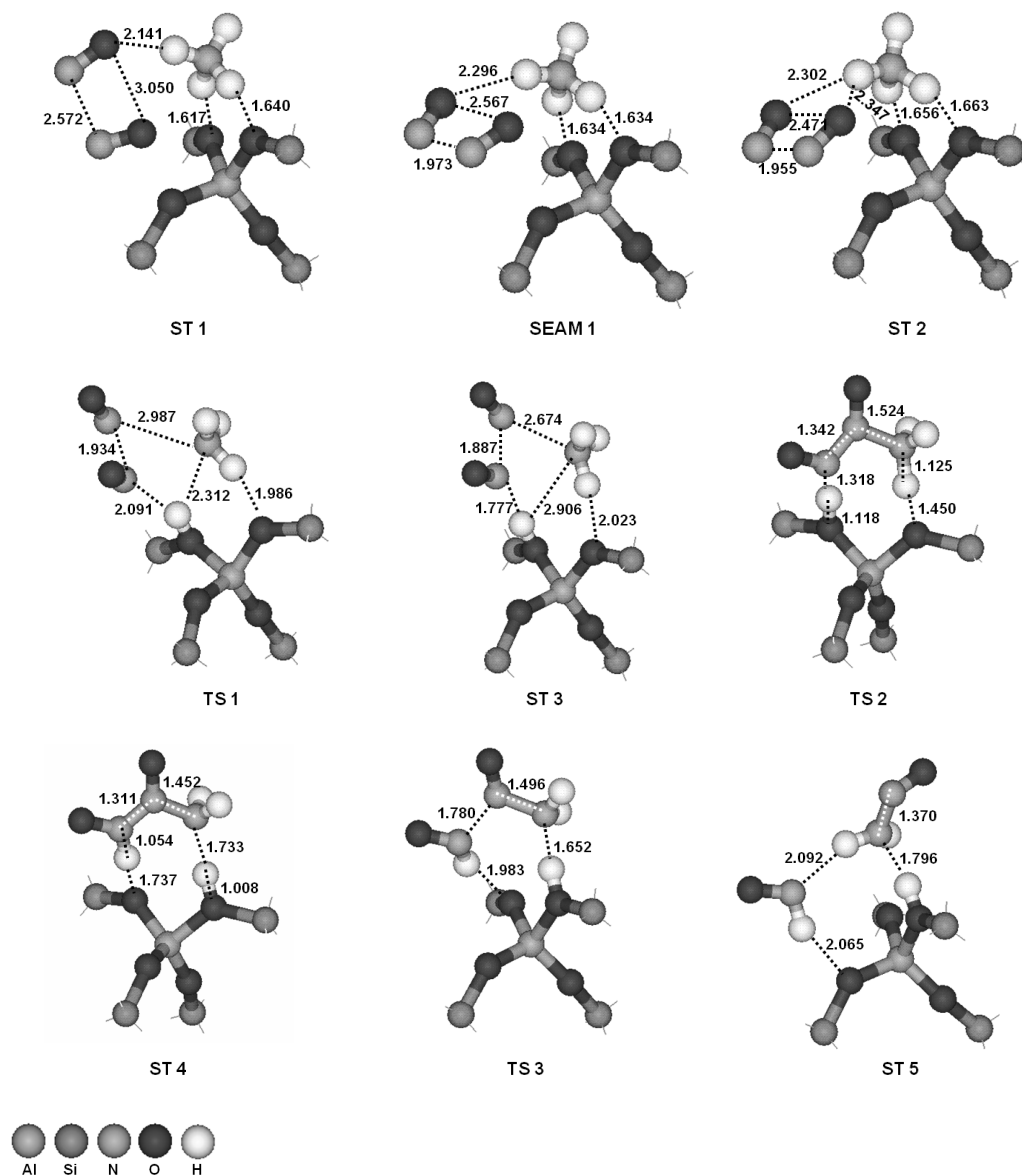


Figure B.7: Geometries of the minima (ST), transition states (TS) and minimum on the seam of two PESs (SEAM) in the formation of NH_2NO from two NO over the zeolite cluster. Bond lengths are in Å. Dangling bonds are not shown.

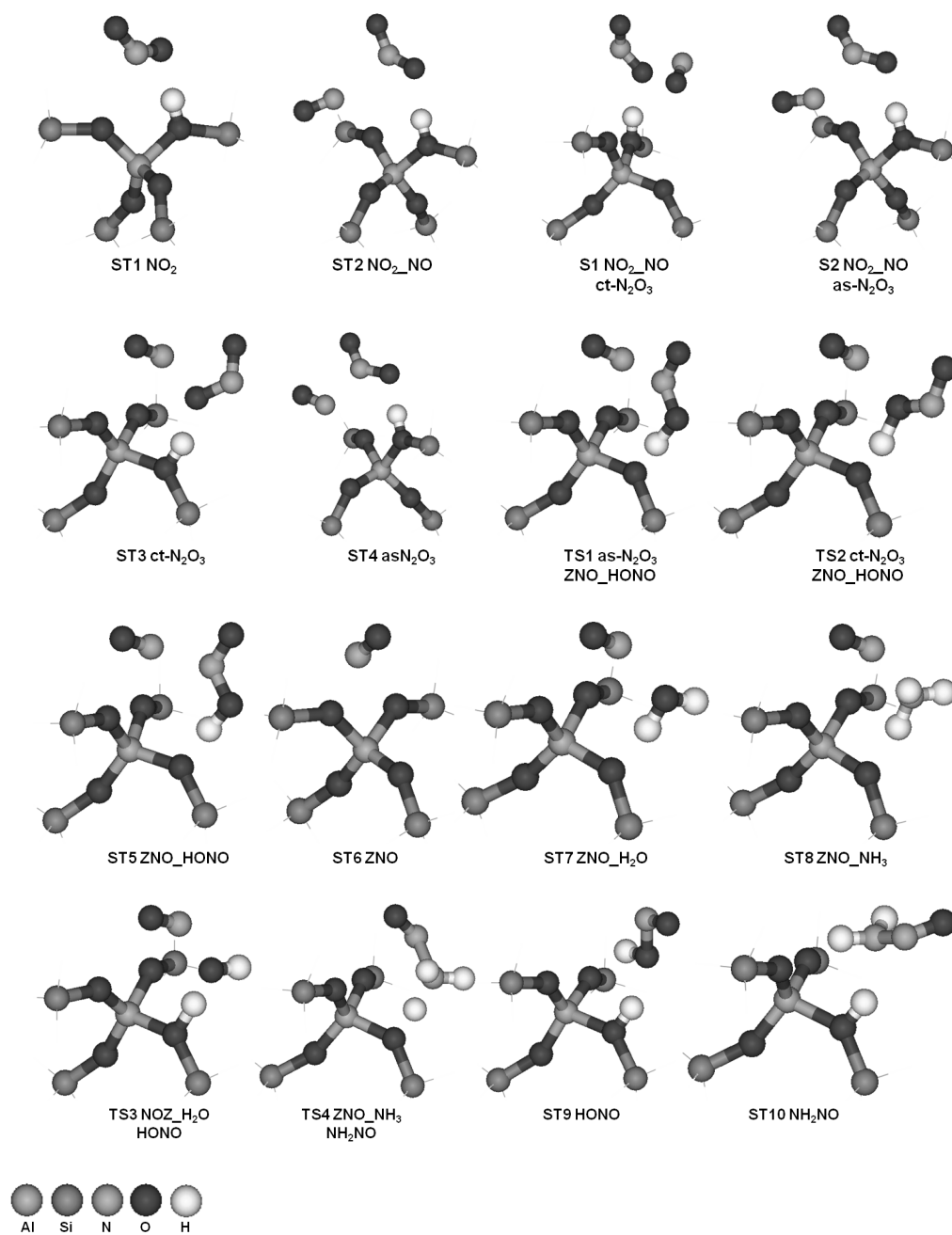


Figure B.8: Geometries of the minima (ST), the minima on the seam of two PESs (S) and the transition states (TS) for the fast SCR via $\text{Z}^-[\text{NO}]^+$. Dangling bonds are not shown.

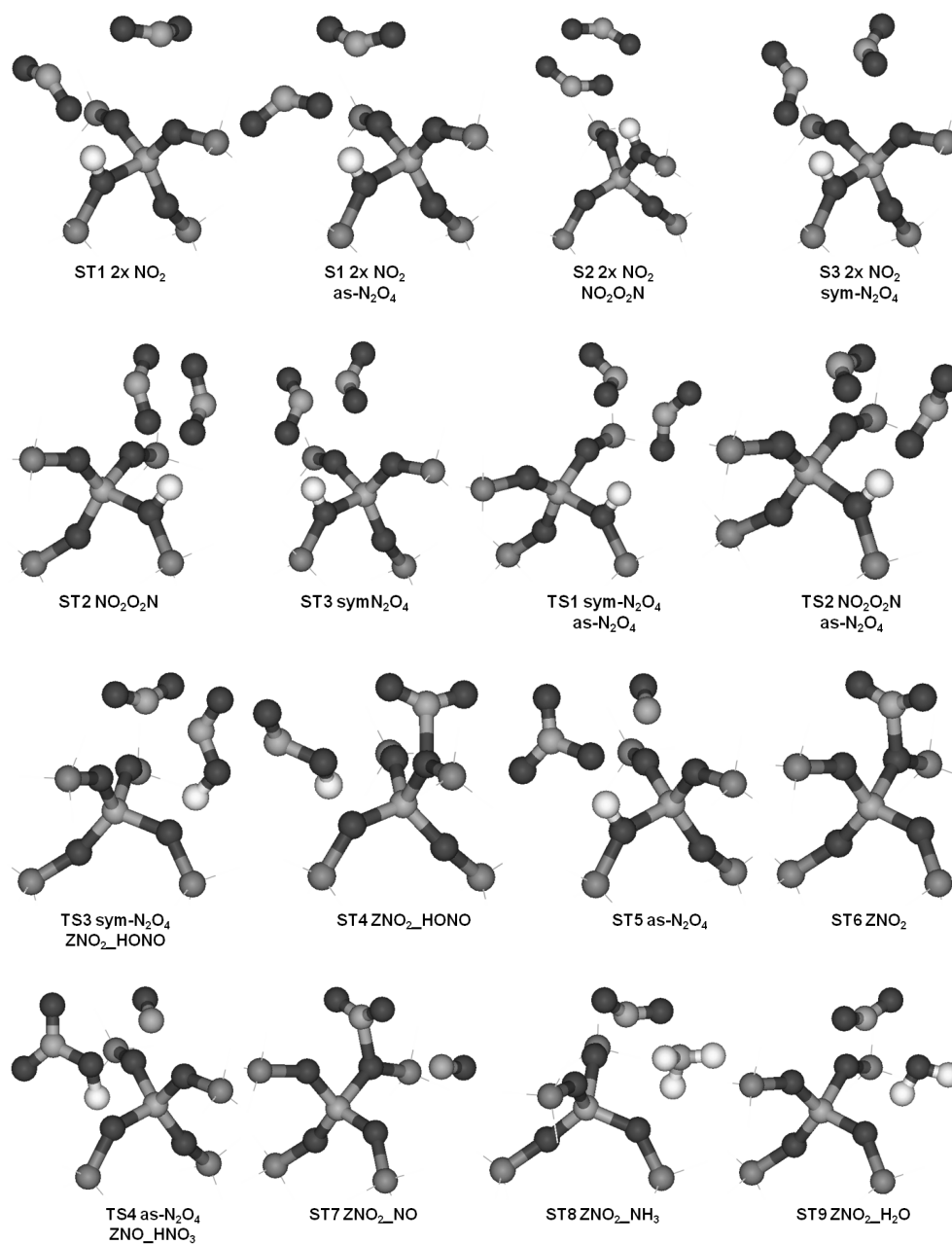


Figure B.9: Part one

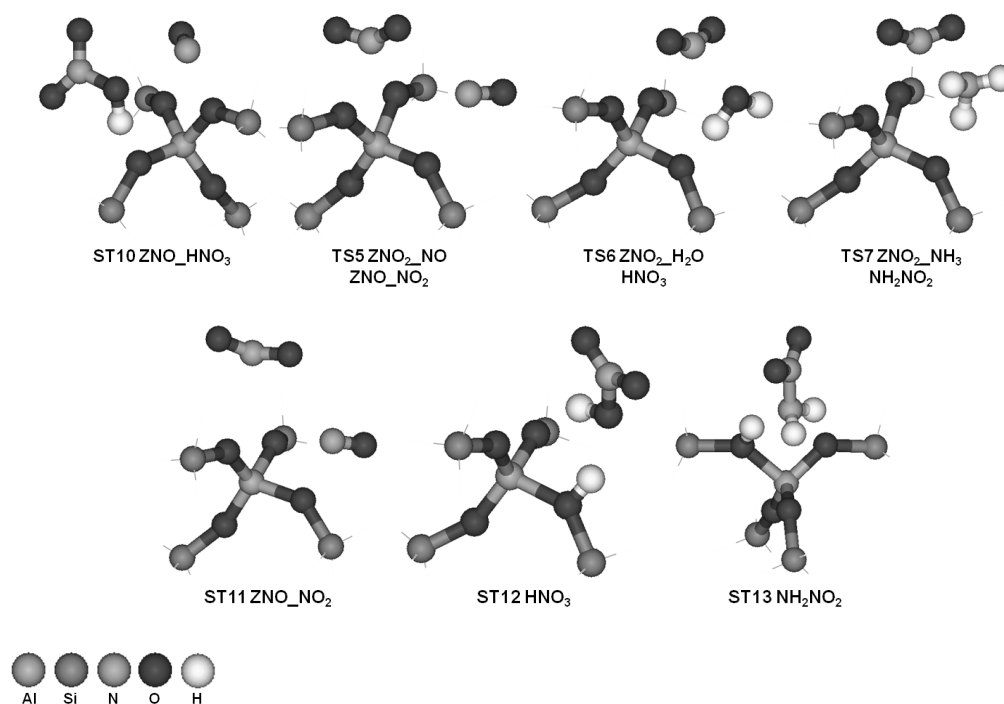


Figure B.9: Geometries of the minima (ST), the minima on the seam of two PESs (S) and the transition states (TS) for the NO₂-SCR via Z⁻[NO₂]⁺. Dangling bonds are not shown.

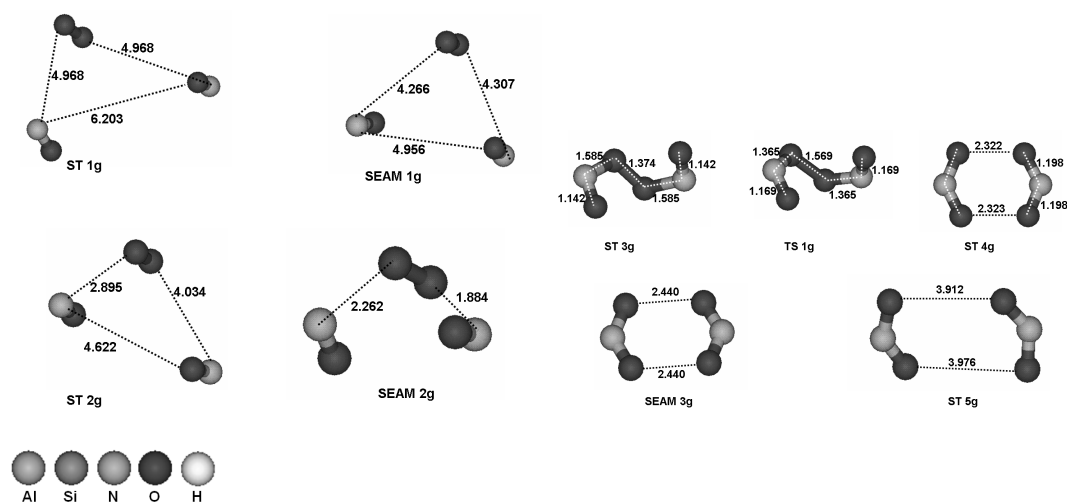


Figure B.10: Geometries of the minima (ST), transition states (TS) and minima on the seam of two PESs (SEAM) in the homogeneous oxidation of NO with O₂. Bond lengths are in Å.

B.2 Decay of HONO and HNO₃

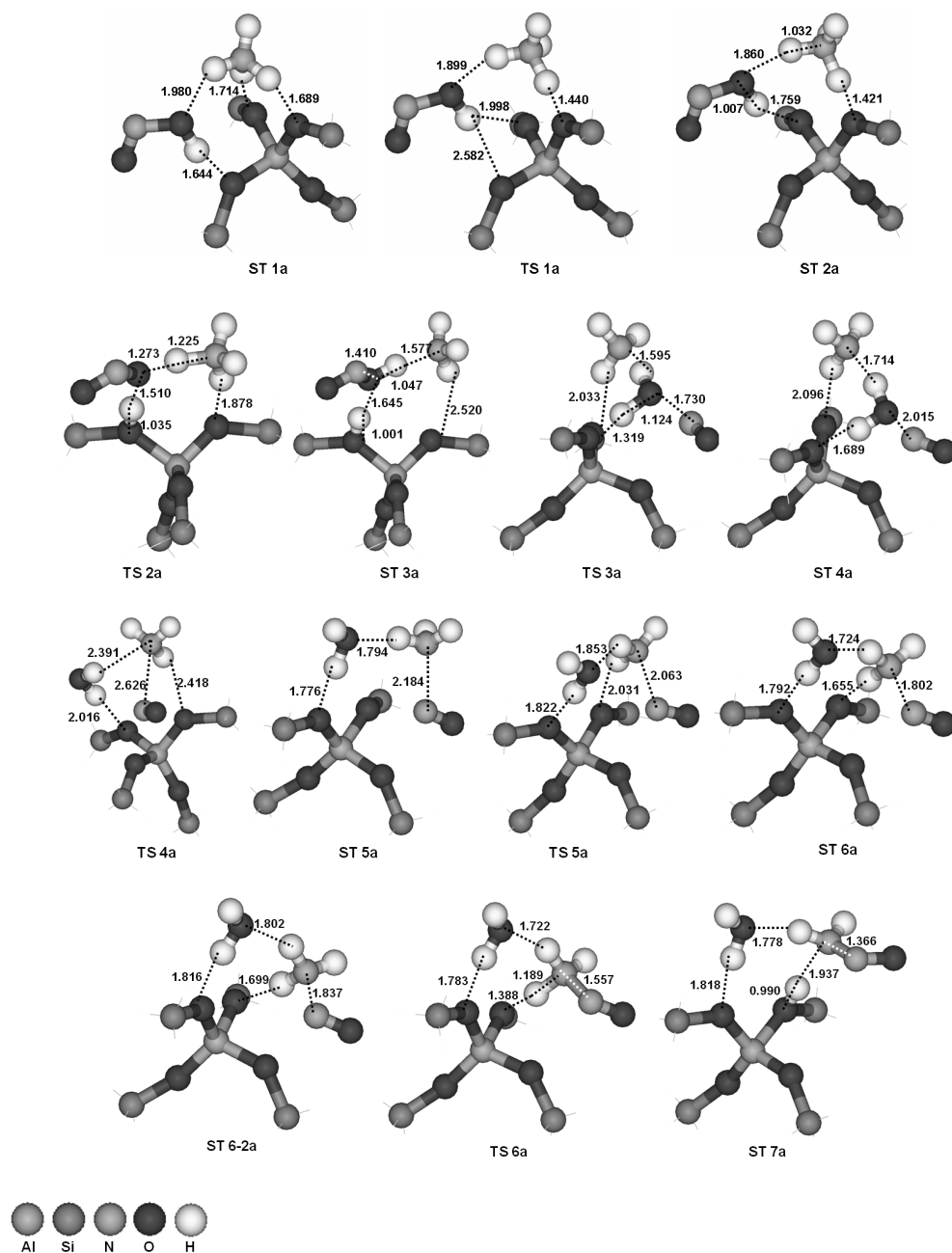


Figure B.11: Geometries of the minima (ST) and the transition states (TS) of the reaction of cis-HONO with NH₃ over the zeolite cluster. Bond lengths are in Å. Dangling bonds are not shown.

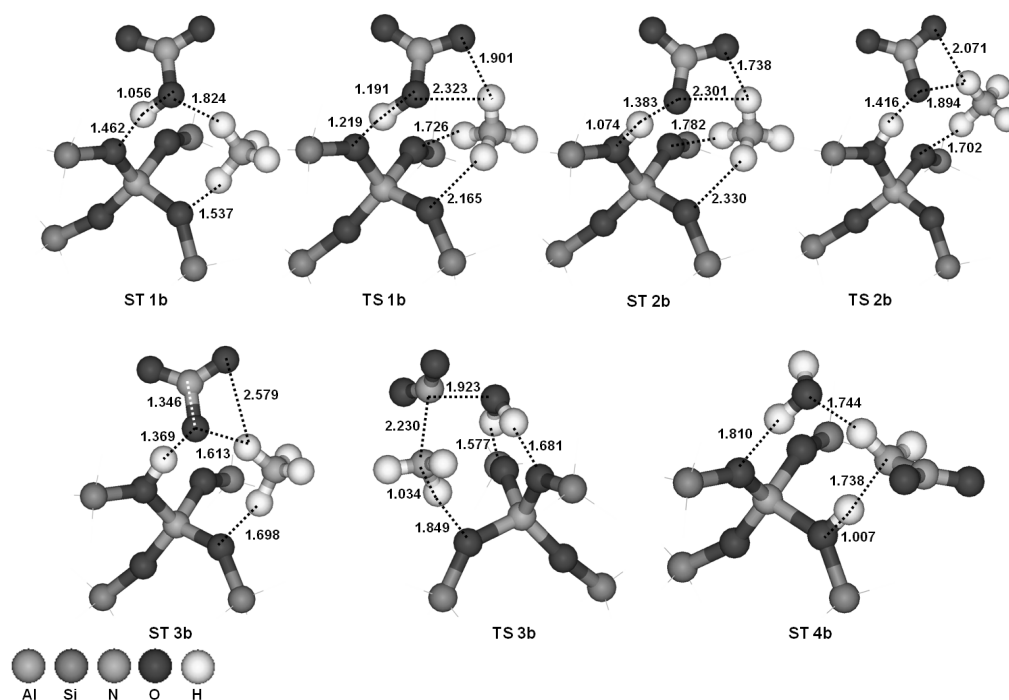


Figure B.12: Geometries of the minima (ST) and the transition states (TS) of the reaction of HNO₃ with NH₃ over the zeolite cluster. Bond lengths are in Å. Dangling bonds are not shown.

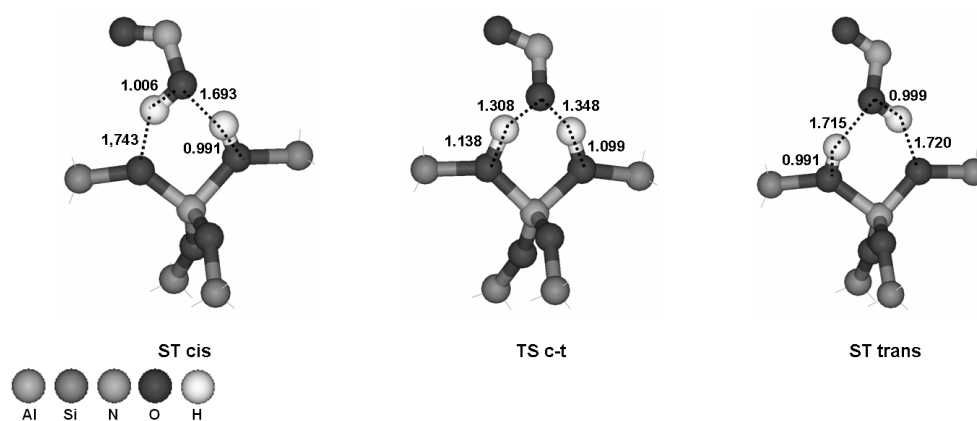


Figure B.13: Geometries of the minima (ST) and the transition state (TS) of the configurational change between trans- and cis-HONO over the zeolite cluster. Bond lengths are in Å. Dangling bonds are not shown.

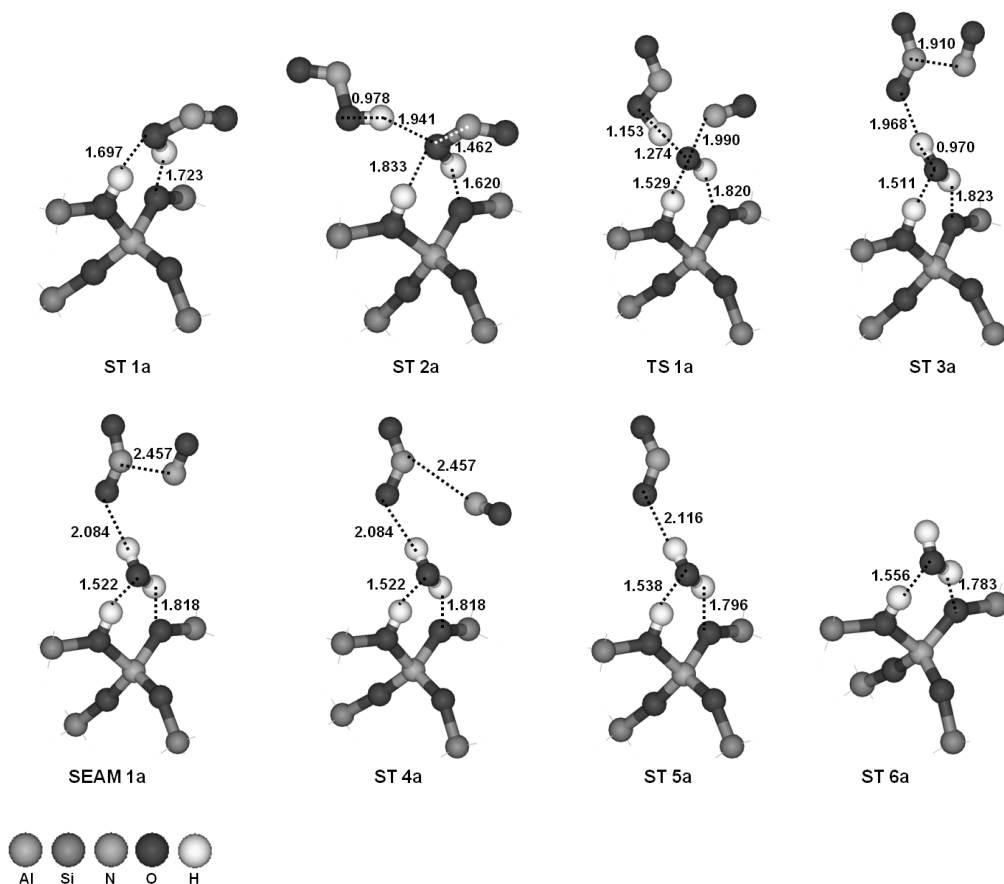


Figure B.14: Geometries of the minima (ST), the transition state (TS) and the minimum on the seam of two PESs (SEAM) of the self-reaction of HONO (cis with trans) in a one-step mechanism over the zeolite cluster. Bond lengths are in Å. Dangling bonds are not shown.

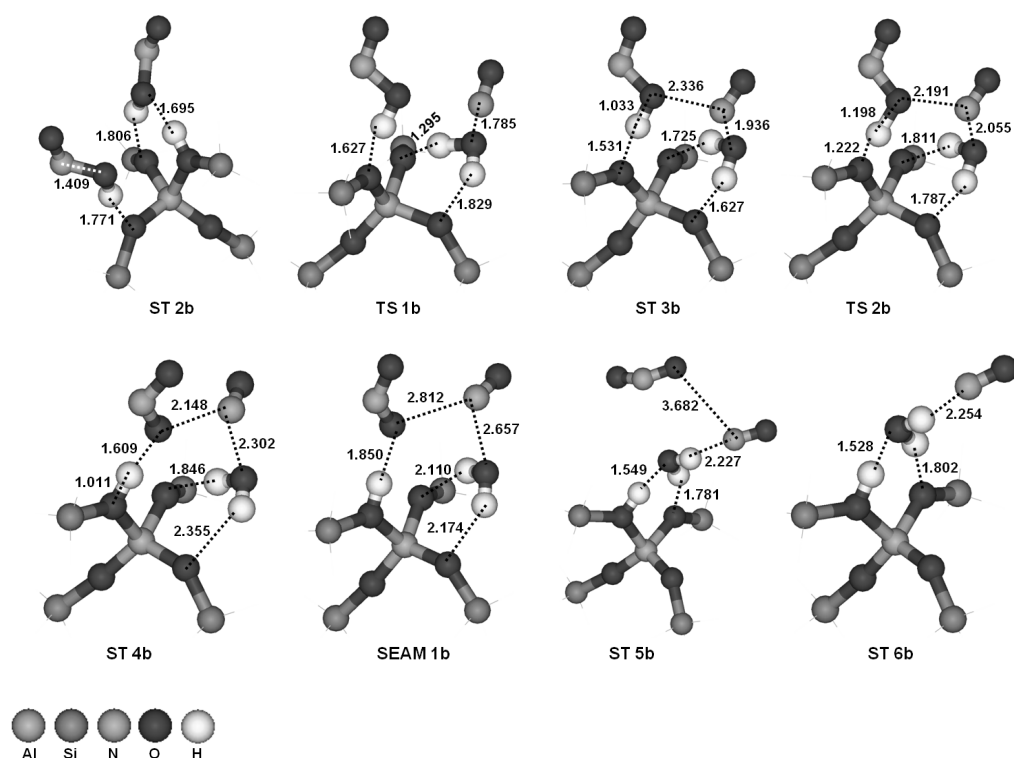


Figure B.15: Geometries of the minima (ST), the transition states (TS) and the minimum on the seam of two PESs (SEAM) of the self-reaction of HONO (trans with trans) in a two-step mechanism over the zeolite cluster. Bond lengths are in Å. Dangling bonds are not shown.

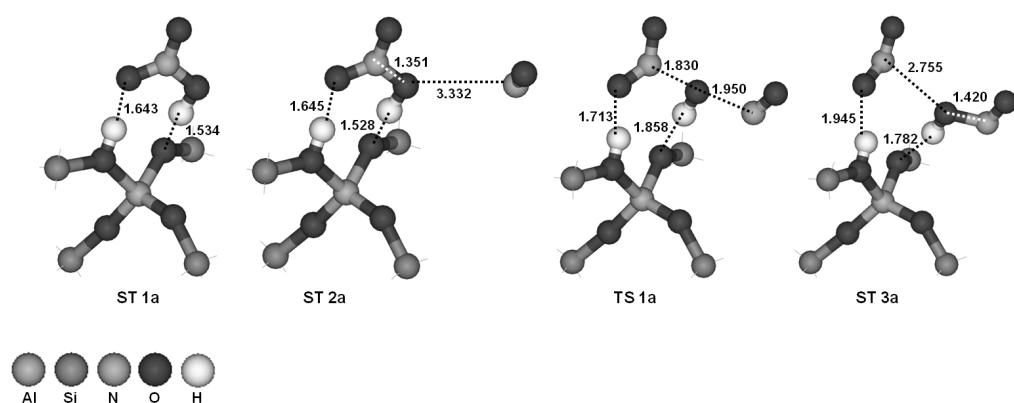


Figure B.16: Geometries of the minima (ST) and the transition state (TS) of the formation of nitrous acid from the reaction of HNO₃ with NO over the zeolite cluster. Bond lengths are in Å. Dangling bonds are not shown.

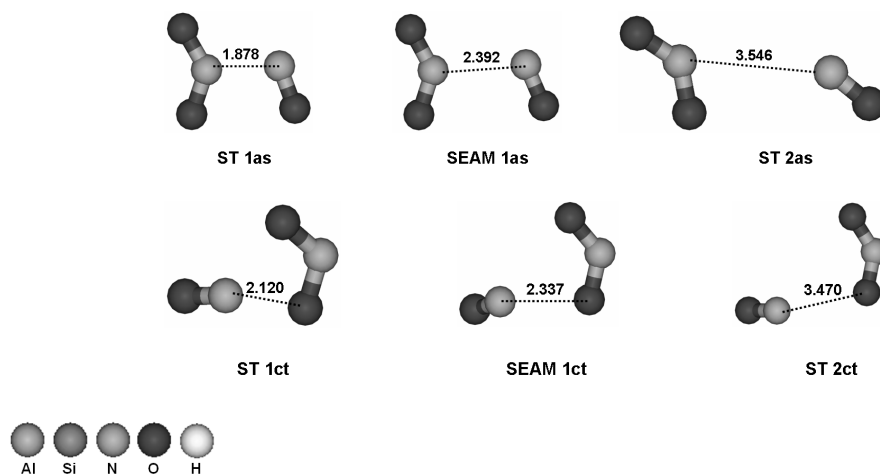


Figure B.17: Geometries of the minima (ST) and the minima on the seam (SEAM) of two PESs (SEAM) of the decomposition of $\text{as-N}_2\text{O}_3$ and $\text{ct-N}_2\text{O}_3$ in the gas-phase. Bond lengths are in Å.

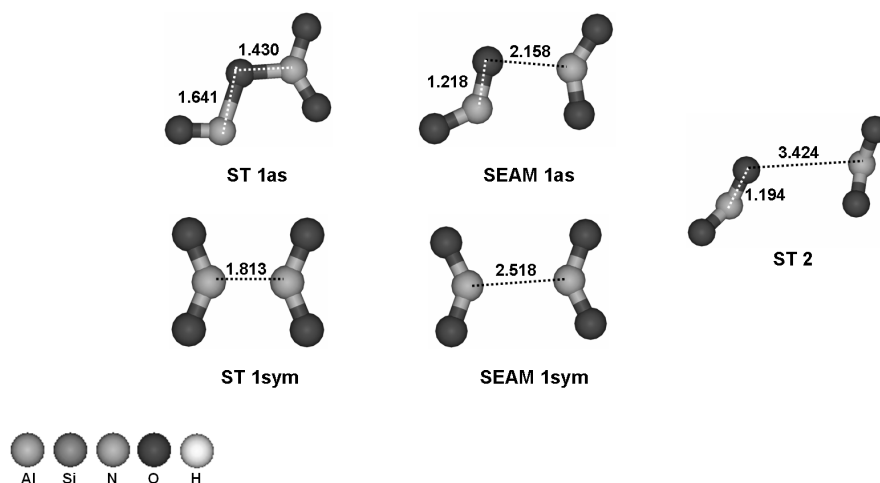


Figure B.18: Geometries of the minima (ST) and the minima on the seam (SEAM) of two PESs (SEAM) of the decomposition of $\text{as-N}_2\text{O}_4$ and $\text{sym-N}_2\text{O}_4$ in the gas-phase. Bond lengths are in Å.

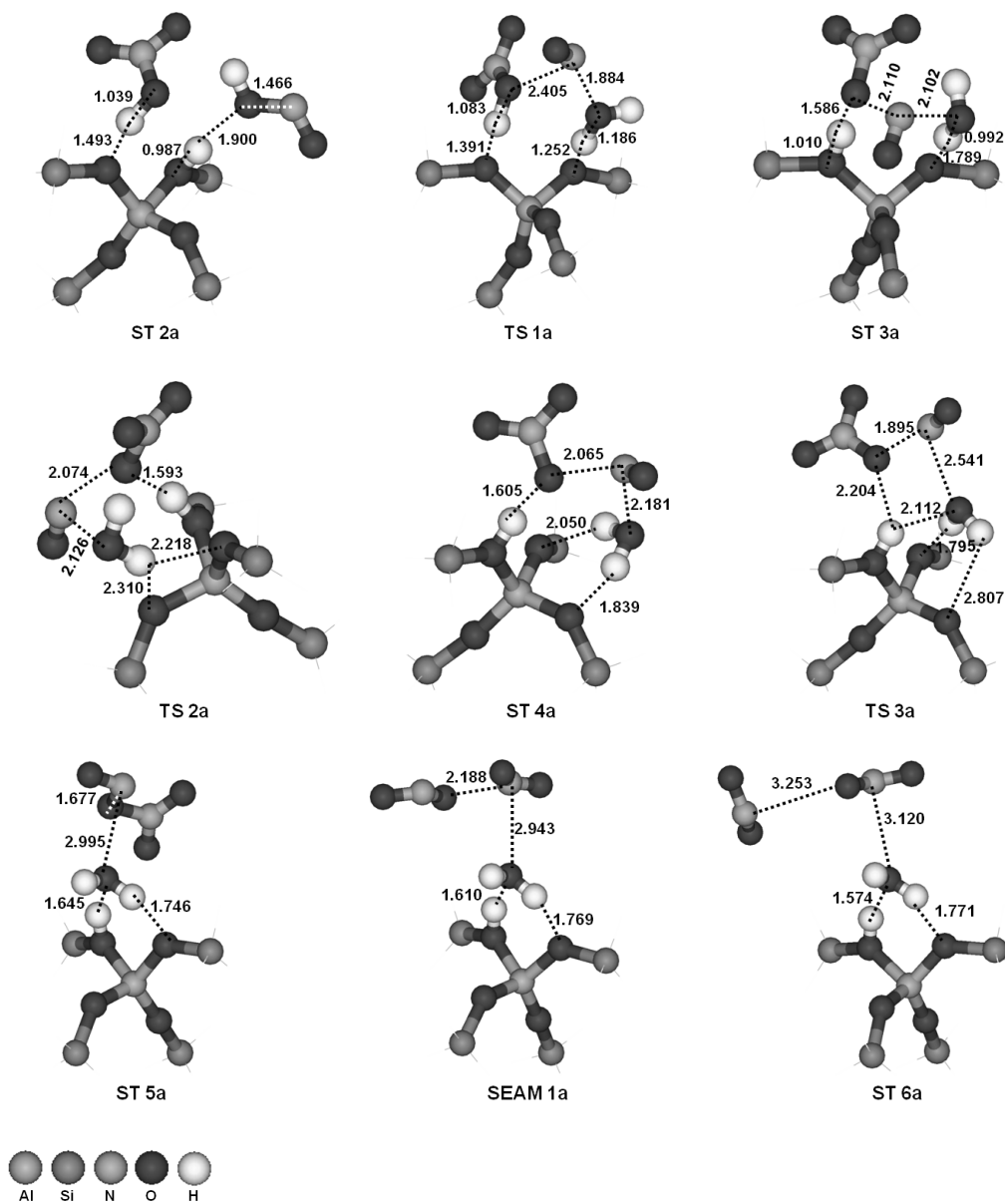


Figure B.19: Geometries of the minima (ST), the transition states (TS) and the minimum on the seam of two PESs (SEAM) in the reaction of trans-HONO with HNO₃ via as-N₂O₄ over the zeolite cluster. Bond lengths are in Å. Dangling bonds are not shown.

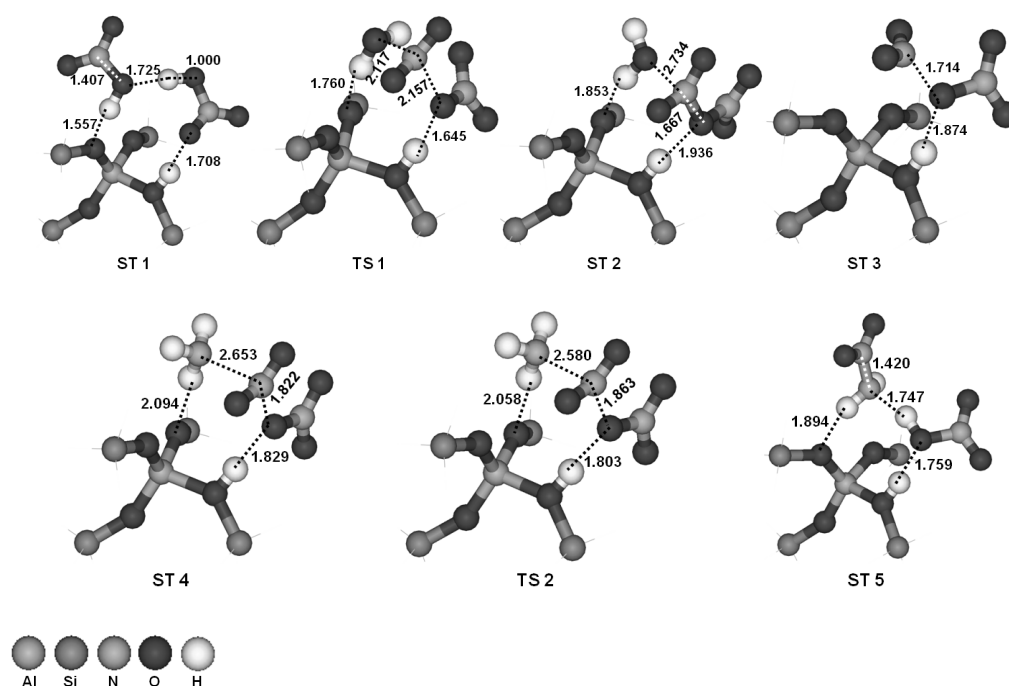


Figure B.20: Geometries of the minima (ST), the transition states (TS) and the minimum on the seam of two PESs (SEAM) in the reaction of trans-HONO with HNO₃ via as-N₂O₄ over the zeolite cluster. Bond lengths are in Å. Dangling bonds are not shown.

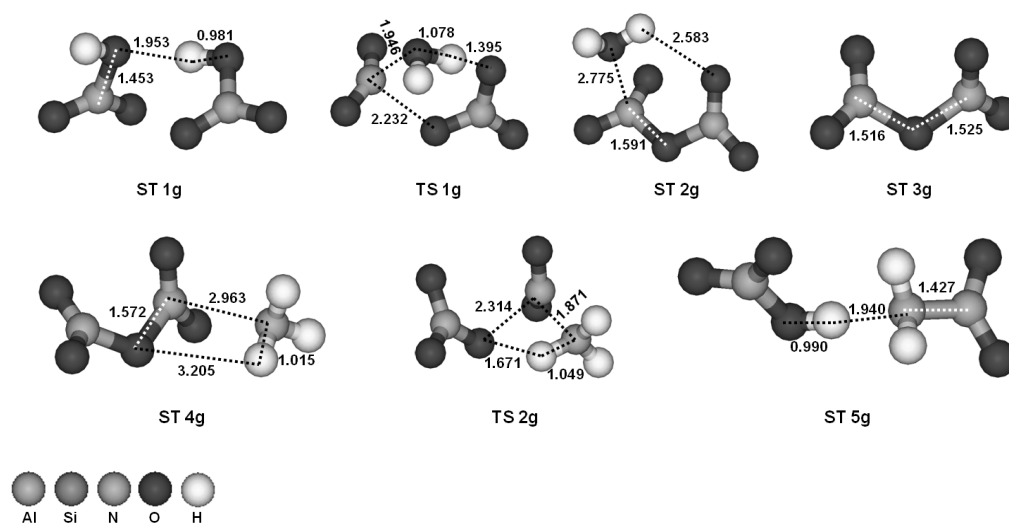


Figure B.21: Geometries of the minima (ST) and the minima on the seam of two PESs (SEAM) of the decomposition of as-N₂O₄ and sym-N₂O₄ in the gas-phase. Bond lengths are in Å.

B.3 Decomposition of NH_2NO_x

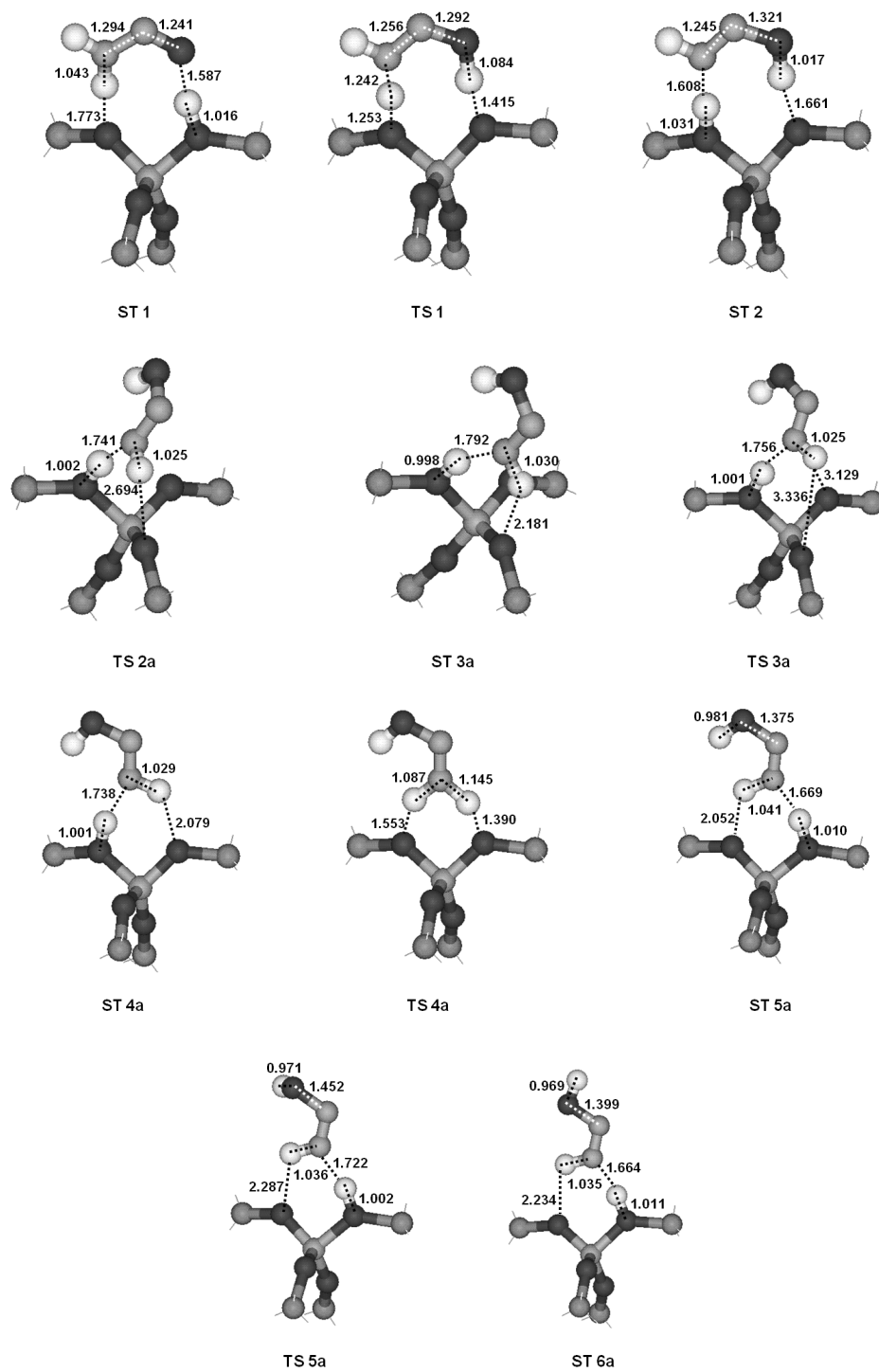


Figure B.22: Part one

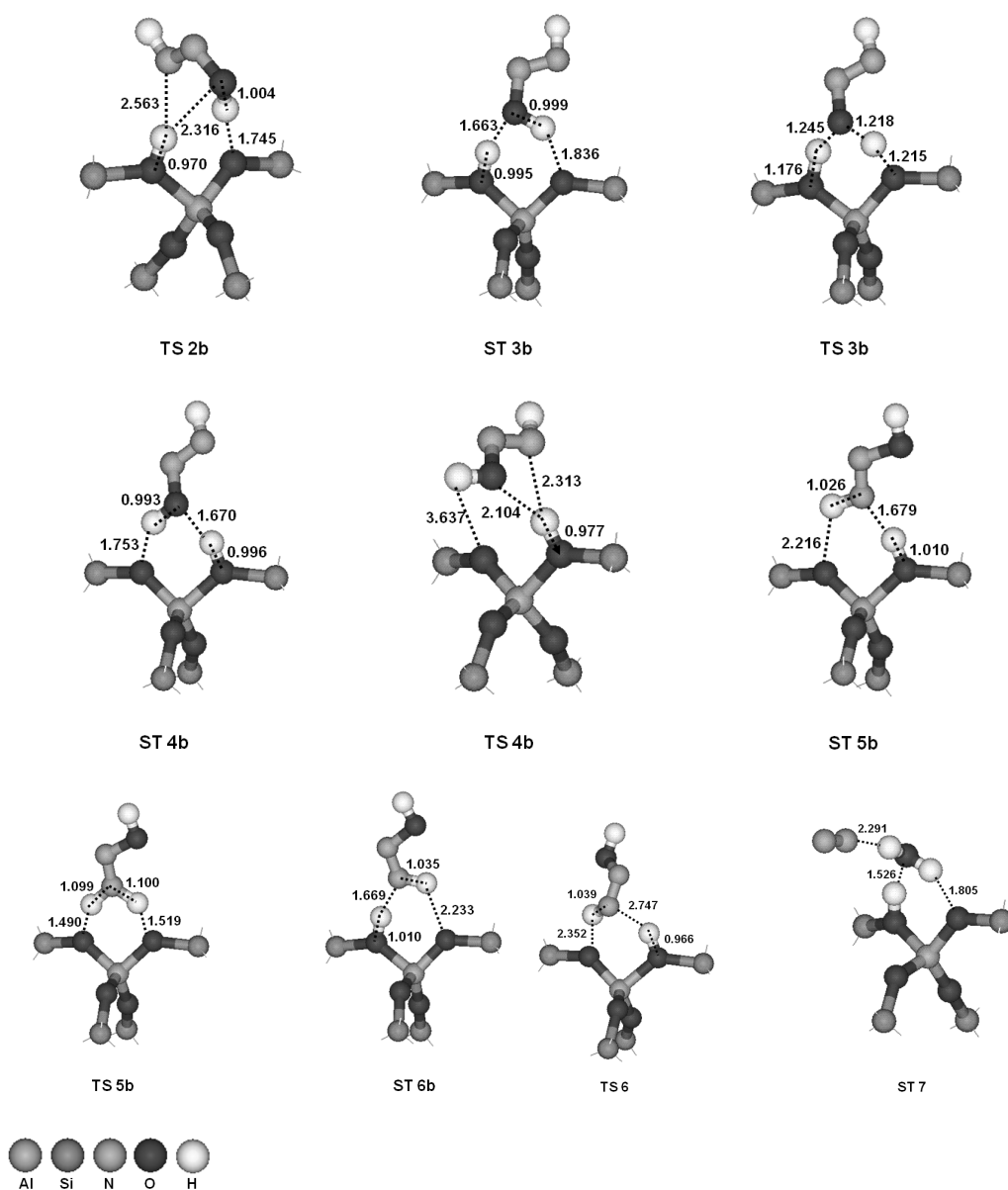


Figure B.22: Geometries of the minima (ST) and transition states (TS) in the decomposition of NH_2NO to N_2 and H_2O for two pathways. Attached “a” refers to “route a”, “b” refers to “route b”. In case of no attachment structures refer to both routes. Bond lengths are in Å. Dangling bonds are not shown.

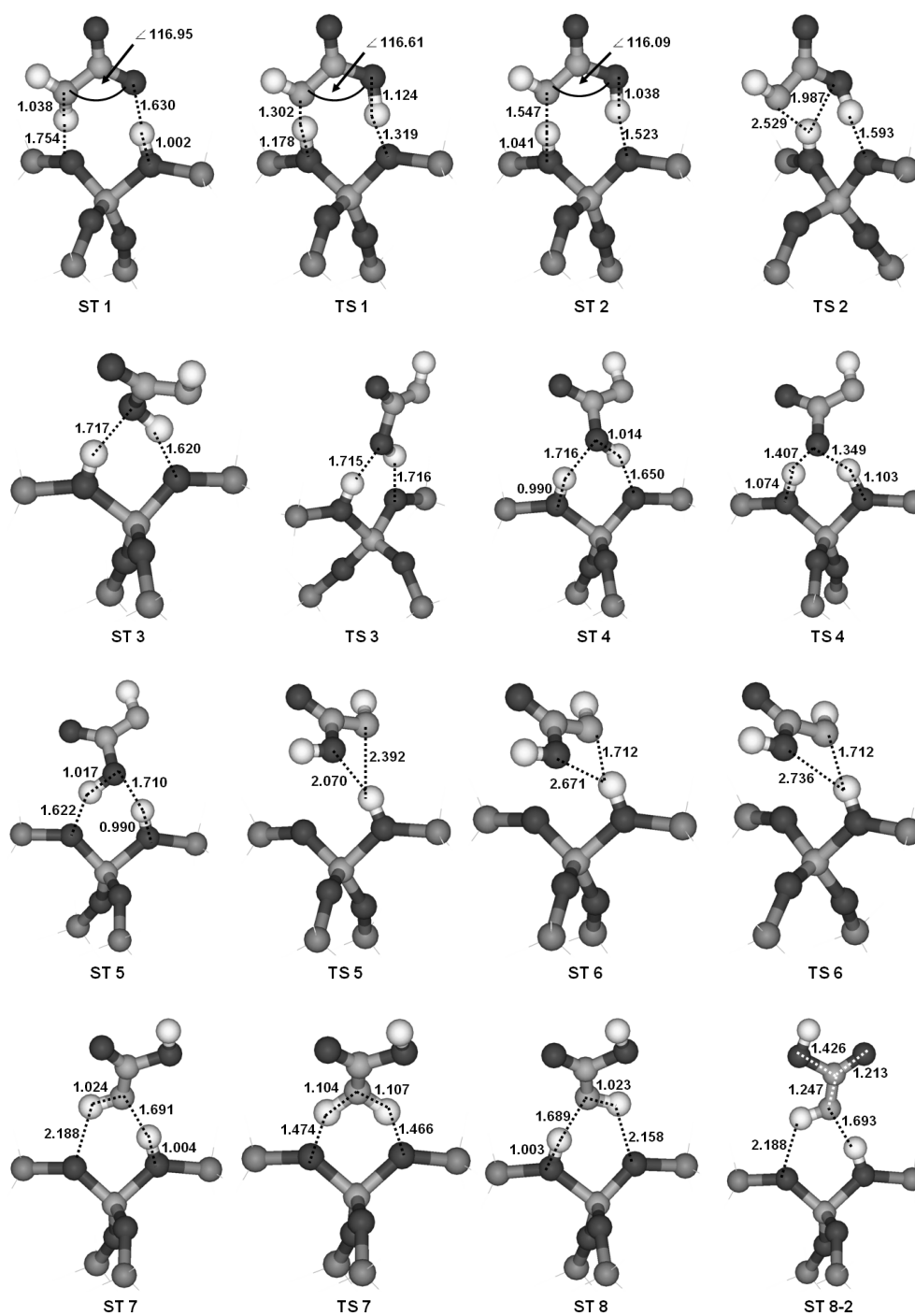


Figure B.23: Part one

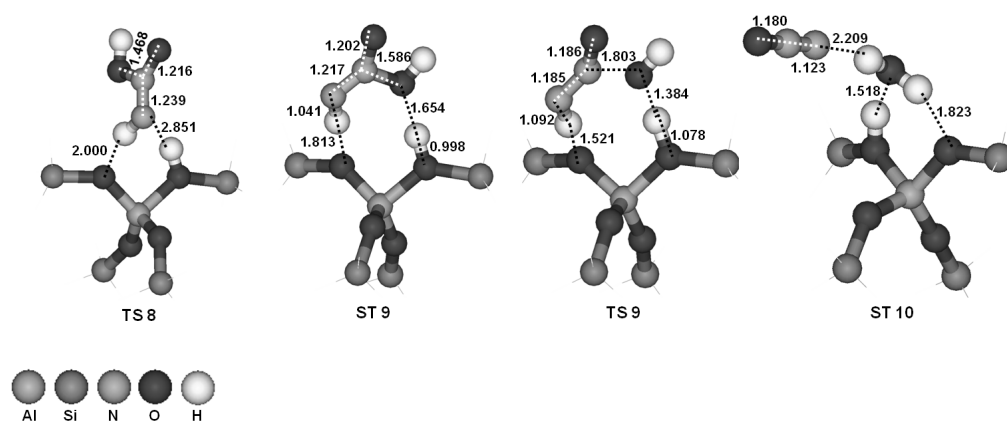


Figure B.23: Geometries of the minima (ST) and the transition states (TS) of the decomposition of NH_2NO_2 over the zeolite cluster. Bond lengths are in Å. Dangling bonds are not shown.

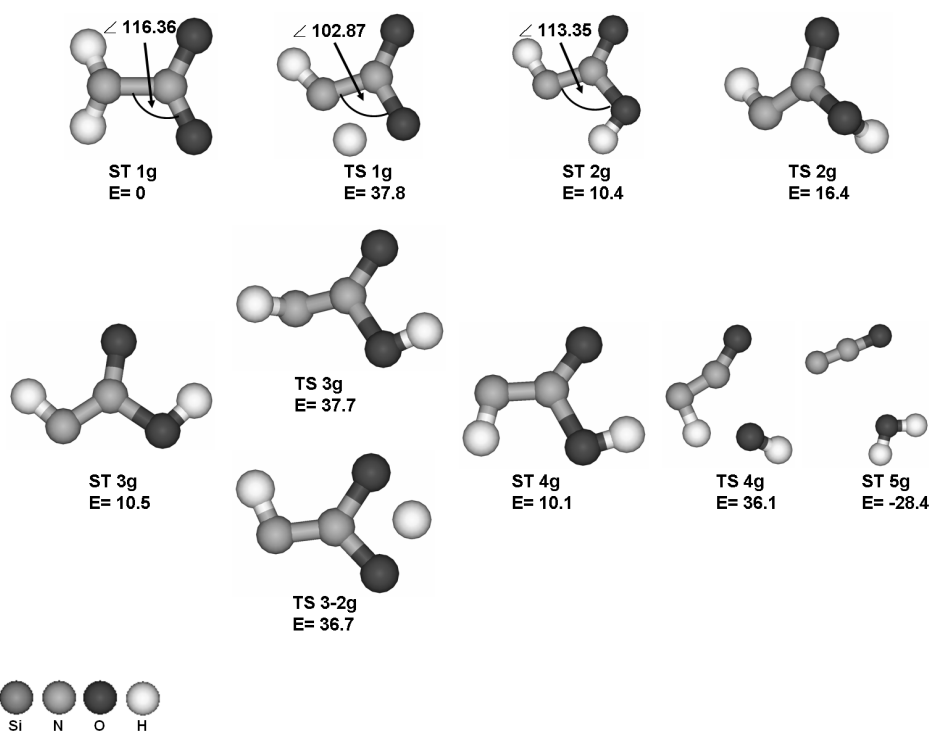


Figure B.24: Geometries of the minima (ST) and the transition states (TS) of the decomposition of NH_2NO_2 in the gas-phase. Energies are in kcal/mol, zero-point corrected and with respect to NH_2NO_2 .

C

Supporting Information for Chapter 5

This appendix contains the structures of the minima, transition states and minimum energy crossing points between two potential energy surfaces corresponding to the discussion of the selective catalytic oxidation on H-form zeolites in chapter 5

C.1 Reaction of NH_3 with O_2

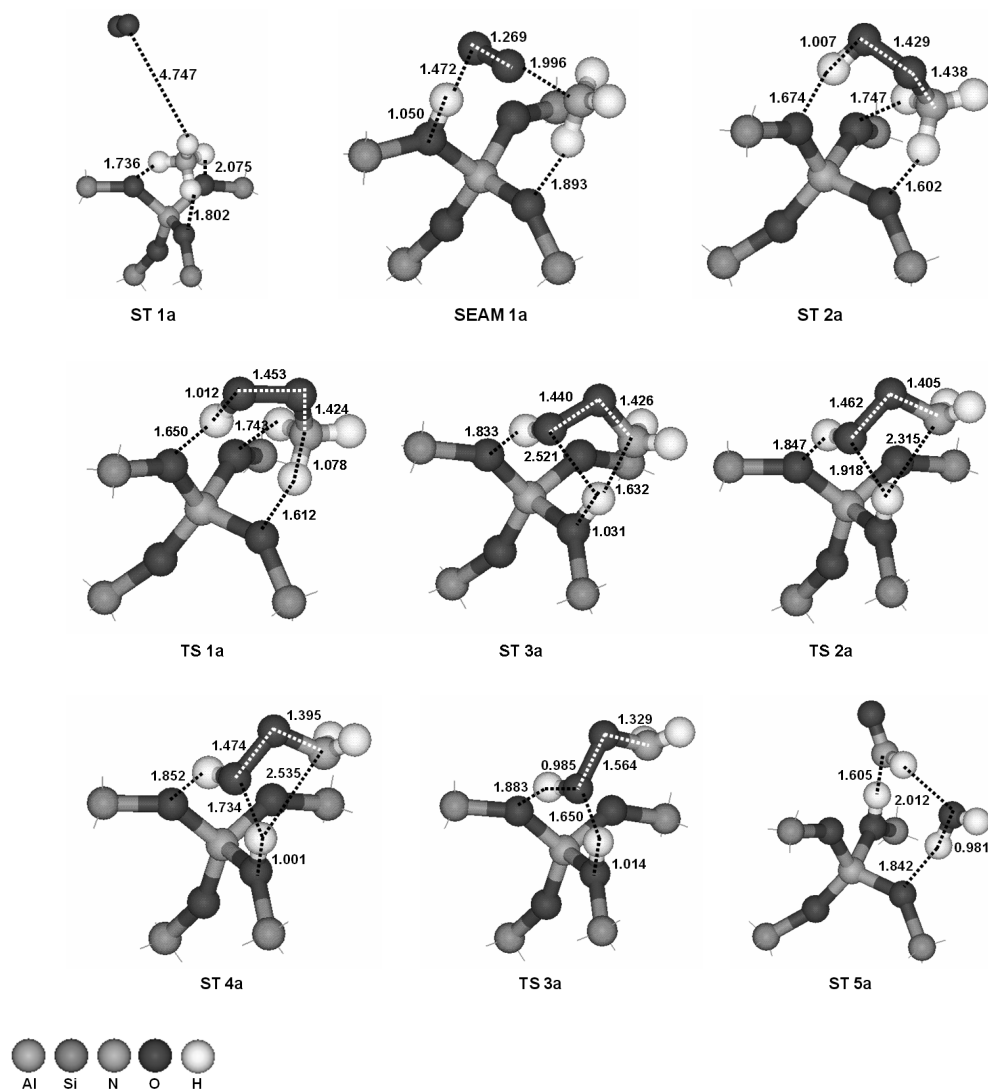


Figure C.1: Geometries of the minima (ST), the transition states (TS) and the minima on the seam of two PESs (SEAM) in the formation of HNO from NH_3 and O_2 over the zeolite cluster. Bond lengths are in Å. Dangling bonds are not shown.

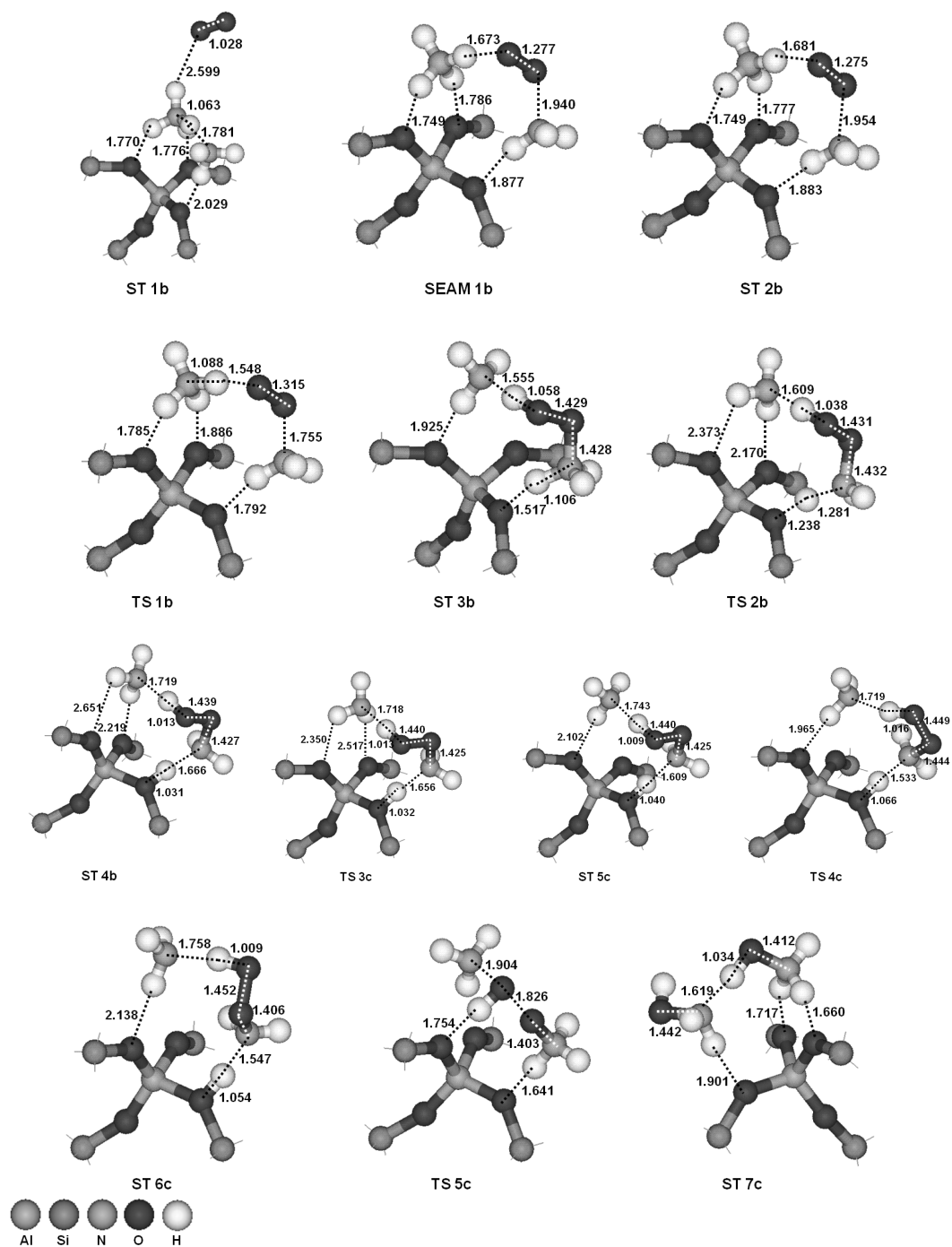


Figure C.2: Geometries of the minima (ST), the transition states (TS) and the minima on the seam of two PESs (SEAM) in the formation of HNO and NH_2OH from $2 \times \text{NH}_3$ and O_2 over the zeolite cluster. Bond lengths are in Å. Dangling bonds are not shown.

C.2 Decay of HNO

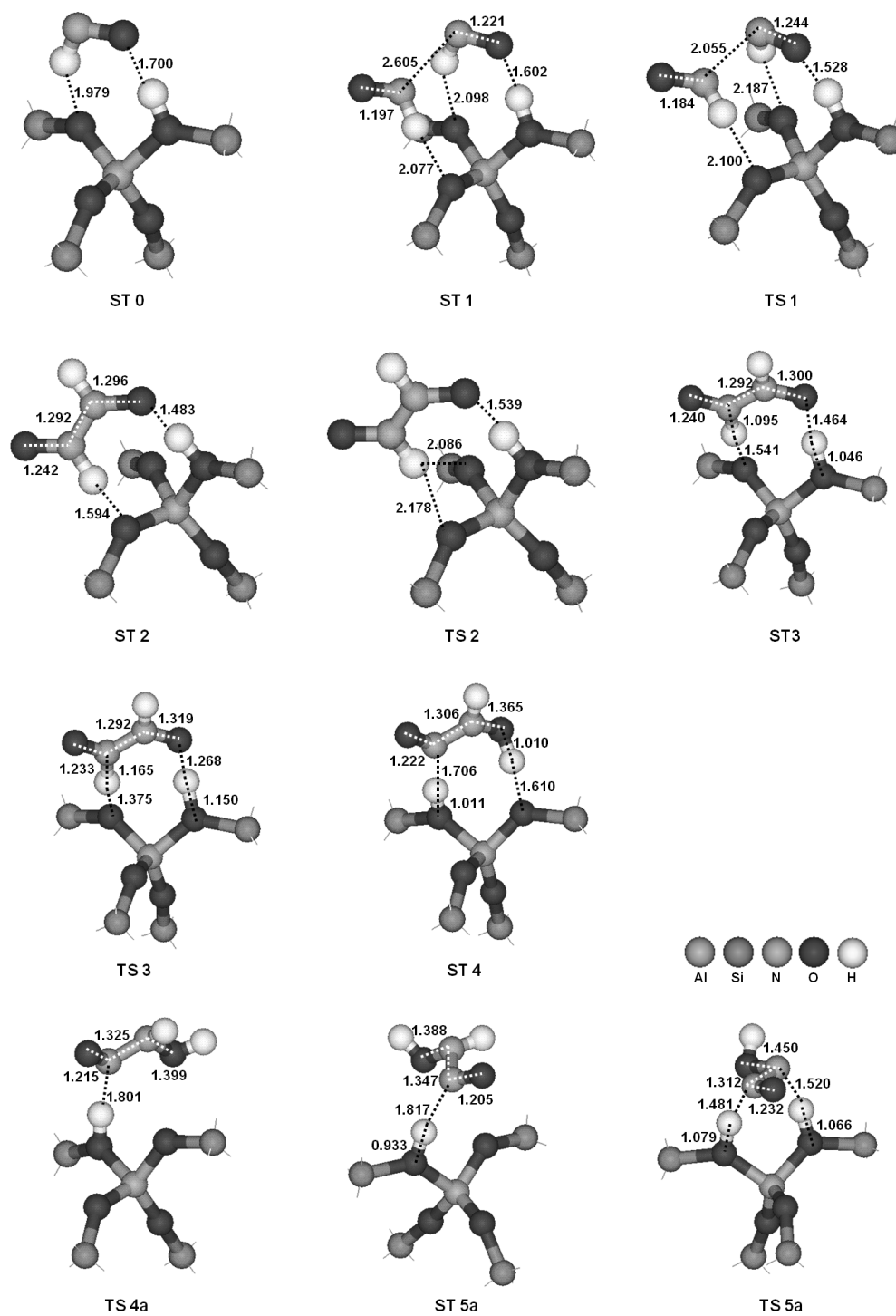


Figure C.3: Part one

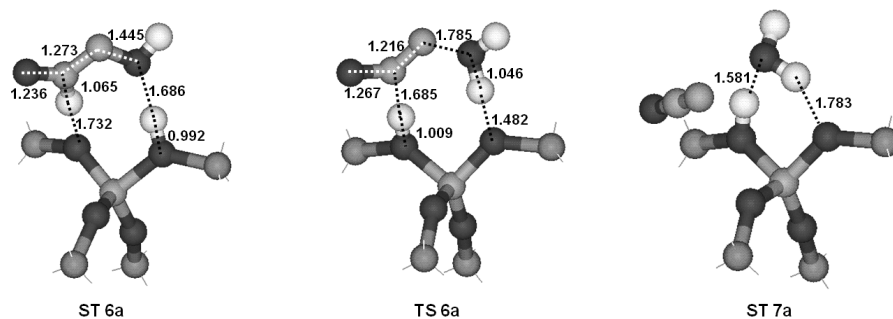


Figure C.3: Geometries of the minima (ST) and the transition states (TS) in the self-reaction of HNO leading to N_2O and H_2O over the zeolite cluster. Bond lengths are in Å. Dangling bonds are not shown.

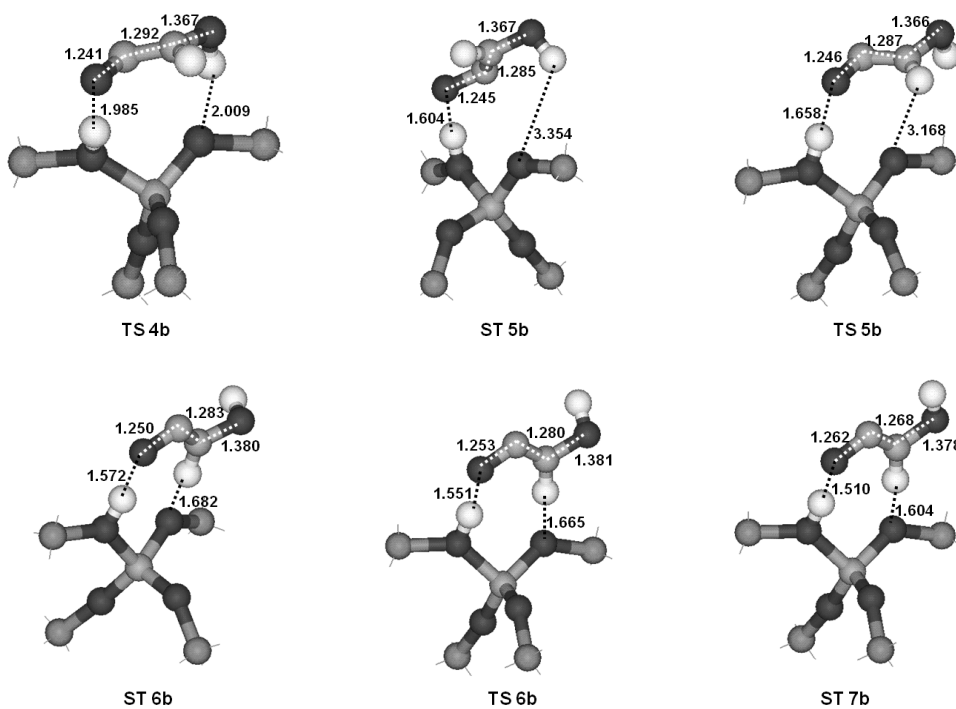


Figure C.4: Part one

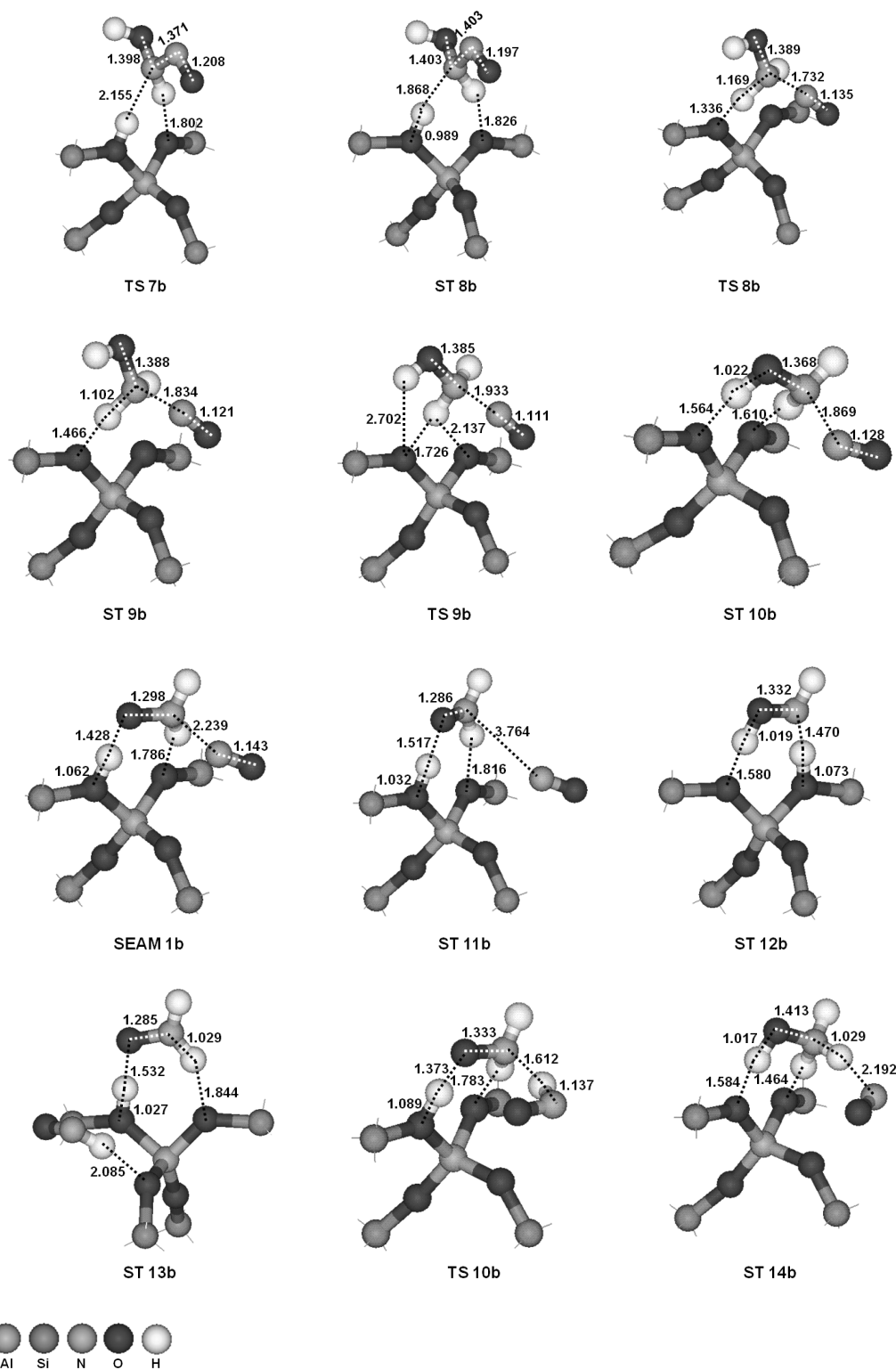


Figure C.4: Geometries of the minima (ST), the transition states (TS) and the minima on the seam of two PESs (SEAM) in the self-reaction of HNO leading to NH₂OH and NO over the zeolite cluster. Bond lengths are in Å. Dangling bonds are not shown.

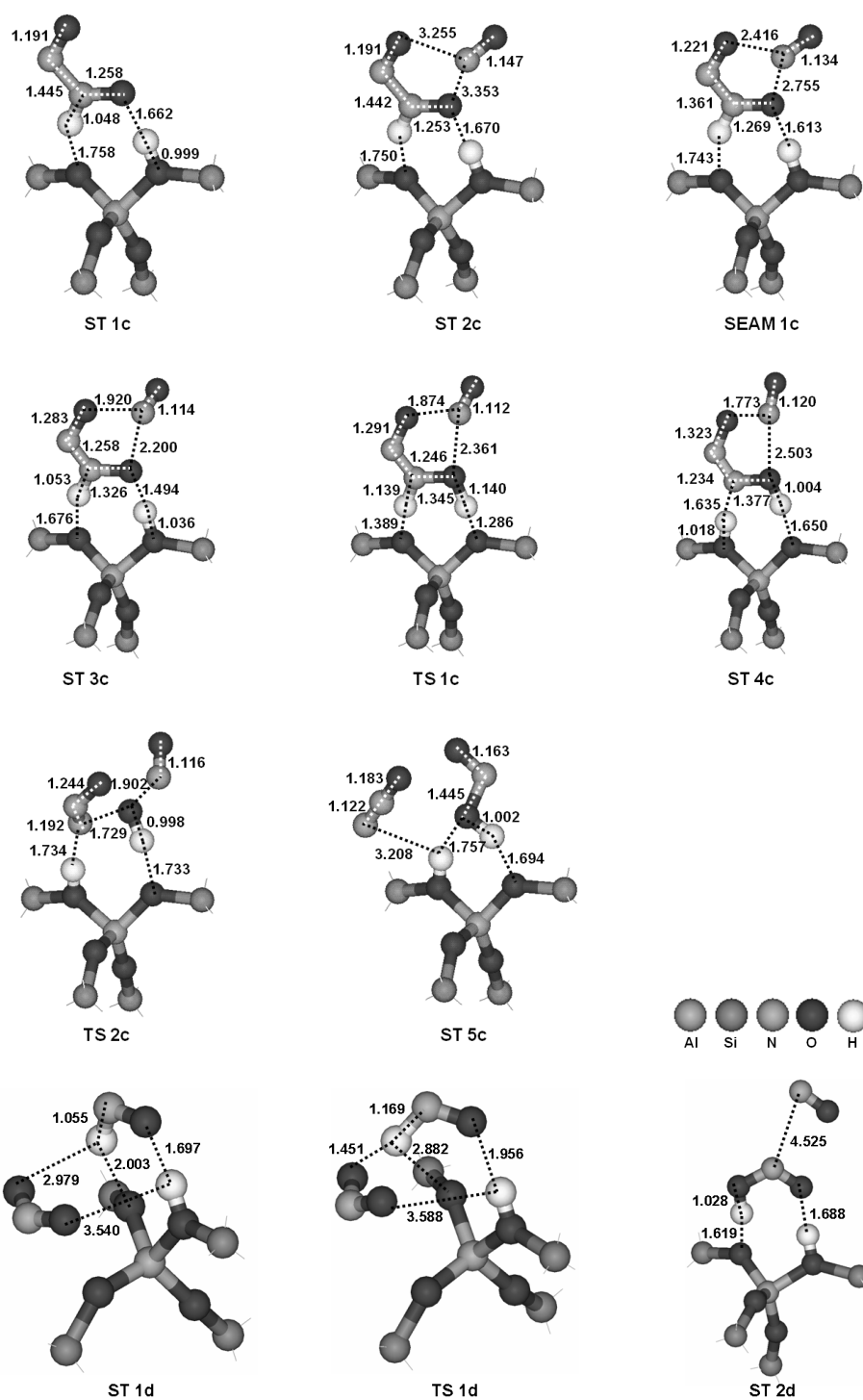


Figure C.5: Geometries of the minima (ST), the transition states (TS) and the minima on the seam of two PESs (SEAM) in the reaction of HNO with 2x NO leading to HONO and N₂O as well as the reaction with NO₂ to HONO and NO over the zeolite cluster. Bond lengths are in Å. Dangling bonds are not shown.

C.3 Decay of NH_2OH

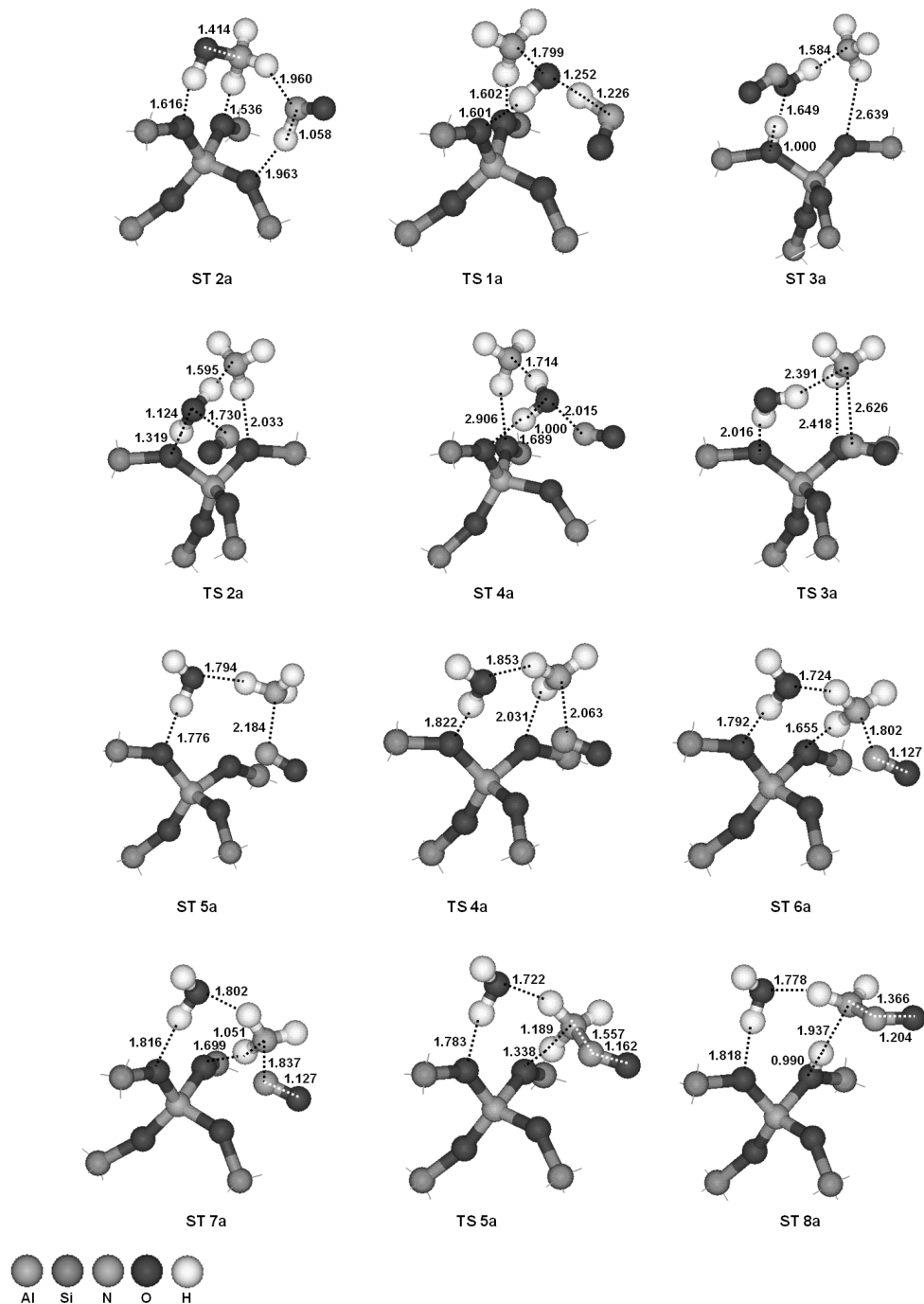


Figure C.6: Geometries of the minima (ST) and the transition states (TS) in the reaction of NH_3OH^+ with HNO over the zeolite cluster. Bond lengths are in Å. Dangling bonds are not shown.

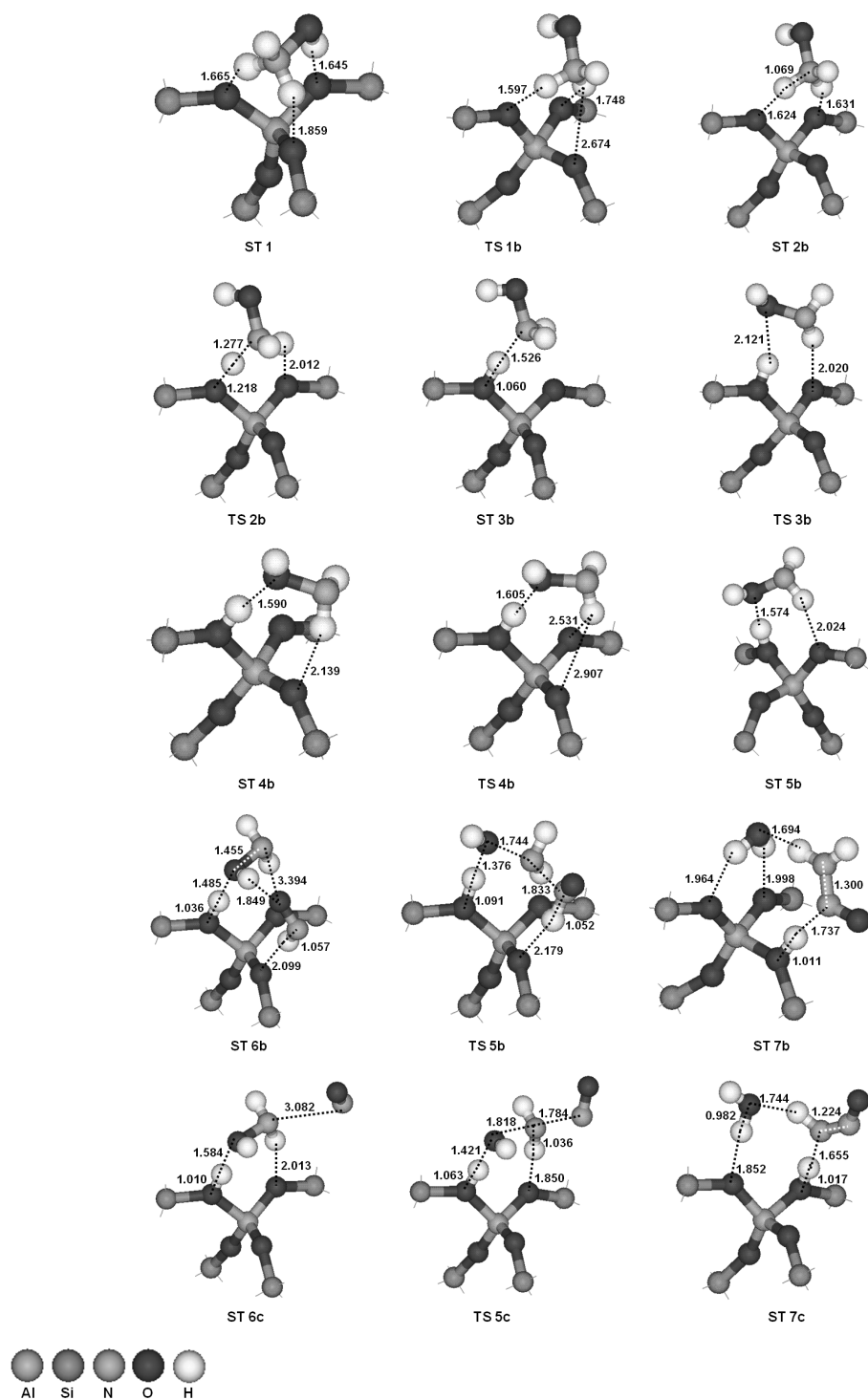


Figure C.7: Geometries of the minima (ST) and the transition states (TS) in the rotation of NH_2OH and its reactions with HNO and NO over the zeolite cluster. Bond lengths are in Å. Dangling bonds are not shown.

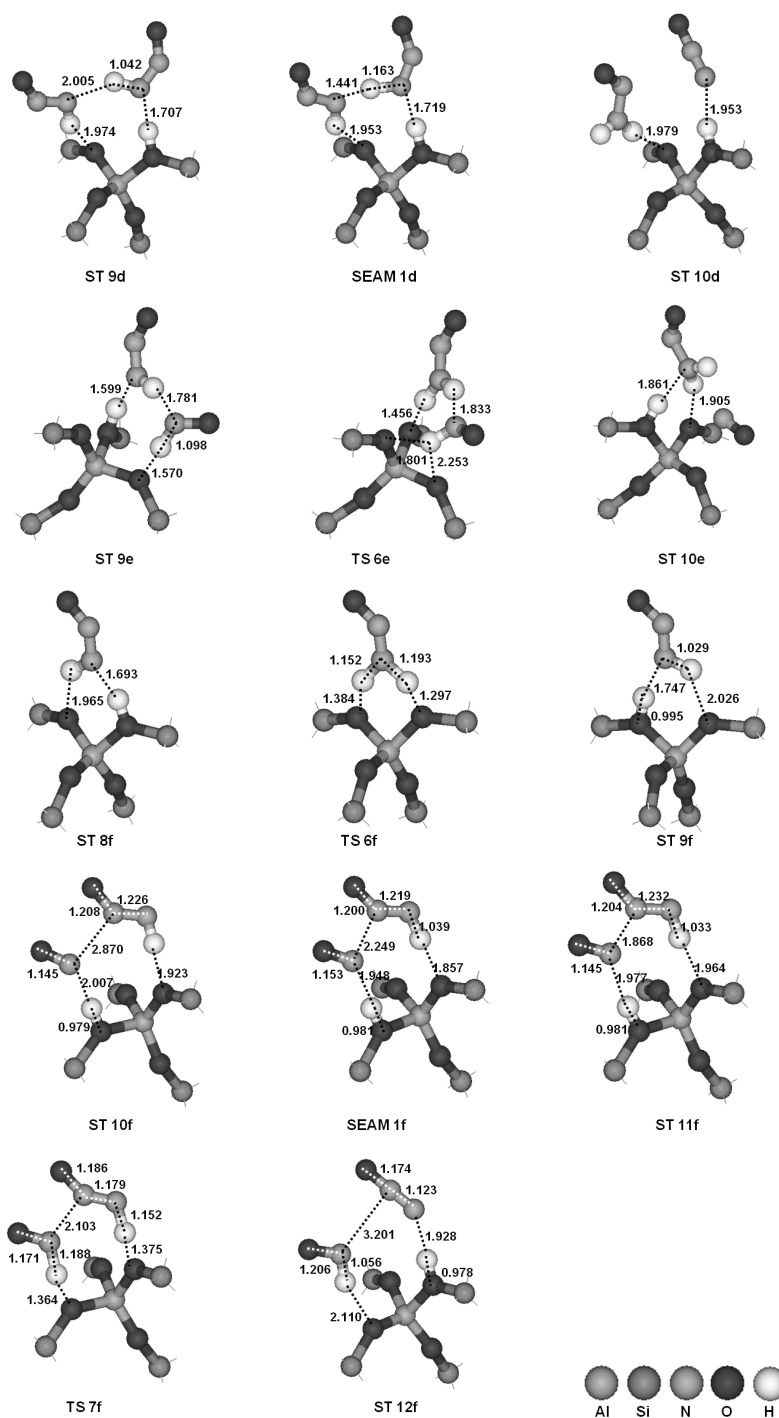


Figure C.8: Geometries of the minima (ST), the transition states (TS) and the minima on the seam of two PESs (SEAM) in the self-reaction of HNNO and the reactions of HNNO with HNO and NO over the zeolite cluster. Bond lengths are in Å. Dangling bonds are not shown.

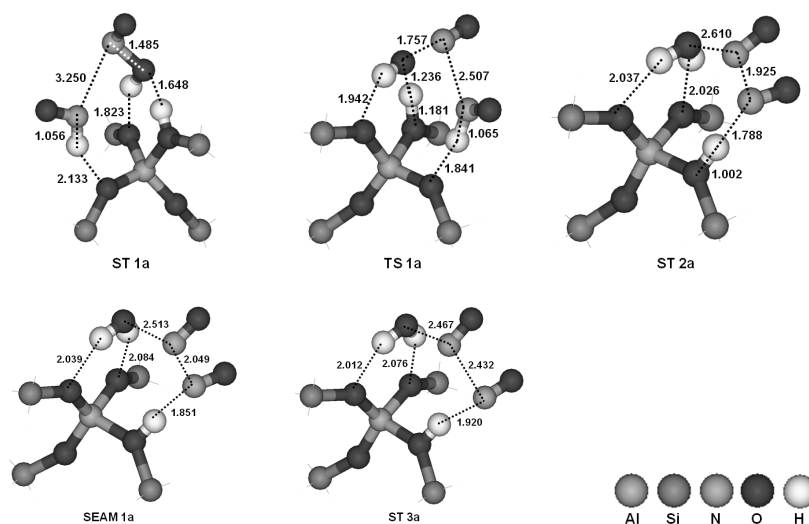
HNO with HONO and HNO_3 

Figure C.9: Geometries of the minima (ST), the transition state (TS) and the minimum on the seam of two PESs (SEAM) of the reaction of HNO with trans-HONO over the zeolite cluster. Bond lengths are in Å. Dangling bonds are not shown.

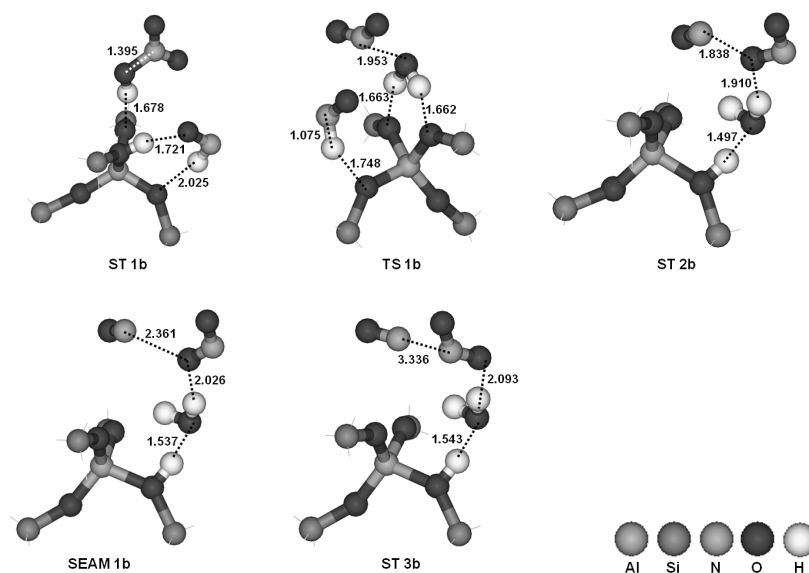


Figure C.10: Geometries of the minima (ST), the transition state (TS) and the minimum on the seam of two PESs (SEAM) of the reaction of HNO with HNO_3 over the zeolite cluster. Bond lengths are in Å. Dangling bonds are not shown.

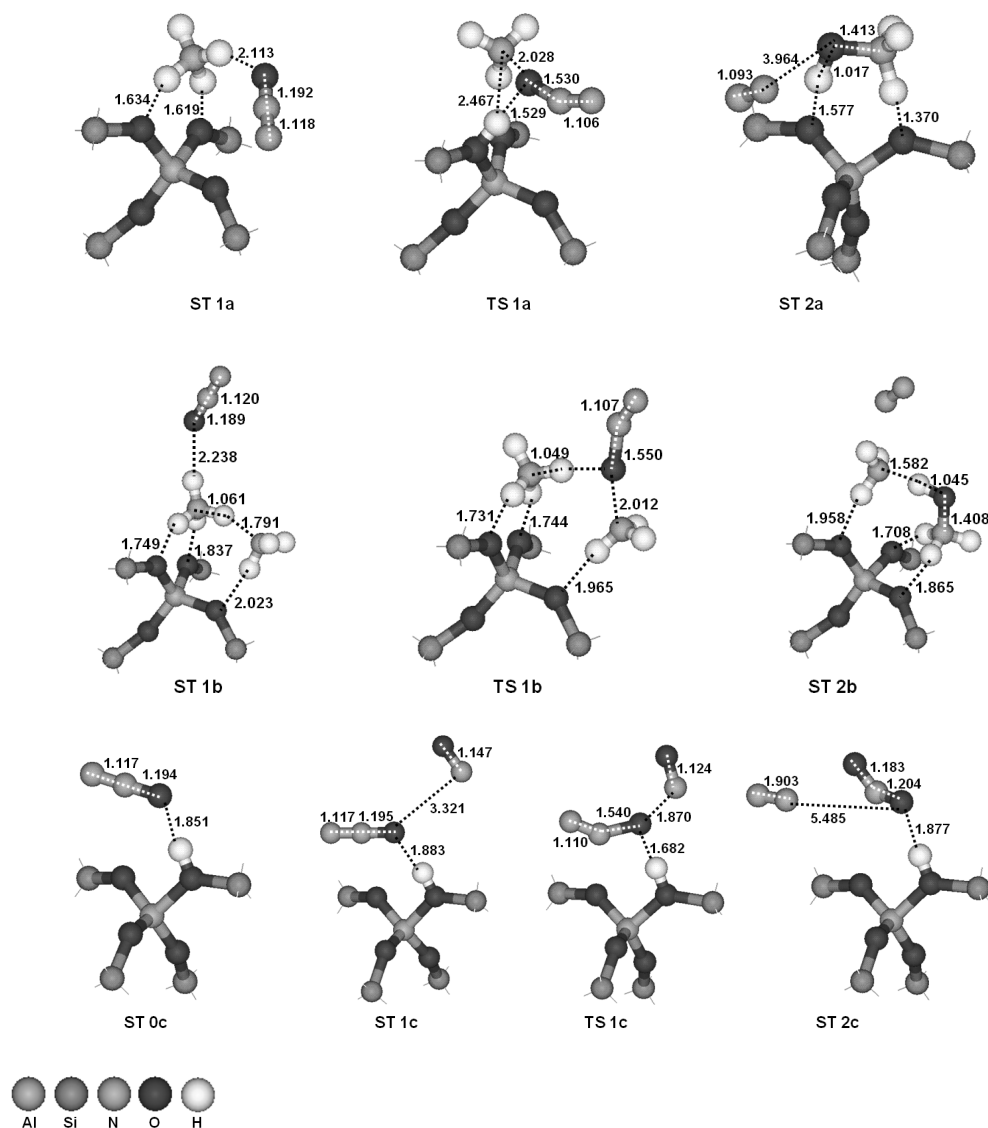
Decay of N_2O 

Figure C.11: Geometries of the minima (ST) and the transition states (TS) of the reactions of N_2O with one and with two ammonia molecules and with NO over the zeolite cluster. Bond lengths are in Å. Dangling bonds are not shown.

D

Supporting Information for Chapter 6

In this section the reaction rate expressions, the thermodynamic data and an overview on the assignment of the heat of formation for all surface species are presented.

Table D.1: Documentation of assignment of the heat of formations of the surface species.

Structure (S)	Cluster E _{elec}	van der Waals	Reference state		Modifications					
			Gas	Site (S)	vdW	ref_add	Enthalpy [kcal/mol] t23_add	extra	Sum	Entropy add [cal/mol/K]
NH3	T23	T23	NH3	H	-5.87		-7.7	2.5	-11.07	3
NH3x2	T23	T23	2x NH3	H	-12.80		-9.8	3.5	-19.10	
NH3x3	T23	T23	3x NH3	H	-19.59		-11.7	1	-30.29	
NH3.NO2	T23	T23	NO2	H	-10.56		-7.7		-18.26	3
HONO	T5	T23	HONO	H	-6.19				-6.19	3
HNO3	T5	T23	HNO3	H	-7.57				-7.57	3
HNO	T5	T23	HNO	H	-5.58				-5.58	3
H2O	T23	T23	H2O	H	-4.39		-3.3		-7.69	
NH2OH	T23	T23	NH2OH	H	-9.31		-5.7		-15.01	
NH2NO	T5	T23	NH2NO	H	-9.14				-9.14	
NH2NO_X	T5	from NH2NO	NH2NO	H	-9.14				-9.14	
NH2NO2	T5	T23	NH2NO2	H	-10.12				-10.12	
NH2NO2_X	T5	from NH2NO2	NH2NO2	H	-10.12				-10.12	
H2O_N2	T5	T5 on H2O	N2	H2O	-0.87	-4.39			-5.26	
H2O_N2O	T5	T5 on H2O	N2O	H2O	-0.90	-4.39			-5.28	
NH3_NH2NO	T5	T5 NH3 on NH2NO	NH2NO	NH3	-3.67	-9.14			-12.81	
NH3_NH2NO2	T5	T5 NH3 on NH2NO2	NH2NO2	NH3	-3.46	-10.12			-13.58	
NO2	T5	T23	NO2	H	-4.81				-4.81	4
NO2.NO	T5	T23	NO2, NO	H	-7.60				-7.60	9
asN2O3	T5	T23	asN2O3	H	-8.78				-8.78	7
ctN2O3	T5	from asN2O3	ctN2O3	H	-8.78				-8.78	7
NO2.NO2	T23	T23	2 NO2	H	-9.35		-1.70	-3	-14.05	12
asN2O4	T5	T23	asN2O4	H	-12.65			-3	-15.65	10
symN2O4	T5	from asN2O4	symN2O4	H	-12.65				-12.65	10
NO2O2N	T5	T23	NO2O2N	H	-8.15				-8.15	10
NOZ	T23	T23	-NH2NO + NH3	H	-2.49		-2.5		-4.99	
NOZ_HONO	T5	T23	t-HONO	NOZ	-8.44	-2.49		-3	-13.92	5
NOZ_HNO3	T5	T23	HNO3	NOZ	-10.49	-2.49		-4	-16.98	5
NOZ_NH3	T23	T23	NH3	NOZ	-7.23	-2.49	-6.9		-16.61	4
NOZ_H2O	T23	T23	H2O	NOZ	-5.73	-2.49	-3.7		-11.91	4
NO	T5	T5	NO	H	-2.04				-2.04	
O2	T5	T23	O2	H	-2.64				-2.64	3
OONO	T5	T23	OONO	H	-6.01				-6.01	5

Table D.1: (continued)

Structure (S)	Cluster E _{elec}	van der Waals	Reference state		Modifications				
			Gas	Site (S)	vdW	Enthalpy [kcal/mol]		Sum	Entropy add [cal/mol/K]
OONO_NO	T5	from ONOONO	NO	ONOO	-8.96		-2	-10.96	10
ONOONO	T5	T23	ONOONO	H	-8.96			-8.96	10
NH3.asN2O4	T23	T23	asN2O4	NH3	-16.34			-20.04	7
NH3.asN2O4_ST3b	T5	T5 on NOZ_NH3	HNO3	NOZ_NH3	-3.69	-9.71		-13.40	
NH2NO_HNO3	T5	T5 on NH2NO	NH2NO, HNO3	H	-3.23	-9.14		-12.37	
NH3.symN2O4	T5	from NH3.asN2O4	NH3, symN2O4	H	-16.34			-20.04	7
symN2O4_ST3	T5	T5 on NH3	NH3, symN2O4	H	-2.46	-5.87		-12.03	
symN2O4_ST4	T5	T5 on NH2NO2	HONO, NH2NO2	H	-2.22	-10.12		-12.34	
NH2NO2_HONO	T5	T5 on NH2NO2	HONO, NH2NO2	H	-2.33	-10.12		-12.44	
NH3.asN2O3	T23	T23	asN2O3, NH3	H	-14.54			-18.10	7
asN2O3_ST3	T5	T5 on asN2O3	asN2O3, NH3	H	-1.88	-8.78		-14.22	
NH2NO_HONO	T5	T5 on NH2NO	NH2NO, HONO	H	-2.46	-9.14		-11.60	
ctN2O3_10c	T5	T5 on NOZ_NH3	NOZ_NH3, HONO	H	-3.82	-9.71		-13.53	
NH3_HONO	T23	T23	NH3, t-HONO	H	-15.32			-17.83	
NH3_HONO.2	T5	T5 +(T23-T5) ST1	NH3, t-HONO	H	-8.00	-6.34		-16.86	
NH4NO2	T5	T5 +(T23-T5) ST1	NH4NO2	H	-5.93	-6.34		-14.78	
NH3_HONO.4	T5	T5 +(T23-T5) ST1	NH3	NOZ_H2O	-9.85	-6.34		-16.20	
NH3_HONO.5	T5	T5 on NOZ_NH3	H2O	NOZ_NH3	-1.80	-9.71		-11.52	
NH3_HONO.6	T5	T5 on NOZ_NH3	H2O	NOZ_NH3	-2.91	-9.71		-12.62	
NH3_HNO3	T23	T23	NH3, HNO3	H	-14.39			-20.71	
NH3_HNO3.2	T5	from ST1	NH3, HNO3	H	-14.39			-20.71	
NH4NO3	T5	from ST1	NH3, HNO3	H	-14.39			-20.71	
NH2NO2_H2O	T5	T5 on NH2NO2	NH2NO2, H2O	H	-3.31	-10.12		-13.43	

Table D.1: (continued)

Structure (S)	Cluster E _{elec}	van der Waals	Gas	Reference state		vdW	Modifications				Entropy add [cal/mol/K]
				Site (S)	Gas		ref_add	t23_add	extra	Sum	
HONO_2a	T5	T5 on HONO	2xt-HONO	H		-2.41	-6.19			-8.60	
H2O_N2O3.a	T5	T5	H2O, asN2O3	H		-4.53				-4.53	
HONO_2b	T5	T5 on HONO	2xt-HONO	H		-3.53	-6.19			-9.72	
HONO_2b-2	T5	T5 on HONO	2xt-HONO	H		-5.87	-6.19			-12.06	
H2O_N2O3.b	T5	T5 on Z.H2O	2xt-HONO	H		-4.45	-4.39			-8.84	
HONO_HNO3	T5	T5 on HNO3	t-HONO, HNO3	H		-2.57	-7.57			-10.14	
HNO3_HONO_3	T5	T5 on H2O	H2O, asN2O4	H		-4.90	-6.19	-3.25		-14.35	
HNO3_HONO_4	T5	T5 on H2O	H2O, asN2O4	H		-4.90	-5.65	-3.25		-13.80	
H2O_asN2O4	T5	T5 on H2O	H2O, asN2O4	H		-4.90	-2.40	-3.25		-10.56	
HNO3x2	T5	T5 on HNO3	2 HNO3	H		-4.38	-7.57			-11.95	
H2O_N2O5	T5	T5 on H2O	H2O, N2O5	H		-4.90	-4.39	-3.25		-12.54	
N2O5	T5	T5 +(T23-T5) asN2O4	N2O5	H		-5.77	-5.26			-11.03	7
NH3_N2O5	T5	T5 on NH3	NH3, N2O5	H		-3.37	-5.87	-3.70		-12.94	
NH2NO2.HNO3	T5	T5 on NH3 on	HNO3, NH2NO2	H		-3.51	-10.12			-13.63	
ZNO2	T5	NH2NO2	-NH2NO2 + NH3	H		-4.23				-4.23	
ZNO2.HONO	T23	T23	HONO	ZNO2		-6.92	-4.23	3.06		-8.09	4
ZNO2.H2O	T23	T23	H2O	ZNO2		-4.74	-4.23	-2.90	-3	-14.87	5
ZNO2.NH3	T23	T23	NH3	ZNO2		-5.60	-4.23	-5.82	-3	-18.65	5
HONO_HNO	T5	T5 on HONO	HONO, HNO	H		-3.01	-6.19			-9.21	
N2O2.H2O	T5	from HONO_HNO	HONO, HNO	H							
HNO_HNO3	T5	T5 on HNO3	HNO, HNO3	H		-3.86	-7.57			-11.43	
H2O.ctN2O3	T5	T5 on H2O	HNO, HNO3	H		-3.70	-4.39			-8.09	
NH3OOH+	T23	T23	HNO, H2O	H		-10.98		-5.58		-16.56	3
NH2OOH	T5	T5 + NH3OOH	HNO, H2O	H		-10.25		-5.58		-15.83	
HNO.H2O	T5	T23-T5 T5 HNO on H2O	HNO, H2O	H		-3.21	-4.39	-3.25		-10.85	
NH3x2_O2	T5	T5 O2 on 2xNH3	O2	NH3x2		-1.68	-12.80			-14.48	
NH3_NH3OOH	T5	T5 O2 on 2xNH3	O2	NH3x2		-2.47	-12.80			-15.28	

Table D.1: (continued)

Structure (S)	Cluster E _{elec}	van der Waals	Gas	Reference state		Modifications			
				Site (S)	vdW	Enthalpy ref_add	t23_add	extra	Sum
NH3_NH2OOH	T5	T5 O2 2xNH3 on	O2	NH3x2	-2.04	-12.80			-14.84
NH3_NH2OOH_2	T5	T5 O2 2xNH3 on	O2	NH3x2	-1.72	-12.80			-14.52
NH2OHx2	T5	T5 O2 2xNH3 on	NH2OH	NH2OH	-2.28	-12.80			-15.08
HN0x2	T5	T5 HNO HNO on	2 HNO	H	-3.63	-5.58		-2	-11.21
HN0x2.2	T5	T5 HNO HNO on	2 HNO	H	-3.60	-5.58			-9.18
HN0x2.3	T5	T5 HNO HNO on	2 HNO	H	-2.92	-5.58			-8.50
HN0x2.4	T5	T5 HNO HNO on	2 HNO	H	-2.96	-5.58			-8.54
HN0x2 5a	T5	T5 HNO HNO on	2 HNO	H	-1.92	-5.58			-7.50
HN0x2 6a	T5	T5 HNO HNO on	2 HNO	H	-2.34	-5.58			-7.93
HN0x2 7b	T5	T5 HNO HNO on	2 HNO	H	-2.44	-5.58			-8.03
HN0x2 8b	T5	T5 HNO HNO on	2 HNO	H	-2.21	-5.58			-7.79
HN0x2 9b	T5	T5 HNO HNO on	2 HNO	H	-4.37	-5.58			-9.95
HN0x2_10b	T5	T5 HNO HNO on	2 HNO	H	-5.50	-5.58			-11.08
HNOH	T5	T5 HNO HNO +NO on	NO -HNO	NH2OH	-1.07	-5.58			-6.65
HNOH_HNO	T5	T5 HNO HNOH on	HNO	HNOH	-2.70	-6.65			-9.35
NH2OH_NO	T5	T5 NO NH2OH on	NO	NH2OH	-0.29	-9.31			-9.60
HN0x2 5f	T5	T5 HNO HNO on	2 HNO	H	-2.55	-5.58			-8.13
HNO_NO	T5	T5 NO HNO on	HNO,NO	H	-2.52	-5.58			-8.10

Table D.1: (continued)

Structure (S)	Cluster E _{elec}	van der Waals	Reference state		Modifications					
			Gas	Site (S)	vdW	Enthalpy [kcal/mol]	extra	Sum	Entropy add [cal/mol/K]	
HNONO	T5	T5 NO on HNO	HNO, NO	H	-1.24	-5.58			-6.82	
HNO ₂ NO	T5	T5 2NO on HNO	HNO, 2NO	H	-3.14	-5.58			-8.73	
HNO ₂ NO ₂	T5	T5 2NO on HNO	HNO, 2NO	H	-2.94	-5.58			-8.52	
NH ₂ OH 2	T5	T5 + NH ₂ OH T23-T5		NH ₂ OH	-5.41	-2.28			-7.69	
NH ₂ OH 3	T5	T5 + NH ₂ OH T23-T5		NH ₂ OH	-4.39	-2.28			-6.67	
NH ₂ OH 4	T5	T5 + NH ₂ OH T23-T5		NH ₂ OH	-5.02	-2.28			-7.30	
NH ₂ OH 5	T5	T5 + NH ₂ OH T23-T5		NH ₂ OH	-4.26	-2.28			-6.55	
NH ₃ OH+HNO NH ₂ OH.HNO	T23	T23 T5 NH ₃ OH+HNO T23-T5	NH ₂ OH, HNO HNO	H	-15.10		-7.15	-3	-25.24	3
	T5			NH ₂ OH	-7.73	-6.41			-14.14	
NH ₂ NO.H ₂ O _b H ₂ O.c-HNNO	T5	T5 on NH ₂ NO T5 on H ₂ O	NH ₂ NO	H ₂ O	-3.46	-9.14			-12.60	
	T5		c-HNNO	H ₂ O	-2.55	-4.39			-6.93	
c-HNNO	T5	T5	c-HNNO	H	-3.61				-3.61	
2xc-HNNO	T5	T5	c-HNNOx2	H	-6.12				-6.12	
NH ₂ NO.N ₂ O	T5	T5 on NH ₂ NO	NH ₂ NO, N ₂ O	H	-1.56	-9.14			-10.70	
HNNO.HNO	T5	T5 on HNO	c-HNNO, HNO	H	-3.96	-5.58			-9.54	
HNNO.NO	T5	T5	c-HNNO, NO	H	-5.53				-5.53	
HNNO.NO ₂	T5	T5	c-HNNO, NO	H	-5.86				-5.86	
NH ₃ .N ₂ O	T5	T5 on NH ₃	N ₂ O	NH ₃	-2.07	-5.87			-7.94	
NH ₃ x2.N ₂ O	T5	T5 on 2xNH ₃	N ₂ O	NH ₃ x2	-0.76	-12.80			-13.56	
NH ₂ OH.NH ₃ N ₂ O	T5	T5 on NH ₂ OH	NH ₂ OH	NH ₃	-2.93	-9.31			-12.24	3
	T5	T5	N ₂ O	H	-2.45				-2.45	

Comments on Table D.1

The column “Cluster” refers to the DFT calculation executed on either the 5 or the 23 T-atoms containing cluster.

In the column “van der Waals” the reference state is stated for which the Grimme add term is calculated. This includes some approximations in the case that no T23 calculation was available. Statements with “from” imply that the vdW energy was taken from a related or similar species. Statements with “T5 on” imply a T5 based vdW energy calculated as the difference of a gas-phase species with respect to the stated reference species, for which a T23 calculation is available. The complete vdW contribution includes then the T5 term plus the T23 addition from the reference state (column ref_add). Finally, the statement “T5 + species T23-T5” implies a comparison of the T5 vdW energies of related structures. To the T5 vdW energy of the species of interest, the difference of the T23 and T5 vdW energy of the related structure is added (column ref_add).

The two columns “Gas” and “Site” define the reference state for the calculation of the heat of formation of the surface species. In case of a surface site other than “H”, which stands for the void active site, the definition of the heat of formation is defined with respect to the adsorption of the stated gas-phase species on the stated surface species. This implies an indirect correction of the heat of formation because via the referencing surface species a T23 cluster contribution is inserted.

In the column “t23_add” either the T23-T5 difference is stated as calculated from DFT (see column “E_{elec}”, it should state T23) or a contribution from a similar structure or potential reference structure is added.

In the column “Extra” the modifications during the fine tuning of the model are stated.

In the column “Entropy” approximated modifications of the entropy of the surface species are stated based on restricted translation and rotation (compare Reyniers et al. [262] and description in section 6.2).

Table D.2: Electronic energy differences for the heat of formation of selected surface species between the 23 T-atoms and the 5 T-atoms containing cluster.

Species [S]	$\Delta T23-T5$ [kcal/mol]	Species [S]	$\Delta T23-T5$ [kcal/mol]
NH3	-7.7	NOZ_HONO	-0.3
NH3x2	-9.8	NOZ_HNO3	1.7
NH3x3	-11.7	NOZ_NH3	-6.9
NH3_NO2	-7.7	NOZ_H2O	-3.7
HONO	-0.7	O2	-0.1
HNO3	1.2	OONO	-0.3
HNO	0.1	ONOONO	-2.2
H2O	-3.3	NH3_asN2O4	-3.7
NH2OH	-5.7	NH3_asN2O3	-3.6
NH2NO	-0.5	NH3_HONO	-2.5
NH2NO2	0.7	NH3_HNO3	-6.3
NO2	0.8	ZNO2	-0.6
NO2_NO	0.8	ZNO2_HONO	3.1
asN2O3	0.6	ZNO2_H2O	-2.9
NO2_NO2	-1.7	ZNO2_NH3	-5.8
asN2O4	3.8	NH3OOH+	-5.6
NO2O2N	0.2	NH3OH+_HNO	-7.1
NOZ	-2.5		

Table D.3: Reaction rates of gas phase and surface reactions.

Reactant	Product	A [1/s]	β [-]	E _a [kcal/mol]	Adjust A x E _a
Gas phase Reactions					
asN2O3	\rightleftharpoons NO + NO2	3.729E+12	1	9.08	10
ctN2O3	\rightleftharpoons NO + NO2	1.692E+12	1	5.55	10
asN2O4	\rightleftharpoons NO2 + NO2	2.256E+12	1	13.81	10 -5
symN2O4	\rightleftharpoons NO2 + NO2	7.577E+13	1	12.36	10 -5
NH4NO2	\rightleftharpoons NH3 + HONO	2.084E+10	1	9.62	
NH4NO3	\rightleftharpoons NH3 + HNO3	2.084E+10	1	12.80	
General Adsorption					
NH3(S) + HZSM5(B)	\rightleftharpoons HZSM5(S) + NH3	2.084E+10	1	32.00	
NH3x2(S)	\rightleftharpoons NH3(S) + NH3	2.084E+10	1	23.45	
NH3x3(S)	\rightleftharpoons NH3x2(S) + NH3	2.084E+10	1	15.85	
NH3_NO2(S)	\rightleftharpoons NH3(S) + NO2	2.084E+10	1	7.25	
HONO(S) + HZSM5(B)	\rightleftharpoons HZSM5(S) + HONO	2.084E+10	1	17.66	
H2O(S) + HZSM5(B)	\rightleftharpoons HZSM5(S) + H2O	2.084E+10	1	22.01	
HZSM5(B) + HNO3(S)	\rightleftharpoons HZSM5(S) + HNO3	2.084E+10	1	19.52	
HNO(S) + HZSM5(B)	\rightleftharpoons HZSM5(S) + HNO	2.084E+10	1	14.71	
HZSM5(B) + NH2OH(S)	\rightleftharpoons HZSM5(S) + NH2OH	2.084E+10	1	35.68	
HZSM5(B) + NH2NO(S)	\rightleftharpoons HZSM5(S) + NH2NO	2.084E+10	1	25.43	

Table D.3: (continued)

Reactant		Product	A [1/s]	β [-]	E _a [kcal/mol]	Adjust A x E _a	
HZSM5(B) + NH2NO2(S)	\rightleftharpoons	HZSM5(S) + NH2NO2	2.084E+10	1	25.69		
NH2NO _{alt} (S) + HZSM5(B)	\rightleftharpoons	HZSM5(S) + NH2NO	2.084E+10	1	15.24		
NH2NO2 _{alt} (S) + HZSM5(B)	\rightleftharpoons	HZSM5(S) + NH2NO2	2.084E+10	1	18.67		
NO2(S) + HZSM5(B)	\rightleftharpoons	HZSM5(S) + NO2	2.084E+10	1	8.24		
NH3_NH2NO(S)	\rightleftharpoons	NH3(S) + NH2NO	2.084E+10	1	18.51		
NH3_NH2NO(S)	\rightleftharpoons	NH2NO(S) + NH3	2.084E+10	1	20.90		
NH3_NH2NO2(S)	\rightleftharpoons	NH3(S) + NH2NO2	2.084E+10	1	18.33		
NH3_NH2NO2(S)	\rightleftharpoons	NH2NO2(S) + NH3	2.084E+10	1	21.10		
NO oxidation							
NO(S) + HZSM5(B)	\rightleftharpoons	HZSM5(S) + NO	2.084E+10	1	4.85		
O2(S) + HZSM5(B)	\rightleftharpoons	HZSM5(S) + O2	2.084E+10	1	3.42		
ONOO(S)	\rightleftharpoons	O2(S) + NO	2.084E+10	1	2.16		
ONOO(S)	\rightleftharpoons	NO(S) + O2	2.084E+10	1	2.16		
ONOO_NO(S)	\rightleftharpoons	ONOO(S) + NO	2.084E+10	1	2.95		
ONOOONO(S)	\rightleftharpoons	ONOO_NO(S)	3.424E+12	1	15.03	10	
ONOOONO(S)	\rightleftharpoons	NO2O2N(S)	1.553E+13	0	5.79		
NO2O2N(S)	\rightleftharpoons	NO2(S) + NO2	2.084E+10	1	0.71		
fast SCR and NO₂ SCR							
NO2_NO(S)	\rightleftharpoons	NO2(S) + NO	2.084E+10	1	8.10		
NO2_NO(S)	\rightleftharpoons	asN2O3(S)	4.232E+10	0	1.43	10	
NO2_NO(S)	\rightleftharpoons	ctN2O3(S)	6.939E+11	0	4.63	10	
asN2O3(S)	\rightleftharpoons	NOZ_HONO(S)	2.084E+10	1	6.05		
ctN2O3(S)	\rightleftharpoons	NOZ_HONO(S)	1.749E+12	0	0.36		
NOZ_HONO(S)	\rightleftharpoons	HONO + NOZ(S)	2.084E+11	1	11.14	10	-7
NOZ_NH3(S)	\rightleftharpoons	NH3 + NOZ(S)	2.084E+11	1	22.89	10	-2
NOZ_H2O(S)	\rightleftharpoons	H2O + NOZ(S)	2.084E+10	1	18.30		
NOZ_NH3(S)	\rightleftharpoons	NH2NO _{alt} (S)	9.614E+12	0	2.96		
NOZ_H2O(S)	\rightleftharpoons	HONO(S)	3.229E+12	0	1.46		
NO2_NO2(S)	\rightleftharpoons	NO2(S) + NO2	2.084E+11	1	8.15	10	-2
asN2O4(S)	\rightleftharpoons	NO2_NO2(S)	1.081E+14	1	22.57	10	-5
NO2_NO2(S)	\rightleftharpoons	symN2O4(S)	7.297E+09	1	1.08	10	-5
asN2O4(S)	\rightleftharpoons	NOZ_HNO3(S)	2.084E+10	1	2.28		
NOZ_HNO3(S)	\rightleftharpoons	HNO3 + NOZ(S)	2.084E+11	1	13.21	10	-10
symN2O4(S)	\rightleftharpoons	ZNO2_HONO(S)	1.609E+11	0	24.92		
ZNO2_HONO(S)	\rightleftharpoons	HONO + ZNO2(S)	2.084E+10	1	7.59		
ZNO2_NH3(S)	\rightleftharpoons	NH3 + ZNO2(S)	2.084E+11	1	9.79	10	-3
ZNO2_H2O(S)	\rightleftharpoons	H2O + ZNO2(S)	2.084E+11	1	6.50	10	-3
ZNO2_NH3(S)	\rightleftharpoons	NH2NO2 _{alt} (S)	5.539E+11	0	0.49		
ZNO2_H2O(S)	\rightleftharpoons	HNO3(S)	2.003E+13	0	2.14		
NO2O2N(S)	\rightleftharpoons	asN2O4(S)	2.519E+11	0	9.21		
symN2O4(S)	\rightleftharpoons	asN2O4(S)	1.255E+15	0	47.16		
NOZ(S) + NO2	\rightleftharpoons	ZNO2(S) + NO	1.789E+08	1	17.87		
asN2O3_ST3(S)	\rightleftharpoons	asN2O3(S) + NH3	2.084E+10	1	6.07		
ctN2O3_10c(S)	\rightleftharpoons	NOZ_HONO(S) + NH3	2.084E+10	1	11.04		
ctN2O3_10c(S)	\rightleftharpoons	NOZ_NH3(S) + HONO	2.084E+10	1	10.53		
ctN2O3_10c(S)	\rightleftharpoons	NH2NO_HONO(S)	1.102E+13	0	0.84		
asN2O4_ST3b(S)	\rightleftharpoons	NOZ_HNO3(S) + NH3	2.084E+10	1	10.17		
asN2O4_ST3b(S)	\rightleftharpoons	NOZ_NH3(S) + HNO3	2.084E+10	1	10.00		
symN2O4_ST3(S)	\rightleftharpoons	symN2O4(S) + NH3	2.084E+10	1	5.77		
NH3_asN2O4(S)	\rightleftharpoons	NH3_NO2(S) + NO2	4.844E+12	1	19.44	10	-5
NH3_asN2O4(S)	\rightleftharpoons	asN2O4_ST3b(S)	2.290E+11	1	19.51		
NH2NO_HNO3(S)	\rightleftharpoons	asN2O4_ST3b(S)	1.869E+11	0	8.85		
NH2NO_HNO3(S)	\rightleftharpoons	NH2NO _{alt} (S) + HNO3	2.084E+10	1	11.11		

Table D.3: (continued)

Reactant	Product	A	β	E_a	Adjust	
		[1/s]	[-]	[kcal/mol]	A x	E _a
NH2NO_HNO3(S)	\rightleftharpoons HNO3(S) + NH2NO	2.084E+10	1	5.54		
NH2NO(S)	\rightleftharpoons NH2NO.alt(S)	2.084E+10	1	10.19		
NH3(S) + NO2	\rightleftharpoons NH2OH(S) + NO	1.599E+07	1	39.13		
NH3_symN2O4(S)	\rightleftharpoons NH3.NO2(S) + NO2	5.207E+13	1	13.45	10	-5
NH3_symN2O4(S)	\rightleftharpoons symN2O4.ST3(S)	1.895E+11	1	16.53		
symN2O4.ST4(S)	\rightleftharpoons symN2O4.ST3(S)	6.910E+10	0	25.84		
symN2O4.ST4(S)	\rightleftharpoons NH2NO2_HONO(S)	2.910E+09	1	8.35		
NH2NO2_HONO(S)	\rightleftharpoons NH2NO2.alt(S) + HONO	2.084E+10	1	8.02		
NH2NO2_HONO(S)	\rightleftharpoons HONO(S) + NH2NO2	2.084E+10	1	6.52		
NH2NO2(S)	\rightleftharpoons NH2NO2.alt(S)	2.084E+10	1	7.02		
NH3_asN2O3(S)	\rightleftharpoons NH3.NO2(S) + NO	3.772E+14	1	14.71	10	
NH3_asN2O3(S)	\rightleftharpoons asN2O3.ST3(S)	1.762E+11	1	23.26		
asN2O3.ST3(S)	\rightleftharpoons NH2NO_HONO(S)	6.037E+11	0	10.29		
NH2NO_HONO(S)	\rightleftharpoons NH2NO.alt(S) + HONO	2.084E+10	1	8.79		
NH2NO_HONO(S)	\rightleftharpoons HONO(S) + NH2NO	2.084E+10	1	4.19		
<u>NH₂NO decomposition</u>						
NH2NO(S)	\rightleftharpoons NH2NO.ST2(S)	2.748E+12	0	3.32		
NH2NO.ST2(S)	\rightleftharpoons NH2NO.ST3b(S)	3.961E+10	1	10.27		
NH2NO.ST3b(S)	\rightleftharpoons NH2NO.ST4b(S)	7.411E+11	0	2.42		
NH2NO.ST4b(S)	\rightleftharpoons NH2NO.ST5b(S)	7.367E+10	1	5.16		
NH2NO.ST6b(S)	\rightleftharpoons NH2NO.ST5b(S)	2.506E+11	0	5.41		
NH2NO.ST6b(S)	\rightleftharpoons H2O.N2(S)	9.572E+10	1	9.81		
H2O.N2(S)	\rightleftharpoons H2O(S) + N2	2.084E+10	1	2.67		
<u>NH₂NO₂ decomposition</u>						
NH2NO2.ST2(S)	\rightleftharpoons NH2NO2(S)	2.084E+10	1	0.85		
NH2NO2.ST2(S)	\rightleftharpoons NH2NO2.ST3(S)	4.354E+10	1	10.71		
NH2NO2.ST3(S)	\rightleftharpoons NH2NO2.ST4(S)	5.524E+12	0	1.82		
NH2NO2.ST5(S)	\rightleftharpoons NH2NO2.ST4(S)	9.157E+11	0	1.31		
NH2NO2.ST5(S)	\rightleftharpoons NH2NO2.ST7(S)	3.265E+11	1	5.33		
NH2NO2.ST7(S)	\rightleftharpoons NH2NO2.ST8(S)	4.704E+11	0	6.60		
NH2NO2.ST8(S)	\rightleftharpoons NH2NO2.ST9(S)	6.935E+09	1	8.20		
NH2NO2.ST9(S)	\rightleftharpoons H2O.N2O(S)	2.084E+10	1	1.19		
H2O.N2O(S)	\rightleftharpoons H2O(S) + N2O	2.084E+10	1	3.49		
<u>NH₃ + HONO / HNO₃</u>						
NH3_HONO(S)	\rightleftharpoons NH3(S) + HONO	2.084E+10	1	21.62		
NH3_HONO(S)	\rightleftharpoons NH3_HONO.2(S)	2.172E+13	0	6.73		
NH4NO2(S)	\rightleftharpoons NH3_HONO.2(S)	2.084E+10	1	1.21		
NH3_HONO.4(S)	\rightleftharpoons NH4NO2(S)	2.084E+10	1	2.36		
NH3_HONO.4(S)	\rightleftharpoons NOZ.H2O(S) + NH3	2.084E+10	1	13.52		
NH3_HONO.4(S)	\rightleftharpoons NH3_HONO.5(S)	9.566E+11	1	12.37		
NH3_HONO.5(S)	\rightleftharpoons NH3_HONO.6(S)	2.754E+12	0	1.92		
NH3_HONO.6(S)	\rightleftharpoons NOZ.NH3(S) + H2O	2.084E+10	1	10.16		
NH3_HONO.6(S)	\rightleftharpoons H2O(S) + NH2NO	2.084E+10	1	1.37		
HZSM5(B) + NH4NO2(S)	\rightleftharpoons HZSM5(S) + NH4NO2	2.084E+10	1	17.00		
NH3.HNO3(S)	\rightleftharpoons NH3(S) + HNO3	2.084E+10	1	21.79		
NH3.HNO3.2(S)	\rightleftharpoons NH3.HNO3(S)	2.084E+10	1	0.31		
NH3.HNO3.2(S)	\rightleftharpoons NH4NO3(S)	7.683E+13	0	4.80		
NH4NO3(S)	\rightleftharpoons NH2NO2.H2O(S)	2.371E+09	1	32.40		
NH2NO2.H2O(S)	\rightleftharpoons NH2NO2.alt(S) + H2O	2.084E+10	1	14.49		
NH2NO2.H2O(S)	\rightleftharpoons H2O(S) + NH2NO2	2.084E+10	1	10.28		
NH4NO3(S) + HZSM5(B)	\rightleftharpoons HZSM5(S) + NH4NO3	2.084E+10	1	26.19		

Table D.3: (continued)

Reactant		Product	A [1/s]	β [-]	E _a [kcal/mol]	Adjust A x E _a	
Bimolecular reactions of HNO_x							
HONOx2_a(S)	\rightleftharpoons	HONO(S) + HONO	2.084E+10	1	4.66		
HONOx2_a(S)	\rightleftharpoons	H2O_N2O3_a(S)	3.736E+10	0	8.64		
H2O_N2O3_a(S)	\rightleftharpoons	H2O(S) + asN2O3	2.084E+10	1	4.96		
HONOx2_b(S)	\rightleftharpoons	HONO(S) + HONO	2.084E+10	1	10.89		
HONOx2_b2(S)	\rightleftharpoons	HONOx2_b(S)	2.084E+10	1	1.26		
HONOx2_b2(S)	\rightleftharpoons	H2O_N2O3_b(S)	2.084E+10	1	1.11		
H2O_N2O3_b(S)	\rightleftharpoons	H2O(S) + ctN2O3	2.084E+10	1	8.59		
HNO3_HONO(S)	\rightleftharpoons	HNO3(S) + HONO	2.084E+10	1	6.79		
HNO3_HONO(S)	\rightleftharpoons	HONO(S) + HNO3	2.084E+10	1	8.97		
HNO3_HONO(S)	\rightleftharpoons	HNO3_HONO_3(S)	8.825E+10	0	4.90		
HNO3_HONO_4(S)	\rightleftharpoons	HNO3_HONO_3(S)	1.028E+12	0	3.25		
H2O_asN2O4(S)	\rightleftharpoons	HNO3_HONO_4(S)	2.084E+10	1	2.13		
H2O_asN2O4(S)	\rightleftharpoons	H2O(S) + asN2O4	2.084E+10	1	7.00		
HNO3x2(S)	\rightleftharpoons	HNO3(S) + HNO3	2.084E+10	1	14.69		
HNO3x2(S)	\rightleftharpoons	H2O_N2O5(S)	4.938E+11	0	24.88		
H2O_N2O5(S)	\rightleftharpoons	N2O5(S) + H2O	2.084E+10	1	9.08		
NH3_N2O5(S)	\rightleftharpoons	N2O5(S) + NH3	2.084E+10	1	6.40		
NH3_N2O5(S)	\rightleftharpoons	NH2NO2_HNO3(S)	2.084E+10	1	0.04		
NH2NO2_HNO3(S)	\rightleftharpoons	HNO3(S) + NH2NO2	2.084E+10	1	11.09		
NH2NO2_HNO3(S)	\rightleftharpoons	NH2NO2.alt(S) + HNO3	2.084E+10	1	13.88		
HONO_HNO(S)	\rightleftharpoons	HONO(S) + HNO	2.084E+10	1	6.44		
HONO_HNO(S)	\rightleftharpoons	HNO(S) + HONO	2.084E+10	1	8.91		
HONO_HNO(S)	\rightleftharpoons	N2O2_H2O(S)	1.269E+11	0	0.74		
N2O2_H2O(S)	\rightleftharpoons	H2O(S) + 2 NO	6.321E+10	1	0.66		
HNO_HNO3(S)	\rightleftharpoons	HNO(S) + HNO3	2.084E+10	1	11.91		
HNO_HNO3(S)	\rightleftharpoons	HNO3(S) + HNO	2.084E+10	1	8.25		
HNO_HNO3(S)	\rightleftharpoons	H2O_ctN2O3(S)	5.032E+07	1	19.94		
H2O_ctN2O3(S)	\rightleftharpoons	H2O(S) + ctN2O3	2.084E+10	1	9.33		
NO + HONO / HNO₃							
HNO(S) + NO2	\rightleftharpoons	HONO(S) + NO	2.150E+09	1	6.23		
HNO3(S) + NO	\rightleftharpoons	HONO(S) + NO2	5.902E+07	1	21.46		
NH₃ + O₂							
NH3OOH+(S)	\rightleftharpoons	NH3(S) + O2	3.345E+12	1	16.25	10	3
NH3OOH+(S)	\rightleftharpoons	NH2OOH(S)	7.700E+13	0	7.47	10	
NH2OOH(S)	\rightleftharpoons	HNO_H2O(S)	2.658E+10	1	3.91		
HNO_H2O(S)	\rightleftharpoons	HNO(S) + H2O	2.084E+10	1	13.59		
HNO_H2O(S)	\rightleftharpoons	H2O(S) + HNO	2.084E+10	1	8.51		
NH3x2_O2(S)	\rightleftharpoons	NH3x2(S) + O2	2.084E+10	1	0.01		
NH3OOH_NH3(S)	\rightleftharpoons	NH3x2_O2(S)	3.000E+10	1	5.56		
NH3OOH_NH3(S)	\rightleftharpoons	NH2OOH_NH3(S)	2.084E+10	1	1.37		
NH2OOH_NH3(S)	\rightleftharpoons	NH2OOH(S) + NH3	2.084E+10	1	9.87		
NH2OOH_NH3(S)	\rightleftharpoons	NH2OOH_NH3_2(S)	4.312E+12	0	8.26		
NH2OOH_NH3_2(S)	\rightleftharpoons	NH2OHx2(S)	3.566E+11	0	22.32		
NH2OHx2(S)	\rightleftharpoons	NH2OH(S) + NH2OH	2.084E+10	1	13.57		
HNO + HNO							
HNOx2(S)	\rightleftharpoons	HNO(S) + HNO	2.084E+11	1	7.62	10	
HNOx2(S)	\rightleftharpoons	HNOx2_2(S)	2.826E+12	0	0.64	10	
HNOx2_2(S)	\rightleftharpoons	HNOx2_3(S)	1.393E+13	0	3.93		
HNOx2_3(S)	\rightleftharpoons	HNOx2_4(S)	2.084E+10	1	0.38		

Table D.3: (continued)

Reactant		Product	A [1/s]	β [-]	E _a [kcal/mol]	Adjust A x E _a
HNOx2.5a(S)	\rightleftharpoons	HNOx2.4(S)	1.123E+13	0	5.33	
HNOx2.6a(S)	\rightleftharpoons	HNOx2.5a(S)	1.516E+12	0	16.41	
HNOx2.6a(S)	\rightleftharpoons	H2O(S) + N2O	8.836E+09	1	13.87	
HNOx2.4(S)	\rightleftharpoons	HNOx2.7b(S)	9.360E+10	1	9.70	
HNOx2.8b(S)	\rightleftharpoons	HNOx2.7b(S)	4.699E+12	0	0.67	
HNOx2.9b(S)	\rightleftharpoons	HNOx2.8b(S)	2.084E+10	1	0.18	
HNOx2.9b(S)	\rightleftharpoons	HNOx2.10b(S)	9.223E+11	0	1.66	
HNOx2.10b(S)	\rightleftharpoons	NOZ(S) + NH2OH	2.084E+10	1	25.66	
HNOx2.10b(S)	\rightleftharpoons	HNOH(S) + NO	1.038E+12	1	9.10	
HNOx2.4(S)	\rightleftharpoons	HNOx2.5f(S)	2.561E+10	1	7.11	
HNOx2.5f(S)	\rightleftharpoons	HNOH(S) + NO	6.234E+10	1	15.85	
HNOH.HNO(S)	\rightleftharpoons	HNOH(S) + HNO	2.084E+10	1	11.67	
HNOH.HNO(S)	\rightleftharpoons	NH2OH.NO(S)	6.223E+10	0	3.56	
NH2OH.NO(S)	\rightleftharpoons	NH2OH(S) + NO	2.084E+10	1	0.80	
HNO + 2 NO						
HNO.NO(S)	\rightleftharpoons	HNO(S) + NO	2.084E+10	1	4.78	
HNO.NO(S)	\rightleftharpoons	HNONO(S)	4.243E+09	0	1.92	
HNO.2NO(S)	\rightleftharpoons	HNONO(S) + NO	1.313E+12	1	15.67	
HNO.2NO(S)	\rightleftharpoons	HNO.2NO.2(S)	2.084E+10	1	1.93	
HNO.2NO.2(S)	\rightleftharpoons	HONO(S) + N2O	2.533E+09	1	7.98	
NH2OH + HNO						
NH3OH+.HNO(S)	\rightleftharpoons	NH2OH(S) + HNO	2.084E+10	1	13.68	
NH3OH+.HNO(S)	\rightleftharpoons	NH4NO2(S)	1.809E+10	1	23.56	-3
NH2OH.2(S)	\rightleftharpoons	NH2OH(S)	9.950E+10	1	0.22	
NH2OH.2(S)	\rightleftharpoons	NH2OH.3(S)	2.084E+10	1	1.03	
NH2OH.3(S)	\rightleftharpoons	NH2OH.4(S)	1.808E+09	1	9.47	
NH2OH.4(S)	\rightleftharpoons	NH2OH.5(S)	7.823E+12	0	1.13	
NH2OH.HNO(S)	\rightleftharpoons	NH2OH.5(S) + HNO	2.084E+10	1	10.16	
NH2OH.HNO(S)	\rightleftharpoons	NH2NO.H2Ob(S)	3.110E+11	0	18.41	
NH2NO.H2Ob(S)	\rightleftharpoons	NH2NO(S) + H2O	2.084E+10	1	11.95	
NH2NO.H2Ob(S)	\rightleftharpoons	H2O(S) + NH2NO	2.084E+10	1	15.75	
NH2OH + NO						
H2O.c-HNNO(S)	\rightleftharpoons	NH2OH.5(S) + NO	3.985E+12	0	39.78	
H2O.c-HNNO(S)	\rightleftharpoons	c-HNNO(S) + H2O	2.084E+10	1	8.78	
H2O.c-HNNO(S)	\rightleftharpoons	H2O(S) + c-HNNO	2.084E+10	1	5.66	
HZSM5(B) + c-HNNO(S)	\rightleftharpoons	HZSM5(S) + c-HNNO	2.084E+10	1	14.58	
HNNOx2(S)	\rightleftharpoons	c-HNNO(S) + c-HNNO	2.084E+10	1	13.43	
HNNOx2(S)	\rightleftharpoons	NH2NO.N2O(S)	9.416E+08	1	4.13	
NH2NO.N2O(S)	\rightleftharpoons	NH2NO.alt(S) + N2O	2.084E+10	1	4.71	
HNNO.HNO(S)	\rightleftharpoons	c-HNNO(S) + HNO	2.084E+10	1	4.52	
HNNO.HNO(S)	\rightleftharpoons	HNO(S) + c-HNNO	2.084E+10	1	6.49	
HNNO.HNO(S)	\rightleftharpoons	NH2NO.alt(S) + NO	1.176E+13	1	0.34	
HNNO.NO(S)	\rightleftharpoons	c-HNNO(S) + NO	2.084E+10	1	3.89	
HNNO.NO(S)	\rightleftharpoons	HNNO.NO.2(S)	5.216E+10	0	2.75	
HNNO.NO.2(S)	\rightleftharpoons	HNO(S) + N2O	2.513E+11	0	11.27	
N2O abatement						
NH3.N2O(S)	\rightleftharpoons	NH3(S) + N2O	2.084E+10	1	5.12	
NH3.N2O(S)	\rightleftharpoons	NH2OH(S) + N2	1.072E+09	1	47.34	
NH3x2.N2O(S)	\rightleftharpoons	NH3x2(S) + N2O	2.084E+10	1	2.24	
NH3x2.N2O(S)	\rightleftharpoons	NH2OH.NH3(S) + N2	9.350E+06	1	41.14	
NH2OH.NH3(S)	\rightleftharpoons	NH2OH(S) + NH3	2.084E+10	1	15.59	
NH2OH.NH3(S)	\rightleftharpoons	NH3(S) + NH2OH	2.084E+10	1	14.81	

Table D.3: (continued)

Reactant	Product	A	β	E_a	Adjust	
		[1/s]	[-]	[kcal/mol]	A x	E_a
HZSM5(B) + N2O(S)	\rightleftharpoons HZSM5(S) + N2O	2.084E+10	1	6.70		
N2O(S) + NO	\rightleftharpoons NO2(S) + N2	7.649E+08	1	37.88		

Comment on Table D.3

The reaction rate is calculated according to

$$k = A \cdot T^\beta \cdot \exp\left(-\frac{E_a}{R \cdot T}\right) \quad (\text{D.1})$$

It should be noted that in this expression the exponent β refers to the absolute temperature in K, not to a relative temperature.

Table D.4: Thermodynamic database of gas and surface species on H-ZSM5 as is used in CHEMKIN.

THERMO							
	300.000	1000.000	5000.000				
HE	L10/90HE	1		G	200.000	6000.000	1000.000
	2.50000000E+00	0.00000000E+00	0.00000000E+00	0.00000000E+00	0.00000000E+00		1
	-7.45375000E+02	9.28723974E-01	2.50000000E+00	0.00000000E+00	0.00000000E+00		2
	0.00000000E+00	0.00000000E+00	-7.45375000E+02	9.28723974E-01	0.00000000E+00		3
	0.00000000E+00	0.00000000E+00	-7.45375000E+02	9.28723974E-01	0.00000000E+00		4
O2	TPIS890	2		G	200.000	3500.000	1000.000
	3.28253784E+00	1.48308754E-03	-7.57966669E-07	2.09470555E-10	-2.16717794E-14		1
	-1.08845772E+03	5.45323129E+00	3.78245636E+00	-2.99673416E-03	9.84730201E-06		2
	-9.68129509E-09	3.24372837E-12	-1.06394356E+03	3.65767573E+00			3
							4
H2O	L 8/89H	20	1	G	200.000	3500.000	1000.000
	3.03399249E+00	2.17691804E-03	-1.64072518E-07	-9.70419870E-11	1.68200992E-14		1
	-3.00042971E+04	4.96677010E+00	4.19864056E+00	-2.03643410E-03	6.52040211E-06		2
	-5.48797062E-09	1.77197817E-12	-3.02937267E+04	-8.49032208E-01			3
							4
NH3	J 6/77N	1H	3	G	200.000	6000.000	1000.00
	0.26344521E+01	0.56662560E-02	-0.17278676E-05	0.23867161E-09	-0.12578786E-13		1
	-0.65446958E+04	0.65662928E+01	0.42860274E+01	-0.46605230E-02	0.21718513E-04		2
	-0.22808887E-07	0.82638046E-11	-0.67417285E+04	-0.62537277E+00			3
							4
N2	121286N	2		G	300.000	5000.000	1000.000
							1

0.02926640E+02	0.14879768E-02	-0.05684760E-05	0.10097038E-09	-0.06753351E-13	2
-0.09227977E+04	0.05980528E+02	0.03298677E+02	0.14082404E-02	-0.03963222E-04	3
0.05641515E-07	-0.02444854E-10	-0.10208999E+04	0.03950372E+02		4
asN203	ownN	20	3	G 300.000 900.000 900.00	1
0.44589581E+01	0.17208337E-01	-0.18228849E-04	0.12087326E-07	-0.39487747E-11	2
0.80152462E+04	0.62234017E+01	0.44589581E+01	0.17208337E-01	-0.18228849E-04	3
0.12087326E-07	-0.39487747E-11	0.80152462E+04	0.62234017E+01		4
ctN203	ownN	20	3	G 300.000 900.000 900.00	1
0.49129524E+01	0.15585551E-01	-0.13010158E-04	0.48387436E-08	-0.53134934E-12	2
0.13181110E+05	0.45915613E+01	0.49129524E+01	0.15585551E-01	-0.13010158E-04	3
0.48387436E-08	-0.53134934E-12	0.13181110E+05	0.45915613E+01		4
asN204	ownN	20	4	G 300.000 900.000 900.00	1
0.29177018E+01	0.27657701E-01	-0.30730848E-04	0.18310383E-07	-0.47370354E-11	2
0.27369185E+04	0.13554673E+02	0.29177018E+01	0.27657701E-01	-0.30730848E-04	3
0.18310383E-07	-0.47370354E-11	0.27369185E+04	0.13554673E+02		4
HNO	ownH	1N	10	1 G 300.000 900.000 900.00	1
0.48118726E+01	-0.75547898E-02	0.22530409E-04	-0.21445428E-07	0.72914172E-11	2
0.10725747E+05	0.55003233E+00	0.48118726E+01	-0.75547898E-02	0.22530409E-04	3
-0.21445428E-07	0.72914172E-11	0.10725747E+05	0.55003233E+00		4
H2NO	ownH	2N	10	1 G 300.000 800.000 800.00	1
0.54949788E+01	-0.78556663E-02	0.31214563E-04	-0.35072443E-07	0.13858958E-10	2
0.41445223E+04	-0.16844634E+01	0.54949788E+01	-0.78556663E-02	0.31214563E-04	3
-0.35072443E-07	0.13858958E-10	0.41445223E+04	-0.16844634E+01		4
HNO3	ownH	1N	10	3 G 300.000 900.000 900.00	1
0.11627672E+01	0.22981426E-01	-0.19329102E-04	0.51195717E-08	0.10053149E-11	2
-0.17372754E+05	0.19402697E+02	0.11627672E+01	0.22981426E-01	-0.19329102E-04	3
0.51195717E-08	0.10053149E-11	-0.17372754E+05	0.19402697E+02		4
HONO	ownH	1N	10	2 G 300.000 900.000 900.00	1
0.21114031E+01	0.15147976E-01	-0.15263788E-04	0.76267635E-08	-0.13395676E-11	2
-0.10417679E+05	0.13957299E+02	0.21114031E+01	0.15147976E-01	-0.15263788E-04	3
0.76267635E-08	-0.13395676E-11	-0.10417679E+05	0.13957299E+02		4
N2O	ownN	20	1	G 300.000 900.000 900.00	1
0.22072581E+01	0.11981395E-01	-0.16470265E-04	0.13526520E-07	-0.47576399E-11	2
0.87988304E+04	0.10925271E+02	0.22072581E+01	0.11981395E-01	-0.16470265E-04	3
0.13526520E-07	-0.47576399E-11	0.87988304E+04	0.10925271E+02		4
NH2NO	ownH	2N	20	1 G 300.000 900.000 900.00	1
0.31167892E+01	0.89948306E-02	0.73587755E-05	-0.18492429E-07	0.92626838E-11	2
0.75946240E+04	0.98634863E+01	0.31167892E+01	0.89948306E-02	0.73587755E-05	3
-0.18492429E-07	0.92626838E-11	0.75946240E+04	0.98634863E+01		4
NH2NO2	ownH	2N	20	2 G 300.000 900.000 900.00	1
0.10556348E+01	0.23384395E-01	-0.11780224E-04	-0.55902046E-08	0.57116615E-11	2
-0.10632378E+04	0.19157917E+02	0.10556348E+01	0.23384395E-01	-0.11780224E-04	3
-0.55902046E-08	0.57116615E-11	-0.10632378E+04	0.19157917E+02		4
c-HNNO	ownH	1N	20	1 G 300.000 900.000 900.00	1
0.29574165E+01	0.59130306E-02	0.82578748E-05	-0.16680459E-07	0.78938262E-11	2
0.25832254E+05	0.11158529E+02	0.29574165E+01	0.59130306E-02	0.82578748E-05	3
-0.16680459E-07	0.78938262E-11	0.25832254E+05	0.11158529E+02		4
NH2OH	ownH	3N	10	1 G 300.000 900.000 900.00	1
0.37440889E+01	-0.43434715E-03	0.27872502E-04	-0.38583574E-07	0.16892271E-10	2

-0.69096614E+04	0.60608528E+01	0.37440889E+01	-0.43434715E-03	0.27872502E-04	3	
-0.38583574E-07	0.16892271E-10	-0.69096614E+04	0.60608528E+01		4	
NH4N02	ownH	4N	20	2	G 300.000 900.000 900.00	1
0.64356725E+01	0.12794692E-01	0.69851431E-05	-0.18386394E-07	0.89658671E-11		2
-0.21796357E+05	-0.27432294E+00	0.64356725E+01	0.12794692E-01	0.69851431E-05		3
-0.18386394E-07	0.89658671E-11	-0.21796357E+05	-0.27432294E+00			4
NH4N03	ownH	4N	20	3	G 300.000 900.000 900.00	1
0.50552872E+01	0.21739979E-01	0.15086560E-05	-0.19502192E-07	0.10681324E-10		2
-0.30330219E+05	0.60864774E+01	0.50552872E+01	0.21739979E-01	0.15086560E-05		3
-0.19502192E-07	0.10681324E-10	-0.30330219E+05	0.60864774E+01			4
N0	ownN	10	1		G 300.000 900.000 900.00	1
0.42220868E+01	-0.45506383E-02	0.10431499E-04	-0.85550037E-08	0.24850503E-11		2
0.97216843E+04	0.22433766E+01	0.42220868E+01	-0.45506383E-02	0.10431499E-04		3
-0.85550037E-08	0.24850503E-11	0.97216843E+04	0.22433766E+01			4
N02	ownN	10	2		G 300.000 900.000 900.00	1
0.39011106E+01	-0.14461602E-02	0.16313410E-04	-0.20952636E-07	0.85468611E-11		2
0.27780600E+04	0.65021481E+01	0.39011106E+01	-0.14461602E-02	0.16313410E-04		3
-0.20952636E-07	0.85468611E-11	0.27780600E+04	0.65021481E+01			4
symN204	ownN	20	4		G 300.000 900.000 900.00	1
0.35221523E+01	0.25869201E-01	-0.25182181E-04	0.13155854E-07	-0.31446438E-11		2
-0.90024613E+03	0.92234989E+01	0.35221523E+01	0.25869201E-01	-0.25182181E-04		3
0.13155854E-07	-0.31446438E-11	-0.90024613E+03	0.92234989E+01			4
NH3(S)	2.5+3H	4N	1		S 300.000 900.000 900.00	1
0.34153955E+01	-0.10909889E-04	0.12879187E-04	-0.10635391E-07	0.24426438E-11		2
-0.21868413E+05	-0.12108870E+02	0.34153955E+01	-0.10909889E-04	0.12879187E-04		3
-0.10635391E-07	0.24426438E-11	-0.21868413E+05	-0.12108870E+02			4
NH3x2(S)	+3.5H	7N	2		S 300.000 900.000 900.00	1
0.53578627E+01	0.12778370E-01	0.83315851E-06	-0.19493208E-08	-0.51970204E-12		2
-0.39986822E+05	-0.20354517E+02	0.53578627E+01	0.12778370E-01	0.83315851E-06		3
-0.19493208E-08	-0.51970204E-12	-0.39986822E+05	-0.20354517E+02			4
NH3x3(S)	H+1H	10N	3		S 300.000 900.000 900.00	1
0.77208748E+01	0.26566341E-01	-0.16922024E-04	0.13519824E-07	-0.60715948E-11		2
-0.56201981E+05	-0.32013985E+02	0.77208748E+01	0.26566341E-01	-0.16922024E-04		3
0.13519824E-07	-0.60715948E-11	-0.56201981E+05	-0.32013985E+02			4
NH3_N02(S)	modH	4N	20	2	S 300.000 900.000 900.00	1
0.81724371E+01	0.28399271E-02	0.21146828E-04	-0.23420743E-07	0.76801273E-11		2
-0.24329964E+05	-0.23659935E+02	0.81724371E+01	0.28399271E-02	0.21146828E-04		3
-0.23420743E-07	0.76801273E-11	-0.24329964E+05	-0.23659935E+02			4
NH3_asN204(S)	modH	4N	30	4	S 300.000 900.000 900.00	1
0.72111864E+01	0.36578763E-01	-0.34491322E-04	0.22640006E-07	-0.75423750E-11		2
-0.28836070E+05	-0.20644593E+02	0.72111864E+01	0.36578763E-01	-0.34491322E-04		3
0.22640006E-07	-0.75423750E-11	-0.28836070E+05	-0.20644593E+02			4
asN204_ST3b(S)	modH	4N	30	4	S 300.000 900.000 900.00	1
0.56623163E+01	0.40424492E-01	-0.32608312E-04	0.13612680E-07	-0.22804832E-11		2
-0.23035883E+05	-0.17512254E+02	0.56623163E+01	0.40424492E-01	-0.32608312E-04		3
0.13612680E-07	-0.22804832E-11	-0.23035883E+05	-0.17512254E+02			4
NH2N0_HN03(S)	modH	4N	30	4	S 300.000 900.000 900.00	1
0.48227961E+01	0.38879585E-01	-0.16524823E-04	-0.13145264E-07	0.11037212E-10		2
-0.23220343E+05	-0.99180624E+01	0.48227961E+01	0.38879585E-01	-0.16524823E-04		3

-0.13145264E-07	0.11037212E-10	-0.23220343E+05	-0.99180624E+01						4
NH2NO_alt(S)	modH	3N	20	1	S	300.000	900.000	900.00	1
0.22719513E+01	0.17531706E-01	-0.53946394E-05	-0.81229042E-08	0.57981895E-11					2
-0.10791971E+03	-0.47767791E+01	0.22719513E+01	0.17531706E-01	-0.53946394E-05					3
-0.81229042E-08	0.57981895E-11	-0.10791971E+03	-0.47767791E+01						4
NH3_asN2O3(S)	modH	4N	30	3	S	300.000	900.000	900.00	1
0.92147709E+01	0.21061026E-01	-0.14756324E-04	0.11562505E-07	-0.55154289E-11					2
-0.22314488E+05	-0.30473234E+02	0.92147709E+01	0.21061026E-01	-0.14756324E-04					3
0.11562505E-07	-0.55154289E-11	-0.22314488E+05	-0.30473234E+02						4
asN2O3_ST3(S)	modH	4N	30	3	S	300.000	900.000	900.00	1
0.72405931E+01	0.33703786E-01	-0.35619363E-04	0.24438978E-07	-0.78235912E-11					2
-0.13864876E+05	-0.24532872E+02	0.72405931E+01	0.33703786E-01	-0.35619363E-04					3
0.24438978E-07	-0.78235912E-11	-0.13864876E+05	-0.24532872E+02						4
NH2NO_HONO(S)	modH	4N	30	3	S	300.000	900.000	900.00	1
0.60333879E+01	0.31589155E-01	-0.16627765E-04	-0.45762382E-08	0.59047686E-11					2
-0.15208713E+05	-0.16360792E+02	0.60333879E+01	0.31589155E-01	-0.16627765E-04					3
-0.45762382E-08	0.59047686E-11	-0.15208713E+05	-0.16360792E+02						4
NH2NO(S)	modH	3N	20	1	S	300.000	900.000	900.00	1
0.26879229E+01	0.98111887E-02	0.14476136E-04	-0.27686806E-07	0.12781457E-10					2
-0.53142617E+04	-0.78215416E+01	0.26879229E+01	0.98111887E-02	0.14476136E-04					3
-0.27686806E-07	0.12781457E-10	-0.53142617E+04	-0.78215416E+01						4
NH2NO_ST2(S)	modH	3N	20	1	S	300.000	900.000	900.00	1
0.29583034E+01	0.46414946E-02	0.28419935E-04	-0.41886824E-07	0.17996162E-10					2
-0.31321372E+04	-0.82993374E+01	0.29583034E+01	0.46414946E-02	0.28419935E-04					3
-0.41886824E-07	0.17996162E-10	-0.31321372E+04	-0.82993374E+01						4
NH2NO_ST3b(S)	modH	3N	20	1	S	300.000	900.000	900.00	1
0.24545049E+01	0.13183122E-01	0.74042203E-05	-0.22418611E-07	0.11522674E-10					2
-0.67489210E+03	-0.54704959E+01	0.24545049E+01	0.13183122E-01	0.74042203E-05					3
-0.22418611E-07	0.11522674E-10	-0.67489210E+03	-0.54704959E+01						4
NH2NO_ST4b(S)	modH	3N	20	1	S	300.000	900.000	900.00	1
0.24552770E+01	0.12797224E-01	0.83321093E-05	-0.23317925E-07	0.11850932E-10					2
-0.14616836E+04	-0.57979224E+01	0.24552770E+01	0.12797224E-01	0.83321093E-05					3
-0.23317925E-07	0.11850932E-10	-0.14616836E+04	-0.57979224E+01						4
NH2NO_ST5b(S)	modH	3N	20	1	S	300.000	900.000	900.00	1
0.30416439E+01	0.10371414E-01	0.12689698E-04	-0.26993767E-07	0.13012027E-10					2
-0.15508989E+04	-0.77140627E+01	0.30416439E+01	0.10371414E-01	0.12689698E-04					3
-0.26993767E-07	0.13012027E-10	-0.15508989E+04	-0.77140627E+01						4
NH2NO_ST6b(S)	modH	3N	20	1	S	300.000	900.000	900.00	1
0.32479181E+01	0.10058691E-01	0.12256716E-04	-0.25725589E-07	0.12304902E-10					2
-0.11406177E+04	-0.85717905E+01	0.32479181E+01	0.10058691E-01	0.12256716E-04					3
-0.25725589E-07	0.12304902E-10	-0.11406177E+04	-0.85717905E+01						4
H2O_N2(S)	modH	3N	20	1	S	300.000	900.000	900.00	1
0.54180329E+01	0.15061519E-01	-0.20065576E-04	0.19008312E-07	-0.75177116E-11					2
-0.43938873E+05	-0.14713401E+02	0.54180329E+01	0.15061519E-01	-0.20065576E-04					3
0.19008312E-07	-0.75177116E-11	-0.43938873E+05	-0.14713401E+02						4
O2(S)	modH	10	2		S	300.000	900.000	900.00	1
0.49376889E+01	-0.21718920E-02	0.89794450E-05	-0.94963208E-08	0.33940720E-11					2
-0.29076932E+04	-0.11184724E+02	0.49376889E+01	-0.21718920E-02	0.89794450E-05					3
-0.94963208E-08	0.33940720E-11	-0.29076932E+04	-0.11184724E+02						4

ON00(S)	modH	1N	10	3	S	300.000	900.000	900.00	1
0.80002591E+01	0.58821967E-02	-0.52284794E-05	0.47152591E-08	-0.22930028E-11					2
0.25365195E+04	-0.23559584E+02	0.80002591E+01	0.58821967E-02	-0.52284794E-05					3
0.47152591E-08	-0.22930028E-11	0.25365195E+04	-0.23559584E+02						4
ON00_NO(S)	-210H	1N	20	4	S	300.000	900.000	900.00	1
0.11263508E+02	0.36951313E-02	0.20420373E-06	0.10607852E-08	-0.16462214E-11					2
0.97484328E+04	-0.25337266E+02	0.11263508E+02	0.36951313E-02	0.20420373E-06					3
0.10607852E-08	-0.16462214E-11	0.97484328E+04	-0.25337266E+02						4
ON00NO(S)	S10H	1N	20	4	S	300.000	900.000	900.00	1
0.50024823E+01	0.38159172E-01	-0.60340545E-04	0.51866366E-07	-0.18365159E-10					2
0.46708919E+04	-0.92228341E+01	0.50024823E+01	0.38159172E-01	-0.60340545E-04					3
0.51866366E-07	-0.18365159E-10	0.46708919E+04	-0.92228341E+01						4
NO202N(S)	S10H	1N	20	4	S	300.000	900.000	900.00	1
0.68612381E+01	0.19577602E-01	-0.10520266E-04	-0.24897842E-08	0.30886997E-11					2
-0.11611615E+04	-0.13485890E+02	0.68612381E+01	0.19577602E-01	-0.10520266E-04					3
-0.24897842E-08	0.30886997E-11	-0.11611615E+04	-0.13485890E+02						4
NO(S)	modH	1N	10	1	S	300.000	900.000	900.00	1
0.41620691E+01	0.17879972E-02	-0.15832619E-05	0.26913049E-08	-0.16267716E-11					2
0.71654398E+04	-0.10813588E+02	0.41620691E+01	0.17879972E-02	-0.15832619E-05					3
0.26913049E-08	-0.16267716E-11	0.71654398E+04	-0.10813588E+02						4
NH3_symN204(S)	modH	4N	30	4	S	300.000	900.000	900.00	1
0.79185976E+01	0.29919529E-01	-0.20005628E-04	0.10184785E-07	-0.37335698E-11					2
-0.30161429E+05	-0.23748319E+02	0.79185976E+01	0.29919529E-01	-0.20005628E-04					3
0.10184785E-07	-0.37335698E-11	-0.30161429E+05	-0.23748319E+02						4
symN204_ST3(S)	modH	4N	30	4	S	300.000	900.000	900.00	1
0.82673409E+01	0.35927688E-01	-0.33100530E-04	0.18276792E-07	-0.47636896E-11					2
-0.17828614E+05	-0.26544433E+02	0.82673409E+01	0.35927688E-01	-0.33100530E-04					3
0.18276792E-07	-0.47636896E-11	-0.17828614E+05	-0.26544433E+02						4
symN204_ST4(S)	modH	4N	30	4	S	300.000	900.000	900.00	1
0.53897166E+01	0.33540944E-01	-0.40969616E-05	-0.25185326E-07	0.15339619E-10					2
-0.22453152E+05	-0.12931292E+02	0.53897166E+01	0.33540944E-01	-0.40969616E-05					3
-0.25185326E-07	0.15339619E-10	-0.22453152E+05	-0.12931292E+02						4
NH2N02_HONO(S)	modH	4N	30	4	S	300.000	900.000	900.00	1
0.51427107E+01	0.38796914E-01	-0.20045861E-04	-0.69003099E-08	0.79203634E-11					2
-0.25315692E+05	-0.11771312E+02	0.51427107E+01	0.38796914E-01	-0.20045861E-04					3
-0.69003099E-08	0.79203634E-11	-0.25315692E+05	-0.11771312E+02						4
NH2N02_alt(S)	modH	3N	20	2	S	300.000	900.000	900.00	1
0.16151176E+01	0.22888501E-01	-0.42455271E-05	-0.15257743E-07	0.96938038E-11					2
-0.10542920E+05	-0.95111757E+00	0.16151176E+01	0.22888501E-01	-0.42455271E-05					3
-0.15257743E-07	0.96938038E-11	-0.10542920E+05	-0.95111757E+00						4
NH3_HONO(S)	modH	5N	20	2	S	300.000	900.000	900.00	1
0.62694876E+01	0.15012702E-01	0.31763386E-05	-0.96300147E-08	0.35434348E-11					2
-0.42300175E+05	-0.23440460E+02	0.62694876E+01	0.15012702E-01	0.31763386E-05					3
-0.96300147E-08	0.35434348E-11	-0.42300175E+05	-0.23440460E+02						4
NH3_HONO_2(S)	modH	5N	20	2	S	300.000	900.000	900.00	1
0.65982149E+01	0.12342515E-01	0.11798175E-04	-0.19696850E-07	0.75152630E-11					2
-0.38689721E+05	-0.22586671E+02	0.65982149E+01	0.12342515E-01	0.11798175E-04					3
-0.19696850E-07	0.75152630E-11	-0.38689721E+05	-0.22586671E+02						4
NH4N02(S)	modH	5N	20	2	S	300.000	900.000	900.00	1

0.60186557E+01	0.13099032E-01	0.99169736E-05	-0.19980651E-07	0.86368497E-11	2
-0.35689580E+05	-0.20850098E+02	0.60186557E+01	0.13099032E-01	0.99169736E-05	3
-0.19980651E-07	0.86368497E-11	-0.35689580E+05	-0.20850098E+02		4
NH3_HONO_4(S)	modH	5N	20	2	1
0.51495317E+01	0.32157434E-01	-0.41795941E-04	0.36265181E-07	-0.13427316E-10	2
-0.37750452E+05	-0.20808094E+02	0.51495317E+01	0.32157434E-01	-0.41795941E-04	3
0.36265181E-07	-0.13427316E-10	-0.37750452E+05	-0.20808094E+02		4
NH3_HONO_5(S)	modH	5N	20	2	1
0.55903040E+01	0.39681580E-01	-0.66141439E-04	0.63204213E-07	-0.23992347E-10	2
-0.35274711E+05	-0.22313727E+02	0.55903040E+01	0.39681580E-01	-0.66141439E-04	3
0.63204213E-07	-0.23992347E-10	-0.35274711E+05	-0.22313727E+02		4
NH3_HONO_6(S)	modH	5N	20	2	1
0.45624875E+01	0.36883601E-01	-0.51368966E-04	0.44451277E-07	-0.16101997E-10	2
-0.37199414E+05	-0.17870182E+02	0.45624875E+01	0.36883601E-01	-0.51368966E-04	3
0.44451277E-07	-0.16101997E-10	-0.37199414E+05	-0.17870182E+02		4
NH3_HNO3(S)	modH	5N	20	3	1
0.56113315E+01	0.18081299E-01	0.11760695E-04	-0.24205204E-07	0.98709214E-11	2
-0.51186245E+05	-0.18669567E+02	0.56113315E+01	0.18081299E-01	0.11760695E-04	3
-0.24205204E-07	0.98709214E-11	-0.51186245E+05	-0.18669567E+02		4
NH3_HNO3_2(S)	modH	5N	20	3	1
0.60086122E+01	0.13556053E-01	0.25794605E-04	-0.41303301E-07	0.17194195E-10	2
-0.50361412E+05	-0.21331889E+02	0.60086122E+01	0.13556053E-01	0.25794605E-04	3
-0.41303301E-07	0.17194195E-10	-0.50361412E+05	-0.21331889E+02		4
NH4NO3(S)	modH	5N	20	3	1
0.60964144E+01	0.12573630E-01	0.28537986E-04	-0.43749004E-07	0.17888039E-10	2
-0.51090795E+05	-0.20537822E+02	0.60964144E+01	0.12573630E-01	0.28537986E-04	3
-0.43749004E-07	0.17888039E-10	-0.51090795E+05	-0.20537822E+02		4
NH2NO2_H2O(S)	modH	5N	20	3	1
0.36020360E+01	0.34772072E-01	-0.20284805E-04	-0.15285178E-08	0.48009754E-11	2
-0.48292657E+05	-0.89256359E+01	0.36020360E+01	0.34772072E-01	-0.20284805E-04	3
-0.15285178E-08	0.48009754E-11	-0.48292657E+05	-0.89256359E+01		4
NH2NO2(S)	modH	3N	20	2	1
0.12846530E+01	0.24179352E-01	-0.66948695E-05	-0.12706411E-07	0.86533322E-11	2
-0.14094796E+05	-0.10984169E+01	0.12846530E+01	0.24179352E-01	-0.66948695E-05	3
-0.12706411E-07	0.86533322E-11	-0.14094796E+05	-0.10984169E+01		4
NH2NO2_ST2(S)	modH	3N	20	2	1
0.16925684E+01	0.16950970E-01	0.12434780E-04	-0.30982149E-07	0.14804488E-10	2
-0.10603704E+05	-0.28454004E+01	0.16925684E+01	0.16950970E-01	0.12434780E-04	3
-0.30982149E-07	0.14804488E-10	-0.10603704E+05	-0.28454004E+01		4
NH2NO2_ST3(S)	modH	3N	20	2	1
0.72599101E+00	0.27315721E-01	-0.11841441E-04	-0.92194577E-08	0.78463665E-11	2
-0.68922273E+04	0.22263483E+01	0.72599101E+00	0.27315721E-01	-0.11841441E-04	3
-0.92194577E-08	0.78463665E-11	-0.68922273E+04	0.22263483E+01		4
NH2NO2_ST4(S)	modH	3N	20	2	1
0.71827702E+00	0.28052878E-01	-0.14073903E-04	-0.67534063E-08	0.68769274E-11	2
-0.65276967E+04	0.26406440E+01	0.71827702E+00	0.28052878E-01	-0.14073903E-04	3
-0.67534063E-08	0.68769274E-11	-0.65276967E+04	0.26406440E+01		4
NH2NO2_ST5(S)	modH	3N	20	2	1
0.69303781E+00	0.27886987E-01	-0.13600650E-04	-0.71409048E-08	0.69803893E-11	2

-0.67101340E+04 0.24816240E+01 0.69303781E+00 0.27886987E-01-0.13600650E-04	3
-0.71409048E-08 0.69803893E-11-0.67101340E+04 0.24816240E+01	4
NH2NO2_ST7(S) modH 3N 20 2 S 300.000 900.000 900.00	1
0.17685816E+01 0.24784918E-01-0.96819516E-05-0.97641597E-08 0.76880121E-11	2
-0.66880330E+04-0.12310580E+01 0.17685816E+01 0.24784918E-01-0.96819516E-05	3
-0.97641597E-08 0.76880121E-11-0.66880330E+04-0.12310580E+01	4
NH2NO2_ST8(S) modH 3N 20 2 S 300.000 900.000 900.00	1
0.17725247E+01 0.26104893E-01-0.13596938E-04-0.55065537E-08 0.60390941E-11	2
-0.69203317E+04-0.10688831E+01 0.17725247E+01 0.26104893E-01-0.13596938E-04	3
-0.55065537E-08 0.60390941E-11-0.69203317E+04-0.10688831E+01	4
NH2NO2_ST9(S) modH 3N 20 2 S 300.000 900.000 900.00	1
0.18115358E+01 0.28865661E-01-0.23054132E-04 0.60769719E-08 0.11268633E-11	2
-0.62871934E+04-0.39389533E+01 0.18115358E+01 0.28865661E-01-0.23054132E-04	3
0.60769719E-08 0.11268633E-11-0.62871934E+04-0.39389533E+01	4
H2O_N20(S) modH 3N 20 2 S 300.000 900.000 900.00	1
0.42209868E+01 0.26154109E-01-0.33323040E-04 0.27049202E-07-0.95499943E-11	2
-0.34461898E+05-0.81730798E+01 0.42209868E+01 0.26154109E-01-0.33323040E-04	3
0.27049202E-07-0.95499943E-11-0.34461898E+05-0.81730798E+01	4
HONOx2_a(S) modH 3N 20 4 S 300.000 900.000 900.00	1
0.64347131E+01 0.30773576E-01-0.25003575E-04 0.83495663E-08-0.77426589E-13	2
-0.32441873E+05-0.16077808E+02 0.64347131E+01 0.30773576E-01-0.25003575E-04	3
0.83495663E-08-0.77426589E-13-0.32441873E+05-0.16077808E+02	4
H2O_N203_a(S) modH 3N 20 4 S 300.000 900.000 900.00	1
0.64299613E+01 0.33665682E-01-0.39199154E-04 0.29197865E-07-0.99597573E-11	2
-0.33783087E+05-0.15326866E+02 0.64299613E+01 0.33665682E-01-0.39199154E-04	3
0.29197865E-07-0.99597573E-11-0.33783087E+05-0.15326866E+02	4
H2O(S) modH 3O 1 S 300.000 900.000 900.00	1
0.95994974E+00 0.13806087E-01-0.17706789E-04 0.14857599E-07-0.53181662E-11	2
-0.41441666E+05-0.35940628E+01 0.95994974E+00 0.13806087E-01-0.17706789E-04	3
0.14857599E-07-0.53181662E-11-0.41441666E+05-0.35940628E+01	4
HONO(S) S+3H 2N 10 2 S 300.000 900.000 900.00	1
0.26541718E+01 0.15925104E-01-0.12039555E-04 0.33031693E-08 0.34211348E-12	2
-0.19462701E+05-0.53207872E+01 0.26541718E+01 0.15925104E-01-0.12039555E-04	3
0.33031693E-08 0.34211348E-12-0.19462701E+05-0.53207872E+01	4
HONOx2_b(S) modH 3N 20 4 S 300.000 900.000 900.00	1
0.59027306E+01 0.32162205E-01-0.25984540E-04 0.76965873E-08 0.68236870E-12	2
-0.35530562E+05-0.15132312E+02 0.59027306E+01 0.32162205E-01-0.25984540E-04	3
0.76965873E-08 0.68236870E-12-0.35530562E+05-0.15132312E+02	4
HONOx2_b2(S) modH 3N 20 4 S 300.000 900.000 900.00	1
0.53958485E+01 0.38415117E-01-0.48890536E-04 0.39047823E-07-0.13722891E-10	2
-0.33454050E+05-0.17610506E+02 0.53958485E+01 0.38415117E-01-0.48890536E-04	3
0.39047823E-07-0.13722891E-10-0.33454050E+05-0.17610506E+02	4
H2O_N203_b(S) modH 3N 20 4 S 300.000 900.000 900.00	1
0.66835513E+01 0.37897624E-01-0.50834240E-04 0.39987808E-07-0.13426698E-10	2
-0.32607369E+05-0.23127625E+02 0.66835513E+01 0.37897624E-01-0.50834240E-04	3
0.39987808E-07-0.13426698E-10-0.32607369E+05-0.23127625E+02	4
HNO3_HONO(S) modH 3N 20 5 S 300.000 900.000 900.00	1
0.50567022E+01 0.38082013E-01-0.24075726E-04-0.11957793E-08 0.53834227E-11	2
-0.41349515E+05-0.11766563E+02 0.50567022E+01 0.38082013E-01-0.24075726E-04	3

-0.11957793E-08 0.53834227E-11-0.41349515E+05-0.11766563E+02	4
HNO3_HONO_3(S) modH 3N 20 5 S 300.000 900.000 900.00	1
0.39720266E+01 0.51355324E-01-0.62059441E-04 0.41277241E-07-0.11584624E-10	2
-0.43041291E+05-0.11679456E+02 0.39720266E+01 0.51355324E-01-0.62059441E-04	3
0.41277241E-07-0.11584624E-10-0.43041291E+05-0.11679456E+02	4
HNO3_HONO_4(S) modH 3N 20 5 S 300.000 900.000 900.00	1
0.43050851E+01 0.53105674E-01-0.69586244E-04 0.50716485E-07-0.15593590E-10	2
-0.44036334E+05-0.12868810E+02 0.43050851E+01 0.53105674E-01-0.69586244E-04	3
0.50716485E-07-0.15593590E-10-0.44036334E+05-0.12868810E+02	4
H2O_asN2O4(S) modH 3N 20 5 S 300.000 900.000 900.00	1
0.60916074E+01 0.44321007E-01-0.52296675E-04 0.35031268E-07-0.10152104E-10	2
-0.41312365E+05-0.13899106E+02 0.60916074E+01 0.44321007E-01-0.52296675E-04	3
0.35031268E-07-0.10152104E-10-0.41312365E+05-0.13899106E+02	4
HNO3(S) S+3H 2N 10 3 S 300.000 900.000 900.00	1
0.15041294E+01 0.22943495E-01-0.12190930E-04-0.39882067E-08 0.46405562E-11	2
-0.27276626E+05 0.45608369E+00 0.15041294E+01 0.22943495E-01-0.12190930E-04	3
-0.39882067E-08 0.46405562E-11-0.27276626E+05 0.45608369E+00	4
HNO3x2(S) modH 3N 20 6 S 300.000 900.000 900.00	1
0.38234608E+01 0.44461183E-01-0.22827933E-04-0.97684891E-08 0.10176807E-10	2
-0.52223729E+05-0.67585788E+01 0.38234608E+01 0.44461183E-01-0.22827933E-04	3
-0.97684891E-08 0.10176807E-10-0.52223729E+05-0.67585788E+01	4
H2O_N2O5(S) modH 3N 20 6 S 300.000 900.000 900.00	1
0.61504142E+01 0.56105880E-01-0.73714636E-04 0.53656860E-07-0.16563924E-10	2
-0.44926631E+05-0.18116992E+02 0.61504142E+01 0.56105880E-01-0.73714636E-04	3
0.53656860E-07-0.16563924E-10-0.44926631E+05-0.18116992E+02	4
N2O5(S) modH 1N 20 5 S 300.000 900.000 900.00	1
0.40231347E+01 0.40055309E-01-0.45227732E-04 0.26977084E-07-0.68637051E-11	2
-0.87271232E+04-0.55960716E+01 0.40231347E+01 0.40055309E-01-0.45227732E-04	3
0.26977084E-07-0.68637051E-11-0.87271232E+04-0.55960716E+01	4
NH3_N2O5(S) modH 4N 30 5 S 300.000 900.000 900.00	1
0.75840930E+01 0.47856634E-01-0.49776743E-04 0.29226765E-07-0.74429196E-11	2
-0.18880017E+05-0.22392371E+02 0.75840930E+01 0.47856634E-01-0.49776743E-04	3
0.29226765E-07-0.74429196E-11-0.18880017E+05-0.22392371E+02	4
NH2NO2_HNO3(S) modH 4N 30 5 S 300.000 900.000 900.00	1
0.38735970E+01 0.45974989E-01-0.19831055E-04-0.15176671E-07 0.12784939E-10	2
-0.35079820E+05-0.60377581E+01 0.38735970E+01 0.45974989E-01-0.19831055E-04	3
-0.15176671E-07 0.12784939E-10-0.35079820E+05-0.60377581E+01	4
HONO_HNO(S) modH 3N 20 3 S 300.000 900.000 900.00	1
0.79981743E+01 0.16825401E-01-0.80572448E-05 0.40195622E-10 0.89948060E-12	2
-0.12180273E+05-0.24687736E+02 0.79981743E+01 0.16825401E-01-0.80572448E-05	3
0.40195622E-10 0.89948060E-12-0.12180273E+05-0.24687736E+02	4
N2O2_H2O(S) modH 3N 20 3 S 300.000 900.000 900.00	1
0.57615260E+01 0.36668148E-01-0.59021028E-04 0.54136071E-07-0.20182215E-10	2
-0.20792368E+05-0.20283338E+02 0.57615260E+01 0.36668148E-01-0.59021028E-04	3
0.54136071E-07-0.20182215E-10-0.20792368E+05-0.20283338E+02	4
HNO_HNO3(S) modH 3N 20 4 S 300.000 900.000 900.00	1
0.57399182E+01 0.26920515E-01-0.12134193E-04-0.49243075E-08 0.47092478E-11	2
-0.20879564E+05-0.16365541E+02 0.57399182E+01 0.26920515E-01-0.12134193E-04	3
-0.49243075E-08 0.47092478E-11-0.20879564E+05-0.16365541E+02	4

H2O_ctN203(S)	modH	3N	20	4	S	300.000	900.000	900.00	1
0.69391080E+01	0.35264507E-01	-0.45401409E-04	0.36083115E-07	-0.12581860E-10					2
-0.34303699E+05	-0.22463673E+02	0.69391080E+01	0.35264507E-01	-0.45401409E-04					3
0.36083115E-07	-0.12581860E-10	-0.34303699E+05	-0.22463673E+02						4
NH300H+(S)	S+3H	4N	10	2	S	300.000	900.000	900.00	1
0.22750966E+01	0.14838587E-01	0.66791039E-05	-0.18438723E-07	0.85551165E-11					2
-0.18584275E+05	-0.65802457E+01	0.22750966E+01	0.14838587E-01	0.66791039E-05					3
-0.18438723E-07	0.85551165E-11	-0.18584275E+05	-0.65802457E+01						4
NH200H(S)	modH	4N	10	2	S	300.000	900.000	900.00	1
0.23199637E+01	0.17109347E-01	0.41786856E-05	-0.20150170E-07	0.10655633E-10					2
-0.18557295E+05	-0.72269543E+01	0.23199637E+01	0.17109347E-01	0.41786856E-05					3
-0.20150170E-07	0.10655633E-10	-0.18557295E+05	-0.72269543E+01						4
HNO_H2O(S)	modH	4N	10	2	S	300.000	900.000	900.00	1
0.57860485E+01	0.15413992E-01	-0.13096384E-04	0.10056301E-07	-0.40603813E-11					2
-0.34768114E+05	-0.20991919E+02	0.57860485E+01	0.15413992E-01	-0.13096384E-04					3
0.10056301E-07	-0.40603813E-11	-0.34768114E+05	-0.20991919E+02						4
NH3x2_O2(S)	modH	7N	20	2	S	300.000	900.000	900.00	1
0.65233435E+01	0.28159509E-01	-0.22415746E-04	0.15976069E-07	-0.61232740E-11					2
-0.24850410E+05	-0.23954866E+02	0.65233435E+01	0.28159509E-01	-0.22415746E-04					3
0.15976069E-07	-0.61232740E-11	-0.24850410E+05	-0.23954866E+02						4
NH300H_NH3(S)	modH	7N	20	2	S	300.000	900.000	900.00	1
0.62201447E+01	0.15429265E-01	0.20416194E-04	-0.33009259E-07	0.13318018E-10					2
-0.27893490E+05	-0.23192433E+02	0.62201447E+01	0.15429265E-01	0.20416194E-04					3
-0.33009259E-07	0.13318018E-10	-0.27893490E+05	-0.23192433E+02						4
NH200H_NH3(S)	modH	7N	20	2	S	300.000	900.000	900.00	1
0.59497959E+01	0.21702710E-01	0.83466076E-05	-0.26704699E-07	0.13285649E-10					2
-0.28016053E+05	-0.20711182E+02	0.59497959E+01	0.21702710E-01	0.83466076E-05					3
-0.26704699E-07	0.13285649E-10	-0.28016053E+05	-0.20711182E+02						4
NH200H_NH3_2(S)	modH	7N	20	2	S	300.000	900.000	900.00	1
0.59686148E+01	0.19140542E-01	0.14993117E-04	-0.32594863E-07	0.15046079E-10					2
-0.29961357E+05	-0.21304854E+02	0.59686148E+01	0.19140542E-01	0.14993117E-04					3
-0.32594863E-07	0.15046079E-10	-0.29961357E+05	-0.21304854E+02						4
NH20Hx2(S)	modH	7N	20	2	S	300.000	900.000	900.00	1
0.78536323E+01	0.15194912E-02	0.55108931E-04	-0.70916698E-07	0.28732267E-10					2
-0.40895646E+05	-0.28115019E+02	0.78536323E+01	0.15194912E-02	0.55108931E-04					3
-0.70916698E-07	0.28732267E-10	-0.40895646E+05	-0.28115019E+02						4
HNO(S)	modH	2N	10	1	S	300.000	900.000	900.00	1
0.34281493E+01	0.40213917E-02	0.28833413E-05	-0.41563808E-08	0.11872508E-11					2
0.32081490E+04	-0.12184076E+02	0.34281493E+01	0.40213917E-02	0.28833413E-05					3
-0.41563808E-08	0.11872508E-11	0.32081490E+04	-0.12184076E+02						4
HNOx2(S)	-25H	3N	20	2	S	300.000	900.000	900.00	1
0.77152867E+01	0.67045438E-02	0.69395781E-05	-0.92238272E-08	0.27294996E-11					2
0.89145574E+04	-0.24843838E+02	0.77152867E+01	0.67045438E-02	0.69395781E-05					3
-0.92238272E-08	0.27294996E-11	0.89145574E+04	-0.24843838E+02						4
HNOx2_2(S)	modH	3N	20	2	S	300.000	900.000	900.00	1
0.34729637E+01	0.10659540E-01	0.20091405E-04	-0.33908132E-07	0.14540900E-10					2
-0.51429833E+04	-0.11767516E+02	0.34729637E+01	0.10659540E-01	0.20091405E-04					3
-0.33908132E-07	0.14540900E-10	-0.51429833E+04	-0.11767516E+02						4
HNOx2_3(S)	modH	3N	20	2	S	300.000	900.000	900.00	1

0.37970500E+01	0.81304392E-02	0.26385224E-04	-0.40144772E-07	0.16756342E-10	2	
-0.51770628E+04	-0.12415098E+02	0.37970500E+01	0.81304392E-02	0.26385224E-04	3	
-0.40144772E-07	0.16756342E-10	-0.51770628E+04	-0.12415098E+02		4	
HNOx2_4(S)	modH	3N	20	2	S 300.000 900.000 900.00	1
0.31067238E+01	0.17423439E-01	0.33477793E-05	-0.18890663E-07	0.98487633E-11	2	
-0.85072492E+04	-0.94740820E+01	0.31067238E+01	0.17423439E-01	0.33477793E-05	3	
-0.18890663E-07	0.98487633E-11	-0.85072492E+04	-0.94740820E+01		4	
HNOx2_5a(S)	modH	3N	20	2	S 300.000 900.000 900.00	1
0.37557539E+01	0.19558377E-01	-0.45073879E-05	-0.11268615E-07	0.73203252E-11	2	
-0.26072512E+04	-0.11099357E+02	0.37557539E+01	0.19558377E-01	-0.45073879E-05	3	
-0.11268615E-07	0.73203252E-11	-0.26072512E+04	-0.11099357E+02		4	
HNOx2_6a(S)	modH	3N	20	2	S 300.000 900.000 900.00	1
0.36180429E+01	0.16831774E-01	0.29766711E-05	-0.18150955E-07	0.95392322E-11	2	
-0.49549402E+04	-0.11691201E+02	0.36180429E+01	0.16831774E-01	0.29766711E-05	3	
-0.18150955E-07	0.95392322E-11	-0.49549402E+04	-0.11691201E+02		4	
HNOx2_7b(S)	modH	3N	20	2	S 300.000 900.000 900.00	1
0.41472448E+01	0.11172694E-01	0.16559348E-04	-0.30303460E-07	0.13387728E-10	2	
-0.89003600E+04	-0.11328874E+02	0.41472448E+01	0.11172694E-01	0.16559348E-04	3	
-0.30303460E-07	0.13387728E-10	-0.89003600E+04	-0.11328874E+02		4	
HNOx2_8b(S)	modH	3N	20	2	S 300.000 900.000 900.00	1
0.39621464E+01	0.19850364E-01	-0.69536674E-05	-0.75542562E-08	0.55914711E-11	2	
-0.23655459E+04	-0.11863475E+02	0.39621464E+01	0.19850364E-01	-0.69536674E-05	3	
-0.75542562E-08	0.55914711E-11	-0.23655459E+04	-0.11863475E+02		4	
HNOx2_9b(S)	modH	3N	20	2	S 300.000 900.000 900.00	1
0.62636204E+01	0.83093532E-02	0.12057281E-04	-0.19963377E-07	0.81454951E-11	2	
-0.10918970E+03	-0.21217573E+02	0.62636204E+01	0.83093532E-02	0.12057281E-04	3	
-0.19963377E-07	0.81454951E-11	-0.10918970E+03	-0.21217573E+02		4	
HNOx2_10b(S)	modH	3N	20	2	S 300.000 900.000 900.00	1
0.42203767E+01	0.15072978E-01	-0.17700740E-06	-0.84175902E-08	0.39266183E-11	2	
-0.50833267E+04	-0.15324919E+02	0.42203767E+01	0.15072978E-01	-0.17700740E-06	3	
-0.84175902E-08	0.39266183E-11	-0.50833267E+04	-0.15324919E+02		4	
HNOH(S)	modH	3N	10	1	S 300.000 900.000 900.00	1
0.25833408E+01	-0.28369833E-02	0.33697573E-04	-0.40662388E-07	0.15820000E-10	2	
-0.79013076E+04	-0.70434145E+01	0.25833408E+01	-0.28369833E-02	0.33697573E-04	3	
-0.40662388E-07	0.15820000E-10	-0.79013076E+04	-0.70434145E+01		4	
HNOH_HNO(S)	modH	4N	20	2	S 300.000 900.000 900.00	1
0.88564201E+01	0.39000826E-02	0.19143226E-04	-0.23731126E-07	0.87176485E-11	2	
-0.35766754E+04	-0.30618911E+02	0.88564201E+01	0.39000826E-02	0.19143226E-04	3	
-0.23731126E-07	0.87176485E-11	-0.35766754E+04	-0.30618911E+02		4	
NH2OH_NO(S)	modH	4N	20	2	S 300.000 900.000 900.00	1
0.64566514E+01	-0.38277181E-02	0.40670010E-04	-0.44861507E-07	0.16098359E-10	2	
-0.15998565E+05	-0.19356067E+02	0.64566514E+01	-0.38277181E-02	0.40670010E-04	3	
-0.44861507E-07	0.16098359E-10	-0.15998565E+05	-0.19356067E+02		4	
HNOx2_5f(S)	modH	3N	20	2	S 300.000 900.000 900.00	1
0.25667818E+01	0.23824493E-01	-0.12425343E-04	-0.36248433E-08	0.44681607E-11	2	
-0.51334493E+04	-0.56936868E+01	0.25667818E+01	0.23824493E-01	-0.12425343E-04	3	
-0.36248433E-08	0.44681607E-11	-0.51334493E+04	-0.56936868E+01		4	
HNO-NO(S)	modH	2N	20	2	S 300.000 900.000 900.00	1
0.86489028E+01	0.17991859E-03	0.13661103E-04	-0.13482363E-07	0.39171719E-11	2	

0.10317904E+05-0.28762764E+02	0.86489028E+01	0.17991859E-03	0.13661103E-04	3	
-0.13482363E-07	0.39171719E-11	0.10317904E+05-0.28762764E+02		4	
HNONO(S)	modH	2N	20 2	S 300.000 900.000 900.00	1
0.36553338E+01	0.17037186E-01-0.64665698E-05-0.51766093E-08	0.39295533E-11			2
0.55491558E+04-0.10488186E+02	0.36553338E+01	0.17037186E-01-0.64665698E-05			3
-0.51766093E-08	0.39295533E-11	0.55491558E+04-0.10488186E+02			4
HNO_2NO(S)	modH	2N	30 3	S 300.000 900.000 900.00	1
0.42791460E+01	0.28211211E-01-0.17891066E-04	0.22181033E-08	0.15019354E-11		2
0.85125669E+04-0.12494618E+02	0.42791460E+01	0.28211211E-01-0.17891066E-04			3
0.22181033E-08	0.15019354E-11	0.85125669E+04-0.12494618E+02			4
HNO_2NO_2(S)	modH	2N	30 3	S 300.000 900.000 900.00	1
0.40855587E+01	0.31983126E-01-0.28066503E-04	0.12296667E-07-0.20271298E-11			2
0.72964504E+04-0.10528739E+02	0.40855587E+01	0.31983126E-01-0.28066503E-04			3
0.12296667E-07-0.20271298E-11	0.72964504E+04-0.10528739E+02				4
NH2OH(S)	modH	4N	10 1	S 300.000 900.000 900.00	1
0.31593311E+01	0.44416721E-04	0.30136543E-04-0.36516672E-07	0.14108545E-10		2
-0.25106083E+05-0.12194312E+02	0.31593311E+01	0.44416721E-04	0.30136543E-04		3
-0.36516672E-07	0.14108545E-10-0.25106083E+05-0.12194312E+02				4
NH2OH_2(S)	modH	4N	10 1	S 300.000 900.000 900.00	1
0.38084549E+01-0.51313715E-02	0.38521031E-04-0.43587860E-07	0.16461609E-10			2
-0.21028411E+05-0.14316506E+02	0.38084549E+01-0.51313715E-02	0.38521031E-04			3
-0.43587860E-07	0.16461609E-10-0.21028411E+05-0.14316506E+02				4
NH2OH_3(S)	modH	4N	10 1	S 300.000 900.000 900.00	1
0.53496965E+01-0.86993633E-02	0.51794456E-04-0.61526692E-07	0.24518007E-10			2
-0.20838027E+05-0.17432483E+02	0.53496965E+01-0.86993633E-02	0.51794456E-04			3
-0.61526692E-07	0.24518007E-10-0.20838027E+05-0.17432483E+02				4
NH2OH_4(S)	modH	4N	10 1	S 300.000 900.000 900.00	1
0.38999998E+01	0.31615372E-02	0.22905956E-04-0.32938619E-07	0.14224001E-10		2
-0.19806743E+05-0.14186818E+02	0.38999998E+01	0.31615372E-02	0.22905956E-04		3
-0.32938619E-07	0.14224001E-10-0.19806743E+05-0.14186818E+02				4
NH2OH_5(S)	modH	4N	10 1	S 300.000 900.000 900.00	1
0.36046575E+01	0.29408151E-02	0.25718549E-04-0.37098858E-07	0.16119193E-10		2
-0.19848982E+05-0.12204254E+02	0.36046575E+01	0.29408151E-02	0.25718549E-04		3
-0.37098858E-07	0.16119193E-10-0.19848982E+05-0.12204254E+02				4
NH2OH_HNO(S)	modH	5N	20 2	S 300.000 900.000 900.00	1
0.76924525E+01	0.53741764E-02	0.30050768E-04-0.41215624E-07	0.16813792E-10		2
-0.16521848E+05-0.27855579E+02	0.76924525E+01	0.53741764E-02	0.30050768E-04		3
-0.41215624E-07	0.16813792E-10-0.16521848E+05-0.27855579E+02				4
NH2NO_H2Ob(S)	modH	5N	20 2	S 300.000 900.000 900.00	1
0.42901490E+01	0.25749253E-01-0.11157015E-04-0.51149932E-08	0.49320679E-11			2
-0.43388385E+05-0.14173030E+02	0.42901490E+01	0.25749253E-01-0.11157015E-04			3
-0.51149932E-08	0.49320679E-11-0.43388385E+05-0.14173030E+02				4
NH3OH+_HNO(S)	-33H	5N	20 2	S 300.000 900.000 900.00	1
0.70199013E+01	0.64843833E-02	0.23244919E-04-0.28375886E-07	0.99537836E-11		2
-0.23797626E+05-0.23555600E+02	0.70199013E+01	0.64843833E-02	0.23244919E-04		3
-0.28375886E-07	0.99537836E-11-0.23797626E+05-0.23555600E+02				4
H2O_c-HNNO(S)	modH	4N	20 2	S 300.000 900.000 900.00	1
0.49121453E+01	0.23099313E-01-0.15206607E-04	0.34989459E-08	0.56559730E-12		2
-0.18690694E+05-0.14750547E+02	0.49121453E+01	0.23099313E-01-0.15206607E-04			3

0.34989459E-08	0.56559730E-12	-0.18690694E+05	-0.14750547E+02						4
c-HNNO(S)	modH	2N	20	1	S	300.000	900.000	900.00	1
0.32712464E+01	0.84441370E-02	0.73571478E-05	-0.16820361E-07	0.79604418E-11					2
0.18332222E+05	-0.85615295E+01	0.32712464E+01	0.84441370E-02	0.73571478E-05					3
-0.16820361E-07	0.79604418E-11	0.18332222E+05	-0.85615295E+01						4
HNNOx2(S)	modH	3N	40	2	S	300.000	900.000	900.00	1
0.79637613E+01	0.11388724E-01	0.25236219E-04	-0.44054953E-07	0.19916487E-10					2
0.37142118E+05	-0.23037886E+02	0.79637613E+01	0.11388724E-01	0.25236219E-04					3
-0.44054953E-07	0.19916487E-10	0.37142118E+05	-0.23037886E+02						4
NH2NO_N2O(S)	modH	3N	40	2	S	300.000	900.000	900.00	1
0.64255390E+01	0.28014772E-01	-0.19290640E-04	0.28957097E-08	0.20038155E-11					2
0.61445936E+04	-0.16606079E+02	0.64255390E+01	0.28014772E-01	-0.19290640E-04					3
0.28957097E-08	0.20038155E-11	0.61445936E+04	-0.16606079E+02						4
HNNO_HNO(S)	modH	3N	30	2	S	300.000	900.000	900.00	1
0.65897168E+01	0.11615105E-01	0.15526002E-04	-0.26824062E-07	0.11056178E-10					2
0.25552495E+05	-0.21716739E+02	0.65897168E+01	0.11615105E-01	0.15526002E-04					3
-0.26824062E-07	0.11056178E-10	0.25552495E+05	-0.21716739E+02						4
HNNO_NO(S)	modH	2N	30	2	S	300.000	900.000	900.00	1
0.84790893E+01	0.80054291E-02	0.82150227E-05	-0.16130472E-07	0.70905460E-11					2
0.25883239E+05	-0.26305906E+02	0.84790893E+01	0.80054291E-02	0.82150227E-05					3
-0.16130472E-07	0.70905460E-11	0.25883239E+05	-0.26305906E+02						4
HNNO_NO_2(S)	modH	2N	30	2	S	300.000	900.000	900.00	1
0.42449710E+01	0.25054114E-01	-0.22340472E-04	0.10565324E-07	-0.21250512E-11					2
0.24647571E+05	-0.12691387E+02	0.42449710E+01	0.25054114E-01	-0.22340472E-04					3
0.10565324E-07	-0.21250512E-11	0.24647571E+05	-0.12691387E+02						4
NH3_N2O(S)	modH	4N	30	1	S	300.000	900.000	900.00	1
0.61618842E+01	0.15551065E-01	-0.10254195E-04	0.96870338E-08	-0.50881427E-11					2
-0.16920316E+05	-0.19193388E+02	0.61618842E+01	0.15551065E-01	-0.10254195E-04					3
0.96870338E-08	-0.50881427E-11	-0.16920316E+05	-0.19193388E+02						4
NH3x2_N2O(S)	modH	7N	40	1	S	300.000	900.000	900.00	1
0.86306452E+01	0.26529925E-01	-0.20074736E-04	0.16613441E-07	-0.73244896E-11					2
-0.33800620E+05	-0.24815478E+02	0.86306452E+01	0.26529925E-01	-0.20074736E-04					3
0.16613441E-07	-0.73244896E-11	-0.33800620E+05	-0.24815478E+02						4
NH2OH_NH3(S)	modH	7N	20	1	S	300.000	900.000	900.00	1
0.60302427E+01	0.77777939E-02	0.27940706E-04	-0.36398628E-07	0.13982413E-10					2
-0.39675214E+05	-0.22977751E+02	0.60302427E+01	0.77777939E-02	0.27940706E-04					3
-0.36398628E-07	0.13982413E-10	-0.39675214E+05	-0.22977751E+02						4
N2O(S)	modH	1N	20	1	S	300.000	900.000	900.00	1
0.26726268E+01	0.15458659E-01	-0.22226913E-04	0.18479440E-07	-0.64676822E-11					2
0.53402334E+04	-0.42629688E+01	0.26726268E+01	0.15458659E-01	-0.22226913E-04					3
0.18479440E-07	-0.64676822E-11	0.53402334E+04	-0.42629688E+01						4
N2O2(S)	modH	1N	10	2	S	300.000	900.000	900.00	1
0.47080697E+01	0.23493158E-02	0.10273021E-04	-0.15824356E-07	0.67719578E-11					2
-0.15015947E+04	-0.10871134E+02	0.47080697E+01	0.23493158E-02	0.10273021E-04					3
-0.15824356E-07	0.67719578E-11	-0.15015947E+04	-0.10871134E+02						4
N2O2_NO(S)	S+9H	1N	20	3	S	300.000	900.000	900.00	1
0.99784625E+01	0.26263955E-03	0.15352116E-04	-0.19071706E-07	0.72563170E-11					2
0.64603915E+04	-0.20836035E+02	0.99784625E+01	0.26263955E-03	0.15352116E-04					3
-0.19071706E-07	0.72563170E-11	0.64603915E+04	-0.20836035E+02						4

asN203(S)	S+7H	1N	20	3	S	300.000	900.000	900.00	1
0.51138711E+01	0.19044502E-01	-0.18135772E-04	0.10930876E-07	-0.34342426E-11					2
-0.21326931E+04	-0.14342027E+02	0.51138711E+01	0.19044502E-01	-0.18135772E-04					3
0.10930876E-07	-0.34342426E-11	-0.21326931E+04	-0.14342027E+02						4
ctN203(S)	S+7H	1N	20	3	S	300.000	900.000	900.00	1
0.58034984E+01	0.18396183E-01	-0.18345838E-04	0.11148009E-07	-0.33241620E-11					2
0.22521649E+04	-0.16245086E+02	0.58034984E+01	0.18396183E-01	-0.18345838E-04					3
0.11148009E-07	-0.33241620E-11	0.22521649E+04	-0.16245086E+02						4
NO2_NO2(S)	-312H	1N	20	4	S	300.000	900.000	900.00	1
0.99114446E+01	0.15453165E-03	0.26711023E-04	-0.35821302E-07	0.14648681E-10					2
-0.31261830E+04	-0.23255248E+02	0.99114446E+01	0.15453165E-03	0.26711023E-04					3
-0.35821302E-07	0.14648681E-10	-0.31261830E+04	-0.23255248E+02						4
asN204(S)	-310H	1N	20	4	S	300.000	900.000	900.00	1
0.39991462E+01	0.31635942E-01	-0.34829609E-04	0.21351964E-07	-0.58444396E-11					2
-0.11498490E+05	-0.72710397E+01	0.39991462E+01	0.31635942E-01	-0.34829609E-04					3
0.21351964E-07	-0.58444396E-11	-0.11498490E+05	-0.72710397E+01						4
symN204(S)	S10H	1N	20	4	S	300.000	900.000	900.00	1
0.50493716E+01	0.26768150E-01	-0.26345097E-04	0.14366517E-07	-0.36968377E-11					2
-0.92342913E+04	-0.96041535E+01	0.50493716E+01	0.26768150E-01	-0.26345097E-04					3
0.14366517E-07	-0.36968377E-11	-0.92342913E+04	-0.96041535E+01						4
NOZ(S)	modN	10	1		S	300.000	900.000	900.00	1
0.20694296E+01	0.88151926E-02	-0.23439092E-04	0.27801307E-07	-0.12014194E-10					2
0.17650991E+05	-0.75653143E+01	0.20694296E+01	0.88151926E-02	-0.23439092E-04					3
0.27801307E-07	-0.12014194E-10	0.17650991E+05	-0.75653143E+01						4
NOZ_HONO(S)	-35H	1N	20	3	S	300.000	900.000	900.00	1
0.55851600E+01	0.18394972E-01	-0.20341705E-04	0.16359272E-07	-0.64691654E-11					2
-0.37396893E+04	-0.17960755E+02	0.55851600E+01	0.18394972E-01	-0.20341705E-04					3
0.16359272E-07	-0.64691654E-11	-0.37396893E+04	-0.17960755E+02						4
NOZ_HNO3(S)	-45H	1N	20	4	S	300.000	900.000	900.00	1
0.47676314E+01	0.27661404E-01	-0.28497962E-04	0.17797086E-07	-0.54483732E-11					2
-0.10994861E+05	-0.12866004E+02	0.47676314E+01	0.27661404E-01	-0.28497962E-04					3
0.17797086E-07	-0.54483732E-11	-0.10994861E+05	-0.12866004E+02						4
NOZ_NH3(S)	S+4H	3N	20	1	S	300.000	900.000	900.00	1
0.34432326E+01	0.23614717E-01	-0.37438054E-04	0.36217036E-07	-0.14169560E-10					2
-0.17259837E+04	-0.11362451E+02	0.34432326E+01	0.23614717E-01	-0.37438054E-04					3
0.36217036E-07	-0.14169560E-10	-0.17259837E+04	-0.11362451E+02						4
NOZ_H2O(S)	S+4H	2N	10	2	S	300.000	900.000	900.00	1
0.27470154E+01	0.28228976E-01	-0.54828740E-04	0.55260800E-07	-0.21532490E-10					2
-0.21950648E+05	-0.93973681E+01	0.27470154E+01	0.28228976E-01	-0.54828740E-04					3
0.55260800E-07	-0.21532490E-10	-0.21950648E+05	-0.93973681E+01						4
ctN203_10c(S)	modH	4N	30	3	S	300.000	900.000	900.00	1
0.64566089E+01	0.33923915E-01	-0.32365730E-04	0.19643541E-07	-0.56804579E-11					2
-0.17672591E+05	-0.23253177E+02	0.64566089E+01	0.33923915E-01	-0.32365730E-04					3
0.19643541E-07	-0.56804579E-11	-0.17672591E+05	-0.23253177E+02						4
ZNO2(S)	modN	10	2		S	300.000	900.000	900.00	1
0.18380622E+01	0.12405259E-01	-0.17012805E-04	0.13947165E-07	-0.51581607E-11					2
0.17454741E+05	-0.52422587E+01	0.18380622E+01	0.12405259E-01	-0.17012805E-04					3
0.13947165E-07	-0.51581607E-11	-0.17454741E+05	-0.52422587E+01						4
ZNO2_HONO(S)	modH	1N	20	4	S	300.000	900.000	900.00	1

0.52419488E+01 0.27098668E-01-0.27487697E-04 0.15182621E-07-0.37525996E-11	2
0.10618470E+04-0.13085625E+02 0.52419488E+01 0.27098668E-01-0.27487697E-04	3
0.15182621E-07-0.37525996E-11 0.10618470E+04-0.13085625E+02	4
ZNO2_H2O(S) -35H 2N 10 3 S 300.000 900.000 900.00	1
0.27643618E+01 0.31989674E-01-0.56703512E-04 0.53938450E-07-0.20393132E-10	2
-0.19356459E+05-0.96183301E+01 0.27643618E+01 0.31989674E-01-0.56703512E-04	3
0.53938450E-07-0.20393132E-10-0.19356459E+05-0.96183301E+01	4
ZNO2_NH3(S) -35H 3N 20 2 S 300.000 900.000 900.00	1
0.57210765E+01 0.21177818E-01-0.26910917E-04 0.23293474E-07-0.88268441E-11	2
0.24526520E+04-0.19078080E+02 0.57210765E+01 0.21177818E-01-0.26910917E-04	3
0.23293474E-07-0.88268441E-11 0.24526520E+04-0.19078080E+02	4
NH3_NH2NO(S) modH 6N 30 1 S 300.000 900.000 900.00	1
0.58276540E+01 0.17377629E-01 0.69614703E-05-0.17699280E-07 0.76602281E-11	2
-0.26457775E+05-0.21329732E+02 0.58276540E+01 0.17377629E-01 0.69614703E-05	3
-0.17699280E-07 0.76602281E-11-0.26457775E+05-0.21329732E+02	4
NH3_NH2NO2(S) modH 6N 30 2 S 300.000 900.000 900.00	1
0.49742474E+01 0.27933099E-01-0.57713958E-05-0.10529971E-07 0.61978183E-11	2
-0.35363964E+05-0.15831413E+02 0.49742474E+01 0.27933099E-01-0.57713958E-05	3
-0.10529971E-07 0.61978183E-11-0.35363964E+05-0.15831413E+02	4
HZSM5(S) ownH 1 S 300.000 900.000 900.00	1
-0.35524778E+01 0.11980479E+00-0.19456364E-03 0.15664527E-06-0.50206795E-10	2
-0.28193329E+04 0.58990408E+01-0.35524778E+01 0.11980479E+00-0.19456364E-03	3
0.15664527E-06-0.50206795E-10-0.28193329E+04 0.58990408E+01	4
HZSM5(B) ownH 0 S 300.000 900.000 900.00	1
-0.35524778E+01 0.11980479E+00-0.19456364E-03 0.15664527E-06-0.50206795E-10	2
-0.28193329E+04 0.58990408E+01-0.35524778E+01 0.11980479E+00-0.19456364E-03	3
0.15664527E-06-0.50206795E-10-0.28193329E+04 0.58990408E+01	4

E

Supporting Information for Chapter 7

This appendix contains the structures of the minima of the active site and the nitrite on a 23 T-atoms containig cluster and a study on the influence of the O-Al-O angle on the adsorption energies for NO.

T21 Cluster

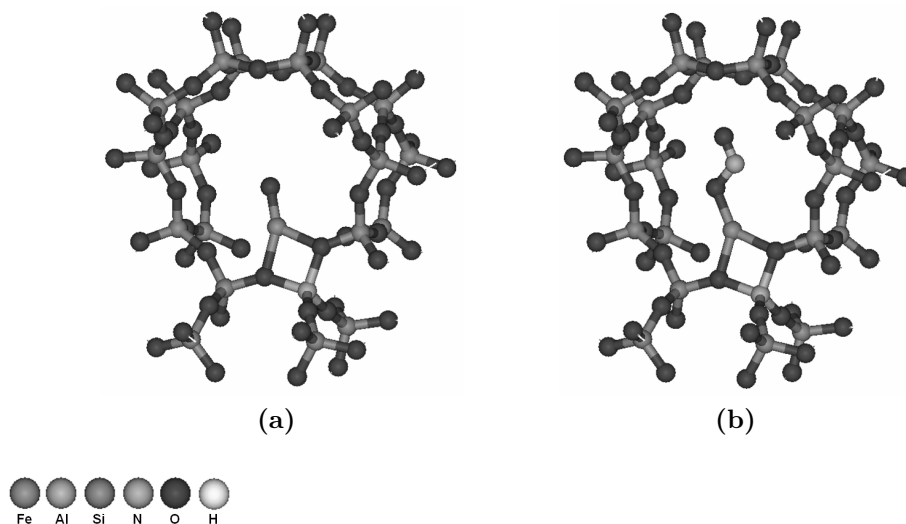


Figure E.1: Geometries of the minima of FeO (a) on the PES with $M_S=6$ and FeONO (b) on the PES with $M_S=5$ on a 21 T-atoms containing cluster of the zeolite. Dangling bonds are not shown.

Table E.1: Influence of the zeolite framework on the adsorption energy of NO on FeO. Angles and bond length refer to the relaxed FeO on the PES with $M_S=6$ (T5-cluster). The energies are the electronic energies only. The third row corresponds to the unperturbed original active site.

O-Al-O	Si-Al-Si	Si-O	O-Al	ΔE_{elec}
[deg]	[deg]	[Å]	[Å]	[kcal/mol]
88.51	130.02	1.67	1.78	-35.19
89.40	132.54	1.67	1.78	-35.02
90.60	135.42	1.68	1.78	-34.83
91.45	137.33	1.68	1.78	-34.71
92.53	139.63	1.69	1.79	-34.56
93.64	141.88	1.69	1.79	-34.42
94.76	144.05	1.70	1.79	-34.28

F

Supporting Information for Chapter 9

In this section the reaction rate expressions and the thermodynamic data for all surface species on Fe-ZSM5 are presented.

Table F.1: Reaction rates of surface reactions on mononuclear iron sites.

Reactant	Product	A [1/s]	β [-]	E _a [kcal/mol]	Adjust A x E _a
NO oxidation on FeO					
FeO_4(S)	\rightleftharpoons FeO_6(S)	2.39E+12	0	1.82	
FeO_NO_7(S)	\rightleftharpoons FeO_6(S) + NO	2.08E+10	1	1.07	
FeONO_5(S)	\rightleftharpoons FeO_4(S) + NO	2.08E+10	1	36.99	
FeO_NO_7(S)	\rightleftharpoons FeONO_5(S)	2.08E+10	1	0.65	
FeONO_5(S)	\rightleftharpoons FeO2N_5(S)	9.14E+12	0	3.51	
O2FeONO_7(S)	\rightleftharpoons FeONO_5(S) + O2	3.89E+10	1	5.93	
O2FeONO_7(S)	\rightleftharpoons O2FeONO_5(S)	2.98E+09	1	11.97	
O2FeONO_5(S)	\rightleftharpoons FeO2_4(S) + NO2	1.16E+14	0	10.53	
O2FeONO_7(S)	\rightleftharpoons FeO2_6(S) + NO2	2.08E+10	1	19.92	
FeO2_4(S)	\rightleftharpoons FeO2_6(S)	8.72E+12	0	2.73	
FeO2_6(S)	\rightleftharpoons OFeO_6(S)	4.99E+12	0	22.04	
OFeO-NO_7(S)	\rightleftharpoons OFeO_6(S) + NO	2.08E+10	1	2.73	
OFeO-NO_7(S)	\rightleftharpoons OFeONO_7(S)	1.03E+13	0	5.46	
OFeONO_7(S)	\rightleftharpoons FeO_6(S) + NO2	2.08E+10	1	5.61	
FeOONO_c_5(S)	\rightleftharpoons FeO2_6(S) + NO	2.01E+13	1	13.14	
FeOONO_t_5(S)	\rightleftharpoons FeO2_4(S) + NO	2.40E+10	1	8.98	
FeOONO_t_5(S)	\rightleftharpoons FeOONO_c_5(S)	8.09E+12	0	9.21	
FeOONO_c_5(S)	\rightleftharpoons FeO_4(S) + NO2	1.32E+12	1	11.73	
O2FeNO_5(S)	\rightleftharpoons FeO2_4(S) + NO	2.08E+11	1	22.52	10
O2FeNO_5(S)	\rightleftharpoons FeONOO_5(S)	2.70E+12	0	25.70	
FeONOO_5(S)	\rightleftharpoons FeOONO_t_5(S)	2.48E+13	0	2.02	
O2FeNO_5(S)	\rightleftharpoons OFeO-NO_5(S)	2.42E+13	0	37.56	
OFeO-NO_5(S)	\rightleftharpoons OFeONO_5(S)	1.36E+12	0	9.19	
OFeONO_7(S)	\rightleftharpoons OFeONO_5(S)	6.00E+13	0	2.07	
OFeONO_5(S)	\rightleftharpoons FeO_4(S) + NO2	2.08E+10	1	20.67	
OFeONO_5(S)	\rightleftharpoons FeO2NO_5(S)	5.46E+12	0	10.80	
NO oxidation on FeONO					
ONFeONO_6(S)	\rightleftharpoons FeONO_5(S) + NO	2.08E+10	1	1.98	
ONFeONO_4(S)	\rightleftharpoons ONFeONO_6(S)	6.17E+12	0	19.72	
ONFeONO_4(S)	\rightleftharpoons FeNO_3(S) + NO2	2.08E+10	1	26.28	
FeNO_O2_5(S)	\rightleftharpoons FeNO_3(S) + O2	2.08E+10	1	0.21	
O2FeNO_5(S)	\rightleftharpoons FeNO_O2_5(S)	1.44E+14	0	13.92	
ONFeONO-O2_6(S)	\rightleftharpoons ONFeONO_4(S) + O2	7.63E+12	0	2.79	
ONFeONO-O2_6(S)	\rightleftharpoons ONOFeOONO_t_6(S)	8.20E+11	0	7.01	
ONOFeOONO_t_6(S)	\rightleftharpoons FeOONO_t_5(S) + NO2	2.08E+10	1	18.50	
O2FeONO-NO_6(S)	\rightleftharpoons O2FeONO_5(S) + NO	2.08E+10	1	19.05	
O2FeONO-NO_6(S)	\rightleftharpoons ONOFeOONO_t_6(S)	6.00E+12	0	9.01	
ONOFeOONO_t_6(S)	\rightleftharpoons ONOFeOONO_c_6(S)	1.03E+13	0	9.90	
ONOFeOONO_c_6(S)	\rightleftharpoons OFeONO_5(S) + NO2	1.08E+13	0	10.48	
ONOFeONO_6(S)	\rightleftharpoons OFeONO_5(S) + NO	2.08E+10	1	32.33	
ONOFeONO_6(S)	\rightleftharpoons FeONO_5(S) + NO2	2.08E+10	1	16.01	
ONFeOONO_t_6(S)	\rightleftharpoons O2FeNO_5(S) + NO	2.16E+13	0	9.64	
ONFeOONO_t_6(S)	\rightleftharpoons ONFeOONO_c_6(S)	7.79E+11	0	9.17	
ONFeOONO_c_6(S)	\rightleftharpoons ONFeO_5(S) + NO2	6.94E+12	0	11.40	
ONFeO_5(S)	\rightleftharpoons FeONO_5(S)	2.32E+12	0	3.93	
NO oxidation on FeO2N					
O2FeO2N_7(S)	\rightleftharpoons FeO2N_5(S) + O2	5.27E+13	0	4.15	
O2FeO2N_5(S)	\rightleftharpoons O2FeO2N_7(S)	2.08E+10	1	0.02	
ONFeO2N_6(S)	\rightleftharpoons FeO2N_5(S) + NO	2.08E+10	1	1.05	
ONFeO2N_4(S)	\rightleftharpoons ONFeO2N_6(S)	1.31E+11	1	18.40	
O2FeO2N_NO_6(S)	\rightleftharpoons O2FeO2N_5(S) + NO	2.08E+10	1	11.94	
O2FeO2N_NO_6(S)	\rightleftharpoons NO2FeOONO_t_6(S)	4.29E+10	1	0.03	
NO2FeOONO_t_6(S)	\rightleftharpoons ONFeO2N_4(S) + O2	1.49E+10	1	12.87	
NO2FeOONO_t_6(S)	\rightleftharpoons NO2FeOONO_c_6(S)	1.10E+12	1	9.18	

Table F.1: (continued)

Reactant	Product	A [1/s]	β [-]	E _a [kcal/mol]	Adjust A x E _a
NO2FeOONO_c.6(S)	\rightleftharpoons NO2FeO_5(S) + NO2	1.72E+13	0	10.34	
NO2FeOONO_c.6(S)	\rightleftharpoons NO2FeOONO_R.6(S)	1.03E+11	0	1.59	
NO2FeOONO_R.6(S)	\rightleftharpoons NO2FeO_5(S) + NO2	2.08E+13	0	13.42	
NO2FeONO_6(S)	\rightleftharpoons NO2FeO_5(S) + NO	2.08E+10	1	34.15	
NO2FeONO_6(S)	\rightleftharpoons FeO2N_5(S) + NO2	2.08E+10	1	14.62	
ONFeONO_6(S)	\rightleftharpoons NO2FeONO_6(S)	8.02E+11	0	0.71	
ONFeONO_4(S)	\rightleftharpoons ONFeONO_c.4(S)	3.96E+12	0	1.89	
ONFeONO_c.4(S)	\rightleftharpoons ONFeO2N_4(S)	5.94E+12	0	4.77	
NO oxidation on FeO₂NO					
O2FeO2NO_7(S)	\rightleftharpoons FeO2NO_5(S) + O2	1.67E+13	0	3.77	
O2FeO2NO_5(S)	\rightleftharpoons O2FeO2NO_7(S)	7.77E+11	0	6.17	
ONFeO2NO_6(S)	\rightleftharpoons FeO2NO_5(S) + NO	2.08E+10	1	1.46	
ONFeO2NO_6(S)	\rightleftharpoons ONFeO2NO_4(S)	2.78E+12	0	2.15	
O2FeO2NO_NO_6(S)	\rightleftharpoons O2FeO2NO_5(S) + NO	2.08E+10	1	5.81	
O2FeO2NO_NO_6(S)	\rightleftharpoons ONO2FeOONO_t6(S)	5.36E+10	1	0.30	
ONO2FeOONO_t6(S)	\rightleftharpoons ONFeO2NO_4(S) + O2	2.63E+11	0	13.78	
ONO2FeOONO_t6(S)	\rightleftharpoons ONO2FeOONO_c6(S)	5.85E+12	0	9.41	
ONO2FeOONO_c6(S)	\rightleftharpoons OFeO2NO_5(S) + NO2	1.55E+13	0	10.10	
ONFeO2NO_6(S)	\rightleftharpoons OFeO2NO_5(S) + NO	2.08E+10	1	37.99	
ONFeO2NO_6(S)	\rightleftharpoons FeO2NO_5(S) + NO2	2.08E+10	1	14.90	
NO2FeONO_6(S)	\rightleftharpoons FeO2NO_5(S) + NO	5.80E+11	0	44.90	
NO oxidation; H₂O influence					
H2OFeO_6(S)	\rightleftharpoons FeO_6(S) + H2O	2.08E+10	1	22.91	
H2OFeO_6(S)	\rightleftharpoons HOFeOH_u.6(S)	2.24E+13	0	14.06	
HOFeOH_4(S)	\rightleftharpoons HOFeOH_u.6(S)	6.45E+12	0	1.01	
HOFeOH-NO_5(S)	\rightleftharpoons HOFeOH_4(S) + NO	2.08E+10	1	17.46	
HOFeOH-NO_5(S)	\rightleftharpoons HONOFeOH_5(S)	6.65E+11	0	9.17	
HONOFeOH_5(S)	\rightleftharpoons FeOH_5(S) + HONO	2.08E+10	1	13.07	
HOFeOH_NO2_5(S)	\rightleftharpoons HOFeOH_4(S) + NO2	2.08E+10	1	15.98	
HOFeOH_NO2_5(S)	\rightleftharpoons HNO3FeOH_5(S)	1.16E+11	0	15.24	
HNO3FeOH_5(S)	\rightleftharpoons FeOH_5(S) + HNO3	2.08E+10	1	12.83	
H2OFeO2N_5(S)	\rightleftharpoons FeO2N_5(S) + H2O	2.08E+10	1	19.81	
HOFeHONO_5(S)	\rightleftharpoons H2OFeO2N_5(S)	6.29E+11	0	3.08	
HOFeHONO_5(S)	\rightleftharpoons FeOH_5(S) + HONO	2.08E+10	1	8.50	
H2OFeO2NO_5(S)	\rightleftharpoons FeO2NO_5(S) + H2O	2.08E+10	1	19.87	
HOFeHNO3_5(S)	\rightleftharpoons H2OFeO2NO_5(S)	5.71E+09	1	3.80	
HOFeHNO3_5(S)	\rightleftharpoons FeOH_5(S) + HNO3	2.08E+10	1	10.89	
NO oxidation on FeOH					
O2FeOH_7(S)	\rightleftharpoons FeOH_5(S) + O2	3.74E+14	0	8.85	
O2FeOH_5(S)	\rightleftharpoons O2FeOH_7(S)	6.26E+12	0	5.19	
O2FeOH_NO_6(S)	\rightleftharpoons O2FeOH_5(S) + NO	2.08E+11	1	5.58	10
O2FeOH_NO_6(S)	\rightleftharpoons HOFeOONO_t.6(S)	3.79E+09	1	0.42	
ONFeOH_6(S)	\rightleftharpoons FeOH_5(S) + NO	2.08E+10	1	3.88	
ONFeOH_6(S)	\rightleftharpoons ONFeOH_4(S)	2.08E+10	0	1.61	
ONFeOH-O2_6(S)	\rightleftharpoons ONFeOH_4(S) + O2	3.52E+13	0	5.29	
ONFeOH-O2_6(S)	\rightleftharpoons O2FeOH_5(S) + NO	2.08E+10	1	6.71	
ONFeOH-O2_6(S)	\rightleftharpoons HOFeOONO_t.6(S)	1.56E+12	0	9.16	
HOFeOONO_t.6(S)	\rightleftharpoons HOFeOONO_c.6(S)	8.09E+13	0	10.00	10
HOFeOONO_c.6(S)	\rightleftharpoons HOFeOONO_cu.6(S)	4.24E+12	0	1.05	
HOFeOONO_c.6(S)	\rightleftharpoons HOFeO_d.5(S) + NO2	5.84E+13	0	10.82	10
HOFeOONO_cu.6(S)	\rightleftharpoons HOFeO_u.5(S) + NO2	8.18E+13	0	10.40	10
HOFeO_d.5(S)	\rightleftharpoons HOFeO_u.5(S)	1.08E+14	0	2.29	
HOFeO_NO_6(S)	\rightleftharpoons HOFeO_u.5(S) + NO	2.08E+10	1	1.52	
HOFeO_NO_6(S)	\rightleftharpoons HOFeONO_u.6(S)	6.89E+12	0	1.29	
HOFeONO_u.6(S)	\rightleftharpoons HOFeONO_d.6(S)	1.23E+13	0	1.12	

Table F.1: (continued)

Reactant	Product	A [1/s]	β [-]	E _a [kcal/mol]	Adjust A x E _a
HOFeONO_u.6(S)	\rightleftharpoons FeOH_5(S) + NO2	2.08E+10	1	19.44	
HOFeONO_d.6(S)	\rightleftharpoons FeOH_5(S) + NO2	2.08E+10	1	19.60	
HOFeO2-NO_6(S)	\rightleftharpoons O2FeOH_7(S) + NO	2.76E+11	1	7.82	
HOFeO2-NO_6(S)	\rightleftharpoons HOFeOONO_t.6(S)	8.15E+12	0	9.37	
HOFeOONO_t.6(S)	\rightleftharpoons HOFeO_d.5(S) + NO2	1.75E+13	0	26.54	
HOFeOONO_t.6(S)	\rightleftharpoons HOFeOONO_R.6(S)	1.57E+12	0	8.29	
HOFeOONO_R.4(S)	\rightleftharpoons HOFeOONO_R.6(S)	2.75E+12	0	0.58	
HOFeOONO_R.4(S)	\rightleftharpoons HOFeO-ONOccd.4(S)	6.42E+13	0	5.64	
HOFeO-ONOccd.4(S)	\rightleftharpoons HOFeO-ONOccu.4(S)	4.92E+13	0	4.54	
HOFeO-ONOccu.4(S)	\rightleftharpoons HOFeO-ONOccu.4(S)	1.20E+13	0	0.94	
HOFeO-N2O3_5(S)	\rightleftharpoons HOFeO-ONOccu.4(S) + NO	2.08E+10	1	13.64	
HOFe(ONO)2_5(S)	\rightleftharpoons HOFeO-N2O3_5(S)	5.20E+11	0	2.64	
HOFe(ONO)2_5(S)	\rightleftharpoons HOFeONO_u.4(S) + NO2	6.25E+12	0	1.71	
HOFeONO_u.4(S)	\rightleftharpoons HOFeONO_u.6(S)	3.46E+12	0	1.70	
HOFeO-ONOccu.6(S)	\rightleftharpoons HOFeO_u.5(S) + NO2	2.08E+10	1	0.23	
HOFeO-ONOccu.4(S)	\rightleftharpoons HOFeO-ONOccu.6(S)	2.08E+10	1	0.15	
HOFeO-ONOccu.4(S)	\rightleftharpoons HOFeO2NO_4(S)	4.60E+12	0	2.70	10 -2
HOFeO2NO_4(S)	\rightleftharpoons HOFeO2NO_6(S)	2.08E+10	1	0.10	
HOFeO2NO-NO_5(S)	\rightleftharpoons HOFeO2NO_4(S) + NO	2.08E+10	1	18.50	
HOFeO2NO-NO_5(S)	\rightleftharpoons HONOFeO2NO_5(S)	4.34E+11	0	4.11	
HONOFeO2NO_5(S)	\rightleftharpoons FeO2NO_5(S) + HONO	2.08E+10	1	15.33	
HONOFeO2NO_5(S)	\rightleftharpoons HOFeONO_u.4(S) + NO2	4.59E+14	1	37.08	
HOFeO2NO_6(S) + NO	\rightleftharpoons HOFeO2N_6(S) + NO2	6.89E+07	1	38.21	
HOFeONO_d.6(S)	\rightleftharpoons HOFeO2N_6(S)	3.83E+11	0	0.63	
ONFeOH-O2_6(S)	\rightleftharpoons HONOFeO2_6(S)	1.51E+11	0	8.69	
HONOFeO2_6(S)	\rightleftharpoons FeO2_6(S) + HONO	2.08E+10	1	14.15	
HOFeO2-NO2_6(S)	\rightleftharpoons O2FeOH_5(S) + NO2	2.08E+10	1	6.20	
HOFeO2-NO2_6(S)	\rightleftharpoons HNO3FeO2_6(S)	7.47E+09	0	15.26	
HNO3FeO2_6(S)	\rightleftharpoons FeO2_6(S) + HNO3	2.08E+10	1	13.11	
HNO3FeO_6(S)	\rightleftharpoons HOFeO2NO_6(S)	7.14E+09	1	15.66	
HNO3FeO_6(S)	\rightleftharpoons FeO_6(S) + HNO3	2.08E+10	1	16.61	
OFeHNO3_6(S)	\rightleftharpoons HOFeO2NO_6(S)	4.68E+11	0	1.84	
OFeHNO3_6(S)	\rightleftharpoons FeO_6(S) + HNO3	2.08E+10	1	8.67	
HOFeONO-NO_5(S)	\rightleftharpoons HOFeONO_u.4(S) + NO	2.08E+10	1	14.40	
HOFeONO-NO_5(S)	\rightleftharpoons HONOFeONO_5(S)	6.48E+11	0	7.25	
HONOFeONO_5(S)	\rightleftharpoons FeONO_5(S) + HONO	2.08E+10	1	14.81	
HOFeONO-NO2_5(S)	\rightleftharpoons HOFeONO_u.4(S) + NO2	2.08E+10	1	12.14	
HOFeONO-NO2_5(S)	\rightleftharpoons HNO3FeONO_5(S)	1.77E+10	0	12.42	
HNO3FeONO_5(S)	\rightleftharpoons FeONO_5(S) + HNO3	2.08E+10	1	13.45	
OFeHONO_6(S)	\rightleftharpoons HOFeONO_u.6(S)	7.87E+11	0	5.96	
OFeHONO_6(S)	\rightleftharpoons FeO_6(S) + HONO	2.08E+10	1	12.59	
HONOFeO_6(S)	\rightleftharpoons HOFeONO_d.6(S)	8.99E+11	0	6.00	
HONOFeO_6(S)	\rightleftharpoons FeO_6(S) + HONO	2.08E+10	1	18.93	
HOFeO2N-NO_5(S)	\rightleftharpoons HOFeO2N_4(S) + NO	2.08E+10	1	16.99	
HOFeO2N-NO_5(S)	\rightleftharpoons HONOFeO2N_5(S)	4.53E+11	0	4.80	
HONOFeO2N_5(S)	\rightleftharpoons FeO2N_5(S) + HONO	2.08E+10	1	15.27	
HOFeO2N_4(S)	\rightleftharpoons HOFeO2N_6(S)	2.08E+10	1	0.07	
HOFeO2N-NO2_5(S)	\rightleftharpoons HOFeO2N_4(S) + NO2	2.08E+10	1	16.62	
HOFeO2N-NO2_5(S)	\rightleftharpoons HNO3FeO2N_5(S)	2.75E+07	1	10.66	
HNO3FeO2N_5(S)	\rightleftharpoons FeO2N_5(S) + HNO3	2.08E+10	1	13.69	
HOFeO2NO-NO25(S)	\rightleftharpoons HOFeO2NO_4(S) + NO2	2.08E+10	1	18.10	
HOFeO2NO-NO25(S)	\rightleftharpoons HNO3FeO2NO_5(S)	2.87E+07	1	10.87	
HNO3FeO2NO_5(S)	\rightleftharpoons FeO2NO_5(S) + HNO3	2.08E+10	1	13.76	

Table F.1: (continued)

Reactant	Product	A	β	E_a	Adjust	
		[1/s]	[-]	[kcal/mol]	A x	E_a
SCR on Fe-ZSM5; Part 1						
NH3FeO.6(S)	\rightleftharpoons FeO.6(S) + NH3	2.08E+10	1	26.75		
NH3FeO.6(S)	\rightleftharpoons NH2FeOH.6(S)	1.31E+10	1	22.81		
NH2FeOH.4(S)	\rightleftharpoons NH2FeOH.6(S)	2.08E+10	1	0.16		
NH2FeOH-NO.5(S)	\rightleftharpoons NH2FeOH.4(S) + NO	2.08E+11	1	13.28	10	-3
NH2FeOH-NO.5(S)	\rightleftharpoons NH2NOFeOH.5(S)	1.83E+12	0	3.24		
NH2NOFeOH.5(S)	\rightleftharpoons FeOH.5(S) + NH2NO	2.08E+10	1	8.51		
NH3FeOH.5(S)	\rightleftharpoons FeOH.5(S) + NH3	2.08E+10	1	20.31		
NH2FeOH2.5(S)	\rightleftharpoons NH3FeOH.5(S)	3.12E+11	0	2.05		
NH2FeOH2.5(S)	\rightleftharpoons FeNH2.5(S) + H2O	2.08E+10	1	9.64		
NH2FeONO.6(S)	\rightleftharpoons FeNH2.5(S) + NO2	2.08E+10	1	24.06		
NH2NOFeO.6(S)	\rightleftharpoons NH2FeONO.6(S)	9.43E+10	1	6.87	10	
NH2NOFeO.6(S)	\rightleftharpoons FeO.6(S) + NH2NO	2.08E+11	1	9.08	10	-3
NH2FeOH.NO2.5(S)	\rightleftharpoons NH2FeOH.4(S) + NO2	2.08E+10	1	13.59		
NH2FeOH.NO2.5(S)	\rightleftharpoons NH2NO2FeOH.5(S)	1.29E+12	0	4.75		
NH2NO2FeOH.5(S)	\rightleftharpoons FeOH.5(S) + NH2NO2	2.08E+10	1	11.41		
NH3FeO2N.5(S)	\rightleftharpoons FeO2N.5(S) + NH3	2.08E+10	1	23.56		
NH2FeHONO.5(S)	\rightleftharpoons NH3FeO2N.5(S)	1.32E+10	1	0.83		
NH2FeHONO.5(S)	\rightleftharpoons FeNH2.5(S) + HONO	2.08E+10	1	7.74		
HONOFeNH2.5(S)	\rightleftharpoons FeNH2.5(S) + HONO	2.08E+10	1	12.54		
HONOFeNH2.5(S)	\rightleftharpoons NH2FeOH-NO.5(S)	1.12E+12	0	5.01		
HNO3FeNH2.5(S)	\rightleftharpoons FeNH2.5(S) + HNO3	2.08E+10	1	12.38		
HNO3FeNH2.5(S)	\rightleftharpoons HOFNH2.NO2.5(S)	1.60E+10	1	8.54		
HOFNH2.NO2.5(S)	\rightleftharpoons NH2FeOH.4(S) + NO2	2.08E+10	1	14.78		
NH2FeHNO.5(S)	\rightleftharpoons FeNH2.5(S) + HNO	2.08E+10	1	20.13		
NH2FeHNO.3(S)	\rightleftharpoons NH2FeHNO.5(S)	9.02E+12	0	0.29		
NH2FeHNO.3(S)	\rightleftharpoons NH3FeNO.3(S)	2.66E+11	1	10.58		
NH3FeNO.3(S)	\rightleftharpoons FeNO.3(S) + NH3	2.08E+10	1	20.66		
SCR on Fe-ZSM5; Part 2						
NH2-ONFeOH.5(S)	\rightleftharpoons NH2FeOH.4(S) + NO2	2.08E+10	1	5.30		
NH2-ONFeOH.5(S)	\rightleftharpoons NH2NO-OFFeOH.5(S)	1.34E+12	0	12.48		
NH2NO-OFFeOH.5(S)	\rightleftharpoons HOFFeO.u.5(S) + NH2NO	2.08E+10	1	8.47		
NH3-HOFFeONO.6(S)	\rightleftharpoons HOFFeONO.u.6(S) + NH3	2.08E+10	1	17.82		
NH3-HOFFeONO.6(S)	\rightleftharpoons NH3FeOH.5(S) + NO2	2.08E+10	1	16.95		
NH3-HOFFeONO.6(S)	\rightleftharpoons NH3-OFFeOH.5(S) + NO	2.08E+10	1	27.46		
NH3-HOFFeONO.6(S)	\rightleftharpoons NH2FeOH-HONO6(S)	1.34E+11	1	25.05		
NH2FeOH-HONO6(S)	\rightleftharpoons NH2FeOH.6(S) + HONO	2.08E+10	1	7.62		
NH2FeOH-HONO6(S)	\rightleftharpoons HOFFeOH-NH2NO6(S)	1.82E+08	1	9.00		
HOFFeOH-NH2NO6(S)	\rightleftharpoons HOFFeOH.u.6(S) + NH2NO	2.08E+10	1	10.15		
NH3-HOFFeONO.6(S)	\rightleftharpoons NH2FeONO-H2O6(S)	2.44E+10	1	21.81		
NH2FeONO-H2O6(S)	\rightleftharpoons NH2FeONO.6(S) + H2O	2.08E+10	1	8.25		
NH3-HOFFeOH.6(S)	\rightleftharpoons HOFFeOH.u.6(S) + NH3	2.08E+10	1	15.24		
NH3-HOFFeOH.6(S)	\rightleftharpoons NH2FeOH-H2O.6(S)	3.05E+10	1	20.92		
NH2FeOH-H2O.6(S)	\rightleftharpoons NH2FeOH.6(S) + H2O	2.08E+10	1	7.76		
NH3-OFFeOH.5(S)	\rightleftharpoons HOFFeO.u.5(S) + NH3	2.08E+10	1	22.71		
NH3-OFFeOH.5(S)	\rightleftharpoons NH2-HOFFeOH.5(S)	6.46E+11	1	36.68		
NH3-OFFeOH.7(S)	\rightleftharpoons NH3-OFFeOH.5(S)	5.37E+11	0	2.20		
NH3-OFFeOH.7(S)	\rightleftharpoons NH2-HOFFeOH.7(S)	9.41E+09	1	20.51		
NH3-OFFeOH.7(S)	\rightleftharpoons NH2FeO-OH2.7(S)	5.51E+09	1	23.67		
NH2FeO-OH2.7(S)	\rightleftharpoons NH2FeO.7(S) + H2O	2.08E+10	1	5.43		
NH2FeO.7(S)	\rightleftharpoons NH2FeO.5(S)	2.08E+10	1	0.92		
NH2-HOFFeOH.7(S)	\rightleftharpoons NH2-HOFFeOH.5(S)	6.33E+11	0	0.81		
NH2-HOFFeOH.5(S)	\rightleftharpoons NH2OHFeOH.5(S)	3.69E+12	0	18.73		
NH2OHFeOH.5(S)	\rightleftharpoons FeOH.5(S) + NH2OH	2.08E+10	1	21.15		
NH2-HOFFeOH.5(S)	\rightleftharpoons NH2FeO-OH2.5(S)	1.57E+12	0	16.02		
NH2FeO-OH2.5(S)	\rightleftharpoons NH2FeO.5(S) + H2O	2.08E+10	1	10.92		

Table F.1: (continued)

Reactant	Product	A [1/s]	β [-]	E _a [kcal/mol]	Adjust A x E _a	
NH ₂ NO ₂ FeO ₂ .6(S)	⇒ NH ₂ FeO ₂ .5(S) + NO ₂	1.80E+13	1	31.70		
NH ₂ NO ₂ FeO ₂ .6(S)	⇒ FeO ₂ .6(S) + NH ₂ NO ₂	2.08E+10	1	14.97		
NH ₂ NO ₂ FeO ₂ -d.6(S)	⇒ NH ₂ FeO ₂ .5(S) + NO ₂	3.50E+10	1	4.71		
NH ₂ NO ₂ FeO ₂ -d.6(S)	⇒ NH ₂ NO-OfFeO ₂ .6(S)	2.14E+10	1	9.14		
NH ₂ NO-OfFeO ₂ .6(S)	⇒ OfFeO ₂ .6(S) + NH ₂ NO	2.08E+10	1	10.26		
SCR on Fe-ZSM5; Part 3						
FeNH ₂ .O ₂ .7(S)	⇒ FeNH ₂ .5(S) + O ₂	2.08E+10	1	0.23		
FeNH ₂ .O ₂ .7(S)	⇒ NH ₂ FeO ₂ .7(S)	1.03E+10	0	0.15		
NH ₂ FeO ₂ .7(S)	⇒ NH ₂ FeO ₂ .5(S)	1.29E+12	0	8.60		
NH ₂ FeNO ₂ .6(S)	⇒ FeNH ₂ .5(S) + NO	2.08E+10	1	4.49		
NH ₂ FeNO ₂ .6(S)	⇒ NH ₂ FeNO ₂ .4(S)	2.08E+10	1	0.64		
NH ₂ -ONFeO ₂ .6(S)	⇒ NH ₂ FeNO ₂ .4(S) + O ₂	2.42E+13	0	5.20		
NH ₂ -ONFeO ₂ .6(S)	⇒ NH ₂ FeO ₂ .5(S) + NO	2.08E+10	1	10.34		
NH ₂ -ONFeO ₂ .6(S)	⇒ NH ₂ NOFeO ₂ .6(S)	3.10E+12	0	3.99		
NH ₂ NOFeO ₂ .6(S)	⇒ FeO ₂ .6(S) + NH ₂ NO	2.08E+10	1	8.42		
NH ₃ FeO ₂ .6(S)	⇒ FeO ₂ .6(S) + NH ₃	2.08E+10	1	22.32		
NH ₃ FeO ₂ .6(S)	⇒ NH ₃ -OfFeO ₂ .6(S)	3.16E+12	0	20.53		
NH ₃ -OfFeO ₂ .6(S)	⇒ OfFeO ₂ .6(S) + NH ₃	2.08E+10	1	24.29		
NH ₂ -OfFeOH ₂ .6(S)	⇒ NH ₃ -OfFeO ₂ .6(S)	2.15E+12	0	21.48		
NH ₂ -OfFeOH ₂ .6(S)	⇒ NH ₂ OHFeO ₂ .6(S)	9.56E+10	0	7.63		
NH ₂ OHFeO ₂ .6(S)	⇒ FeO ₂ .6(S) + NH ₂ OH	2.08E+10	1	27.84		
NH ₂ -OfFeOH ₂ .6(S)	⇒ NH ₂ -OfFeOH ₂ .4(S)	2.39E+13	0	0.73		
NH ₂ -HOFeONO ₂ .5(S)	⇒ NH ₂ -OfFeOH ₂ .4(S) + NO	2.08E+10	1	41.85		
NH ₃ -OfFeONO ₂ .7(S)	⇒ NH ₃ -OfFeO ₂ .6(S) + NO	2.08E+10	1	15.58		
NH ₃ -OfFeONO ₂ .7(S)	⇒ NH ₃ FeO ₂ .NO ₂ .7(S)	1.77E+09	1	2.20		
NH ₃ FeO ₂ .NO ₂ .7(S)	⇒ NH ₃ FeO ₂ .6(S) + NO ₂	2.08E+10	1	3.14		
NH ₃ -OfFeONO ₂ .7(S)	⇒ NH ₂ FeOH ₂ .6(S) + NO ₂	5.78E+10	1	18.53		
NH ₃ -OfFeONO ₂ .7(S)	⇒ NH ₃ -OfFeONO ₂ .5(S)	2.08E+10	1	0.55		
NH ₃ -OfFeONO ₂ .5(S)	⇒ NH ₃ FeO ₂ .4(S) + NO ₂	2.08E+10	1	23.30		
NH ₃ FeO ₂ .4(S)	⇒ NH ₃ FeO ₂ .6(S)	1.65E+10	1	6.53		
NH ₃ FeO ₂ .4(S)	⇒ FeO ₂ .4(S) + NH ₃	2.08E+10	1	22.13		
NH ₃ -OfFeONO ₂ .5(S)	⇒ NH ₂ -HOFeONO ₂ .5(S)	1.51E+10	1	29.36		
NH ₂ -HOFeONO ₂ .5(S)	⇒ NH ₂ FeOH ₂ .4(S) + NO ₂	2.08E+10	1	2.37		
NH ₃ -OfFeONO ₂ .5(S)	⇒ OfFeONO ₂ .5(S) + NH ₃	2.08E+10	1	24.77		
NH ₃ -OfFeONO ₂ .7(S)	⇒ OfFeONO ₂ .7(S) + NH ₃	2.08E+10	1	19.64		
NH ₂ FeO ₂ .NO ₂ .6(S)	⇒ NH ₂ FeO ₂ .5(S) + NO	2.08E+10	1	10.06		
NH ₂ FeO ₂ .NO ₂ .6(S)	⇒ NH ₂ FeOONO ₂ .t.6(S)	1.69E+12	1	4.16		
NH ₂ FeOONO ₂ .t.6(S)	⇒ NH ₂ FeOONO ₂ .c.6(S)	3.66E+11	1	10.96		
NH ₂ FeOONO ₂ .c.6(S)	⇒ NH ₂ FeO ₂ .NO ₂ .6(S)	2.47E+09	1	10.45		
NH ₂ FeO ₂ .NO ₂ .6(S)	⇒ NH ₂ FeO ₂ .5(S) + NO ₂	2.08E+10	1	2.03		
NH ₂ FeONO ₂ .6(S)	⇒ NH ₂ FeO ₂ .5(S) + NO	2.08E+10	1	31.68		
NH ₃ -HOFeNO ₂ .4(S)	⇒ ONFeOH ₂ .4(S) + NH ₃	2.08E+10	1	14.22		
NH ₃ -HOFeNO ₂ .4(S)	⇒ NH ₂ FeNO-H ₂ O ₂ .4(S)	1.09E+10	1	18.39		
NH ₂ FeNO-H ₂ O ₂ .4(S)	⇒ NH ₂ FeNO ₂ .4(S) + H ₂ O	2.08E+10	1	3.20		
NH ₂ FeNO ₂ .2(S)	⇒ NH ₂ FeNO ₂ .4(S)	2.08E+10	1	0.23		
NH ₂ FeNO-NO ₂ .3(S)	⇒ NH ₂ FeNO ₂ .2(S) + NO	2.08E+10	1	21.34		
NH ₂ FeNO-NO ₂ .3(S)	⇒ NH ₂ NOFeNO ₂ .3(S)	1.93E+12	0	3.50		
NH ₂ NOFeNO ₂ .3(S)	⇒ FeNO ₂ .3(S) + NH ₂ NO	2.08E+10	1	8.51		
SCR on Fe-ZSM5; Part 4						
NH ₂ FeO ₂ .5(S)	⇒ NH ₂ OOfFe ₂ .5(S)	1.90E+14	0	20.12	10	-3.5
FeOONH ₂ .5(S)	⇒ NH ₂ OOfFe ₂ .5(S)	4.14E+12	0	0.52	10	
FeOONH ₂ .5(S)	⇒ FeO ₂ .4(S) + H ₂ NO	2.08E+10	1	1.64		
NH ₂ FeO ₂ .5(S)	⇒ NH ₂ -OfFeO ₂ .5(S)	4.25E+09	1	34.05		
NH ₂ -OfFeO ₂ .5(S)	⇒ OfFeH ₂ NO ₂ .5(S)	6.36E+09	1	8.19		
OfFeH ₂ NO ₂ .5(S)	⇒ FeO ₂ .4(S) + H ₂ NO	2.08E+10	1	28.01		

Table F.1: (continued)

Reactant		Product	A [1/s]	β [-]	E _a [kcal/mol]	Adjust A x E _a
H2NOFeO.5(S)	\rightleftharpoons	FeO.4(S) + H2NO	2.08E+10	1	28.25	
H2NOFeO.7(S)	\rightleftharpoons	FeO.6(S) + H2NO	2.08E+11	1	23.80	10
H2NOFeO.7(S)	\rightleftharpoons	H2NOFeO.5(S)	2.08E+10	1	0.32	
H2NOFeO.5(S)	\rightleftharpoons	HNOFeOH.5(S)	2.93E+11	0	5.16	
HNOFeOH.5(S)	\rightleftharpoons	FeOH.5(S) + HNO	2.08E+10	1	12.21	
HOFeHNO.5(S)	\rightleftharpoons	FeOH.5(S) + HNO	2.08E+10	1	20.27	
HOFeHNO.3(S)	\rightleftharpoons	HOFeHNO.5(S)	2.08E+10	0	1.20	
HOFeHNO.3(S)	\rightleftharpoons	H2OFeNO.3(S)	1.03E+12	1	7.49	
H2OFeNO.3(S)	\rightleftharpoons	FeNO.3(S) + H2O	2.08E+10	1	16.65	
HOFeONH2.6(S)	\rightleftharpoons	FeOH.5(S) + H2NO	2.08E+10	1	19.47	
HOFeONH2.6(S)	\rightleftharpoons	HOFeONH2.4(S)	2.08E+10	1	1.94	
HOFeONH2.4(S)	\rightleftharpoons	HOFeH2NO.4(S)	6.21E+09	1	9.16	
NH2-OFeOH.4(S)	\rightleftharpoons	HOFeH2NO.4(S)	9.00E+12	0	9.28	
HOFeONH2-NO.5(S)	\rightleftharpoons	HOFeONH2.4(S) + NO	2.08E+10	1	1.52	
HOFeONH2-NO.5(S)	\rightleftharpoons	HOFeO-NH2NO.5(S)	7.21E+08	1	18.63	
HOFeO-NH2NO.5(S)	\rightleftharpoons	HOFeO.d.5(S) + NH2NO	2.08E+10	1	8.59	
OFeHNO.4(S)	\rightleftharpoons	FeO.4(S) + HNO	2.08E+10	1	27.73	
OFeHNO.4(S)	\rightleftharpoons	ONFeOH.4(S)	3.52E+11	1	16.78	
H2NOFeNO.4(S)	\rightleftharpoons	FeNO.3(S) + H2NO	2.08E+10	1	21.50	
H2NOFeNO.4(S)	\rightleftharpoons	OFeNH2NO.4(S)	4.68E+11	0	12.49	
OFeNH2NO.4(S)	\rightleftharpoons	FeO.4(S) + NH2NO	2.08E+10	1	20.92	
HOFeH2NO.4(S)	\rightleftharpoons	H2OFeHNO.4(S)	3.87E+11	1	19.95	
H2OFeHNO.4(S)	\rightleftharpoons	FeHNO.4(S) + H2O	2.08E+10	1	15.13	
HOFeONH2.4(S)	\rightleftharpoons	FeHNO.4(S) + H2O	6.76E+07	1	17.31	
O2FeHNO.6(S)	\rightleftharpoons	FeHNO.4(S) + O2	2.08E+10	1	4.08	
O2FeHNO.6(S)	\rightleftharpoons	FeO2.6(S) + HNO	2.08E+10	1	12.77	
FeOH.5(S) + N2O	\rightleftharpoons	HOFeO.u.5(S) + N2	4.01E+08	1	21.78	
OFeONN.6(S)	\rightleftharpoons	FeO.6(S) + N2O	2.08E+10	1	5.69	
OFeONN.6(S)	\rightleftharpoons	OFeO.6(S) + N2	2.55E+09	1	30.84	
NH2FeONN.5(S)	\rightleftharpoons	FeNH2.5(S) + N2O	2.08E+10	1	1.58	
NH2FeONN.5(S)	\rightleftharpoons	NH2FeO.5(S) + N2	1.49E+09	1	19.01	

Table F.2: Thermodynamic database of the surface species on Fe-ZSM5 as is used in CHEMKIN.

THERMO							
	300.000	1000.000	5000.000				
FeO ₆ (S)	own0	1		S	300.000	800.000	800.00
	0.21207151E+01	0.10463324E-01	-0.21954231E-04	0.20932753E-07	-0.77637614E-11		1
	-0.94108211E+03	-0.40356463E+01	0.21207151E+01	0.10463324E-01	-0.21954231E-04		2
	0.20932753E-07	-0.77637614E-11	-0.94108211E+03	-0.40356463E+01			3
							4
FeO ₄ (S)	own0	1		S	300.000	800.000	800.00
	0.18243632E+01	0.14561339E-01	-0.33628357E-04	0.34182593E-07	-0.13176580E-10		1
	0.93479793E+03	-0.42422156E+01	0.18243632E+01	0.14561339E-01	-0.33628357E-04		2
	0.34182593E-07	-0.13176580E-10	0.93479793E+03	-0.42422156E+01			3
							4
FeO _{NO} _7(S)	ownN	10	2	S	300.000	800.000	800.00
	0.61483594E+01	0.95567718E-02	-0.19335407E-04	0.20122510E-07	-0.82097635E-11		1
	0.81389168E+04	-0.14203773E+02	0.61483594E+01	0.95567718E-02	-0.19335407E-04		2
	0.20122510E-07	-0.82097635E-11	0.81389168E+04	-0.14203773E+02			3
							4
FeONO ₅ (S)	ownN	10	2	S	300.000	800.000	800.00
	0.39963600E+01	0.21291353E-01	-0.37341429E-04	0.33371560E-07	-0.12088795E-10		1
	-0.79744861E+04	-0.93199498E+01	0.39963600E+01	0.21291353E-01	-0.37341429E-04		2
	0.33371560E-07	-0.12088795E-10	-0.79744861E+04	-0.93199498E+01			3
							4
FeO _{2N} _5(S)	H+2N	10	2	S	300.000	800.000	800.00
	0.42023246E+01	0.15973858E-01	-0.20205617E-04	0.12949136E-07	-0.35764082E-11		1
	-0.98004851E+04	-0.11033868E+02	0.42023246E+01	0.15973858E-01	-0.20205617E-04		2
	0.12949136E-07	-0.35764082E-11	-0.98004851E+04	-0.11033868E+02			3
							4
O2FeONO ₇ (S)	ownN	10	4	S	300.000	800.000	800.00
	0.64258586E+01	0.34169647E-01	-0.59802087E-04	0.53263595E-07	-0.19163123E-10		1
	-0.11480552E+05	-0.18703416E+02	0.64258586E+01	0.34169647E-01	-0.59802087E-04		2
	0.53263595E-07	-0.19163123E-10	-0.11480552E+05	-0.18703416E+02			3
							4
O2FeONO ₅ (S)	ownN	10	4	S	300.000	800.000	800.00
	0.55585411E+01	0.39848957E-01	-0.72524296E-04	0.65808105E-07	-0.23812376E-10		1
	-0.53666423E+04	-0.16954712E+02	0.55585411E+01	0.39848957E-01	-0.72524296E-04		2
	0.65808105E-07	-0.23812376E-10	-0.53666423E+04	-0.16954712E+02			3
							4
FeO ₂ _4(S)	own0	2		S	300.000	800.000	800.00
	0.16674785E+01	0.24941799E-01	-0.48984580E-04	0.45392764E-07	-0.16454451E-10		1
	-0.33971065E+04	-0.36151541E+01	0.16674785E+01	0.24941799E-01	-0.48984580E-04		2
	0.45392764E-07	-0.16454451E-10	-0.33971065E+04	-0.36151541E+01			3
							4
FeO ₂ _6(S)	own0	2		S	300.000	800.000	800.00
	0.32052407E+01	0.17528495E-01	-0.34489113E-04	0.32209258E-07	-0.11832585E-10		1
	-0.40644325E+04	-0.82474520E+01	0.32052407E+01	0.17528495E-01	-0.34489113E-04		2
	0.32209258E-07	-0.11832585E-10	-0.40644325E+04	-0.82474520E+01			3
							4
OFeO ₆ (S)	own0	2		S	300.000	800.000	800.00
	0.15038051E+01	0.26998854E-01	-0.54327781E-04	0.51007470E-07	-0.18606385E-10		1
	-0.21694553E+03	-0.21470075E+01	0.15038051E+01	0.26998854E-01	-0.54327781E-04		2
	0.51007470E-07	-0.18606385E-10	-0.21694553E+03	-0.21470075E+01			3
							4
OFeO-NO ₇ (S)	ownN	10	3	S	300.000	800.000	800.00
	0.62152100E+01	0.28001727E-01	-0.56300715E-04	0.55074597E-07	-0.20974987E-10		1
							2

0.79994855E+04-0.17027756E+02 0.62152100E+01 0.28001727E-01-0.56300715E-04	3
0.55074597E-07-0.20974987E-10 0.79994855E+04-0.17027756E+02	4
OFeONO_7(S) ownN 10 3 S 300.000 800.000 800.00	1
0.49485643E+01 0.32736454E-01-0.62658976E-04 0.58847884E-07-0.21795225E-10	2
-0.74658572E+03-0.13496201E+02 0.49485643E+01 0.32736454E-01-0.62658976E-04	3
0.58847884E-07-0.21795225E-10-0.74658572E+03-0.13496201E+02	4
Fe0ONO_c_5(S) ownN 10 3 S 300.000 800.000 800.00	1
0.27579648E+01 0.34752536E-01-0.62709752E-04 0.56551088E-07-0.20377757E-10	2
0.10143065E+04-0.55227383E+01 0.27579648E+01 0.34752536E-01-0.62709752E-04	3
0.56551088E-07-0.20377757E-10 0.10143065E+04-0.55227383E+01	4
Fe0ONO_t_5(S) ownN 10 3 S 300.000 800.000 800.00	1
0.42403832E+01 0.32431765E-01-0.58192280E-04 0.52452764E-07-0.18941709E-10	2
0.24794221E+04-0.94327145E+01 0.42403832E+01 0.32431765E-01-0.58192280E-04	3
0.52452764E-07-0.18941709E-10 0.24794221E+04-0.94327145E+01	4
O2FeNO_5(S) ownN 10 3 S 300.000 800.000 800.00	1
0.60157020E+01 0.26801012E-01-0.52228795E-04 0.50945227E-07-0.19584678E-10	2
-0.52335882E+04-0.19679097E+02 0.60157020E+01 0.26801012E-01-0.52228795E-04	3
0.50945227E-07-0.19584678E-10-0.52335882E+04-0.19679097E+02	4
FeONOO_5(S) ownN 10 3 S 300.000 800.000 800.00	1
0.33189773E+01 0.35645988E-01-0.62799490E-04 0.55548686E-07-0.19743699E-10	2
0.25640491E+04-0.72577304E+01 0.33189773E+01 0.35645988E-01-0.62799490E-04	3
0.55548686E-07-0.19743699E-10 0.25640491E+04-0.72577304E+01	4
OFeO-NO_5(S) ownN 10 3 S 300.000 800.000 800.00	1
0.50077347E+01 0.33981320E-01-0.68709818E-04 0.67177043E-07-0.25521209E-10	2
0.43634366E+04-0.16450712E+02 0.50077347E+01 0.33981320E-01-0.68709818E-04	3
0.67177043E-07-0.25521209E-10 0.43634366E+04-0.16450712E+02	4
OFeONO_5(S) ownN 10 3 S 300.000 800.000 800.00	1
0.38120429E+01 0.34726412E-01-0.62964094E-04 0.56997810E-07-0.20596857E-10	2
-0.63799605E+04-0.10307760E+02 0.38120429E+01 0.34726412E-01-0.62964094E-04	3
0.56997810E-07-0.20596857E-10-0.63799605E+04-0.10307760E+02	4
FeO2NO_5(S) ownN 10 3 S 300.000 800.000 800.00	1
0.26419489E+01 0.29431186E-01-0.38827995E-04 0.25900134E-07-0.71970674E-11	2
-0.19041518E+05-0.42449962E+01 0.26419489E+01 0.29431186E-01-0.38827995E-04	3
0.25900134E-07-0.71970674E-11-0.19041518E+05-0.42449962E+01	4
ONFeONO_6(S) ownN 20 3 S 300.000 800.000 800.00	1
0.86672760E+01 0.21625105E-01-0.36633894E-04 0.34087808E-07-0.13050244E-10	2
0.48797111E+03-0.26930845E+02 0.86672760E+01 0.21625105E-01-0.36633894E-04	3
0.34087808E-07-0.13050244E-10 0.48797111E+03-0.26930845E+02	4
ONFeONO_4(S) ownN 20 3 S 300.000 800.000 800.00	1
0.63031002E+01 0.33808618E-01-0.62274959E-04 0.59128166E-07-0.22416216E-10	2
-0.79928216E+04-0.19287468E+02 0.63031002E+01 0.33808618E-01-0.62274959E-04	3
0.59128166E-07-0.22416216E-10-0.79928216E+04-0.19287468E+02	4
ONFeONO-02_6(S) ownN 20 5 S 300.000 800.000 800.00	1
0.10492078E+02 0.38115137E-01-0.67340016E-04 0.62404713E-07-0.23359075E-10	2
-0.19893359E+04-0.34700052E+02 0.10492078E+02 0.38115137E-01-0.67340016E-04	3
0.62404713E-07-0.23359075E-10-0.19893359E+04-0.34700052E+02	4
ONFeOONO_t_6(S) ownN 20 5 S 300.000 800.000 800.00	1
0.73096029E+01 0.50462730E-01-0.86749527E-04 0.76611090E-07-0.27357121E-10	2
-0.42450482E+04-0.18990303E+02 0.73096029E+01 0.50462730E-01-0.86749527E-04	3

0.76611090E-07-0.27357121E-10-0.42450482E+04-0.18990303E+02	4
ONFe00NO_c_6(S) ownN 20 5 S 300.000 800.000 800.00	1
0.67716724E+01 0.53246831E-01-0.92506822E-04 0.82099271E-07-0.29360008E-10	2
-0.53920189E+04-0.16539427E+02 0.67716724E+01 0.53246831E-01-0.92506822E-04	3
0.82099271E-07-0.29360008E-10-0.53920189E+04-0.16539427E+02	4
O2Fe0NO-NO_6(S) ownN 20 5 S 300.000 800.000 800.00	1
0.67329992E+01 0.55493213E-01-0.10025214E-03 0.91546309E-07-0.33340472E-10	2
-0.52084558E+04-0.18535869E+02 0.67329992E+01 0.55493213E-01-0.10025214E-03	3
0.91546309E-07-0.33340472E-10-0.52084558E+04-0.18535869E+02	4
ONFe0NO_6(S) ownN 20 4 S 300.000 800.000 800.00	1
0.66310434E+01 0.43243989E-01-0.76122444E-04 0.68693812E-07-0.24967436E-10	2
-0.12944977E+05-0.16799831E+02 0.66310434E+01 0.43243989E-01-0.76122444E-04	3
0.68693812E-07-0.24967436E-10-0.12944977E+05-0.16799831E+02	4
FeNO_3(S) ownN 10 1 S 300.000 800.000 800.00	1
0.36455396E+01 0.14848880E-01-0.33247664E-04 0.35452308E-07-0.14422153E-10	2
0.25733511E+04-0.10934190E+02 0.36455396E+01 0.14848880E-01-0.33247664E-04	3
0.35452308E-07-0.14422153E-10 0.25733511E+04-0.10934190E+02	4
FeNO_O2_5(S) ownN 10 3 S 300.000 800.000 800.00	1
0.80405605E+01 0.10913374E-01-0.20875255E-04 0.22678366E-07-0.97922799E-11	2
0.13173504E+04-0.21016198E+02 0.80405605E+01 0.10913374E-01-0.20875255E-04	3
0.22678366E-07-0.97922799E-11 0.13173504E+04-0.21016198E+02	4
ONFe00NO_t_6(S) ownN 20 4 S 300.000 800.000 800.00	1
0.88438779E+01 0.33302042E-01-0.58635167E-04 0.54301935E-07-0.20339958E-10	2
0.99060431E+04-0.24817405E+02 0.88438779E+01 0.33302042E-01-0.58635167E-04	3
0.54301935E-07-0.20339958E-10 0.99060431E+04-0.24817405E+02	4
ONFe00NO_c_6(S) ownN 20 4 S 300.000 800.000 800.00	1
0.84713643E+01 0.35356071E-01-0.62938894E-04 0.58384438E-07-0.21812047E-10	2
0.84429178E+04-0.21900553E+02 0.84713643E+01 0.35356071E-01-0.62938894E-04	3
0.58384438E-07-0.21812047E-10 0.84429178E+04-0.21900553E+02	4
ONFe0_5(S) ownN 10 2 S 300.000 800.000 800.00	1
0.54918143E+01 0.19156061E-01-0.40624234E-04 0.41610253E-07-0.16443892E-10	2
0.16710581E+04-0.17106348E+02 0.54918143E+01 0.19156061E-01-0.40624234E-04	3
0.41610253E-07-0.16443892E-10 0.16710581E+04-0.17106348E+02	4
ONFe0NO_c_4(S) ownN 20 3 S 300.000 800.000 800.00	1
0.49326486E+01 0.34442160E-01-0.61428626E-04 0.56753082E-07-0.21114288E-10	2
-0.84050405E+04-0.15027185E+02 0.49326486E+01 0.34442160E-01-0.61428626E-04	3
0.56753082E-07-0.21114288E-10-0.84050405E+04-0.15027185E+02	4
O2Fe02N_7(S) ownN 10 4 S 300.000 800.000 800.00	1
0.66446068E+01 0.27340469E-01-0.37549115E-04 0.26614547E-07-0.80140302E-11	2
-0.12559984E+05-0.20378781E+02 0.66446068E+01 0.27340469E-01-0.37549115E-04	3
0.26614547E-07-0.80140302E-11-0.12559984E+05-0.20378781E+02	4
O2Fe02N_5(S) ownN 10 4 S 300.000 800.000 800.00	1
0.50757772E+01 0.35926547E-01-0.55410409E-04 0.43516999E-07-0.14116928E-10	2
-0.71851228E+04-0.16952717E+02 0.50757772E+01 0.35926547E-01-0.55410409E-04	3
0.43516999E-07-0.14116928E-10-0.71851228E+04-0.16952717E+02	4
ONFe02N_6(S) ownN 20 3 S 300.000 800.000 800.00	1
0.93374503E+01 0.14526742E-01-0.16534281E-04 0.11189203E-07-0.36910640E-11	2
-0.17598138E+04-0.25389203E+02 0.93374503E+01 0.14526742E-01-0.16534281E-04	3
0.11189203E-07-0.36910640E-11-0.17598138E+04-0.25389203E+02	4

ONFe02N_4(S)	ownN	20	3	S	300.000	800.000	800.00	1
0.64241703E+01	0.28356629E-01	-0.44275044E-04	0.37537225E-07	-0.13389639E-10				2
-0.10746240E+05	-0.20652498E+02	0.64241703E+01	0.28356629E-01	-0.44275044E-04				3
0.37537225E-07	-0.13389639E-10	-0.10746240E+05	-0.20652498E+02					4
O2Fe02N_NO_6(S)	ownN	20	5	S	300.000	800.000	800.00	1
0.94305505E+01	0.33251456E-01	-0.49316372E-04	0.39641070E-07	-0.13534892E-10				2
-0.36308298E+04	-0.30769102E+02	0.94305505E+01	0.33251456E-01	-0.49316372E-04				3
0.39641070E-07	-0.13534892E-10	-0.36308298E+04	-0.30769102E+02					4
N02Fe00NO_t_6(S)	ownN	20	5	S	300.000	800.000	800.00	1
0.63142363E+01	0.44994688E-01	-0.67772457E-04	0.53410418E-07	-0.17552769E-10				2
-0.60559341E+04	-0.18250632E+02	0.63142363E+01	0.44994688E-01	-0.67772457E-04				3
0.53410418E-07	-0.17552769E-10	-0.60559341E+04	-0.18250632E+02					4
N02Fe00NO_c_6(S)	ownN	20	5	S	300.000	800.000	800.00	1
0.65945373E+01	0.48626565E-01	-0.75250125E-04	0.60546935E-07	-0.20164276E-10				2
-0.74212449E+04	-0.17707251E+02	0.65945373E+01	0.48626565E-01	-0.75250125E-04				3
0.60546935E-07	-0.20164276E-10	-0.74212449E+04	-0.17707251E+02					4
N02Fe00NO_R_6(S)	ownN	20	5	S	300.000	800.000	800.00	1
0.45595185E+01	0.53838814E-01	-0.77954467E-04	0.57609062E-07	-0.17631432E-10				2
-0.81193907E+04	-0.12691440E+02	0.45595185E+01	0.53838814E-01	-0.77954467E-04				3
0.57609062E-07	-0.17631432E-10	-0.81193907E+04	-0.12691440E+02					4
N02Fe0_5(S)	ownN	10	3	S	300.000	800.000	800.00	1
0.32773925E+01	0.31179037E-01	-0.46506129E-04	0.35188304E-07	-0.11032953E-10				2
-0.76301586E+04	-0.91858413E+01	0.32773925E+01	0.31179037E-01	-0.46506129E-04				3
0.35188304E-07	-0.11032953E-10	-0.76301586E+04	-0.91858413E+01					4
N02Fe0NO_6(S)	ownN	20	4	S	300.000	800.000	800.00	1
0.65489569E+01	0.38070772E-01	-0.57649402E-04	0.45957996E-07	-0.15340611E-10				2
-0.15104409E+05	-0.18990319E+02	0.65489569E+01	0.38070772E-01	-0.57649402E-04				3
0.45957996E-07	-0.15340611E-10	-0.15104409E+05	-0.18990319E+02					4
O2Fe02NO_7(S)	ownN	10	5	S	300.000	800.000	800.00	1
0.53693406E+01	0.39323690E-01	-0.53198416E-04	0.36802446E-07	-0.10647671E-10				2
-0.21151754E+05	-0.13990390E+02	0.53693406E+01	0.39323690E-01	-0.53198416E-04				3
0.36802446E-07	-0.10647671E-10	-0.21151754E+05	-0.13990390E+02					4
O2Fe02NO_5(S)	ownN	10	5	S	300.000	800.000	800.00	1
0.51308626E+01	0.40642571E-01	-0.55908653E-04	0.39323165E-07	-0.11541754E-10				2
-0.18841709E+05	-0.14720054E+02	0.51308626E+01	0.40642571E-01	-0.55908653E-04				3
0.39323165E-07	-0.11541754E-10	-0.18841709E+05	-0.14720054E+02					4
O2Fe02NO_NO_6(S)	ownN	20	6	S	300.000	800.000	800.00	1
0.86899586E+01	0.42270297E-01	-0.58382736E-04	0.43203323E-07	-0.13651624E-10				2
-0.12164627E+05	-0.25474215E+02	0.86899586E+01	0.42270297E-01	-0.58382736E-04				3
0.43203323E-07	-0.13651624E-10	-0.12164627E+05	-0.25474215E+02					4
ONFe02NO_6(S)	ownN	20	4	S	300.000	800.000	800.00	1
0.69332431E+01	0.27116544E-01	-0.33346934E-04	0.22433512E-07	-0.66996480E-11				2
-0.10208654E+05	-0.17595831E+02	0.69332431E+01	0.27116544E-01	-0.33346934E-04				3
0.22433512E-07	-0.66996480E-11	-0.10208654E+05	-0.17595831E+02					4
ONFe02NO_4(S)	ownN	20	4	S	300.000	800.000	800.00	1
0.52458114E+01	0.39877211E-01	-0.58847666E-04	0.46558187E-07	-0.15550177E-10				2
-0.18905592E+05	-0.14846311E+02	0.52458114E+01	0.39877211E-01	-0.58847666E-04				3
0.46558187E-07	-0.15550177E-10	-0.18905592E+05	-0.14846311E+02					4
ON02Fe00NO_t6(S)	ownN	20	6	S	300.000	800.000	800.00	1

0.57869277E+01 0.58408560E-01-0.86561114E-04 0.66723346E-07-0.21365571E-10	2
-0.14718783E+05-0.12646506E+02 0.57869277E+01 0.58408560E-01-0.86561114E-04	3
0.66723346E-07-0.21365571E-10-0.14718783E+05-0.12646506E+02	4
ON02Fe00NO_c6(S) ownN 20 6 S 300.000 800.000 800.00	1
0.54739537E+01 0.59800733E-01-0.89104407E-04 0.68896014E-07-0.22083634E-10	2
-0.15885032E+05-0.11775918E+02 0.54739537E+01 0.59800733E-01-0.89104407E-04	3
0.68896014E-07-0.22083634E-10-0.15885032E+05-0.11775918E+02	4
OFe02NO_5(S) ownN 10 4 S 300.000 800.000 800.00	1
0.20182036E+01 0.43480678E-01-0.63078882E-04 0.46334115E-07-0.14020607E-10	2
-0.14076082E+05-0.31216845E+01 0.20182036E+01 0.43480678E-01-0.63078882E-04	3
0.46334115E-07-0.14020607E-10-0.14076082E+05-0.31216845E+01	4
ON0Fe02NO_6(S) ownN 20 5 S 300.000 800.000 800.00	1
0.52020255E+01 0.50439428E-01-0.74007782E-04 0.56722563E-07-0.18151054E-10	2
-0.23474092E+05-0.11874914E+02 0.52020255E+01 0.50439428E-01-0.74007782E-04	3
0.56722563E-07-0.18151054E-10-0.23474092E+05-0.11874914E+02	4
FeOH_5(S) H+3H 10 1 S 300.000 800.000 800.00	1
0.21914037E+01 0.21425091E-01-0.46471913E-04 0.45729947E-07-0.17087810E-10	2
-0.24858774E+05-0.56566541E+01 0.21914037E+01 0.21425091E-01-0.46471913E-04	3
0.45729947E-07-0.17087810E-10-0.24858774E+05-0.56566541E+01	4
O2FeOH_7(S) ownH 10 3 S 300.000 800.000 800.00	1
0.42644485E+01 0.34627488E-01-0.67565913E-04 0.62976992E-07-0.22839491E-10	2
-0.31430316E+05-0.13443324E+02 0.42644485E+01 0.34627488E-01-0.67565913E-04	3
0.62976992E-07-0.22839491E-10-0.31430316E+05-0.13443324E+02	4
O2FeOH_5(S) ownH 10 3 S 300.000 800.000 800.00	1
0.45135276E+01 0.33371003E-01-0.64843988E-04 0.60223452E-07-0.21776026E-10	2
-0.29019892E+05-0.14362266E+02 0.45135276E+01 0.33371003E-01-0.64843988E-04	3
0.60223452E-07-0.21776026E-10-0.29019892E+05-0.14362266E+02	4
O2FeOH_NO_6(S) H-2H 1N 10 4 S 300.000 800.000 800.00	1
0.78933498E+01 0.36000402E-01-0.69514392E-04 0.66310942E-07-0.24729432E-10	2
-0.23257668E+05-0.25608915E+02 0.78933498E+01 0.36000402E-01-0.69514392E-04	3
0.66310942E-07-0.24729432E-10-0.23257668E+05-0.25608915E+02	4
ONFeOH_6(S) ownH 1N 10 2 S 300.000 800.000 800.00	1
0.67833130E+01 0.22665470E-01-0.47878559E-04 0.48594262E-07-0.18881920E-10	2
-0.18793819E+05-0.20827651E+02 0.67833130E+01 0.22665470E-01-0.47878559E-04	3
0.48594262E-07-0.18881920E-10-0.18793819E+05-0.20827651E+02	4
ONFeOH_4(S) ownH 1N 10 2 S 300.000 800.000 800.00	1
0.40176462E+01 0.35608260E-01-0.73779886E-04 0.73101511E-07-0.27846447E-10	2
-0.26427128E+05-0.12802367E+02 0.40176462E+01 0.35608260E-01-0.73779886E-04	3
0.73101511E-07-0.27846447E-10-0.26427128E+05-0.12802367E+02	4
ONFeOH-O2_6(S) ownH 1N 10 4 S 300.000 800.000 800.00	1
0.81663124E+01 0.39761534E-01-0.78268865E-04 0.75707299E-07-0.28513866E-10	2
-0.22938166E+05-0.28937495E+02 0.81663124E+01 0.39761534E-01-0.78268865E-04	3
0.75707299E-07-0.28513866E-10-0.22938166E+05-0.28937495E+02	4
HOFe00NO_t_6(S) H-1H 1N 10 4 S 300.000 800.000 800.00	1
0.48696548E+01 0.51835033E-01-0.95806751E-04 0.87218896E-07-0.31281048E-10	2
-0.24700010E+05-0.12517658E+02 0.48696548E+01 0.51835033E-01-0.95806751E-04	3
0.87218896E-07-0.31281048E-10-0.24700010E+05-0.12517658E+02	4
HOFe00NO_c_6(S) ownH 1N 10 4 S 300.000 800.000 800.00	1
0.41566270E+01 0.55362997E-01-0.10287870E-03 0.93819947E-07-0.33654894E-10	2

-0.25353738E+05-0.91336573E+01 0.41566270E+01 0.55362997E-01-0.10287870E-03	3
0.93819947E-07-0.33654894E-10-0.25353738E+05-0.91336573E+01	4
H0Fe00NO_cu_6(S) ownH 1N 10 4 S 300.000 800.000 800.00	1
0.43466444E+01 0.54629586E-01-0.10169470E-03 0.92897108E-07-0.33367653E-10	2
-0.25291978E+05-0.10235379E+02 0.43466444E+01 0.54629586E-01-0.10169470E-03	3
0.92897108E-07-0.33367653E-10-0.25291978E+05-0.10235379E+02	4
H0Fe0_d_5(S) ownH 10 2 S 300.000 800.000 800.00	1
0.77503566E+00 0.35542563E-01-0.66231227E-04 0.59023247E-07-0.20548734E-10	2
-0.23106675E+05 0.19712669E-01 0.77503566E+00 0.35542563E-01-0.66231227E-04	3
0.59023247E-07-0.20548734E-10-0.23106675E+05 0.19712669E-01	4
H0Fe0_u_5(S) ownH 10 2 S 300.000 800.000 800.00	1
0.70387949E+00 0.35626152E-01-0.66027964E-04 0.58550307E-07-0.20300742E-10	2
-0.26380649E+05 0.58701411E+00 0.70387949E+00 0.35626152E-01-0.66027964E-04	3
0.58550307E-07-0.20300742E-10-0.26380649E+05 0.58701411E+00	4
H0Fe0_NO_6(S) ownH 1N 10 3 S 300.000 800.000 800.00	1
0.54784083E+01 0.35009662E-01-0.62957925E-04 0.56699524E-07-0.20203591E-10	2
-0.17494667E+05-0.13271652E+02 0.54784083E+01 0.35009662E-01-0.62957925E-04	3
0.56699524E-07-0.20203591E-10-0.17494667E+05-0.13271652E+02	4
H0Fe0NO_u_6(S) ownH 1N 10 3 S 300.000 800.000 800.00	1
0.40547622E+01 0.44625369E-01-0.84345939E-04 0.77956081E-07-0.28251495E-10	2
-0.33036723E+05-0.10698641E+02 0.40547622E+01 0.44625369E-01-0.84345939E-04	3
0.77956081E-07-0.28251495E-10-0.33036723E+05-0.10698641E+02	4
H0Fe0NO_d_6(S) ownH 1N 10 3 S 300.000 800.000 800.00	1
0.41938812E+01 0.44231166E-01-0.83928221E-04 0.77802238E-07-0.28257878E-10	2
-0.33109066E+05-0.10273916E+02 0.41938812E+01 0.44231166E-01-0.83928221E-04	3
0.77802238E-07-0.28257878E-10-0.33109066E+05-0.10273916E+02	4
H0Fe00NO_R_6(S) ownH 1N 10 4 S 300.000 800.000 800.00	1
0.23040203E+01 0.59900891E-01-0.10460287E-03 0.90171884E-07-0.30901647E-10	2
-0.27084651E+05-0.49757608E+01 0.23040203E+01 0.59900891E-01-0.10460287E-03	3
0.90171884E-07-0.30901647E-10-0.27084651E+05-0.49757608E+01	4
H0Fe00NO_R_4(S) ownH 1N 10 4 S 300.000 800.000 800.00	1
0.37410985E+00 0.67310373E-01-0.11729072E-03 0.10077394E-06-0.34400987E-10	2
-0.19901638E+05 0.15331218E+01 0.37410985E+00 0.67310373E-01-0.11729072E-03	3
0.10077394E-06-0.34400987E-10-0.19901638E+05 0.15331218E+01	4
H0Fe0-ON0cd_4(S) ownH 1N 10 4 S 300.000 800.000 800.00	1
0.44145886E+01 0.45613523E-01-0.73924868E-04 0.61320706E-07-0.20639466E-10	2
-0.22778647E+05-0.12733346E+02 0.44145886E+01 0.45613523E-01-0.73924868E-04	3
0.61320706E-07-0.20639466E-10-0.22778647E+05-0.12733346E+02	4
H0Fe0-ON0cu_4(S) ownH 1N 10 4 S 300.000 800.000 800.00	1
0.40166682E+01 0.47074392E-01-0.76225893E-04 0.63029388E-07-0.21135302E-10	2
-0.25332580E+05-0.10970512E+02 0.40166682E+01 0.47074392E-01-0.76225893E-04	3
0.63029388E-07-0.21135302E-10-0.25332580E+05-0.10970512E+02	4
H0Fe0-ON0tu_4(S) H-3H 1N 10 4 S 300.000 800.000 800.00	1
0.54624848E+01 0.39628668E-01-0.60735589E-04 0.48103970E-07-0.15620956E-10	2
-0.25470935E+05-0.14377284E+02 0.54624848E+01 0.39628668E-01-0.60735589E-04	3
0.48103970E-07-0.15620956E-10-0.25470935E+05-0.14377284E+02	4
H0Fe0-N203_5(S) ownH 1N 20 5 S 300.000 800.000 800.00	1
0.51949945E+01 0.64569171E-01-0.11015994E-03 0.96333028E-07-0.33896814E-10	2
-0.21150099E+05-0.16166399E+02 0.51949945E+01 0.64569171E-01-0.11015994E-03	3

0.96333028E-07-0.33896814E-10-0.21150099E+05-0.16166399E+02	4
HOFe(ONO)2_5(S) ownH 1N 20 5 S 300.000 800.000 800.00	1
0.48328984E+01 0.73646737E-01-0.13553699E-03 0.12411727E-06-0.44891638E-10	2
-0.21947867E+05-0.14631650E+02 0.48328984E+01 0.73646737E-01-0.13553699E-03	3
0.12411727E-06-0.44891638E-10-0.21947867E+05-0.14631650E+02	4
HOFeONO_u_4(S) ownH 1N 10 3 S 300.000 800.000 800.00	1
0.16196437E+01 0.52287305E-01-0.94832128E-04 0.84795629E-07-0.29948197E-10	2
-0.27335539E+05-0.30387063E+01 0.16196437E+01 0.52287305E-01-0.94832128E-04	3
0.84795629E-07-0.29948197E-10-0.27335539E+05-0.30387063E+01	4
HOFeO-ON0tu_6(S) ownH 1N 10 4 S 300.000 800.000 800.00	1
0.55440201E+01 0.39134785E-01-0.59594090E-04 0.46923438E-07-0.15162728E-10	2
-0.23914017E+05-0.13829708E+02 0.55440201E+01 0.39134785E-01-0.59594090E-04	3
0.46923438E-07-0.15162728E-10-0.23914017E+05-0.13829708E+02	4
HOFeO2NO_4(S) ownH 1N 10 4 S 300.000 800.000 800.00	1
0.59130039E+00 0.56938026E-01-0.86917777E-04 0.66979576E-07-0.20898842E-10	2
-0.35583178E+05 0.10981124E+01 0.59130039E+00 0.56938026E-01-0.86917777E-04	3
0.66979576E-07-0.20898842E-10-0.35583178E+05 0.10981124E+01	4
HOFeO2NO_6(S) H+3H 1N 10 4 S 300.000 800.000 800.00	1
0.31391986E+01 0.49487878E-01-0.77673883E-04 0.61748977E-07-0.19906686E-10	2
-0.42774365E+05-0.75076051E+01 0.31391986E+01 0.49487878E-01-0.77673883E-04	3
0.61748977E-07-0.19906686E-10-0.42774365E+05-0.75076051E+01	4
HOFeO2NO-NO_5(S) ownH 1N 20 5 S 300.000 800.000 800.00	1
0.67742594E+01 0.55652187E-01-0.90109536E-04 0.75875046E-07-0.26021237E-10	2
-0.35505354E+05-0.22071530E+02 0.67742594E+01 0.55652187E-01-0.90109536E-04	3
0.75875046E-07-0.26021237E-10-0.35505354E+05-0.22071530E+02	4
HOFeO2N_6(S) ownH 1N 10 3 S 300.000 800.000 800.00	1
0.45768467E+01 0.36662085E-01-0.60305665E-04 0.49947467E-07-0.16692725E-10	2
-0.35342730E+05-0.14293025E+02 0.45768467E+01 0.36662085E-01-0.60305665E-04	3
0.49947467E-07-0.16692725E-10-0.35342730E+05-0.14293025E+02	4
HONOFeO2_6(S) ownH 1N 10 4 S 300.000 800.000 800.00	1
0.63395793E+01 0.35468916E-01-0.54846826E-04 0.45531006E-07-0.15638450E-10	2
-0.21899517E+05-0.18815897E+02 0.63395793E+01 0.35468916E-01-0.54846826E-04	3
0.45531006E-07-0.15638450E-10-0.21899517E+05-0.18815897E+02	4
HNO3FeO_6(S) ownH 1N 10 4 S 300.000 800.000 800.00	1
0.41063860E+01 0.35254353E-01-0.41881346E-04 0.26457459E-07-0.71532426E-11	2
-0.26891291E+05-0.95778188E+01 0.41063860E+01 0.35254353E-01-0.41881346E-04	3
0.26457459E-07-0.71532426E-11-0.26891291E+05-0.95778188E+01	4
OFeHNO3_6(S) ownH 1N 10 4 S 300.000 800.000 800.00	1
0.43331739E+01 0.40484971E-01-0.58254962E-04 0.43713597E-07-0.13578642E-10	2
-0.22858141E+05-0.67676346E+01 0.43331739E+01 0.40484971E-01-0.58254962E-04	3
0.43713597E-07-0.13578642E-10-0.22858141E+05-0.67676346E+01	4
HONOFeO2NO_5(S) ownH 1N 20 5 S 300.000 800.000 800.00	1
0.50316043E+01 0.46414476E-01-0.57519985E-04 0.37655407E-07-0.10405348E-10	2
-0.37461117E+05-0.14132425E+02 0.50316043E+01 0.46414476E-01-0.57519985E-04	3
0.37655407E-07-0.10405348E-10-0.37461117E+05-0.14132425E+02	4
HOFeONO-NO_5(S) ownH 1N 20 4 S 300.000 800.000 800.00	1
0.77435873E+01 0.50782071E-01-0.96993268E-04 0.92411757E-07-0.34521235E-10	2
-0.25141195E+05-0.25408190E+02 0.77435873E+01 0.50782071E-01-0.96993268E-04	3
0.92411757E-07-0.34521235E-10-0.25141195E+05-0.25408190E+02	4

HONOFONO_5(S)	ownH	1N	20	4	S	300.000	800.000	800.00	1
0.73217008E+01	0.37946897E-01	-0.54269081E-04	0.42656030E-07	-0.14175591E-10					2
-0.26124813E+05	-0.20954574E+02	0.73217008E+01	0.37946897E-01	-0.54269081E-04					3
0.42656030E-07	-0.14175591E-10	-0.26124813E+05	-0.20954574E+02						4
HONOFEO_6(S)	ownH	1N	10	3	S	300.000	800.000	800.00	1
0.49970786E+01	0.30584067E-01	-0.47602155E-04	0.39535175E-07	-0.13510467E-10					2
-0.21172713E+05	-0.14363602E+02	0.49970786E+01	0.30584067E-01	-0.47602155E-04					3
0.39535175E-07	-0.13510467E-10	-0.21172713E+05	-0.14363602E+02						4
OFehONO_6(S)	ownH	1N	10	3	S	300.000	800.000	800.00	1
0.54166346E+01	0.33064066E-01	-0.56956659E-04	0.50204573E-07	-0.17743086E-10					2
-0.17961874E+05	-0.13855104E+02	0.54166346E+01	0.33064066E-01	-0.56956659E-04					3
0.50204573E-07	-0.17743086E-10	-0.17961874E+05	-0.13855104E+02						4
HOFEO2N-NO_5(S)	ownH	1N	20	4	S	300.000	800.000	800.00	1
0.83226824E+01	0.42542908E-01	-0.72586664E-04	0.64227121E-07	-0.22946184E-10					2
-0.26572762E+05	-0.29253619E+02	0.83226824E+01	0.42542908E-01	-0.72586664E-04					3
0.64227121E-07	-0.22946184E-10	-0.26572762E+05	-0.29253619E+02						4
HONOFEO2N_5(S)	ownH	1N	20	4	S	300.000	800.000	800.00	1
0.69561367E+01	0.36423355E-01	-0.46471187E-04	0.32270013E-07	-0.96500193E-11					2
-0.29201065E+05	-0.21599777E+02	0.69561367E+01	0.36423355E-01	-0.46471187E-04					3
0.32270013E-07	-0.96500193E-11	-0.29201065E+05	-0.21599777E+02						4
H2OFeO_6(S)	ownH	20	2		S	300.000	800.000	800.00	1
0.24504107E+01	0.32360586E-01	-0.58546202E-04	0.53050896E-07	-0.18870977E-10					2
-0.42881102E+05	-0.74718589E+01	0.24504107E+01	0.32360586E-01	-0.58546202E-04					3
0.53050896E-07	-0.18870977E-10	-0.42881102E+05	-0.74718589E+01						4
HOFEOH_u_6(S)	H+3H	20	2		S	300.000	800.000	800.00	1
0.24579138E+01	0.43231984E-01	-0.89695574E-04	0.86300091E-07	-0.31679981E-10					2
-0.52114984E+05	-0.74326478E+01	0.24579138E+01	0.43231984E-01	-0.89695574E-04					3
0.86300091E-07	-0.31679981E-10	-0.52114984E+05	-0.74326478E+01						4
HOFEOH_4(S)	ownH	20	2		S	300.000	800.000	800.00	1
0.35025128E+00	0.49142716E-01	-0.96034426E-04	0.88608237E-07	-0.31522767E-10					2
-0.46456804E+05	0.53561347E+00	0.35025128E+00	0.49142716E-01	-0.96034426E-04					3
0.88608237E-07	-0.31522767E-10	-0.46456804E+05	0.53561347E+00						4
HOFEOH-NO_5(S)	ownH	2N	10	3	S	300.000	800.000	800.00	1
0.50878847E+01	0.53785306E-01	-0.11033370E-03	0.10776249E-06	-0.40355219E-10					2
-0.45836458E+05	-0.17705469E+02	0.50878847E+01	0.53785306E-01	-0.11033370E-03					3
0.10776249E-06	-0.40355219E-10	-0.45836458E+05	-0.17705469E+02						4
HONOFEOH_5(S)	ownH	2N	10	3	S	300.000	800.000	800.00	1
0.55176822E+01	0.37910560E-01	-0.63021581E-04	0.54727870E-07	-0.19103666E-10					2
-0.43630155E+05	-0.16790924E+02	0.55176822E+01	0.37910560E-01	-0.63021581E-04					3
0.54727870E-07	-0.19103666E-10	-0.43630155E+05	-0.16790924E+02						4
H2OFeO2N_5(S)	ownH	2N	10	3	S	300.000	800.000	800.00	1
0.40999588E+01	0.39118833E-01	-0.58690351E-04	0.46714210E-07	-0.15282760E-10					2
-0.51148321E+05	-0.12918045E+02	0.40999588E+01	0.39118833E-01	-0.58690351E-04					3
0.46714210E-07	-0.15282760E-10	-0.51148321E+05	-0.12918045E+02						4
HOFEOHNO_5(S)	ownH	2N	10	3	S	300.000	800.000	800.00	1
0.50233632E+01	0.41210501E-01	-0.69639182E-04	0.60206399E-07	-0.20786677E-10					2
-0.41266570E+05	-0.13115974E+02	0.50233632E+01	0.41210501E-01	-0.69639182E-04					3
0.60206399E-07	-0.20786677E-10	-0.41266570E+05	-0.13115974E+02						4
H2OFeO2NO_5(S)	ownH	2N	10	4	S	300.000	800.000	800.00	1

0.29973049E+01	0.50033452E-01	-0.71705049E-04	0.54056844E-07	-0.16783969E-10	2	
-0.59417371E+05	-0.70310970E+01	0.29973049E+01	0.50033452E-01	-0.71705049E-04	3	
0.54056844E-07	-0.16783969E-10	-0.59417371E+05	-0.70310970E+01		4	
HOFeHNO3_5(S)	ownH	2N	10	4	S 300.000 800.000 800.00	1
0.30195219E+01	0.43590898E-01	-0.56672765E-04	0.38675452E-07	-0.10894456E-10	2	
-0.49285622E+05	-0.21167023E+01	0.30195219E+01	0.43590898E-01	-0.56672765E-04	3	
0.38675452E-07	-0.10894456E-10	-0.49285622E+05	-0.21167023E+01		4	
HOFeO2N_4(S)	ownH	1N	10	3	S 300.000 800.000 800.00	1
0.27332606E+01	0.43444597E-01	-0.71249435E-04	0.58498966E-07	-0.19320774E-10	2	
-0.27469335E+05	-0.83621143E+01	0.27332606E+01	0.43444597E-01	-0.71249435E-04	3	
0.58498966E-07	-0.19320774E-10	-0.27469335E+05	-0.83621143E+01		4	
HOFeONO-N02_5(S)	ownH	1N	20	5	S 300.000 800.000 800.00	1
0.84037702E+01	0.45946491E-01	-0.73900372E-04	0.62799996E-07	-0.21889915E-10	2	
-0.30853311E+05	-0.20357669E+02	0.84037702E+01	0.45946491E-01	-0.73900372E-04	3	
0.62799996E-07	-0.21889915E-10	-0.30853311E+05	-0.20357669E+02		4	
HN03FeONO_5(S)	ownH	1N	20	5	S 300.000 800.000 800.00	1
0.63678503E+01	0.43485978E-01	-0.51241413E-04	0.32748095E-07	-0.91321390E-11	2	
-0.32328545E+05	-0.15915887E+02	0.63678503E+01	0.43485978E-01	-0.51241413E-04	3	
0.32748095E-07	-0.91321390E-11	-0.32328545E+05	-0.15915887E+02		4	
HOFeO2N-N02_5(S)	ownH	1N	20	5	S 300.000 800.000 800.00	1
0.82986493E+01	0.40311464E-01	-0.53691161E-04	0.37887475E-07	-0.11326524E-10	2	
-0.33204224E+05	-0.21236858E+02	0.82986493E+01	0.40311464E-01	-0.53691161E-04	3	
0.37887475E-07	-0.11326524E-10	-0.33204224E+05	-0.21236858E+02		4	
HN03FeO2N_5(S)	ownH	1N	20	5	S 300.000 800.000 800.00	1
0.59755949E+01	0.41827778E-01	-0.42600328E-04	0.21203828E-07	-0.41031015E-11	2	
-0.35291317E+05	-0.16753585E+02	0.59755949E+01	0.41827778E-01	-0.42600328E-04	3	
0.21203828E-07	-0.41031015E-11	-0.35291317E+05	-0.16753585E+02		4	
HOFeO2NO-N025(S)	ownH	1N	20	6	S 300.000 800.000 800.00	1
0.69584655E+01	0.52619731E-01	-0.69919525E-04	0.48535825E-07	-0.14098636E-10	2	
-0.42129794E+05	-0.14817175E+02	0.69584655E+01	0.52619731E-01	-0.69919525E-04	3	
0.48535825E-07	-0.14098636E-10	-0.42129794E+05	-0.14817175E+02		4	
HN03FeO2NO_5(S)	ownH	1N	20	6	S 300.000 800.000 800.00	1
0.48617786E+01	0.52718654E-01	-0.55495735E-04	0.28431178E-07	-0.55714555E-11	2	
-0.43571177E+05	-0.10885604E+02	0.48617786E+01	0.52718654E-01	-0.55495735E-04	3	
0.28431178E-07	-0.55714555E-11	-0.43571177E+05	-0.10885604E+02		4	
HOFeOH_N02_5(S)	ownH	2N	10	4	S 300.000 800.000 800.00	1
0.52334650E+01	0.50668212E-01	-0.89582273E-04	0.79577983E-07	-0.28028067E-10	2	
-0.51851293E+05	-0.12100507E+02	0.52334650E+01	0.50668212E-01	-0.89582273E-04	3	
0.79577983E-07	-0.28028067E-10	-0.51851293E+05	-0.12100507E+02		4	
HN03FeOH_5(S)	ownH	2N	10	4	S 300.000 800.000 800.00	1
0.43889477E+01	0.44169421E-01	-0.61132703E-04	0.45628117E-07	-0.14273131E-10	2	
-0.50389560E+05	-0.11099914E+02	0.43889477E+01	0.44169421E-01	-0.61132703E-04	3	
0.45628117E-07	-0.14273131E-10	-0.50389560E+05	-0.11099914E+02		4	
HOFeO2_N02_6(S)	ownH	1N	10	5	S 300.000 800.000 800.00	1
0.86768427E+01	0.39788131E-01	-0.63864916E-04	0.53505413E-07	-0.18357387E-10	2	
-0.29456888E+05	-0.24813208E+02	0.86768427E+01	0.39788131E-01	-0.63864916E-04	3	
0.53505413E-07	-0.18357387E-10	-0.29456888E+05	-0.24813208E+02		4	
HN03FeO2_6(S)	ownH	1N	10	5	S 300.000 800.000 800.00	1
0.55559514E+01	0.39383881E-01	-0.47466114E-04	0.31231036E-07	-0.90507273E-11	2	

-0.28304517E+05-0.15766296E+02 0.55559514E+01 0.39383881E-01-0.47466114E-04	3
0.31231036E-07-0.90507273E-11-0.28304517E+05-0.15766296E+02	4
H0Fe02-NO_6(S) ownH 1N 10 4 S 300.000 800.000 800.00	1
0.41366106E+01 0.57951393E-01-0.11201031E-03 0.10506189E-06-0.38417715E-10	2
-0.24948743E+05-0.11648385E+02 0.41366106E+01 0.57951393E-01-0.11201031E-03	3
0.10506189E-06-0.38417715E-10-0.24948743E+05-0.11648385E+02	4
NH3Fe0_6(S) ownH 3N 10 1 S 300.000 800.000 800.00	1
0.36030296E+01 0.25201202E-01-0.36971948E-04 0.31039902E-07-0.10721575E-10	2
-0.21298195E+05-0.11409781E+02 0.36030296E+01 0.25201202E-01-0.36971948E-04	3
0.31039902E-07-0.10721575E-10-0.21298195E+05-0.11409781E+02	4
NH3Fe0_4(S) ownH 3N 10 1 S 300.000 800.000 800.00	1
0.30659433E+01 0.25620179E-01-0.35372801E-04 0.28122009E-07-0.93219095E-11	2
-0.17056280E+05-0.10199019E+02 0.30659433E+01 0.25620179E-01-0.35372801E-04	3
0.28122009E-07-0.93219095E-11-0.17056280E+05-0.10199019E+02	4
NH2FeOH_6(S) H+2H 3N 10 1 S 300.000 800.000 800.00	1
0.22844753E+01 0.46645883E-01-0.92046564E-04 0.87573118E-07-0.32022878E-10	2
-0.26263477E+05-0.65439888E+01 0.22844753E+01 0.46645883E-01-0.92046564E-04	3
0.87573118E-07-0.32022878E-10-0.26263477E+05-0.65439888E+01	4
NH2FeOH_4(S) ownH 3N 10 1 S 300.000 800.000 800.00	1
0.16805328E-01 0.52385141E-01-0.97080914E-04 0.88146996E-07-0.31128827E-10	2
-0.20280823E+05 0.18253085E+01 0.16805328E-01 0.52385141E-01-0.97080914E-04	3
0.88146996E-07-0.31128827E-10-0.20280823E+05 0.18253085E+01	4
NH2FeOH-NO_5(S) H-3H 3N 20 2 S 300.000 800.000 800.00	1
0.52674592E+01 0.55784643E-01-0.10994934E-03 0.10653531E-06-0.39832758E-10	2
-0.20628533E+05-0.18431313E+02 0.52674592E+01 0.55784643E-01-0.10994934E-03	3
0.10653531E-06-0.39832758E-10-0.20628533E+05-0.18431313E+02	4
NH2NOFeOH_5(S) ownH 3N 20 2 S 300.000 800.000 800.00	1
0.52182240E+01 0.37116534E-01-0.49620449E-04 0.35986309E-07-0.10785151E-10	2
-0.23214686E+05-0.15805850E+02 0.52182240E+01 0.37116534E-01-0.49620449E-04	3
0.35986309E-07-0.10785151E-10-0.23214686E+05-0.15805850E+02	4
FeNH2_5(S) ownH 2N 1 S 300.000 800.000 800.00	1
0.26515498E+01 0.21983616E-01-0.43369652E-04 0.42049544E-07-0.15678749E-10	2
0.18275656E+04-0.70689323E+01 0.26515498E+01 0.21983616E-01-0.43369652E-04	3
0.42049544E-07-0.15678749E-10 0.18275656E+04-0.70689323E+01	4
NH2FeONO_6(S) ownH 2N 20 2 S 300.000 800.000 800.00	1
0.39754122E+01 0.47196474E-01-0.84330802E-04 0.76517195E-07-0.27479475E-10	2
-0.75506005E+04-0.10065903E+02 0.39754122E+01 0.47196474E-01-0.84330802E-04	3
0.76517195E-07-0.27479475E-10-0.75506005E+04-0.10065903E+02	4
NH2NOFeO_6(S) ownH 2N 20 2 S 300.000 800.000 800.00	1
0.47222310E+01 0.28718510E-01-0.31302679E-04 0.17889086E-07-0.41487223E-11	2
0.38719546E+03-0.13496777E+02 0.47222310E+01 0.28718510E-01-0.31302679E-04	3
0.17889086E-07-0.41487223E-11 0.38719546E+03-0.13496777E+02	4
NH2-ONOFEOH_5(S) ownH 3N 20 3 S 300.000 800.000 800.00	1
0.34732537E+01 0.70907081E-01-0.12919379E-03 0.11742649E-06-0.41886862E-10	2
-0.20434872E+05-0.11496343E+02 0.34732537E+01 0.70907081E-01-0.12919379E-03	3
0.11742649E-06-0.41886862E-10-0.20434872E+05-0.11496343E+02	4
NH2NO-OFEOH_5(S) ownH 3N 20 3 S 300.000 800.000 800.00	1
0.25208385E+01 0.57454009E-01-0.82213990E-04 0.61672657E-07-0.18848381E-10	2
-0.23219714E+05-0.64893997E+01 0.25208385E+01 0.57454009E-01-0.82213990E-04	3

0.61672657E-07-0.18848381E-10-0.23219714E+05-0.64893997E+01	4
NH3-HOFeONO ₆ (S) ownH 4N 20 3 S 300.000 800.000 800.00	1
0.40030922E+01 0.62137456E-01-0.98113629E-04 0.82247535E-07-0.27845674E-10	2
-0.49212904E+05-0.12326341E+02 0.40030922E+01 0.62137456E-01-0.98113629E-04	3
0.82247535E-07-0.27845674E-10-0.49212904E+05-0.12326341E+02	4
NH2FeOH-HONO6(S) ownH 4N 20 3 S 300.000 800.000 800.00	1
0.36751905E+01 0.63044422E-01-0.10234735E-03 0.86803420E-07-0.29491769E-10	2
-0.41598054E+05-0.67363778E+01 0.36751905E+01 0.63044422E-01-0.10234735E-03	3
0.86803420E-07-0.29491769E-10-0.41598054E+05-0.67363778E+01	4
NH2FeONO-H2O6(S) ownH 4N 20 3 S 300.000 800.000 800.00	1
0.55027758E+01 0.66019518E-01-0.11779430E-03 0.10736394E-06-0.38564142E-10	2
-0.42251554E+05-0.19363655E+02 0.55027758E+01 0.66019518E-01-0.11779430E-03	3
0.10736394E-06-0.38564142E-10-0.42251554E+05-0.19363655E+02	4
HOFeOH-NH2NO6(S) ownH 4N 20 3 S 300.000 800.000 800.00	1
0.30684117E+01 0.65061579E-01-0.98191111E-04 0.77108722E-07-0.24383801E-10	2
-0.51049124E+05-0.51346092E+01 0.30684117E+01 0.65061579E-01-0.98191111E-04	3
0.77108722E-07-0.24383801E-10-0.51049124E+05-0.51346092E+01	4
NH3-HOFeOH ₆ (S) ownH 5N 10 2 S 300.000 800.000 800.00	1
0.18763189E+01 0.66405309E-01-0.11979283E-03 0.10944610E-06-0.39064727E-10	2
-0.68032599E+05-0.61479267E+01 0.18763189E+01 0.66405309E-01-0.11979283E-03	3
0.10944610E-06-0.39064727E-10-0.68032599E+05-0.61479267E+01	4
NH2FeOH-H2O ₆ (S) ownH 5N 10 2 S 300.000 800.000 800.00	1
0.22764859E+01 0.71937142E-01-0.13749177E-03 0.12910541E-06-0.46824155E-10	2
-0.61564122E+05-0.79732135E+01 0.22764859E+01 0.71937142E-01-0.13749177E-03	3
0.12910541E-06-0.46824155E-10-0.61564122E+05-0.79732135E+01	4
NH3-OfFeOH ₅ (S) ownH 4N 10 2 S 300.000 800.000 800.00	1
0.14137927E+01 0.54101555E-01-0.88412116E-04 0.75435941E-07-0.25671994E-10	2
-0.44679433E+05-0.39695170E+01 0.14137927E+01 0.54101555E-01-0.88412116E-04	3
0.75435941E-07-0.25671994E-10-0.44679433E+05-0.39695170E+01	4
NH3-OfFeOH ₇ (S) ownH 4N 10 2 S 300.000 800.000 800.00	1
0.38451383E+01 0.49519532E-01-0.88143305E-04 0.80920788E-07-0.29169015E-10	2
-0.36962393E+05-0.13014312E+02 0.38451383E+01 0.49519532E-01-0.88143305E-04	3
0.80920788E-07-0.29169015E-10-0.36962393E+05-0.13014312E+02	4
NH2-HOFeOH ₇ (S) ownH 4N 10 2 S 300.000 800.000 800.00	1
0.21857504E+01 0.70552279E-01-0.13993451E-03 0.13291314E-06-0.48447735E-10	2
-0.38170032E+05-0.65348763E+01 0.21857504E+01 0.70552279E-01-0.13993451E-03	3
0.13291314E-06-0.48447735E-10-0.38170032E+05-0.65348763E+01	4
NH2-HOFeOH ₅ (S) ownH 4N 10 2 S 300.000 800.000 800.00	1
0.74506022E+00 0.72714889E-01-0.13814138E-03 0.12722067E-06-0.45301186E-10	2
-0.37947455E+05-0.15383066E+01 0.74506022E+00 0.72714889E-01-0.13814138E-03	3
0.12722067E-06-0.45301186E-10-0.37947455E+05-0.15383066E+01	4
NH2OHFeOH ₅ (S) ownH 4N 10 2 S 300.000 800.000 800.00	1
0.44131805E+01 0.35706997E-01-0.47575772E-04 0.35153172E-07-0.10707608E-10	2
-0.44061935E+05-0.13483057E+02 0.44131805E+01 0.35706997E-01-0.47575772E-04	3
0.35153172E-07-0.10707608E-10-0.44061935E+05-0.13483057E+02	4
NH2-ONFeO2 ₆ (S) ownH 2N 20 3 S 300.000 800.000 800.00	1
0.71136178E+01 0.47711482E-01-0.89881394E-04 0.85800225E-07-0.32099846E-10	2
0.40704679E+04-0.25262658E+02 0.71136178E+01 0.47711482E-01-0.89881394E-04	3
0.85800225E-07-0.32099846E-10 0.40704679E+04-0.25262658E+02	4

NH2NOFeO2_6(S)	ownH	2N	20	3	S	300.000	800.000	800.00	1
0.59288515E+01	0.35244460E-01	-0.42872147E-04	0.28389206E-07	-0.79821252E-11					2
-0.90437719E+03	-0.18260005E+02	0.59288515E+01	0.35244460E-01	-0.42872147E-04					3
0.28389206E-07	-0.79821252E-11	-0.90437719E+03	-0.18260005E+02						4
NH3FeO2_6(S)	ownH	3N	10	2	S	300.000	800.000	800.00	1
0.47911867E+01	0.31857766E-01	-0.48999218E-04	0.42142620E-07	-0.14821657E-10					2
-0.22210249E+05	-0.16204197E+02	0.47911867E+01	0.31857766E-01	-0.48999218E-04					3
0.42142620E-07	-0.14821657E-10	-0.22210249E+05	-0.16204197E+02						4
NH3-0FeO_6(S)	ownH	3N	10	2	S	300.000	800.000	800.00	1
0.28648758E+01	0.43389095E-01	-0.73754867E-04	0.65840301E-07	-0.23416276E-10					2
-0.19371615E+05	-0.10163758E+02	0.28648758E+01	0.43389095E-01	-0.73754867E-04					3
0.65840301E-07	-0.23416276E-10	-0.19371615E+05	-0.10163758E+02						4
NH2-0FeOH_6(S)	ownH	3N	10	2	S	300.000	800.000	800.00	1
0.27679648E+01	0.58362543E-01	-0.11507568E-03	0.10911442E-06	-0.39823323E-10					2
-0.71565960E+04	-0.89274295E+01	0.27679648E+01	0.58362543E-01	-0.11507568E-03					3
0.10911442E-06	-0.39823323E-10	-0.71565960E+04	-0.89274295E+01						4
NH2-0FeOH_4(S)	ownH	3N	10	2	S	300.000	800.000	800.00	1
0.39884185E-01	0.64640515E-01	-0.11912196E-03	0.10737998E-06	-0.37729215E-10					2
-0.12350138E+05	0.86187534E+00	0.39884185E-01	0.64640515E-01	-0.11912196E-03					3
0.10737998E-06	-0.37729215E-10	-0.12350138E+05	0.86187534E+00						4
NH3FeO2N_5(S)	ownH	3N	20	2	S	300.000	800.000	800.00	1
0.55742552E+01	0.30963705E-01	-0.35707930E-04	0.23659763E-07	-0.68142818E-11					2
-0.29545574E+05	-0.18184084E+02	0.55742552E+01	0.30963705E-01	-0.35707930E-04					3
0.23659763E-07	-0.68142818E-11	-0.29545574E+05	-0.18184084E+02						4
NH2FeHONO_5(S)	ownH	3N	20	2	S	300.000	800.000	800.00	1
0.33555081E+01	0.41585182E-01	-0.61085716E-04	0.49395311E-07	-0.16460828E-10					2
-0.12549175E+05	-0.55108785E+01	0.33555081E+01	0.41585182E-01	-0.61085716E-04					3
0.49395311E-07	-0.16460828E-10	-0.12549175E+05	-0.55108785E+01						4
NH3FeOH_5(S)	ownH	4N	10	1	S	300.000	800.000	800.00	1
0.39274250E+01	0.35248349E-01	-0.60186596E-04	0.55021448E-07	-0.19866815E-10					2
-0.43463358E+05	-0.13065948E+02	0.39274250E+01	0.35248349E-01	-0.60186596E-04					3
0.55021448E-07	-0.19866815E-10	-0.43463358E+05	-0.13065948E+02						4
NH2FeOH2_5(S)	ownH	4N	10	1	S	300.000	800.000	800.00	1
0.32034561E+01	0.44831208E-01	-0.84281136E-04	0.79630197E-07	-0.29129544E-10					2
-0.33376914E+05	-0.85522749E+01	0.32034561E+01	0.44831208E-01	-0.84281136E-04					3
0.79630197E-07	-0.29129544E-10	-0.33376914E+05	-0.85522749E+01						4
NH2FeO2_7(S)	ownH	2N	10	2	S	300.000	800.000	800.00	1
0.39517685E+01	0.38904799E-01	-0.71762180E-04	0.65997571E-07	-0.23808940E-10					2
-0.46399270E+04	-0.11920889E+02	0.39517685E+01	0.38904799E-01	-0.71762180E-04					3
0.65997571E-07	-0.23808940E-10	-0.46399270E+04	-0.11920889E+02						4
NH2FeO2_5(S)	H-3H	2N	10	2	S	300.000	800.000	800.00	1
0.22453537E+01	0.47492186E-01	-0.88888659E-04	0.81783819E-07	-0.29403493E-10					2
-0.16436651E+04	-0.66934205E+01	0.22453537E+01	0.47492186E-01	-0.88888659E-04					3
0.81783819E-07	-0.29403493E-10	-0.16436651E+04	-0.66934205E+01						4
NH2FeNO_6(S)	ownH	2N	20	1	S	300.000	800.000	800.00	1
0.61803924E+01	0.28352492E-01	-0.55122995E-04	0.54778802E-07	-0.21112975E-10					2
0.90808090E+04	-0.19840413E+02	0.61803924E+01	0.28352492E-01	-0.55122995E-04					3
0.54778802E-07	-0.21112975E-10	-0.90808090E+04	-0.19840413E+02						4
NH2FeNO_4(S)	ownH	2N	20	1	S	300.000	800.000	800.00	1

0.37879470E+01 0.39344011E-01-0.76892306E-04 0.75190956E-07-0.28518113E-10	2
-0.39592663E+02-0.11858795E+02 0.37879470E+01 0.39344011E-01-0.76892306E-04	3
0.75190956E-07-0.28518113E-10-0.39592663E+02-0.11858795E+02	4
NH2OHFeO_6(S) ownH 3N 10 2 S 300.000 800.000 800.00	1
0.38531398E+01 0.27099232E-01-0.27751892E-04 0.14765525E-07-0.29818486E-11	2
-0.22005356E+05-0.10865008E+02 0.38531398E+01 0.27099232E-01-0.27751892E-04	3
0.14765525E-07-0.29818486E-11-0.22005356E+05-0.10865008E+02	4
FeNH2_O2_7(S) ownH 2N 10 2 S 300.000 800.000 800.00	1
0.80545644E+01 0.17957437E-01-0.30784164E-04 0.29063139E-07-0.10968663E-10	2
0.55663721E+03-0.19111500E+02 0.80545644E+01 0.17957437E-01-0.30784164E-04	3
0.29063139E-07-0.10968663E-10 0.55663721E+03-0.19111500E+02	4
NH2FeOH_N02_5(S) ownH 3N 20 3 S 300.000 800.000 800.00	1
0.68265612E+01 0.46961031E-01-0.79321299E-04 0.70042546E-07-0.24732813E-10	2
-0.24589215E+05-0.17839622E+02 0.68265612E+01 0.46961031E-01-0.79321299E-04	3
0.70042546E-07-0.24732813E-10-0.24589215E+05-0.17839622E+02	4
NH2N02FeOH_5(S) ownH 3N 20 3 S 300.000 800.000 800.00	1
0.43517294E+01 0.45132630E-01-0.55707262E-04 0.36791555E-07-0.10065947E-10	2
-0.33390527E+05-0.11302075E+02 0.43517294E+01 0.45132630E-01-0.55707262E-04	3
0.36791555E-07-0.10065947E-10-0.33390527E+05-0.11302075E+02	4
OFeONN_6(S) ownN 2D 2 S 300.000 800.000 800.00	1
0.51023943E+01 0.26744546E-01-0.48017900E-04 0.44061060E-07-0.16150014E-10	2
0.47960457E+04-0.12979824E+02 0.51023943E+01 0.26744546E-01-0.48017900E-04	3
0.44061060E-07-0.16150014E-10 0.47960457E+04-0.12979824E+02	4
NH3-OFeONO_5(S) ownH 3N 20 3 S 300.000 800.000 800.00	1
0.43758599E+01 0.52114330E-01-0.80479719E-04 0.67490378E-07-0.23166322E-10	2
-0.26103959E+05-0.14152674E+02 0.43758599E+01 0.52114330E-01-0.80479719E-04	3
0.67490378E-07-0.23166322E-10-0.26103959E+05-0.14152674E+02	4
NH2-HOFeONO_5(S) ownH 3N 20 3 S 300.000 800.000 800.00	1
0.36462050E+01 0.69936141E-01-0.12705594E-03 0.11520127E-06-0.41007956E-10	2
-0.18913283E+05-0.10549160E+02 0.36462050E+01 0.69936141E-01-0.12705594E-03	3
0.11520127E-06-0.41007956E-10-0.18913283E+05-0.10549160E+02	4
NH3-OFeONO_7(S) ownH 3N 20 3 S 300.000 800.000 800.00	1
0.60152806E+01 0.47792205E-01-0.75818316E-04 0.65472077E-07-0.23011730E-10	2
-0.17854728E+05-0.18071859E+02 0.60152806E+01 0.47792205E-01-0.75818316E-04	3
0.65472077E-07-0.23011730E-10-0.17854728E+05-0.18071859E+02	4
NH2-HOFeONO_7(S) ownH 3N 20 3 S 300.000 800.000 800.00	1
0.47722630E+01 0.67369472E-01-0.12534386E-03 0.11574453E-06-0.41777168E-10	2
-0.19862795E+05-0.13837361E+02 0.47722630E+01 0.67369472E-01-0.12534386E-03	3
0.11574453E-06-0.41777168E-10-0.19862795E+05-0.13837361E+02	4
NH3FeO_N02_7(S) ownH 3N 20 3 S 300.000 800.000 800.00	1
0.87778202E+01 0.27434358E-01-0.28206372E-04 0.17264381E-07-0.47982459E-11	2
-0.20284435E+05-0.26433057E+02 0.87778202E+01 0.27434358E-01-0.28206372E-04	3
0.17264381E-07-0.47982459E-11-0.20284435E+05-0.26433057E+02	4
NH2FeO2_N0_6(S) ownH 2N 20 3 S 300.000 800.000 800.00	1
0.60119441E+01 0.34179441E-01-0.62336430E-04 0.59028335E-07-0.22018733E-10	2
0.43972628E+04-0.18954118E+02 0.60119441E+01 0.34179441E-01-0.62336430E-04	3
0.59028335E-07-0.22018733E-10 0.43972628E+04-0.18954118E+02	4
NH2FeOON0_t_6(S) ownH 2N 20 3 S 300.000 800.000 800.00	1
0.37340012E+01 0.54987048E-01-0.97374100E-04 0.87547152E-07-0.31224343E-10	2

0.22030458E+04-0.90471610E+01 0.37340012E+01 0.54987048E-01-0.97374100E-04	3
0.87547152E-07-0.31224343E-10 0.22030458E+04-0.90471610E+01	4
NH2Fe00N0_c_6(S) ownH 2N 20 3 S 300.000 800.000 800.00	1
0.40255796E+01 0.58641670E-01-0.10493432E-03 0.94766967E-07-0.33865181E-10	2
0.85278830E+03-0.76294451E+01 0.40255796E+01 0.58641670E-01-0.10493432E-03	3
0.94766967E-07-0.33865181E-10 0.85278830E+03-0.76294451E+01	4
NH2Fe0_N02_6(S) ownH 2N 20 3 S 300.000 800.000 800.00	1
0.67971998E+01 0.37253492E-01-0.53043344E-04 0.40808277E-07-0.13073362E-10	2
0.68135765E+03-0.17165599E+02 0.67971998E+01 0.37253492E-01-0.53043344E-04	3
0.40808277E-07-0.13073362E-10 0.68135765E+03-0.17165599E+02	4
NH2Fe0_5(S) ownH 2N 10 1 S 300.000 800.000 800.00	1
0.15116954E+01 0.35884628E-01-0.63721860E-04 0.56386397E-07-0.19637876E-10	2
-0.92667627E+03-0.32332813E+01 0.15116954E+01 0.35884628E-01-0.63721860E-04	3
0.56386397E-07-0.19637876E-10-0.92667627E+03-0.32332813E+01	4
NH2Fe0_7(S) ownH 2N 10 1 S 300.000 800.000 800.00	1
0.23508654E+01 0.37382061E-01-0.73997135E-04 0.70887366E-07-0.26181122E-10	2
0.51434800E+04-0.59226199E+01 0.23508654E+01 0.37382061E-01-0.73997135E-04	3
0.70887366E-07-0.26181122E-10 0.51434800E+04-0.59226199E+01	4
NH2Fe0NN_5(S) ownH 2N 30 1 S 300.000 800.000 800.00	1
0.57089642E+01 0.37578199E-01-0.67890767E-04 0.63745500E-07-0.23569937E-10	2
0.96719448E+04-0.14718880E+02 0.57089642E+01 0.37578199E-01-0.67890767E-04	3
0.63745500E-07-0.23569937E-10 0.96719448E+04-0.14718880E+02	4
NH2N02Fe0_6(S) ownH 2N 20 3 S 300.000 800.000 800.00	1
0.39330047E+01 0.35721708E-01-0.34248593E-04 0.14897989E-07-0.18102541E-11	2
-0.97642204E+04-0.90715060E+01 0.39330047E+01 0.35721708E-01-0.34248593E-04	3
0.14897989E-07-0.18102541E-11-0.97642204E+04-0.90715060E+01	4
NH2N02Fe0-d_6(S) ownH 2N 20 3 S 300.000 800.000 800.00	1
0.57185112E+00 0.59791153E-01-0.87463854E-04 0.65879609E-07-0.20197597E-10	2
0.63174811E+04 0.14017882E+01 0.57185112E+00 0.59791153E-01-0.87463854E-04	3
0.65879609E-07-0.20197597E-10 0.63174811E+04 0.14017882E+01	4
NH2N0-0Fe0_6(S) ownH 2N 20 3 S 300.000 800.000 800.00	1
0.39251428E+01 0.46762540E-01-0.67386202E-04 0.51793951E-07-0.16458652E-10	2
0.19987817E+04-0.12159306E+02 0.39251428E+01 0.46762540E-01-0.67386202E-04	3
0.51793951E-07-0.16458652E-10 0.19987817E+04-0.12159306E+02	4
NH2Fe0-OH2_7(S) ownH 4N 10 2 S 300.000 800.000 800.00	1
0.30645629E+01 0.51653496E-01-0.99809797E-04 0.95415233E-07-0.35188508E-10	2
-0.28038763E+05-0.10553439E+02 0.30645629E+01 0.51653496E-01-0.99809797E-04	3
0.95415233E-07-0.35188508E-10-0.28038763E+05-0.10553439E+02	4
NH2Fe0-OH2_5(S) ownH 4N 10 2 S 300.000 800.000 800.00	1
0.23125502E+01 0.58357710E-01-0.10502124E-03 0.95047317E-07-0.33686705E-10	2
-0.36636112E+05-0.71276773E+01 0.23125502E+01 0.58357710E-01-0.10502124E-03	3
0.95047317E-07-0.33686705E-10-0.36636112E+05-0.71276773E+01	4
NH3-H0FeN0_4(S) ownH 4N 20 2 S 300.000 800.000 800.00	1
0.52296250E+01 0.51373668E-01-0.90281015E-04 0.84203969E-07-0.31061287E-10	2
-0.40444743E+05-0.18616584E+02 0.52296250E+01 0.51373668E-01-0.90281015E-04	3
0.84203969E-07-0.31061287E-10-0.40444743E+05-0.18616584E+02	4
NH2FeN0-H20_4(S) ownH 4N 20 2 S 300.000 800.000 800.00	1
0.53145555E+01 0.57522922E-01-0.10816819E-03 0.10342437E-06-0.38479175E-10	2
-0.32082563E+05-0.17617307E+02 0.53145555E+01 0.57522922E-01-0.10816819E-03	3

0.10342437E-06-0.38479175E-10-0.32082563E+05-0.17617307E+02	4
NH2FeNO_2(S) ownH 2N 20 1 S 300.000 800.000 800.00	1
0.13311269E+01 0.47785644E-01-0.89741344E-04 0.84682769E-07-0.31278732E-10	2
0.97678959E+04-0.33003705E+01 0.13311269E+01 0.47785644E-01-0.89741344E-04	3
0.84682769E-07-0.31278732E-10 0.97678959E+04-0.33003705E+01	4
NH2FeNO-NO_3(S) ownH 2N 30 2 S 300.000 800.000 800.00	1
0.70884556E+01 0.47271512E-01-0.92596036E-04 0.92225197E-07-0.35674203E-10	2
0.83585547E+04-0.25304127E+02 0.70884556E+01 0.47271512E-01-0.92596036E-04	3
0.92225197E-07-0.35674203E-10 0.83585547E+04-0.25304127E+02	4
NH2NOFeNO_3(S) ownH 2N 30 2 S 300.000 800.000 800.00	1
0.67118331E+01 0.30196527E-01-0.35617826E-04 0.25017086E-07-0.78993676E-11	2
0.57017665E+04-0.21671064E+02 0.67118331E+01 0.30196527E-01-0.35617826E-04	3
0.25017086E-07-0.78993676E-11 0.57017665E+04-0.21671064E+02	4
NH200Fe_5(S) ownH 2N 10 2 S 300.000 800.000 800.00	1
0.24522669E+01 0.32219290E-01-0.42882571E-04 0.29793041E-07-0.84385914E-11	2
0.34335555E+04-0.42352629E+01 0.24522669E+01 0.32219290E-01-0.42882571E-04	3
0.29793041E-07-0.84385914E-11 0.34335555E+04-0.42352629E+01	4
Fe00NH2_5(S) H-3H 2N 10 2 S 300.000 800.000 800.00	1
0.25747003E+01 0.29046843E-01-0.39486000E-04 0.28529934E-07-0.84872715E-11	2
0.50489500E+04-0.52877810E+01 0.25747003E+01 0.29046843E-01-0.39486000E-04	3
0.28529934E-07-0.84872715E-11 0.50489500E+04-0.52877810E+01	4
HOFeHNO_3(S) ownH 2N 10 2 S 300.000 800.000 800.00	1
0.13360514E+01 0.43934656E-01-0.73494800E-04 0.62878458E-07-0.21537319E-10	2
-0.20281412E+05-0.35298862E+01 0.13360514E+01 0.43934656E-01-0.73494800E-04	3
0.62878458E-07-0.21537319E-10-0.20281412E+05-0.35298862E+01	4
HOFeHNO_5(S) ownH 2N 10 2 S 300.000 800.000 800.00	1
0.42744107E+01 0.35908592E-01-0.65309082E-04 0.60414363E-07-0.22048377E-10	2
-0.25905907E+05-0.12784640E+02 0.42744107E+01 0.35908592E-01-0.65309082E-04	3
0.60414363E-07-0.22048377E-10-0.25905907E+05-0.12784640E+02	4
H2NOFeO_7(S) ownH 2N 10 2 S 300.000 800.000 800.00	1
0.47042286E+01 0.25372403E-01-0.35625032E-04 0.28075534E-07-0.93250818E-11	2
-0.89009454E+04-0.14322794E+02 0.47042286E+01 0.25372403E-01-0.35625032E-04	3
0.28075534E-07-0.93250818E-11-0.89009454E+04-0.14322794E+02	4
H2NOFeO_5(S) ownH 2N 10 2 S 300.000 800.000 800.00	1
0.51045538E+01 0.23473760E-01-0.31795293E-04 0.24418239E-07-0.79757041E-11	2
-0.92407438E+04-0.15890399E+02 0.51045538E+01 0.23473760E-01-0.31795293E-04	3
0.24418239E-07-0.79757041E-11-0.92407438E+04-0.15890399E+02	4
HNOFeOH_5(S) ownH 2N 10 2 S 300.000 800.000 800.00	1
0.48919836E+01 0.34890091E-01-0.63925317E-04 0.58715835E-07-0.21184231E-10	2
-0.21894496E+05-0.15441897E+02 0.48919836E+01 0.34890091E-01-0.63925317E-04	3
0.58715835E-07-0.21184231E-10-0.21894496E+05-0.15441897E+02	4
H20FeNO_3(S) ownH 2N 10 2 S 300.000 800.000 800.00	1
0.42997908E+01 0.34715949E-01-0.65402893E-04 0.63313664E-07-0.23989199E-10	2
-0.36205053E+05-0.14975507E+02 0.42997908E+01 0.34715949E-01-0.65402893E-04	3
0.63313664E-07-0.23989199E-10-0.36205053E+05-0.14975507E+02	4
HOFeONH2_6(S) ownH 3N 10 2 S 300.000 800.000 800.00	1
0.47421800E+01 0.36530130E-01-0.60163887E-04 0.52266085E-07-0.18198517E-10	2
-0.32083107E+05-0.13939939E+02 0.47421800E+01 0.36530130E-01-0.60163887E-04	3
0.52266085E-07-0.18198517E-10-0.32083107E+05-0.13939939E+02	4

HOFeONH2_4(S)	ownH	3N	10	2	S	300.000	800.000	800.00	1
0.51832510E+01	0.33996580E-01	-0.55542289E-04	0.48765028E-07	-0.17238412E-10					2
-0.31372537E+05	-0.16891631E+02	0.51832510E+01	0.33996580E-01	-0.55542289E-04					3
0.48765028E-07	-0.17238412E-10	-0.31372537E+05	-0.16891631E+02						4
HOFeH2NO_4(S)	H+3H	3N	10	2	S	300.000	800.000	800.00	1
0.11708976E+01	0.46184496E-01	-0.69050132E-04	0.53337932E-07	-0.16556980E-10					2
-0.27845778E+05	-0.12780820E+01	0.11708976E+01	0.46184496E-01	-0.69050132E-04					3
0.53337932E-07	-0.16556980E-10	-0.27845778E+05	-0.12780820E+01						4
HOFeONH2-NO_5(S)	ownH	3N	20	3	S	300.000	800.000	800.00	1
0.53610253E+01	0.47167771E-01	-0.69975965E-04	0.57427721E-07	-0.19519406E-10					2
-0.22347609E+05	-0.15065738E+02	0.53610253E+01	0.47167771E-01	-0.69975965E-04					3
0.57427721E-07	-0.19519406E-10	-0.22347609E+05	-0.15065738E+02						4
HOFeO-NH2NO_5(S)	ownH	3N	20	3	S	300.000	800.000	800.00	1
0.38046522E+01	0.49198565E-01	-0.62773637E-04	0.41501779E-07	-0.11039942E-10					2
-0.20678098E+05	-0.74182658E+01	0.38046522E+01	0.49198565E-01	-0.62773637E-04					3
0.41501779E-07	-0.11039942E-10	-0.20678098E+05	-0.74182658E+01						4
OFeHNO_4(S)	ownH	1N	10	2	S	300.000	800.000	800.00	1
0.27995303E+01	0.28487284E-01	-0.43655224E-04	0.35436296E-07	-0.11888448E-10					2
-0.23056324E+04	-0.81023508E+01	0.27995303E+01	0.28487284E-01	-0.43655224E-04					3
0.35436296E-07	-0.11888448E-10	-0.23056324E+04	-0.81023508E+01						4
HONOFeNH2_5(S)	ownH	3N	20	2	S	300.000	800.000	800.00	1
0.57661852E+01	0.39565608E-01	-0.62379987E-04	0.53622739E-07	-0.18715134E-10					2
-0.15199315E+05	-0.18421948E+02	0.57661852E+01	0.39565608E-01	-0.62379987E-04					3
0.53622739E-07	-0.18715134E-10	-0.15199315E+05	-0.18421948E+02						4
HN03FeNH2_5(S)	ownH	3N	20	3	S	300.000	800.000	800.00	1
0.46858314E+01	0.45652584E-01	-0.60158739E-04	0.44102920E-07	-0.13679702E-10					2
-0.21991326E+05	-0.12657461E+02	0.46858314E+01	0.45652584E-01	-0.60158739E-04					3
0.44102920E-07	-0.13679702E-10	-0.21991326E+05	-0.12657461E+02						4
HOFeNH2-NO2_5(S)	ownH	3N	20	3	S	300.000	800.000	800.00	1
0.55257918E+01	0.52298167E-01	-0.89004708E-04	0.78550791E-07	-0.27668472E-10					2
-0.25906220E+05	-0.13111636E+02	0.55257918E+01	0.52298167E-01	-0.89004708E-04					3
0.78550791E-07	-0.27668472E-10	-0.25906220E+05	-0.13111636E+02						4
NH2FeHNO_5(S)	ownH	3N	20	1	S	300.000	800.000	800.00	1
0.46633377E+01	0.36984277E-01	-0.63086967E-04	0.57321592E-07	-0.20765204E-10					2
0.23777882E+04	-0.13660734E+02	0.46633377E+01	0.36984277E-01	-0.63086967E-04					3
0.57321592E-07	-0.20765204E-10	-0.23777882E+04	-0.13660734E+02						4
NH2FeHNO_3(S)	ownH	3N	20	1	S	300.000	800.000	800.00	1
0.21703672E+01	0.44803218E-01	-0.73609998E-04	0.63846595E-07	-0.22241091E-10					2
0.61370109E+04	-0.74111889E+01	0.21703672E+01	0.44803218E-01	-0.73609998E-04					3
0.63846595E-07	-0.22241091E-10	-0.61370109E+04	-0.74111889E+01						4
NH3FeNO_3(S)	ownH	3N	20	1	S	300.000	800.000	800.00	1
0.55012430E+01	0.27711708E-01	-0.44450747E-04	0.42021732E-07	-0.16128942E-10					2
-0.14718543E+05	-0.19222488E+02	0.55012430E+01	0.27711708E-01	-0.44450747E-04					3
0.42021732E-07	-0.16128942E-10	-0.14718543E+05	-0.19222488E+02						4
NH2-OFeO_5(S)	ownH	2N	10	2	S	300.000	800.000	800.00	1
0.16798346E+01	0.47252251E-01	-0.84271753E-04	0.74623461E-07	-0.26010533E-10					2
0.10032829E+05	-0.47245588E+01	0.16798346E+01	0.47252251E-01	-0.84271753E-04					3
0.74623461E-07	-0.26010533E-10	-0.10032829E+05	-0.47245588E+01						4
OFeH2NO_5(S)	ownH	2N	10	2	S	300.000	800.000	800.00	1

0.22750273E+01 0.32824925E-01-0.43657399E-04 0.30141405E-07-0.84489946E-11	2
-0.88817043E+04-0.45052776E+01 0.22750273E+01 0.32824925E-01-0.43657399E-04	3
0.30141405E-07-0.84489946E-11-0.88817043E+04-0.45052776E+01	4
H2NOFeNO_4(S) ownH 2N 20 2 S 300.000 800.000 800.00	1
0.70099243E+01 0.22897547E-01-0.28527153E-04 0.21666703E-07-0.73046565E-11	2
-0.41380899E+04-0.22312266E+02 0.70099243E+01 0.22897547E-01-0.28527153E-04	3
0.21666703E-07-0.73046565E-11-0.41380899E+04-0.22312266E+02	4
OFeNH2NO_4(S) ownH 2N 20 2 S 300.000 800.000 800.00	1
0.26631377E+01 0.39363089E-01-0.53304970E-04 0.38907609E-07-0.11908408E-10	2
-0.25686260E+04-0.76505864E+01 0.26631377E+01 0.39363089E-01-0.53304970E-04	3
0.38907609E-07-0.11908408E-10-0.25686260E+04-0.76505864E+01	4
FeHNO_4(S) ownH 1N 10 1 S 300.000 800.000 800.00	1
0.24068906E+01 0.22540598E-01-0.37220934E-04 0.31717594E-07-0.10937082E-10	2
0.75335802E+04-0.60949102E+01 0.24068906E+01 0.22540598E-01-0.37220934E-04	3
0.31717594E-07-0.10937082E-10 0.75335802E+04-0.60949102E+01	4
H2OFeHNO_4(S) ownH 3N 10 2 S 300.000 800.000 800.00	1
0.39409313E+01 0.36867539E-01-0.58696009E-04 0.50982888E-07-0.17984197E-10	2
-0.30516457E+05-0.11220464E+02 0.39409313E+01 0.36867539E-01-0.58696009E-04	3
0.50982888E-07-0.17984197E-10-0.30516457E+05-0.11220464E+02	4
O2FeHNO_6(S) ownH 1N 10 3 S 300.000 800.000 800.00	1
0.58745125E+01 0.29591231E-01-0.47148645E-04 0.39442922E-07-0.13538484E-10	2
0.11284829E+03-0.18579245E+02 0.58745125E+01 0.29591231E-01-0.47148645E-04	3
0.39442922E-07-0.13538484E-10 0.11284829E+03-0.18579245E+02	4
Alternative assignment with Bulk species for Iron:	
FeO_6(S) ownO 1 S 300.000 800.000 800.00	1
0.11204458E+00 0.11947028E+00-0.19081333E-03 0.15090565E-06-0.47480764E-10	2
-0.40710169E+04-0.45946458E+01 0.11204458E+00 0.11947028E+00-0.19081333E-03	3
0.15090565E-06-0.47480764E-10-0.40710169E+04-0.45946458E+01	4
FeO_6(B) ownO 1 S 300.000 800.000 800.00	1
-0.35524778E+01 0.11980479E+00-0.19456364E-03 0.15664527E-06-0.50206795E-10	2
-0.28193329E+04 0.58990408E+01-0.35524778E+01 0.11980479E+00-0.19456364E-03	3
0.15664527E-06-0.50206795E-10-0.28193329E+04 0.58990408E+01	4

Comment on Table F.2

The original FeO_6(S) as used in this work is implemented without the use of a bulk species in CHEMKIN. However, an alternative set is supplied as well for FeO_6, together with a corresponding bulk species which should enable a transfer.

Bibliography

- [1] GECATS (ed.), *Roadmap der deutschen Katalyseforschung: Katalyse, eine Schlüsseltechnologie für nachhaltiges Wirtschaftswachstum*, vol. 2010, 3rd ed., **2010**.
- [2] F. Schüth, Heterogene Katalyse. Schlüsseltechnologie der Chemischen Industrie, *Chem. unserer Zeit* **2006**, 40, 2, 92.
- [3] B. Lindstrom, L. J. Pettersson, A brief history of catalysis, *CATTECH* **2003**, 7, 4, 130.
- [4] M. Roberts, Birth of the catalytic concept: To understand science it is necessary to know its history, *Catal. Lett.* **2000**, 67, 1, 1.
- [5] R. Schlögl, Katalytische Ammoniaksynthese – eine “unendliche Geschichte?”, *Angew. Chem.* **2003**, 115, 18, 2050.
- [6] A. Mittasch, *Geschichte der Ammoniaksynthese*, Verl. Chemie, Weinheim, **1951**.
- [7] O. Deutschmann, H. Knözinger, K. Kochloeff, T. Turek, *Heterogeneous Catalysis and Solid Catalysts: Ullmann’s Encyclopedia of Industrial Chemistry*, Wiley-VCH Verlag GmbH & Co. KGaA, **2000**.
- [8] I. Chorkendorff, J. W. Niemantsverdriet, *Concepts of modern catalysis and kinetics*, 2nd ed., Wiley-VCH, Weinheim, **2007**.
- [9] I. Langmuir, Chemical Reactions at Low Pressures.1, *J. Am. Chem. Soc.* **1915**, 37, 5, 1139.
- [10] I. Langmuir, The Evaporation, Condensation and Reflection of Molecules and the Mechanism of Adsorption, *Phys. Rev.* **1916**, 8, 2, 149.
- [11] K. M. Watson, O. A. Hougen, *Chemical process principles*, Wiley, New York [u.a.], **1956**.
- [12] A. Wheeler, Reaction Rates and Selectivity in Catalyst Pores, vol. 3 of *Advances in Catalysis*, Academic Press, **1951**, pp. 249–327.
- [13] J. F. Haw, *In-situ spectroscopy in heterogeneous catalysis*, Wiley-VCH, Weinheim, **2004**.
- [14] S. T. Bromley, C. R. A. Catlow, T. Maschmeyer, Computational Modeling of Active Sites in Heterogeneous Catalysts, *CATTECH* **2003**, 7, 164.

- [15] K. E. Gubbins, J. D. Moore, Molecular Modeling of Matter: Impact and Prospects in Engineering, *Ind. Eng. Chem. Res.* **2010**, 49, 7, 3026.
- [16] Ansgar Schäfer, Katalyse auf molekularer Ebene: Tieferes Verständnis durch theoretische Methoden; Pressemitteilung, BASF SE, Ludwigshafen, **2008**.
- [17] J. Caruthers, Catalyst design: knowledge extraction from high-throughput experimentation, *J. Catal.* **2003**, 216, 1-2, 98.
- [18] G. Ertl, Elementarschritte bei der heterogenen Katalyse, *Angew. Chem.* **1990**, 102, 11, 1258.
- [19] C. J. Cramer, *Essentials of computational chemistry: Theories and models*, 2nd ed., Wiley, Chichester, **2009**.
- [20] J. P. Dahl, B. Amstrup, *Introduction to the quantum world of atoms and molecules*, World Scientific, Singapore; River Edge, NJ, **2001**.
- [21] D. Wolf, G. Münster, M. Kremer, *NIC Symposium 2006: Symposium, 01.-02. March 2006, Forschungszentrum Julich : proceedings*, John von Neumann-Institut für Computing, Julich, Germany, **2006**.
- [22] D. Frenkel, *Understanding molecular simulation: From algorithms to applications*, Academic Press, San Diego, **2002**.
- [23] L. J. Broadbelt, R. Q. Snurr, Applications of molecular modeling in heterogeneous catalysis research, *Appl. Catal., A* **2000**, 200, 1-2, 23.
- [24] R. I. Masel, *Chemical kinetics and catalysis*, Wiley-Interscience, New York, **2001**.
- [25] R. A. van Santen, M. Neurock, *Molecular heterogeneous catalysis: A conceptual and computational approach*, 1st ed., Wiley-VCH-Verl, Weinheim, **2006**.
- [26] K. Skalska, J. S. Miller, S. Ledakowicz, Trends in NO_x abatement: A review, *Sci. Total Environ.* **2010**, 408, 19, 3976.
- [27] S. Roy, A. Baiker, NO_x Storage-Reduction Catalysis: From Mechanism and Materials Properties to Storage-Reduction Performance, *Chem. Rev.* **2009**, 109, 9, 4054.
- [28] S. Roy, M. S. Hegde, G. Madras, Catalysis for NO_x abatement, *Appl. Ener.* **2009**, 86, 11, 2283.
- [29] M. Schwefer, R. Siefert, M. Groves, R. Maurer, Kombinierte N₂O- und NO_x-Beseitigung im HNO₃-Prozess: Neue Anforderungen an die katalytische NO_x-Reduktion, *Chem. Ing. Tech.* **2004**, 76, 9, 1283.
- [30] Clean Air Technology Center, Nitrogen Oxides (NO_x), Why and How They are Controlled; Technical Bulletin of US Environmental Protection Agency, **1999**.
- [31] Z. M. Liu, S. I. Woo, Recent advances in catalytic DeNO_x science and technology, *Catal. Rev. Sci. Eng.* **2006**, 48, 1, 43.
- [32] Y. Hu, K. Griffiths, P. R. Norton, Surface science studies of selective

- catalytic reduction of NO: Progress in the last ten years, *Surf. Sci.* **2009**, 603, 10-12, Sp. Iss. SI, 1740.
- [33] G. Busca, L. Lietti, G. Ramis, F. Berti, Chemical and mechanistic aspects of the selective catalytic reduction of NO_x by ammonia over oxide catalysts: A review, *Appl. Catal., B* **1998**, 18, 1-2, 1.
- [34] S. Brandenberger, O. Kröcher, A. Tissler, R. Althoff, The State of the Art in Selective Catalytic Reduction of NO_x by Ammonia Using Metal-Exchanged Zeolite Catalysts, *Catal. Rev. Sci. Eng.* **2008**, 50, 4, 492.
- [35] C. Baerlocher, W. M. Meier, D. Olson, *Atlas of zeolite framework types*, 5th ed., Elsevier, Amsterdam; New York, **2001**.
- [36] S. Brandenberger, O. Kröcher, A. Tissler, R. Althoff, The determination of the activities of different iron species in Fe-ZSM-5 for SCR of NO by NH₃, *Appl. Catal. B* **2010**, 95, 3-4, 348.
- [37] M. Schwidder, S. Heikens, A. d. Toni, S. Geisler, M. Berndt, A. Brueckner, W. Gruenert, The role of NO₂ in the selective catalytic reduction of nitrogen oxides over Fe-ZSM-5 catalysts: Active sites for the conversion of NO and of NO/NO₂ mixtures, *J. Catal.* **2008**, 259, 1, 96.
- [38] M. Devadas, O. Kröcher, M. Elsener, A. Wokaun, N. Söger, M. Pfeifer, Y. Demel, L. Mussmann, Influence of NO₂ on the selective catalytic reduction of NO with ammonia over Fe-ZSM5, *Appl. Catal. B* **2006**, 67, 3-4, 187.
- [39] S. Stevenson, J. C. Vartuli, The Selective Catalytic Reduction of NO₂ by NH₃ over HZSM-5, *J. Catal.* **2002**, 208, 1, 100.
- [40] M. Iwasaki, H. Shinjoh, A comparative study of “standard”, “fast” and “NO₂” SCR reactions over Fe/zeolite catalyst, *Appl. Catal. A* **2010**, 390, 1-2, 71.
- [41] A. Heyden, *Theoretical investigation of the nitrous oxide decomposition over iron zeolite catalysts. Ph.D. Thesis, TUHH*, **2005**.
- [42] A. Akah, C. Cundy, A. Garforth, The selective catalytic oxidation of NH₃ over Fe-ZSM-5, *Appl. Catal. B* **2005**, 59, 3-4, 221.
- [43] G. S. Qi, R. T. Yang, Selective catalytic oxidation (SCO) of ammonia to nitrogen over Fe/ZSM-5 catalysts, *Appl. Catal., A* **2005**, 287, 1, 25.
- [44] A. R. Leach, *Molecular modelling: Principles and applications*, 2nd ed., Prentice Hall, Harlow, **2001**.
- [45] F. Jensen, *Introduction to computational chemistry*, Wiley, Chichester; New York, **1999**.
- [46] I. N. Levine, *Quantum chemistry*, 6th ed., Pearson Education International, Upper Saddle River, N.J., **2009**.
- [47] A. Szabo, N. S. Ostlund, *Modern quantum chemistry*, republication of the 1. ed., rev. ed., Dover Publications, New York, **1996**.

- [48] T. Helgaker, P. Jørgensen, J. Olsen, *Molecular electronic-structure theory*, Wiley-VCH, Chichester; New York, **2000**.
- [49] M. Born, Physical Aspects of Quantum Mechanics, *Nature* **1927**, 119, 2992, 354.
- [50] E. Schrödinger, Quantisierung als Eigenwertproblem, *Ann. Phys.* **1926**, 384, 4, 361.
- [51] M. Born, R. Oppenheimer, Zur Quantentheorie der Molekeln, *Ann. Phys.* **1927**, 389, 20, 457.
- [52] W. Demtröder, *Molekülphysik: Theoretische Grundlagen und experimentelle Methoden*, Oldenbourg, München, **2003**.
- [53] H. Nakamura, *Nonadiabatic transition: Concepts, basic theories and applications*, World Scientific, River Edge, NJ, **2002**.
- [54] E. E. Nikitin, Nonadiabatic Transitions: What We Learned from Old Masters and How Much We Owe Them, *Annu. Rev. Phys. Chem.* **1999**, 50, 1, 1.
- [55] J. N. Harvey, Understanding the kinetics of spin-forbidden chemical reactions, *Phys. Chem. Chem. Phys.* **2007**, 9, 3, 331.
- [56] D. Fedorov, S. Koseki, M. Schmidt, M. Gordon, Spin-orbit coupling in molecules: Chemistry beyond the adiabatic approximation, *Int. Rev. Phys. Chem.* **2003**, 22, 3, 551.
- [57] K. Drukker, Basics of Surface Hopping in Mixed Quantum/Classical Simulations, *J. Comput. Phys.* **1999**, 153, 2, 225.
- [58] G. A. Worth, L. S. Cederbaum, Beyond Born-Oppenheimer: Molecular Dynamics Through a Conical Intersection, *Annu. Rev. Phys. Chem.* **2004**, 55, 1, 127.
- [59] P. Ehrenfest, Ersetzung der Hypothese vom unmechanischen Zwang durch eine Forderung bezüglich des inneren Verhaltens jedes einzelnen Elektrons, *Die Naturwissenschaften* **1925**, 13, 47, 953.
- [60] W. Pauli, Zur Quantenmechanik des magnetischen Elektrons, *Z. Phys.* **1927**, 43, 9-10, 601.
- [61] D. A. McQuarrie, J. D. Simon, *Physical Chemistry: A Molecular Approach*, University Science Books, Sausalito, **1997**.
- [62] P. A. M. Dirac, On the Theory of Quantum Mechanics, *Proc. R. Soc. London Ser. A* **1926**, 112, 762, 661.
- [63] J. Slater, Atomic Shielding Constants, *Phys. Rev.* **1930**, 36, 1, 57.
- [64] S. F. Boys, Electronic Wave Functions. I. A General Method of Calculation for the Stationary States of Any Molecular System, *Proc. R. Soc. London Ser. A* **1950**, 200, 1063, 542.
- [65] W. J. Hehre, Stewart R. F., Pople J. A., Self-Consistent Molecular-Orbital Methods. I. Use of Gaussian Expansions of Slater-Type Atomic Orbitals, *J. Chem. Phys.* **1969**, 51, 6, 2657.

- [66] A. Schäfer, C. Huber, R. Ahlrichs, Fully optimized contracted Gaussian basis sets of triple zeta valence quality for atoms Li to Kr, *J. Chem. Phys.* **1994**, 100, 8, 5829.
- [67] R. Krishnan, J. S. Binkley, R. Seeger, J. A. Pople, Self-consistent molecular orbital methods. XX. A basis set for correlated wave functions, *J. Chem. Phys.* **1980**, 72, 1, 650.
- [68] D. R. Hartree, The Wave Mechanics of an Atom with a Non-Coulomb Central Field. Part I. Theory and Methods, *Math. Proc. Cambridge Philos. Soc.* **1928**, 24, 01, 89.
- [69] J. Slater, Note on Hartree's Method, *Phys. Rev.* **1930**, 35, 2, 210.
- [70] V. Fock, Näherungsmethode zur Lösung des quantenmechanischen Mehrkörperproblems, *Z. Phys.* **1930**, 61, 1-2, 126.
- [71] C. Roothaan, New Developments in Molecular Orbital Theory, *Rev. Mod. Phys.* **1951**, 23, 2, 69.
- [72] G. G. Hall, The Molecular Orbital Theory of Chemical Valency. VIII. A Method of Calculating Ionization Potentials, *Proc. R. Soc. London Ser. A* **1951**, 205, 1083, 541.
- [73] J. A. Pople, R. K. Nesbet, Self-Consistent Orbitals for Radicals, *J. Chem. Phys.* **1954**, 22, 3, 571.
- [74] L. H. Thomas, The calculation of atomic fields, *Math. Proc. Cambridge Philos. Soc.* **1927**, 23, 05, 542.
- [75] E. Fermi, Un Metodo Statistico per la Determinazione di alcune Proprietà dell'Atomo, *Rend. Accad. Naz. Lincei* **1927**, , 6, 602.
- [76] P. Hohenberg, Inhomogeneous Electron Gas, *Phys. Rev.* **1964**, 136, 3B, B864.
- [77] W. Kohn, L. J. Sham, Self-Consistent Equations Including Exchange and Correlation Effects, *Phys. Rev.* **1965**, 140, 4A, A1133.
- [78] D. M. Ceperley, Ground State of the Electron Gas by a Stochastic Method, *Phys. Rev. Letters* **1980**, 45, 7, 566.
- [79] J. Slater, A Simplification of the Hartree-Fock Method, *Phys. Rev.* **1951**, 81, 3, 385.
- [80] S. Vosko, L. Wilk, M. Nusair, Accurate spin-dependent electron liquid correlation energies for local spin density calculations: a critical analysis, *Can. J. Phys.* **1980**, 58, 8, 1200.
- [81] A. D. Becke, Density-functional exchange-energy approximation with correct asymptotic behavior, *Phys. Rev. A* **1988**, 38, 6, 3098.
- [82] A. D. Becke, Density-functional thermochemistry. I. The effect of the exchange-only gradient correction, *J. Chem. Phys.* **1992**, 96, 3, 2155.
- [83] C. Lee, W. Yang, R. G. Parr, Development of the Colle-Salvetti correlation-energy formula into a functional of the electron density, *Phys. Rev. B* **1988**, 37, 2, 785.

- [84] P. J. Stephens, F. J. Devlin, C. F. Chabalowski, M. J. Frisch, Ab Initio Calculation of Vibrational Absorption and Circular Dichroism Spectra Using Density Functional Force Fields, *J. Phys. Chem.* **1994**, 98, 45, 11623.
- [85] A. D. Becke, A new mixing of Hartree–Fock and local density-functional theories, *J. Chem. Phys.* **1993**, 98, 2, 1372.
- [86] A. D. Becke, Density-functional thermochemistry. III. The role of exact exchange, *J. Chem. Phys.* **1993**, 98, 7, 5648.
- [87] J. P. Perdew, K. A. Jackson, M. R. Pederson, D. J. Singh, C. Fiolhais, Atoms, molecules, solids, and surfaces: Applications of the generalized gradient approximation for exchange and correlation, *Phys. Rev. B* **1992**, 46, 11, 6671.
- [88] S. F. Sousa, P. A. Fernandes, M. J. Ramos, General Performance of Density Functionals, *J. Phys. Chem. A* **2007**, 111, 42, 10439.
- [89] J. B. Foresman, E. Frisch, *Exploring chemistry with electronic structure methods*, 2nd ed., Gaussian, Pittsburgh, Pa, **1996**.
- [90] J. W. Ochterski, G. A. Petersson, J. A. Montgomery, A complete basis set model chemistry. V. Extensions to six or more heavy atoms, *J. Chem. Phys.* **1996**, 104, 7, 2598.
- [91] J. A. Montgomery, M. J. Frisch, J. W. Ochterski, G. A. Petersson, A complete basis set model chemistry. VI. Use of density functional geometries and frequencies, *J. Chem. Phys.* **1999**, 110, 6, 2822.
- [92] J. A. Montgomery, M. J. Frisch, J. W. Ochterski, G. A. Petersson, A complete basis set model chemistry. VII. Use of the minimum population localization method, *J. Chem. Phys.* **2000**, 112, 15, 6532.
- [93] M. J. Frisch, G. W. Trucks, H. B. Schlegel, G. E. Scuseria, M. A. Robb, J. R. Cheeseman, J. J. A. Montgomery, T. Vreven, K. N. Kudin, J. C. Burant, J. M. Millam, S. S. Iyengar, J. Tomasi, V. Barone, B. Mennucci, M. Cossi, G. Scalmani, N. Rega, G. A. Petersson, H. Nakatsuji, M. Hada, M. Ehara, K. Toyota, R. Fukuda, J. Hasegawa, M. Ishida, T. Nakajima, Y. Honda, O. Kitao, H. Nakai, M. Klene, X. Li, J. E. Knox, H. P. Hratchian, J. B. Cross, V. Bakken, C. Adamo, J. Jaramillo, R. Gomperts, R. E. Stratmann, O. Yazyev, A. J. Austin, R. Cammi, C. Pomelli, J. W. Ochterski, P. Y. Ayala, K. MOROKUMA, G. A. Voth, P. Salvador, J. J. Dannenberg, V. G. Zakrzewski, S. Dapprich, A. D. Daniels, M. C. Strain, O. Farkas, D. K. Malick, A. D. Rabuck, K. Raghavachari, J. B. Foresman, J. V. Ortiz, Q. Cui, A. G. Baboul, S. Clifford, J. Cioslowski, B. B. Stefanov, G. Liu, A. Liashenko, P. Piskorz, I. Komaromi, R. L. Martin, D. J. Fox, T. Keith, M. A. Al-Laham, C. Y. Peng, A. Nanayakkara, M. Challacombe, P. M. W. Gill, B. Johnson, W. Chen, M. W. Wong, C. Gonzalez, J. A. Pople,

- Gaussian 03, Revision C.02.
- [94] W. J. Hehre, *A guide to molecular mechanics and quantum chemical calculations*, Wavefunction, Irvine, CA, **2003**.
 - [95] D. J. Wales, *Energy landscapes*, Cambridge University Press, Cambridge, UK; New York, **2003**.
 - [96] G. Henkelman, H. Jonsson, Improved tangent estimate in the nudged elastic band method for finding minimum energy paths and saddle points, *J. Chem. Phys.* **2000**, 113, 22, 9978.
 - [97] G. Henkelman, B. P. Uberuaga, H. Jonsson, A climbing image nudged elastic band method for finding saddle points and minimum energy paths, *J. Chem. Phys.* **2000**, 113, 22, 9901.
 - [98] W. E, W. Ren, E. Vanden-Eijnden, String method for the study of rare events, *Phys. Rev. B* **2002**, 66, 5.
 - [99] B. Peters, A. Heyden, A. T. Bell, A. Chakraborty, A growing string method for determining transition states: Comparison to the nudged elastic band and string methods, *J. Chem. Phys.* **2004**, 120, 17, 7877.
 - [100] A. Goodrow, A. T. Bell, M. Head-Gordon, Development and application of a hybrid method involving interpolation and ab initio calculations for the determination of transition states, *J. Chem. Phys.* **2008**, 129, 17, 174109.
 - [101] A. Goodrow, A. T. Bell, M. Head-Gordon, Transition state-finding strategies for use with the growing string method, *J. Chem. Phys.* **2009**, 130, 24, 244108.
 - [102] A. Goodrow, A. T. Bell, M. Head-Gordon, A strategy for obtaining a more accurate transition state estimate using the growing string method, *Chem. Phys. Lett.* **2010**, 484, 4-6, 392.
 - [103] J. Baker, An algorithm for the location of transition states, *J. Comput. Chem.* **1986**, 7, 4, 385.
 - [104] G. Henkelman, H. Jonsson, A dimer method for finding saddle points on high dimensional potential surfaces using only first derivatives, *J. Chem. Phys.* **1999**, 111, 15, 7010.
 - [105] A. Heyden, A. T. Bell, F. J. Keil, Efficient methods for finding transition states in chemical reactions: Comparison of improved dimer method and partitioned rational function optimization method, *J. Chem. Phys.* **2005**, 123, 22, 224101.
 - [106] J. Kästner, P. Sherwood, Superlinearly converging dimer method for transition state search, *J. Chem. Phys.* **2008**, 128, 1, 014106.
 - [107] J. N. Harvey, M. Aschi, Modelling spin-forbidden reactions: recombination of carbon monoxide with iron tetracarbonyl, *Faraday Discuss.* **2003**, 124, 129.
 - [108] J. N. Harvey, M. Aschi, Spin-forbidden dehydrogenation of methoxy

- cation: a statistical view, *Phys. Chem. Chem. Phys.* **1999**, 1, 24, 5555.
- [109] Q. Cui, K. Morokuma, J. M. Bowman, S. J. Klippenstein, The spin-forbidden reaction $\text{CH}(^2\Pi) + \text{N}_2 \rightarrow \text{HCN} + \text{N}(^4S)$ revisited. II. Nonadiabatic transition state theory and application, *J. Chem. Phys.* **1999**, 110, 19, 9469.
- [110] F. McLafferty, T. George, On nonadiabatic transition state theory, *Chem. Phys. Lett.* **1976**, 37, 1, 67.
- [111] J. N. Harvey, M. Aschi, H. Schwarz, W. Koch, The singlet and triplet states of phenyl cation. A hybrid approach for locating minimum energy crossing points between non-interacting potential energy surfaces, *Theor. Chem. Acc.* **1998**, 99, 2, 95.
- [112] N. Koga, K. Morokuma, Determination of the lowest energy point on the crossing seam between two potential surfaces using the energy gradient, *Chem. Phys. Lett.* **1985**, 119, 5, 371.
- [113] D. R. Yarkony, Systematic determination of intersections of potential energy surfaces using a Lagrange multiplier constrained procedure, *J. Phys. Chem.* **1993**, 97, 17, 4407.
- [114] F. Jensen, Locating minima on seams of intersecting potential energy surfaces. An application to transition structure modeling, *J. Am. Chem. Soc.* **1992**, 114, 5, 1596.
- [115] S. Madsen, F. Jensen, Locating seam minima for macromolecular systems, *Theor. Chem. Acc.* **2009**, 123, 5-6, 477.
- [116] A. Farazdel, M. Dupuis, On the determination of the minimum on the crossing seam of two potential energy surfaces, *J. Comput. Chem.* **1991**, 12, 2, 276.
- [117] J. M. Anglada, J. M. Bofill, A reduced-restricted-quasi-Newton-Raphson method for locating and optimizing energy crossing points between two potential energy surfaces, *J. Comput. Chem.* **1997**, 18, 8, 992.
- [118] M. J. Bearpark, M. A. Robb, H. Bernhard Schlegel, A direct method for the location of the lowest energy point on a potential surface crossing, *Chem. Phys. Lett.* **1994**, 223, 3, 269.
- [119] A. Heyden, B. Peters, A. T. Bell, F. J. Keil, Comprehensive DFT Study of Nitrous Oxide Decomposition over Fe-ZSM-5, *J. Phys. Chem. B* **2005**, 109, 5, 1857.
- [120] D. G. Truhlar, B. C. Garrett, S. J. Klippenstein, Current Status of Transition-State Theory, *J. Phys. Chem.* **1996**, 100, 31, 12771.
- [121] D. G. Truhlar, B. C. Garrett, Variational Transition State Theory, *Annu. Rev. Phys. Chem.* **1984**, 35, 1, 159.
- [122] D. G. Truhlar, B. C. Garrett, Variational transition-state theory, *Acc. Chem. Res.* **1980**, 13, 12, 440.

- [123] B. C. Garrett, D. G. Truhlar, Generalized transition state theory. Classical mechanical theory and applications to collinear reactions of hydrogen molecules, *J. Phys. Chem.* **1979**, 83, 8, 1052.
- [124] B. C. Garrett, D. G. Truhlar, Criterion of minimum state density in the transition state theory of bimolecular reactions, *J. Chem. Phys.* **1979**, 70, 4, 1593.
- [125] J. C. Keck, Variational Theory of Chemical Reaction Rates Applied to Three-Body Recombinations, *J. Chem. Phys.* **1960**, 32, 4, 1035.
- [126] P. W. Atkins, C. A. Trapp, M. Zillgitt, *Physikalische Chemie*, 3rd ed., VCH, Weinheim [u.a.], **2001**.
- [127] M. Tuckerman, *Statistical mechanics and molecular simulations*, Oxford University Press, Oxford, UK, **2007**.
- [128] W. Göpel, H.-D. Wiemhöfer, *Statistische Thermodynamik*, Spektrum, Akad. Verl., Heidelberg; Berlin, **2000**.
- [129] J. W. Gibbs, *Elementary principles in statistical mechanics: Developed with especial reference to the rational foundation of thermodynamics*, Ox Bow Press, Woodbridge, Conn, **1981**.
- [130] C. E. Housecroft, A. G. Sharpe, *Inorganic chemistry*, 3rd ed., Pearson Prentice Hall, Harlow, England; New York, **2008**.
- [131] A. Fernández-Ramos, B. A. Ellingson, R. Meana-Pañeda, J. M. C. Marques, D. G. Truhlar, Symmetry numbers and chemical reaction rates, *Theor. Chem. Acc.* **2007**, 118, 4, 813.
- [132] H. Eyring, The Activated Complex and the Absolute Rate of Chemical Reactions, *Chem. Rev.* **1935**, 17, 1, 65.
- [133] M. G. Evans, M. Polanyi, Some applications of the transition state method to the calculation of reaction velocities, especially in solution, *Trans. Faraday Soc.* **1935**, 31, 875.
- [134] P. Pechukas, Transition State Theory, *Annu. Rev. Phys. Chem.* **1981**, 32, 1, 159.
- [135] D. G. Truhlar, W. L. Hase, J. T. Hynes, Current status of transition-state theory, *J. Phys. Chem.* **1983**, 87, 15, 2664.
- [136] K. J. Laidler, M. C. King, Development of transition-state theory, *J. Phys. Chem.* **1983**, 87, 15, 2657.
- [137] K. J. Laidler, *Chemical Kinetics*, 3rd ed., Harper & Row, New York, **1987**.
- [138] M. Page, J. W. McIver, On Evaluating the Reaction-Path Hamiltonian, *J. Chem. Phys.* **1988**, 88, 2, 922.
- [139] A. E. Stearn, H. Eyring, Nonadiabatic Reactions. The Decomposition of N₂O, *J. Chem. Phys.* **1935**, 3, 12, 778.
- [140] R. J. Kee, F. M. Rupley, J. A. Miller, *Chemkin-II: A FORTRAN chemical kinetics package for the analysis of gas phase chemical kinetics*.

- SAND89-8009*, Livermore, CA, **1991**.
- [141] M. E. Coltrin, R. J. Kee, F. M. Rupley, *Surface Chemkin: A FORTRAN package for analyzing heterogeneous chemical kinetics at a solid-surface – gas phase interface*. *SAND90-8003B*, Livermore, CA, **1991**.
- [142] P. Spitzer, C. Zierhofer, E. Hochmair, Algorithm for multi-curve-fitting with shared parameters and a possible application in evoked compound action potential measurements, *Biomed. Eng. Online* **2006**, 5.
- [143] M. Saliccioli, Y. Chen, D. G. Vlachos, Microkinetic Modeling and Reduced Rate Expressions of Ethylene Hydrogenation and Ethane Hydrogenolysis on Platinum, *Ind. Eng. Chem. Res.* **2011**, 50, 1, 28.
- [144] R. Q. Long, R. T. Yang, Catalytic Performance of Fe-ZSM-5 Catalysts for Selective Catalytic Reduction of Nitric Oxide by Ammonia, *J. Catal.* **1999**, 188, 2, 332.
- [145] S. Stevenson, J. C. Vartuli, Kinetics of the Selective Catalytic Reduction of NO over HZSM-5, *J. Catal.* **2000**, 190, 2, 228.
- [146] M. Koebel, M. Elsener, G. Madia, Reaction pathways in the selective catalytic reduction process with NO and NO₂ at low temperatures, *Ind. Eng. Chem. Res.* **2001**, 40, 1, 52.
- [147] M. Koebel, G. Madia, M. Elsener, Selective catalytic reduction of NO and NO₂ at low temperatures, *Catal. Today* **2002**, 73, 3-4, 239.
- [148] D. T. Pence, T. R. Thomas, *Proc. AEC Pollut. Control Conf.* **1972**, 115.
- [149] S. Stevenson, J. C. Vartuli, S. B. Sharma, The Effects of Steaming and Sodium Exchange on the Selective Catalytic Reduction of NO and NO₂ by NH₃ over HZSM-5, *J. Catal.* **2002**, 208, 1, 106.
- [150] J. Eng, C. H. Bartholomew, Kinetic and Mechanistic Study of NO_x Reduction by NH₃ over H-Form Zeolites, *J. Catal.* **1997**, 171, 1, 14.
- [151] J. Eng, C. H. Bartholomew, Kinetic and Mechanistic Study of NO_x Reduction by NH₃ over H-Form Zeolites, *J. Catal.* **1997**, 171, 1, 27.
- [152] M. Richter, R. Eckelt, B. Parlitz, R. Fricke, Low-temperature conversion of NO_x to N₂ by zeolite-fixed ammonium ions, *Appl. Catal. B* **1998**, 15, 1-2, 129.
- [153] M. Wallin, C. Karlsson, M. Skoglundh, A. Palmqvista, Selective catalytic reduction of NO_x with NH₃ over zeolite H-ZSM-5: influence of transient ammonia supply, *J. Catal.* **2003**, 218, 2, 354.
- [154] M. Wallin, C.-J. Karlsson, A. Palmqvist, M. Skoglundh, Selective Catalytic Reduction of NO_x over H-ZSM-5 Under Lean Conditions Using Transient NH₃ Supply, *Top. Catal.* **2004**, 30/31, 107.
- [155] R. Long, R. T. Yang, Characterization of Fe-ZSM-5 Catalyst for Selective Catalytic Reduction of Nitric Oxide by Ammonia, *J. Catal.* **2000**, 194, 1, 80.

- [156] R. Long, R. T. Yang, Reaction Mechanism of Selective Catalytic Reduction of NO with NH₃ over Fe-ZSM-5 Catalyst, *J. Catal.* **2002**, 207, 2, 224.
- [157] V. Sanchez-Escribano, T. Montanari, G. Busca, Low temperature selective catalytic reduction of NO by ammonia over H-ZSM-5: an IR study, *Appl. Catal. B* **2005**, 58, 1-2, 19.
- [158] K. Rahkamaa-Tolonen, T. Maunula, M. Lomma, M. Huuhtanen, R. Keiski, The effect of NO₂ on the activity of fresh and aged zeolite catalysts in the NH₃-SCR reaction, *Catal. Today* **2005**, 100, 3-4, 217.
- [159] V. M. Mastikhin, S. V. Filimonova, ¹⁵N nuclear magnetic resonance studies of the NO-O₂-NH₃ reaction over ZSM-5 zeolites, *J. Chem. Soc., Faraday Trans.* **1992**, 88, 10, 1473.
- [160] J. R. Klovsky, P. B. Koradia, C. T. Lim, Evaluation of a New Zeolitic Catalyst for NO_x Reduction with NH₃, *Ind. Eng. Chem. Prod. RD* **1980**, 19, 2, 218.
- [161] R. Q. Long, R. T. Yang, Temperature-Programmed Desorption/Surface Reaction (TPD/TPSR) Study of Fe-Exchanged ZSM-5 for Selective Catalytic Reduction of Nitric Oxide by Ammonia, *J. Catal.* **2001**, 198, 1, 20.
- [162] G. Qi, R. Yang, Ultra-active Fe/ZSM-5 catalyst for selective catalytic reduction of nitric oxide with ammonia, *Appl. Catal. B* **2005**, 60, 1-2, 13.
- [163] O. Kröcher, M. Devadas, M. Elsener, A. Wokaun, N. Söger, M. Pfeifer, Y. Demel, L. Mussmann, Investigation of the selective catalytic reduction of NO by NH₃ on Fe-ZSM5 monolith catalysts, *Appl. Catal. B* **2006**, 66, 3-4, 208.
- [164] M. Schwidder, M. S. Kumar, K. Klementiev, M. Pohl, A. Brückner, W. Grünert, Selective reduction of NO with Fe-ZSM-5 catalysts of low Fe content: Part I. Relations between active site structure and catalytic performance, *J. Catal.* **2005**, 231, 2, 314.
- [165] K. Krishna, M. Makkee, Preparation of Fe-ZSM-5 with enhanced activity and stability for SCR of NO_x, *Catal. Today* **2006**, 114, 1, 23.
- [166] T. Komatsu, M. Nunokawa, I. S. Moon, T. Takahara, S. Namba, T. Yashima, Kinetic Studies of Reduction of Nitric Oxide with Ammonia on Cu₂⁺-Exchanged Zeolites, *J. Catal.* **1994**, 148, 2, 427.
- [167] E. M. El-Malki, R. A. van Santen, W. M. H. Sachtler, Introduction of Zn, Ga, and Fe into HZSM-5 Cavities by Sublimation: Identification of Acid Sites, *J. Phys. Chem. B* **1999**, 103, 22, 4611.
- [168] A. Grossale, I. Nova, E. Tronconi, D. Chatterjee, M. Weibel, The chemistry of the NO/NO₂-NH₃ "fast" SCR reaction over Fe-ZSM5 investigated by transient reaction analysis, *J. Catal.* **2008**, 256, 2, 312.

- [169] A. Grossale, I. Nova, E. Tronconi, Ammonia blocking of the “Fast SCR” reactivity over a commercial Fe-zeolite catalyst for Diesel exhaust aftertreatment, *J. Catal.* **2009**, 265, 2, 141.
- [170] A. Grossale, I. Nova, E. Tronconi, Role of Nitrate Species in the “NO₂-SCR” Mechanism over a Commercial Fe-zeolite Catalyst for SCR Mobile Applications, *Catal. Lett.* **2009**, 130, 3-4, 525.
- [171] M. Schwidder, M. S. Kumar, U. Bentrup, J. Pérez-Ramírez, A. Brückner, W. Grünert, The role of Brønsted acidity in the SCR of NO over Fe-MFI catalysts, *Microporous and Mesoporous Materials* **2008**, 111, 1-3, 124.
- [172] S. Brandenberger, O. Kröcher, A. Wokaun, A. Tissler, R. Althoff, The role of Brønsted acidity in the selective catalytic reduction of NO with ammonia over Fe-ZSM-5, *J. Catal.* **2009**, 268, 2, 297.
- [173] M. J. Li, J. Henao, Y. Yeom, E. Weitz, W. M. Sachtler, Low activation energy pathway for the catalyzed reduction of nitrogen oxides to N₂ by ammonia, *Catal. Lett.* **2004**, 98, 1, 5.
- [174] M. Li, Y. Yeom, E. Weitz, W. M. H. Sachtler, An acid catalyzed step in the catalytic reduction of NO_x to N₂, *Catal. Lett.* **2006**, 112, 3-4, 129.
- [175] I. Halasz, A. Brenner, K. Y. Simon Ng, Active sites of H-ZSM5 catalysts for the oxidation of nitric oxide by oxygen, *Catal. Lett.* **1995**, 34, 1-2, 151.
- [176] B. J. Adelman, G.-D. Lei, W. M. H. Sachtler, Co-adsorption of nitrogen monoxide and nitrogen dioxide in zeolitic DeNO_x catalysts, *Catal. Lett.* **1994**, 28, 2-4, 119.
- [177] Q. Sun, Z. X. Gao, B. Wen, W. M. Sachtler, Spectroscopic evidence for a nitrite intermediate in the catalytic reduction of NO_x with ammonia on Fe/MFI, *Catal. Lett.* **2002**, 78, 1-4, 1.
- [178] A. Grossale, I. Nova, E. Tronconi, Study of a Fe-zeolite-based system as NH₃-SCR catalyst for diesel exhaust aftertreatment, *Catal. Today* **2008**, 136, 1-2, 18.
- [179] M. Anstrom, Density functional theory studies of mechanistic aspects of the SCR reaction on vanadium oxide catalysts, *J. Catal.* **2003**, 213, 2, 115.
- [180] S. Soyer, A. Uzun, S. Senkan, I. Onal, A quantum chemical study of nitric oxide reduction by ammonia (SCR reaction) on V₂O₅ catalyst surface, *Catal. Today* **2006**, 118, 3-4, 268.
- [181] J. Li, S. Li, New insight into selective catalytic reduction of nitrogen oxides by ammonia over H-form zeolites: a theoretical study, *Phys. Chem. Chem. Phys.* **2007**, 9, 25, 3304.
- [182] D. Tantanak, I. H. Hillier, M. A. Vincent, A theoretical study of the

- formation of a nitrogen–nitrogen triple bond from RNH_2 and NO species: implications for the selective catalytic reduction of nitrogen oxides, *J. Mol. Struct.-Theochem* **2003**, 626, 1-3, 239.
- [183] N. H. Morgon, A. R. d. Souza, J. R. Sambrano, $\text{NH}_3 + \text{N}_2\text{O}_3$ reaction. High level calculations, *J. Mol. Struct.-Theochem* **2006**, 759, 1-3, 189.
- [184] A. M. Mebel, M. C. Lin, C. F. Melius, Rate Constant of the $\text{HONO} + \text{HONO} \rightarrow \text{H}_2\text{O} + \text{NO} + \text{NO}_2$ Reaction from ab Initio MO and TST Calculations, *J. Phys. Chem. A* **1998**, 102, 10, 1803.
- [185] R. Wieczorek, Z. Latajka, J. Lundell, Quantum chemical study of the bimolecular complex of HONO , *J. Phys. Chem. A* **1999**, 103, 31, 6234.
- [186] A. Chou, Zhiru, F.-M. Tao, Density Functional Studies of the Formation of Nitrous Acid from the Reaction of Nitrogen Dioxide and Water Vapor, *J. Phys. Chem. A* **1999**, 103, 39, 7848.
- [187] D. Hanway, F. M. Tao, A density functional theory and ab initio study of the hydrolysis of dinitrogen pentoxide, *Chem. Phys. Lett.* **1998**, 285, 5-6, 459.
- [188] R. N. Musin, M. C. Lin, Novel bimolecular reactions between NH_3 and HNO_3 in the gas phase, *J. Phys. Chem. A* **1998**, 102, 10, 1808.
- [189] A. M. Mebel, C.-C. Hsu, M. C. Lin, K. Morokuma, An ab initio molecular orbital study of potential energy surface of the $\text{NH}_2 + \text{NO}_2$ reaction, *J. Chem. Phys.* **1995**, 103, 13, 5640.
- [190] C. Frenck, W. Weisweiler, Modeling the reactions between ammonia and dinitrogen pentoxide to synthesize ammonium dinitramide, *Chem. Eng. Technol.* **2002**, 25, 2, 123.
- [191] X. Lu, R. N. Musin, M. C. Lin, Gas-phase reactions of HONO with HNO and NH_3 : an ab initio MO/TST study, *J. Phys. Chem. A* **2000**, 104, 21, 5141.
- [192] X. Lu, J. Park, M. C. Lin, Gas Phase Reactions of HONO with NO_2 , O_3 , *J. Phys. Chem. A* **2000**, 104, 38, 8730.
- [193] K. Hadjiivanov, J. Saussey, J. L. Freysz, J. C. Lavalley, FT-IR study of $\text{NO} + \text{O}_2$ co-adsorption on H-ZSM-5: re-assignment of the 2133 cm^{-1} band to NO^+ species, *Catal. Lett.* **1998**, 52, 1-2, 103.
- [194] B. Pommier, P. Gelin, Infrared and volumetric study of NO adsorption on Pd-H-ZSM-5, *Phys. Chem. Chem. Phys.* **2001**, 3, 6, 1138.
- [195] J. Szanyi, J. H. Kwak, R. A. Moline, C. H. Peden, The adsorption of NO_2 and the $\text{NO} + \text{O}_2$ reaction on Na-Y,FAU: an in situ FTIR investigation, *Phys. Chem. Chem. Phys.* **2003**, 5, 18, 4045.
- [196] I. Perdana, D. Creaser, O. Ohrman, J. Hedlund, A comparison of NO_x adsorption on Na, H and BaZSM-5 films, *Appl. Catal., B* **2007**, 72, 1-2, 82.
- [197] D. H. Olson, G. T. Kokotailo, S. L. Lawton, W. M. Meier, Crystal

- structure and structure-related properties of ZSM-5, *J. Phys. Chem.* **1981**, 85, 15, 2238.
- [198] D. H. Olson, N. Khosrovani, A. W. Peters, B. H. Toby, Crystal Structure of Dehydrated CsZSM-5 (5.8Al): Evidence for Nonrandom Aluminum Distribution, *J. Phys. Chem. B* **2000**, 104, 20, 4844.
- [199] M. S. Stave, J. B. Nicholas, Density Functional Studies of Zeolites. 2. Structure and Acidity of [T]-ZSM-5 Models (T = B, Al, Ga, and Fe), *J. Phys. Chem.* **1995**, 99, 41, 15046.
- [200] R. Ahlrichs, M. Bär, M. Haser, H. Horn, C. Kolmel, Electronic structure calculations on workstation computers: The program system turbomole, *Chem. Phys. Lett.* **1989**, 162, 3, 165.
- [201] O. Treutler, R. Ahlrichs, Efficient molecular numerical integration schemes, *J. Chem. Phys.* **1995**, 102, 1, 346.
- [202] H. Tsukahara, Gas-Phase Oxidation of Nitric Oxide: Chemical Kinetics and Rate Constant, *Nitric Oxide* **1999**, 3, 3, 191.
- [203] E. H. Teunissen, R. A. van Santen, A. P. J. Jansen, F. B. van Duijneveldt, Ammonium in zeolites: coordination and solvation effects, *J. Phys. Chem.* **1993**, 97, 1, 203.
- [204] E. D. Glendening, A. M. Halpern, Ab initio calculations of nitrogen oxide reactions: Formation of N_2O_2 , N_2O_3 , N_2O_4 , N_2O_5 , and N_4O_2 from NO, NO_2 , NO_3 , and N_2O , *J. Chem. Phys.* **2007**, 127, 16, 164307.
- [205] T. C. Brüggemann, M.-D. Przybylski, S. P. Balaji, F. J. Keil, Theoretical Investigation of the Mechanism of the Selective Catalytic Reduction of Nitrogen Dioxide with Ammonia on H-Form Zeolites and the Role of Nitric and Nitrous Acids as Intermediates, *J. Phys. Chem. C* **2010**, 114, 14, 6567.
- [206] A. Savara, M.-J. Li, W. M. Sachtler, E. Weitz, Catalytic reduction of NH_4NO_3 by NO: Effects of solid acids and implications for low temperature DeNO_x processes, *Appl. Catal. B* **2008**, 81, 3-4, 251.
- [207] A. M. Mebel, M. C. Lin, K. Morokuma, C. F. Melius, Theoretical-Study of the Gas-Phase Structure, Thermochemistry, and Decomposition Mechanisms of NH_4NO_2 and $\text{NH}_4\text{N}(\text{NO}_2)_2$, *J. Phys. Chem.* **1995**, 99, 18, 6842.
- [208] T. W. Kirchstetter, R. A. Harley, D. Littlejohn, Measurement of nitrous acid in motor vehicle exhaust, *Environ. Sci. Technol.* **1996**, 30, 9, 2843.
- [209] K. A. Ramazan, D. Syomin, B. J. Finlayson-Pitts, The photochemical production of HONO during the heterogeneous hydrolysis of NO_2 , *Phys. Chem. Chem. Phys.* **2004**, 6, 14, 3836.
- [210] J. Calvert, G. Yarwood, A. Dunker, An Evaluation of the Mechanism of Nitrous Acid Formation in the Urban Atmosphere, *Res. Chem. Intermed.* **1994**, 20, 3, 463.

- [211] P. Wiesen, J. Kleffmann, R. Kurtenbach, K. H. Becker, Mechanistic study of the heterogeneous conversion of NO₂ into HONO and N₂O on acid surfaces, *Faraday Discuss.* **1995**, 100, 121.
- [212] B. J. Finlayson-Pitts, L. M. Wingen, A. L. Sumner, D. Syomin, K. A. Ramazan, The heterogeneous hydrolysis of NO₂ in laboratory systems and in outdoor and indoor atmospheres: An integrated mechanism, *Phys. Chem. Chem. Phys.* **2003**, 5, 2, 223.
- [213] A. L. Goodman, G. M. Underwood, V. H. Grassian, Heterogeneous reaction of NO₂: Characterization of gas-phase and adsorbed products from the reaction, 2 NO₂(g)+H₂O(a)→ HONO(g)+HNO₃(a) on hydrated silica particles, *J. Phys. Chem. A* **1999**, 103, 36, 7217.
- [214] J. A. Harrison, R. G. A. R. Maclagan, A. R. Whyte, Structures, energies, and vibrational frequencies of intermediates and transition states in the reaction of amidogen and nitric oxide, *J. Phys. Chem.* **1987**, 91, 27, 6683.
- [215] S. P. Walch, Theoretical characterization of the reaction NH₂+NO → products, *J. Chem. Phys.* **1993**, 99, 7, 5295.
- [216] E. W.-G. Diau, S. C. Smith, Theoretical investigation of the potential energy surface for the NH₂+NO reaction via density functional theory and ab initio molecular electronic structure theory, *J. Chem. Phys.* **1997**, 106, 22, 9236.
- [217] A. C. Akah, G. Nkeng, A. A. Garforth, The role of Al and strong acidity in the selective catalytic oxidation of NH₃ over Fe-ZSM-5, *Appl. Catal., B* **2007**, 74, 1-2, 34.
- [218] T. Curtin, S. Lenihan, Copper exchanged beta zeolites for the catalytic oxidation of ammonia, *Chem. Commun.* **2003**, , 11, 1280.
- [219] G. S. Qi, J. E. Gatt, R. T. Yang, Selective catalytic oxidation (SCO) of ammonia to nitrogen over Fe-exchanged zeolites prepared by sublimation of FeCl₃, *J. Catal.* **2004**, 226, 1, 120.
- [220] R. Q. Long, R. T. Yang, Selective Catalytic Oxidation (SCO) of Ammonia to Nitrogen over Fe-Exchanged Zeolites, *J. Catal.* **2001**, 201, 1, 145.
- [221] R. Q. Long, R. T. Yang, Superior ion-exchanged ZSM-5 catalysts for selective catalytic oxidation of ammonia to nitrogen, *Chem. Commun.* **2000**, , 17, 1651.
- [222] R. Q. Long, R. T. Yang, Noble metal (Pt, Rh, Pd) promoted Fe-ZSM-5 for selective catalytic oxidation of ammonia to N₂ at low temperatures, *Catal. Lett.* **2002**, 78, 1-4, 353.
- [223] S. Nassos, E. E. Svensson, M. Boutonnet, S. Järas, The influence of Ni load and support material on catalysts for the selective catalytic oxidation of ammonia in gasified biomass, *Appl. Catal. B* **2007**, 74,

- 1-2, 92.
- [224] R. Burch, B. Southward, A Novel Application of Trapping Catalysts for the Selective Low-Temperature Oxidation of NH_3 to N_2 in Simulated Biogas, *J. Catal.* **2000**, 195, 1, 217.
- [225] L. Andrussov, Über die schnell verlaufenden katalytischen Prozesse in strömenden Gasen und die Ammoniak-Oxydation (V), *Ber. dtsh. Chem. Ges. A/B* **1927**, 60, 8, 2005.
- [226] R. Imbihl, A. Scheibe, Y. F. Zeng, S. Günther, R. Kraehnert, V. A. Kondratenko, M. Baerns, W. K. Offermans, A. P. J. Jansen, R. A. van Santen, Catalytic ammonia oxidation on platinum: mechanism and catalyst restructuring at high and low pressure, *Phys. Chem. Chem. Phys.* **2007**, 9, 27, 3522.
- [227] Y. J. Li, J. N. Armor, Selective NH_3 oxidation to N_2 in a wet stream, *Appl. Catal., B* **1997**, 13, 2, 131.
- [228] J. Jones, M. Pourkashanian, A. Williams, R. Backreedy, L. Darvell, P. Simell, K. Heiskannen, P. Kilpinen, The selective oxidation of ammonia over alumina supported catalysts—experiments and modelling, *Appl. Catal. B* **2005**, 60, 1-2, 139.
- [229] T. Curtin, F. O' Regan, C. Deconinck, N. Knuttel, B. K. Hodnett, The catalytic oxidation of ammonia: influence of water and sulfur on selectivity to nitrogen over promoted copper oxide/alumina catalysts, *Catal. Today* **2000**, 55, 1-2, 189.
- [230] L. Gang, J. van Grondelle, B. G. Anderson, R. A. van Santen, Selective low temperature NH_3 oxidation to N_2 on copper-based catalysts, *J. Catal.* **1999**, 186, 1, 100.
- [231] H. M. Kusar, A. G. Ersson, M. Vosecky, S. G. Jaras, Selective catalytic oxidation of NH_3 to N_2 for catalytic combustion of low heating value gas under lean/rich conditions, *Appl. Catal., B* **2005**, 58, 1-2, 25.
- [232] L. S. Escandon, S. Ordonez, F. V. Diez, H. Sastre, Ammonia oxidation over conventional combustion catalysts, *React. Kinet. Catal. Lett.* **2002**, 76, 1, 61.
- [233] N. N. Sazonova, A. V. Simakov, T. A. Nikoro, G. B. Barannik, V. F. Lyakhova, V. I. Zheivot, Z. R. Ismagilov, H. Veringa, Selective catalytic oxidation of ammonia to nitrogen, *React. Kinet. Catal. Lett.* **1996**, 57, 1, 71.
- [234] M. Amblard, A study of the mechanism of selective conversion of ammonia to nitrogen on $\text{Ni}/\gamma\text{-Al}_2\text{O}_3$ under strongly oxidising conditions, *Catal. Today* **2000**, 59, 3-4, 365.
- [235] L. Chmielarz, P. Kustrowski, A. Rafalska-Lasocha, R. Dziembaj, Selective oxidation of ammonia to nitrogen on transition metal containing mixed metal oxides, *Appl. Catal. B* **2005**, 58, 3-4, 235.

- [236] G. Ramis, L. Yi, G. Busca, Ammonia activation over catalysts for the selective catalytic reduction of NO_x and the selective catalytic oxidation of NH_3 . An FT-IR study, *Catal. Today* **1996**, 28, 4, 373.
- [237] L. Gang, B. G. Anderson, J. van Grondelle, R. A. van Santen, Intermediate species and reaction pathways for the oxidation of ammonia on powdered catalysts, *J. Catal.* **2001**, 199, 1, 107.
- [238] M. Bodenstein, Einzelvorträge: Herr Max Bodenstein-Berlin: Über den Mechanismus der katalytischen Ammoniakverbrennung, *Z. Elektrochem. angew. phys. Chem.* **1935**, 41, 7, 466.
- [239] M. Bodenstein, Einige Reaktionen des Hydroxylamins und die Katalytische Ammoniakoxydation, *Z. Elektrochem. angew. phys. Chem.* **1941**, 47, 7, 501.
- [240] O. Skreiberg, P. Kilpinen, P. Glarborg, Ammonia chemistry below 1400 K under fuel-rich conditions in a flow reactor, *Combust. Flame* **2004**, 136, 4, 501.
- [241] D. A. Dixon, J. S. Francisco, Y. Alexeev, Thermochemical Properties of H_xNO Molecules and Ions from ab Initio Electronic Structure Theory, *J. Phys. Chem. A* **2006**, 110, 1, 185.
- [242] S. G. Cheskis, V. A. Nadtochenko, O. M. Sarkisov, Study of the $\text{HNO} + \text{HNO}$ and $\text{HNO} + \text{NO}$ Reactions by Intra-Cavity Laser Spectroscopy, *Int. J. Chem. Kinet.* **1981**, 13, 10, 1041.
- [243] M. C. Lin, Y. S. He, C. F. Melius, Theoretical Interpretation of the Kinetics and Mechanisms of the $\text{HNO} + \text{HNO}$ and $\text{HNO} + 2\text{NO}$ Reactions with a Unified Model, *Int. J. Chem. Kinet.* **1992**, 24, 5, 489.
- [244] E. W. Diau, M. C. Lin, Y. He, C. F. Melius, Theoretical Aspects of H/N/O-Chemistry Relevant to the Thermal Reduction of NO by H_2 , *Prog. Energy Combust. Sci.* **1995**, 21, 1, 1.
- [245] A. M. Mebel, K. Morokuma, M. C. Lin, C. F. Melius, Potential-Energy Surface of the $\text{HNO} + \text{NO}$ Reaction – An Ab-Initio Molecular-Orbital Study, *J. Phys. Chem.* **1995**, 99, 7, 1900.
- [246] Am Mebel, M. C. Lin, K. Morokuma, Ab initio MO and TST calculations for the rate constant of the $\text{HNO} + \text{NO}_2 \rightarrow \text{HONO} + \text{NO}$ reaction, *Int. J. Chem. Kinet.* **1998**, 30, 10, 729.
- [247] K. Ruud, T. Helgaker, E. Uggerud, Mechanisms, energetics and dynamics of a key reaction sequence during the decomposition of nitromethane: $\text{HNO} + \text{HNO} \rightarrow \text{N}_2\text{O} + \text{H}_2\text{O}$, *J. Mol. Struc.-Theochem* **1997**, 393, 1-3, 59.
- [248] O. P. Strausz, H. E. Gunning, Reactions of Electronically Excited Nitric Oxide Molecules with Hydrocarbons, *Can. J. Chem.* **1963**, 41, 5, 1207.
- [249] O. P. Strausz, H. E. Gunning, Reaction of Hydrogen Atoms with Nitric Oxide, *Trans. Faraday Soc.* **1964**, 60, 4942, 347.

- [250] J. L. Holmes, E. V. Sundaram, Gas Phase Photolysis of Hydrogen Iodide. I. Inhibition with Nitric Oxide at 25 Degrees C, *Trans. Faraday Soc.* **1966**, 62, 520P, 910.
- [251] J. L. Holmes, E. V. Sundaram, Gas-Phase Photolysis of Hydrogen Iodide. 2. Effect of Nitric Oxide at 6 and -20 Degrees C, *Trans. Faraday Soc.* **1966**, 62, 523P, 1822.
- [252] T. C. Brüggemann, F. J. Keil, Theoretical Investigation of the Mechanism of the Selective Catalytic Oxidation of Ammonia on H-Form Zeolites, *J. Phys. Chem. C* **2009**, 113, 31, 13860.
- [253] L. Cisneros, W. J. Rogers, M. S. Mannan, Adiabatic calorimetric decomposition studies of 50 wt. % hydroxylamine/water, *J. Hazard. Mater.* **2001**, 82, 1, 13.
- [254] S. R. Saraf, W. J. Rogers, M. S. Mannan, M. B. Hall, L. M. Thomson, Theoretical Thermochemistry: Ab Initio Heat of Formation for Hydroxylamine, *J. Phys. Chem. A* **2003**, 107, 8, 1077.
- [255] D. Feller, D. A. Dixon, A Nonparametrized Ab Initio Determination of the Heat of Formation of Hydroxylamine, NH_2OH , *J. Phys. Chem. A* **2003**, 107, 48, 10419.
- [256] A. B. Mhadeshwar, D. G. Vlachos, Hierarchical multiscale mechanism development for methane partial oxidation and reforming and for thermal decomposition of oxygenates on Rh, *J. Phys. Chem. B* **2005**, 109, 35, 16819.
- [257] A. B. Mhadeshwar, H. Wang, D. G. Vlachos, Thermodynamic consistency in microkinetic development of surface reaction mechanisms, *J. Phys. Chem. B* **2003**, 107, 46, 12721.
- [258] N. Hansen, A. Heyden, A. T. Bell, F. J. Keil, Microkinetic modeling of nitrous oxide decomposition on dinuclear oxygen bridged iron sites in Fe-ZSM-5, *J. Catal.* **2007**, 248, 2, 213.
- [259] A. A. Gokhale, S. Kandoi, J. P. Greeley, M. Mavrikakis, J. A. Dumesic, Molecular-level descriptions of surface chemistry in kinetic models using density functional theory, *Chem. Eng. Sci.* **2004**, 59, 22-23, 4679.
- [260] N. Hansen, T. Kerber, J. Sauer, A. T. Bell, F. J. Keil, Quantum Chemical Modeling of Benzene Ethylation over H-ZSM-5 Approaching Chemical Accuracy: A Hybrid MP2:DFT Study, *J. Am. Chem. Soc.* **2010**, 132, 33, 11525.
- [261] S. Grimme, Semiempirical GGA-type density functional constructed with a long-range dispersion correction, *J. Comput. Chem.* **2006**, 27, 15, 1787.
- [262] B. A. d. Moor, M.-F. Reyniers, G. B. Marin, Physisorption and chemisorption of alkanes and alkenes in H-FAU: a combined ab initio-statistical thermodynamics study, *Phys. Chem. Chem. Phys.* **2009**, 11,

- 16, 2939.
- [263] M. Frenklach, H. Wang, M. Goldenberg, G. P. Smith, D. M. Golden, C. T. Bowman, R. K. Hanson, W. C. Gardiner, V. Lissianski, GRI-Mechs An Optimized Detailed Chemical Reaction Mechanism for Methane Combustion. Available via the Internet at http://www.me.berkeley.edu/gri_mech/ (Accessed February 1, 2009).
- [264] B. E. Poling, J. P. O'Connell, J. M. Prausnitz, *The properties of gases and liquids*, 5th ed., McGraw-Hill, New York, NY [u.a.], **2001**.
- [265] M. J. Chase, NIST-JANAF Thermochemical Tables, Fourth Edition, *J. Phys. Chem. Ref. Data, Monograph* **1998**, 9, 1.
- [266] L. Shirazi, E. Jamshidi, M. R. Ghasemi, The effect of Si/Al ratio of ZSM-5 zeolite on its morphology, acidity and crystal size, *Cryst. Res. Technol.* **2008**, 43, 12, 1300.
- [267] D. J. Parrillo, R. J. Gorte, W. E. Farneth, A Calorimetric Study of Simple Bases in H-ZSM-5 - A Comparison with Gas-Phase and Solution-Phase Acidities, *J. Am. Chem. Soc.* **1993**, 115, 26, 12441.
- [268] J. Valyon, G. Onyestyak, L. V. Rees, Study of the dynamics of NH₃ adsorption in ZSM-5 zeolites and the acidity of the sorption sites using the frequency-response technique, *J. Phys. Chem. B* **1998**, 102, 45, 8994.
- [269] F. Lonyi, J. Valyon, A TPD and IR study of the surface species formed from ammonia on zeolite H-ZSM-5, H-mordenite and H-beta, *Thermochim. Acta* **2001**, 373, 1, 53.
- [270] F. Lonyi, J. Valyon, On the interpretation of the NH₃-TPD patterns of H-ZSM-5 and H-mordenite, *Microporous Mesoporous Mater.* **2001**, 47, 2-3, 293.
- [271] M. Armandi, B. Bonelli, I. Bottero, C. O. Arean, E. Garrone, Thermodynamic Features of the Reaction of Ammonia with the Acidic Proton of H-ZSM-5 As Studied by Variable-Temperature IR Spectroscopy, *J. Phys. Chem. C* **2010**, 114, 14, 6658.
- [272] B. Bonelli, M. Armandi, C. O. Arean, E. Garrone, Ammonia-Solvated Ammonium Species in the NH₄-ZSM-5 Zeolite, *ChemPhysChem* **2010**, 11, 15, 3255.
- [273] B. Hunger, J. Hoffmann, Kinetic-Analysis of NH₃ Temperature Programmed Desorption (TPD) on a HZSM-5 Zeolite, *Thermochim. Acta* **1986**, 106, 133.
- [274] B. Hunger, J. Hoffmann, O. Heitzsch, M. Hunger, Temperature-Programmed Desorption (TPD) of Ammonia from HZSM-5 Zeolites, *J. Therm. Anal.* **1990**, 36, 4, 1379.
- [275] S. B. Sharma, B. L. Meyers, D. T. Chen, J. Miller, J. A. Dumesic, Characterization of Catalyst Acidity by Microcalorimetry and Temperature-

- Programmed Desorption, *Appl. Catal., A* **1993**, 102, 2, 253.
- [276] B. Dragoi, A. Gervasini, E. Dumitriu, A. Auroux, Calorimetric determination of the acidic character of amorphous and crystalline aluminosilicates, *Thermochim. Acta* **2004**, 420, 1-2, Sp. Iss. SI, 127.
- [277] J. Datka, B. Gil, Heterogeneity of OH groups in HZSM-5 zeolites. IR studies of ammonia adsorption and desorption, *J. Mol. Struct.* **2001**, 596, Sp. Iss. SI, 41.
- [278] R. Atkinson, D. L. Baulch, R. A. Cox, J. N. Crowley, R. F. Hampson, R. G. Hynes, M. E. Jenkin, M. J. Rossi, J. Troe, Evaluated kinetic and photochemical data for atmospheric chemistry: Volume I - gas phase reactions of O_x, HO_x, NO_x and SO_x species, *Atmos. Chem. Phys.* **2004**, 4, 6, 1461.
- [279] Y. Yeom, J. Henao, M. Li, W. Sachtler, E. Weitz, The role of NO in the mechanism of reduction with ammonia over a BaNa-Y catalyst, *J. Catal.* **2005**, 231, 1, 181.
- [280] A. Savara, W. M. Sachtler, E. Weitz, TPD of NO₂⁻ and NO₃⁻ from Na-Y: The relative stabilities of nitrates and nitrites in low temperature DeNO_x catalysis, *Appl. Catal. B* **2009**, 90, 1-2, 120.
- [281] I. Nova, C. Ciardelli, E. Tronconi, D. Chatterjee, M. Weibel, NH₃-NO/NO₂ SCR for diesel exhausts after treatment: mechanism and modelling of a catalytic converter, *Top. Catal.* **2007**, 42-43, 1-4, 43.
- [282] G. Delahay, D. Valade, A. Guzmán-Vargas, B. Coq, Selective catalytic reduction of nitric oxide with ammonia on Fe-ZSM-5 catalysts prepared by different methods, *Appl. Catal. B* **2005**, 55, 2, 149.
- [283] H. Y. Huang, R. Q. Long, R. T. Yang, Kinetics of selective catalytic reduction of NO with NH₃ on Fe-ZSM-5 catalyst, *Appl. Catal. A* **2002**, 235, 1-2, 241.
- [284] H. Y. Chen, T. Voskoboinikov, W. M. Sachtler, Reduction of NO_x over Fe/ZSM-5 catalysts: Adsorption complexes and their reactivity toward hydrocarbons, *J. Catal.* **1998**, 180, 2, 171.
- [285] L. J. Lobree, I. C. Hwang, J. A. Reimer, A. T. Bell, An in situ infrared study of NO reduction by C₃H₈ over Fe-ZSM-5, *Catal. Lett.* **1999**, 63, 3-4, 233.
- [286] R. Brosius, D. Habermacher, J. A. Martens, L. Vradman, M. Herskowitz, L. Capek, Z. Sobalik, J. Dedeczek, B. Wichterlova, V. Tokarova, O. Gonsiorova, NO oxidation kinetics on iron zeolites: influence of framework type and iron speciation, *Top. Catal.* **2004**, 30-1, 1-4, 333.
- [287] L. Capek, L. Vradman, P. Sazama, M. Herskowitz, B. Wichterlova, R. Zukerman, R. Brosius, J. Martens, Kinetic experiments and modeling of NO oxidation and SCR of NO_x with decane over Cu- and Fe-MFI catalysts, *Appl. Catal. B* **2007**, 70, 1-4, 53.

- [288] R. Giles, N. W. Cant, M. Kogel, T. Turek, D. L. Trimm, The effect of SO₂ on the oxidation of NO over Fe-MFI and Fe-ferrierite catalysts made by solid-state ion exchange, *Appl. Catal., B* **2000**, 25, 2-3, L75.
- [289] H. Sjövall, R. J. Blint, A. Gopinath, L. Olsson, A Kinetic Model for the Selective Catalytic Reduction of NO_x with NH₃ over an Fe-zeolite Catalyst, *Ind. Eng. Chem. Res.* **2010**, 49, 1, 39.
- [290] S. Brandenberger, O. Kröcher, A. Tissler, R. Althoff, Estimation of the fractions of different nuclear iron species in uniformly metal-exchanged Fe-ZSM-5 samples based on a Poisson distribution, *Appl. Catal. A* **2010**, 373, 1-2, 168.
- [291] G. D. Pirngruber, P. K. Roy, R. Prins, On determining the nuclearity of iron sites in Fe-ZSM-5 – a critical evaluation, *Phys. Chem. Chem. Phys.* **2006**, 8, 34, 3939.
- [292] H. Y. Chen, E. M. El-Malki, X. Wang, R. A. van Santen, W. M. Sachtler, Identification of active sites and adsorption complexes in Fe/MFI catalysts for NO_x reduction, *J. Mol. Catal. A: Chem.* **2000**, 162, 1-2, 159.
- [293] M. S. Kumar, M. Schwidder, W. Grünert, A. Brückner, On the nature of different iron sites and their catalytic role in Fe-ZSM-5 DeNO_x catalysts: new insights by a combined EPR and UV/VIS spectroscopic approach, *J. Catal.* **2004**, 227, 2, 384.
- [294] M. S. Kumar, M. Schwidder, W. Grünert, U. Bentrup, A. Brückner, Selective reduction of NO with Fe-ZSM-5 catalysts of low Fe content: Part II. Assessing the function of different Fe sites by spectroscopic in situ studies, *J. Catal.* **2006**, 239, 1, 173.
- [295] A. Zecchina, M. Rivallan, G. Berlier, C. Lamberti, G. Ricchiardi, Structure and nuclearity of active sites in Fe-zeolites: comparison with iron sites in enzymes and homogeneous catalysts, *Phys. Chem. Chem. Phys.* **2007**, 9, 27, 3483.
- [296] G. Berlier, A. Zecchina, G. Spoto, G. Ricchiardi, S. Bordiga, C. Lamberti, The role of Al in the structure and reactivity of iron centers in Fe-ZSM-5-based catalysts: a statistically based infrared study, *J. Catal.* **2003**, 215, 2, 264.
- [297] A. Rosa, G. Ricciardi, E. J. Baerends, Is [FeO]²⁺ the Active Center Also in Iron Containing Zeolites? A Density Functional Theory Study of Methane Hydroxylation Catalysis by Fe-ZSM-5 Zeolite, *Inorg. Chem.* **2010**, 49, 8, 3866.
- [298] L. J. Lobree, I. C. Hwang, J. A. Reimer, A. T. Bell, Investigations of the state of Fe in H-ZSM-5, *J. Catal.* **1999**, 186, 2, 242.
- [299] A. Sierralta, Theoretical Study of NO₂ Adsorption on a Transition-Metal Zeolite Model, *J. Catal.* **2002**, 205, 1, 107.

- [300] A. Heyden, N. Hansen, A. T. Bell, F. J. Keil, Nitrous Oxide Decomposition over Fe-ZSM-5 in the Presence of Nitric Oxide: A Comprehensive DFT Study, *J. Phys. Chem. B* **2006**, 110, 34, 17096.
- [301] N. Hansen, A. Heyden, A. T. Bell, F. J. Keil, A reaction mechanism for the nitrous oxide decomposition on binuclear oxygen bridged iron sites in Fe-ZSM-5, *J. Phys. Chem. C* **2007**, 111, 5, 2092.
- [302] H. Guesmi, D. Berthomieu, L. Kiwi-Minsker, Nitrous Oxide Decomposition on the Binuclear $[\text{Fe}^{\text{II}}(\mu\text{-O})(\mu\text{-OH})\text{Fe}^{\text{II}}]$ Center in Fe-ZSM-5 Zeolite, *J. Phys. Chem. C* **2008**, 112, 51, 20319.
- [303] J. G. Fripiat, F. Bergerandre, J. M. Andre, E. G. Derouane, Non-Empirical Quantum Chemical Calculation on Pentasil-Type Zeolites, *Zeolites* **1983**, 3, 4, 306.
- [304] E. G. Derouane, J. G. Fripiat, Non-Empirical Quantum Chemical Study of the Siting and Pairing of Aluminum in the MFI Framework, *Zeolites* **1985**, 5, 3, 165.
- [305] S. Lonsinger, A. K. Chakraborty, D. N. Theodorou, A. T. Bell, The Effects of Local Structural Relaxation on Aluminum Siting Within H-ZSM-5, *Catal. Lett.* **1991**, 11, 2, 209.
- [306] A. Redondo, P. J. Hay, Quantum-Chemical Studies of Acid Sites in Zeolite ZSM-5, *J. Phys. Chem.* **1993**, 97, 45, 11754.
- [307] A. Chatterjee, A. K. Chandra, Fe and B substitution in ZSM-5 zeolites: A quantum-mechanical study, *J. Mol. Catal. A: Chem.* **1997**, 119, 1-3, 51.
- [308] D. Zhou, Y. Bao, M. Yang, N. He, G. Yang, DFT studies on the location and acid strength of Brønsted acid sites in MCM-22 zeolite, *J. Mol. Catal. A: Chem.* **2006**, 244, 1-2, 11.
- [309] Y. Zhao, N. González-García, D. G. Truhlar, Benchmark Database of Barrier Heights for Heavy Atom Transfer, Nucleophilic Substitution, Association, and Unimolecular Reactions and Its Use to Test Theoretical Methods, *J. Phys. Chem. A* **2005**, 109, 9, 2012.
- [310] S. Shaik, S. Cohen, Y. Wang, H. Chen, D. Kumar, W. Thiel, P450 Enzymes: Their Structure, Reactivity, and Selectivity—Modeled by QM/MM Calculations, *Chem. Rev.* **2010**, 110, 2, 949.
- [311] I. Zilberberg, R. W. Gora, G. M. Zhidomirov, J. Leszczynski, Bonding in the oxo ferrous iron species: A complete active-space self-consistent-field theory verification of the molecular-oxygen-like pattern, *J. Chem. Phys.* **2002**, 117, 15, 7153.
- [312] M. Radon, E. Broclawik, K. Pierloot, Electronic Structure of Selected $\{\text{FeNO}\}$ 7, *J. Phys. Chem. B* **2010**, 114, 3, 1518.
- [313] H. Chen, J. Song, W. Lai, W. Wu, S. Shaik, Multiple Low-Lying States for Compound I of P450 cam and Chloroperoxidase Revealed from Mul-

- reference Ab Initio QM/MM Calculations, *J. Chem. Theory Comput.* **2010**, 6, 3, 940.
- [314] A. Heyden, A. Bell, F. Keil, Kinetic modeling of nitrous oxide decomposition on Fe-ZSM-5 based on parameters obtained from first-principles calculations, *J. Catal.* **2005**, 233, 1, 26.
- [315] H. Guesmi, D. Berthomieu, B. Bromley, B. Coq, L. Kiwi-Minsker, Theoretical evidence of the observed kinetic order dependence on temperature during the N₂O decomposition over Fe-ZSM-5, *Phys. Chem. Chem. Phys.* **2010**, 12, 12, 2873.
- [316] T. C. Brüggemann, F. J. Keil, Theoretical Investigation of the Mechanism of the Oxidation of Nitrogen Oxide on Iron-Form Zeolites in the Presence of Water, *J. Phys. Chem. C* **2011**, 115, 5, 2114.
- [317] O. Kröcher, M. Elsener, Combination of V₂O₅/WO₃-TiO₂, Fe-ZSM5, and Cu-ZSM5 Catalysts for the Selective Catalytic Reduction of Nitric Oxide with Ammonia, *Ind. Eng. Chem. Res.* **2008**, 47, 22, 8588.
- [318] M. Iwasaki, K. Yamazaki, H. Shinjoh, NO_x reduction performance of fresh and aged Fe-zeolites prepared by CVD: Effects of zeolite structure and Si/Al₂ ratio, *Appl. Catal. B* **2011**, 102, 1-2, 302.
- [319] A. Grossale, I. Nova, E. Tronconi, D. Chatterjee, M. Weibel, NH₃-NO/NO₂ SCR for Diesel Exhausts Aftertreatment: Reactivity, Mechanism and Kinetic Modelling of Commercial Fe- and Cu-Promoted Zeolite Catalysts, *Top. Catal.* **2009**, 52, 13-20, 1837.
- [320] A. L. Kustov, K. Egeblad, M. Kustova, T. W. Hansen, C. H. Christensen, Mesoporous Fe-containing ZSM-5 zeolite single crystal catalysts for selective catalytic reduction of nitric oxide by ammonia, *Top. Catal.* **2007**, 45, 1-4, 159.
- [321] E. Lima, A. Guzmán-Vargas, J. Méndez-Vivar, H. Pfeiffer, J. Fraissard, Fe-ZSM-5 Catalysts: Preparation in Organic Media, Fe-particle Morphology and NO_x Reduction Activity, *Catal. Lett.* **2008**, 120, 3-4, 244.
- [322] S. Brandenberger, O. Kröcher, A. Tissler, R. Althoff, Effect of Structural and Preparation Parameters on the Activity and Hydrothermal Stability of Metal-Exchanged ZSM-5 in the Selective Catalytic Reduction of NO by NH₃, *Ind. Eng. Chem. Res.* **2011**, 50, 8, 4308.
- [323] L. Capek, V. Kreibich, J. Dedecek, T. Grygar, B. Wichterlova, Z. Sobalik, J. Martens, R. Brosius, V. Tokarova, Analysis of Fe species in zeolites by UV-VIS-NIR, IR spectra and voltammetry. Effect of preparation, Fe loading and zeolite type, *Microporous Mesoporous Mater.* **2005**, 80, 1-3, 279.
- [324] M. Iwasaki, K. Yamazaki, K. Banno, H. Shinjoh, Characterization of Fe/ZSM-5 DeNO_x catalysts prepared by different methods: Relation-

- ships between active Fe sites and NH_3 -SCR performance, *J. Catal.* **2008**, 260, 2, 205.
- [325] M. Iwasaki, H. Shinjoh, NO evolution reaction with NO_2 adsorption over Fe/ZSM-5: In situ FT-IR observation and relationships with Fe sites, *J. Catal.* **2010**, 273, 1, 29.
- [326] A. d. Toni, M. Schwidder, W. Grünert, A. Brückner, Zentrenstruktur und Vergiftungswirkungen bei der selektiven katalytischen Reduktion von NO mit Ammoniak an Fe-ZSM-5-Katalysatoren, *Chem. Ing. Tech.* **2007**, 79, 6, 871.
- [327] J. Sullivan, O. Keane, The role of Brønstead acidity in poisoning the SCR-urea reaction over FeZSM-5 catalysts, *Appl. Catal. B* **2005**, 61, 3-4, 244.
- [328] A. Schuler, M. Votsmeier, P. Kiwic, J. Gieshoff, W. Hauptmann, A. Drochner, H. Vogel, NH_3 -SCR on Fe zeolite catalysts – From model setup to NH_3 dosing, *Chem. Eng. J.* **2009**, 154, 1-3, 333.
- [329] J.-Y. Luo, X. Hou, P. Wijayakoon, S. J. Schmieg, W. Li, W. S. Epling, Spatially resolving SCR reactions over a Fe/zeolite catalyst, *Appl. Catal. B* **2011**, 102, 1-2, 110.
- [330] P. S. Metkar, N. Salazar, R. Muncrief, V. Balakotaiah, M. P. Harold, Selective catalytic reduction of NO with NH_3 on iron zeolite monolithic catalysts: Steady-state and transient kinetics, *Appl. Catal. B* **2011**, 104, 110.
- [331] A. Schuler, A. Drochner, H. Vogel, S. Malmberg, M. Votsmeier, J. Gieshoff, N. Söger, L. Mußmann, Transiente Effekte der NH_3 -SCR an Fe-Zeolithen – Experimente und Computersimulation, *Chem. Ing. Tech.* **2006**, 78, 9, 1246.
- [332] M. Devadas, O. Kröcher, M. Elsener, A. Wokaun, G. Mitrikas, N. Söger, M. Pfeifer, Y. Demel, L. Mussmann, Characterization and catalytic investigation of Fe-ZSM5 for urea-SCR, *Catal. Today* **2007**, 119, 1-4, 137.
- [333] M. Iwasaki, K. Yamazaki, H. Shinjoh, Transient reaction analysis and steady-state kinetic study of selective catalytic reduction of NO and $\text{NO} + \text{NO}_2$ by NH_3 over Fe/ZSM-5, *Appl. Catal. A* **2009**, 366, 1, 84.
- [334] P. Forzatti, I. Nova, E. Tronconi, Enhanced NH_3 Selective Catalytic Reduction for NO_x Abatement, *Angew. Chem. Int. Ed.* **2009**, 48, 44, 8366.
- [335] P. Forzatti, I. Nova, E. Tronconi, New “Enhanced NH_3 -SCR” Reaction for NO_x Emission Control, *Ind. Eng. Chem. Res.* **2010**, 49, 21, 10386.
- [336] B. Coq, M. Mauvezin, G. Delahay, S. Kieger, Kinetics and Mechanism of the N_2O Reduction by NH_3 on a Fe-Zeolite-Beta Catalyst, *J. Catal.* **2000**, 195, 2, 298.

- [337] A. Guzmán-Vargas, G. Delahay, B. Coq, Catalytic decomposition of N_2O and catalytic reduction of N_2O and $\text{N}_2\text{O} + \text{NO}$ by NH_3 in the presence of O_2 over Fe-zeolite, *Appl. Catal. B* **2003**, 42, 4, 369.
- [338] B. Coq, M. Mauvezin, G. Delahay, J.-B. Butet, S. Kieger, The simultaneous catalytic reduction of NO and N_2O by NH_3 using an Fe-zeolite-beta catalyst, *Appl. Catal. B* **2000**, 27, 3, 193.
- [339] G. Delahay, M. Mauvezin, B. Coq, S. Kieger, Selective Catalytic Reduction of Nitrous Oxide by Ammonia on Iron Zeolite Beta Catalysts in an Oxygen Rich Atmosphere: Effect of Iron Contents, *J. Catal.* **2001**, 202, 1, 156.
- [340] A. Ates, Characteristics of Fe-exchanged natural zeolites for the decomposition of N_2O and its selective catalytic reduction with NH_3 , *Appl. Catal. B* **2007**, 76, 3-4, 282.
- [341] K. Sugawara, T. Nobukawa, M. Yoshida, Y. Sato, K. Okumura, K. Tomishige, K. Kunimori, The importance of Fe loading on the N_2O reduction with NH_3 over Fe-MFI: Effect of acid site formation on Fe species, *Appl. Catal. B* **2007**, 69, 3-4, 154.
- [342] J. Li, S. Li, A DFT Study toward Understanding the High Activity of Fe-Exchanged Zeolites for the “Fast” Selective Catalytic Reduction of Nitrogen Oxides with Ammonia, *J. Phys. Chem. C* **2008**, 112, 43, 16938.
- [343] M. Schwidder, M. S. Kumar, A. Brückner, W. Grünert, Active sites for NO reduction over Fe-ZSM-5 catalysts, *Chem. Commun.* **2005**, , 6, 805.
- [344] D. Chatterjee, P. Kočí, V. Schmeißer, M. Marek, M. Weibel, B. Krutzsch, Modelling of a combined NO_x storage and NH_3 -SCR catalytic system for Diesel exhaust gas aftertreatment, *Catal. Today* **2010**, 151, 3-4, 395.
- [345] B. Ramachandran, Testing zeolite SCR catalysts under protocol conditions for NO_x abatement from stationary emission sources, *Catal. Today* **2000**, 55, 3, 281.
- [346] P. Kern, M. Klimczak, T. Heinzelmann, M. Lucas, P. Claus, High-throughput study of the effects of inorganic additives and poisons on NH_3 -SCR catalysts. Part II: Fe-zeolite catalysts, *Appl. Catal. B* **2010**, 95, 1-2, 48.
- [347] M. Devadas, O. Kröcher, A. Wokaun, Catalytic investigation of Fe-ZSM5 in the selective catalytic reduction of NO_x with NH_3 , *React. Kinet. Catal. Lett.* **2005**, 86, 2, 347.
- [348] S. Malmberg, M. Votsmeier, J. Gieshoff, N. Söger, L. Mußmann, A. Schuler, A. Drochner, Dynamic phenomena of SCR-catalysts containing Fe-exchanged zeolites – experiments and computer simulations,

- Top. Catal.* **2007**, 42-43, 1-4, 33.
- [349] I. Nova, D. Bounechada, R. Maestri, E. Tronconi, A. K. Heibel, T. A. Collins, T. Boger, Influence of the Substrate Properties on the Performances of NH_3 , *Ind. Eng. Chem. Res.* **2011**, 50, 1, 299.
- [350] D. Danovich, S. Shaik, Spin–Orbit Coupling in the Oxidative Activation of H–H by FeO^+ . Selection Rules and Reactivity Effects, *J. Am. Chem. Soc.* **1997**, 119, 7, 1773.
- [351] A. Goodrow, A. T. Bell, M. Head-Gordon, Are Spin-Forbidden Crossings a Bottleneck in Methanol Oxidation?, *J. Phys. Chem. C* **2009**, 113, 45, 19361.
- [352] M. Colombo, I. Nova, E. Tronconi, A comparative study of the NH_3 -SCR reactions over a Cu-zeolite and a Fe-zeolite catalyst, *Catal. Today* **2010**, 151, 3-4, 223.

Published work

- J.A. Federici, D.G. Norton, **T. C. Brüggemann**, K.W. Voit, E.D. Wetzel, and D.G. Vlachos,
Catalytic microcombustors with integrated thermoelectric elements for portable power production
J. Power Sources **2006**, 161, 1469–1478.
- N. Hansen, **T. C. Brüggemann**, A. T. Bell, and F. J. Keil,
Theoretical investigation of benzene alkylation with ethene over H-ZSM-5,
J. Phys. Chem. C **2008**, 112, 15402–15411.
- **T. C. Brüggemann**, F. J. Keil,
Theoretical investigation of the selective catalytic reduction of nitric oxide with ammonia on H-form zeolites
J. Phys. Chem. C **2008**, 112, 17378–17387.
- **T. C. Brüggemann**, F. J. Keil,
Theoretical investigation of the selective catalytic oxidation of ammonia on H-form zeolites
J. Phys. Chem. C **2009**, 113, 13860–13876.
- **T. C. Brüggemann**, M-D. Przybylski, S. P. Balaji, F. J. Keil,
Theoretical investigation of the selective catalytic reduction of nitric dioxide with ammonia on H-form zeolites and the role of nitric and nitrous acids as intermediates
J. Phys. Chem. C **2010**, 114, 6567–6587.

- **T. C. Brüggemann**, F. J. Keil,
Theoretical investigation of the mechanism of the oxidation of nitrogen oxide on Fe-form zeolites in the presence of water
J. Phys. Chem. C **2011**, 115, 2114–2133.
- **T. C. Brüggemann**, F. J. Keil, D. G. Vlachos,
Microkinetic modeling of the fast selective catalytic reduction of nitrogen oxide with ammonia on H-ZSM5 based on first principles
J. Catal. **2011**, 283, 178–191
- **T. C. Brüggemann**, F. J. Keil,
Theoretical investigation of the mechanism of the selective catalytic reduction of nitrogen oxide with ammonia on Fe-form zeolites
J. Phys. Chem. C **2011**, 115, 23854–23870.

Conferences

- T.C. Brüggemann, F.J. Keil, “Theoretische Untersuchung des Reaktionsmechanismus der selektiven katalytischen Reduktion von Stickstoffmonoxid mit Ammoniak am H-ZSM5”, 42. Jahrestreffen deutscher Katalytiker, Weimar, 10.–13. Mrz 2009
- T.C. Brüggemann, F.J. Keil, “Theoretische Untersuchung der selektiven katalytischen Reduktion von Stickstoffmonoxid mit Ammoniak in Kombination mit der selektiven katalytischen Oxidation von Ammoniak am H-ZSM5”, Jahrestreffen Reaktionstechnik 2009, Würzburg, 8.–10. Juni 2009
- T.C. Brüggemann, F. J. Keil, “Theoretical Investigation of the Mechanism of the Selective Catalytic Reduction of Nitric Oxide with Ammonia in the Presence of Oxygen on H-form Zeolites”, 2009 Aiche Annual Meeting, Nashville, TN, 8.–13. Nov. 2009

Lebenslauf

Persönliche Daten

Name	Till Christian Brüggemann
Geburtsdatum	22.11.1979
Geburtsort	Karlsruhe

Schulausbildung

08/1986 – 07/1990	Werner von Siemens Grundschule Karlsruhe
08/1990 – 06/1999	Humboldt Gymnasium Karlsruhe
06/1999	Abschluss: Abitur

Zivildienst

08/1999 – 07/2000	Alten- und Pflegewohnheim Benckiser-Stift der Evangelischen Stadtmission in Karlsruhe
-------------------	--

Studium

10/2000 – 08/2003	Verfahrenstechnik an der TU Hamburg-Harburg
09/2003 – 06/2004	Chemical Engineering an der University of Delaware, Newark, USA
08/2004 – 04/2006	Verfahrenstechnik an der TU Hamburg-Harburg
04/2006	Abschluss: Diplom-Ingenieur

Wissenschaftliche Tätigkeit

06/2006 – 06/2011	Wissenschaftlicher Mitarbeiter an der TU Hamburg-Harburg, Institut für Chemische Reaktionstechnik
03/2010 – 05/2010	Forschungsaufenthalt an der University of Delaware, Newark, USA